NASA/CP–2000–209967

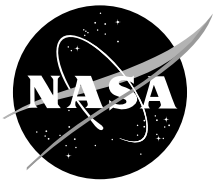

21st Space Simulation Conference
The Future of Space Simulation Testing in the 21st Century

Compiled by
Joseph L. Stecher III
Applied Engineering and Technology Directorate
NASA Goddard Space Flight Center, Greenbelt, Maryland

Sponsored by:
National Aeronautics and Space Administration
Institute of Environmental Sciences and Technology
American Institute for Aeronautics and Astronautics
American Society for Testing and Materials
Canadian Space Agency

National Aeronautics and
Space Administration

Goddard Space Flight Center
Greenbelt, Maryland 20771

October 2000

The NASA STI Program Office … in Profile

Since its founding, NASA has been dedicated to the advancement of aeronautics and space science. The NASA Scientific and Technical Information (STI) Program Office plays a key part in helping NASA maintain this important role.

The NASA STI Program Office is operated by Langley Research Center, the lead center for NASA's scientific and technical information. The NASA STI Program Office provides access to the NASA STI Database, the largest collection of aeronautical and space science STI in the world. The Program Office is also NASA's institutional mechanism for disseminating the results of its research and development activities. These results are published by NASA in the NASA STI Report Series, which includes the following report types:

- TECHNICAL PUBLICATION. Reports of completed research or a major significant phase of research that present the results of NASA programs and include extensive data or theoretical analysis. Includes compilations of significant scientific and technical data and information deemed to be of continuing reference value. NASA's counterpart of peer-reviewed formal professional papers but has less stringent limitations on manuscript length and extent of graphic presentations.
- TECHNICAL MEMORANDUM. Scientific and technical findings that are preliminary or of specialized interest, e.g., quick release reports, working papers, and bibliographies that contain minimal annotation. Does not contain extensive analysis.
- CONTRACTOR REPORT. Scientific and technical findings by NASA-sponsored contractors and grantees.
- CONFERENCE PUBLICATION. Collected papers from scientific and technical conferences, symposia, seminars, or other meetings sponsored or cosponsored by NASA.
- SPECIAL PUBLICATION. Scientific, technical, or historical information from NASA programs, projects, and mission, often concerned with subjects having substantial public interest.
- TECHNICAL TRANSLATION. English-language translations of foreign scientific and technical material pertinent to NASA's mission.

Specialized services that complement the STI Program Office's diverse offerings include creating custom thesauri, building customized databases, organizing and publishing research results . . . even providing videos.

For more information about the NASA STI Program Office, see the following:

- Access the NASA STI Program Home Page at http://www.sti.nasa.gov/STI-homepage.html
- E-mail your question via the Internet to help@sti.nasa.gov
- Fax your question to the NASA Access Help Desk at (301) 621-0134
- Telephone the NASA Access Help Desk at (301) 621-0390
- Write to:
  NASA Access Help Desk
  NASA Center for AeroSpace Information
  7121 Standard Drive
  Hanover, MD 21076–1320

Acknowledgments

This paper was not possible without the development of the Poseidon GCM by Paul Schopf, George Mason University Center for Ocean-Land-Atmospheres, and the provision of code for integration. Michele Rienecker, NASA/GSFC, provided meaningful insight into the GCM results and dynamics. The NASA/Goddard Space Flight Center Distributed Active Archive Center provided the CZCS data that was used for comparison. Margarita E. Conkright (NODC/OCL) provided *in situ* nitrate seasonal climatologies. This work was supported under NASA Grant (RTOP) 971-622-51-31.

Available from:

NASA Center for AeroSpace Information
7121 Standard Drive
Hanover, MD 21076–1320
Price Code: A17

National Technical Information Service
5285 Port Royal Road
Springfield, VA 22161
Price Code: A10

COMMITTEES FOR
21st SPACE SIMULATION CONFERENCE

MEETING MANAGEMENT COMMITTEE

General Chairman:	John D. Hazen, Boeing Phantom Works
Technical Program:	Terry C. Fisher, Jet Propulsion Laboratory
IES Meeting Chair:	John D. Campbell, Consultant
Publication Chairman:	Joseph L. Stecher III, NASA Goddard Space Flight Center
IEST Executive Director:	Julie Kendrick, Institute of Environmental Sciences and Technology
Facilities Chairman:	Russell T. Hollingsworth, Consultant
Tutorial Co-Chair:	John Packard, Mantech/NSI
Tutorial Co-Chair:	William O. Wilkinson, Johns Hopkins University Applied Physics Laboratory
Publicity Chairman:	Harold G. Fox, Johns Hopkins University Applied Physics Laboratory

TECHNICAL PROGRAM COMMITTEE

Dr. Raj K. Singhal, Canadian Space Agency

Peter W. Brinkman, ESA/ESTEC

Robert L. Tomkiewicz, Johns Hopkins University, Applied Physics Laboratory

Donald M. Benson, Northrup Grumann

Robert G. Moss, Space Systems/Loral

Patrick F. Neary, TRW

William N. Breeden III, Lockheed Martin Astronautics

Rick Lehmann, Hughes Space and Communications

JOINT POLICY COMMITTEE

IES

John D. Campbell, Consultant
Joseph L. Stecher III, NASA Goddard Space Flight Center

ASTM

Robert G. Moss, Space Systems/Loral
Eugene N. Borson, Consultant

AIAA

Terry Fisher, Jet Propulsion Laboratory

Page intentionally left blank

TABLE OF CONTENTS

SESSION 1: DYNAMICS

SESSION 2A: THERMAL VACUUM TESTING

SESSION 2B: THERMAL VACUUM TESTING (continued)

SESSION 3A: NEW CAPABILITIES

SESSION 3B: NEW CAPABILITIES (continued)

SESSION 4: INSTRUMENTATION/DATA ACQUISITION/NETWORKING

SESSION 5A: SPECIAL TOPICS

SESSION 5B: SPECIAL TOPICS (continued)

INPE/LIT New Facility for Vibration and Acoustics Tests - Novel Ideas and Lessons Learned

Elbert E. N. Macau and Rovilson E. Silva
Laboratório de Integração e Testes - LIT
Instituto Nacional de Pesquisas Espaciais - INPE
São José dos Camapos, SP, Brazil

ABSTRACT

The Brazilian Institute of Space Research/Integration and Testing Laboratory (INPE/LIT) is conducting a project to implement a new large facility for vibration and acoustic tests of spacecrafts. This new facility was designed to provide an integrated environment where simultaneous tests can be conducted with efficiency, while multiple test results can be easily analyzed and compared, allowing an incremental mechanical structural development. The facility provides resources that allow the running of automatic pretest checks, and fully automatic system and subsystems calibration procedures. Artificial Intelligence technology supports system supervision and helps system operation and data result analysis. Budget constraints required that subsystems of the current vibration facility were used wherever possible. The system is scheduled to be operational in November 2000. In this work we present the system architecture and the novel ideas that have been used in this new facility.

INTRODUCTION

The *Integration and Testing Laboratory* (*LIT*) is the *Brazilian Institute for Space Research* (*INPE*) laboratory complex where the satellite assembly, integration and test activities take place [1]. It started operating in 1987 to allow the development of satellites for the Brazilian Space Program. At first, LIT facilities were designed to allow the development of small satellites. With the success and continuity of the Brazilian Space Program, there has been a necessity to improve LIT facilities to support assembly, integration and test activities on large satellites. Thus, a 160 KN electrodynamic shaker was installed in 1993, and projects to implement new, larger facilities for vibration and acoustic tests are being conducted [2,3].

The current data acquisition and control system for vibration tests has been operating since 1987. Initially, it was designed to allow the operation of two electrodynamic shakers, one of 13 KN and other of 80 KN. With the installation of the 160 KN shaker, small changes were made to the system to allow the operation of this large shaker. However, the following reasons have contributed to the need for a new data acquisition and control system for satellite vibration and acoustic test, afterwards referred to by the acronymous *VIBSIS*: The increasing number of failures experimented these days by the dedicated computers that are used for controlling and data analysis; The necessity for having more channels available in the data acquisition and control system; The requirement for supporting three dynamical tests running simultaneously; The desire of the development teams to have the most advanced tools for visualization and analysis available on the system; The plans for building an acoustic chamber.

In this paper, we present the system architecture and the novel ideas that are being used in the design of this new data acquisition and control system. The new data acquisition subsystem will be used to support both vibration and acoustic tests. We also report the difficulties that we are facing during the phases that we have passed through in the development of the project.

THE CURRENT SYSTEM

The current Vibration Test Facility is illustrated schematically in Fig. 1. Physically, it is divided into four areas: The *High Bay*, where the shakers and the strain-gauge conditioners are installed; The *Control Room*, where two control systems (GenRad-2514), charge amplifiers for control channels, and the shakers actuators control system are located; The *Data Acquisition Room*, where the data analyzer system, the charge amplifier, and the data recorder system are placed; The *Shaker Power Amplifier Room*, where the power amplifiers that drive the shakers are installed. The signals that come from the strain-gauge senors are conditioned in the High Bay by home-made conditioners. The signals that come from the accelerometers as well as the conditioned signal from the strain-gauge sensors are wired to the control system or to the data acquisition system through a connection panel. In the control room, the signals from the control accelerometers are amplified and are connected to one of the controllers. In the

Data Acquisition Room, the signals from the accelerometers are properly conditioned. The conditioned signals from the accelerometers and strain-gauge sensors pass through a multiplex system that multiplex then in groups of four (4 x 1, PCM). The multiplexed signals are stored in two tape recorders. Two demultiplexers (1 x 4) allow the recovery of eight signals, that can be analyzed by the data analyzer system (GenRad 2515). During the test, it is possible to connect in parallel up to sixteen of the signals to the data analyzer system to allow on-line monitoring of these channels during the vibration test and immediate analysis and report generation on them just after the end of the test. The rest of the stored signals must be recover from the tape recorders through the demultiplexers, in groups of eight signals. Up to sixteen channels can be connected to a homemade maximum amplitude selector system which generates a signal that is sent to the Control Room to be used as a notching input signal. The tape recorders also provide two FM recorder channels to be used to store reference signals. The signals recorded in FM mode can be accessed at any time without passing by demultiplexing.

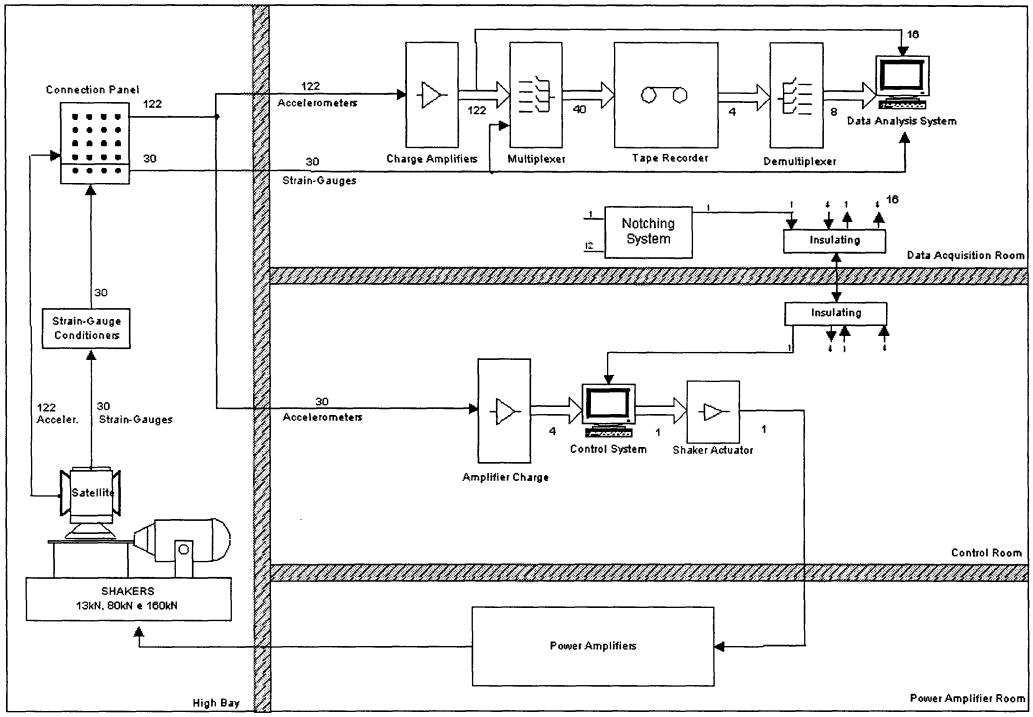

Figure 1: The current Vibration Test Facility

CONSTRAINTS ON THE CURRENT SYSTEM

After operating for more than thirteen years, the current vibration system is almost in the limit of its life time. Comparing the technology and concepts that were used in its design with nowadays technology, concepts and tools available for signal processing we can compile the following list of constraints in related to the system:

a) Hardware maintenance: the majority of the hardware used in our system is now out of production, and the manufactures do not support them anymore. For some of them, as is the case of the GenRad equipments, even new circuit boards or subsystems to replace malfunction parts are unavailable. We are keeping the equipments in good operational conditions due to our spare parts and our good maintenance team. However, our supply of spare parts is coming to the end as the system malfunctions become more frequent. At the same time, the confidence in using our equipments is reducing proportionally to the increase of the number of failures.

b) Impossibility of using advantage softwares: the GenRad equipments do not support the new releases of the top softwares for signal processing, control, data analysis and modal analysis. Their limitation in memory, disk space and speed impose prohibitive barriers for using or even developing those enhanced software solutions.

c) Poor real time capability of visualization: In real time, the system just allows the visualization of up to four channels. It is impossible to follow the history of other channels or even impose safety limits for more channels.

d) Excessive post-test processing time: During the vibration test, up to four channels can be processed by the controller and up to sixteen by the data analyzer system. At the end of the test, the results on those "real-time" channels can be displayed immediately and printed in about ten minutes. For the other channels that were stored into the tape recorders using a multiplexer scheme, they can be recovered to be processed by the GenRad 2514 in groups of eight and using the same speed rate that were used during the test. This constraint means for a test involving 150 channels, an analysis and print time of more than three hours.

e) Reduced automation capability: The system architecture imposes several restrictions to implement automatic procedures for calibration procedures, test set up, start and end of test, check up system conditions. The system operation requires from the operating team attention all the time, besides the execution of many time intensive and manual tasks. Furthermore, the overall system calibration requires many weeks or intensive work.

f) Impossibility of real-time channel check: When all the accelerometers and strain-gauges are connected to the system channels, it is impossible to check if all the channels are properly operating. As the majority of the channels goes straightforward to the tape recorder system, they are unaccessible until after the end of the test, during the post test analysis phase.

g) Tape recorder instability: The tape recorders fine-tunning is a challenger. It requires a long time of hard and tired work. As they are very sensitive to environmental changes, tunning and calibration procedures must be repeated very often to minimize the occurrence of drop outs.

REQUIREMENTS FOR A NEW SYSTEM

Based on our experience in working with the current system, on the top available technology, on the necessity to have a system that supports both vibration and acoustic tests and on the necessities of the structural development team, we came to the following specifications for a new data acquisition and control system for satellite vibration and acoustic tests:

a. Physically, the *VIBSIS* will extended over five places, as depicted in Fig 2: The *High Bay*, the *Control Room*, the *Data Acquisition Room*, the *Visualization Room*, the *Acoustic Chamber*, and the *Shaker Power Amplifier Room*;

b. Development team and LIT external persons will follow the test from the Visualization Room. In that room will be installed all the facilities needed for following the test, for performing the post test data analysis, and for cross-comparing test results with structural model outcomes. Communication system with audio and video resources will provide full access to the groups in the outer places, while a video system will provide full view of the specimen being tested;

c. The system will be implemented using a distributed architecture for processing and modular implementation so that each functional module can individually perform control or data acquisition tasks or operate interconnected as necessary;

d. Synchronous operation among the modules, with real-time data channels overall measurement and intercommunications to allow the implementation of flexible notching strategies;

e. 390 measurement channels available, with at least two modules with 32 measurement channels to be used as solo vibration controllers; 32 of this channels will have programable bandwidth from 2 Hz to 40 kHz (at least), while the other from 2 Hz to 4 KHz; The anti-alias filters will selectable between Elliptical with 135 dB/Octave of roll-off (or better) and eight order Bessel (or better); Simultaneous samples in all channels;

f. Support for perform random, sine, shock, transient, sine-on-random, random-on-random, and modal analysis tests. Processing tools for analysis in time domain, frequency domain; transfer function generation, wavelet analysis, modal analysis, and structural parametric identification;

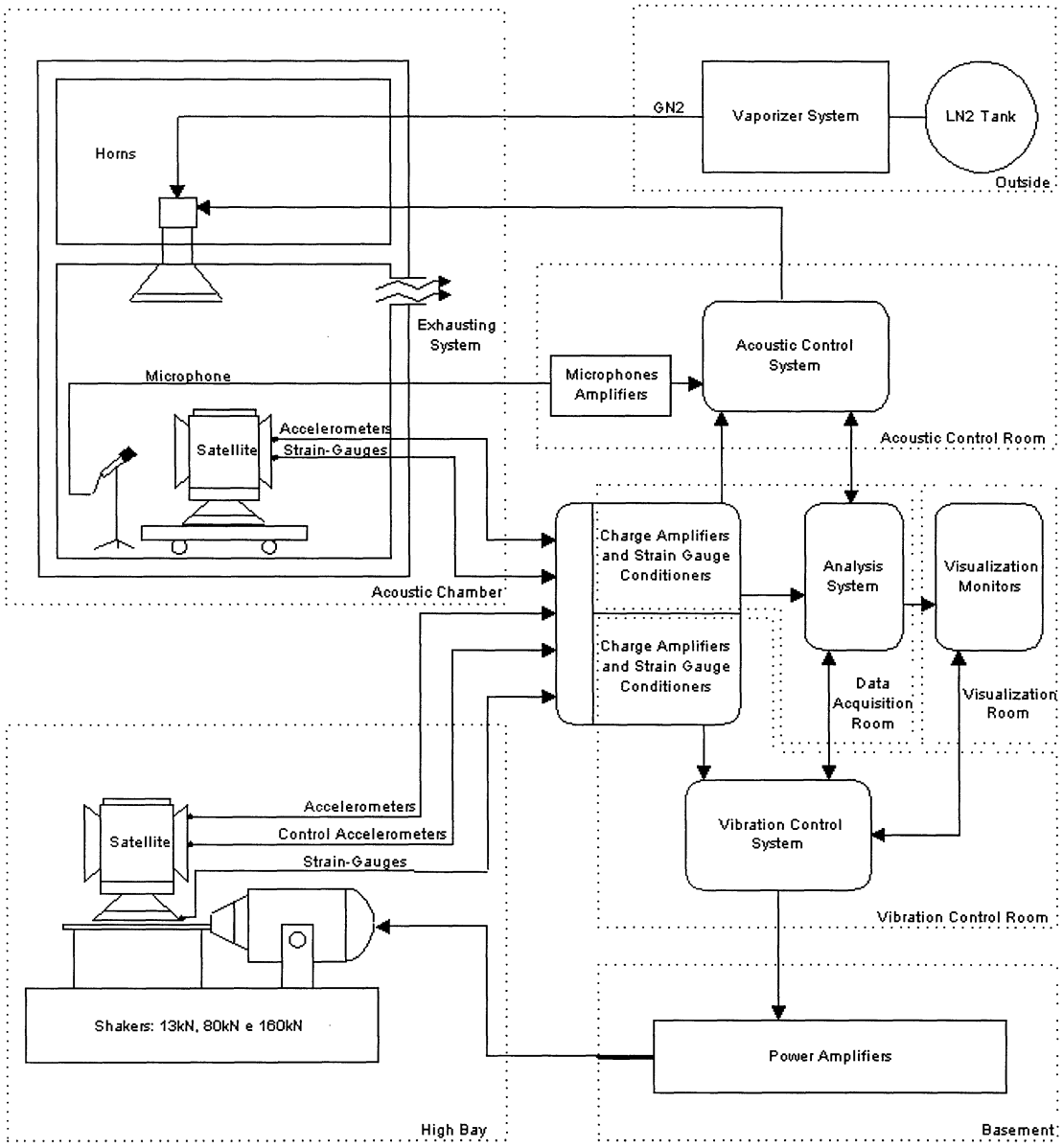

Figure 2: The new Vibration Test Facility

g. Parallel data digital storage of raw data and data analysis with associated visualization on all the channels and in real-time. The digital media will support raw data storage for at least 30 minutes of test, with system in the full capability configuration;

h. Data storage files importable and exportable form the following formats: UFF, Word, Excell, MatLab, Mathematica, Grapher Ansy, Nastran. The data files will be accessed from external computer using NFS and ftp protocols;

i.The time interval for overall data reduction and post test analysis using the system in a full configuration will be no longer than fifteen minutes;

j. All system and subsystems calibrations, functional diagnostics, and performance tests will be executed totally automatic; Hardware and software support for programming customized procedures;

k. *Series Voltage Insertion Method* for overall accelerometer-channel-system status check will be supported on all the accelerometer channels;

l. Auxiliary instrumentation will support automatized calibration procedures and allow to follow in real-time all the channels, with data analysis being executed both in time and frequency domains;

m. All the cabling routing interconnection will be implemented by using electronic switch subsystems;

n. The charge amplifiers that are used in the current data acquisition system will continue to be used in the new system. The other charge amplifiers will come from a home-made development, as well as the strain-gauge amplifier to be used in the project;

o. Artificial Intelligence technology will support system supervision and will help system operation and data result analysis.

p. The current tape recorders will be integrated to the system to allow the reproduction of old data previously stored in tape by using the new system, when necessary.

FROM THE SPECIFICATIONS TO THE NEW SYSTEM

A bid was performed on 1998 to choose the main contractor responsible for supplying and integrating all the system. The main international companies on vibration and acoustic data acquisition and control system replied the bid. The Spectral Dynamics was the winner. That company presented the best technical project with a reasonable price. The system integration and acceptance test will be hold on next November. Figure 3 presents a detailed block diagram of the new system.

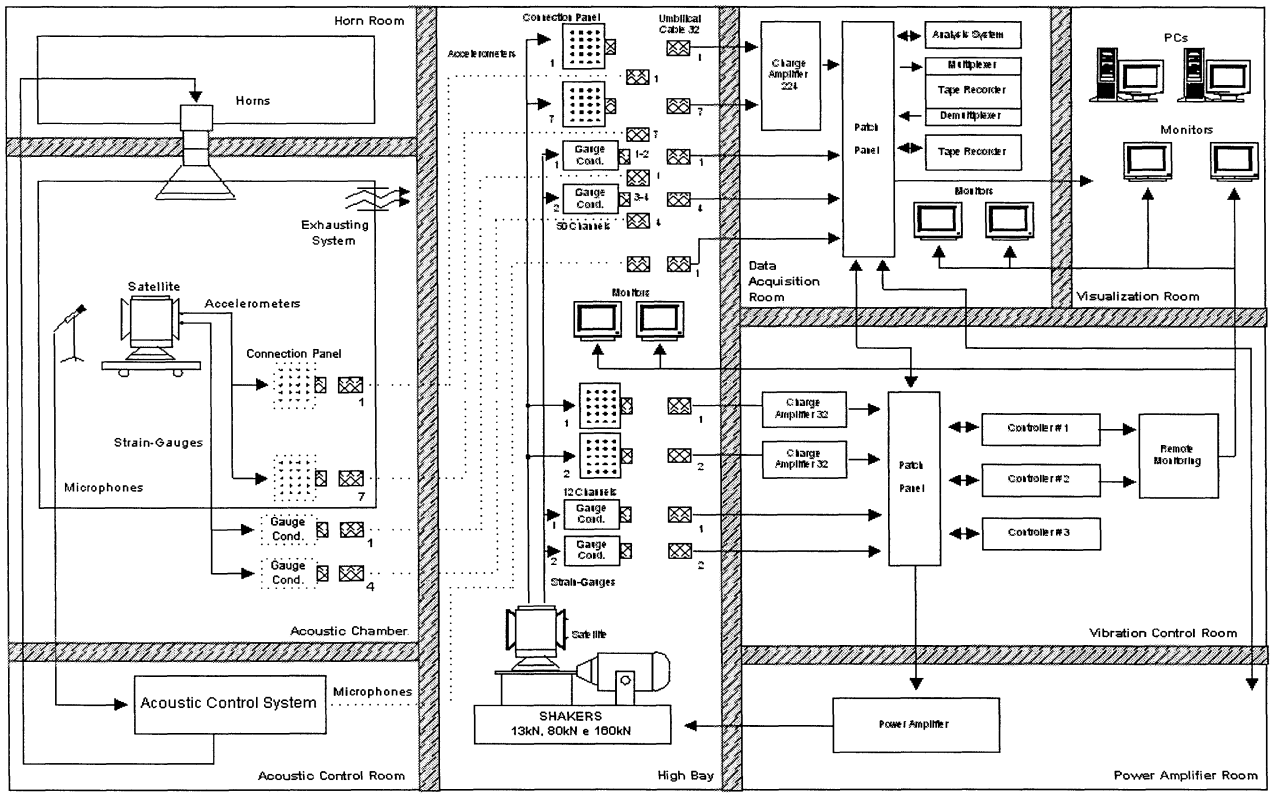

Figure 3: Detailed diagram of the new Vibration Test Facility

Budget and technology restrictions imposed changes regarding the above specifications as well as introduced additional constraints to the project concepts, as described bellows:

a. The system will be implemented, as requested, using a distributed architecture for processing and modular implementation so that each functional module can individually performs control or data acquisition tasks as well as operates interconnected with the other modules as necessary; However, in our configuration, we are limited to conduct (control) up to three tests in parallel because of the number of workstations (three) that are integrated in the system. If more workstations are added, more simultaneous tests can be performed in parallel, up to eight;

b. The system can store raw data digitally for up to 45 minutes. When the throughput hard disks are full, the data must be transfer to the long term data storage system. After that, the throughput hard disks can be released to be used again, overwriting the old data. A long term data storage system for both raw and processed data and was not included in the original system specifications. In accordance with the requirements for long term data storage, many options are available. It can be random or sequential access. If the system is intended for permanent archive with rare recall of the data, then sequential access systems such as DAT tape drives may be adequate and cost efficient. If random access is critical, then either magnetic disk media or optical media must be used. The volume of data to be managed or archived is key to defining the design of any system regardless of the type of media. Volume management of data can be handled with either single drive devices or with multiple drives or jukebox systems. Costs vary significantly between the two. Another issue to be considered is if the stored date is to be used for central file management or to make files available to a large number of users served by one common system. In the latter case, speed, access, and usually smaller file sizes are more important. As we intend to have the data available for a large number of users that could access it both locally or remotely, we decide to use a file server with magnetic disks;

c. It is not feasible to have all the cabling routing interconnection implemented by using electronic switch subsystems. The costs involved in it would be prohibited large. It would require a very large switching matrix located in the data acquisition room. While electronic switching will be extensively used, it will be necessary to have one large patch panel responsible for the main interconnections. However, in the control room, just electronic switches will be used;

d. Because a patch panel will be used, it is impossible to have just automatic procedures for system verification and calibration. Those procedures, however, can be automatically performed in sets of sixteen channels. Thus, manual intervention will be necessary for cabling set up and interconnections for each group of sixteen channels in the data acquisition system. In the control room all the procedures for system verification and calibration will be performed automatically;

e. In the data acquisition room, the auxiliary instrumentation can be used to follow the channels in real-time in groups of sixteen. Thus, before the start of the test, up to sixteen channels can be chosen to be monitored using the auxiliary instrumentation. All the auxiliary instrumentations are assembled in mobile carts that can support all the system's requirements in related to calibration, verification and channel monitoring. Those carts are located in the high bay, in the control room, and in the data acquisition room, and can be remotely operated by network. Furthermore, all the test procedures can be programmed using an object-oriented language for instrumentation;

f. Besides the courses that were requested in the bid specifications, specific training courses on the workstations' operational system utilization, management, network interconnection, and program development will be necessary. Those courses will be given by the workstations manufacture. The expenses with those courses were not foresighted in the original budget;

g. Completely new channel wiring will be used. Old cables that support the current system will be removed. Because of the wiring, the system integration will take twice more time than it was originally foresighted for it in the bid specifications. During this time, all the vibration system will be shutdown;

h. Artificial intelligence system to help system supervision, system operation and data result analysis will be developed by LIT team. The development will start after the system acceptance.

i..Delays from third part suppliers postpone the system integration and acceptance test in LIT from September to November this year.

CONCLUSION

Nowadays technology enables us to design a data acquisition and control system for satellite vibration and acoustic tests that is incomparably more advanced and efficient than those systems based on previously available technologies. It is possible to have a fully automated distributed and scalable system that operates with the supervision of an artificial intelligent system, thus making all the tasks easy, efficient and reliable. This system can provide enhanced visualization and analysis capacity, with remarkable response time. In this system, human interfaces are required just to care out the test set up. It is even possible to integrate this system with CAE systems so that they interact in refining structural and dynamical models. Budget constraints, however, are a severe obstacle to implement this system, as well as the requirement of a huge development team with experts in many areas. A complex system like this requires more support subsystems than can be previously foreseen, which implies in budget overpasses. Special attention must be paid to the team training and to the development of operational procedures for the system.

REFERENCES

[1] Lino, C. O., Silveira, V. B., Galvão, B. S. M. C., Sakita, M. T., Garcia, E. C., and Kakizaki, M., "Users Manual - Laboratory of Integration and Testing", LIT15-LIT00-MM-001, INPE, December, 1998.

[2] Macau, E. E. N. M., "Specifications for the new LIT Vibration Control and Data Acquisition System", LIT21-LIT00-EM-002, INPE, June, 1998.

[3] Sakita, M., Figueiroa, J. G. S., and Fuliene, C. A. V., "Acoustic Test Facility for Space Applications - Detailed Technical Specifications", LIT02-LIT00-TE-004, July, 200.

[4] J. E. Rhodes, *Piezoelectric Transducer Calibration Simulation Method Using Series Voltage Insertion*, Endevco TP216.

Page intentionally left blank

FEEDBACK AND COMPRESSION PARAMETERS FOR SPACECRAFT SINE VIBRATION TESTING USING EXPERIMENTAL METHODS

B S Jagadesh Babu*, J N Hemanta Kumar*, C V R Reddy and N K Mishra***
*Environmental Test Facilities, ISRO Satellite Centre, Bangalore-560017, India
**Structures Group, ISRO Satellite Centre, Bangalore-560017, India

ABSTRACT

This paper presents an account of the extensive experiments carried out for firming up the feedback loop parameter settings in the SD2550B Digital Vibration Control System from M/s Spectral Dynamics for Sine Vibration testing of a Spacecraft. The Control system offers programmability over compression rate and control amplitude estimation in terms of number of cycles over which the estimation is carried out. An essential feature of the control during sine vibration testing is a stable system performance with minimal amplitude excursions. Instability of control during automatic notching as well as the overshoot immediately after notching, typically observed during the tests, is of serious concern.

A systematic study was initiated to quantify the sensitivity of varying the compression rate and amplitude estimation period parameters of the control system. A series of experiments were performed for this purpose on simple and complex structures with varying natural frequencies and damping factors at different sweep rates. Assessment of control system performance in terms of stability and amplitude excursions over the pre-set levels were made and optimum system parameter settings were evolved. The same has been effectively used during spacecraft tests.

INTRODUCTION

The phenomena of limiting dynamic responses of a large spacecraft during ground vibration tests is well understood in order to protect the spacecraft from exceeding dynamic responses beyond what is anticipated in flight. The basic test specification for the spacecraft sinusoidal vibration testing does not account for this phenomenon. However this is taken care by implementing the automatic notching as part of the control process. Notching or the reduction in the input to the shaker is intentionally done during sine sweep to limit a particular level of response at all identified critical locations of the spacecraft. These levels are obtained by the coupled load analysis of the spacecraft with the launcher.

Almost all the manufacturers of the control systems provide peak response limiting feature in the control systems. However, the process of implementing such a feature is different from one manufacturer to the other. Understanding the implementation is very much essential to get better performance from the control system. Two issues that need to be addressed in this

regard are stability and notching overshoot. Over emphasis on either will tend to undermine the other, which is not acceptable. The setting of the control parameters are accordingly to be arrived at keeping in mind both the factors to achieve an optimum combination.

The vibration lab at ISRO Satellite Centre is equipped with several generations of control systems. Tests on several spacecraft systems meant for scientific, remote sensing and communication applications have been conducted with the many genres of control systems. The latest in the series of control systems in the stable is the SD2550B 32 Channel control system from M/s Spectral Dynamics. The SD2550B of the former M/s Generad design was a major shift in terms of the technology and testing concepts from the earlier 1200/1500 series of control systems from M/s Spectral Dynamics. With respect to notching the system differed very much by not providing the adaptive control that was available in the earlier systems. In the earlier control methodology, the control system has several compression curves defined. The compression curve is defined in terms of dB/sec, which increases linearly over the frequency range. Several such curves with fixed offsets are available. In the Adaptive control the control algorithm would measure the input signal, derive the information in terms of quality factor and select an appropriate curve, with an higher or lower compression rate, and apply the control signal accordingly over the entire sweep in the frequency range of testing.

In the SD2550B, this feature is replaced by giving the control operator more flexibility in selecting the appropriate compression in terms of percentage. One can also set different compression rates over the frequency range in fixed steps. Apart from this, the estimation duration can also be set. The estimation duration by definition refers to for how long the input signal is sampled before the amplitude estimation is arrived at. The sampling frequency is constant and 51.2 kHz over the entire sweep frequency range. The estimation duration is specified in terms of cycles per second ranging from 255 millicycles to several kilocycles. The estimation duration can only be set at the time of programming the test and remains constant through out the frequency range. The compression can be varied from 0% to 200%.

Experiments were carried out on simple beam specimens with varying fundamental frequencies and different damping coefficients. Tests were carried out varying the parameters such as sweep rate, compression and the estimation duration. The optimum control parameters were arrived at based on synthesis of results and used for testing satellites.

OBJECTIVE

The basic objective of the work is to optimise the Control parameter settings, in respect of feed back parameters (amplitude estimation period and compression speed) at different Sweep rates, to achieve control stability and minimum response amplitude excursions for notching. This is particularly in view of Lack of adaptive control i.e. provision of control system to sense the on line change in behaviour of response and effect varied Control System settings during the sweep.

CONTROL SYSTEM DESCRIPTION

SD2550B Digital Vibration Control system perform control and Data acquisition functions during Sine, Random and Shock tests. The system facilitates simulating swept sine, frequency dwell, tracked resonance dwell, random, classical shock and SRS tests in the frequency range of 0.1 Hz to 10,000 Hz. The shaker system safety is protected using in-built shaker safety features limiting the maximum displacement or velocity or acceleration as per user definition. Data storage modes are simplified by providing simple data acquisition methods, which specify various data storage modes.

The system provides an in-built calibration Software package to periodically calibrate and store the calibration constants to maintain the required accuracy. The 16 bit ADC per input channel provides for high precision measurement process. Powerful DSP processors per 4-channel card and the main MDSP processor aid the fast processing of incoming signals. The host workstation is left with the job of programming the MDSP card for operation, receiving the processed data from the front end and storing and display of data. The system is versatile and provides, an experienced user, several options to conduct the test with flexibility.

During Sine testing the swept sine signal is generated using modified phase accumulator method The generated drive signal is attenuated to the required level by means of two stages, coarse and fine, of attenuators. The amplitude estimation is synchronised with the sweeping frequency. There are three methods of processing the input signal for amplitude estimation. They are Peak, RMS and Tracking Filter processing. For Spacecraft testing the BB RMS processing method is chosen. This is to account for the out of band energy that may be present during resonance. Otherwise, it may result in over testing of the structure. The input signal is sampled at a constant rate of 51000 samples per second. The RMS value is computed within the duration as per user selection made during initial set-up. The estimation duration can be selected from 255 millicycles to 3.31 kilocycles. Error signal is computed with reference to the set level. The percentage of error that is used for correction is termed as Compression. The manufacturer given general guidelines for selecting Compression speeds are primarily based on the frequency region (low, mid and high) and the sweep rate.

EXPERIMENTAL SET-UP

A simple experimental set-up is devised to simulate typical situations as seen during Spacecraft tests like global resonant frequencies and associated modal damping, simulation of closely spaced modes, etc.

The experimental set-up consisted of several beams made of different materials and having different lengths mounted on a vibration fixture. Aluminium, Polycarbonate and Acrylic (Methyl-metha-acralite) materials were chosen for the beams. The effective lengths of beams were chosen so as to have the beams fundamental frequency lie between 20 Hz. to 100 Hz. and the damping values ranged from 1% to 4%. All the beams of different lengths made of different materials are mounted on a rigid vibration fixture, which in turn is interfaced with

the shaker. Centre of the vibration fixture is chosen as the location of the control accelerometer.

Ling Electronics 8 Ton shaker system was used for providing base excitation input to the specimen. Endevco 2226C accelerometers were used for response measurement. Endevco 3090C low noise cabling was used to connect the accelerometers to the Endevco 2275A signal conditioners. All the transducers signal conditioners and equipments used for the testing were calibrated prior to the experiments.

DETAILS OF TESTS

Following section describes the details of tests performed and the test results as a part of control system parametric evaluation.

Structural Characterisation Tests

In the first test the set of beams specimens were characterised for their vibration behaviour. The structural characteristics are extracted from the following tests.

A low-level swept Sine Test was carried with the following specifications.

- Frequency Range : 5 Hz. – 100 Hz
- Input Amplitude : 0.5g
- Sweep rate : 4 Oct/min

The Test definition was based on the actual Spacecraft Test frequency range and sweep rate to evaluate the response of the control system for actual conditions.

Table - 1

Beam ID	Measured resonant response of Beams		
	Frequency (Hz.)	β - Amplification Factor	ζ – Damping Ratio %
Beam 1	33.89	7.96	1.28
Beam 2	26.36	16.94	1.28
Beam 3	46.67	31.04	0.76
Beam 4	58.06	69.50	1.01
Beam 5	90.71	52.12	1.01
Beam 6	20.71	23.82	1.53
Beam 7	58.36	23.77	1.01
Beam 8	52.40	13.31	1.02
Beam 9	23.79	11.22	3.87
Coupled Beam - 10	21.95 25.50	10.26 8.36	2.35 3.07

Table-1 gives the fundamental bending frequencies of the beams and amplification factors (β) with respect to the input. The fundamental Frequencies of the beams have been tuned keeping in mind typical spacecraft resonant frequencies. The 'Q' factor and the damping coefficients associated with the fundamental mode for different beams are calculated using half power bandwidth method and is presented in the same table. For a typical Control system setting of 255milliCycles Estimation duration and 100% Compression, the percentage overshoot of the notched responses beyond the pre-set levels are given in Table-2.

Table – 2

Beam No.	Set Notch Level 'g'	Notched Level 'g'	Percentage Overshoot
1	6	6.68	11.33
2	12	14.35	18.62
3	16	18.53	15.81
4	16	27.99	75.00
5	16	24.72	54.50
6	10	12.88	28.80
7	12	Not Notched*	Not Notched*
8	10	11.40	14.00

* The channel did not notch as the level reached was well below the set notch level.

Control System Parametric studies on 4% Damping Ratio Beam

In the second set of tests, a beam with damping ratio of 4% was used for extensive characterisation of the notching performance with wider compression variations and at selected estimation period intervals. The details of tests performed with different combinations of estimation periods, Percentage Compression and Sweep rates are as given below.

Estimation Periods considered: 255millicycles, 509millicycles, 1.02 cycles and 2.04 cycles
Compression Rates considered: 50%, 75%, 100%, 125%, 150%, 175% and 200%
Sweep Rates considered: 1 Octaves/min, 2 Octaves/min and 4 Octaves/min

- Tests were conducted in the 3 Sweep rate settings.
- To reduce the number of tests successive doubling of Estimation periods were chosen. Tests were stopped at 2.04 cycles as error in terms of percentage overshoot was successively increasing and any experiment beyond this was not considered useful.
- The compression percentage was started at 50% and increased up to 200% in steps of 25 to get better approximation of the effect of compression on notching.

Typical response plots keeping estimation period of 509milliCycles with varying compression speeds from 50% to 200% and at 4 Octaves/min sweep rate is shown in Figure-1. The deviation of the response beyond the pre-set Notch levels is clearly brought out in the

figure. Figures 2, 3 and 4 show the details of the Percentage deviation of the response from the set notch levels for different combinations of compression speeds at sweep rates of 1, 2 and 4 Octaves/min.

Control System Parametric studies on Low Damped Beam

In the third set of tests, a single beam representing a damping of 1.6% was used to a narrowed down set of fine tuned tests to get the notching performance for low damped structures. The details of tests performed with different combinations of estimation periods, Percentage Compression and Sweep rates are as given below.

Estimation Periods considered: 255millicycles, 509millicycles, 1.02 cycles and 2.04 cycles
Compression Rates considered: 75%, 100%, 125%, 150% and 175%
Sweep Rate considered: 4 Octaves/min

The tests were narrowed to,

- 4 Octaves/min Sweep rates as all Flight units of spacecraft are tested at this Sweep rate.
- 50% and 200% Compression rates were eliminated as 50% compression was leading to under correction and 200% compression was leading to instability even with a higher damped system.

The deviation of response beyond the pre-set Notch levels for this low damped beam is shown in Figure-5 considering Sweep rate of 4 Octaves/min.

Control System Parametric studies on Coupled Beam

In the fourth set of tests, a complex structure was simulated with closely spaced dual resonances and different damping coefficients. The tests were devised to understand the behaviour of the Control system while testing complex structures. The details of tests performed with different combinations of estimation periods, Percentage Compression and Sweep rates are as given below.

Estimation Periods considered: 255millicycles, 509millicycles, 1.02 cycles and 2.04 cycles
Compression Rates considered: 75%, 100%, 125%, 150% and 175%
Sweep Rate considered: 4 Octaves/min

The tests were continued as per the following settings,

- 4 Octaves/min Sweep rates as this is the normal rate of testing on spacecraft
- 50% and 200% Compression rates were eliminated as 50% compression was leading to under correction and 200% compression was leading to instability even with a higher damped system.
- A complex structure with closely spaced resonances was chosen to study the effect of control parameter settings on the notching performance.

Figure-8 shows typical response plots for the coupled beam with notching for the tests with 125% compression and at four different estimation periods. The deviation of the responses beyond the pre-set notch levels for the first and the second peaks is shown in the Figures 6 and 7 respectively.

DISCUSSION OF RESULTS

The results of the structural characterisation tests performed described in Tables 1 and 2 show that frequency range covered for the study extends from 20Hz. to 100 Hz. The modal damping associated with the fundamental mode ranges from 1% to 4% with amplification factors ranging from 8 to 70. Such structural characteristics are typically encountered during spacecraft tests. With the default settings of the percentage compression and the estimation duration of the control system the notched test results as given in Table-2 indicate higher over shoot as the as the Q factor increases. The percentage overshoot seen in the results of the default settings are not acceptable for tests on spacecraft.

The results of the tests on beam with 4% damping have been summarised below,

- Comparison of the effectiveness of performance of notching in terms of percentage Overshoot/Undershoot
- Apparent instability in the notch zone show that,
  - For all the 3 Sweep rates considered (viz. 1, 2 & 4 Octaves/min), choosing a compression value between 125% to 150% appears to be better for all the estimation periods i.e. 255 millicycles, 509millicycles, 1.02cycles and 2.04cycles
- It is evident from the observations that for the chosen Compression speed, the estimation period of 509 millicycles setting with 125% compression and all sweep rates from 1, 2 & 4 Oct/min the percentage overshoot is least along with least apparent instability.
- It is evident from the observation that the control performance in terms of percentage overshoot is least at slower sweep rates as compared to higher sweep rates.
- Selection of 509 or 255 millicycles at different compressions show that 509 millicycles has least percentage overshoot / Undershoot (least over/under test) from the set notch level. Though 255milliCycles appears like having flat platone, because of larger percentage overshoot this estimation period is not preferable.

The results of the tests on beam having low damping (1.5%) show that,

- Compression of 125 and 150% appear to give the lowest percentage overshoot for all the estimation periods considered namely, 255millicycles, 509millicycles, 1.02cycles and 2.04cycles and for the sweep rate of 4 Octaves/min.
- Keeping compression at 125%, the shape of response curve shows that,
  - The resonant response crossing the set threshold is picked up fast when lower estimation periods are chosen. Subsequently the Control System tries to dip the input and hence the response. This is reflected as dip in response immediately

after notching, which is clearly seen in the results of the tests with estimation period of 255millicycles as compared to estimation periods in excess of 255millicycles.
    - The off resonant response curve is smoother.
- Higher compression is not proving to be helpful in view of second overshoot which is larger than the first overshoot in the notch duration.
- Recommended setting is 509milliCycles at 125% or 255 millicycles at 150%.

The results of the tests on coupled beam with closely spaced modes show that,

- With respect to the Estimation period, 255 millicycles or 509 millicycles show lower percentage Overshoot.
- Percentage Compression between 125 and 150 appears to yield better results.
- General observation what is seen earlier with simple beam is applicable here also with respect to compression settings.

CONCLUSION

The efforts to optimise amplitude Estimation Period and Compression Speed parameters of the SD2550B, 32 Channel control system from M/s Spectral Dynamics by a series of extensive swept sine tests reveal that,

- Best results in terms of control stability and least percentage overshoot is obtained when the estimation Period is 509millicycle and the associated percentage Compression is 125% to 150%. These results are applicable for test specimens having resonance peaks in the frequency range of 20Hz. to 100Hz. and for damping ratios ranging from 1% to 4%.
- For complex structures exhibiting closely spaced resonant peaks, the Estimation Period and Compression settings applicable for simple beams are valid at 4 Octaves/min.
- The above conclusions have been drawn with RMS processing which is generally used with tests on complex structures like spacecraft.

REFERENCES

System Manuals of SD2550B Digital Vibration Control System and associated literature of the manufacturer.

Figure - 1 Notched Response Plots on a beam

4% Damping Ratio, Sweep Rate - 4 Oct/Min

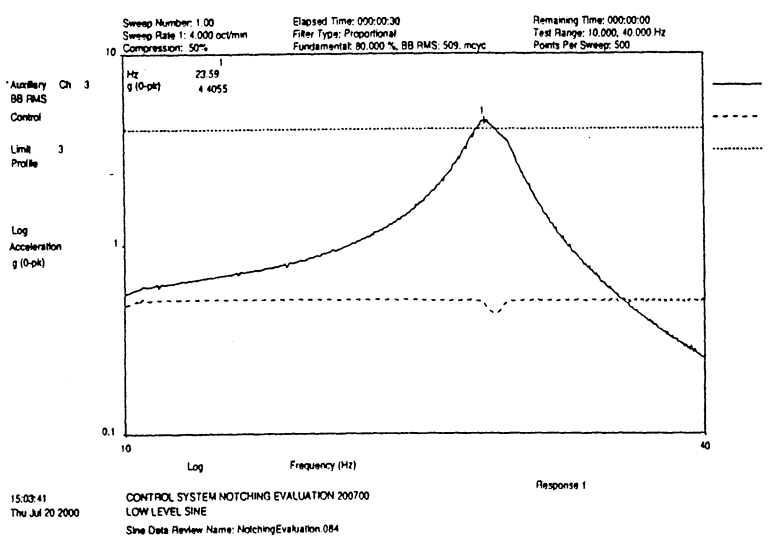

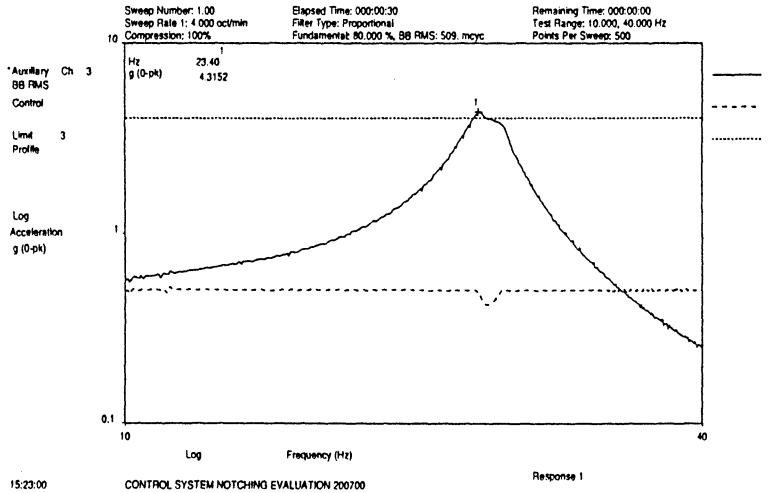

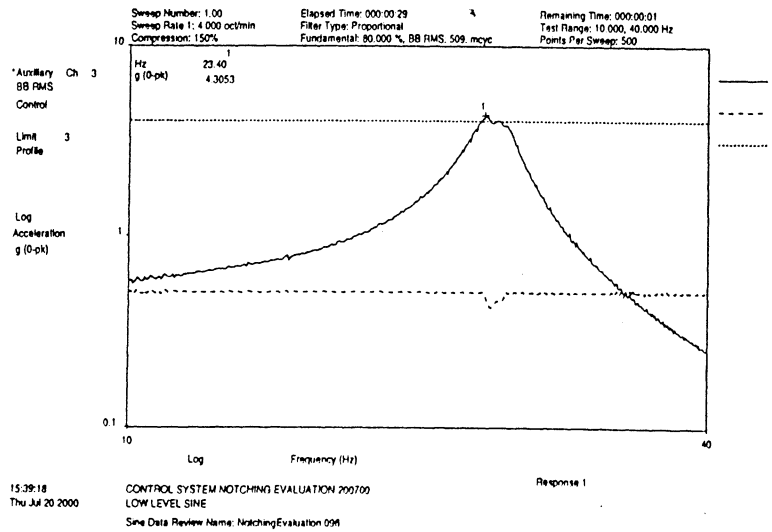

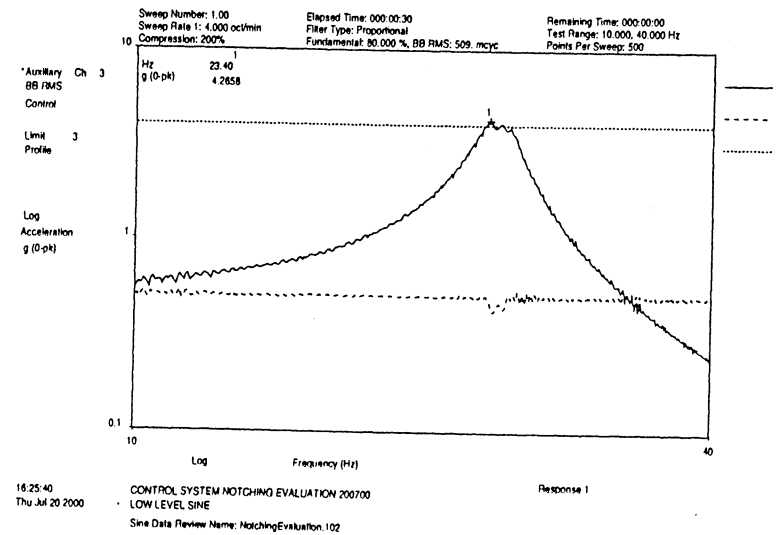

Figure - 2 Deviation observed in the Notched respnse

Damping Ratio-4%, Sweep Rate-1 Octave/Min

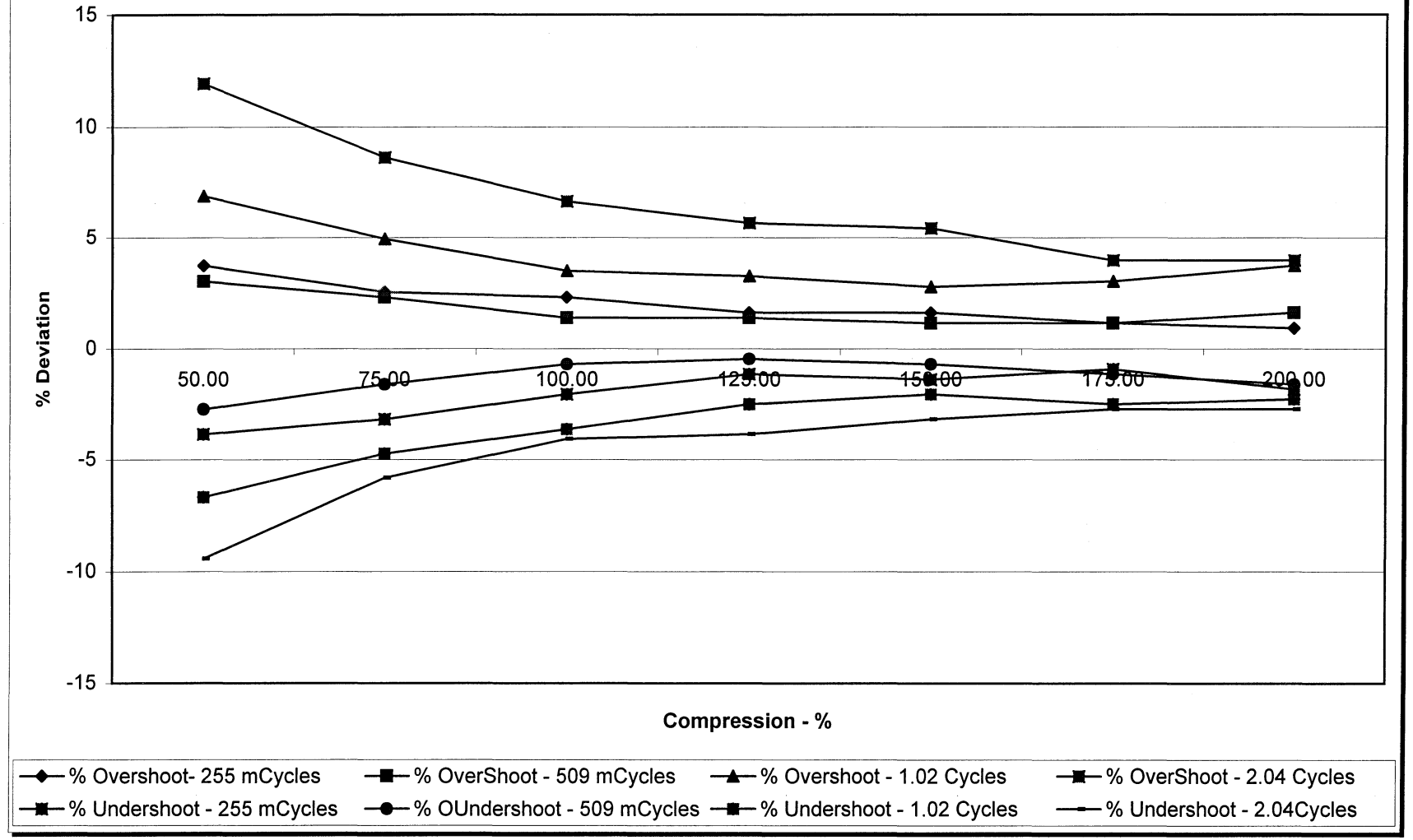

Figure - 3 Deviation observed in the Notched respnse

Damping Ratio-4%, Sweep Rate-2 Octave/Min

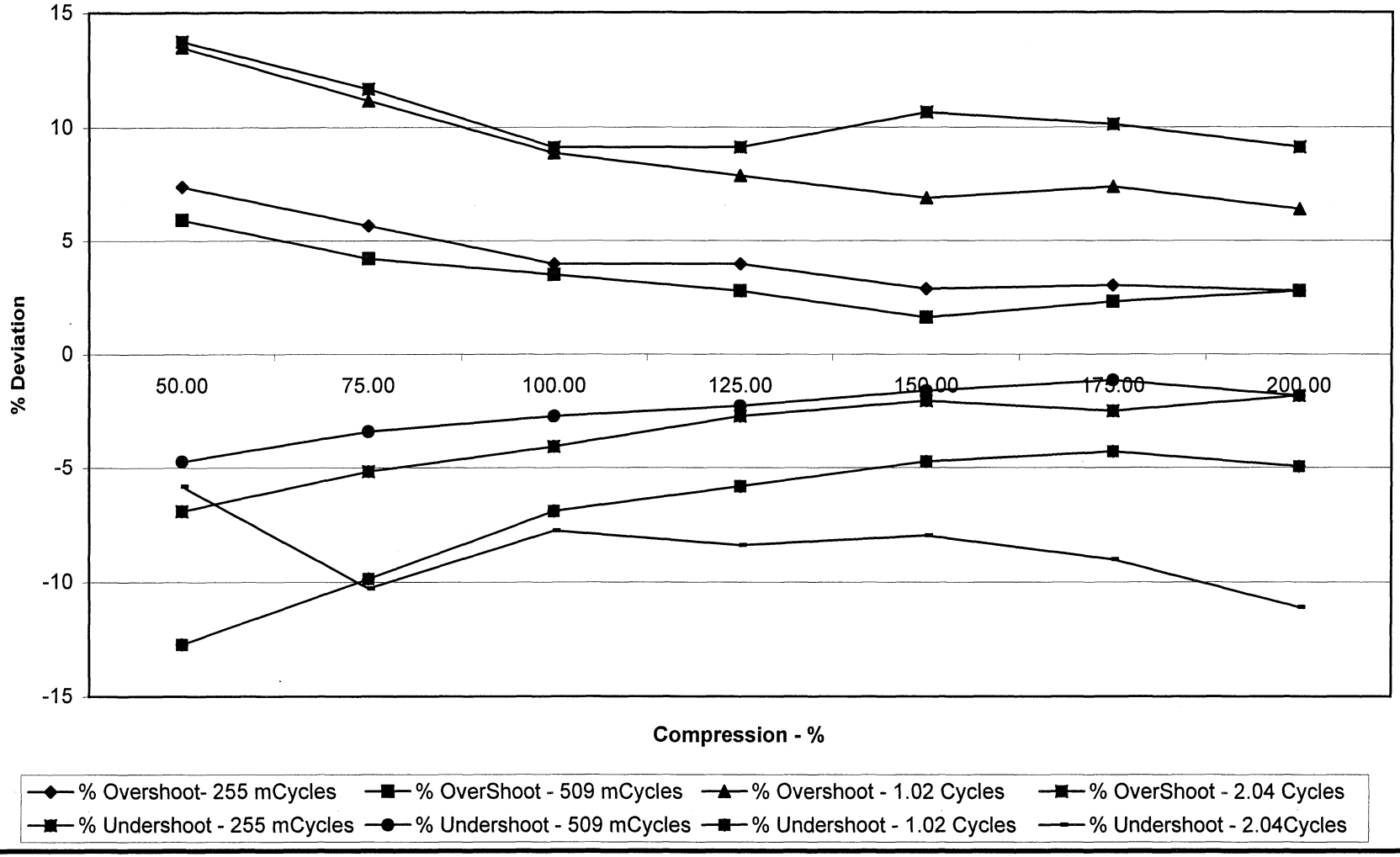

Figure - 4 Deviation observed in the Notched respnse

Damping Ratio-4%, Sweep Rate-4 Octave/Min

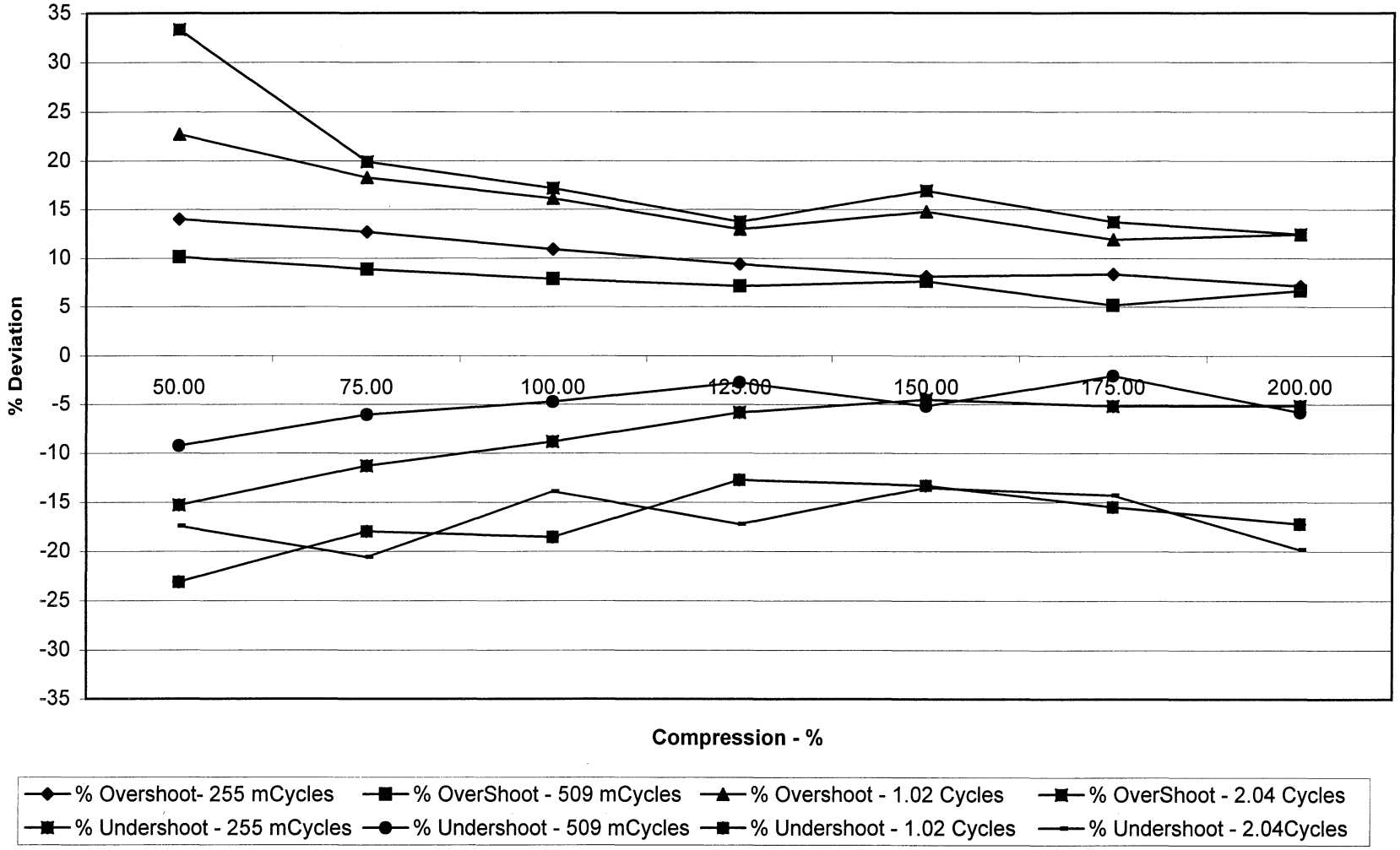

Figure - 5 Deviation observed in the Notched respnse

Damping Ratio-1.5%, Sweep Rate-4 Octave/Min

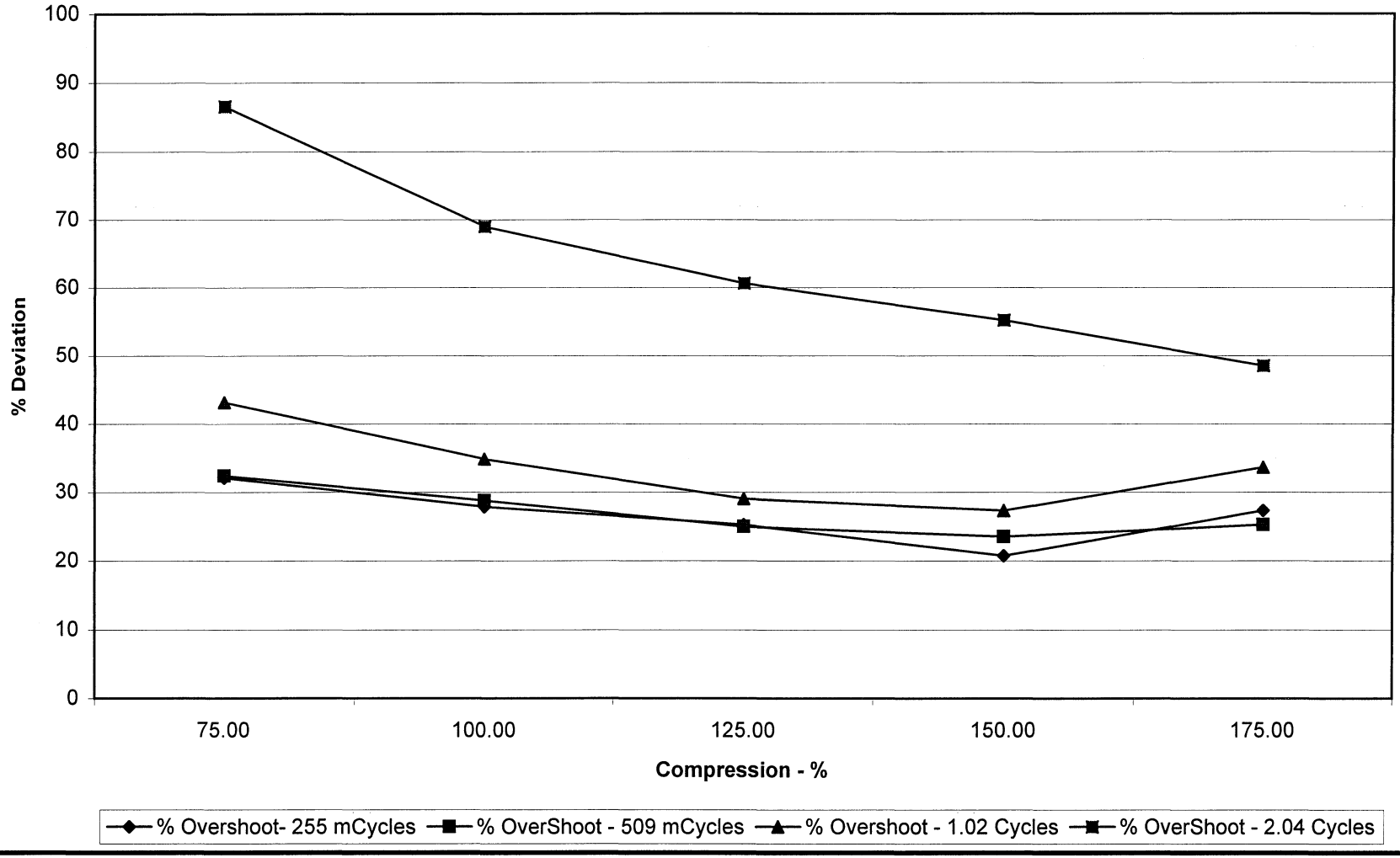

Figure - 6 Deviation observed in the Notched Respnse of Coupled Beam

Damping Ratio-2.6%, Sweep Rate-4 Octave/Min, Peak-1

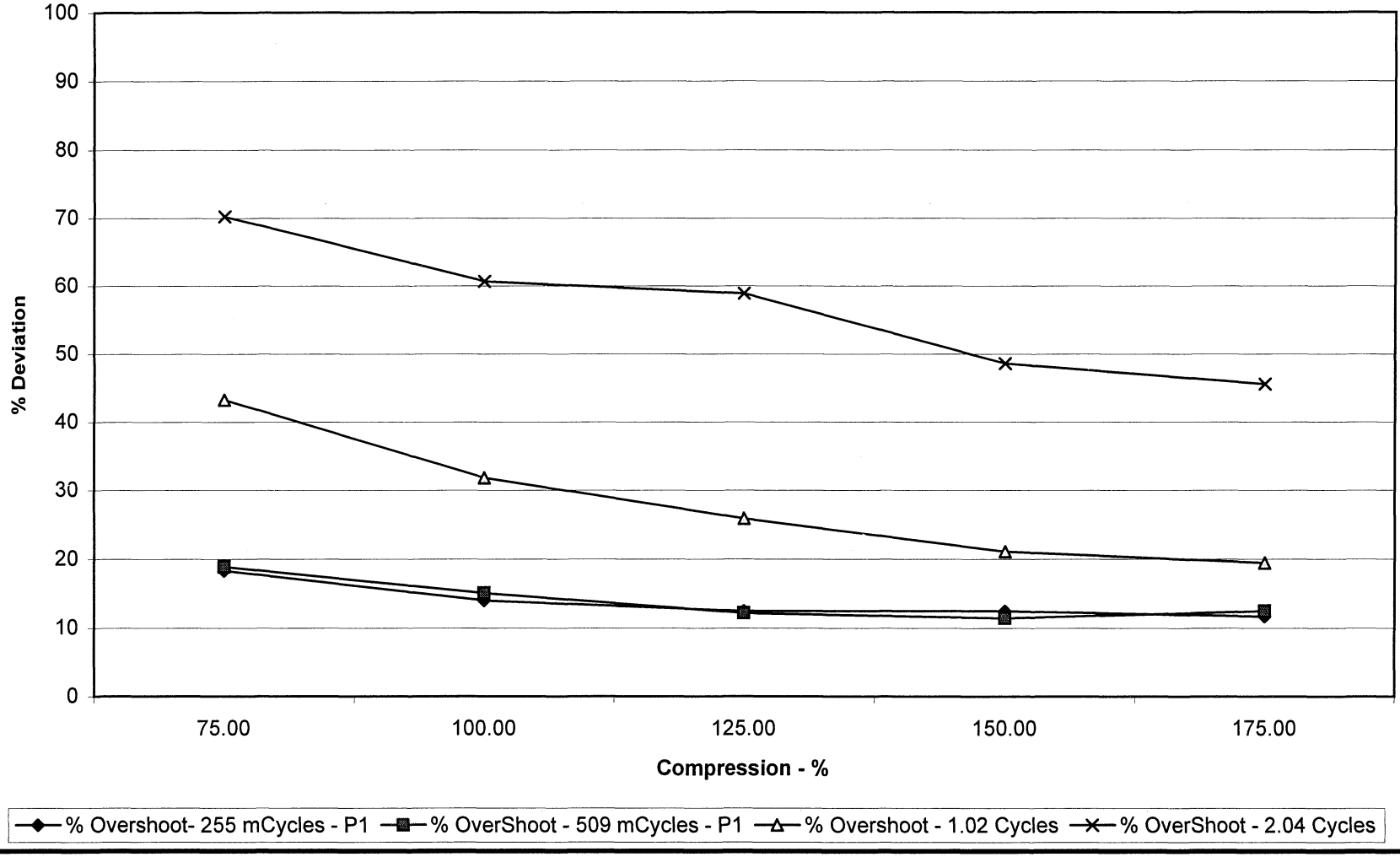

Figure - 7 Deviation observed in the Notched respnse of Coupled Beam

Damping Ratio-3.07%, Sweep Rate-4 Octave/Min, Peak-2

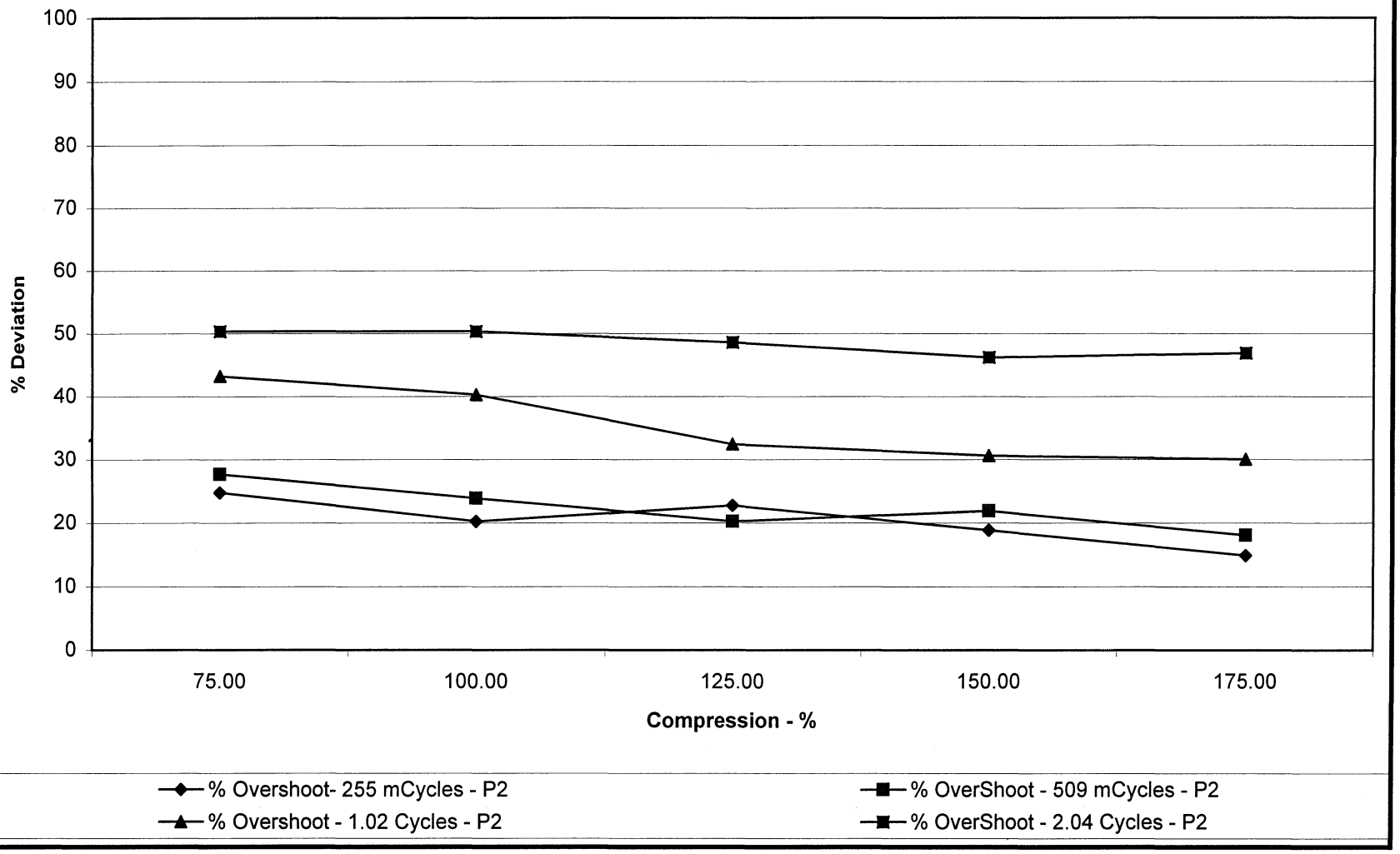

Figure - 8 Notched Response Plots on Coupled Beam

2.34% and 3.07% Damping Ratio, Sweep Rate - 4 Oct/Min

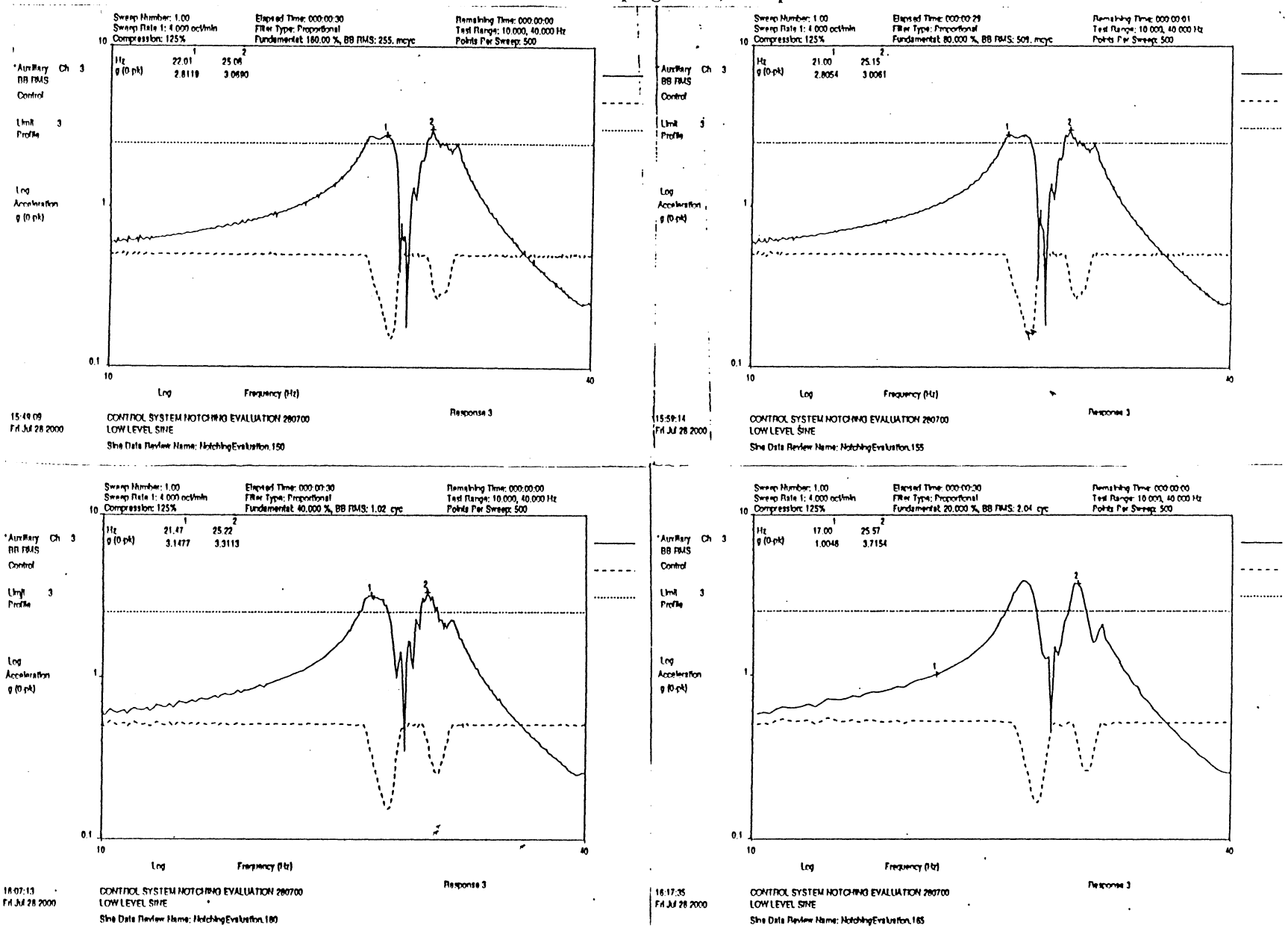

REDUCTION OF COOLER INDUCED VIBRATIONS BY MEANS OF AN ADAPTIVE ADD-ON SYSTEM

Tobias Melz, Jörg Melcher, Delf Sachau

German Aerospace Center e.V. (DLR), Institute of Structural Mechanics

ABSTRACT

Future space missions' requirements on high precision structures get continuously more challenging with respect to structural accuracy. With classical structural technology coming to its limits, adaptive structure technology offers the potential to solve a variety of quasistatic and dynamic problems.

With respect to the dynamic excitation of sensitive equipment, mechanical cryocooler systems, which are often used in aerospace applications to cool specific equipment to their cryogenic working temperatures, represent a typical dynamic disturbance source within a satellite. They either directly excite vibrations at the attached, cryogenic equipment or indirectly by exciting elastic interface structures leading to vibrations of one or multiple remote systems.

One approach to compensate for cryocooler vibrations utilizing adaptive structure technologies is presented in the paper. Within a typical small satellite project, two infrared detectors have to be mechanically cooled by two independent miniature Stirling cryocoolers. The induced cooler vibrations critically excite the detectors, leading to a severe reduction of the quality of the scientific results. Opposite alignment of the coolers was impractical due to mission constraints. Within an ESA project, DLR developed an add-on, long life adaptive vibration compensation system that removes critical vibratory energy and works without launch locking devices. The system has been designed and qualified for general space applications on material and system level. Functional demonstration proved a vibration reduction by 53 dB, representing a significant improvement on the general acceptance specifications for residual cryocooler vibration force levels for future missions. Long life testing showed no performance degradation after more than 10^8 cycles. The system was designed to be easily transferred to other applications.

INTRODUCTION

Adaptive structural technology offers a tremendous potential to cope with the manifold structural problems of modern space systems especially when compared to adequate conventional technological approaches. Typical problems arise from a variety of disturbance sources – either by the natural space environment e.g. thermal irradiation or artificially generated e.g. mechanical cryocoolers – which lead to performance degradations of quasistatic or dynamic nature. Typical effects are degradations of surface precision, dimensional stability, and pointing accuracy resulting in non-optimal radiation pattern, reduced system efficiency, fatigue, or reduced system lifetime, to name a few. Creating an adaptive structure means to realize a *"... load bearing or shape defining system with the ability to measure what is happening to itself (the system) and decide on and undertake counteracting action to bring and then keep the system in the desired*

state" (ref. 1). In comparison to a passive structure, the adaptive or smart structure is equipped with sensors, actuators and an adaptive control system which is self-optimizing and highly non-linear. Such adaptive structures allow performance levels that are not achievable by passive systems. Additionally, such a system is characterized by its adaptability: it can adjust to changing requirements or even compensate for errors.

This possibility also implies that in comparison to an advanced passive design it could be possible to achieve equivalent system capabilities at a cheaper price with an adaptive structural solution. These price savings could come up at different time periods: during design, validation, manufacturing, assembly, operation or maintenance.

Within the space area adaptive structural technology is expected to be of major importance for future missions for e.g.

- *active vibration control and isolation,*

  at/ of disturbance sources like cryocoolers or solar arrays, sensible equipment like infrared detectors or within the transmission path like truss structures (SRTM, L/PL interface) to improve system performance, lower structural loads, increase service life

- *active shape control,*

  of optical surfaces and booms for optical data transmission and interferometry (active/adaptive optics), to reduce rigid, heavy, expensive structures and use flexible ones

- *online health monitoring* and *system identification,*

  to increase service life, call for required maintenance missions, study structural mechanical interaction

- *active positioning* and *pointing,*

  of instruments, e.g. transmitters, receivers, detectors

- *precision deployment of large structures* and

  to deploy, put into position and correct the shape of structures like wide-area surfaces of modern space interferometers

- *active compensation of manufacturing errors.*

  to allow for small manufacturing errors, correct them by active means and with that reduce costs

The following paper concentrates on adaptive vibration control at a typical satellite disturbance source interconnected to sensitive equipment. DLR is engaged in the development of a variety of systems to cope with the above listed research areas.

MICROVIBRATIONS ABOARD A SMALL SATELLITE APPLICATION

Microvibrations aboard spacecraft are generated by moving mechanisms like antenna pointing mechanisms or mechanical coolers. The respective vibrational energy is being transferred over the satellite structure via structural paths which, for lightweight satellite structures, are usually poorly damped so that the disturbance energy will not be dissipated. With the stringent demands of modern satellites the residual vibrations

more often lead to critical excitations of sensitive equipment significantly degrading their performance. In the past spacecraft designs have been rendered useless due to incomplete vibration consideration.

The classical approach to the problem is to simulate the complex structural characteristics as accurately as possible. Since the models generally cannot be correlated with the real hardware during the design phase and moreover, with the structure being subject to design modifications which have to be updated in the models, this procedure leads to intensive analyses and design uncertainties. Eventually, this results in more or less conservative, oversized final designs of host structure and instruments as well as high design and verification costs.

In order to increase functional performance of systems, to significantly reduce analysis efforts, simplify structural design and thus reduce future mission costs it is increasingly important to control microvibrations aboard spacecraft. Since passive isolation basing on soft mounts is not straightforward within a space application with respect to launch loads (displacements) and e.g. pointing stability (accuracy) requirements, it is quite challenging to develop advanced structural systems to actively control microvibrations. This brings the potential to realize much higher levels of vibration reduction as well as reduce or omit heavy, expensive, rigid structures and realize flexible structural systems.

The primary goal of the presented work was to develop an adaptive microvibration control (MVC) structure for a demanding small satellite application to cancel critical vibrations at the disturbance source/-sensitive equipment. It was of major interest to prove that the smart structure is capable to withstand all relevant environmental loads and function reliably in the extreme space environment.

The mission's primary payload consists of two infrared sensors, a Medium (MWIR) and a Long Wave Infrared (LWIR) detectors. The satellite is planned to weight about 80 kg, and measure about 500 mm on each side before solar panel and antenna deployment. The major scientific-technical mission objectives are to perform earth observation e.g. for detection of hot spots and to develop next generation IR-sensors.

Due to the weight and volume restrictions, it was decided to use cryocoolers instead of cryostats to ensure the necessary operating temperatures for the IR-sensors. Small tactical cryocoolers (Signal USFA type 7058) have been preselected. These mechanical cryocoolers induce axial forces into the satellite due to their function i.e. due to the movement of piston arms and additional pumping actions. More critically, due to the coupling of the cooling arm to the upper dewar / sensor housing, there is the danger that the sensor orientation will not be fixed to the desired accuracy leading to potential reductions of the usefulness of the scientific results.

The cyrocooler is shown in figure 1. The larger part is the compressor, the smaller is the pump with attached cold finger. Compressor and pump are split to keep residual disturbances at the cryogenic interface as low as possible. A flexible metal tube interconnection serves to transfer the cooling fluid back and forth between the two components.

Experiments did show a drift of the disturbance signal phase and amplitude during cooler operation, with the major disturbance at the cooler's drive frequency and its higher harmonics. Moreover, there is the danger that system parameters will be shifted during launch loading as well as that external disturbance sources excite the sensor head. This led to the decision to implement an adaptive compensation to cancel any vibrations at the infrared detector.

ADAPTIVE MICROVIBRATION CONTROL STRUCTURE

The primary goal was to develop a system that can drastically reduce the cryocooler induced forces, and resulting vibrations, of the cooler pump by destructive interference. - The MVC system was intended not only to solve mission specific problems but moreover to offer a solution potential for similar applications. – Preceding measurements with a representative test set-up have shown that the primary disturbance forces can be up to 4 N at 50 Hz with displacements in the sub-millimeter range. Thus, the MVC system, which was to be designed without launch locking devices with a tuned first eigenfrequency above launch load excitation, was to operate at the disturbance frequency far below structural resonance as a compensation system. A force output of 4.4 N at 50 Hz was to be generated. Major design goals were to

- introduce a drastic, fast vibration reduction that is adaptable to changing operational conditions,
- build a very robust system that comes without launch locking devices,
- realize a system which is compatible with the operational environment (e.g. EMC, thermal),
- design a modular add-on system that can easily be transferred into different applications,
- offer a quasi-standard system to be used for uni- or multiaxial vibration control,
- allow broadband or multifrequent vibration control,
- consider general space constraints ,
- qualify the system for general space applications using elevated test parameters,
- base the system on a rather simple pattern,
- design small lightweight system this especially wrt the robust design,
- allow for future design optimization and to
- realize a system with long service life.

Figure 2 shows a simple scheme of the adaptive MVC concept. Here, the force is generated by activating a modified piezoceramic stack actuator (axial stiffness c_A) which has been qualified as a part of this project. This solid state actuator accelerates its inherent mass plus an additional compensation mass. The reactive control force will be transferred to the cooler pump via a flexible tip (axial stiffness c_F) which serves to keep critical bending loads from the stack. The additional compensation mass sheaths the actuator, being connected to its base. The complete actuator-compensation mass assembly is supported to an external housing by use of patented springs (ref. 7) (axial stiffness c_S). The disturbing vibration force between optic's housing (right of figure 2) and MVC system shall be compensated with the piezoceramic stack producing at least the same force with an opposite phase. This meant to control the actuator such that no residual displacement is left at the camera head.

Control forces can be adjusted by variation of the compensation mass and / or the mass and stroke of the actuator. With the help of analytical models the system parameters have been calculated. A piezoceramic stack actuator with a free stroke of 120 µm has been designed. The compensation mass was set to 700 g with a required low axial stiffness of the spring mount of 10^4 N/mm at maximum.

Actuator components have been tested on a material level for outgassing characteristics according to ESA specifications (ref. 2, 6). Basing on thermal vacuum test results a standard actuator was properly modified. Within the final actuator design, all insulation and adhesive materials were replaced by a qualified epoxy material or omitted where possible. To improve the actuator's mechanical robustness wrt survivability during launch, a high pre-stress of 1000 N was introduced. Moreover, the stack was laterally stiffened with a suitable silicon compound filling also improving the heat removal from the stack. Electric wiring was done through a bore in the actuator's base.

The MVC structure set-up is shown in an exploded view in figure 3. The compensation mass is attached to the piezoceramic actuator at its left side. In order to minimize the mass moments of inertia, a rotational symmetrical geometry was realized with the force being generated in the middle of the assembly. Compensation mass and actuator are rested on star-shaped springs made of X12CrNi17 7, shown in figure 4 and 5. Due to the spring's special design, the required low axial stiffness (c_S = 35 N/mm) was realized allowing at the same time for the desired high lateral stiffness (c_{Sl} = 20100 N/mm) to absorb launch loads. Piezoceramic sensors, a PCB force sensor type M208B01 mounted between camera and MVC structure and a PCB accelerometer type 306M118 are employed. The force sensor provides the reference signal for the adaptive feedback controller, the accelerometer is used as error signal.

Figure 7 shows the manufactured MVC-structure being connected to a mock-up of the IR-camera with integrated cooler system. The left picture displays the inner structure, compare to figure 3, whereas the right view shows displays the complete structure with all sensors connected.

The structure has been numerically analysed assuming quasi-static comparative design launch loads of 50 g. To determine maximum stress, displacement and screw forces, eight potentially critical load cases have been verified. Figure 6 indicates the respective loading cases. Having determined the respective forces at the threaded fasteners, a design and strength verification analysis has been performed according to VDI 2230 for the fasteners.

The transfer functions of the MVC system have been determined by exciting the actuator with a pseudo random noise signal in a frequency range from 0 to 2000 Hz with a voltage of 20 Vp. The frequency response spectra of the force sensor and the axial acceleration sensor have been monitored. The system's main natural frequency is at 945 Hz. This data serves as a reference for monitoring the structural and functional integrity during the qualification phase.

ADAPTIVE DIGITAL CONTROLLER EXPERIMENTS

Figure 8, left, shows the equivalent block diagram of the adaptively controlled system. The different blocks represent the continuous transfer functions P1(s), S1(s), P2(s), and S2(s) which are defined in the analogous s-plane and represent the relationships between the appropriate forces and accelerations. The discrete transfer function H(z) gives the relationship between the measurable control output y and the force f (ref. 3). To simplify the block diagram, all A/D and D/A converters have been omitted here.

Functional demonstration was performed at DLR Braunschweig, Institute of Structural Mechanics. For the real-time controller realization, a digital system was chosen within a PC environment, consisting of an AT&T DSP32C Floating Point Signal Processor with 16-bit A/D and D/A converters containing two AT&T DSP16a digital signal processors and an in-house development environment. The controller mentioned above

was programmed in C language, down-loaded in the signal processors, and monitored with a further C program running on the PC processor.

Different tests have been performed to check the quality of the control circuit and to record the transients and spectra of forces and accelerations of the system. Figure 8, right, compares the error signal in the frequency domain with and without control. A very fast microvibration reduction of 53dB was realized.

ADAPTIVE MICROVIBRATION CONTROL STRUCTURE QUALIFICATION

Environmental testing has been performed wrt general ESA test requirements specifications (ref. 4) in the laboratories of DLR Berlin, Institute of Space Sensors. Long-time functional testing was done at DLR Braunschweig.

To observe the structure's retention of its functional and structural integrity during all different qualification test sequences, structural mechanical tests to check the functional characteristics of the MVC system have been performed. These functional verification tests have been done, depending on the test type, before, within and / or after each test sequence as well as before and after completion of all tests. The functional tests have been done by exciting the actuator with a pseudo random noise signal, s. above.

Dynamic launch load testing was performed using an electrodynamic shaker system TIRAVIB 51010/LS with a slip table for testing of payloads and subsystems by TIRA Maschinenbau GmbH. The MVC structure, mounted for horizontal testing (here z-axis), is shown in figure 9, left. Random vibration and pyrotechnic shock testing was performed with test parameters given in figure 10. The latter was performed as Shock Response Spectrum (SRS) tests to simulate the structural response of the MVC structure to pyrotechnic shocks. Three shocks per axis have been applied. Overall and intermediate dynamic functional verification tests as well as the resonance survey test, see above, have been performed. No damage was detected.

In addition to launch load testing the MVC structure has been qualified for in orbit environmental thermal and vacuum loading. For this, a vacuum temperature cycling test has successfully been performed. Figure 11 displays the test pattern according to ref. 4. To increase thermal loading on the active elements within the MVC demonstrator structure, additional conductors of heat, copper cables and sheets, have been added to the structure, s. figure 9, right. To simulate the system's in orbit function the MVC system was operated druing VTC testing with characteristic drive signals. To check for functional or structural degradations, initial and final dynamic functional verification tests as described above have been performed prior to and after the VTC test, i.e. before and after vacuum has been applied at ambient temperature. Moreover, functional tests have been done as indicated in figure 11. No damage was detected which is in accordance to overall functional tests performed at DLR Braunschweig prior to and after all environmental tests.

Qualification was completed with a long-time functional test. For this, the MVC system was continuously operated for 72 days. To simulate the disturbance the MVC structure was excited with a LDS shaker system, the piezoceramic stack was driven with a high voltage sinusoidal signal. Functional performance was checked prior, within and after the test. No damages have been detected.

SUMMARY

For a typical small satellite application, here a scientific DLR satellite, the operational vibration levels of a mechanical cryocooler system excite an attached infrared detector. There is the danger that the quality of the scientific results would be critically reduced. To reduce these microvibrations an adaptively controlled robust add-on structure was developed employing piezoceramic actuators and sensors. Functional demonstration of the system was successfully performed leading to a vibration reduction of 53 dB! The structure was successfully qualified for launch and space environmental loads as well as for long-time functional performance.

Current DLR activities led to a variety of new MVC designs. Work is focussed on optimizing mass, volume and power demands wrt the original system as well as on performing broadband and/or multifrequency vibration control. One solution is displayed in figure 12.

REFERENCES

1. Breitbach, E., *Research Status on Adaptive Structures in Europe*, Proceedings of the 2nd Int. Conf. on Adaptive Structures, Nagoya, Japan (1991)

2. ESA PSS-01-702, Issue 2, A Thermal Vacuum Test for the Screening of Space Materials (1994)

3. Melcher, J., Active Vibration Isolation Using Multifunctional Interfaces and Adaptive Digital Controllers, 3rd Int. Conf. On Adaptive Structures, San Diego, USA (1992)

4. ESA PSS-01-802, Draft 1, Test Requirements Specifications for Space Equipment (1993)

5. Melz, T, Sachau, D., Melcher, J., Breitbach, E., *An Add-On Adaptive Proof Mass System to Reduce Cryocooler Induced Vibration*, 4th International Conference on Dynamics and Control of Structures in Space, Cranfield, 1999

6. Thermal Vacuum Test for the Screening of Space Materials, ESA, Draft, ECSS-Q-70-02, in review, (2000)

7. Breitbach, E.; Breitbach, H.: Deutsches Patent, Nr. 19723515, *Elastisches Element mit Blattfedern*

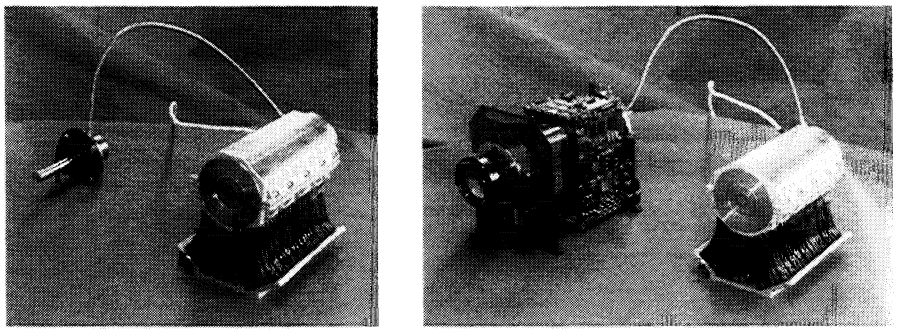

Figure 1: Engineering model of the cooler and its integration within the infrared sensor

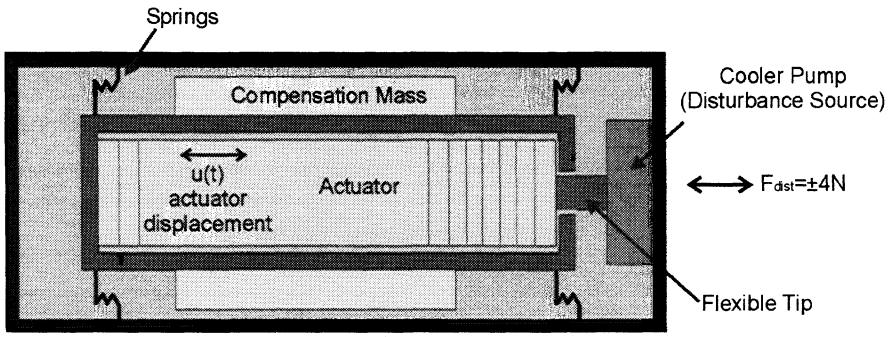

Figure 2: Scheme of adaptive MVC system

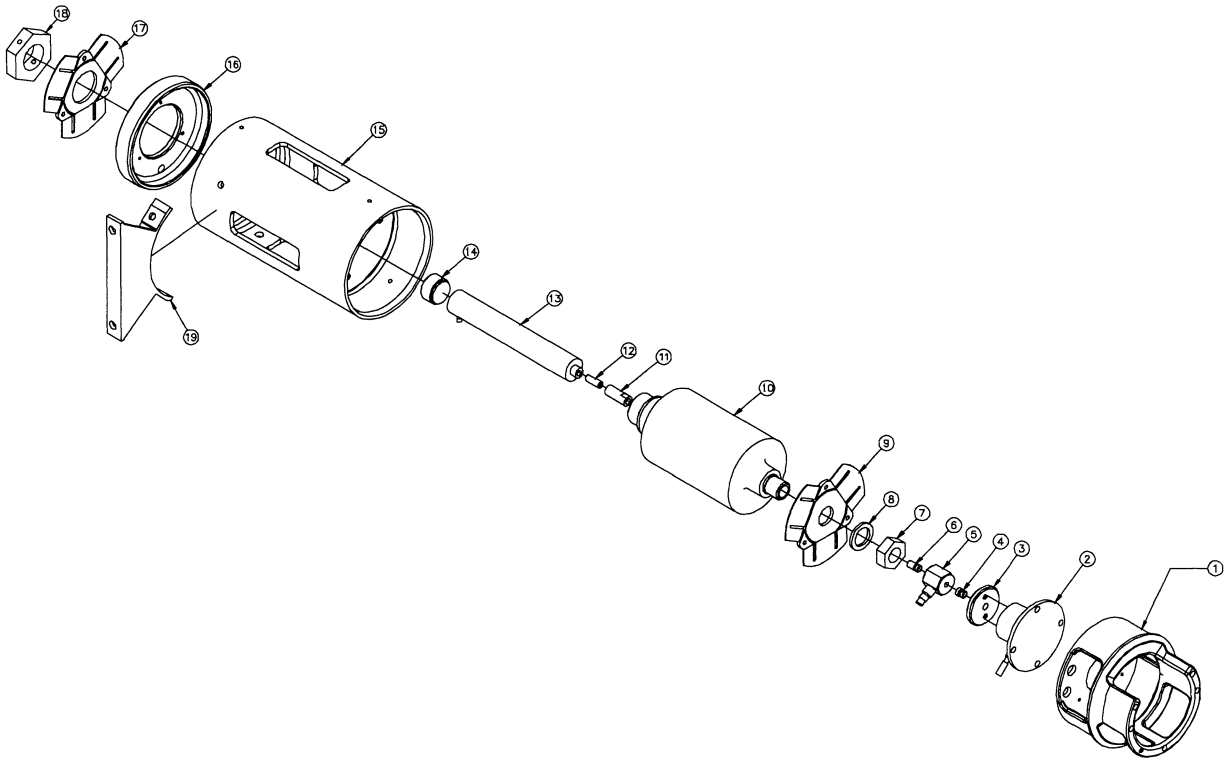

Figure 3: Assembly drawing of MVC structure

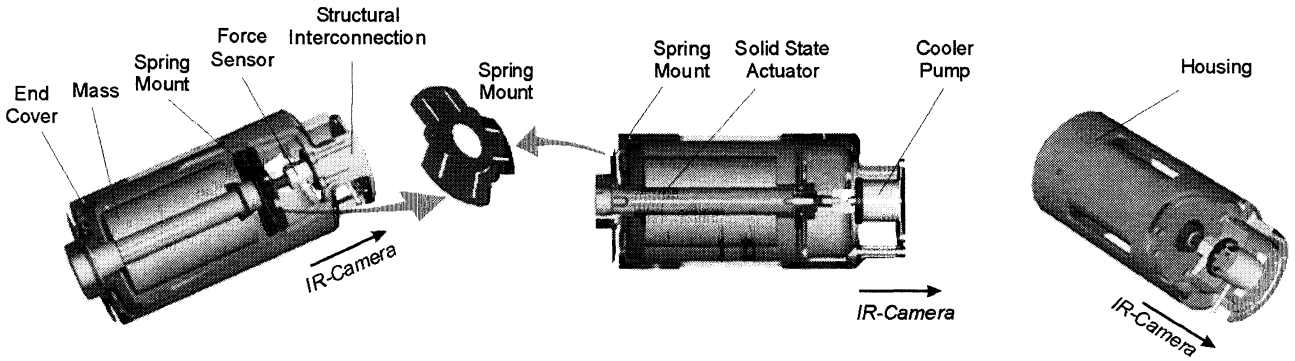

Figure 4: Cut views of MVC structure assembly

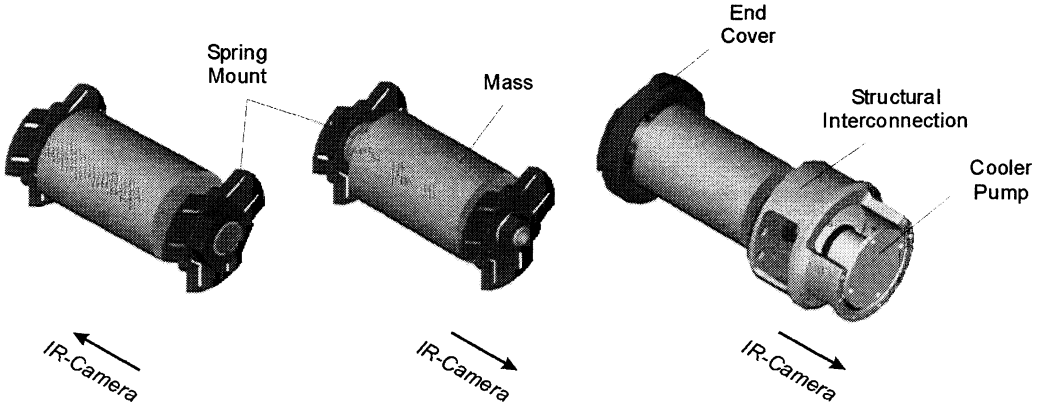

Figure 5: Inner MVC structure assembly, looking from actuator bottom (left), actuator head (middle, right)

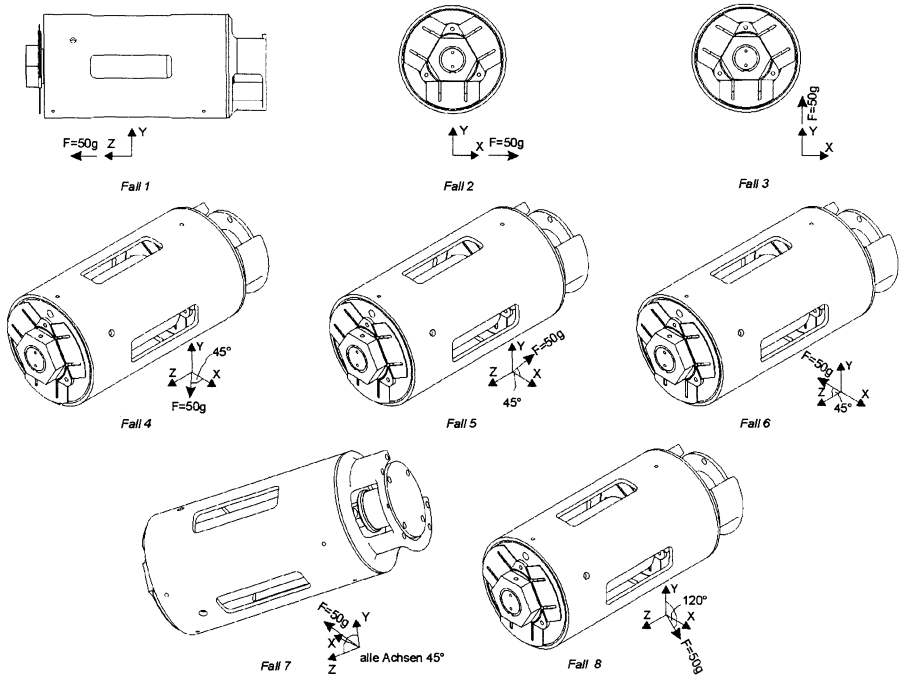

Figure 6: Loadcases for FEM calculations

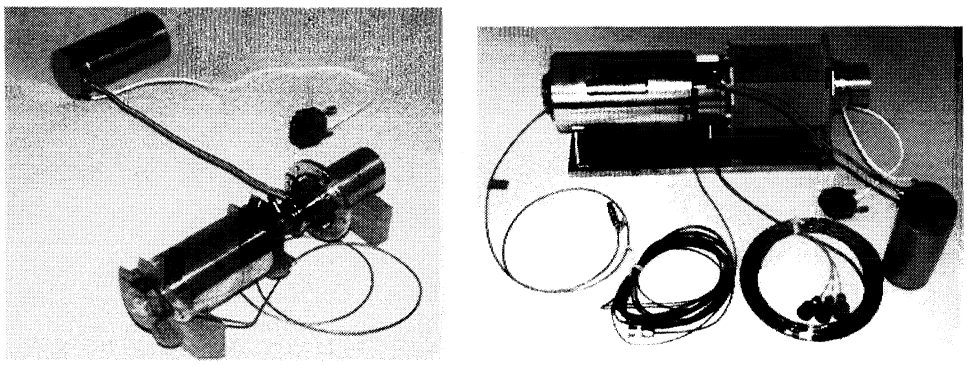

Figure 7: Manufactured MVC structure with IR-sensor mock-up

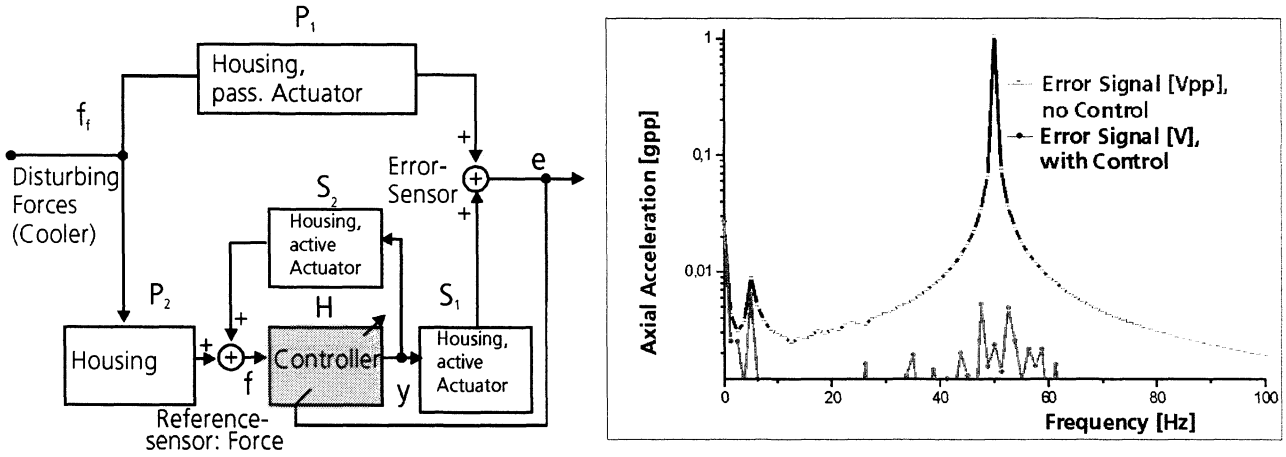

Figure 8: Adaptive feedback control block diagram (left), MVC test results (right)

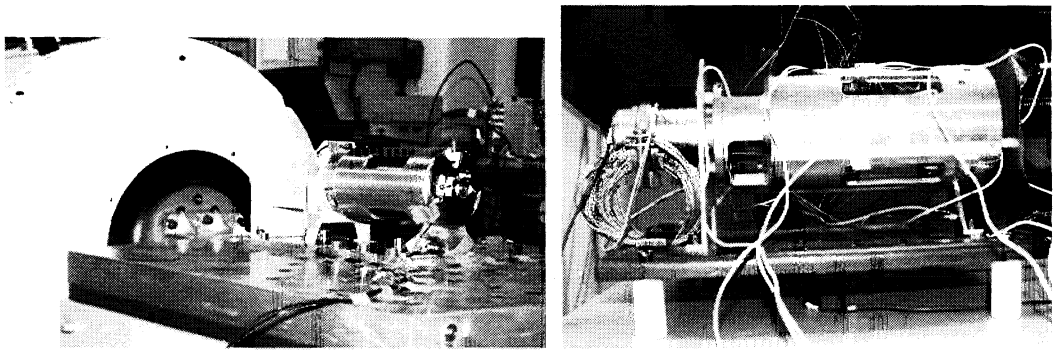

Figure 9: Test assembly for vibration testing, z-axis (left), and for VTC

Frequency range	PSD Spectrum
20 - 50 Hz	+6 dB/oct
50 - 500 Hz	0.4 g^2/Hz
500 - 2000 Hz	-6 dB/oct.
Overall	20.8 g
test duration	120 s
Vibration in all 3 orthogonal axes	

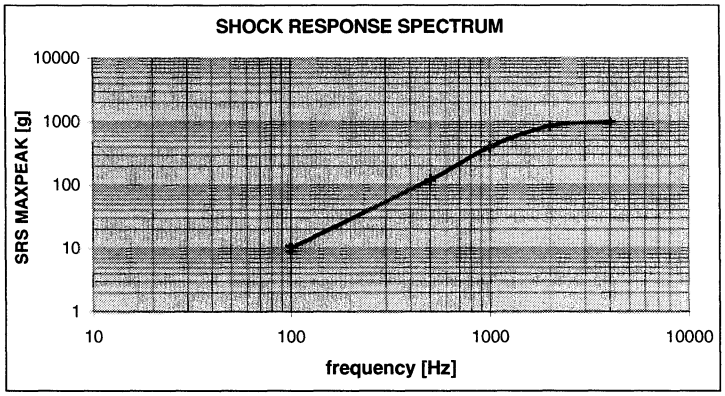

Figure 10: Random vibration and shock testing

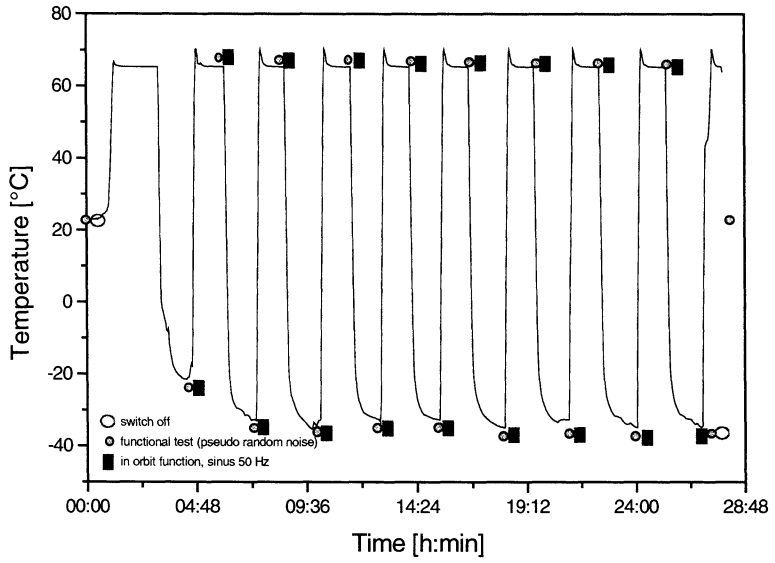

Temperature Extremes	-35...+65 °C
Pressure	$<10^{-5}$ torr
Temperature Gradient dT/dt	10 K/min
Number of Cycles	8
Dwell Time	> 60 min.

Figure 11: VTC-Test sequence and parameters

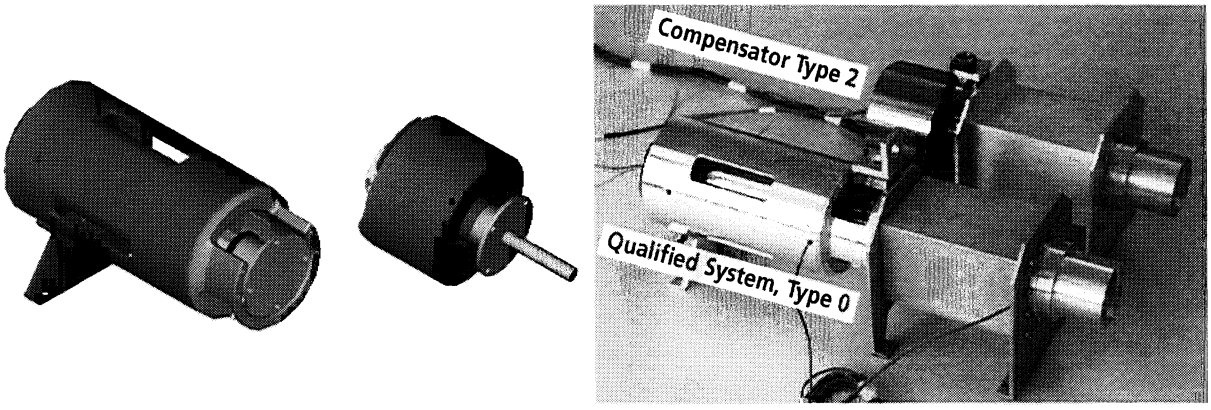

Figure 12: Two MVC systems

Page intentionally left blank

SOFTWARE FOR VIBRO ACOUSTIC DATA BANK

V Ramesh Naidu,
J N Hemanta Kumar,
B S Jagadesh Babu,
N K Mishra,
ISRO Satellite Centre, Bangalore, India.

ABSTRACT

This paper discusses the development of the software for Vibro-Acoustic Data Bank being setup at Shock and Vibration Test Facility, ISRO Satellite Centre. The data bank will facilitate management of vibration and acoustic test data of all the tests, carried out on various satellites and their subsystems.

The software will provide the user a set of comprehensive tools to access and analyze the test data over the network at his/her desktop. It consists of a File System in which the data is archived and organized for easy access, and an Application Server. The application server is designed as web-based application using 3-tier architecture. JAVA programming and principles of Artificial Intelligence and Expert System are employed in the development.

Three layers of the application server consist of client software in the form of applets that provide user friendly GUI, a server module that manages the request, uploads the applets onto client computers, invokes either search engine to obtain the requested data or analysis tool to carry out a given analysis on the selected set of data, and a set of library functions that consist of analysis tools and the search engine. The querying and some of the functions requiring human intelligence and domain expertise are implemented using Artificial Intelligence principles.

INTRODUCTION

Dynamic testing of satellites and their subsystems involve measurement of a large number of responses and analysis of the data resulting out of this measurement. This analysis process is critical to ensure qualification of the specimen for dynamic loads and, to verify its mechanical integrity and electrical functionality. This process involves comparison of signature tests to verify the mechanical integrity, computation of various modal parameters, and computation of stress levels at various locations on the specimen, etc. The process may also involve comparison of the test results with results of earlier tests conducted on similar satellite/subsystem or on qualification model of the specimen. This requires accessing and analysing the required test data. Structural Analysts were required to frequent the test facilities for looking up of data and to carry out the analysis of earlier test data. It would be convenient to the users if the data, along with necessary analysis tools, is available at their desktop for analysis.

Considering this requirement, vibration and acoustic test data is placed on a network enabled mass storage media and users are provided with web enabled tools to access and analyze the data. The Vibro-Acoustic Data Bank is located at Shock and Vibration Test Facility and is connected to the Facility's LAN. The LAN is part of the Intranet of ISRO Satellite Centre, enabling the users to access the data bank across the Intranet. The mass storage media consists of Jukebox of re-writable Magneto-Optical (MO) disks supervised by a dedicated NFS Server. Data is stored in NFS format in the jukebox. A Windows NT Server sits above the NFS Server and acts as a proxy server while hosting the application server software for the data bank. The software facilitates access to the data bank over the network and provides tools for data search and analysis. An overview of the data bank and its connectivity across the network is shown in Figure 1.

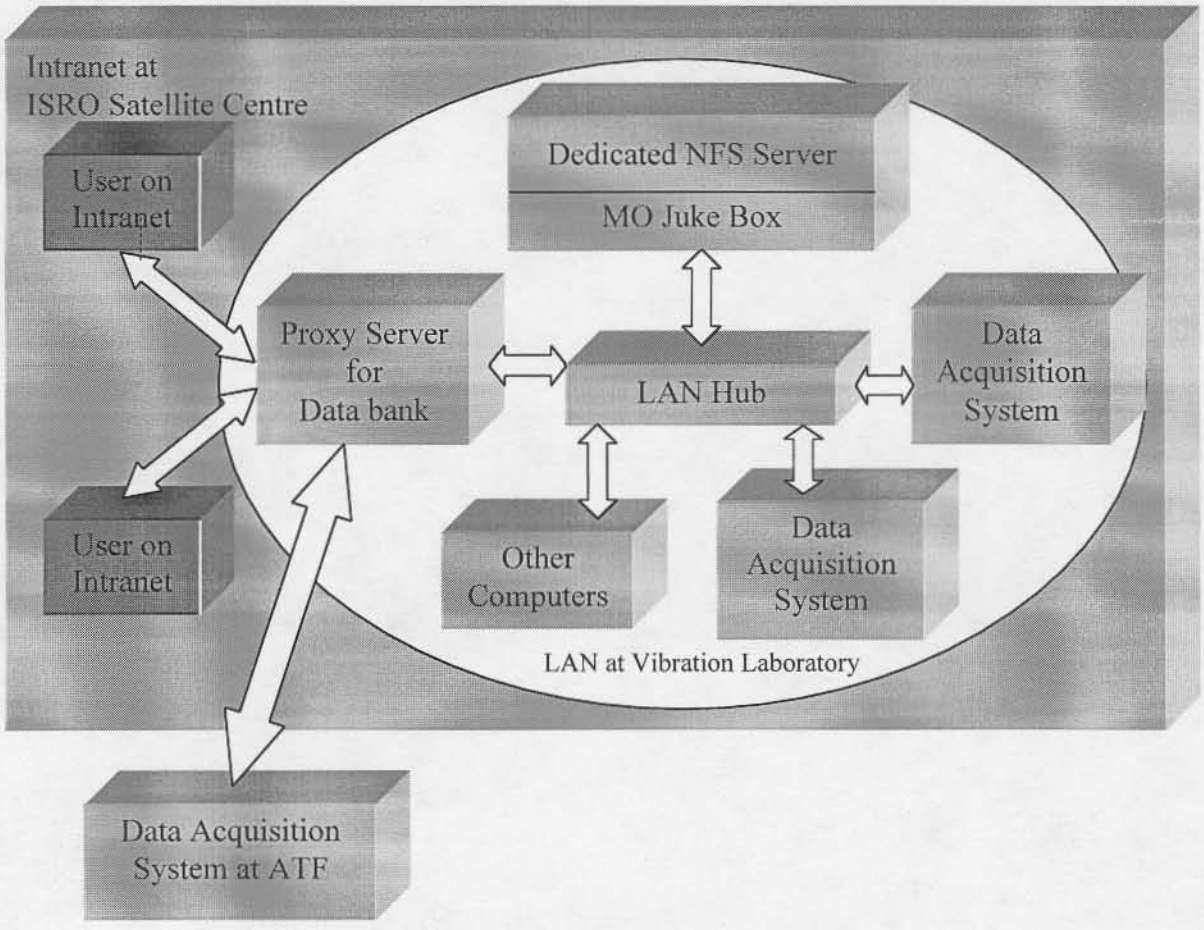

Figure 1 : Network Connectivity and Data Bank Configuration

SOFTWARE REQUIREMENTS

Software for the data bank resides in the server that supervises the data bank. It archives and organises the data for easy access. It also provides the user a set of comprehensive tools to access and analyze the test data over network at his/her desktop. Requirements of the software are

- Data archival and management involving,
  - Definition of a unified file format to store the data.
  - Development of file filters for conversion of the data acquisition system specific flat file formats to the unified file format.
  - Conversion of data of all the tests conducted on various satellites/subsystems into unified file format and archival of the same onto the jukebox.
  - Regular updation of the data bank.
- Development of a web enabled server that provides following facilities to the user.
  - Enable the user to access the server through Home Page of Shock and Vibration Test Facility.
  - Search for the required data using either specifying the details of the data or through query in natural language.
  - Enable the user to carry out analysis on selected set of data. Various analysis tools that are provided are as follows.
    - Specifications derivation for subsystems from transmissibility data of low level sine tests of satellite. Also deriving specifications from the PSD data of low level random or acoustic tests.
    - Verification of interchangeability of qualification programs for subsystems of different satellite projects (to enable using subsystems of one project in another project without further additional testing). Similarly verification of the qualification program (specifications) of a subsystem due to revision in the input level (specifications) of a project.
    - Check for the over test and under test of the satellite and subsystems using the response data of acceptance or qualification level sine tests.
    - Provide assistance to the user to verify the mechanical integrity by comparing the results of low level (sine or random) test data.
    - To compute the stress levels and Bending Moments from the strain information.
    - Response prediction for a given test profile.
    - Notching level prediction from the low-level data.
    - Identification of modes (both global and local) and mode shapes using the transmissibility and phase information.
    - Calculation of damping and Q-factors.
    - From the acoustic test data,
      - Check whether the subsystems' actual responses are well within the specification.
      - Check for the under test and over test.
      - Provision for bandwidth analysis with different resolutions.
      - Verifying linearity from low to high in octave band.

OVERVIEW OF THE SOFTWARE

The entire data is stored in a file system hierarchy within NFS specifically defined for the purpose. No commercially available DBMS software is being used, as the data cannot be represented in the table format. A separate file system with specific file formats (i.e., Unified File Format) is defined to store the data. Details of the file system and file formats are explained in the following section.

Aforesaid software requirements can be classified into two categories. First one, involving creation and maintenance of the data bank, is handled by File System Manager. Responsibilities of this software include, accessing the data acquisition systems over network for test data of a specific system/subsystem, converting it into the unified file format and archiving it on to the MO jukebox.

Second one involves facilitating the user to access and analyze required data. These features are implemented as Application Server. This software provides client interface with the data bank, capability to search the required data and tools to perform analysis on selected data. This software sits in the server computer and supervises the data bank activities involving client requests.

The software is designed to be modular for easy maintenance and augmentation of the software system, enabling new features such as new analysis tools and improvisation of the existing features to be added easily without affecting other modules of the software. These modules are implemented using Java, as the development involves network and applet programming. As Java provides platform independence, the server computer can be changed at any later date without concern for the platform. Following sections detail these modules.

FILE SYSTEM MANAGER

File System Manager incorporates file filters, GUIs for interface to input details of the test specimen, various tests carried out and listing of source data files, and networking interface to two data acquisition systems to get the source data files and to the MO jukebox for archiving the data in unified file format. The software is used only by the data bank administrator who has access to the server directly. It is not accessed across the network. Also, there would be only one local administrator taking care of the data bank management activities. Hence it is implemented as stand-alone application.

File Filters

Each of the two data acquisition systems stores the data of sine, random and shock tests using separate flat file formats for each of the data type. If data in these flat file formats are archived directly, development of modules that access the data bank would have to be developed 6 times one for each of the file formats. This problem is overcome by storing the data in a single file format for all the three data types and for the two data acquisition systems. For this, a unified file format is defined.

The file system is organized as hierarchical directories corresponding to satellite programmes, individual satellite projects, and their subsystems. Files corresponding to test data of a satellite/subsystem are stored in the respective directory. Two files are defined to store the data, viz., Master File and Data Files. Master file is an ASCII file and is unique for every satellite/subsystem. It stores general information about the test specimen, details of the tests carried out and details of the response locations. Data file is of flat file format and stores entire data of one test. Data file consists of a header in ASCII format, and stores information about the details of the test and responses monitored in the test. Actual data of the test is stored in binary format after the header.

File filters that are developed, to convert data from data type specific file formats to unified file format, include filters for sine, random and shock data.

GUI for File System Manager

Graphical User Interface (GUI) is provided to enter details of the test specimen and test details. Data bank administrator can methodically enter the information pertaining to the test specimen such as project name, model name, satellite serial number, subsystem name and serial number (if applicable), zone details of the specimen, etc. The administrator can also feed in details of the test carried out, viz., type of the test, test name, number of responses monitored, name of the response channel, response location details, etc. Once the administrator inputs these details, he has to provide list of data files corresponding to the test. The Software, using network interface, obtains the data files from the data acquisition system. File filter corresponding to the test type is invoked and files are passed onto it. Resulting master and data files are written to the MO juke box, using the network interface software module. In case of existing test specimen, the master file in MO jukebox is updated with the test details provided. GUI to enter the information about test specimen is updated with the information from the master file and displayed.

Network Interface

File system manager has to extract the source data files from two data acquisition systems and required master file from MO jukebox through network connectivity. It writes the converted data files and master files onto the MO jukebox. It uses the network interface for this purpose. As the network interface is required only for file transfer between the data acquisition systems, server computer and MO Jukebox, FTP is employed for the purpose. Separate functions are defined for file transfer between data acquisition system and server computer, and MO jukebox and server computer. These functions are invoked as and when required.

APPLICATION SERVER

Application server software provides interface to the Vibro-Acoustic Data Bank. It is accessed by the users sitting across the network. This necessitates development of the software using client-server model. However, if traditional client-server model is adopted, client software needs to be loaded onto the computer at the users' end. This has two

drawbacks. The user has to be bound to a particular computer where the client software is loaded, which will not allow him/her to switch over to an arbitrary computer to access the data bank. Also, whenever there is an updation of the software resulting due to addition of new features or due to fixing of any hitherto unforeseen bugs, client software is to be upgraded at every client computer, which is a tedious job. To circumvent these problems web technology is employed and the software is implemented as web application server using 3-tier architecture containing following modules.

a. Client software in the form of applets that provide user friendly GUI,
b. A server module that manages the request, uploads the applets onto client computers, invokes either search engine to obtain the requested data or analysis tool to carry out a given analysis on the selected set of data, and,
c. A set of library functions consisting of analysis tools and the search engine.

The client requires only web browser and network connectivity to the Intranet to access the data bank, thus avoiding the client software distribution. Software modules implementing these layers are explained in detail in the following sections.

Client Applets

Interface for the users are in the form of applets, which get downloaded to users' computer, when the user logs in. These applets form first tier of the application server. Applets provide web browser based user front-ends to search data, select data of interest, display the selected data, and carryout analysis on the selected data. Facility is provided for new user to sign in. A small database of the users is created in which users' details such as user ID, password, etc., are stored. The password is encrypted using IDEA algorithm. A variation of the algorithm is adopted wherein the sub-keys required for encryption are generated using alpha-numerical words. This makes the encryption process more secure. Some of the applets also perform certain basic computations using client computer's computational power. These computations include, computation of transmissibility, computation of rms value of random data, encryption of the password and other necessary information.

Server

Server module, sitting in the second tier, is the broker between client and the data bank. It provides interface to the search engine and analysis tools. This relation is depicted in Figure 2. Any request from the client, for data or for invoking an analysis tool, has to go through the server module. Search engine and analysis tools do not interact with each other, as well as with the client directly. This design avoids any direct communication between client and search engine/analysis tools, resulting in systematic flow of information between modules. Any new addition of analysis tool or client interface, and improvements in search engine, can be carried out independent of other modules, as long as the addition/modification is within the server module interface definition.

The module receives request from the client, and uploads the required applet. When data search is requested for, it invokes the search engine, by passing information about the

data required. Data obtained from search engine is passed back onto the client. If the request is for analysis, first the required data is obtained by invoking search engine, then, the corresponding analysis tool is invoked and data is passed onto it. Result of the analysis is sent to the client for his perusal.

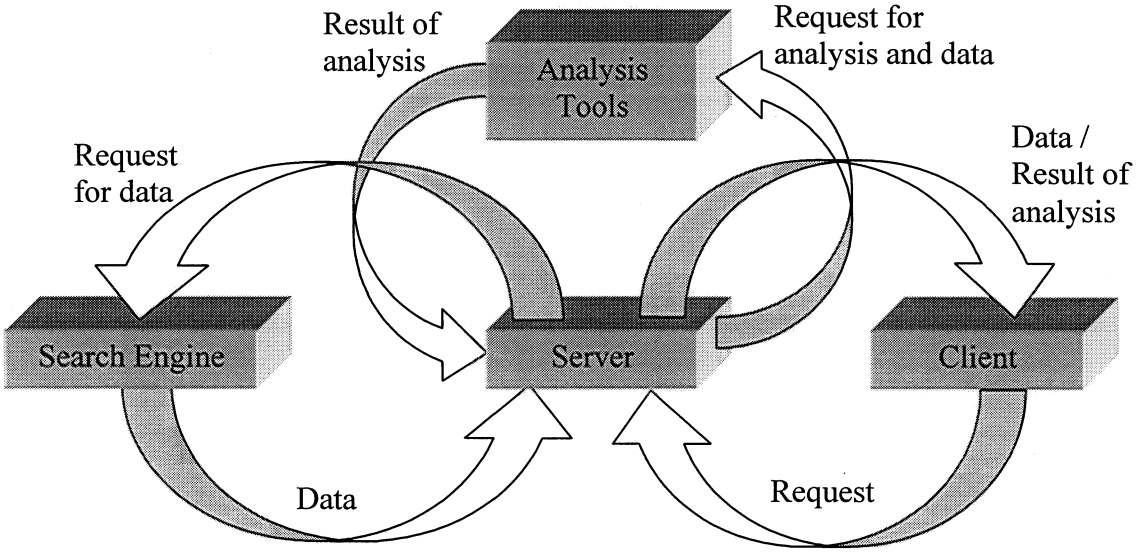

Figure 2 : Flow between different entities in the software

Search Engine

Search Engine module, as part of the 3rd tier, services requests for the data by searching through the data bank, retrieving the requested data and passing it to the server. The module is the only interface between the server module and data bank, wherein the data is archived. It communicates only with the server module to receive the request for data transfer and send the data retrieved from the data bank. Search engine provides the capability for searching the required data. Data can be obtained either by providing complete information (such as response name, test name, satellite name, etc.) or by navigating through the data bank in a step by step manner. The module provides following search capabilities.

Generic Search

User can interactively select a data set by progressively selecting the satellite name, subsystem name (if applicable), test name and the response location name. Data can also be obtained by giving all these information at one step using the GUI.

Subsystemwise Search

For each of the satellite tests carried out, information about the response channels monitored around a particular subsystem is stored in the data bank. Data of all the response channels pertaining to a subsystem for a particular test can be obtained.

Zonewise Search

Similar to the subsystemwise organization of the test data, information about the data channels identified under a particular zone of the satellite is also stored in the data bank. Hence responses monitored in a particular zone of a satellite for a test can be obtained.

Query using NLP

If the user does not have complete information about the data required, or does not want to use the above search capabilities, he/she can query the data bank in the natural language about the required data. This capability is implemented using Natural Language Processing (NLP) principles.

Approach of combined syntactic (structural) and semantic directed analysis is used. With this approach, information conveyed in the sentence is extracted using syntactical and semantical analysis of the input sentence. This involves analysing the sentence using parser, generating the template for sentence by replacing the key words with their syntactic equivalents and semantic tags from lexicon, and extracting the information. Lexicon is a dictionary of words that may appear as part of the query sentence and information about each of the word. This information consists of parts of speech of the word (syntactic information), and a semantic tag that defines meaning of the word. Syntactic parsing verifies grammatical correctness of the sentence and, if found correct, generates the template. A Grammar is defined for this purpose. Grammar is a formal specification of the sentence structures that are allowable in the language. Semantic parsing extracts the information. For this, semantic information is also encoded into the grammar, and the grammar is used to perform syntactic as well as semantic parsing.

The search engine module receives the sentence; using combined syntactic and semantic directed analysis, it attempts to extract the information about the data to be searched in the data bank. If the information is complete, the data is retrieved from the data bank and sent to the client. Otherwise, if ambiguity is encountered, the ambiguity is presented to the user for more clear information about the data required. This continues until all ambiguities are cleared so that the search engine could collect complete information needed for data retrieval.

Analysis Tools

Analysis tools provide user the capability to perform various analyses on selected set of vibro-acoustic test data. These tools, along with the search engine, sit in the third and last tier of the application server. Earlier section on requirements of the software has defined list of analysis tools.

Performing some of these analysis functions require domain expert knowledge and human judgement. Hence these expert system tools are implemented using principles of Artificial Intelligence and Expert Systems. Notable functions among these are,

- Derivation of specifications for a satellite/subsystem from the low level test data,

- Verification of interchangeability of qualification programs for subsystems of different satellite projects.
- Verification of mechanical integrity of the test specimen by comparing results of signature tests.

The expert system tools are implemented using the concept of Knowledge Based Expert System. This form of expert system consists of a knowledge base and an inference engine. The knowledge base imbibes domain knowledge. Analysis function and Domain Expertise required to perform the analysis are encoded into the Inference engine, which uses knowledge base to carry out the analysis. Rules, a Non-formal representation of knowledge, are used to encode the vibro-acoustic domain knowledge. Here, knowledge base is represented in the form of a set of rules. Advantages of such a Rule Based Expert System include modular nature of knowledge representation and similarity of such an expert system to human cognitive process.

The user supplies the information about data on which the analysis is to be performed through applet. The Server module invokes the search engine and retrieves the data. It then invokes the required expert system tool and provides the data. The Inference engine processes the data with the help of the knowledge base and produces results of the analysis to the server module. The server module presents the results to the user using appropriate applet.

CONCLUSION

From the simple goal of providing network access to the data bank, software for the Vibro-Acoustic Data Bank has evolved into a comprehensive system. It organizes archival of vibro-acoustic test data and provides numerous facilities to the user to access and analyze the data across the network using web tools. Modular design concept is adopted as it helps easy maintenance and upgradation. Application of various fields such as expert system design, networking programming, web technology, etc., has culminated into the present system. Design of the software using the concept of web application server has resulted in easy access of the data bank using web browser. It has also eliminated the necessity of software distribution among the users. Implementation of analysis tools such as expert system tools has resulted in dissemination of the domain expertise reducing the burden on the domain experts. Non-experts / semi-experts who are in need of the experts can use these tools, cutting down analysis time and improving efficiency. Updation of the knowledge base is manual at present. Updation of the lexicon for the NLP based query in search engine is also manual. However, Machine Learning can be employed to automate these updation processes.

REFERENCES

1. Valerie C Thomas, A Vibro-Acoustic Database Management Centre for Shuttle and Expendable Launch Vehicle Payloads, The Journal of Environmental Sciences, November/December 1987, pp. 24 - 26.

2. W Henricks and Y Albert Lee, A Vibro-Acoustic Database Management System and its Application for a Pyroshock Database, Shock and Vibration Bulletin, part 3, 1986, pp. 63 – 68.

3. Dan W Patterson, Introduction to Artificial Intelligence and Expert Systems, prentice-Hall Inc., 1990.

4. Dr Sunil Vadera (Ed), Expert System Applications, Sigma Press, First Edition, 1989

5. J C Giarratano, G D Riley, Expert Systems : Principles and Programming, PWS publishing Company, Second Edition, 1994.

6. Michael A Carrico, John E Girard, Jennifer P Jones, Building Knowledge Systems, Developing and Managing Rule-based Applications, Intertext Publications, McGraw Hill Book Company, First Edition, 1989.

7. T J M Bench Capon, Knowledge Representation, an approach to Artificial Intelligence, Academic Press, First Edition, 1990.

8. Cay S Horstman and Gary Cornell, Core Java, Volume I and II, SunSoft Press, Java Series, Second Edition, 1999.

9. Patrick Naughton and Herbert Schildt, Java : The Complete Reference, Tata McGraw Hill Publications, Second Edition, 1999.

10. Jim Farley, Java Distributed Computing, O'Reilly and Associates Inc., First Edition, 1998.

11. Elliotte Rusty Harold, Java Network Computing, O'Reilly and Associates Inc., First Edition, 1997.

12. Bruce Schneier, Applied Cryptography, John Wiley and Sons, Inc., Second Edition, 1996.

13. Roger S Pressman, Software Engineering : A Practitioner's Approach, McGraw Hill Publications, Third Edition, 1996.

Multiple Pages Intentionally Left Blank

THERMAL VACUUM TESTING OF THE HEAT REJECTION SYSTEM RADIATOR FOR THE INTERNATIONAL SPACE STATION

Duane Beach, Jerry Carek, and Robert Ziemke
NASA Glenn Research Center, Plum Brook Station

ABSTRACT

The International Space Station (ISS) is designed with large deployable radiator panels that are used to reject waste heat from the habitation modules. A system level test was performed in a thermal vacuum environment to demonstrate the ability to deploy these radiators once on-orbit. A Heat Rejection System (HRS) radiator successfully passed deployment tests at the extreme thermal conditions expected during the assembly of the ISS. Testing was conducted in the Space Power Facility (SPF) located at the NASA Glenn Research Center (GRC) Plum Brook Station in Sandusky, Ohio. The radiator system was installed in the 30.5m (100ft) diameter by 37.2m (122ft) tall vacuum chamber on a special deployment track that simulated weightless conditions. A large cryoshroud was used to simulate the cold space environment conditions, while a quartz lamp heater array was used to simulate the hot space environment conditions. Radiator deployments were performed at several thermal conditions using both the primary deployment mechanism and the back-up deployment mechanism. Special thermal vacuum compatible test hardware was developed to simulate the astronauts EVA drive tool for the back-up deployment mechanism. This paper discusses the test set-up, the test conditions, and the test results. The test results yield a high level of confidence for successful deployment and retraction of the ISS radiators at all expected on-orbit conditions.

INTRODUCTION

The International Space Station (ISS) is designed with large, deployable radiator panels that are used to reject waste heat from the habitation modules and the power generation equipment. A total of six Heat Rejection System (HRS) radiators and four Photovoltaic Radiators (PVR) will be used on the completed ISS. Critical thermal vacuum qualification testing of these radiators occurred over the last 5 years at the NASA Glenn Research Center's (GRC) Plum Brook Station Space Power Facility (SPF) in Sandusky, Ohio. A wide range of hot and cold thermal environments will be encountered by the radiator during its on-orbit lifetime. To simulate the on-orbit environment, unique test support hardware was developed by both NASA and Lockheed Martin to create the appropriate thermal conditions for the radiator. A gaseous nitrogen cryoshroud was run at approximately -129^{0}C (–200^{0}F) to simulate cold deployment conditions. Hot deployment conditions were simulated by an infrared heater system which enclosed the stowed radiator system until deployment. Just prior to deployment, the front of the heater system swung open on hinges to provide a clear deployment path for the radiator. A gaseous nitrogen pressurization system was built to pressurize the radiator and provide the proper system stiffness. A radiator deployment track was used to minimize gravity effects during deployment, enabling accurate measurement of deployment torques, and verification of the deploy/retract system performance.

TEST FACILITY AND TEST SUPPORT EQUIPMENT

Space Power Facility Overview

The SPF is the world's largest space environment test chamber, measuring 30.5m (100 ft) in diameter by 37.2m (122 ft) high (see Figure 1). The facility was designed to test space hardware in a simulated LEO environment. The test chamber has two 15.2m (50 ft) square doors and may be run at pressures as low as 1x10-6 torr. Solar radiation can be simulated via a 4 MW quartz heat lamp array or a 400 kW arc lamp. A variable geometry thermal shroud is used to provide simulated space environment temperatures from ambient to -195^{0}C (-320^{0}F).

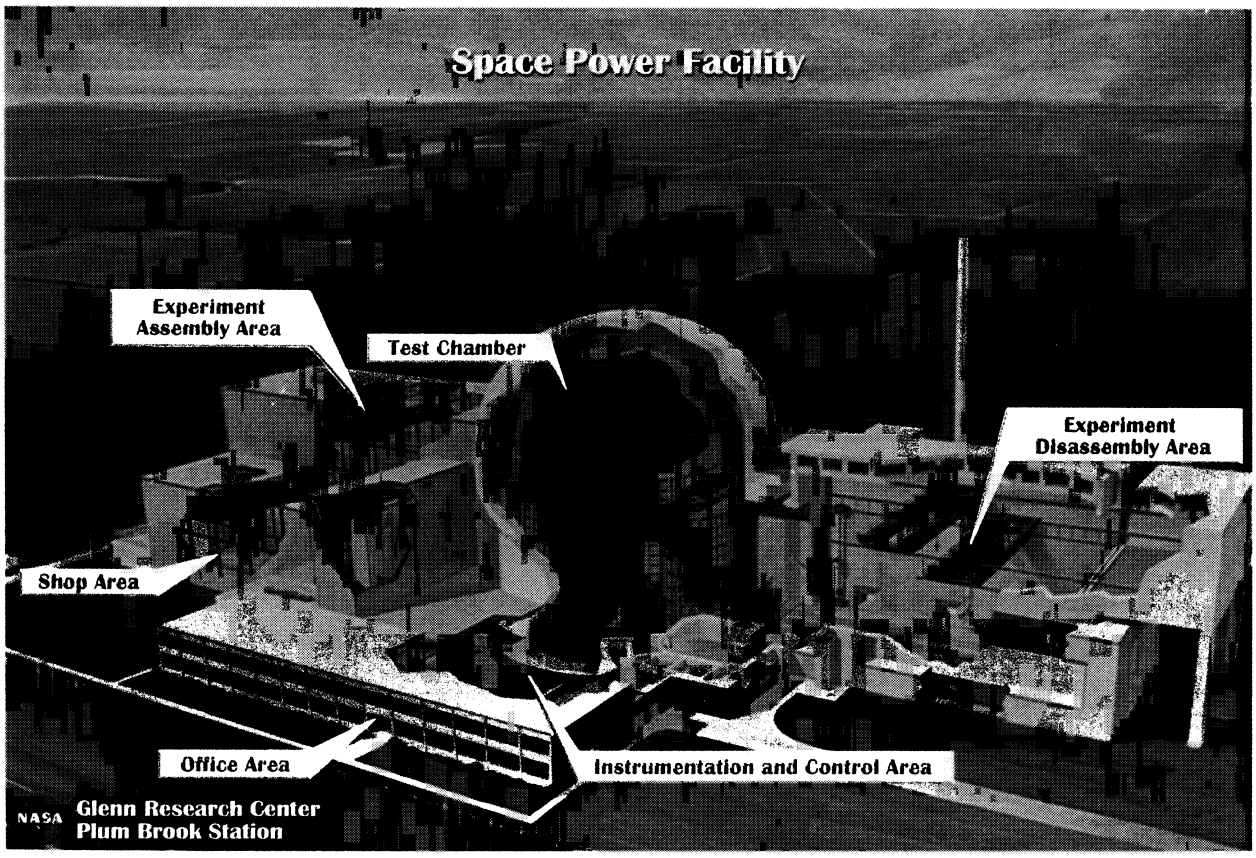

Figure 1. Cutaway View of the Space Power Facility

The test chamber is composed of an aluminum chamber surrounded by a vacuum-tight, thick-walled, concrete enclosure. This unique configuration is essentially an aluminum vacuum chamber enclosed within a larger concrete vacuum chamber. The concrete chamber serves as the primary vacuum barrier from atmospheric pressure. It has a 39.6m (130 ft) inside diameter and a 40.2m (132 ft) inside height. The concrete thickness varies from 1.8 m to 2.1 m (6 ft to 7 ft) and contains a leak-tight 6.3 mm (0.25 in) steel containment barrier embedded within. Like the aluminum test chamber, the concrete chamber doors have 15.2 m by 15.2 m (50 ft by 50 ft) openings, which are sealed with inflatable seals. The space between the concrete enclosure and the aluminum test chamber is pumped down to a pressure of 20 torr during a test such that the majority of the atmospheric pressure load is carried on the concrete enclosure. The chamber vacuum pumping system utilizes oil diffusion pumps backed by roughing pumps.

The mechanical roughing pump system consists of two systems with five stages each, having a total pumping capacity 61,000 liters/sec (130,000 cfm). The hard vacuum system consists of thirty-two 122cm (48 in) diameter oil diffusion pumps mounted in the chamber floor. Each diffusion pump is LN2-baffled , electrically heated, and has a pumping capacity of 43,000 liters/sec.

The SPF is flanked by two high-bay areas, the assembly area, located on the east side of the test chamber, and the disassembly area on the chamber's west side. The assembly area is 22.9m (75 ft) wide by 45.7m (150 ft) long and has a steel frame superstructure with a clear height of 24.4m (80 ft). Test hardware in the assembly area may be lifted with a 25-ton overhead bridge crane, or rolled on three sets of parallel railroad tracks that extend into the test chamber. The disassembly area has epoxy coated concrete walls and is 21.3m (70 ft) wide by 45.7m (150 ft) long with a clear height of 23.2m (76 ft). A remotely controlled 20-ton overhead bridge crane services the disassembly area. The railroad tracks from the assembly area and chamber continue through the dissassembly area, thus providing a rolling transport capability the entire length of the facility.

14 MW of utility power is available to the SPF, redundantly fed from two, independent power grids. In addition to utility power, emergency backup power is available from a diesel power generator and an on-line uninterruptable power supply (UPS) consisting of a battery bank and a 15 kVA dc to ac inverter. The UPS system is configured to supply power to critical instrumentation and critical control systems.

Cryoshroud

The SPF has a large removable cryoshroud to simulate cold LEO thermal conditions. The cryoshroud is 12.8 m (42 ft) wide by 24.4m (80 ft) long with a ceiling height of 6.7m (22 ft). It has a removable floor section that is 12.2 m (40 ft) wide by 24.4 m (80 ft) long. The cryoshroud floor is mounted on trolleys which ride on rails extending through the chamber and both high-bays. This configuration permitted build-up of test hardware in the disassembly area on the cryoshroud floor. Hard attachment points at various locations on the cryoshroud floor were used to mount the HRS radiator test hardware. The cryoshroud floor and test hardware were then rolled directly into the chamber. The cryoshroud is shown in Figure 2. inside the test chamber without the end panels installed.

Figure 2. Cryoshroud inside SPF chamber

The SPF cryogenic system is supplied by two liquid nitrogen storage vessels with capacities of 821 kilolitres (217,000 gal.) and 106 kilolitres (28,000 gal.). The system is capable of removing up to 14 MW (47.8 x 106 BTU/hr) of heat from the cryoshrouds. Fill pumps circulate liquid nitrogen to the cryoshroud and to the diffusion pump baffles. Liquid nitrogen is used in the diffusion pump baffles to minimize the potential of backstreaming silicon oil vapor into the chamber during high vacuum conditions. Two 11,000 cfm nitrogen compressors circulate gaseous nitrogen through the cryoshroud. The temperature of the shroud can be controlled by adjusting the cold nitrogen gas flow rate. During the cold temperature testing of the radiators, over 3785 litres/hour (1000 gallons/hour) of liquid nitrogen was required to maintain the desired cold soak test temperature of -87^0C (-125^0F).

HRS Pressurization System

Accurate simulation of on-orbit radiator deployment torques required that the radiator fluid passages be at working pressure to provide proper system stiffness. A gaseous nitrogen supply panel available from earlier radiator tests was modified for the HRS radiator test to supply clean, gaseous nitrogen at 586-655 kPa (85-95 psig). The system incorporated redundant pressure relief devices and pressure transducers to ensure accurate radiator pressurization, while guarding against over-pressurization. Nitrogen was supplied to the panel at high pressure from facility storage bottles. The storage bottles were charged by vaporizing liquid nitrogen from the facility storage dewar. Several steps were taken to ensure that clean nitrogen was supplied to the radiator. Gas samples were first drawn both at the SPF high-pressure storage bottles and again just downstream of the supply panel. The samples were tested to verify the gas was of Grade B quality (per military specification mil-p-27401c) and that contaminants were not being introduced at the panel. Additional samples were taken at the radiator connection fitting prior to hook up, and again at the conclusion of testing. All samples were well within specification limits. Further protection was provided by a two micron filter installed at the radiator connection fitting prior to connecting the nitrogen supply to the radiator.

IR Lamp System

An infrared heat lamp system was used in conjunction with the cryoshroud to provide the proper thermal environment for the HRS radiator deployment tests. The heater system was designed to uniformly heat each face of the stowed radiator at a sufficient rate (approximately 10^0F per minute) to achieve the required temperature conditions for each deployment test. The system was used to provide constant temperature hot soaks as well as temperature gradients across opposite faces of the stowed radiator. The heat flux required for the stowed radiator surfaces ranged from 0.34 (watts/sq. inch) for the top and sides, to 1.30 (watts/sq inch) for the front panel surface. The heater arrays were designed with a 50 percent power margin to cover the uncertainty in the radiator surface emissivity at the dominant wavelength radiated by the lamps (1.3 microns).

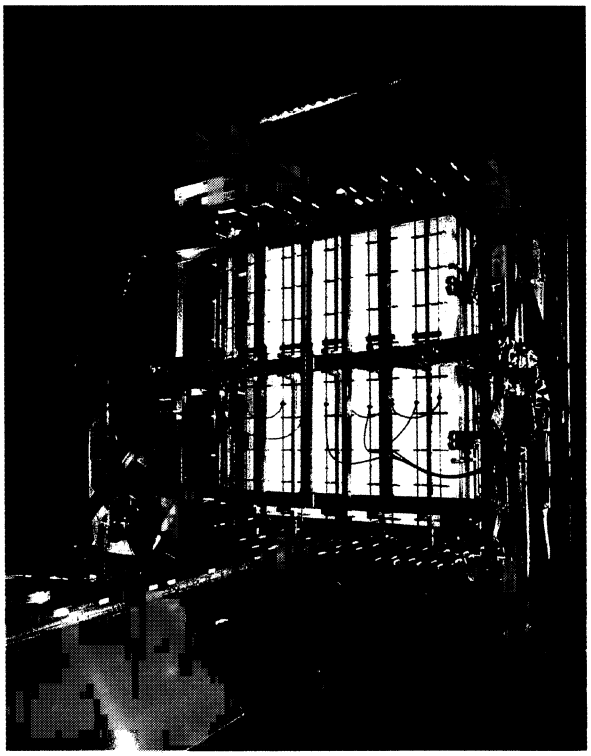

Figure 3. Stowed HRS inside IR lamp system

The heater system, which was designed and built in-house, used 203 quartz-tungsten filament lamps arranged in six planar arrays, one for each face of the stowed radiator. An aluminum support structure was constructed to enclose the stowed radiator and support six banks of lamps, one for each side of HRS as shown in Figure 3. The lamp assemblies were Research, Inc., model 5236 space thermal simulation modules with quartz-tungsten, linear filament lamps at 500 and 1000 watts. The support structure was made adjustable so that the smaller PVR could also be accommodated. High thermal emissivity plastic tape was applied to the aluminum structure surfaces to enhance the structure's cool-down rate.

The infrared lamp arrays were powered by six, 3-phase, 480-volt, SCR phase-angle controlled, AC power supplies. These are part of an existing 18 zone, 7.2 MW, SCR-controlled power supply located in the SPF. Each zone controller is protected by subcycle rectifier fuses, ground

fault trips, and a high chamber pressure trip. For each array, the lamp-to-lamp spacing and lamp-to-radiator distance were designed to provide the required heat flux level and uniformity.

The front array was split into two halves to form a double door which opened by remote controlled electric actuators just prior to radiator deployment (See Figure 4). The electric door actuators were extensively tested in the laboratory before being installed. A cold environment was established in which the actuators were cycled 100 times while driving an inertial and resistance load which greatly exceeded the anticipated door load.

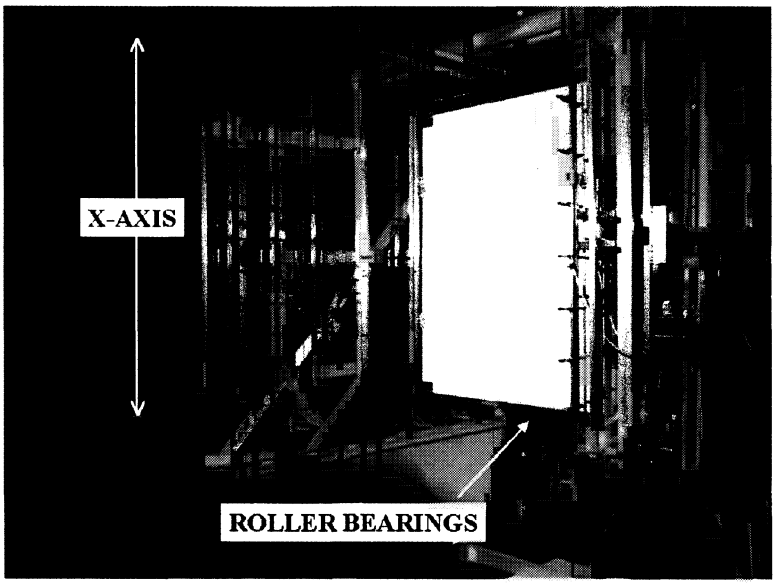

Figure 4. IR lamp system doors open, ready for HRS deployment

Each face of the stowed radiator was equipped with a primary and backup control thermocouple. These were used in conjunction with six PID temperature controllers and the SCR-controlled power supplies to regulate the surface temperature of each zone. The set point control for each zone was manually set to the desired surface temperature. The temperature controllers were also equipped with adjustable voltage and current limits, which were used to control the rate of radiator temperature rise and to limit the in-rush current to the IR lamp filaments. When the cryoshroud was operated below -125^{0}F, the IR lamps at the base of the stowed radiator were needed to augment the on-board DC heaters. Without this augmentation, it was possible for the temperature of the on-board electronics to drop below its qualified limit. To further insure that this low temperature limit was not exceeded, provision was made, in the event of a power outage, to operate the heat lamps at the base via diesel generator backup power.

EVA Drive System

It was required to fully deploy and retract the radiator under cold soak conditions using the on-board EVA override drive mechanism. Since the on-orbit, hand-held EVA drive tool used as a back-up deployment mechanism was not available, a custom-made remote controlled drive system was developed at Plum Brook Station, specifically for the deploy/retract tests.

The back-up radiator deployment mechanism simulator drive system incorporated a stepper motor, a planetary speed reducing gearbox, a pillow block stabilizer bearing, and an extension shaft which coupled the drive system to the EVA hex drive shaft on the radiator base. All of the drive components except the extension shaft were mounted on a heavy aluminum base plate (See Figure 5). Drive component temperatures were maintained by equipping the base plate with temperature-controlled strip heaters and shrouding the components with a vented aluminum cover to minimize radiated heat loss. Additionally, a magnetic wheel with a dual-element magnetic pickup was used for measuring the speed, direction, and number of turns of the output shaft. Also included were two torque transducers: one for precise "torque out" control, and the other for an ultimate over-torque safety trip.

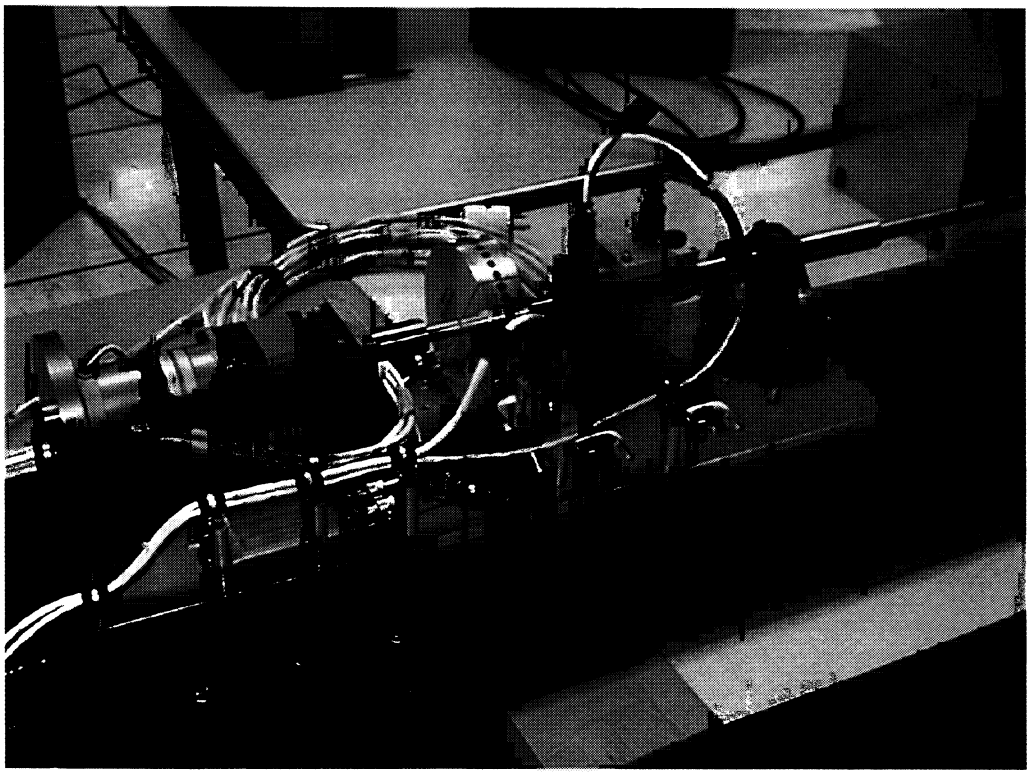

Figure 5. EVA Overide drive system with cover removed

The "torque out" control mode was accomplished by electronically comparing the output shaft torque to a manually adjusted set-point. When the torque exceeded the set-point, the stepper motor de-energized and had to be manually reset to resume operation.

The stepper motor speed and direction was controlled by a manually-operated, variable frequency stepper motor driver. The upper limit of the speed adjustment range was limited to prevent inadvertent over-speed operation. An ultimate overspeed safety trip based on stepper motor drive frequency was also provided. A stop and hold feature was provided whereby, when manually commanded, the stepper motor ramped down to zero speed but remained energized so that it would hold torque without slipping.

Since the on-board EVA override drive mechanism had limited life, only one ambient EVA deploy of the radiator was permitted as a final check of the facility EVA override drive system. Therefore, a dynamic load test bed was constructed to develop and verify the performance. (See Figure 6). The test bed components simulated, as accurately as possible, the dynamic loading of the on-board EVA drive mechanism. Installed on the test bed were the facility EVA override drive system, the extension shaft, a replica of the on-board EVA flex shaft, and a high ratio gear motor acting as a variable load. The flex shaft was oriented and rigidly held in position with the same bends as in the flight hardware. It was discovered early in the development testing that a high frequency, torsional resonance condition existed in the stepper motor drive train which prevented the system from delivering the required torque (120 in-lb) at the high speed (20 rpm). The problem was corrected by installing an elastomer damper and flywheel on the stepper motor shaft.

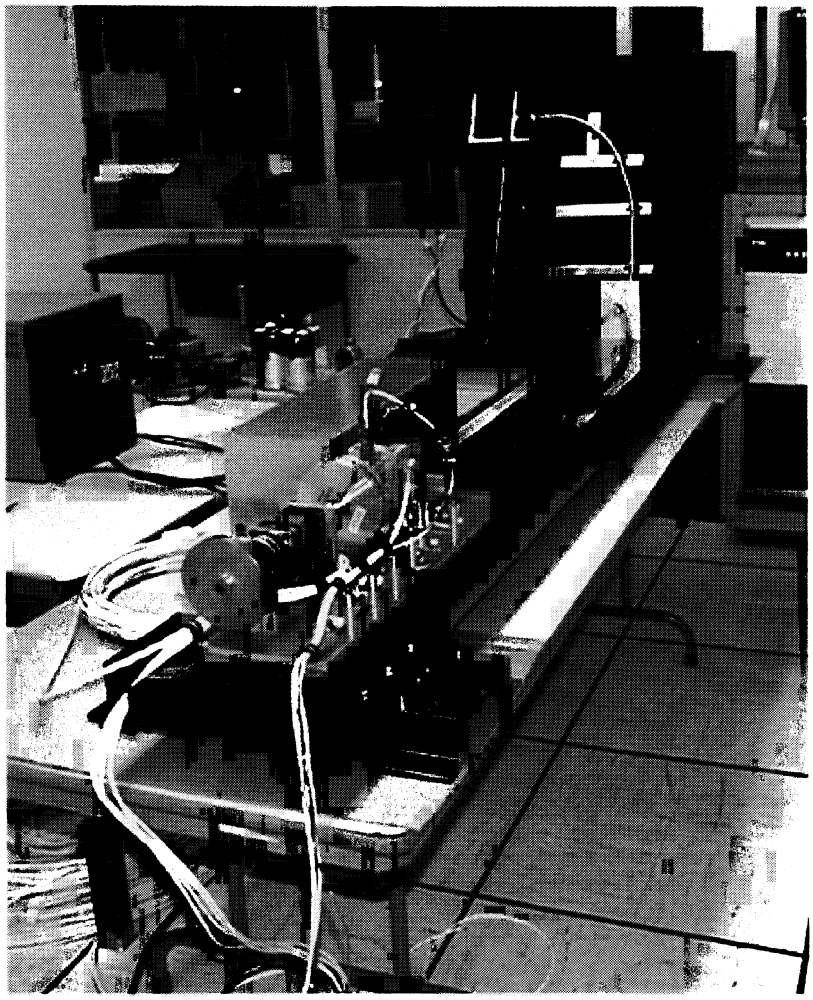

Figure 6. EVA Override dynamic load test bed

Data Acquisition

A system based on the Escort D System maintained by GRC in Cleveland, Ohio, was used for data acquisition during testing at Plum Brook. The system has 512 reconfigurable channels of which 92 were used for the HRS test with a recorded sample rate of 1 Hz. Ungrounded thermocouples were used to minimize noise pickup from the IR lamp SCR power control system. To compensate for temperature-induced strain gauge errors, dual-element strain gauges were used. Real-time engineering unit conversions were made and displayed on-screen in the control room in both tabular and trend plot format. To guard against catastrophic loss of data, data was stored redundantly on local and remote Unix-based machines and also backed up onto magnetic tape. Data was archived and delivered to the customer on CD-ROM, with a capacity of 45 days of testing data.

International Space Station Radiator Description

Six HRS radiators will be used to reject waste heat from the ISS habitation modules. Each radiator consists of a base assembly with a primary and back-up deployment mechanism, and eight panels that deploy with a scissors-arm

mechanism. When fully deployed, the radiators are about 23m (75ft) long. A deployed radiator inside the SPF chamber is shown in Figure 4. A full description of the HRS radiator is contained in Reference 3.

Radiator Deployment Track

A special 24 m (80 ft) long radiator deployment track was designed to minimize gravity effects on the test article mechanisms while testing. Frictionless rollers were attached to the pivot pins on the scissors-arm mechanism at the bottom of the panels. The rollers, which carry the weight of the panels, roll down the deployment track with minimal resistance during deployment of the radiator. A second track was erected above the radiator to restrict side to side radiator movement at the top of the scissors-arm mechanism. High emissivity tape was applied to the entire structure to speed its rate of cooling and permit it to reach thermal equilibrium quickly.

THERMAL VACUUM TEST

Objectives

Testing of the HRS radiator had three objectives. The first was to demonstrate the radiators ability to deploy and retract its panels under worst case hot soak, cold soak, and temperature gradient conditions using the flight Integrated Motor Controller Assembly (IMCA). Secondly, the retract and deploy capability was to be demonstrated using the backup EVA manual override feature under worst case cold soak conditions. Lastly, the test was to provide data to support delta qualification of the IMCA, gear/brake, and heater control assemblies.

Facility Performance and Test Results

Following a pre-vacuum radiator system checkout, vacuum conditions were established in the chamber. Radiator pressure was established at 448-517 kPa (65-75 psia) by the nitrogen pressurization system and a hot soak with the IR lamp system initiated. The hot soak of the radiator was successfully achieved by maintaining the radiator external temperatures at approximately 46^0C (115^0F) until the radiator internal temperature rate-of-change lowered to within test limits. At hot soak conditions, the IR lamp doors were opened and a successful deploy and retract of the radiator was conducted using the IMCA.

Subsequent to the radiator hot deploy/retract test, the SPF cryoshroud was chilled down to approximately -128^0C (-200^0F) to establish the radiator cold soak thermal conditions. As the radiator cooled, individual IR lamp zones were gradually powered on to maintain radiator surface temperatures at -87^0C (-125^0F). All six sides were maintained at -87^0C (-125^0F) until the temperature rate-of-change had decreased to within test limits. At this point, the delta qualification of the IMCA, gear/brake, and heater control assemblies were successfully conducted. The radiator cold retract/deploy capability was then demonstrated using the IMCA. As with the hot deploy/retract demonstration, system performance was nominal with all torques and strains meeting requirements.

Following the successful IMCA deploy/retract sequence, the IR lamp doors were closed and cold soak thermal conditions were reestablished in preparation to demonstrate radiator deploy/retract capability using the backup EVA manual override feature. At cold soak conditions, the EVA drive was engaged and the radiator was extended to a fully-deployed condition, followed by a complete retraction to its stowed configuration. Radiator torques and strains again met their required values, indicating a successful demonstration.

For the final tests , the IR lamps were adjusted to establish two radiator thermal gradient conditions, one for deploy and one for retract. The deployment test required establishing a temperature gradient from the front to back (Z axis,

through the stowed panels). This was accomplished by maintaining the radiator backside at 21^{0}C (70^{0}F) and the front side at -23^{0}C (-10^{0}F) to establish a gradient of 11-16^{0}C (51-60^{0}F) between panels seven and eight. Upon establishing this condition, the radiator was successfully deployed using the IMCA. With the radiator deployed, a temperature gradient of approximately 71^{0}C (160^{0}F) between the radiator base and panel 1 was established by warming the radiator base to no greater than 49^{0}C (120^{0}F) while allowing panel to cool. With a 71^{0}C (160^{0}F) temperature gradient, the radiator was successfully retracted to the stowed condition using the IMCA. This concluded the HRS radiator thermal vacuum demonstration testing.

CONCLUSIONS

The testing of the ISS HRS radiator was successfully completed and all test objectives were met. All facility systems and test support hardware performed as designed, successfully simulating predicted on-orbit conditions for the HRS radiators. As a result of these tests, NASA acquired a high degree of confidence that all six radiator units will deploy flawlessly once on-orbit during the construction of the ISS.

REFERENCES

1. Voss, F.E.: Thermal Vacuum Qualification Testing for the International Space Station Heat Rejection System Radiators. SAE Paper 98ES-34, July 1998.

2. Test Requirements Document for Space Station HRS Radiator Thermal Vacuum Demonstration Test at NASA's Plum Brook Space Power Facility. Report No. 3-47300H/8R-001, August 4, 1998.

3. Oren, J.A; Howell, H. R; Space Station Heat Rejection Subsystem Radiator Assembly Design and Development. SEA Paper 951651, July 1995.

Page intentionally left blank

MERCURY THERMAL TESTING WITH USE OF IR TECHNIQUES

Pietro GIORDANO[1], Giuseppe ANDRINA[1], Luca CANE[2], Bruno PANELLA[2]

[1]ALENIA SPAZIO
TORINO – Italy

[2]POLITECNICO DI TORINO
TORINO – Italy

ABSTRACT

The Mercury Cornerstone mission will be the first mission in the inner solar system after two decades.

The probe will face a 12 S.C. environment whose simulation, during system thermal tests, forces to explore thermal testing methods that take into account space budget issues.

The InfraRed Heating Technique evolution can now help in proposing this technique as a reasonable alternative testing method to Solar Simulation since it offers several advantages like a good simulation of albedo and of planet shine radiation.

A study has been carried on focusing:

- the analysis of the correlation data between Solar Simulation and IR test data for previous missions (e. g. Helios);
- the comparison of Helios probe with Mercury/BepiColombo probe condition to find out similarities and differences;
- the complete study on peculiarities of IR thermal testing;

This paper summarizes the results of the study comparing also orbital data and the two simulation test techniques: Solar Simulation and InfraRed Heating Simulation.

Keywords: Infrared Test, Thermal Test Mercury, Helios.

INTRODUCTION

The Mercury Cornerstone is a mission to planet Mercury designed by ESA to improve our understanding of the planet and its surroundings by a wide variety of techniques, from remote sensing to particle and field detectors, as well as to conduct fundamental physics experiments by radio science.

To honour the memory of the great Italian scientist Giuseppe Colombo, ESA call it the BepiColombo Project.

Launch is foreseen to take place before 2012: it will be the first mission in the inner solar system after two decades: the last two probes that approached the Sun so much were Mariner 10 (1974) and Helios (1974 and 1976).

The mission design is still in a early phase A, nevertheless it could be important to evaluate the different thermal testing approaches, in order to optimize the design avoiding problems

connected with appendages or large apertures positioning.

A particularly interesting technique for the Mercury/BepiColombo mission could be represented by the Infrared Heating, an absorbed fluxes approach that could allow the simulation of orbital fluxes in a European chamber, with a consistent and consequent testing cost reduction.

THE MERCURY PROJECT

The Mercury system configuration is based on the concept of modular mission elements; the whole probe consists in:

- a Solar Electric Propulsion Module (SEPM);
- a Chemical Propulsion Module (CPM);
- a 3-axis stabilized Orbiter;
- a spinning Magnetospheric Satellite;
- a Mercury Surface Element (MSE).

Fig. 1 – Mercury Cruise Configuration

The composite of the five elements forms the cruise configuration. Each of the propulsion modules is jettisoned when its function has been performed: the SEPM just before Mercury capture, the CPM after capture and acquisition of the Magnetospheric Satellite and Orbiter orbits. During the planetary orbit, each module is controlled by the main one: Orbiter module acts as communications relay.

A brief description of topical aspects in the configuration of the three modules and in thermal control system used is given in the following paragraphs.

Orbiter

The Orbiter element is dedicated to remote sensing observations, but is also the focus of a set of radio science experiments; it requires a polar orbit.

The configuration of the Orbiter is driven by the thermal design, the purpose of which is to reject as much as possible the very large heat inputs from the sun and the planet by means of highly efficient insulation all over the body and a large radiator shielded from direct solar and planetary radiation.

The external shape is a flat prism with slanting sides, tilted by 20° to reduce the view factor to the planet.

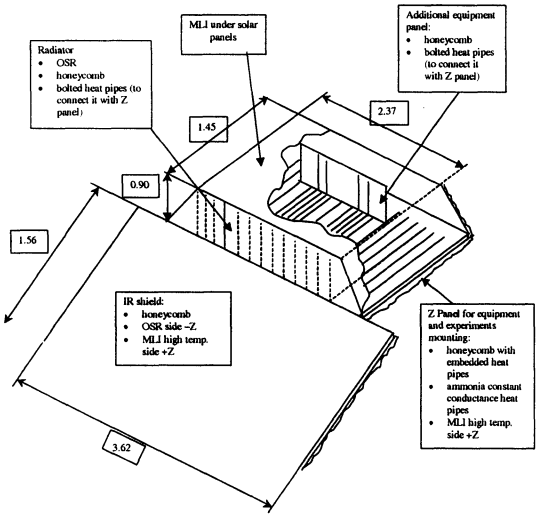

Fig. 2 – Orbiter Thermal Design Overview

Three sides are partially covered with solar cells mounted on an Aluminium substrate, with 30% cell filling factor; the remaining 70% of the surface is covered with OSRs.

The peculiarities of the Orbiter design from the Thermal Testing point of view are: **the large dimensions** of the main module (approximately 4 x 3 x 1 m), **the dishomogeneity** and **the difference in thermo-optical properties** for the different surfaces (e.g. in three sides there are both OSR and solar cells), a Thermal Control System based on **the use of heat pipes, OSR/MLI and a large radiator** protected from IR planetary fluxes by a IR shield.

The thermal analysis confirms that the chosen solutions success in assuring acceptable temperature limits.

Magnetospheric Satellite

The Magnetospheric Satellite is devoted to fields and particles science; in the mission scenario assumed for this study, it is regarded as a physically small component of the total mission, not in science return but in comparison to the main Orbiter satellite.

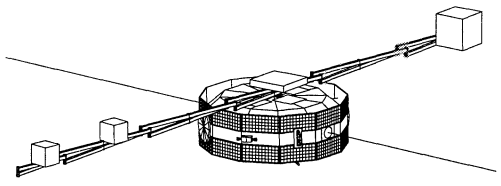

Fig. 3 – Magnetospheric Satellite Configuration

This module is a spinning satellite with spin rate around 15 rpm; in this case, too, the key design driver is the thermal environment in the neighbourhood of Mercury, with very high fluxes when the probe face the sun and the planet, practically nil fluxes when the probe is in eclipse.

The external shape is a cylinder 0.3 m high and with a diameter of 0.9 m: the reduced dimensions has driven the design to miniaturize the equipment and payload.

The primary aim of the satellite thermal design is to attempt to create near-Earth-temperature conditions for the electronic mounted in the interior of the satellite body; this is to reduce or eliminate development cost for high temperature electronics.

The peculiarities of this module from the Thermal Testing point of view are: **the simple cylindrical shape**, **the uniformity of the surfaces thermo-optical properties** (external surfaces are covered with 100% solar cells), **the use of two radiators** thermally coupled in the top and bottom of the body to spread heat into cold space.

The thermal analysis indicates that the average internal temperatures and the environment for the electronic is relatively stable and appears within the range of present technology capability.

Surface Element

The Surface Element is conceived as a simple short-lived probe for the determination of the physical properties of the planet surface; it will be deployed from the Orbiter into an impact orbit to a high latitude landing site where the environmental condition are acceptable.

The Surface Element is designed to achieve a significant scientific return with scarce resources.

The external shape is cylindrical, divided in two parts with boxes for electronics and instruments: the upper part separates from the

main body upon surface impact and penetrates the surface.

The design goals are: **the survival on the surface for at least 7 days** and **a ratio of payload to total mass not less than 1:4**; the Surface Element does not present particular problems concerned with Thermal Testing due to its reduced dimensions, and the thermal analysis is subordinated to structural aspects.

THERMAL TESTING IN HARD DEMANDING ENVIRONMENT

The choice of the experimental technique that has to be preferred for the execution of Thermal Testing on space probes cannot be separated from the analysis of the mission peculiar characteristics: a solution providing good results with acceptable investment costs has to be chosen.

Due to the high impinging fluxes on bodies orbiting around planet Mercury, the only techniques that seem to be suitable for thermal testing are:

- Solar Simulation Technique (SST);
- Infrared Heating Technique (IRT).

The Solar Simulation Technique is an *incident energy approach* and allows simulation through the creation of a uniform, collimated beam, spectrally similar to the solar one.

The Infrared Heating Technique is an *absorbed energy approach* in which the infrared radiation source has to provide the equivalent heat to be absorbed at the spacecraft surface.

Although the first method is more experienced, the IR heating technique could represents a great change for those situations in which the spacecraft shape is simple, the apertures total area on the probe external surface is not too wide and the thermal load arrives both from the sun and the albedo or IR emission from the planet.

The main constraints to a useful application of this technique are:

1. No beam parallelism required; that is true when shadowing effects due to appendages and multiple reflections are not important.
2. Spacecraft simple shape required; that is to avoid hot spots during the IR heating, in addition to the need of eliminating as much as possible the shadowing effects.
3. Surfaces thermo-optical properties yet known and not too different among each other, at least for the covering of the same surface.
4. Higher design margins required; that is to take into account the uncertainties associated with this kind of testing procedure.

Sometimes the Solar Simulation in existing chambers could be unable to reach the required fluxes values for a complete and correct reproduction of the orbital environment encountered by a satellite: this is the case of the mission to planet Mercury.

A great chance to compare with each other these two simulation methods was represented by thermal testing performed on Helios solar probe: initially SST was asked to validate IRT results, then IRT was chosen to simulate the 12 S.C. environment encountered by the probe during its perihelion, an extreme condition that SST did not allow to reproduce on the whole spacecraft at the required intensities.

The spacecraft shape was simple – a double reversed cone – and the IR radiation source used to heat the surface was a Thermal Canister: it

consists of a thin aluminium sheet structure, with heater foils glued to the outside of its surface.

A total of nine different models were used during the Test Phase.

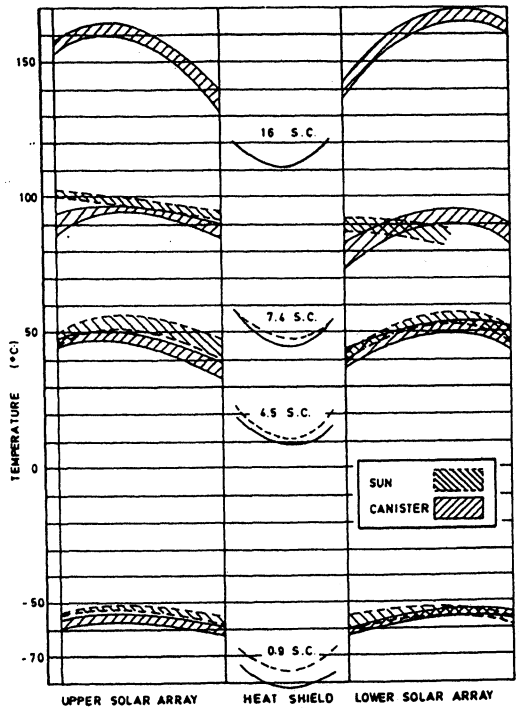

Fig. 4 – Helios Test Temperatures

The comparison performed at the end of that Phase showed a very good agreement between SST and IRT result.

It can be seen a good correspondence in the data measured with the two simulation methods, even if the comparison has to stop at a 7.4 S.C. (or 11 S.C. on a partially illuminated model) due to the not big enough dimension of the solar beam generated by xenon arc lamps.

The orbital data confirms a quite good agreement with testing results: as shown in the two pictures below, temperature differences between orbital data and values measured using SST or IRT always remain in an acceptably narrow range. ΔT statistical distribution for IR testing compared with Helios orbital data presents a percentage of 88% in the – 4°C / + 4°C range, while for Solar Simulation that value is equal to 81% in the – 2°C / +6°C range.

Although the important differences in the Helios and Mercury design that have to be considered, these results clearly show that IR

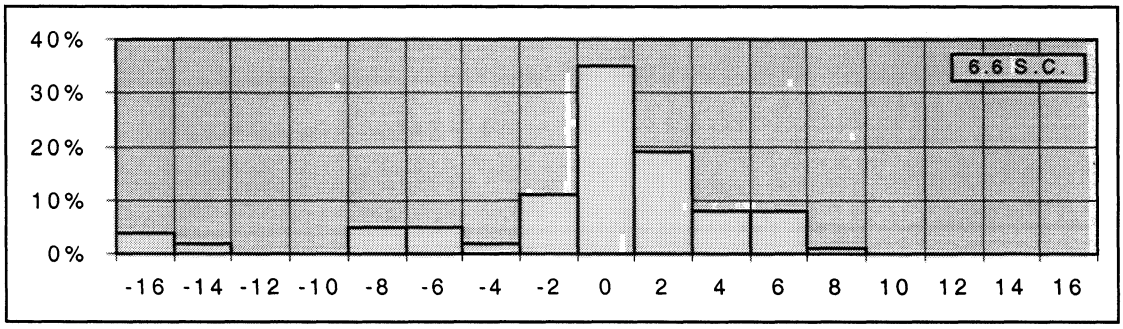

Fig. 5 – Distribution of ΔT between orbital data and test prediction using SST

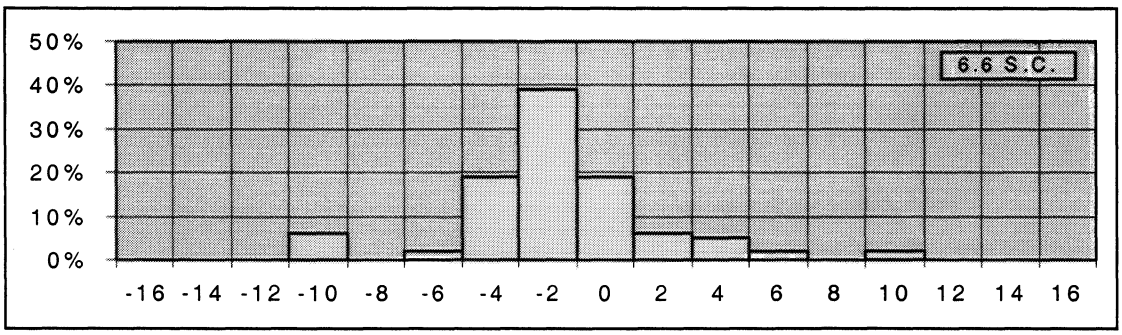

Fig. 6 – Distribution of ΔT between orbital data and test prediction using IRT

technique could really represent a valid alternative to the Solar Simulation technique.

IR TECHNIQUES ADVANTAGES AND DISADVANTAGES

The Infrared Heating Techniques for thermal testing are not as known as the SST, but present a number of peculiar advantages, the most important of whom are:

- simulation of albedo and planetary IR radiation;
- simulation of end-of-life conditions for surface materials;
- reduction of thermal test duration;
- lower capital investment and operating costs.

In particular, for what concerns cost reduction it has to be underlined that the investment costs of a solar simulation chamber is approximately an order of magnitude larger than a IR one, and this gap grows for increasing chamber size.

The feasibility of this kind of IR space simulation method is strictly connected with the characteristics of the spacecraft that have to be tested: when applied on complicated geometries, for example, it requires a not negligible additional analytical effort, so particular care has to be taken in avoiding or minimizing surfaces multireflection effects.

Nevertheless, lessons learned from the several testing campaigns performed in the past using these two space thermal simulation methods (e.g. Helios, Olympus and many others) allow to point out that the IRT and SST testing results are similar and that sometimes the IR Technique can replace the Solar Simulation at all.

The main differences between SST and IRT are summarized below:

SST	IRT
Incident energy approach	Absorbed energy approach
Solar radiation simulation	Solar radiation *effects* simulation
Good spectral match	Poor spectral match
Unidirectional collimated beam	Multidirectional uncollimated beam
View factors verification	No view factors verification
Thermo-optical properties verification	No thermo-optical properties verification
No EOL simulation	EOL simulation
No albedo, shine radiation and seasonal variation simulation	Albedo, shine radiation and seasonal variation simulation
Vacuum breaking for functional testing	No vacuum breaking for functional testing
Large chamber size compared to satellite dimensions	Small chamber size compared with satellite dimensions
Higher investment and operating costs	Lower investment and operating costs
Lower analysis costs	Higher analysis costs

Another interesting aspect of the IR heating technique is a relatively simple testing lay-out when heat pipes are used; whereas SST requires the satellite to be moved to reach the correct inclination with respect to the incident simulated solar beam, using IRT the probe remains in a horizontal position, so heat pipes can work at their best.

It is important to underline that it doesn't exist one IR source alone: it is possible to make a choice amongst different kind of heat sources, in order to allow a good simulation of space environmental conditions; the most important IR sources are:

- IR lamps;
- IR skin heaters;

- Rod and wire heaters;
- Thermal panels.

Any of them have its peculiar characteristic.

Tables presented in this page are intended to show advantages and disadvantages of each IR source and of a SST xenon arc lamps source.

Solar Simulation using Xenon arc lamps	
Advantages	**Disadvantages**
• Good spectral match and local distribution of radiation • Simulation of multireflections and shadowing effects • Useful to verify the thermo-optical properties • View factors verification	• High investment and operating costs • Large facility required • Do not allow the simulation of EOL conditions for optical materials • Difficulties in simulating albedo, planet shine radiation and seasonal variation • Reduced functional testing due to movements

IR Simulation using IR lamps	
Advantages	**Disadvantages**
• Useful to simulate albedo, planet shine radiation and seasonal variation • Simulation of EOL conditions • Allow to perform functional tests without breaking vacuum • Fast heat-up • Low chamber size • Low investment and operating costs	• Do not allow thermo-optical properties verification • External surface thermo-optical properties and absorbed flux must be well known • Shadowing effects and multireflections due to appendages are difficult to consider • Cold shroud blockage from IR lamps structure (approximately lower than 10%)

IR Simulation using skin heaters	
Advantages	**Disadvantages**
• High efficiency • Simulation of varying heat fluxes • Surface absorbed flux surely known • Fast heat-up • No cold shroud blockage	• Need a precise preparation and calibration • Glued on the surfaces to be heat • Additional flying mass

IR Simulation using rod and wire heaters	
Advantages	**Disadvantages**
• Small size • Simple test set-up • No cold shroud blockage • Aperture testing possible	• Cross-talk between elements • Difficult simulation on surfaces with different thermo-optical properties

IR Simulation using thermal panels	
Advantages	**Disadvantages**
• High reliability	• Cross-talk between panels
• Simple design	• Cold shroud blockage
• Direct plates refrigeration	• Low temperature transients

APPLICABILITY OF IR TESTING ON MERCURY MODULES

A mission to planet Mercury presents particular and very hard environmental conditions, due to its vicinity to the sun: the IR flux emitted from the planet surface, the direct solar and the albedo radiation are difficult to simulate using usual methods.

	Perihelion	Aphelion
Heat flux	14.5 kW/m^2	6.3 kw/m^2
Solar Constant	10.7 SC	4.6 SC
Planet IR flux, hot side	13.6 kW/m^2 $\cong$ 10 SC	7.4 kW/m^2 $\cong$ 5.5 SC
Hot side T	700 K	600 K
Planet IR flux, cold side	0.006 kW/m^2	0.006 kW/m^2
Cold side T	100 K	100 K
Albedo	0.11	0.11

The simulation of these conditions requires a testing technique alternative to SST, at least for the highest values, because existing chambers equipped with xenon arc lamps do not generate such high thermal fluxes: the world's biggest Solar Simulation facility – the JPL Solar Simulator – reach 13 SC on a 2.6 m solar beam diameter, 7.8 SC on a 3.35 m beam diameter and 2.7 SC if it grows till 5.6 m.

Only few SST chambers success in reach these thermal flux values, but in that case dimensions are really small.

Scaled models of the spacecraft are not reliable because they can lead to uncorrected results e.g. with an error too large to be accepted.

For that reasons, too, it is important to analyze the applicability of an IR technique on the Mercury/BepiColombo probe: this Cornerstone Mission certainly represents an important challenge for European Space Agency and for that reason it has to be chosen a testing philosophy that take into account space budget issues, allowing at the same time to obtain reliable results with a correct environmental simulation.

Therefore, with regard to the particular design features for this probe, it is important to analyze the project from the IR constraints point of view: the simple probe shape, the minimization of the apertures areas, the thermal decoupling of each module from the others and the higher-than-normal margin adopted for the Mercury BepiColombo project are all design elements directed to that kind of thermal testing, in order to simplify its setting up, laying out and performing.

Thermal testing should be performed on each of the three modules, even not connected to the others due to their physical separation with not

continuos but discrete links.

The main module dimension is the first problem to consider; a vacuum chamber large enough has to be equipped with IR devices of the chosen type. Mainly, considering the spacecraft design there are three possible choices:

1. IR lamps;
2. IR thermal plates;
3. Resistance heaters glued behind the spacecraft surfaces.

Taking into account the Helios background, it can be foreseen that problems will possibly derive from appendages and apertures: even if the Orbiter apertures total area is small in comparison with total module surface, particular care must be taken in fluxes simulation on these elements.

To reduce costs and to perform thermal tests without damaging external components, at least in the qualification test phase, it could be possible to use a dummy model of the spacecraft equipped with the most important component or with something that replace them, like an aluminium layer for the simulation of the solar arrays behaviour when irradiated: obviously, simulation is better done as much as the material properties of the real surface and of the dummy element are similar.

The Orbiter thermal testing could be performed with two different IR testing set-up:

- using IR lamps and surface skin heaters in a vacuum chamber with LN_2 cooled walls; skin heaters are used to prevent vacuum chamber overheating caused by the lamps used to reproduce orbital very high thermal fluxes.

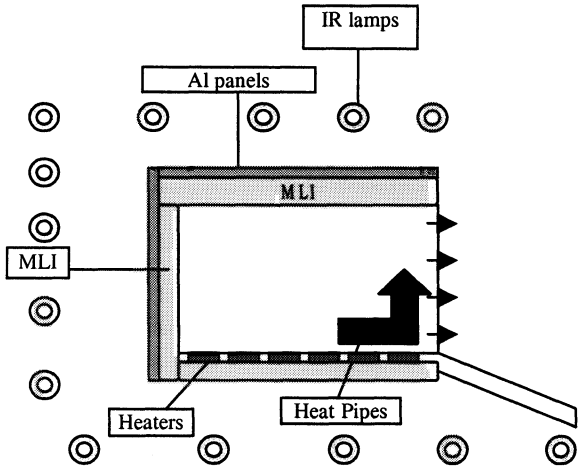

Fig. 7 – IR lamps testing set-up

- using thermal plates (IR shrouds) and separation baffles in a vacuum chamber with LN_2 cooled walls;

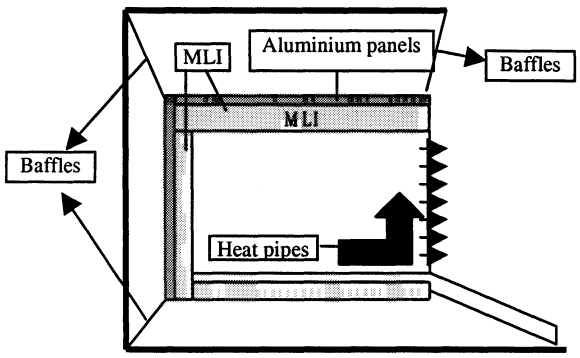

Fig. 8 – Thermal plates testing set-up

Radiator must not be heated during thermal testing because it has never been irradiated, in orbit, by direct solar radiation (because of a particular attitude strategy), nor planet shine emission (because of IR shield).

The Magnetospheric Satellite and the Surface Element do not represent a problem for testing

because their dimensions are small enough to be contained in existing European Solar Simulation chambers; nevertheless, the design of modules is not yet completed and it is possible that Magnetospheric Satellite dimensions, in particular, will become larger than now: in any case, both for Surface Element and for Magnetospheric Satellite, it would be possible to adopt the IR heating technique for Thermal Testing because of their simple shape.

Nevertheless, the SST have to be used for external surfaces thermo-optical properties evaluation, and could be used in the early phase of the testing campaign for simulation on spacecraft surfaces representative samples, in order to have surely known data for the Mercury/BepiColombo probe and establish a direct correlation between a solar simulation performed only at lower intensities and a complete IR simulation.

Using SST for small components or complicated elements testing, and IRT for each module testing, the verification campaign could be fully performed in European facilities, with consequent and consistent cost reduction.

CONCLUSIONS

The development of an IR Heating Technique for Thermal Testing is a great chance for spacecraft space simulation; thermal testing using IR techniques seems to be a viable alternative to Solar Simulation, even if it still represent an important touchstone for particularly complicated spacecraft or payload elements.

At the moment, the IR simulation seems to be an obliged but reliable enough solution for thermal testing on Mercury BepiColombo probe; even considering a potential increasing in the analytical effort required to reduce risk connected with the novelty of such a technique, the IR heating allows to reduce investment and operating costs with respect to Solar Simulation.

Particular care has to be taken in testing appendages or apertures, in order to avoid multireflections and shadowing effects, making the IR simulation effective.

REFERENCES

1. *Mercury Cornerstone System and Technology Study-Final Technical Report*, Alenia Spazio, 1999.
2. H.Nuss, his letter to Alenia Spazio Torino, November 11, 1999.
3. J.Gülpen - W.Lorenz - B.Schwarz K.Beckmann - D.Stümpel, *Results and experiences of the Helios solar probe Thermal Control System operating in flight*, XXVIth Intern. Astronautical Congress, Lisbon, 1975.
4. J.Gülpen - W.Lorenz, *Method and results of IR testing of the Helios solar probe*, 7th Space Simulation Conference, 1973.
5. A.Santovincenzo, *Mercury CS - IR approach to spacecraft thermal testing*, ESA/Alenia internal paper.
6. E.Choueiry - M.Donato, *Spacecraft thermal design verification in Canada*, 6th CASI Conference on Astronautics, 1990
7. J.Redor, *Satellite Thermal Balance Testing using the IR approach*, ESA, 1981
8. *Design model and test working group*, ESA, 1978.

THERMAL VACUUM TEST FACILITY DESIGN CONSIDERATIONS FOR THE NEXT GENERATION SPACE TELESCOPE

David A. McWilliams and Y. Roberto Than
Chart Inc. - Process Systems Division

ABSTRACT

The study presents several design options for a thermal system that can produce the required space environment for testing of the Next Generation Space Telescope (NGST). Because of the large size of the thermal vacuum environment and the required sink temperature, a large cryogenic refrigeration system is required, resulting in a system that is costly, with high power and liquid nitrogen use. The goal is to minimize parasitic heat loads thus keeping the cryogenic system small. The challenge is to achieve a design that is economical in terms of both initial capital investment and utility consumption. In addition, the thermal shroud system should be able to be used for other space vehicle tests with minimal, or no, rework. Thermal system design issues studied and the implications on the vacuum performance include: 1) active shielding utilizing liquid nitrogen, 2) passive shielding using multi-layer insulation (MLI), 3) thermal zone configurations, 4) refrigeration system tradeoffs. Relative operating costs are also presented.

INTRODUCTION

The NGST is an 8m diameter telescope with spectral coverage from .6 to 28μm. The orbit has been chosen to allow the optical telescope assembly (OTA) to operate at a temperature of less than 40K. Thermal balance testing of the OTA and critical subassemblies will be required. The large size and low operating temperature of the OTA require a thermal shroud and refrigeration system capable of operation at about 20K. This is beyond the operating range of existing large thermal vacuum chambers. The characteristics of the OTA from the Goddard Space Flight Center Reference Design are:

Primary Mirror Diameter	8m
Length	20m
Operating Temperature	30K
Mass	1750 kg
Active Load	750-1000 W

SHROUD SHIELD CONFIGURATION OPTIONS

20K Thermal Shroud Size

The study is based on a typical cylindrical shroud with the following characteristics range shown in the table below. The weight of the shroud will depend on the size, structural, and thermal requirements of the shroud system.

Shroud Dimensions and Weight

Type	Cylinder		
Dimensions		**Weight**	
Diameter	9 to 10 m	Low estimate	10,000 kg
Length	15 to 25 m	High estimate	20,000 kg
End surface	66 to 79 m^2	**Average**	**15,000 kg**
Cylinder surface	425 to 785 m^2		
Total area	**550 to 945 m^2**		

20K Shroud with Liquid Nitrogen Cooled Shield/Shroud.

The chamber radiant load will be the dominant part of the 20K thermal load if something is not done to mitigate this large load. A way to accomplish this is to have a liquid nitrogen cooled shield surrounding the 20K-shroud system. This will cut the radiant load to the backside of the 20K shroud to a few hundred watts. Thus, this configuration will give the smallest 20K load, but it may be the most expensive option. In most situations, an existing facility will be used, and consequently the existing shroud can be used to function as the (liquid) nitrogen cooled shield, and a new 20K shroud is added on the inside of the existing shroud.

20K Shroud with MLI Shield

This concept involves employing MLI between the 20K shroud and the chamber wall. This approach was used for the NGST prototype 2m mirror segment testing at NASA MSFC, Huntsville, AL. A 20K shroud enclosed the primary mirror. A 1.2m diameter aperture at one end of the shroud provided access for instrumentation. The shroud and mirror segments were supported on ambient temperature rail carts. The entire assembly was installed inside the existing X-Ray Calibration Facility (XRCF) chamber. The chamber contained an existing shroud/heater panel designed to operate at slightly below room temperature. The existing shroud/heater panel was left in place because it was too costly to remove for one test. The 20Kshroud assembly was comprised of a rectangular box 3m x 3m x 10m long with a total surface area of about 150 m^2. The 20K shroud was wrapped with 30 layers double aluminized mylar with 3% perforations. Heat leak through the large instrument aperture was reduced using a cylindrical LN2 cooled shade. Although the radiant heat load using MLI will be much higher than for an LN2 cooled shield, the overall 20 K load may not be very different depending on the size of the other 20K loads. This option is best employed where an existing shroud is used.

20K Shroud with Combination of LN2 Cooled Shield and MLI Shield.

This option of employing an actively cooled shield is useful where an existing shroud is used as the 20K shroud and where parts of the existing shroud need to be replaced / reworked. an actively cooled shield can be added and installed along with the new / reworked shroud. MLI could be added to shroud sections that are not removed. In order to benefit from this option, the goal is to have at least 50% of the 20K shroud shielded with actively cooled shields.

20K THERMAL LOADS

The thermal load on the 20K helium refrigerator system consists of the following:
1) Radiant load from the actively cooled/passive shield
2) Heat leak from the supports for the 20K shroud. This is minimized by employing liquid nitrogen cooled heat intercepts.
3) Heat load from the 20K intercepts for the Primary Mirror supports if required. This may be required if a temporary support structure is used to carry the primary mirror, and heat leak will be above the emissive capacity of the mirror.
4) Active loads from the primary mirror and other equipment inside the 20K shroud.

20K Loads

	No Shield	Active LN2 Cooled Shield	Passive 30 Layer MLI	Combo 50%/50% LN2 Shield / MLI system
LOADS	W	W	W	W
Radiant	22,000	200	1600	900
Shroud Supports	320	320	320	320
Mirror Intercepts	120	120	120	120
Active Load	1000	1000	1000	1000
TOTAL	**23,440**	**1640 W**	**3040 W**	**2340 W**

COOLDOWN

Because 90% of the thermal capacity is above 85K, a relatively large cooling capacity is required to achieve a reasonable cooldown time. Due to the small cooling capacity of the typical 20K helium refrigerator system above 80K, additional cooling capacity needs to be designed into the system.

An LN_2 cooled, recirculating gas, thermal-conditioning unit typically used for temperature control of shrouds between 100K and 400K is considered here to aid the cooling of the 20K shroud from ambient to 85K. Cooling is accomplished with high mass flow rate and at relatively small temperature gradients.

Cooldown From 300K to 85K

Cooldown of the 20K Shroud

Cooldown of the shroud is most efficiently accomplished using a large thermal conditioning unit that uses helium as the working fluid. With a net cooling capacity of 50kW the shroud can be cooled to liquid nitrogen temperatures in less than a day. There may be however, cooldown rate limitations imposed by the test article that will extend the cooldown time.

Thermal Characteristics 20K Shroud (300K–85K)

	Average	High	Low
Shroud Mass	15,000 kg	20,000 kg	10,000 kg
Thermal Capacity xCpdT 300K-85	2.5E+09 Joules	3.4E+09 Joules	1.7E+09 Joules
Cooldown Time @ 50 kW Capacity	15 hrs	20 hrs	10 hrs

HELIUM REFRIGERATOR OPTIONS and COOLDOWN 85K to 20K

Thermal Characteristics 20K Shroud (85K–20K)

	Average	High	Low
Shroud Mass	15,000 kg	20,000 kg	10,000 kg
Thermal Capacity xCpdT 85K-20K	1.8E+08 Joules	2.4E+08 Joules	1.2E+08 Joules
Cooldown time with 2 kW system	18 hours		

20K Helium Refrigeration System Options

	Active LN2 Cooled Shield	Passive 30 Layer MLI	Combo 50%/50% LN2 Shield / MLI system
Capacity at 20K	2000 W	4000 W	3000 W
20K Load	1700 W	3100 W	2400 W

Cooldown Capacity of 20K Helium Refrigerator

Capacity is limited at higher operating temperatures by the expanders that are essentially constant volumetric flow devices (i.e. turbines or piston expanders that are speed limited) sized to handle the work extraction at their steady state operating point. No additional capacity can be obtained at higher temperatures. One way to increase expander capacity at temperatures above 20K is to have a second expander set in parallel that operates during cooldown and will serve as a back-up expander. No additional compressors are required because there is sufficient flow to supply both expander sets during cooldown. This option will more than double available ***net*** cooling capacity (available cooling minus active steady state load).

Figure1 shows the cooling capacities for three 20K helium refrigerator sizes, 2 kW, 3 kW, 4 kW. The 20K helium refrigerator size is dictated by the shielding method employed for the 20K shroud. The net capacity available during cooldown for the large system employing two sets of expanders is an additional 2.5 kW, and 5 kW above the steady state capacity for the 3 kW and 4 kW systems respectively, and can shorten the cooldown time considerably. The extra 2kW available above the steady state load is sufficient to cool the shroud in less than a day and any more will result in shorter cooling time.

Cooling of the 20K Shroud

Figure 2 shows the cooling of the shroud with a mass of 15,000 kg of aluminum and an active load of 1.8 kW of a 2 kW helium refrigerator with two expander sets operating during cooldown. The resulting cooldown time is almost one day. The cooldown rate accelerates as the temperature drops due to the

decrease of the specific heat of aluminum with decreasing temperature and the availability of the extra expander capacity during cooldown.

Optics Bench

If an optics bench is required, its thermal mass could be of the same order of magnitude as the shroud. If the optics bench needs to be cooled, a second thermal conditioning unit and 20 K refrigerator is required to maintain a similar cooldown time. If the required cooldown time is extended, a 2 kW helium system with extra expander is sufficient to cool both the shroud and optics bench as long as the 20K steady state load is less than that currently budgeted for the 2 kW system.

SHROUD ZONE CONFIGURATIONS

Because the refrigerator used for cooling from ambient to 85 K has very different flow and head characteristics from the 20K refrigerator, consideration must be given to how to best arrange the shroud zones to optimize performance.

Parallel Configuration

This configuration (Figure 3), which feeds all zones in parallel, will give low heat transfer coefficients but also low pressure drops. This matches best with the operating conditions of the thermal conditioning unit, but since the flow of the helium refrigerator will be much smaller than the thermal conditioning unit, heat transfer coefficients will be low. Because the heat fluxes are low, the heat transfer gradients may still be reasonable and will depend on the particular shroud design. Due to the parallel configuration, if shroud zones are of unequal size, flow balancing valves are required.

Series Configuration

This configuration (Figure 4) in practice will give the best heat transfer coefficients, but also the highest pressure drops.

Again, due to the large difference in flows between the thermal conditioning unit and helium refrigerator, the heat transfer for the helium refrigerator loop will suffer if the shroud system is designed for the pressure drop capability of the thermal conditioning unit.

Dual Configuration

This configuration (Figure 5) matches the thermal conditioning unit characteristics in its parallel mode, and it matches the helium refrigerator in its series mode, and provides optimum heat transfer performance for both cooling systems at the desired hydraulic resistance.

Series with Recooling Configuration

This configuration (Figure 6) is required when a separate thermal conditioning unit is not desired. No thermal conditioning unit is used, only the 20K helium refrigerator compressor is used for circulation. LN2 cooled heat exchangers are installed between used between shroud sections for recooling. The recooling heat exchangers are operated from 300K to 85K. This configuration will most likely be employed when an existing shroud designed for pumped LN2 is reused, and hydraulic resistance is too high to employ a thermal conditioning unit.

VACUUM GAS LOADS

For systems with large 20K surfaces, vacuum pressure is typically not a problem due to the high pumping speeds. In the case of a 20K shroud shielded by a liquid nitrogen cooled shield, the most significant outgassing source is most likely the test article whose outgassing will decay as it gets colder. For a system insulated with MLI, due to the large quantities of aluminized mylar surfaces, the outgassing rates can be significant, and thus a closer look is required for a system utilizing MLI.

Thus for 30 layers at 800 m^2 each side the total outgassing surface is 480x 10^6 cm^2 of double aluminized mylar. At 1 hour no additional pumping is present except for that by the cryo-pump / contamination panel. At 10 hours, the main 20K shroud and or active shield is cold enough to pump water vapor. At 100 hours the 20K shroud is cold enough to pump air. The 20K shroud has to be at least 27K to reach $1x10^{-5}$ Torr; at least 25K to reach $1x10^{-6}$ Torr; and at least 22K to reach $1x10^{-7}$ Torr. Thus, from the analysis, the MLI will not present any vacuum problems at the present. The remaining concern is related to the large quantities of MLI that need to be vacuum-baked to reduce contamination problems inside the chamber.

Time	1 hr $q_{@1hr}=1x\ 10^{-7}$ Torr-L/s-cm^2	10 hr $q_{@10hr}=5x\ 10^{-9}$ Torr-L/s- cm^2	100 hr $q_{@100hr}=1x\ 10^{-10}$ Torr-L/s- cm^2
Outgassing Loads			
Water	48 Torr-L/s	2.4 Torr-L/s	0.048 Torr-L/s
Air	2.4 Torr-L/s	0.12 Torr-L/s	0.0024 Torr-L/s
Pumping Speeds (L/s)			
Water	32,000 L/s *	118 $x10^{6}$ **	118 $x10^{6}$ **
Air	25,000 L/s *	25,000 L/s	90 $x10^{6}$ ***
Pressure (Torr)			
Water	1.5 x 10^{-3}	2 x 10^{-8}	2 x 10^{-8}
Air	1 x 10^{-4}	1 x 10^{-4}	<1 x 10^{-8}
Total	1.6 x 10^{-3}	1 x 10^{-4}	2x 10^{-8}

* Assumed net pumping speed of cryopumps on the inside of 20K shroud.
** Water; Shroud <150K
*** Shroud @20K

UTILITIES

	Cooldown		
	Low	High	Ave
	10,000 kg	20,000 kg	15,000 kg
20K Shroud Cooldown 300K–85K	7200 liters	14400 liters	11800 liters
Cooldown LN2 shield			7200 liters

	Steady State			
20 K Refrigerator Capacity	**25 kW**	**2 kW**	**3 kW**	**4 kW**
Refrigerator Utilities				
Electric Power	1750 kW	240 kW	360 kW	480 kW
LN_2	625 LPH	50 LPH	75 LPH	100 LPH
LN2 shield	0 LPH	500 LPH	500 LPH	500 LPH
Total LN2 /day	15000 l	13200 L	13800 L	14400 L
Daily Operating Cost				
Electricity @ $0.1/kWh	$4200	$580	$870	$1150
LN2 @ $0.1/L	$1500	$1320	$1380	$1440
Total	**$5700**	**$1900**	**$2250**	**$2600**

SUMMARY

Shielding

The type of shielding used is relatively unimportant from a capital and operating cost viewpoint. Either type will reduce the 20K load sufficiently to allow standard 20K helium refrigerators to be used. These will be much less costly than a large custom helium refrigerator that would be required if no additional shielding is used.

The largest difference will be the practicality and performance of the system when operated at LN2 temperatures and warmer. Because the shroud will not cryopump air at 80K, and because there will be high outgassing from the MLI, there may be may not be adequate pumping speed available to maintain the chamber at the required pressure.

Shroud Zone Configuration

The choice of flow configuration may be determined by whether a new or existing shroud is used. The hydraulic characteristics of a new shroud can be tailored to match the refrigerator requirements. If an existing LN_2 shroud is adapted, then multiple recoolers may be required. The 20K helium refrigerator design may also need to be modified to operate with a high hydraulic resistance shroud design.

REFERENCES

1. NGST Monograph No. 5 "NGST Reference Design Requirements, Recommendations and Guidelines", J. Mather , et al., Next Generation Space Telescope Project Study office, Goddard Space Flight Center.

2. "Lockheed Martin Team's Next Generation Space Telescope (NGST) Reference Architecture", Frank Martin et al., http://www.ngst.external.lmco.com

3. A. P. M. Glassford and C. K. Liu, "Outgassing rate of multi layer insulation material at ambient temperature," *J. Vac. Science and Technology* 17(3), May/June 1980.

4. "NGST OTA Optical Testing," Ritva Keski-Ruha (NASA GSFC), Hyannis Presentation, September 16, 1999.

HELIUM REFRIGRATOR

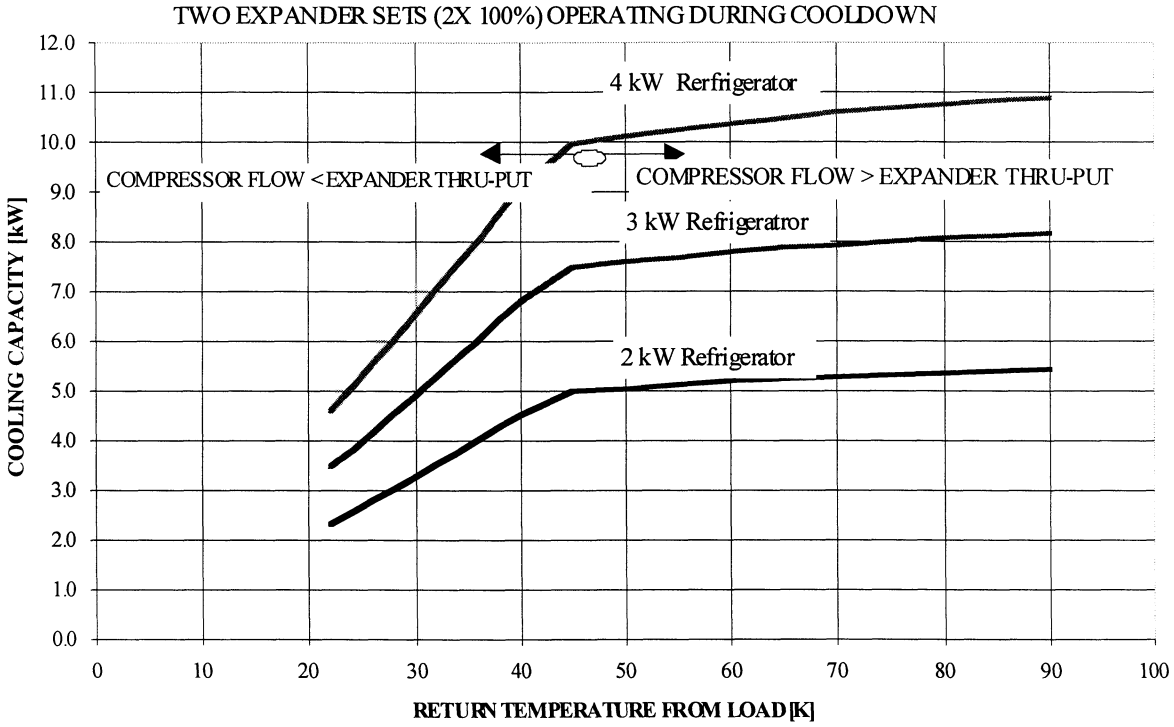

Figure 1

COOLDOWN 85K-20K

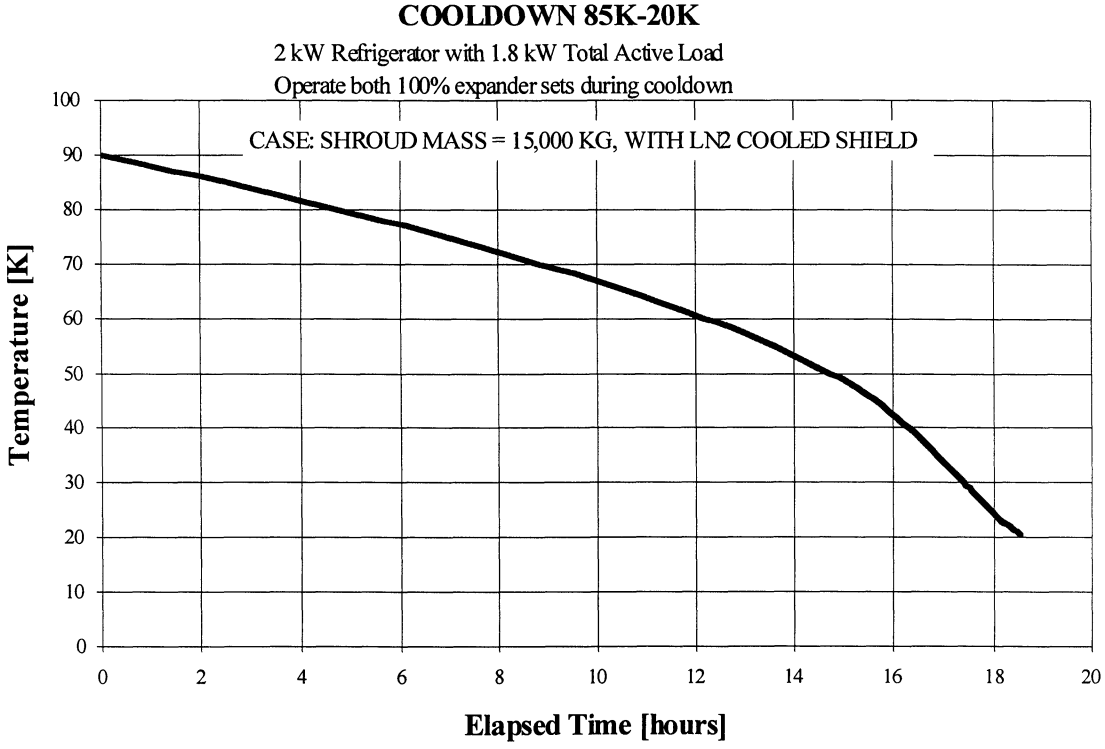

Figure 2

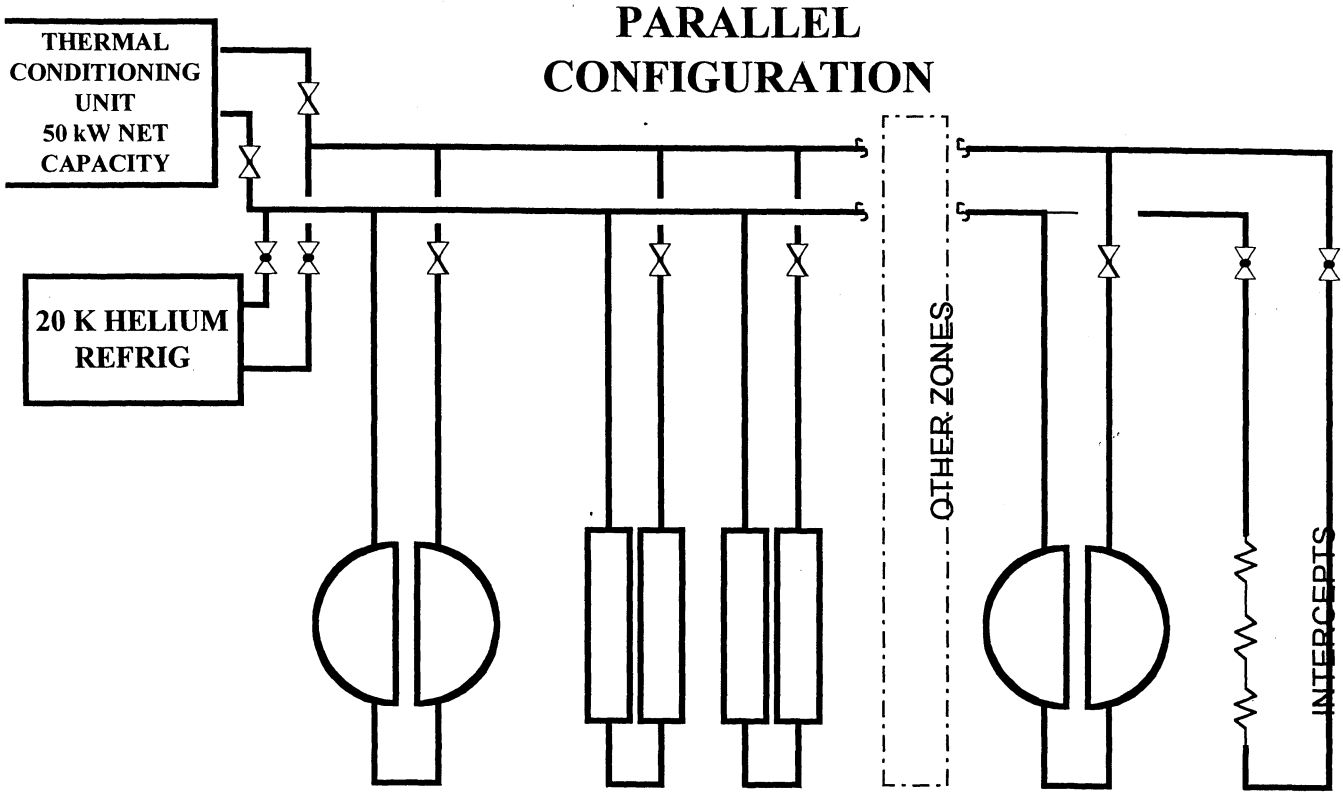

Figure 3

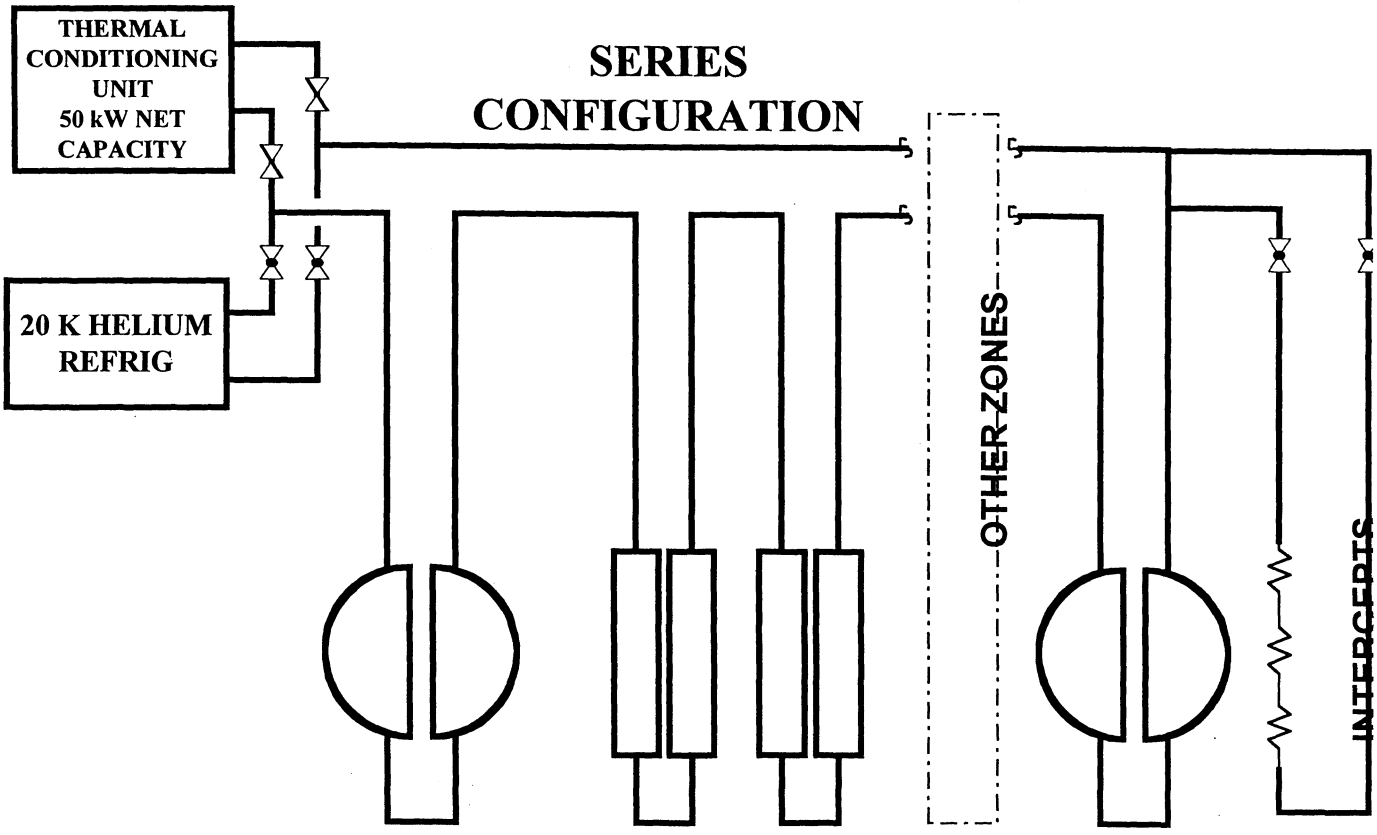

Figure 4

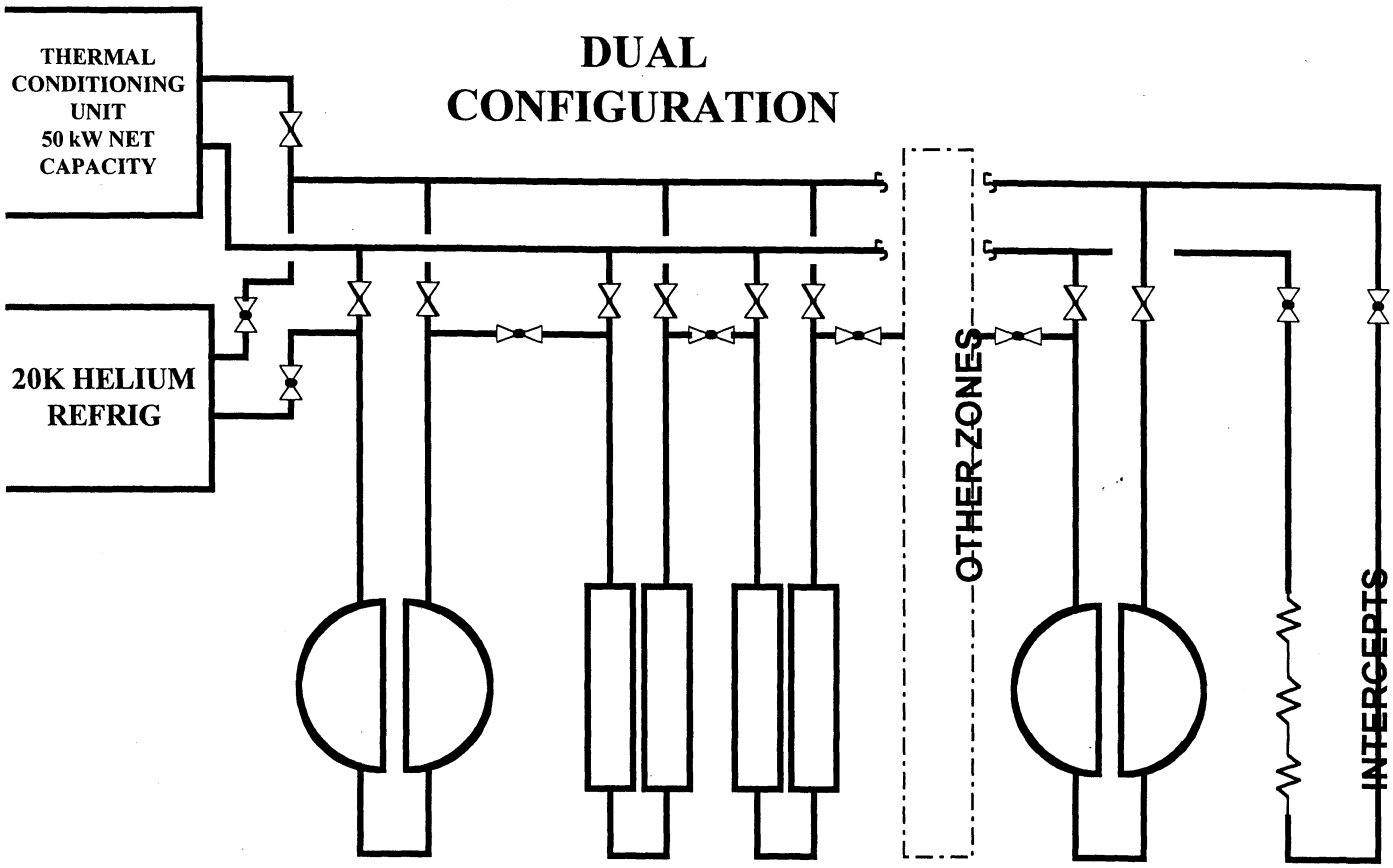

Figure 5

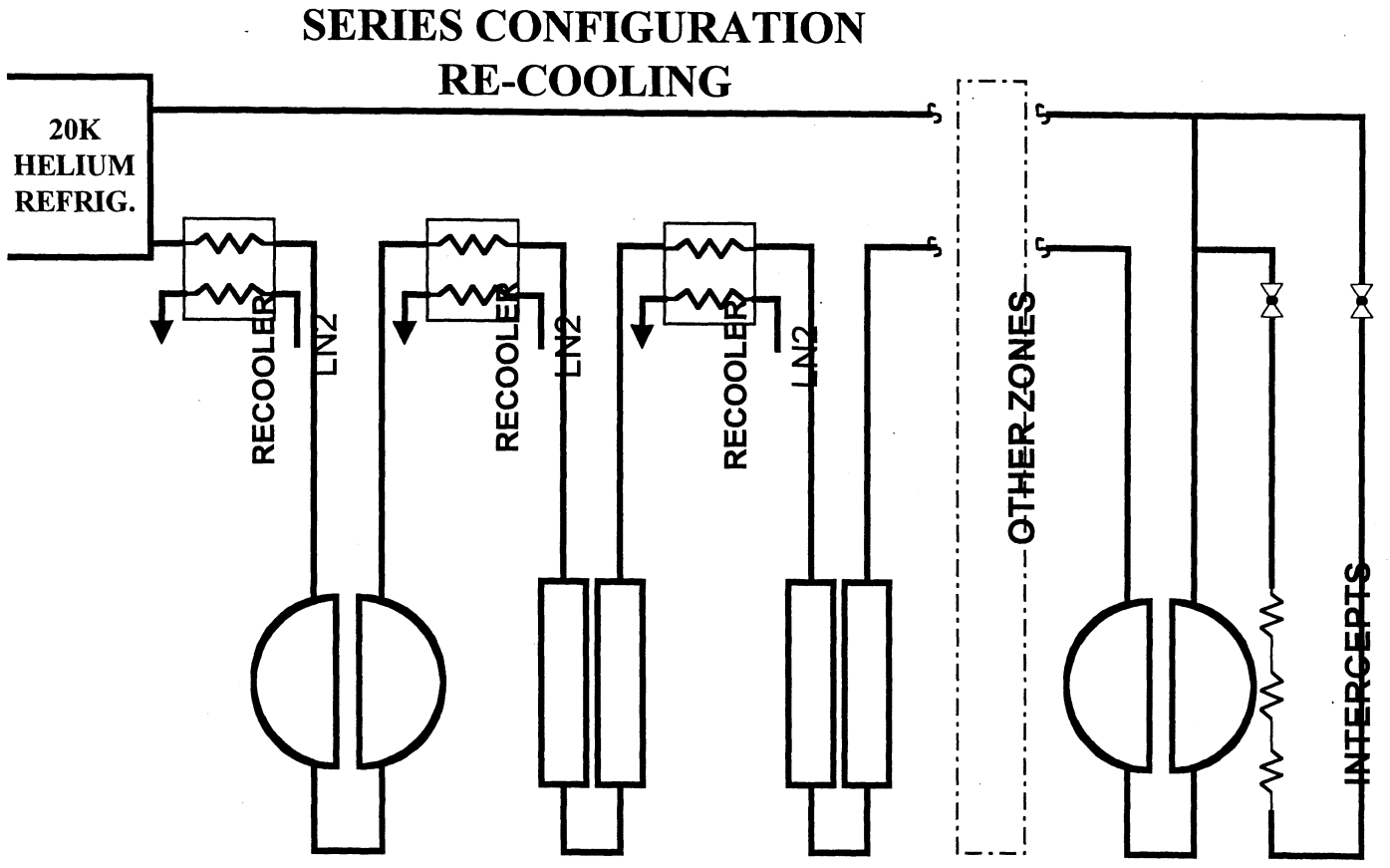

Figure 6

THERMAL CYCLING TEST FACILITY FOR SPACE MATERIALS AND LIFE TIME RESEARCH

Prof. Dr.-Ing. Wilfried Ley
Dipl.-Ing. Engelbert Plescher

University of Applied Sciences Aachen
Department 6 Aeronautical and Astronautical Technology
Hohenstaufenallee 6, D-52064 Aachen, Germany
Phone: ++49 (0) 241/6009-2343, Fax: -2680, E-mail: Ley@fh-aachen.de

ABSTRACT

During in-orbit operations the spacecrafts surface materials receive thermal loads from sun and earth. The frequent change of sun and shadow phases leads to temperature changes at the structural materials, e.g. solar cells, carbon fiber materials and coatings, insulation materials, actuators and functional parts in the order of up to 300 °C or more. This results in an important mechanical, thermal driven load for the materials. Cause due to this an increase of the precipitated material degradation leads to negative effects on mechanical and thermal properties up to damage or failure of functional parts.
With the Thermal Cycling Test Facility (TCTF) such changing of thermal loads can be simulated under vacuum conditions next to real space operations. Infrared irradiation and a low temperature background by LN_2 cold shrouds can be simulated in a ground test facility. Correlated with the real thermal load, the cycling time can be varied to compress long duration tests during simulation. During the test both the mechanical and thermal material behavior is monitored and therefore variations are detected.
The paper presents a description of the upgraded TCTF, preliminary test results and perspectives for future test opportunities.

CONTENTS

1.0 INTRODUCTION

The Thermal Cycling Test Facility (TCTF) is the only test chamber of that kind in Europe. The chamber was designed and built up for the first time at DFVLR (Deutsche Forschungsanstalt für Luft- und Raumfahrt, Cologne – Germany) in the 70`s. At this time all materials for space, especially solar cells are subjected to thermal cycling tests in vacuum.
The test principles and the technical realization are proved during operation at DFVLR. Several basic research and qualification tests for ESA and industrial partners were performed successfully during this phase.
In 1994 the Fachhochschule/University of Applied Sciences Aachen received this facility. Studying the relevant publications showed, that such a facility may have several interesting aspects for education and further test campaigns.
Therefore several studies were performed to bring the upgraded facility once again in operation. That concerns the LN_2 supply, the cycling mechanisms and the control unit for the vacuum system. But they indicated several difficulties with the old technics and equipment going in operation.
In 1998 the decision was made to upgrade the complete control part to a computer based system. All actuators and sensors as well as the measurement technics had to be changed to computer conform signal lines. As operating system the software package LabVIEW was chosen. All activities, controls and measurements had to be managed under this software using a user-friendly software interface.

2.0 Simulation Background

During the operation of a satellite in orbit the surface materials, e.g. solar cells, insulation materials, windows, metallic and non-metallic structures as well as functional parts (actuators, sensors, ...) are extremely exposed to changing the thermal radiation background. This means sun and shadow phases during one orbit or the motion behavior of the satellite itself. This changing thermal radiation influences the design and operation of each satellite significantly. Therefore intensive studies have to be performed by numerical calculations and for validation by test and qualification procedures. Several software packages, e.g. SINDA, NASTRAN, ... deliver the opportunity to calculate the temperature influence. For special applications, e.g. Tether Systems self written software fulfills this need and delivers design and test parameters. Typically, the temperature behavior changes with

- geometry of the satellite (system)
- orbit parameters
- launch side and launch time.

Figure 1 shows typical temperature curves for a Tethered Satellite System (TSS) with different tether materials in LEO, launched in Plesetsk/Russia at 0^{00} h on the 13^{th} of April 1995.

Changing the launch time results in a shift of the space fixed orbit related to the sun. Therefore the thermal radiation over one orbit changes also. *Figure 2* shows for the same orbital parameters as above the change in temperature behavior depending on the launch time.

The simulation aim using the thermal cycling test facility is to perform the same thermal loads for a sample as calculated by software or known from objects in orbit.

To test the long time behavior of materials or components the cycles have to be shrunken in time spanned over the thermal load equivalent to the reality.

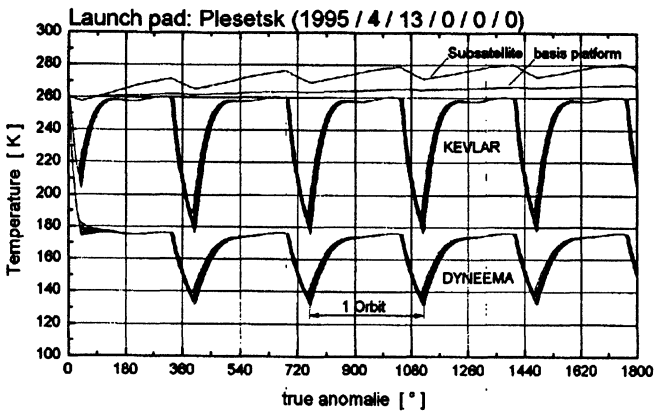

Figure 1 Temperature Behavior of a Tethered Satellite System

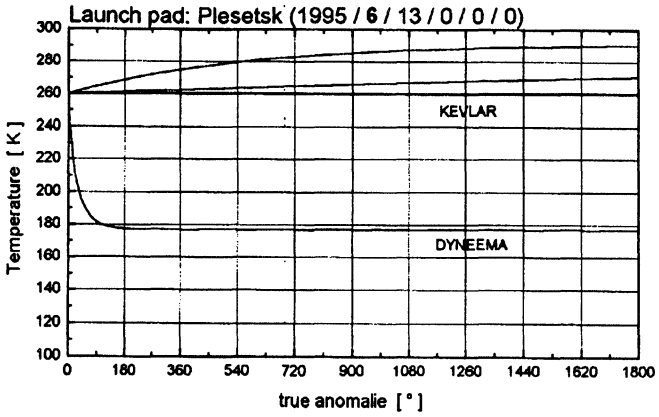

Figure 2 Temperature Behavior for different Launch Times *(launch date: 13.06.95)*

3.0 Description of the Thermal Cycling Test Facility

The following description presents the upgraded Thermal Cycling Test Facility (TCTF) which is now operative and ready for qualification and tests within national and international programs.

3.1 In General

The facility consists of a vertical cylindrical vacuum chamber with an inner diameter of 1000 mm and a height of 2000 mm. *Figure 3* shows this vacuum chamber with lifted upper lid adapted to the Thermal Cycling Unit (TCU) and the vacuum pumping system, the power conversion and supply and the computer control boards including the measurement unit packed in a 19" rack. The chamber is equipped with proper flange studs for the vacuum connection, the torque feedthrough for the reversing operation of the sample support structure (TCU), the LN_2 supply lines, and Deutsch-plugs for the thermocouple feedthrough lines. The LN_2-storage tank is next to the chamber in order to lower the evaporation of LN_2 in those lines.

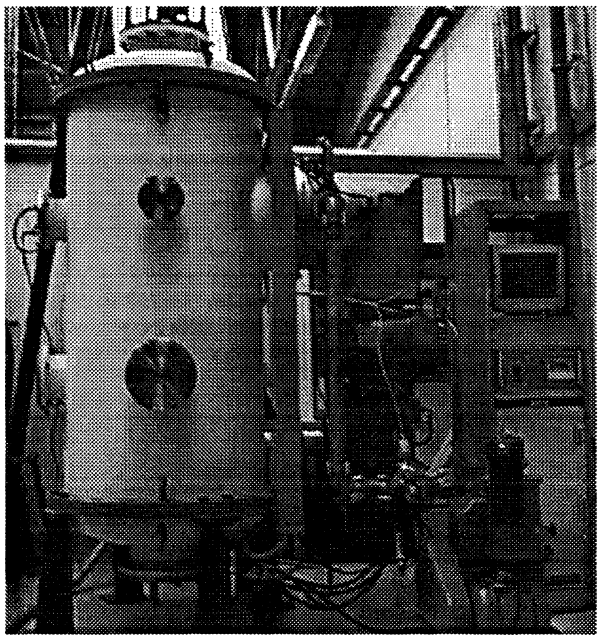

Figure 3 View of the Thermal Cycling Test Facility with necessary Peripherals.

3.2 Vacuum Pumping System

The vacuum system of the TCTF, which is schematically drawn in *Figure 4*, consists of the following components:

A = Two-stage rotary vane pump as pre-vacuum pump (1000 l/h)
B = Three-stage water-cooled oil diffusion pump for the high vacuum operation (5200 l/s)
C = Water-cooled baffle
D = Electro-pneumatically operated gate valve
E = Electro-pneumatically operated bypass valve for the pre-evacuation of the oil diffusion pump
F = Electro-pneumatically operated pre-vacuum valve for the test chamber
G = Gauge tube for measuring the pressure during operating corresponding to the chamber pressure (10^{5} to 10^{-7} Pa)
H = Gauge tube for controlling the operation pressure of the gate valve (1 to 10^{-7} Pa)
I = Pre-vacuum gauge tube controlling the pre-evacuation of the diffusion pump (10^{5} to 10^{-1} mbar)
J = Air inlet valves

During the upgrade of the facility all components are directly connected to the I/O board of the computer based control unit. The gauge tubes offer computer compatible signal outputs which allow to control the actual pressure in real time. The operation of the pumps is controlled and switched by computer according to a logic for save operation. For the oil diffusion pump the cooling water cycle is controlled too, to protect the pump against overheating.
All important vacuum components are blocked against abnormal events. Endangered parts of the facility and the samples are protected.
In case of operation difficulties of the facility, a change-over to an uncritical state for the experiment is ensured.
Using the actual pump system, the chamber can be evacuated up to $5*10^{-2}$ Pa in 30 minutes. After 24 hours of operation the pressure in the chamber decreases to $5*10^{-3}$ Pa. The outgasing of all interior parts can be minimized by pre-heating during the first evacuation phase.

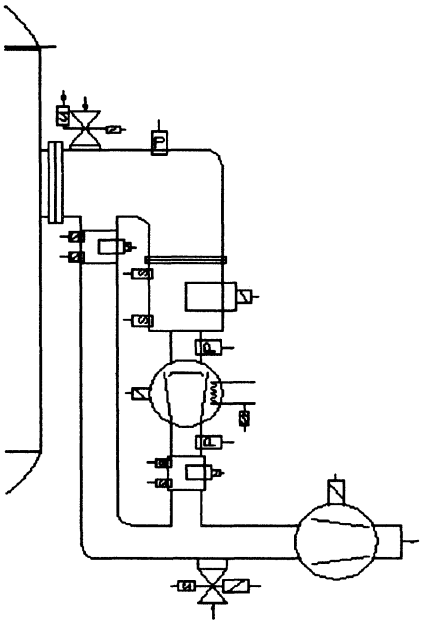

Figure 4 Scheme of the Computer controlled Vacuum Pumping System

3.3 LN_2 Supply Unit

For tempering the cooling areas, an open pressureless cooling cycle supplied by liquid nitrogen (-196 °C) is chosen. The LN_2 is stored in a vacuum insulated transportable tank with 1000 liter volume. A vacuum insulated tube connects the tank to the LN_2 inlet control unit. This part consists of an electrical actuated main valve and safety valves. Through a hermetic sealed feedthrough flange the LN_2 flows to the TCTU. The supply tubes to the different cooling panels are arranged in a rising way in order to avoid vapor lock formation. After cooling the TCTU the nitrogen flows through a drain off line

outside the vacuum chamber and is blown into the air. The necessary flow rate is controlled by a manual valve to lower the rate of evaporation during the sample cooling.

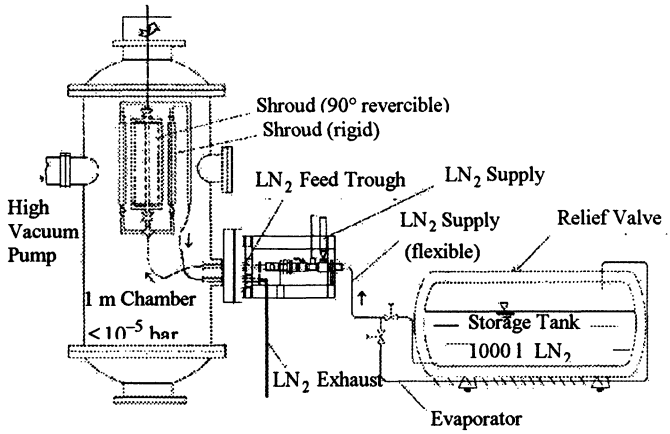

Figure 5 Scheme of the LN_2 Cycles for Cooling.

3.4 Pneumatic Cycling Unit

The rotation (reversing by ± 90°) of the central sample support is performed by a pneumatic rotary cylinder outside the vacuum chamber. The exact position after a turn of 90° is given by adjustable non-contacting end-sensors. An electro-pneumatically driven 5/3-line valve holds the end-position independent until the next electrical command. The period for hot and cold phases, respectively, can be adjusted and varied by the software. Due to an hermetic sealed rotary high vacuum feedthrough the rotation is transferred directly to the inner sample support structure.

3.5 Electrical Supply Unit

The complete control of the TCTF is handled by software. Therefore all low voltage converters for sensors, actuators and the computer system are arranged in one 19" rack compatible plug-in drawer. All lines to the computer are protected against overload. Digital and analog output lines of the computer board control the power settings. The high voltage power supplies for the vacuum pumps and the internal heater are separately fused and switched by relays controlled by I/O lines of the data acquisition of the computer system. In case of power failure the entire system switches over into a system safe position.

3.6 PC Operating and Control System

The main hardware part for controlling the TCTF is a personal computer based on a Pentium system equipped with VGA board, IDE storage components and a medium RAM comparing the requirements of the operating software.
Additional to the PC components two plug-in boards are installed. The first one is a National Instruments Inc. (NI) multi I/O-board which is disposed to acquire and actuate signals. This board is used to operate the facility and to control the main parameters.
For converting the low current signals, which are exclusively processed by the board, several relay boards are specially designed and connected.
The second board is a data acquisition board for thermocouples. Basically the board disposes 16 thermocouple lines. Upgraded with expansion boards 64 thermocouple lines are now available.
As operating software LabVIEW Vision 5.01, as well a product of NI, was selected. This should secure the compatibility of hardware and software.
All operating commands are programmed within LabVIEW and can only be changed by the user interface. This allows the automation of the processes at a high safety level for the TCTF and the samples.

3.7 Data Acquisition Unit

During the operation of the TCTF all facility related parameters are controlled and stored on disc.
In testing samples the mechanical, electrical and temperature behavior is of interest. Therefore several sensor lines are available and mounted to the TCTU. Additional to the copper lines for electrical power a large number of thermocouples is integrated. The measured points at the sample support structure are user dependent. The connection point to the data acquisition unit is the cold contact compensation point and all lines can be compared easily. The type of thermocouples is Copper - Constantan (type T, DIN) and the conversion from voltage to temperature is performed during the sampling of each channel to the board. If necessary additional types of temperature sensors may be integrated.
The accuracy is ± 1,5°C for the data acquisition board and additional ± 1,5°C for the thermocouples itself. The maximum sampling rate by the board is 2 measurements of each channel per second (up to 64 measurement lines via multiplexer). The data's are blockwise stored on a disk together with the time information.
The analysis of the overall behavior may be done after the test using all stored measurement data and the operational data.

3.8 Description of the Test Set-up

Figure 6 shows the TCTU (without outer MLI radiation protection for the hot part) with the upper chamber lift carrying the pneumatic cycle control. *Figure 7* represents the schematic cross section of the test set-up.

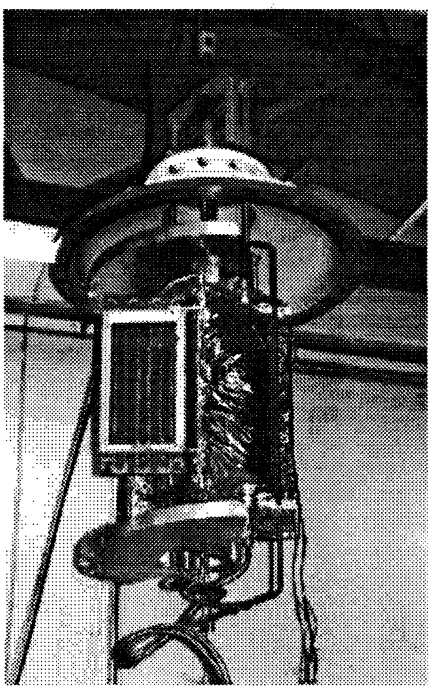

Figure 6 Thermal Cycling Test Unit (TCTU) without surrounding Vacuum Chamber

The supporting scaffolding is rigidly connected with the upper chamber lid. The inner cage consists of 4 LN_2 cooled copper sheets (640x180x1.5 mm), two situated opposite to each other at a time functioning as sample support.
The 4 copper plates of the inner cage are sprayed on both side with black 3M-varnish and are thermally insulated (glass fiber reinforced Teflon) and connected with each other. The plates are cooled down during the test approximately to the temperature of the liquid nitrogen by the copper tubes soldered on to the backside; these copper tubes are connected with the LN_2-cycle. The inner cage performs reversing rotations of ± 90° by the pneumatic cycle unit.
The 2 areas of the 4 copper plates, which are not covered by samples, are coated by a five layer super insulating foil. They are furthermore coated by a covering foil made of glass silk reinforced Kapton .
The two cold phase regions (at the top and at the bottom) and the hot phase regions (left and right) are separated by LN_2 cooled copper sheets, which are sprayed on both sides by 3M varnish. These separating sheets are covered up by a 24 layer super insulating foil in the hot phase region. An additional flexible packing washer consisting of a 12 layer super insulating foil seals the hot phase region from the cold phase.

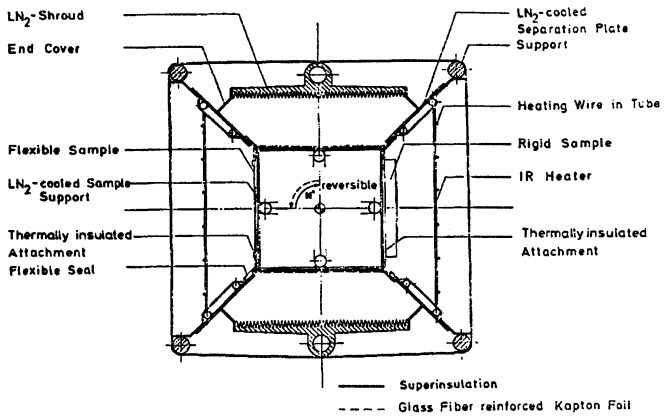

Figure 7 Schematic Cross Section of TCTF; Sample position during hot phase.

The LN_2 cooled shroud, which shows a cog profile, is sprayed black on the front side. The total test facility is surrounded by a radiation protection consisting of a 7 layer super insulation foil.

3.8.1 Cooling System

Within the chamber the following areas must be cooled down by liquid nitrogen:

- Copper sheets of the inner cage (4 pieces)
- Separating sheets between warm and cold phases
- Shroud cog profiles

The tubes to the various cooling areas are designed that the sufficient flow-through of liquid nitrogen cools the areas to be cooled down to the temperature of liquid nitrogen. The rising arrangement shall prevent vapor lock formation and thus contribute to a uniform cool-down of the cooling areas which is shown in *Figure 8.*

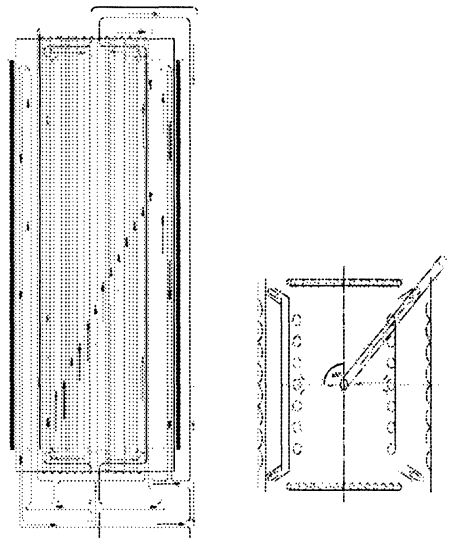

Figure 8 The rising Way of the liquid Nitrogen through the different Cooling Panels within the Sample Support Structure.

3.8.2 Infrared Heating Cycle

The infrared heater consists of copper sheets in the size of 640x290x2 mm. The plane side is sprayed by black 3M-varnish. About 5.5 m cover heating were soldered on the polished backside in regular distances.
The temperature of the heating plate is controlled by a software based PID-controller and a high power TRIAC. The necessary temperature for the heating plate is calculated based on the required radiation per area for the sample.
The following calculation represents the estimation of the necessary heater plate power for a flexible solar cell sample at a maximum tolerable sample temperature of 70°C [1].

ε_H = 0.9 $\quad$ $_P$ = probe
ε_{PS} = 0.8 (solar cell) $\quad$ $_H$ = heater
ε_{PK} = 0.65 (Kapton)
A_H = 0.186 m^2
A_P = 0.1152 m^2
T_P = 70 °C ≅ 343 K

The form factor between heater plate and sample amounts to $\Phi_{H\text{-}P} = 0.51$. In order to keep the sample at the temperature T_P the heat dissipation Q_P at the sample arises to:

$$Q_P = \delta \cdot T_p^4 \cdot A_p \cdot (\varepsilon_{PS} + \varepsilon_{PK}) = 133.4 \text{ W}$$

To obtain this heat dissipation, the heater plate must reach the temperature T_H:

$$T_H^4 = \frac{133.4}{\delta \cdot A_H \cdot \varepsilon_H \cdot \varepsilon_{PS} \cdot \Phi_{H\text{-}P}}$$

$$T_H = 156 \text{ °C}$$

This results in a heater output power necessary for the calculated heater temperature of T_H = 156°C by

$$Q_H = T_H^4 \cdot A_H \cdot \delta \cdot \varepsilon_H + (T_H^4 - T_U^4) \cdot A_H \cdot \delta \cdot \varepsilon_{H^*}$$
$$= A_H \cdot \delta \cdot \varepsilon_H \cdot (2 \cdot T_H^4 - T_U^4)$$

$$Q_H = 576 \text{ W}$$

For an ambient temperature T_U (temperature of the vacuum chamber) of 300 K and a maximum possible heat exchange with the surrounding the heater output power amounts to Q_H = 576 W.
The emissivity on the heater backside ε_{H^*} is assumed to be 0,9 too. By lowering the emissivity on the heater back side (e.g. by a polished surface) and by an additional radiation screen between infrared heater and vacuum chamber, the heater output can be reduced.

4.0 Description of the Control Software

The selected software for operation, control and data acquisition is the National Instruments software package LabVIEW, version 5.01 including several libraries and a stand alone opportunity. Compatible with the multi I/O board, the system runs on a Pentium based computer. The Professional Development Tool was used to design and program a 32-bit solution of the TCTF operating software. Data exchange via Intranet was provided.

LabVIEW is an object orientated software tool (VI's) which offers many features for easy programming of data acquisition. In case of system controlling via LabVIEW a more detailed basic programming is necessary, and the internal structure of the software has to be acquainted too.
For the operator and user of the TCTF the operation should be run independent and safe. The control and input interface is limited to the main parameters for adequate testing. Therefore the communication with the program is limited due to the displayed input interface.

4.1 LabVIEW Control Strategy

The implemented control strategy is based on a safe operation of the facility and the sample for each status of the system. Therefore all facility relevant parameters (e.g. vacuum pressure, temperature, position of valves, status of pumps, ...) are continuously controlled by software (*Figure 9*).

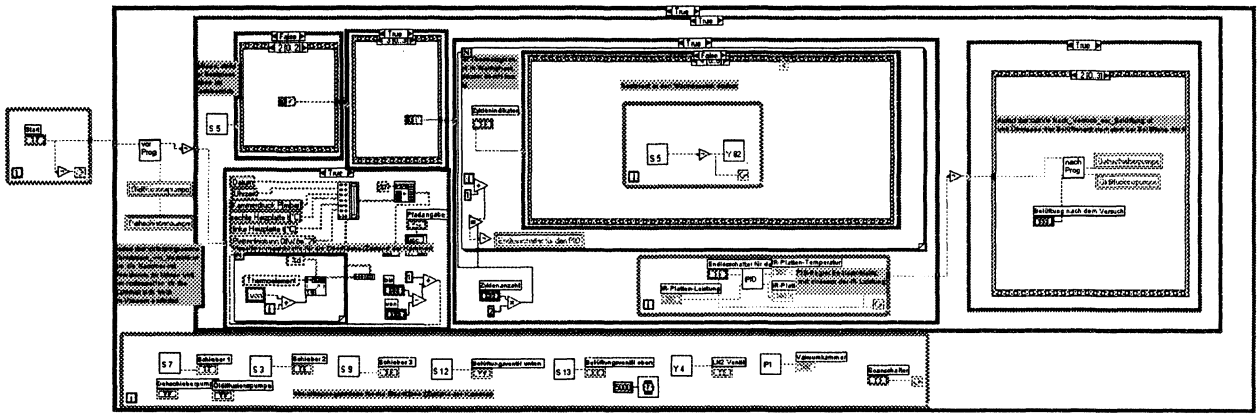

Figure 9 Flow chart for the control via LabVIEW

The operation of the two vacuum pumps depends on the pressure level inside the chamber and for the diffusion pump, also the water cooling system is monitored. Starting at a pressure level lower than $5^* 10^{-2}$ Pa the LN_2 cooling cycle and the heating unit is available. The actual temperature at the sample support structure and the sample itself is monitored and correlated to the required test temperatures. The LN_2 cooling cycle operates at lowest temperatures as possible (e.g. –180 °C during former solar cell tests), depending on internal heat input. The heating plate consists of an electrical resistant wire. The measured feedback temperature of the heating plate itself or a measurement point at the sample are inputs for the software adapted PID-controller. Input for the user is only the required radiation power per area coming from the front of the heating plate.
All parameters necessary for operation are displayed by a start up screen (*Figure 10*) and selectable:

- Measurement start pressure
- Status of the vacuum system at the end of the test or in case of a failure
- Necessary resources activated ?
  (water cooling cycle, air pressure, ...)
- Path of data file storage

Feedback lines shown at the screen are:

- LN_2 temperature at the sample support structure
- Heater temperature
- Status of pumps and valves (red/green indicated)
- Actual pressure in the chamber

If all parameters are selected at the start-up screen the process can be started by the START button and than runs automatically.

4.2 LabVIEW Data Acquisition

In parallel to the facility control LabVIEW runs in the background to sample all selected measurement lines. Therefore the second plug-in board is used. Depending on the software features it is necessary to switch between the data acquisition board and the multi I/O board to store the sampled data's on hard disc. Using a sampling rate of 2 measurements per seconds for each channel (up to 64 lines) the switching leads to no data leg. Due to the specifics of the board 32 or 64 thermocouple lines are available. The number of scanned lines (in serial) is selectable during the initialization with the start-up screen. The data's are stored on hard disc as ASCII data set. The data sets are time correlated to the operational data set.

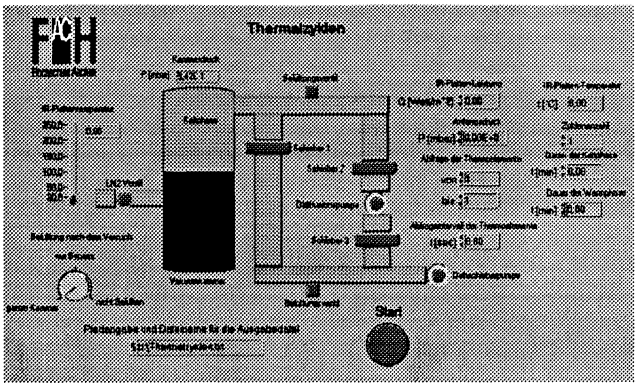

Figure 10 Main System Control Screen for Thermal Cycling.

4.3 Software Handling and User Interface

Due to the desired limited opportunity to change the basic operation code (in LabVIEW) the user has only four different screens to communicate and change the control parameters.
The screens are designed for visual control of operation and measurement. During the test period normally no changes are necessary and also possible. In case of emergency a stop button (on screen and in hardware) may stop all activities and transfer the facility in a save status.

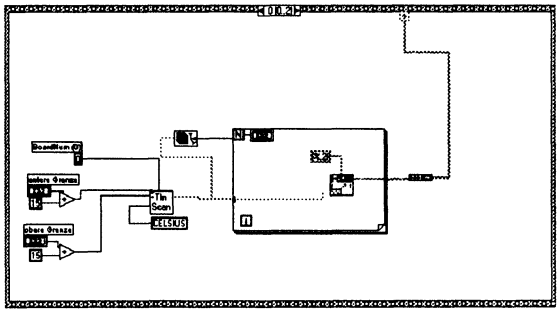

Figure 11 Flow Chart for Sampling 32/64 Thermo-couple Lines in parallel to the Control Activities.

A restart is possible without data loss.
The interface screens are:

- General system setup and start-up screen
- Vacuum operation status screen
- Thermal cycling test operation status screen
- Measurement data/control screen

5.0 Test Capability

5.1 Former Test Subjects

The TCTF was designed and built up for the first time at the DFVLR in the 70`s. At this time all materials for space, especially solar cells are subjected to thermal cycling tests in vacuum between e.g. - 180°C and +70°C with cooling and heating periods of e.g. 72 min and 18 min respectively. The objective was to compare the thermal cycling capabilities of the respective designs; particularly with respect to the most critical failure modes of cell to cell interconnected ruptures, cracking of cover slides and solar cells, and delamination of adhesives.

During 2500 temperature cycles solar cell panels from different European manufacturers were tested simultaneously. Additional tests at room temperature were investigated at predetermined intervals for optical, electrical and mechanical differences [1,2]. The temperature - time profile was similar to the calculated curves for typical solar cell panels. The average initial temperature rates of change from cold to hot phase were up to 50 °C / minute. The results have shown an decreasing of maximum power of up to 5%. The thermographical investigations on the panels showed no defect in the electrical circle of the solar cell module or separation of the solar cell from the substrate

5.2 Qualification Tests

Since there were made no changes in the sample support structure, the internal LN_2 cooling loop and the heater arrangement the same temperatures were assumed as during the former tests at DFVLR.

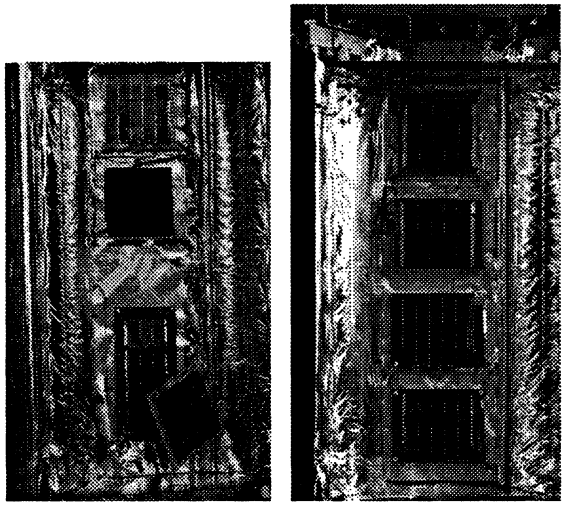

Figure 12 Test Configuration for flexible and rigid Solar Cell Panels /lit. 1,2/.

Indeed, the required temperatures [1] in the hot phase (+70°C) and in the cold phase (-180°C) could be obtained.
Dependent on the test duration the temperatures in the cold phase were measured in the range of –180 °C to +160 °C.
In the hot phase the equilibrium temperature was already obtained after 10 min. By changing the heat out-put of the infrared heater during the cold phase for the sample this desired final temperature could be reached. As shown in *Figure 13* the thermal cycles are well in time and the amount is at the same level as required.

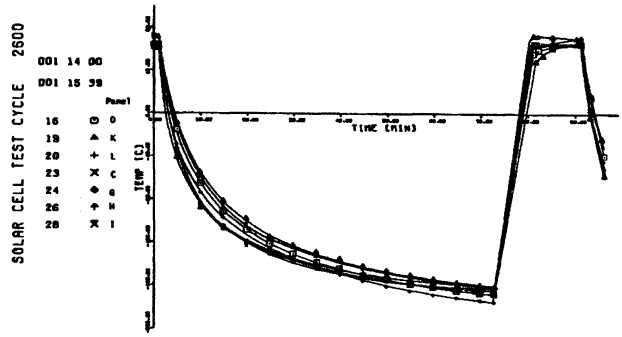

Figure 13 Plot of Temperature Variation

Qualification tests for the upgraded computer controlled facility are running at time.
The control strategy of the vacuum operation works well and the final vacuum pressure reaches the 10^{-3} Pa region. At the time several defined samples are mounted for a facility verifying long term test.

5.3 Future Test Capability

Up to now the upgraded Thermal Cycling Test Facility offers a wide range of different possibilities for testing materials and components in high vacuum providing alternating thermal loads.

Possible applications of the TCTF:

- Test of electrical and mechanical parameters of samples
- Verification of insulation effectiveness and heat transfer rates
- Functional tests on sensors and actuators
- Design optimization
- Verification of numerical calculations
- Qualification of spacecraft hardware

In the case of testing material properties, the classical application of solar cell (panel) test is discussed further more for new materials and designs of substrates.
Lightweight structure materials are often composite materials. New technologies offer new solutions for spacecraft application. The materials itself and their bonding have to be verified for spacecraft application. More and more components are glued for reducing mass. Therefore several bonding technologies and compositions have to be mechanically verified and for long time applications investigated.
Electronic components e.g. computer boards have to prove their vacuum and thermal compatibility and reliability during full operation.
New insulation's and radiator concepts for passive and active thermal control can be verified.
Due to the miniaturization of spacecraft components the overall design size decreases by increasing perfor-mance. Therefore several mechanical components (e.g. motors, gears, bearings, connectors, ...) are shrinking to a size also feasible for quick testing under vacuum or by thermal cycling conditions in the TCTF.
In parallel to the numerical calculation and simulation the TCTF offers the opportunity to verify this results before the next step in design optimization starts.
After test and qualification of our TCTF according to international standards, the facility offers the opportunity to qualify small spacecraft hardware for their space employment.

The automation of the operation of the TCTF offers the opportunity for long term tests with minimized operator activities. Due to the possibility to shrink the test time retaining the thermal load to the sample, also life time research will be possible according to the predicted realistic application of the sample.
Additional to the TCTF several tests can be offered for detailed investigation:

- Mass spectrometric analysis of outgasing products
- Electronic particle radiation charge (in discussion)
- Thermooptical properties
- Infrared temperature distribution visualization on the sample surface

6.0 Summary

The Thermal Cycling Test Facility at the University of Applied Sciences in Aachen, Germany makes it possible to conduct reproducible comparison measurements of any solar cell panel, materials or mechanism for the use in space. The decisive environmental conditions met outside the earth's atmosphere, which have a certain influence on the lifetime and the efficiency of solar cell panels and spacecraft materials are simulated by a vacuum down to $5*10^{-4}$ mbar and any chosen number of hot to cold cycles.
Also the space environment on the moon surface:

−178°C to +110°C

and on Mars:

−133°C to +17°C

can be simulated using a special LN_2 reduce valve.
In addition it is possible to test electrical and mechanical components under simulated space conditions. As shown the simulation principle works well and the desired low and high temperatures can be achieved at the sample.
The upgrade of the TCTF offers now the opportunity to test autonomously over a long term period with nearly no operator activities. Data sampling offers a complete test history available for further analysis.

Literature

(1) *Ley, Wilfried*
DFVLR FACILITY FOR THERMAL CYCLING TESTS ON SOLAR CELL PANEL SAMPLES UNDER VACUUM CONDITION.
DFVLR, Space Simulation Institute, Köln-Porz
February 1976

(2) *Ley, Wilfried*
ADDITIONAL THERMAL CYCLING TESTS ON SOLAR CELL PANEL SAMPLES UNDER VACUUM CONDITIONS.
DFVLR, Space Simulation Institute, Köln-Porz
IB 353-78/1, Final Report 1978

(3) *Rehmann, K. V.*
VACUUM THERMAL CYCLING TEST ON SOLAR PANEL SAMPLES.
DFVLR, Space Simulation Institute, Köln-Porz
ESA/ESTEC Contract, 1982

(4) *Rehmann, K.V.*
LEBENSDAUERUNTERSUCHUNGEN IN EINER THERMISCHEN ZYKLENTESTANLAGE
DFVLR, Institut für Raumsimulation, Köln-Porz, März 1984

(5) *Ley, Wilfried; Hallmann, W.; Plescher, E.*
Umgebungssimulation von Raumflugkörpern
4. Raumfahrt-Kolloquium an der FH Aachen, 28. Nov. 1991, DGLR-Bericht 92-01

(6) *Justen, B., Hallmann, W.*
Bahnmechanik und Erdschattenphasen bei seilgefesselten Systemen - *Tethersystem*
DGLR-JT 1994, Erlangen

(7) *Sürül T.; Ley, W.; Plescher, E.*
Einsatzspektrum, Ausbaumöglichkeiten und wissenschaftliche Zielsetzung für die Tieftemperatur-Zyklentestanlage
Diplomarbeit FH Aachen, FB6 , Januar 1996

(8) *Zaske, Uwe*
Automatisierung des Betriebs und der Datenerfassung der Hochvakuum-Anlage (Thermal-Zyklen-Testanlage) mittels LabVIEW.
Diplomarbeit FH Aachen, FB6, Sept. 1999

Page intentionally left blank

THE USE OF ENVIRONMENTAL TEST FACILITIES FOR PURPOSES BEYOND THEIR ORIGINAL DESIGN

Terry C. Fisher and W.J. Marner
Jet Propulsion Laboratory
California Institute of Technology

ABSTRACT

Increasing demands from space flight project offices are requiring environmental testing facilities to become more versatile with increased capabilities. At the same time, maintaining a cost-effective approach to test operations has driven efforts to use these facilities for purposes beyond their original design. This paper presents an overview of the Jet Propulsion Laboratory's efforts to provide JPL's space flight projects with test facilities to meet unique test requirements and to serve the needs of selected outside customers. The large number of recent Mars Missions, including the Mars Pathfinder project, have required testing of components and systems in a Martian surface environment in facilities originally designed for deep space testing. The unique problems associated with performing these tests are discussed, along with practical solutions. Other unique test requirements are discussed including the use of space simulation chambers for testing high altitude balloon gondolas and the use of vacuum chambers for system level test firing of an ion propulsion engine.

INTRODUCTION

Aerospace environmental testing has seen many innovations from the early days of aircraft testing, through the early years of the "space race" to the present day of "faster, better, cheaper". During all of these phases of testing aerospace hardware for flight operations, there has always been a need for engineers in the test community to work with the project scientists and engineers to provide test facilities and test methodologies that would meet all the requirements for a successful test program. In today's ever-changing world of spacecraft testing, it has become even more important for the testing community to respond to the requirements of flight projects community to ensure successful test results that meet the project's requirements. Many unusual and unique test requirements have been levied on environmental test labs in recent years due to the renewed interest in the exploration of the Martian surface. These requirements along with the thrust for "faster, better, cheaper" projects have led to new and innovative test techniques.

BRIEF HISTORY OF AEROSPACE ENVIRONMENTAL TESTING

Environmental testing of components and systems has taken place since the early days of aircraft design and production but really came of age during the early years of the jet aircraft. When the Russians put Sputnik in orbit in 1956, the aircraft industry had in place advanced methods of vibration, shock, aerodynamic and thermal testing; however, testing of hardware that would be exposed to space opened a new era in environmental testing. The dynamics test field needed only minor adjustments to transition from aircraft testing to launch vehicle testing but the deep space environment was much more than just high altitude testing and a new field of simulating the space environment was born. New fields of testing included the use of cryogenic fluids to simulate the cold of outer space, higher levels of vacuum, and the great-unknown solar radiation effects in space. In recent years the increased use of optical components in space flight instruments has levied a whole new set of cleanliness requirements on environmental test laboratories. Working closely with the projects, new methods of contamination control and ultra clean vacuum systems have been implemented in aerospace test laboratories. In addition "faster, better, cheaper" has given rise to many new challenges to both the science community and the test community.

THE JPL ENVIRONMENTAL TEST FACILITIES

The Jet Propulsion Laboratory (JPL), an operating division of the California Institute of Technology (Caltech), is a lead research center for the National Aeronautics and Space Administration (NASA). JPL has a wide-ranging charter for Solar System exploration, earth observation, and technology development.

As part of this charter, JPL maintains NASA owned environmental test facilities for its research and development programs. These facilities include thermal vacuum test chambers, vibration tables, an acoustic chamber, and two large space simulation chambers. The Environmental Test Laboratory (ETL) at JPL has numerous horizontal thermal vacuum chambers ranging in size from 3 ft by 3 ft to 11 ft by 11 ft. These chambers are capable of providing an outer space environment of better than $1x10^{-6}$ Torr at –185°C. The thermal vacuum lab also has several vacuum bakeout chambers, capable of attaining high vacuum at temperatures of over 100°C. The ETL has vibration and acoustic test systems for simulating space flight launch environments. The vibration systems range in size from 5,000 to 40,000 pounds of force. The acoustic test facility is a 10,900 cubic foot chamber capable of noise levels up to 155 dB. The ETL operates and maintains both 25-ft and 10-ft Space Simulator Facilities. These two large vertical thermal vacuum chambers are capable of providing an outer space environment of better than $1x10^{-6}$ Torr at –185°C. The 25-ft Space Simulator (See Figure 1) is 85 ft in height and has the added capability

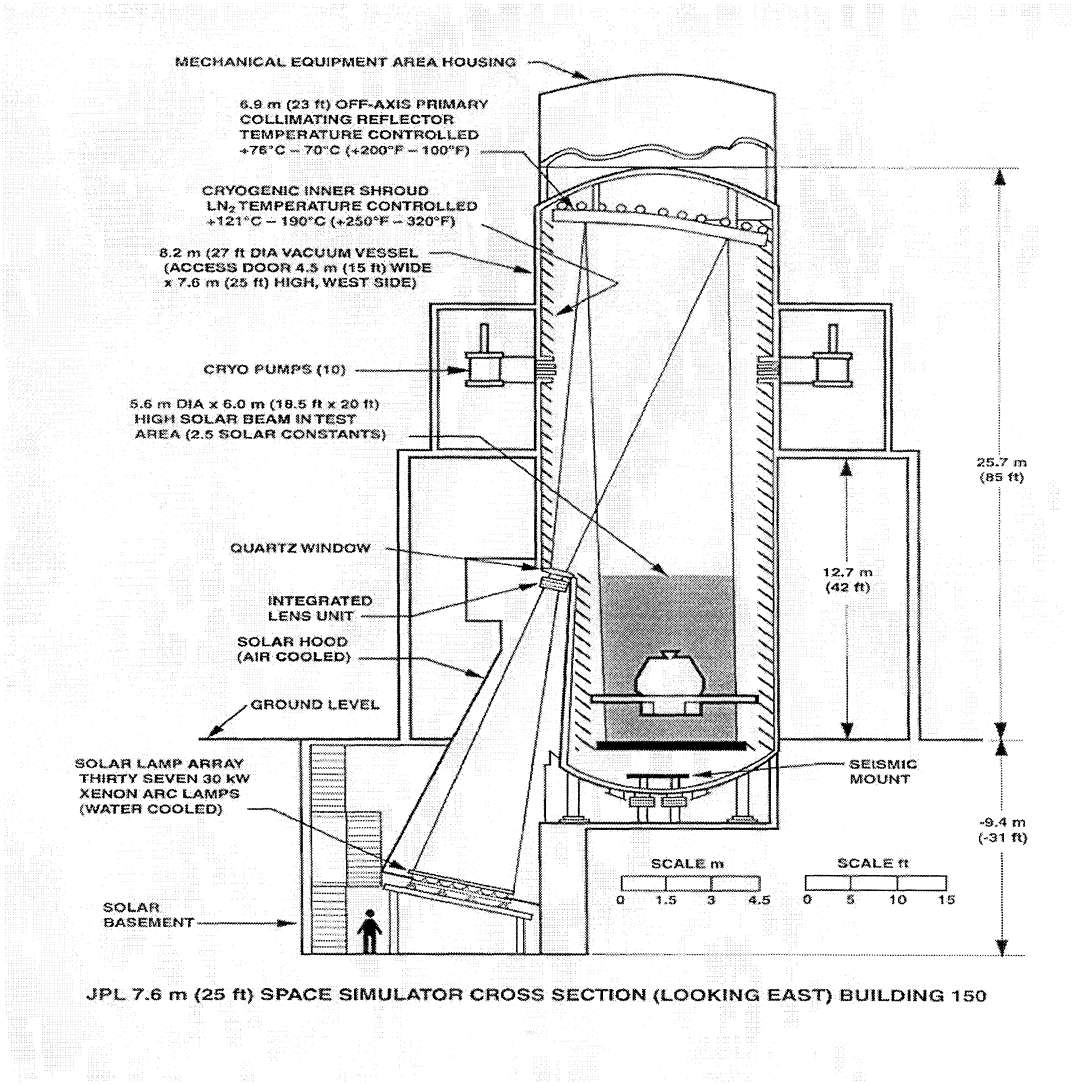

Figure 1: The JPL 25-ft Space Simulator Facility

of producing a 19-ft diameter solar beam with radiation levels greater than 2.5 solar constants. Also included in this facility is the Satellite Test Assistant Robot (STAR) system, a remote controlled video imaging and infrared camera system, designed to aid test personnel in monitoring their test article in the chamber.

UNIQUE REQUIREMENTS FOR SPACECRAFT TESTING

Recent requirements to perform thermal vacuum tests in a simulated Martian surface environment have presented many new challenges to the environmental test community. Requirements such as operating a Mars lander and rover vehicle at 7 Torr and –100°C or performing thermal vacuum tests with a 20 meter/second wind in a CO_2 environment were some of the challenges during the Mars Pathfinder test program which led to the very successful landing on Mars in July, 1997. Another unique test requirement was the firing of an ion thruster engine during the space simulation test program for the Deep Space-1 (DS-1) flight spacecraft. Ion engines had successfully been tested in specially designed vacuum chambers in a stand-alone configuration, but never in a space simulation chamber as an integral part of a system level flight acceptance test. During the design and development of the Hubble Space Telescope, the scientists designing the optical imaging systems presented the test community with the challenge of providing ultra clean vacuum tests and vacuum bakeout testing. These more stringent tests were necessary to ensure spacecraft cleanliness to levels never previously attempted. All of these unique test requirements and the desire of NASA to perform all new missions in a "faster, better, cheaper" mode have necessitated innovative and creative problem solving on the part of the environmental test community.

THE CHALLENGES AND THE PROBLEMS

In order to meet the challenges of these new and unique test requirements, there were many opportunities for test personnel to become involved with the project personnel in the early stages of program development. This collaboration proved to be very beneficial to all parties as the test requirements could be developed and test facilities modified as the project evolved. Because of the emphasis on doing things in a more cost-effective manner, it was decided early on to utilize existing facilities to the greatest extent possible in order to save schedule, time, and money.

In the case of simulating a Martian surface environment, it was determined that testing should be done in existing vacuum chambers because it would be cost prohibitive to build new chambers of various sizes to support the total test program. The major challenge was the fact that thermal vacuum and space simulation chambers are designed to provide a deep space environment of high vacuum ($1x10^{-6}$ Torr) and –185°C temperatures. However, the Martian surface pressure is approximately 7 Torr, with CO_2 as the major gas component, and a surface temperature that varies from –40°C to –130°C depending on the time of day. At these conditions of pressure and temperature, the stainless steel vacuum vessel walls become very cold due to gas conduction between the chamber cryogenic shroud and the vessel. When the mild steel structural members of the vacuum vessel cool below –40°C they become brittle. Also, when the vessel becomes cold, condensation forms on the exterior of the vacuum vessel and moisture can penetrate electrical connectors and cables. Another problem appears when using the standard technique in thermal vacuum testing of using a liquid nitrogen flooded "scavenger plate" or "cold finger" to trap contamination and water vapor in the vacuum chamber. It was discovered that CO_2 at 7 Torr solidifies at approximately –120°C and the chamber could not be maintained at 7 Torr because a block of frozen CO_2 would form.

Contamination of optical surfaces and space flight components in environmental test programs presented many challenges to JPL, other NASA centers and commercial aerospace contractors during the testing of the Wide Field Planetary Camera and other Hubble Space Telescope instruments. It became necessary to devise methods of baking spacecraft components in vacuum chambers in order to ensure that contamination would not be deposited on optical surfaces once the instrument was on-orbit, and test methods needed to be changed to provide a contamination free test program. Some specific test requirements included: (1) the test hardware must not be re-contaminated at anytime during a bakeout or post test chamber shut-down, (2) the background emission rate of the chamber must be

significantly below that of the test hardware i.e. the chamber must initially be very clean, and (3) the contamination measurements must accurately verify that hardware cleanliness specifications have been met. Meeting contamination control requirements again necessitated creative engineering on the part of the environmental test facilities personnel.

During the space simulation test program of the Deep Space 1 (DS-1) spacecraft in 1998 (See Figure 2) the project engineers were concerned about the effects of the ion thruster engine on other spacecraft systems and the fact that the thruster had never been operated at the system level. The ion propulsion system had undergone extensive testing in a specially designed vacuum chamber, but had never been operated as a system with the spacecraft and flight software. The major concern of the space simulation operations personnel was the effect of the stream of ionized xenon gas coming from the engine, as it could erode the surface of the chamber cryogenic shroud and contaminate the optical components of the solar simulation system.

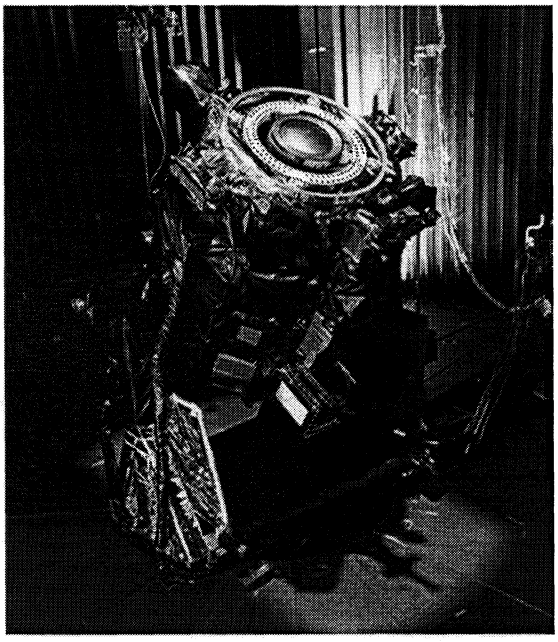

Figure 2: Deep Space 1 Spacecraft in the JPL 25-ft Space Simulation Chamber

The final case presented similar problems to those encountered during the simulation of the Mars surface environment. In late 1998 the Environmental Test Laboratory at JPL was requested to assist in the testing of a high altitude, manned balloon gondola. The primary mission goal was to be the first manned flight around the world and to set a manned ballooning altitude record. The gondola was designed to fly at elevations up to 130,000 ft where temperatures can go as low as –135°C. Since the designers had only limited experience in the design of hardware for such a mission, an accurate simulation of the flight environment was essential. The goals of the tests were to obtain information regarding the thermal characteristics of the gondola and validate thermal models and predictions. A secondary goal was to provide information pertaining to arcing susceptibility of the electrical systems at predicted flight pressures.

DEVELOPING PRACTICAL SOLUTIONS

In the early days of the Mars Pathfinder project the problem of using CO_2 gas in vacuum chambers presented problems as previously discussed. Working with project thermal analysts it was determined that for some test cases nitrogen gas was a suitable replacement for CO_2. The thermal properties of nitrogen were sufficiently close to the Martian gas composition to provide a fairly accurate simulation; therefore, nitrogen was used to maintain the 7 Torr

pressure in the vacuum chambers for most of the test programs. An experimental wind machine (See Figure 3) was used in several tests in an attempt to simulate Martian winds. This machine was developed through collaboration

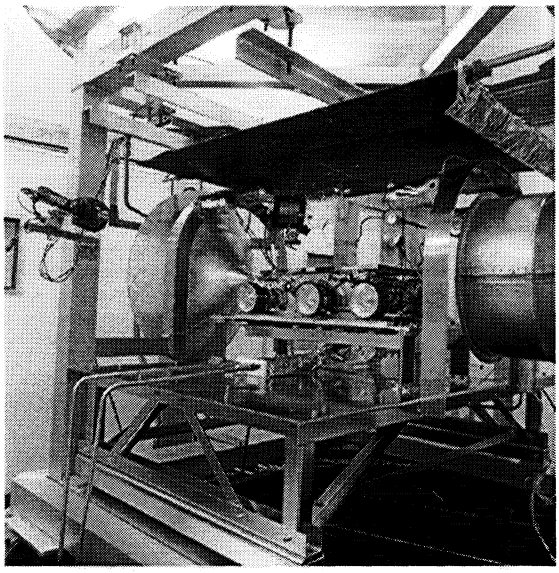

Figure 3: The Mars Pathfinder Rover and Wind Machine in the JPL 10-ft Space Simulator

between the environmental test facility personnel and the project engineering personnel; however, because of a lack of time and budget these tests were only partially successful, due to problems with the motor used to drive the fan that created the winds. However, sufficient data was collected to verify the scientist's computer models and to confirm that the thermal design would be effective for maintaining critical components within tolerance.

To meet the requirements of operating the Mars rover during system level solar-thermal-vacuum testing (See Figure 4), a special floor for the 25-ft Space Simulator was designed through a joint effort of the facility personnel and the project engineers.

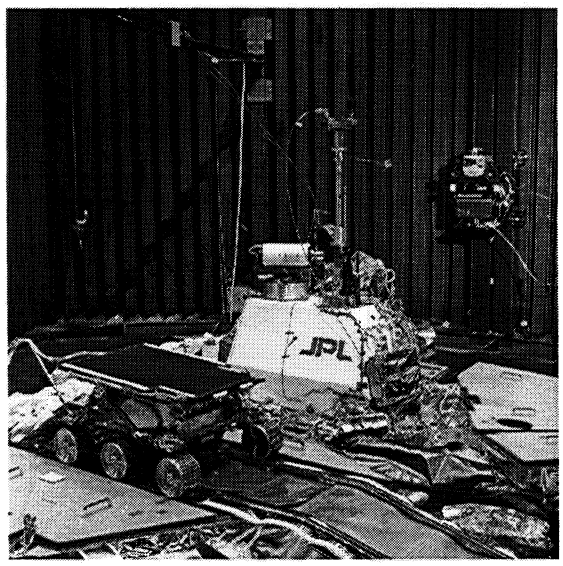

Figure 4: The Mars Pathfinder Spacecraft and the Mars Rover "Sojourner" in the JPL 25-ft Space Simulator

Potentially, the most serious problem encountered during the Mars Pathfinder test program was that of the structural members of the thermal vacuum chambers becoming so cold that the mild steel could fracture. To counter this problem, several practical solutions were developed by the space simulator facilities personnel. The first step was to instrument the vacuum vessel walls and mild steel structural members with thermocouples to alert the chamber operators when the temperatures approached –40°C. With this warning in place, steps could be undertaken to initiate a chamber warm-up if required. Second, the operations crew conducted hourly walk-around inspection tours of the facility and used hand-held non-contact temperature indicators to check areas that appeared to be getting too cold. Electrical heaters were used in the area of the chamber electrical penetration ports to eliminate condensation in the areas of cables and connectors. Last, fans were used to circulate air in the areas where condensation appeared on external surfaces of the chamber. All of these steps proved to be very effective and, although vacuum vessel external temperatures approached –40°C on several occasions, the testing programs were completed without interruptions.

During the test program for the Re/Max balloon gondola (See Figure 5), many of the same techniques developed for the Mars programs were implemented to protect the facilities.

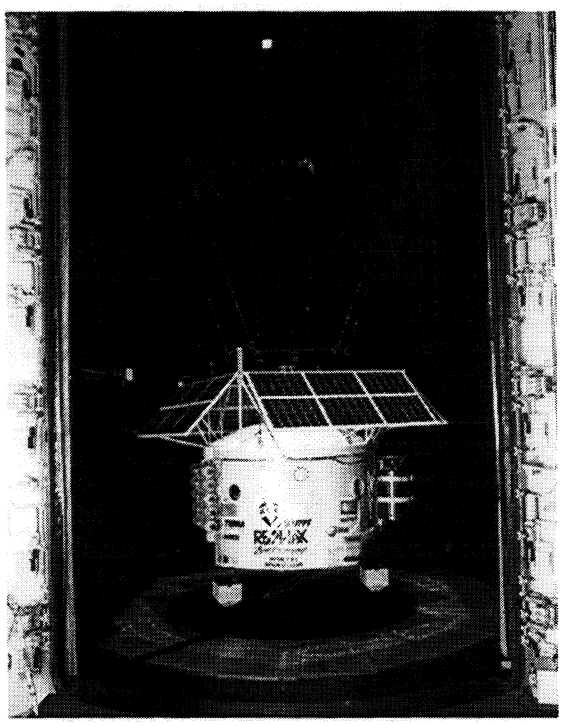

Figure 5: High Altitude Balloon Gondola in the JPL 25-ft Space Simulator

In addition, a unique partnership arrangement was developed. In this case the designers and developers of the balloon flight project had little or no experience in building equipment designed to fly at the edge of space, so they approached experienced personnel at Lockheed Martin in Denver for assistance. The design and test team in Denver and the facilities test team at JPL provided the ballooning company with the expertise needed to successfully complete their design, fabrication, and test project.

To protect the vacuum chamber shrouds during the DS-1 ion thruster firing tests in the 25-ft Space Simulator (See Figure 6), a special target was fabricated from pure graphite foil and secured to an aluminum frame in front of the chamber cryogenic shroud. To protect the 23-ft diameter collimating mirror from any potential contamination in the chamber, a special cover was fabricated from carbon impregnated Kapton thermal blanket material. This cover was designed by the engineers in the thermal blanket and radiation shield shop at JPL, using their years of experience in

designing and fabricating thermal blankets and radiation shields for spacecraft.

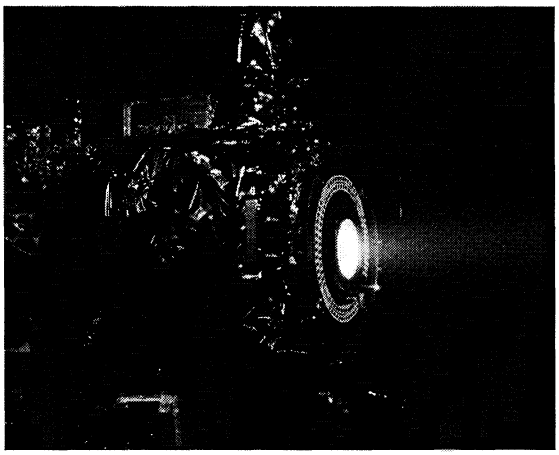

Figure 6: Deep Space-1 Ion Thruster Firing in the JPL 25-ft Space Simulator

During the fabrication and test programs for the Hubble Space Telescope, many new innovations were required in the world of environmental test due to the contamination control requirements developed by the project scientists. The techniques employed ranged from very simple to very complex. One simple solution was involved in preventing contamination of optical surfaces during vibration testing. Even when located in a Class 10,000 clean room there are enough oil vapors present in the vicinity of the shake table to contaminate sensitive optical components. The method to prevent contamination involved wrapping the test article in clean static dissipative material and introducing a purge of high purity nitrogen gas. This approach provided a simple, cost effective solution to the problem. In the case of verifying cleanliness specifications in the vacuum chamber, special instrumentation was used to monitor the outgasing rates of both the chamber and the test article. Residual Gas Analyzers (RGAs) and Quartz Crystal Microbalances (QCMs) were used to measure high level and low level contamination levels during vacuum bake out testing. Data from these instruments were analyzed by project contamination control engineers to determine when the proper levels of cleanliness had been obtained. Since the project scientists were required to make the final determination of the effectiveness of the bakeout, it was imperative to establish a very close working relationship between the scientists and the test lab personnel.

In order to meet all of the contamination control requirements during the Wide Field Planetary Camera 2 (WF/PC II) project, JPL personnel determined that conventional vacuum chambers could not be used to obtain the desired bakeout results and at the same time meet the very stringent project requirements. A new chamber design concept evolved from these requirements to effectively bake out hardware to levels required by the project. This new design used a test article containment system that is placed inside of the vacuum chamber shroud to prevent re-contamination of the test hardware. By enclosing the hardware in a stainless steel enclave (See Figure 7), and by always maintaining the enclave temperature above that of the shroud, the outgased contaminants are prevented from condensing on the test hardware. Contaminants exit the enclave through orifices in the enclave and are removed from the chamber by either the vacuum pumping system or by condensing on the cryogenic shroud. During return to ambient conditions, the time when contamination is most likely to be re-condensed on the test hardware, the shroud is slowly warmed, then the enclave is slowly cooled and a purge of high purity nitrogen gas is introduced into the enclave. The combination of the purge and the slow warm up of the shroud minimizes the back flow of contamination into the enclave.

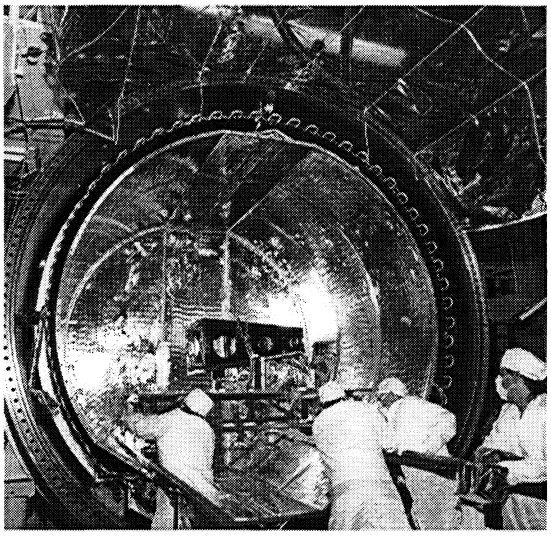

Figure 7: Wide Field/Planetary Camera II Optical Bench in the JPL 10-ft Thermal Vacuum Chamber with Enclave

SUMMARY

Unique test requirements will continue to be the norm in this ever-changing era of space flight programs. The continued exploration of Mars, the increased use of sensitive optical systems, and the decreasing size of test budgets will continue to present numerous technical challenges to environmental testing facilities around the world.

REFERENCES

Johnson, K.R. October 1996. "Mars Pathfinder Spacecraft, Lander and Rover Testing in Simulated Deep Space and Mars Surface Environments." *Proceedings, 19th Space Simulation Conference.*

Johnson, K.R. Taylor, Dr. D.M. Lane, R.W. Cortez, M.G. and Anderson, M. R. November 1992. "A New Approach for Performing Contamination Control Bakeouts in the JPL Thermal Vacuum Test Chambers". *Proceedings, 17th Space Simulation Conference.*

Johnson, K. Wen, L. Kwack, E. and Noller, E. January 1995. "Simulation of Mars Surface Conditions for Characterization of the Mars Rover Thermal Response". *Proceedings, 16th Aerospace Testing Seminar.*

* The research described in this paper was carried out by the Jet Propulsion Laboratory, California Institute of Technology, under a contract with the National Aeronautics and Space Administration.

Networked Vibration Testing And Analysis Using Industry Standard Network Protocols

Thomas J. Reilly
Spectral Dynamics, Inc.
San Jose, CA 95131

Biography

Thomas Reilly received a BS degree in Mechanical Engineering from Virginia Polytechnic Institute and State University in 1983. After working several years in the field of vibration and acoustic analysis of U.S. Navy ships, Thomas joined GenRad (now Spectral Dynamics) in 1988. Thomas has spent 12 years with Spectral Dynamics focusing on signal analysis and vibration control system products. He is currently Product Manager for the PUMA Vibration Control and Analysis System Group.

Abstract

This paper outlines an innovative approach using standard network technologies to streamline testing and data acquisition, distribute signal processing and analysis, and enhance the creation and distribution of test results. The TCP/IP-based data server architecture and industry standard inter-process communication protocols, ActiveX and Component Object Model are explained. This architecture allows remote control of testing using standard Ethernet networks. The data server also allows live data analysis on Microsoft Windows-based computers across the local area network or the Internet. Data sharing on the network allows independent data processing on the remote computer and maximizes processing performance.

Keywords

Vibration, Test, Network, TCP/IP, COM, DCOM, ActiveX, OLE, Internet

Introduction

Typically, vibration testing is only one part of product testing and qualification. Often multiple tests must be run simultaneously. Examples include combined thermal and vibration testing, product functional testing during vibration, and measurement of dynamic data with static data. Most test laboratories link test systems with older TTL, RS-232, or GPIB interfaces. These interfaces have limitations in both performance and flexibility.

This paper outlines an innovative approach using standard network technologies to streamline test and data acquisition, distribute signal processing and analysis, and enhance the creation and distribution of test results.

Objectives

There are four main objectives in designing a distributed vibration data acquisition and analysis system.

a. Flexible remote control of testing – Provide remote control of testing using standard Ethernet connections and communication protocols. This includes both limited control (Test start/stop) and complete control of the dynamic test application.

b. Real-time access to live test data – Again using standard Ethernet protocols, users should be able to view live data from anywhere on the local area network or the Internet.

c. Remote data processing and analysis – Data transfer must be possible from the test system to other computers on the network to distribute the processing load and permit more flexible real-time processing of test data.

d. Test automation and laboratory integration – Network test control and data analysis must be able to be integrated into other test applications like Visual Basic, Visual C++, JAVA, or National Instruments LabView™ to automate multiple test functions.

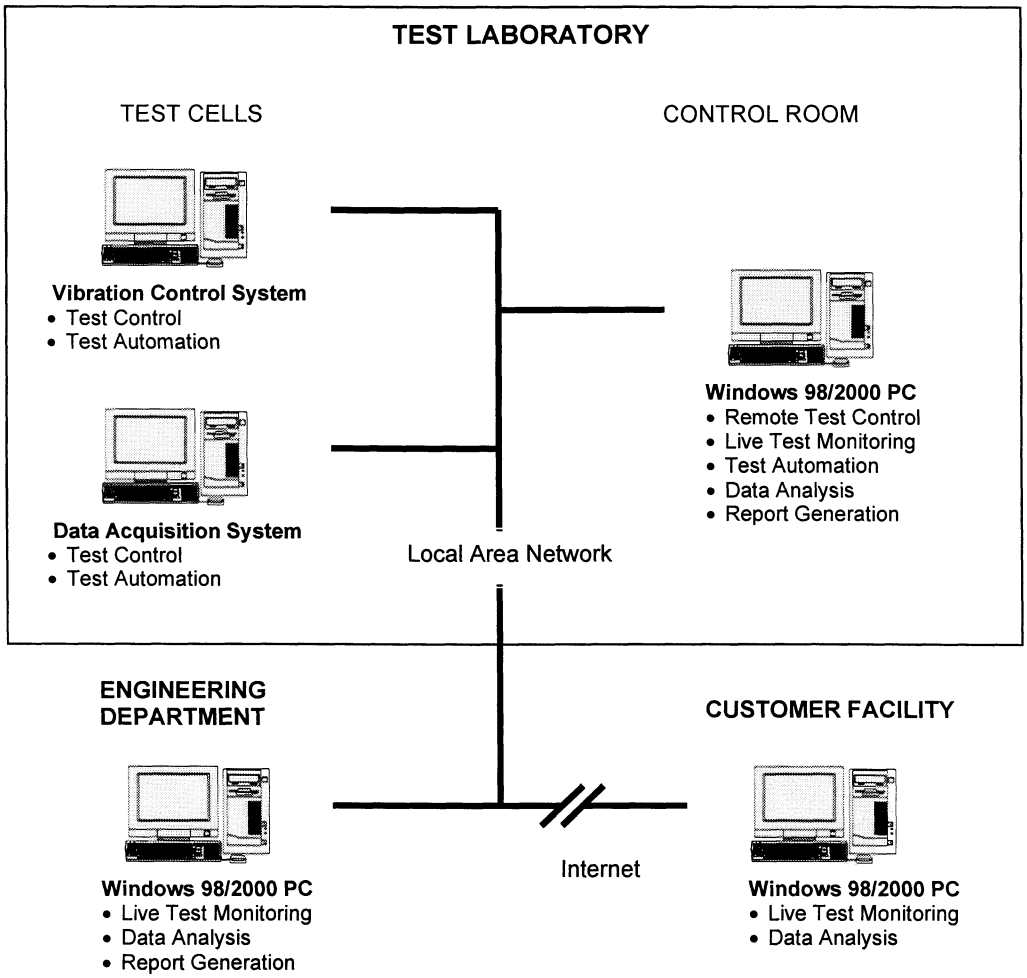

Figure 1. Networked Test Laboratory

Client/Server Architecture

The basis of this client/server architecture is the data server. The data server runs on the test system and serves as the interface between the graphical user interface and the system DSP hardware. To simplify implementation, all communication with the data server both across the network and within the test system uses TCP/IP protocol (see Figure 1). TCP/IP is the standard network protocol that is

used on the Internet. Use of TCP/IP in this manner provides inherent network functionality. The same test control and data viewing software can be used across the network as on the test system. In addition to simplifying implementation of network capabilities this ensures that all of the capabilities of the test system are available in network operation. The TCP/IP communication also makes operation across the Internet possible.

The data server is responsible for all test supervision and local data storage. Tolerance and safety checks are performed in test system DSP hardware. This design ensures test control and data storage are not compromised.

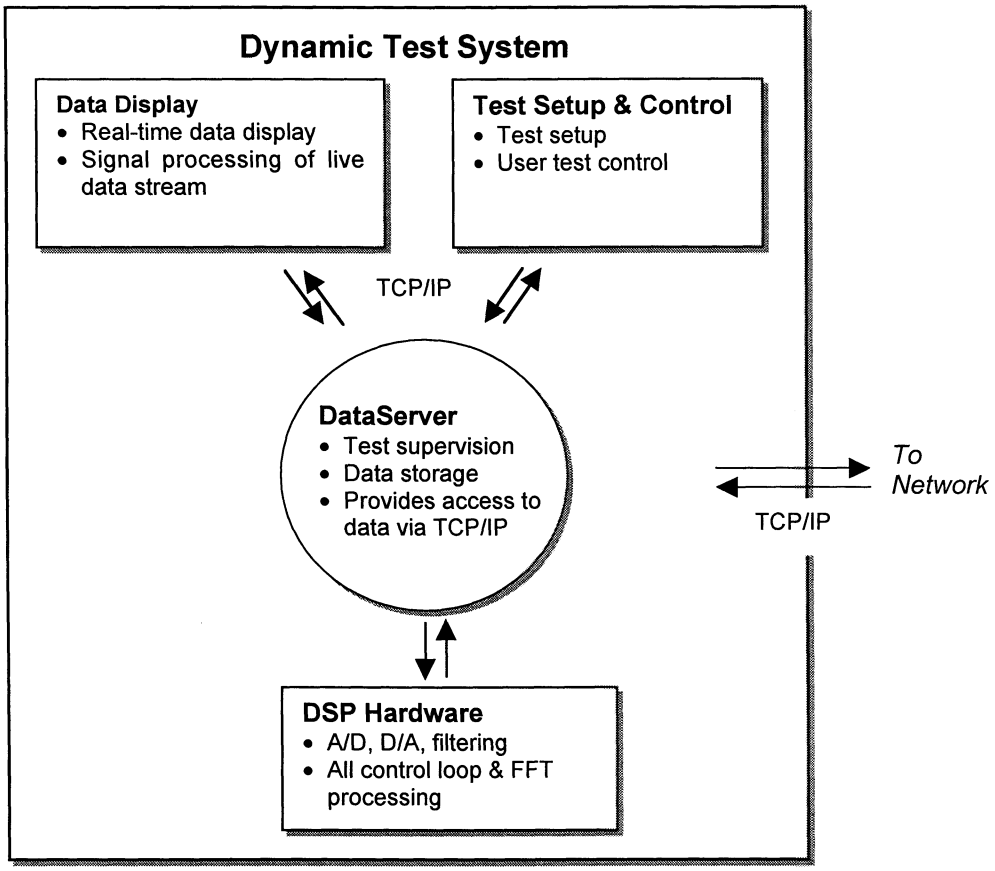

Figure 2. Client/Server Architecture

The primary benefit of the data server architecture over typical network architectures is that the data is transmitted across the network. Typical network implementations only share displays of data across the network. All processing of data is still performed on the test system. Sharing data allows independent data processing and analysis on each remote station. In addition to providing more flexibility for real-time analysis, this increases processing performance by distributing the load. Additional processing on remote computers does not compromise critical test signal processing.

The Component Object Model (COM)

The most widely used technology for inter-process communication is the Component Object Model (COM). COM is a software architecture that allows components made by different vendors to be combined in a variety of applications. It defines a standard for component interoperability. COM has

evolved over the past decade from Dynamic Data Exchange (DDE), Object Linking and Embedding (OLE), Component Object Model, and ActiveX (COM enabled for the Internet).

COM provides the low level binding mechanism that enables objects to communicate with each other. The Component Object Model provides several significant benefits to developing networked dynamic test capability. COM is scalable, enabling the developer to use the same technology for communication within the same process, between multiple processes on the same machine and (using Distributed COM) between processes on different machines.

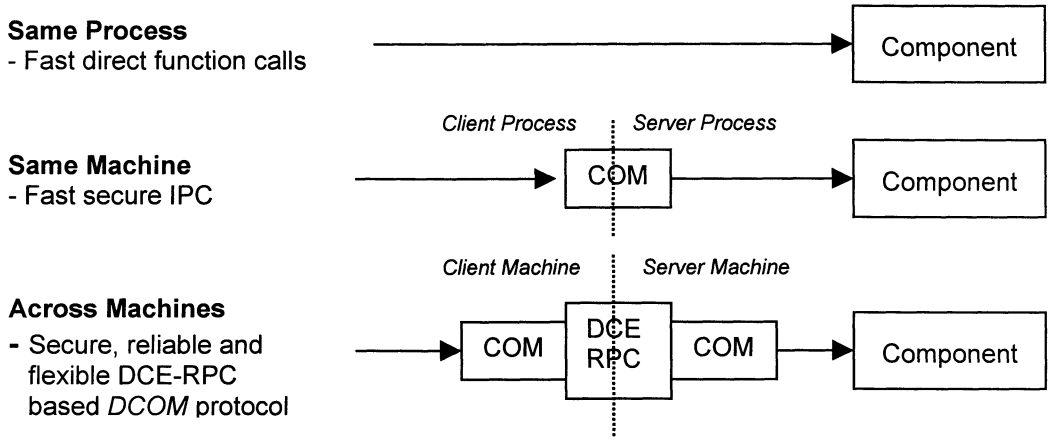

Figure 3. Accessing COM Services

COM is the basis for a large majority of new code for Microsoft Windows and Windows 2000 operating system created by Microsoft and third party vendors. COM is now even supported on Sun and HP UNIX platforms.

The two most widely used COM-based technologies are Object Linking and Embedding (OLE), and ActiveX. OLE allows COM based applications to be embedded within each other. OLE is optimized for end-user usability and integration of desktop applications. An example of OLE is embedding a spreadsheet within a word processor document. Double-clicking on the spreadsheet within the word processor enables all of the spreadsheet functions.

ActiveX is OLE controls that have been extended for the Internet environment. ActiveX is optimized for size and speed for Internet applications. These same attributes make ActiveX ideal for network control of dynamic test applications.

Remote Test Monitoring

The client/server data architecture has inherent remote test monitoring and control capability. Test setup and control processes act like Internet "browsers," connecting to data server processes by specifying the target IP address. The communication is identical whether attaching to a local data server on the test system or attaching to a data server across the Internet.

Figures 4 and 5 shows application of client server data architecture to remote monitoring of testing. In these examples viewing of the data does not affect the control of the test. Control is managed from the local test system and one or more data analysis and display processes are launched from a remote PC. The IP address of the target test system is selected to connect to the data server process. Multiple PC's may connect to the same data server or a single PC may connect to data servers on multiple test systems to monitor multiple tests.

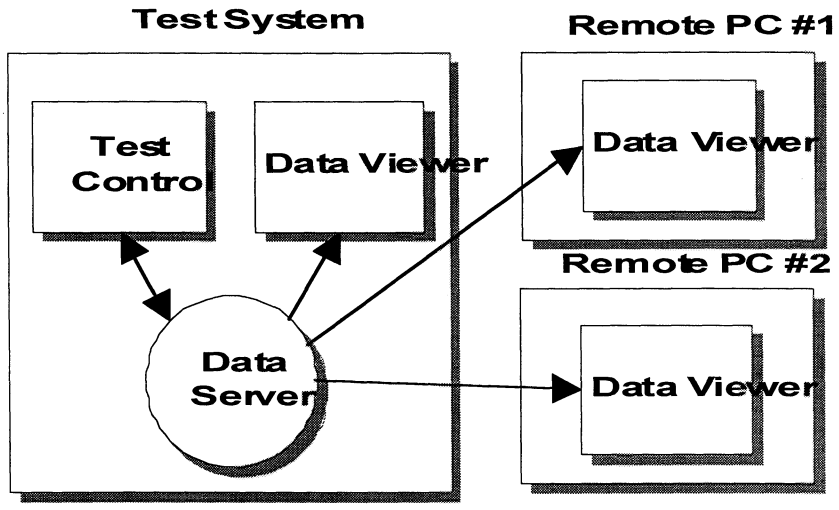

Figure 4. Remote Monitoring of a Vibration Test System from Two PC's

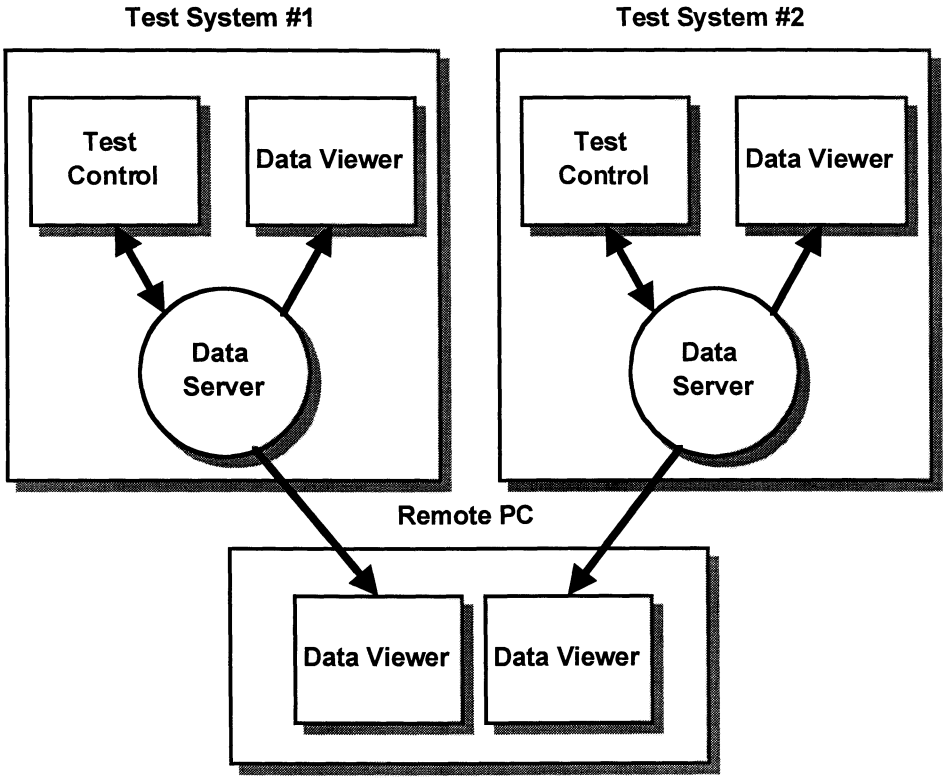

Figure 5. Monitoring Multiple Vibration Test Systems from a Single PC

Independent data viewer processes provides the benefit of complete independent control of data viewing and analysis while control by test operators is unimpeded. Because the data is networked, instead of just the graphical user interface, additional signal processing may be performed on the remote PC without degrading performance on the test system.

Remote Test Control

For remote control of a test system one only needs to have a data server running on the test system as shown in Figure 4. The test control process can be launched from another PC anywhere on the network, attaching to the data server on the remote test system. The test operation and performance is the same as if the test were being executed locally. This capability has obvious advantages when testing and data acquisition must be made in areas that are inaccessible or may be hazardous to the test operator.

Remote test control allows the data acquisition hardware to be located close to the measurement sensors to reduce the impact that external noise would have on analog signals.

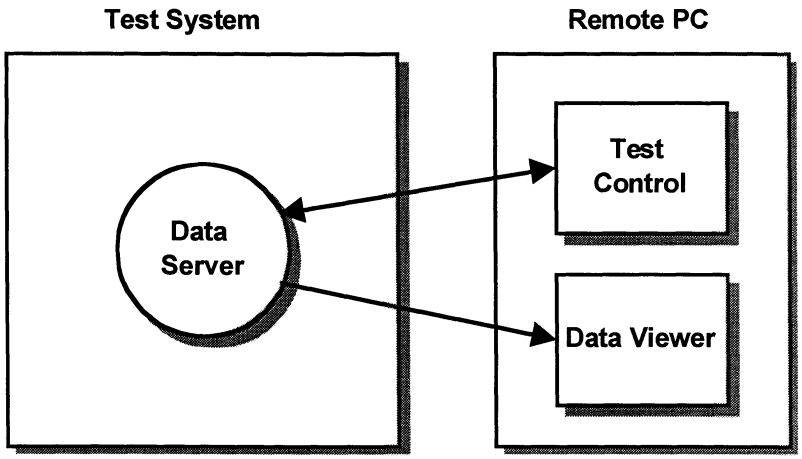

Figure 5. Remote Test Control

Test Automation using ActiveX

ActiveX provides a library of vibration test function calls to provide the ability for limited control of testing from an external program. Using ActiveX, the user can write applications to monitor and process real-time test data, make decisions, and execute test functions automatically. ActiveX also allows the user to bring together control of multiple test systems in a single test program to streamline complex or repetitive tests involving a variety of test systems. Thermal cycling, vibration, and functional testing can all be combined in a single test program. ActiveX can also be used to create a custom graphical user interface or embed vibration control into another ActiveX compliant application.

ActiveX components are self-registering and can be written in C++, Visual Basic, JAVA. They are also supported by higher-level instrument programming languages such as National Instruments LabView™.

The example in Figure 6 shows a simple LabView™ Virtual Instrument, which provides limited control and monitoring of a vibration control test from across the network. Control of the vibration testing equipment can be easily integrated into a LabView-based functional test program.

In the case of a large test facility,

the combination of ActiveX automation and remote data analysis and viewing software can be used to bring control and management of multiple test cells to a single control room.

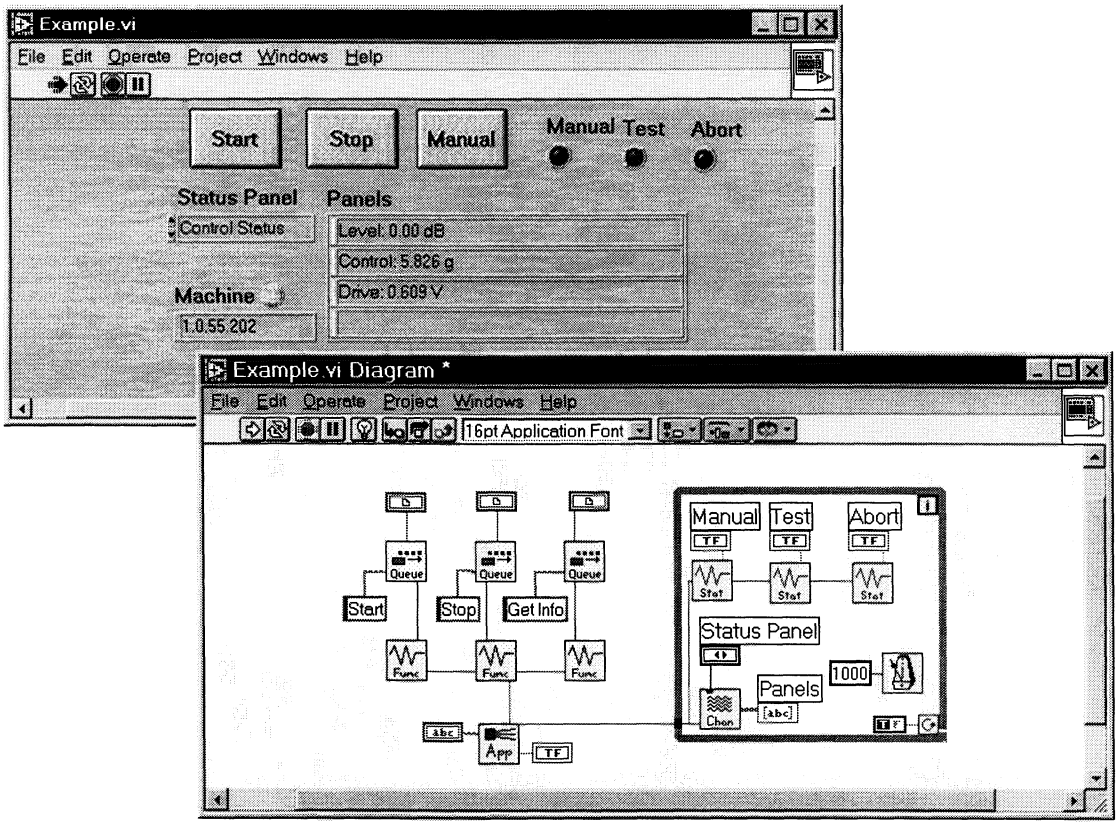

Figure 6. LabView™ ActiveX Example

Reporting Test Results

Because COM is the basis of much of the new code for the Windows 98 and Windows 2000 operating system, COM-based applications can have complete compatibility with other desktop applications.

Using COM technology, publishing of test results is enhanced as well. Test results can be embedded into Object Linking and Embedding (OLE) compliant documents. This provides a seamless integration into the Microsoft Windows environment.

Data plots may be embedded in electronic documents like word processors or spreadsheets by simple cutting and pasting. Once pasted the plot, and the data are embedded objects within the document. Unlike pictures, double clicking on the object in the document activates embedded object. The application that created the object is launched allowing the data to be further analyzed by the recipient of the report. OLE applications may be both embedded objects and containers for embedded documents. For example, images or video may be embedded in a vibration data analysis document, which may, in turn, be embedded in a word processing, or presentation document.

By creating electronic documents, test results may be quickly and easily transmitted over the Internet to anywhere in the world.

Summary

This paper has presented an approach to using industry standard network protocols in the test laboratory to automate testing and analysis of vibration data. Ethernet connectivity provides significant benefit over TTL, RS-232, and GPIB solutions.

A TCP/IP based data server architecture is described for remote test control, remote test monitoring and distributed data processing. This architecture provides inherent network capability and flexibility.

The Component Object Model, ActiveX and Object Linking and Embedding are explained. ActiveX can be used to communicate with the vibration test process to automate multiple test functions on different test systems.

Object Linking and Embedding provides seamless integration of vibration data analysis and report generation in the with desktop publishing applications in the Microsoft Windows environment. Creation of electronic documents allows test results to be quickly transmitted any where in the world.

References

1. Williams, Sara and Kindel, Charlie, (1994), "The Component Object Model: A Technical Overview," Microsoft Corporation
2. Microsoft Corporation, (1996) "DCOM Technical Overview"

THERMAL VACUUM TESTING OF THE TIMED SPACECRAFT INSIDE AN ENCLOSURE IN A WARM CHAMBER

Bruce D. Williams
Johns Hopkins University Applied Physics Laboratory

ABSTRACT

The Thermosphere-Ionoshpere-Mesosphere-Energetics and Dynamics (TIMED) spacecraft will be placed in a 625 km, 74.1 degree inclination low earth orbit, with four scientific instruments on board. The TIMED spacecraft will be launched from Vandenberg Air Force Base on a Delta II rocket. The TIMED spacecraft is a co-manifested launch with the JASON spacecraft (TOPEX follow-on). The TIMED spacecraft will be encapsulated in a Dual Payload Attach Fitting (DPAF), with the JASON spacecraft mounting to the top of the DPAF. The TIMED instruments are designed to characterize the Earth's upper atmosphere using visible, UV and IR sensors. Due to the stringent thermal requirements for the instruments, the spacecraft must maintain an anti-sun side, as well as a Nadir pointing side. These basic requirements, along with instrument field of view requirements have resulted in a very interesting spacecraft design and thermal vacuum testing.

The TIMED spacecraft was scheduled to be thermal vacuum tested in the large Space Environment Simulation Chamber (SES 290) at the Goddard Space Flight Center starting on Dec. 10, 1999. However, six weeks prior, during a verification of the newly upgraded thermal system in the SES chamber, a part within a steam heat exchange failed. The steam heat exchanger is used to flush the liquid nitrogen from the chamber cold walls and warm the walls back up to ambient temperature. Without the steam heat exchange, the cold wall could not be flooded for the next test, which was the TIMED spacecraft test. Within 6 weeks, the thermal shroud used for MSX spacecraft was fitted with cryo panels. The thermal shroud enclosure was used to surround the TIMED spacecraft providing the necessary environment for both thermal balance and thermal cycle testing. This paper will discuss this interesting test configuration, successful test results and correlation between model predictions and test data.

INTRODUCTION

The TIMED Spacecraft was successfully exposed to the thermal vacuum environment in the large vacuum chamber (No. 290, Space Environmental Simulation) at the Goddard Space Flight Center from December 10 to the 21, 1999 and again from February 10 to the 29, 2000. The first test was the thermal balance portion of the thermal environmental testing, which covered 6 flight-like cases, ranging from an extreme cold hard safe mode to a hot case with all redundant spacecraft components powered. Figure 1 shows the spacecraft in the launch stowed configuration for information, which is similar to the test setup. Figure 2 shows the profile followed for the thermal balance and thermal cycle portions of the test. Note that the spacecraft components and instruments experienced a cold turn-on during the test at the end of case 2. The goal of the thermal balance portion was to verify the thermal design of the spacecraft, as well as, provide the needed temperature data to correlate the spacecraft thermal math model. The test was completed on time and with no serious problems. The thermal systems on the spacecraft performed as designed, maintaining the spacecraft within acceptable temperature ranges throughout the test. The thermal environments applied to the spacecraft were more extreme than those predicted on orbit. The test validated the thermal stability and robustness of the spacecraft thermal design.

For background information on the TIMED spacecraft, the "SPACECRAFT DESCRIPTION", "SPACECRAFT THERMAL DESIGN REQUIREMENTS" AND "THERMAL DESIGN DESCRIPTION" sections of this paper are replicated here, in part, from the paper "The TIMED Spacecraft: A Thermal Design Perspective". [1]

SPACECRAFT DESCRIPTION

The TIMED spacecraft contains most of the usual hardware found on board any scientific spacecraft, which includes, attitude control systems, communications, power systems, thermal systems, main structure and more. The spacecraft has an irregular octagon shape, with small, permanent, corner panels and wide side panels. The small panels support the top deck during integration when the side panels are removed for package integration. The spacecraft is 46" across the flats of the octagon and over 100" tall. The coordinate system for the spacecraft is +Z to Nadir, +Y cold side (sun keep out zone) and +X to velocity vector, as shown in Figure 1.

The TIMED spacecraft structure has been designed to reject the heat generated inside the electronics boxes and instruments, as well as carry everything safely into space. The main structural components start with the payload adapter ring, which attaches to the DPAF, the launch vehicle interface for the TIMED mission. The +Z bottom deck, which is bolted to the adapter ring, is a machined aluminum deck with a round honeycomb inner panel. The machined deck transmits all the spacecraft loads down into the adapter ring, while the round deck supports the GUVI instrument on the bottom (outside) and the four reaction wheels on the top (inside). The four permanent corner panels, which support the –Z top deck, are aluminum honeycomb 1" thick with 0.015" thick aluminum facesheets. The four side panels and the round bottom deck have a similar construct to the corner panels. The top deck is also aluminum honeycomb, but is 2" thick. The ±X panels have a large opening to allow the two battery halves to be inserted in the spacecraft from the outside and mount flush with the panels. The +Y IEM panel is a short panel mounted just below the top deck, leaving open the lower portion of the +Y side for the SABER instrument to be installed. The –Y panel (sun side), is removable to allow access to the interior of the spacecraft.

Most electronics boxes on the TIMED spacecraft are mounted to the aluminum honeycomb side panels, on the inside, with the outside of the panels used at thermal radiators. However, there are several boxes mounted to the inside of the top and bottom decks, which have no direct connection to thermal radiators. Heat from these boxes must be transported to the back of the spacecraft (+Y side) for rejection to space. Table 1 contains all the hardware on the TIMED spacecraft by subsystem, including spacecraft mounting location, maximum and minimum orbit average heat dissipations, and operating and non-operating test temperature ranges. Several instrument components are conductively mounted to the spacecraft, as noted in the table. The heat from these boxes is absorbed by the spacecraft thermal design, as described below.

The TIMED spacecraft sports a 23" X 45" X 1.75" thick graphite epoxy optical bench, which supports two star trackers, four TIDI telescopes and two GPS antennas. The optical bench maintains arc-second level alignment between the trackers and the rest of the components on the bench over the expected operating temperature range. The optical bench is mounted on the top deck, along with the TIDI profiler, the SEE instrument and two S-band antennas.

SPACECRAFT THERMAL DESIGN REQUIREMENTS

Thermal design systems evolve from the requirements imposed on the thermal engineer by various subsystems throughout the spacecraft design and development process. One of the major thermal design drivers is the desired operating temperature range of electronic packages and sensors on board the spacecraft. Running a close second is the heat generated inside components, the location of these sources relative to the available heat sinking areas and the variation in the heat dissipation as a function of time, orbit and life of the mission. Mission requirements, like orbit altitude and inclination, dictate the orbital environment, which imposes solar and earth fluxes onto the spacecraft. Other requirements include, s/c geometry, resulting in radiator field of view (FOV) blockage, instrument FOV's (apertures and radiators), the availability of vacuum and space compatible materials, and many more secondary requirements.

Once the locations for all the electronics packages and instruments on the spacecraft have been initialized, the thermal designer can begin the process of thermal management. By using the thermal data for each package, as shown in Table 1, each spacecraft panel and deck can be analyzed to determine the feasibility of maintaining each package and interface within their required operating and non-operating ranges. Table 2

summarizes the temperature requirements imposed onto the TIMED spacecraft thermal design. The Thermal Control Design Range represents the maximum allowable analytically predicted temperatures, while the Package Test Range is the range over which the packages are tested in thermal vacuum conditions. The difference between the two ranges is the thermal margin, which is usually 10 °C, 5 °C on the cold end when heaters are used to control the minimum temperature. The most tightly controlled spacecraft component is the 50 Amp-hour, Nickel-Hydrogen battery. The battery consists of 22 Individual Pressure Vessels (IPV) divided into two halves of 11 cells each. The two halves are mounted on opposite sides of the spacecraft due to volume constraints. The 22 cells are connected in series to provide over 400 watts of power to the spacecraft during the 2.5 hour launch cycle and the 40 minute effective eclipse time during Beta 0 orbits. As shown in Table 2, the battery bulk temperature of each half must be maintained between –5 and +10 °C.

The thermal placement of packages on panels and decks is driven by several factors; the amount of heat the packages dissipate and the amount of environmental loading onto the local thermal radiators. Table 3 shows the predicted steady state orbit average heat dissipated from the packages inside the TIMED spacecraft per panel and deck, which must be rejected to space from available radiators. Note the hot and cold case differences. The asterisks in Table 3 indicate the components are thermally isolated from the spacecraft but are included for completeness.

In general, the spacecraft thermal design has been created primarily from the steady state orbit average conditions, as opposed to the orbit transient effects. However, the time-varying sources must be considered to verify the peak temperatures for each package. There are four sources of time varying heat generators on the spacecraft. The battery heat dissipation changes due to the charge, discharge and trickle charge nature of eclipsing spacecraft. The heat from the peak power tracker converter modules (PPTCM), which maximizes the power produced from the solar arrays during low beta angles, also varies with time. The power system electronics (PSE) exhibits the same characteristics as the PPTCM. The Integrated Electronics Module (IEM) contains the S-band transmitters, which are powered up to 20 minutes out of every 97-minute orbit.

THERMAL DESIGN DESCRIPTION

Now that the many requirements have been defined and the package locations have been organized on the spacecraft, the real thermal design must be completed. The thermal design philosophy is to reject the heat from the packages to space by creating the shortest possible path between the packages and a usable radiator. With this in mind, the packages on the inside of ± X panels and the +Y panel have direct connection to a viable radiator, which is the outside of each panel. These spacecraft panels are fairly self-contained, since they have their own radiators and heater systems, which will be discussed later. So the thermal management of these panels is fairly straightforward. However, several electronics boxes are mounted to both sides of the bottom and top decks.

The bottom deck has no direct access to usable radiator area due to external blockage. Thus heat pipes are employed as a conduction enhancement method. Four ammonia-filled heat pipes were embedded in the honeycomb round deck, under the reaction wheel brackets, to transport the 26 watts from the wheels to the +Y side adapter ring for rejection. The heat from the reaction wheels must be conducted down the support brackets and into the heat pipes for transfer to the edge of the round deck. The heat must then travel across the joint between the round deck and the machined deck and then down to the adapter ring. Both joints are bolted interfaces with numerous fasteners. This heat flow path is long, but usable, for the reaction wheel heat dissipation, made possible by the use of the heat pipes.

Similarly, the top deck supports several boxes that have no direct access to viable radiators. The top deck supports the two Inertial Reference Units (IRU or Gyros), which produces 23 watts each, but not simultaneously. The heat from the IRU's is conducted to the +Y IEM panel for rejection via a 0.062" thick aluminum doubler bonded between the IRU's and the top deck facesheet. Detailed analyses showed that the 0.015" aluminum facesheets and honeycomb core were not sufficient to maintain adequate margin on the IRU's. The other packages conductively mounted to the top deck can be maintained within operating range with just the aluminum honeycomb panel.

As briefly discussed above, the optical bench is mounted to the top deck of the spacecraft. A titanium kinematic mounting system thermally isolates the bench from the spacecraft. However, to minimize the bulk temperature change of the bench, the bottom of the bench is allowed to radiatively view the top deck, which is painted black to enhance radiation heat transfer. In other words, no MLI blanket is placed between the bench and the top deck. The top and sides of the bench are covered with MLI blankets to isolate the bench from the varying external environment. The thermal design of the bench is totally passive. No heaters or radiators are used to heat or cool the bench. The components mounted to the bench are thermally isolated from the bench or produce little or no heat, preventing local thermal distortions of the bench.

The two star trackers are mounted to the top of the optical bench via three titanium bi-pods and a spacecraft supplied graphite epoxy bracket. The trackers have their own thermal control design with radiators and heaters, including a Thermal Electric Cooler (TEC) to maintain the CCD below 20 °C.

Due to their tight temperature requirements, the two battery halves are thermally isolated from the spacecraft using G-10 isolators. The battery halves are individually wrapped with MLI blankets, radiatively isolating the battery from the spacecraft interior. The baseplate of each battery is used as a thermal radiator to reject the internal heat dissipation. Two redundant heater and electronic thermostat circuits were designed to, not only maintain the battery above –5 °C, but maintain the bulk temperature difference between the two halves below 3 °C. Mechanical thermostats are employed to protect both the hot and cold extremes of the battery, in case both electronic heater circuits should fail.

Most of the instruments are thermally isolated from the spacecraft with Titanium or G-10 mounting feet. The instrument interface temperatures must be maintained within operating and non-operating ranges in order to facilitate the thermal performance of the instruments. SABER and SEE are thermally isolated from the spacecraft, with their own thermal design systems to maintain the desired temperatures. The TIDI profiler and TIDI telescopes are also isolated from the spacecraft and have their own thermal control, but the TIDI electronics box is conductively mounted to the underside of the top deck near the IRU's. The GUVI SIS housing is also thermally isolated from the spacecraft bottom deck and thermally self-contained. However, the rest of the GUVI packages (HVPS, FPE 1 and 2, SIS E-box and ECU) are all conductively mounted to the spacecraft. Interesting enough, the GUVI SIS scan motor is actually thermally isolated from the SIS housing and the four watts generated by the motor is conducted to the spacecraft via a copper strap. The spacecraft thermal design adequately accommodates the heat from these packages and maintains the desired temperature ranges.

Now that the locations of all the thermal radiators have been specified and the heat rejection capability is adequate, the judicious use of heater power to maintain minimum temperatures can be investigated. MLI blankets are used, not only to isolate the spacecraft from the sun, like on the –Y panel, but also to close down the radiator area saving heater power. The electronics radiators on the ± X panels are designed to allow multiple boxes to use the same radiator area, as opposed to separate cutouts in the MLI blanket. By opening only one hole in the MLI, the MLI efficiency is increased, as well as the fabrication of the blanket simplified. The more efficient the MLI blankets, the smaller the heater power requirements. The hole in the MLI is sized to expose the appropriate amount of area to maintain the panel, and the attach packages, below the maximum operating temperature during the hot case and also, if possible, eliminate any operational heaters for the cold case. Thus, a passive thermal design has been created for most of the spacecraft components.

Survival (or non-operating) heaters and mechanical thermostats are employed to protect the spacecraft minimum operational temperatures. Each panel and deck, except the –Y panel, has a redundant set of heaters and thermostats, which are continuously powered, to provide 100% protection from exposure to minimum temperatures. The survival thermostat set points are staggered to allow both heater circuit relays to be enabled, with only one circuit drawing current. Should a failure occur in the thermal system, the redundant set of thermostats and heaters are available to protect the spacecraft. The star trackers have a similar redundant set of heater circuits, with thermostat set points below the predicted operating temperatures. The battery operational heater circuits are the only operational circuits used to control a spacecraft component. The instruments have both operational and survival heater circuits.

Selection of external material properties is typically the most difficult of the thermal hardware due to the lack of choices. Basically, there are paints, conversion coatings (anodizes), thin films (rigid and flexible) and MLI blankets. The spacecraft is using Silver Teflon as the radiator surface of choice and for the outer layer of the MLI blankets as well. Silver Teflon has a very low solar absorptivity, while maintaining a reasonably high emissivity. Silver Teflon can be applied at any time in the integration process, and with the use of a transfer adhesive, can easily be applied just prior to launch to maintain cleanliness. Where available radiator area is limited, like the two battery halves and +Y IEM radiators, 0.01" thick Silver Teflon is used to maximize the emissivity. Where radiator area is relatively more abundant, like on the ± X panels and on the outside of the adapter ring, 0.005" thick Silver Teflon is used. 0.002" thick Silver Teflon is used as the outer layer of the MLI blankets to minimize the outer layer temperature. In terms of paints, the S-Band antenna radomes, the GNS antenna ground planes and antenna elements, the back of the solar arrays and the solar array yoke assemblies are coated with A276 Aeroglaze white paint. SABER radiators and the TIDI profiler radiator and earth shade are covered with Z93-P white paint to take advantage of the paints very high emissivity and the relatively low absorptivity, especially at temperatures below –60 °C. SABER and the TIDI profiler radiators are in the sun keep out zone, so absorptivity is less a concern than the high emissivity. The SEE instrument radiator, the GUVI SIS housing radiator and two of the TIDI telescope sunshades are covered with 0.005" thick Silver Teflon.

The TIMED spacecraft is covered with MLI blankets to protect it from the sun and insulate it from the cold of deep space. The MLI layout consists of 18 inner layers of 0.001" thick Dacron mesh separating 0.0025" thick double aluminized Mylar. The inner most layer is a 0.002" thick Dacron sailcloth, which is very durable and flexible. In terms of the outer layer, there will actually be two. First, a 0.001" thick single aluminized Kapton sheet, Kapton side out, will be used as the outer layer for the initial MLI blanket construction and used up through the spacecraft thermal vacuum test. Then, the blankets will be removed and a 0.002" thick sheet of Silver Teflon will be attached to the outside of the blankets. This will preserve the Teflon from being damaged due to the normal handling that occurs during spacecraft integration and test. The blankets will be installed at the launch facility just prior to integration on the DPAF.

MLI blankets cover the outside of the top deck, underneath the SEE instrument and the TIDI profiler. Blankets are wrapped around the S-band antenna masts, leaving only the cylindrical radomes exposed on top. The Optical bench top and sides are covered with MLI, as mentioned above, and the GNS antennas masts are covered up to the bottom side of the ground planes. The SEE instrument, the TIDI profiler and the TIDI telescopes all have some MLI blankets. The –Y panel and the four corner panels are completely covered with MLI. The outside of the bottom deck, both inside and outside of the payload adapter ring, is also completely covered with MLI, except for some of the GUVI SIS housing. The SIS housing has an external radiator and a larger aperture door, which opens after launch. The ±X panels are covered with MLI blankets, with holes cut in the blankets to expose the radiator surfaces.

THERMAL VACUUM SHROUD TEST SETUP

The TIMED spacecraft was scheduled for testing inside the SES chamber at the GSFC in greenbelt, MD. The plan was to use an existing shroud enclosure developed for the Mid-course Surveillance Experiment (MSX) spacecraft to surround the top portion of the TIMED spacecraft. The enclosure looks like an eight-sided gazebo, were panels can be installed into the sides and top to provide a variety of environmental conditions. The initial shroud configuration consisted of a 66" tall lower frame section, an 81" upper frame section and a crown, or lid, on the top. The 66" section and the lower part of the 81" section were to be left open such that the spacecraft could have a large view to the chamber cold wall. An enclosure would be created around the top of the spacecraft, consisting of 17" tall cryo panels, which would be installed at the top of the 81" section, the crown, which contains 8 triangular cryo panels, plus a closeout MLI blanket between the bottom of the 17" panels and the spacecraft top deck. Figure 3 shows the proposed setup. This shroud arrangement would allow the components on the top deck to view a common environment inside the top enclosure, while the rest of the spacecraft would view the cold wall.

All the cryo panels were built and ready for integration into the shroud. However, six weeks prior, during a verification of the newly upgraded thermal system in the SES chamber, a part within a steam heat exchange failed. The steam heat exchanger is used to flush the liquid nitrogen from the chamber cold walls and warm the walls back up to ambient temperature. Without the steam heat exchange, the cold wall could not be flooded for the next test, which was the TIMED spacecraft test in just 6 short weeks. The steam heat exchanger would be out of commission for at least 10-12 weeks and the chamber would have to be requalified prior to the start of our test. We had a **BIG** problem.

After several days of discussions with the Goddard personnel, it was decided to fabricate enough cryo panels to completely enclose the TIMED spacecraft in the MSX shroud. Twelve 61" tall cryo panels would be installed in the 66" lower portion and the 81" upper portion would be populated with twelve 76" tall cryo panels. These cryo panels, once flooded with liquid nitrogen, would hopefully simulate the cold wall. Unfortunately, by installing the 76" panels in the upper section, the 17" panels originally designed for the top enclosure no longer fit. So, heater panels were installed on the inside of the 81" section, at the top, providing the sides for the top enclosure. (These replaced the 17" cryo panels mentioned above). Brackets were created that suspend the heater panels from the top of the 81" section. The back of the heater panels were covered with MLI to isolated them from the 76" panel directly behind. Figure 4 shows the final configuration used for the TIMED spacecraft test. Two of the 61" cryo panels were plumbed used flexible lines, which enable them to be opened, allowing personnel access inside the shroud without disconnecting any plumbing. (An excellent, timesaving idea). The rest of the cryo panels were hard plumbed together.

The shroud frames were constructed of C channels welded together into modular section that heater or cryo panels could be installed inside the open frames creating the enclosure. Normally, these C-channels are looking at the flooded cold wall of the chamber, and thus would be very cold relative to the spacecraft. Therefore, the channels could be neglected in the thermal balance condition. However, with the chamber cold wall not flooded with liquid nitrogen, these channels would be looking at a warm chamber wall. Special care had to be taken to blanket the inside of the channels, such that the spacecraft had no view to these channels. Aluminized Mylar "V's" were placed over each channel, on the inside of the enclosure, to minimize the view from s/c radiators to the channels. Additionally, an aluminized Mylar sheet was draped around the outside of the entire enclosure to block any direct view that the s/c might have to the warm wall and also reduce the liquid nitrogen usage in the shroud. Furthermore, MLI was also placed on the floor of the chamber to radiatively isolate the spacecraft from the warm payload table (chamber floor).

The sides and top of the spacecraft would now view the inside of the shroud enclosure. But, the bottom of the spacecraft must also be controlled. Thus, two cryo panels were installed on the bottom of the chamber floor inside the enclosure. Two, you ask? The first cryo panel was placed on top of Teflon block and on top of the floor MLI to provide a cold sink for the spacecraft test stand. This 47" diameter cryo panel also doubled as a cold trap for contamination collection during chamber warm up, since the normal cold trap was outside the shroud enclosure next to the chamber wall. The second cryo panel sat on top of the first panel and would provided the radiation environment for the GUVI instrument inside the spacecraft adapter ring. This cryo panel was designed with retractable legs to allow the spacecraft test stand to be install over the lowered cryo panel, then the panel would be raised into position just below the GUVI instrument.

One additional cold plate was required for the TIMED spacecraft test. The TIDI profiler required an liquid nitrogen panel to be placed a few inches from their radiator. To meet this requirement, a separate cryo panel was suspended from a C-channel that ran across the top of the 81" section. Therefore a total of 35 individual cryo panels and 8 heater panels were used to control to the TIMED spacecraft TV test.

The shroud enclosure and the other cryo panels created a total of 4 zones. The first zone is the top deck enclosure, which consists of the crown, the side heater panels and the top deck closeout MLI. The 61" cryo panels and the lower portion of the 76" Liquid Nitrogen-filled cryo panels provide the "cold wall" for the spacecraft sides. The GUVI cryo panel provides the environment for the GUVI Spectrograph. As shown in Figure 4, the top deck enclosure was controlled between –70 ^{o}C and +10 ^{o}C during different portions of the test. A thermal control unit (TCU) was used to control the crown temperatures, with the heater panels set to the same temperature as the

TCU. The GUVI cryo panel was controlled between –40 °C and +30 °C, by employing another stand-alone TCU. The TCU's flow gaseous nitrogen through the Crown and GUVI cryo panels controlling the panel temperatures . The fourth zone was the cryo panel in front of the TIDI profiler CCD radiator and it was set to –186 °C the entire test. This cryo panel is actually inside the top deck enclosure and had to be externally blanketed to prevent other top deck components from viewing this cold plate.

After several weeks of very busy activity by APL and Goddard personnel, the shroud was finally assembled, plumbed and leak checked outside the chamber. All the heater panels were installed and the thermocouples integrated onto the shrouds and panels. MLI blankets were installed on the inside of the channels, with the "V's" to be installed later. Once the two cryo panel that resting on the chamber floor were installed, the enclosure was placed into the chamber, without the spacecraft, for a verification of the shroud thermal design. During the shroud thermal verification, several things became obvious. It appeared that the design would work to provide the necessary environments. But, the 61" cryo panels were being starved of liquid nitrogen and thus did not reach –186 °C as expected. By quickly replumbing the panels to allow two fluid circuits instead of one, the system could completely flood. Now the shroud was ready for the spacecraft to arrive.

SPACECRAFT TV PREPARATIONS

At the same time that the shroud was being configured and assembled, the spacecraft was in the GSFC cleanroom being prepared for the TV test. The first step was to remove the solar arrays from the spacecraft since the stowed arrays blocked the spacecraft and battery thermal radiators. A heater plate was bolted to the solar array interface to the spacecraft to provide the predicted solar array heat loading into the solar array drive motor. 150 Thermocouples were installed on the spacecraft to monitor the critical temperatures during the testing. The four S-band antennas were enclosed in hat couplers allowing RF communication during all testing phases. Heaters and MLI blankets were installed on the bottom (NADIR) two hat couplers to protect them against the cold shroud temperatures. The top two hat couplers did not require supplemental heaters. The two star tracker stimulators were removed for the thermal balance test to insure a proper thermal balance of the trackers and the optical bench. The GNS antenna hat couplers were also remove for thermal balance testing.

Kapton themofoil heaters were used to control the temperature of the spacecraft bus, control the test stand, simulate the environmental heating rates and provide zero flux controls at critical interfaces. Some of the heaters where placed on the outside of the spacecraft, on the honeycomb panels, in place of the thermal radiators. These heaters acted as the radiator surfaces, as well as, provide the ability to apply the expected orbital loading directly to the spacecraft, as opposed to using Infrared lamps. The +/- X spacecraft panels, the two battery half radiators and the +Y IEM panel were covered with heaters, which double as radiators. Heaters where installed on the inside of the top and bottom decks, on the inside the payload adapter fitting (PAF) and on the test stand. A total of 17 flux heater circuits where used to apply a given heat load to the spacecraft, while 14 temperature control heater circuits where used to either set a boundary temperature or interface temperature or establish zero heat flow (Zero-Q) interfaces.

The zero-Q interfaces were established to zero out the heat flow across certain spacecraft interfaces in order to obtain a good thermal balance condition. By placing heaters on each side of an interface, the temperature across the interface can be controlled, assuming there is a local radiator available to cool down the interfaces. The top edge of the stand, which was painted white, was left open to view the cold shroud to act as a radiator. Heaters where placed on the top of the stand and on the inside of the spacecraft adapter ring (the dummy PAF) to control the temperatures. Furthermore, heaters were place on each of the eight stand legs, at the bottom, to control the bottom of the stand relative to the top of the stand. The temperature difference across the interface between the bottom of the dummy PAF and the top of the stand was held to less that 0.5 C throughout the thermal balance portion. Other than the top edge of the stand, the rest of the stand was blanketed to minimize the heater power required to heater the stand. Both the inside and outside of the dummy PAF were also blanketed. Additionally, four wire bundles were zero-Q'd as the bundles came off of the spacecraft bottom deck. All the heaters on the stand were installed in the cleanroom, while the wire bundle heaters were installed on the spacecraft inside the chamber.

Now that all the heaters and thermocouples where installed on the spacecraft, the MLI blankets could be installed around the spacecraft. Finally a bag was placed over the entire spacecraft to maintain cleanliness during the trip over to the chamber.

SPACECRAFT INSTALLATION INTO TV CHAMBER

To install the spacecraft into the chamber, the chamber top was removed, and then the crown was removed from the top of the shroud. The TIDI cold plate and support beam were unbolted and set aside. The test stand, on which the spacecraft rests, was lowered into the chamber and placed on four large G-10 blocks to isolated the stand from the chamber floor. The stand was clamped to the floor across the G-10 blocks. Small holes were cut in the floor MLI to accommodate the clamps. The spacecraft was then lowered into the chamber and onto the stand with 6 small G-10 blocks used to isolate the spacecraft from the stand. Once the spacecraft was securely bolted to the test stand, the TIDI Profiler cryo panel was install and finally the crown section was reinstall, completing the enclosure. After the chamber top was closed and particle counts where taken to verify cleanliness levels, the bag used to protect the spacecraft from contamination was removed. Finally, the drape that covered the outside of the entire enclosure was put back in place, leaving a flap open to access the inside of the enclosure through the two movable 61" panels.

Now that the access to the spacecraft was available by removing the contamination bag, the final thermal preparations could begin. The GUVI cryo panel was raised up to close off the top of the test stand. MLI blankets where installed around the edge of the GUVI cryo panel over to the top of the stand providing an enclosure inside the spacecraft adapter ring. Furthermore, the stand legs and base were wrapped in MLI blankets. All spacecraft thermocouples and heater circuits were hooked up and checked out. Note that the shroud heaters, thermocouples and fluid circuits were checked out during the chamber/shroud verification test. The top deck enclosure closeout MLI was one of the last pieces to be installed, prior to the start of the TV test. Once the two 61" cryo panels were closed and the outer drape tape closed, the chamber door could be close in preparation for pump down.

THERMAL BALANCE TESTING

Figure 2 shows the thermal balance and thermal cycle temperature profile to which the spacecraft was exposed. The thermal balance portion of the test lasted for 9 days, while the thermal cycle portion lasted for 19 days. Six different thermal balance cases where performed attempting to verify the spacecraft thermal design system, as well as, provide valuable data for the model correlation effort. The test began with the start of the chamber turbo pumps, at which time the spacecraft was configured for a launch simulation. As the chamber pumped down simulating the assent of the spacecraft, the on-line battery provided all the electrical power for the spacecraft components. Two and half hours after the start of pump down, the battery was recharged then taken off-line and then the spacecraft was configured for the first balance case.

A cold survival case, Case 1, was performed which configured the spacecraft into a cold safe mode condition with the absolute minimum electronics operating. The power supplies, which provide the electrical power to the spacecraft in the TV chamber, were adjusted to provide the minimum bus voltage of 24.5 Volts. The instrument and spacecraft survival heater circuits were activated to verify the ability of the thermal system to protect the spacecraft during worst case orbit conditions. The test showed that the thermal design successfully maintained all components within their non-operating ranges if off, and for those components still operating, within their operating ranges. It should be noted that this test represents a last-ditch condition on the spacecraft to recover from a low voltage condition, which should never happen on orbit. But, the spacecraft was designed and now tested to that condition.

A few anomalies occurred during the balance test, as occurs during any test, and they include a lower than expected heat dissipation by the spacecraft electronics boxes in the order of 40 Watts. This lower than expected heat resulted in the spacecraft survival heaters consuming more than their predicted power in order to maintain minimum temperatures. In order to push the spacecraft thermal system, Case 1 intentionally set the spacecraft bus voltage to 24.5 Volts. By combining the low bus voltage, the minimum predicted environmental

heat loads and the lower than expected box heat dissipations, several survival thermostats ran at 100% duty cycle. No critical minimum temperatures were exceeded and the survival heaters maintained the bus temperatures. Another point that should be stated is that the test environment does not provide the solar loading on the MLI blankets, which allowed the spacecraft to cool down further than actual on-orbit conditions. This test provided a great deal of confidence in the spacecraft's ability to thermally survival on-orbit.

The second thermal balance condition, Case 2, was another cold survival condition, but less severe than Case 1, in that the bus voltage was raised to 26.3 Volts, one AIU turned off and one IEM was brought on line. This condition simulates what happens during an attitude safe mode, as opposed to a low voltage safe mode. The test case showed the appropriate decrease in heater duty cycles occurred associated with the voltage increase and the IEM heat generation. Table 4 shows a summary off all internal heat dissipated, the environmental heat load applied and the flight heater power applied to the spacecraft during each test case.

Case 3 represents the first full spacecraft operating condition, with the instruments coming on-line for the first time. The bus voltage was set to 29 volts. The environmental load applied was consistent with the predicted absorbed heat based on Beginning of Life (BOL) optical properties for the external surfaces of the spacecraft. Additionally, the battery has been off-line, in trickle charge, since shortly after the beginning of the test, which produces only minimal amounts of internal heat.

Case 4 was similar to Case 3 in the components that were powered, but the environment was raised to represent the End of Life (EOL) conditions and the hottest predicted environmental heat loading. Furthermore, the battery was brought on-line for the first time since the launch simulation at the beginning of the test, which resulted in the bus voltage being clamped to the battery voltage of 33 Volts. This balance case verified that an adequate amount of radiator was exposed to allow the rejection of both the internal heat dissipation and the absorbed environmental loading.

The goal for Case 6 was to establish a flight-like orbit simulation by varying the power input into the spacecraft from the solar array simulator. A 90-minute orbit simulation was created that cycled the power into the power system to determine the thermal effect on the spacecraft bus. The Battery, PPTCM and the PSE were directly effected by the varying input power. Additionally, the transmitter in the IEM was cycled once per orbit, on for 20 minutes, off for 70 minutes, to see the transient effects on the bus. The results showed a 4 ^{o}C peak to peak oscillation on the PPTCM, which is smaller than expected. This result makes sense based on the reduced amount of heat actually dissipated from PPTCM observed in earlier cases. The same environment loading and spacecraft load were maintained as in case 4, except for those transient components stated.

Case 5 provided the maximum steady state hot case conditions for the spacecraft bus. The predicted on-orbit environmental loading was increased by 20%, as well as all redundant units powered, to create the worst hot case for the spacecraft. Additionally, one transmitter was turned on for the entire test case to provide the maximum IEM dissipation. Unfortunately, the second Inertial Reference Unit (IRU's or Gyros), was inadvertently turned off half way through the case and thus the maximum temperatures were not obtained. But, the trend showed that both IRU's would have operated fine in the hot test condition. Note in Table 4 the 627 Watts of total heat load on the spacecraft bus for this case versus the 382 Watts associated with Case 1. The test did show that enough radiator area is exposed on the spacecraft to reject the internal heat, as well as more than the expected environmental loading. The 20% increase should allow for the on-orbit MLI heat loading not tested.

The thermal balance testing provide a very good dry run for the on orbit conditions in terms of component temperature limits. The balance test pushed the extremes of many components right to their yellow limits and sometimes, almost to their red limit. For example, the GUVI ECU, during the cold survival case saw –33 °C, with a survival test limit of –34 °C. The GUVI personnel saw this as no risk to the box, so no action was taken. This was one result of the lower heat dissipation from spacecraft boxes. But, the results of the test forced a hard look at all the temperature limits to see if they really apply.

The thermal balance test revealed that the spacecraft thermal system could adequately protect the spacecraft subsystem, especially given the fact that the internal heat dissipation was 40 Watts less that expected.

Furthermore, the test showed that enough radiator is available to reject the environmental and internal heat in the hottest conditions. The thermal balance portion was completed ahead of schedule, just in time for the Christmas holidays. Once the test was completed and the chamber brought back to ambient conditions, the spacecraft was configured over the next few days for the thermal cycling test. The Star Tracker Simulators were installed on the end of the sunshades and G-negated to minimize the loading on the Trackers. The GPS hat couplers were install to provide signals to the GPS navigation system. The SEE and GUVI instruments installed stimulator lamps facing their apertures.

THERMAL CYCLE TESTING

After the Y2K NASA facility shutdown, the TIMED spacecraft was powered up and checked out in preparation for the start of the cycling portion. A repeat of the launch simulation was conducted during chamber pump down to again verify operation of components during the "launch assent". The thermal cycle portion of the thermal testing sailed through with very few thermal glitches. The spacecraft bus was cycled 4 times between –15 °C and +30 °C, with most components performing as expected. The exceptions, and there are always exceptions, include the Star Trackers Thermal Electric Cooler set points which were 3, 20 and 42 °C, instead of the 0, 20 and 30 °C as expected. Furthermore, the flight PT1000 temperature sensor on the TIDI Telescope #2 show an inaccurate reading at least once during one of the cold transitions.

The thermal shrouds and heater circuits were used to cycle the spacecraft over the desired temperature ranges. A majority of the flux heater circuits were converted over to temperature control circuits for ease of operation during the cycle portion. This allowed almost a hands-off control for the spacecraft temperatures. The cycle portion was completed on schedule.

THERMAL VACUUM TESTING TEMPERATURE RESULTS AND MODEL CORRELATION

Upon completion of the thermal balance portion of the TV testing, the correlation effort was started. Figures 5-9 show the actual temperature data as compared to the correlated model steady state temperature results. The correlation effort was concluded when all the spacecraft test temperatures matched the model predictions within +/- 3 °C, while the heat balance for each case was well within 10%. The figures illustrate the close relationship between the model results and test data. Note the –30 to +30 °C temperature range for the spacecraft panels. Figure 9 shows the battery radiator temperature comparison, with the temperature range between –13 and -2 °C as desired. The correlated model will be used to predict on-orbit temperatures for the TIMED spacecraft for comparison against actual flight data.

CONCLUSION

In general, the thermal vacuum testing at GSFC was very successful. The few anomalies experienced during the test resulted in several actions. First, one additional flight heater was added to the +X and –X survival heater circuits to insure proper heater duty cycles on-orbit. And secondly, after a thorough investigation, the TIMED team could not find any apparent problem with the TIDI Telescope flight temperature sensor or associated harness.

The GSFC chamber facility crews need to be recognized for their hard work and dedication to the testing efforts. I'd further like to thank the other APL thermal engineers and APL test personnel who helped make the test such a success. Everything went as planned largely due to people who kept the ball rolling, especially during the extremely hazardous weather conditions we experienced. Thanks again for all the help. The TIMED spacecraft is now ready for launch on a Delta II rocket, which is scheduled for later February 2001, along with the JASON Spacecraft. I look for to an exciting launch.

REFERENCES

1. Bruce Williams: *The TIMED Spacecraft: A Thermal Design Perspective*, 29th International Conference on Environmental Systems, July 12-15, 1999, 1999-01-2133.

Table 1
TIMED Spacecraft Component Locations, Heat Dissipation and Test Temperature Ranges

Subsystem and Components	Location on spacecraft	Beta Angle Max & Min Orbit Average Heat Dissipation (W)	Operating Test Range (°C)	Non-operating Test Range (°C)
Power System				
Peak Power Tracker Converter Modules (PPTCM), 2 units	1 on +X panel, in 1 on –X panel, in	46.7/15.5	-29/+55	-34/+60
Power System Electronics & Distribution Unit (PSE/DU)	+X panel, in	28.3/16.7	-29/+55	-34/+60
Fuse Junction Boxes, 2 units	1 on +X panel, in 1 on –X panel, in	1	-29/+55	-34/+60
64.6 sq. ft. solar array wings, 2 wings	1 on +X side, out 1 on -X side, out	0	-80/+100	-80/+100
Solar array drive motors, 2 units	1 on +X side, out 1 on -X side, out	0	-29/+55	-34/+60
Solar array drive control unit	-Z deck, in	1	-29/+55	-34/+60
22 cell 50 Amp-Hr Ni-H Battery (2 X 11 cell halves)	1 on +X panel, in 1 on –X panel, in	40/16	-10/+20	-20/+30
Attitude Control System				
Star Tracker, 2 units, TEC on for max.	Optical Bench, out	16.31/12.31	-30/+50	-40/+60
Attitude Interface Units (AIU), 2 units in Chassis (Both units on for max.)	+X panel, in	22.4/11.2	-29/+55	-34/+60
Attitude Flight Computers (AFC), 2 units stacked (Both units on for max.)	-X panel, in	14.64/7.32	-29/+55	-34/+60
Inertial Reference Units (IRU), 2 units	-Z deck, in	23	-30/+70	-40/+75
Momentum Reaction Wheels, 4 units	+Z deck, in	26	-23/+55	-34/+60
Torque Rods, 3 units	-Y, +X & Corner Panel	3	-40/+60	-50/+80
Sun sensors, 4 units	2 on –Y panel 2 on +Y corners	0	-100/+100	-100/+100
Magnetometers, 2 units	+Z deck, out	0	-40/+60	-50/+80
Magnetometer electronics, 2 units	Corner panel, in	1.96	-40/+60	-50/+80
C&DH System				
S-Band Antennas, 2 Zenith and 2 Nadir units	-Z deck, out +Z deck, out	0	-100/+75	-100/+75
GPS Antennas, 2 units	Optical Bench	0	-100/+75	-100/+75
Integrated Electronics Module (IEM), 2 units	+Y panel, in	94.95/65.65	-29/+55	-34/+60
Remote Interface Units (RIU), 6 units	Scattered around	3.96	-29/+55	-34/+60

Table 2
TIMED Spacecraft Temperature Requirements Summary

Location	Thermal Control Design Ranges		Package Test Ranges	
	Operating Temperature (°C)	Non-Operating Temperature (°C)	Operating Temperature (°C)	Non-Operating Temperature (°C)
+X Panel	-14 to +45	-19 to +50	-24 to +55	-29 to +60
-Y Panel	-19 to +45	-24 to +50	-29 to +55	-34 to +60
-X Panel	-19 to +45	-24 to +50	-29 to +55	-34 to +60
+Y Panel (@ IEM)	-19 to +45	-24 to +50	-29 to +55	-34 to +60
-Z Deck (@ IRU)	-20 to +60	-30 to +65	-30 to +70	-40 to +75
+Z Deck	-13 to +45	-19 to +50	-23 to +55	-29 to +60
Optical bench	-5 to +35	-20 to +30	-15 to +45	-30 to +40
Star Trackers	-25 to +40	-30 to +45	-30 to +50	-35 to +55
Batteries	-5 to +10	-15 to +20	-10 to +20	-20 to +30
Solar arrays	-70 to +90	-70 to +90	-80 to +100	-80 to +100
Antenna	-90 to +65	-90 to +65	-100 to +75	-100 to +75

Table 3
TIMED Spacecraft Internal Heat Dissipation Summary

Component	Hot Case Internal Heat Diss. Beta=0 (W)	Hot Case Internal Heat Diss. Beta=90 (W)	Cold Case Internal Heat Diss. Beta=0 (W)	Cold Case Internal Heat Diss. Beta=90 (W)
+X Panel	75.1	58.2	48.9	35.7
-Y Panel	1.0	1.0	0.0	0.0
-X Panel	52.9	37.3	42.0	29.9
+Y Panel	87.9	87.9	62.1	62.1
+Z Deck	32.6	32.6	32.6	32.6
-Z Deck	32.2	32.2	32.2	32.2
Corner Panels	3.3	3.3	2.3	2.3
Optical bench	1.3	1.3	1.3	1.3
Star Trackers (2)*	24.6	24.6	24.6	24.6
Battery Halves (2)*	33.0	16.0	33.0	16.0
GUVI SIS Motor	4.0	4.0	4.0	4.0
GUVI SIS*	0.4	0.4	0.2	0.2
SABER*	58.7	58.4	58.6	59.2
SEE*	16.4	16.4	12.5	12.5
TIDI telescopes*	1.2	1.2	1.2	1.2
TIDI profiler*	0.6	0.6	0.5	0.5
Total Heat	419.9	370.1	350.8	309.1

*Components are thermally isolated from spacecraft.

Table 4
TIMED Spacecraft Test Heat Summary

Internal Heat	Case 1	Case 2	Case 3	Case 4	Case 5	Case 6
+X Bat.	6.13	6.58	7.26	8.25	8.31	8.25
-X Bat	6.13	6.58	7.26	8.25	8.31	8.25
+X Panel	44.29	34.42	35.30	36.55	59.07	36.36
-X Panel	6.13	6.58	23.94	31.93	38.80	32.16
+Y Panel	23.20	47.93	49.37	51.79	97.00	51.49
Adapter & +Z deck	14.37	16.22	24.32	28.22	29.70	27.82
-Z deck	22.27	22.76	37.37	39.15	40.41	38.94
Total	122.51	141.08	184.80	204.15	281.60	203.27
Flight Heaters						
+X Bat.	30.66	25.90	27.12	9.11	0.00	5.38
-X Bat	30.66	25.90	27.12	9.11	0.00	5.38
+X Panel	10.26	23.11	13.40	0.00	0.00	0.00
-X Panel	30.78	30.97	6.53	0.00	0.00	0.00
+Y Panel	2.52	0.00	0.00	0.00	0.00	0.00
Adapter & +Z deck	17.65	19.88	0.00	0.00	0.00	0.00
-Z deck	13.65	11.56	0.00	0.00	0.00	0.00
Total	136.19	137.33	74.17	18.22	0.00	10.75
Internal and Flight Heater Total	258.70	278.41	258.98	222.36	281.60	214.03
Test Heater						
+X Bat.	24.03	24.14	24.15	46.60	57.96	46.63
-X Bat	24.30	24.32	24.26	47.14	58.66	47.14
+X Panel	17.97	15.30	22.47	64.24	78.38	64.75
-X Panel	13.42	13.40	16.90	43.44	52.19	43.68
+Y Panel	16.82	16.98	14.25	21.34	25.13	20.91
Adapter & +Z deck	26.92	26.96	29.96	56.29	73.45	56.24
-Z deck	0.00	0.00	0.00	0.00	0.00	0.00
Test Heater Total	123.46	121.11	131.98	279.04	345.78	279.34
Int/Flt/Test Heater Totals	382.16	399.52	390.95	501.41	627.38	493.37

Figure 2
TIMED S/C THERMAL VACUUM TEST PROFILE

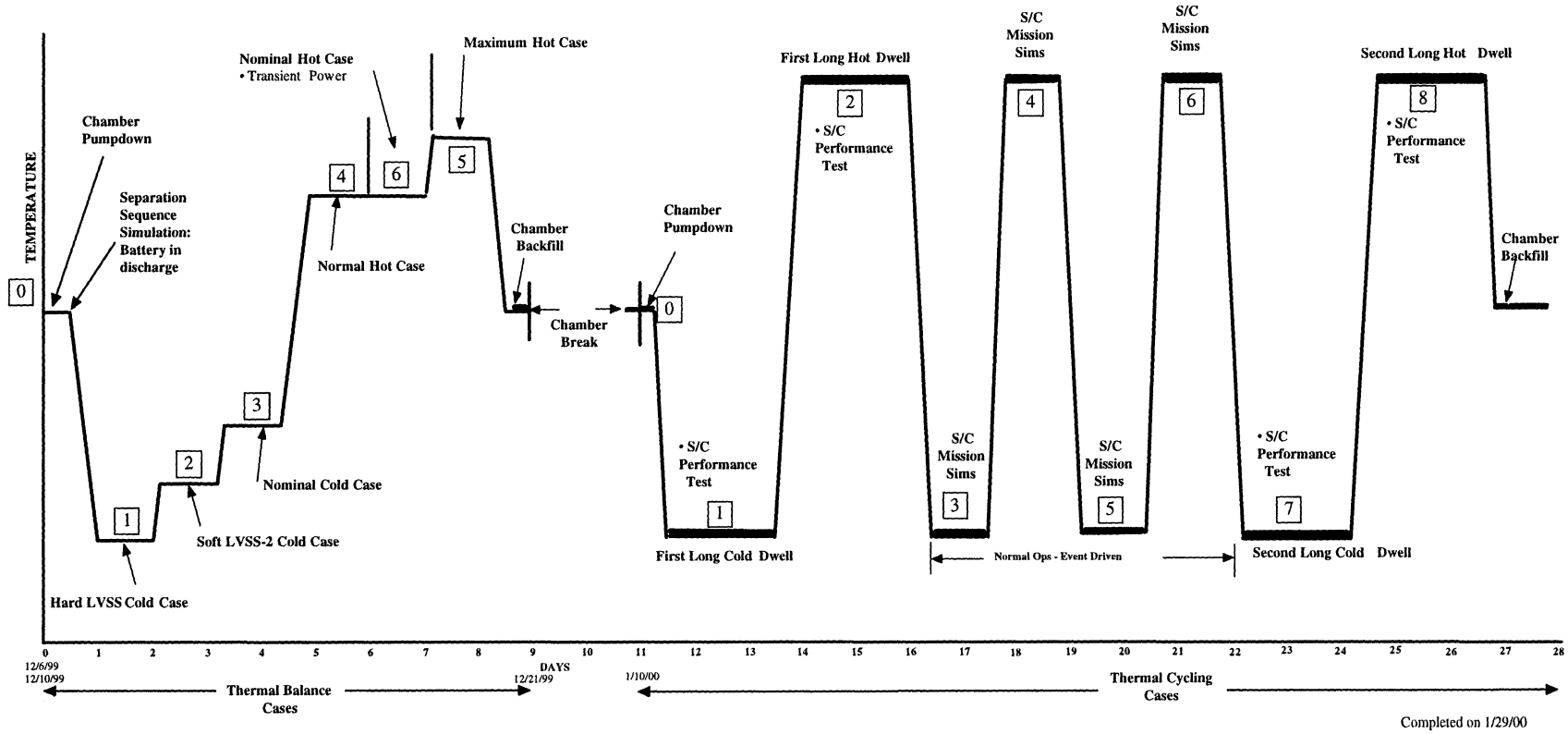

Completed on 1/29/00

Figure 1
TIMED Spacecraft in Stowed Configuration

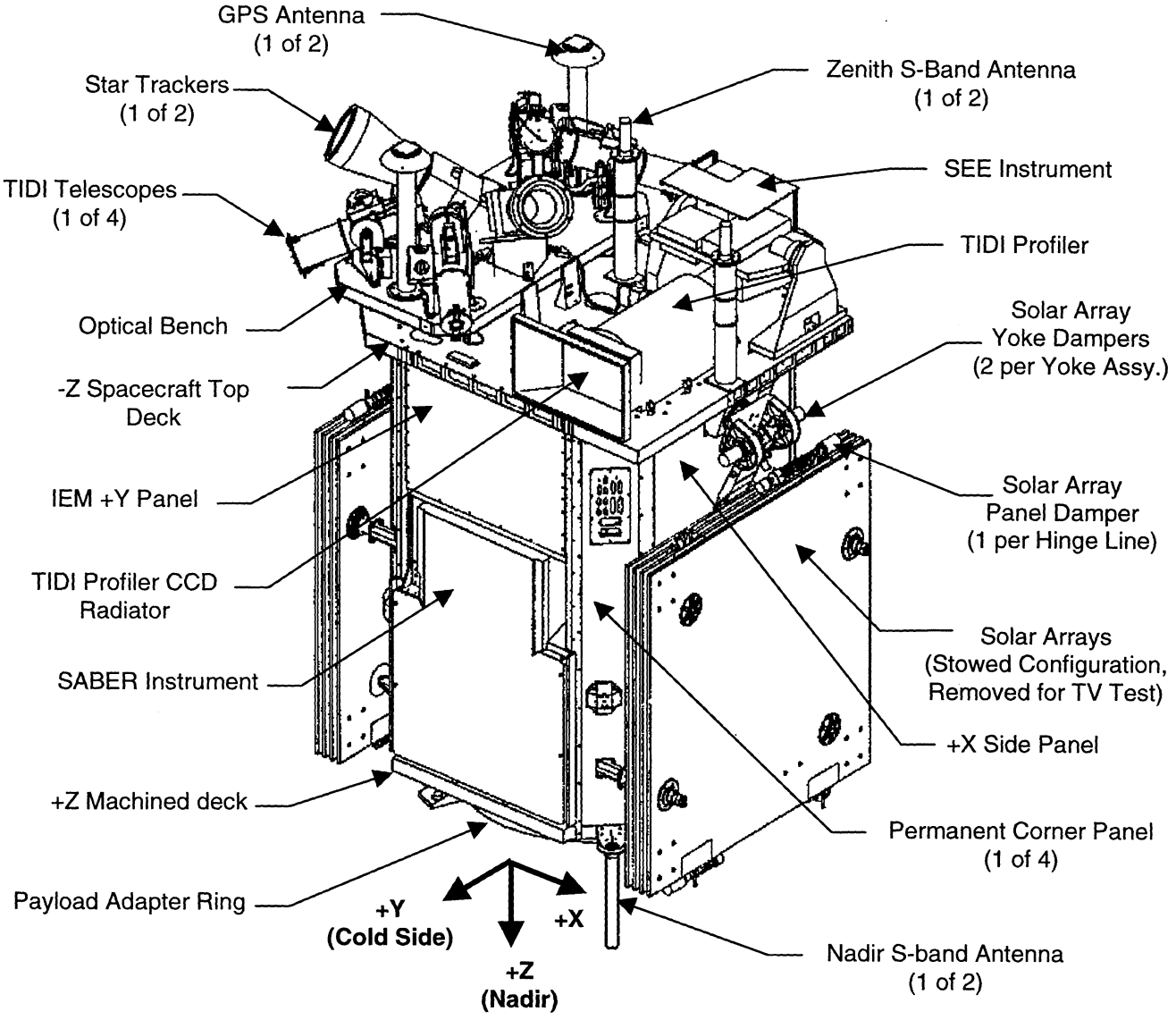

Figure 3
TIMED Spacecraft Initial TV Test Configuration
(Top Cavity Only with Open frames)

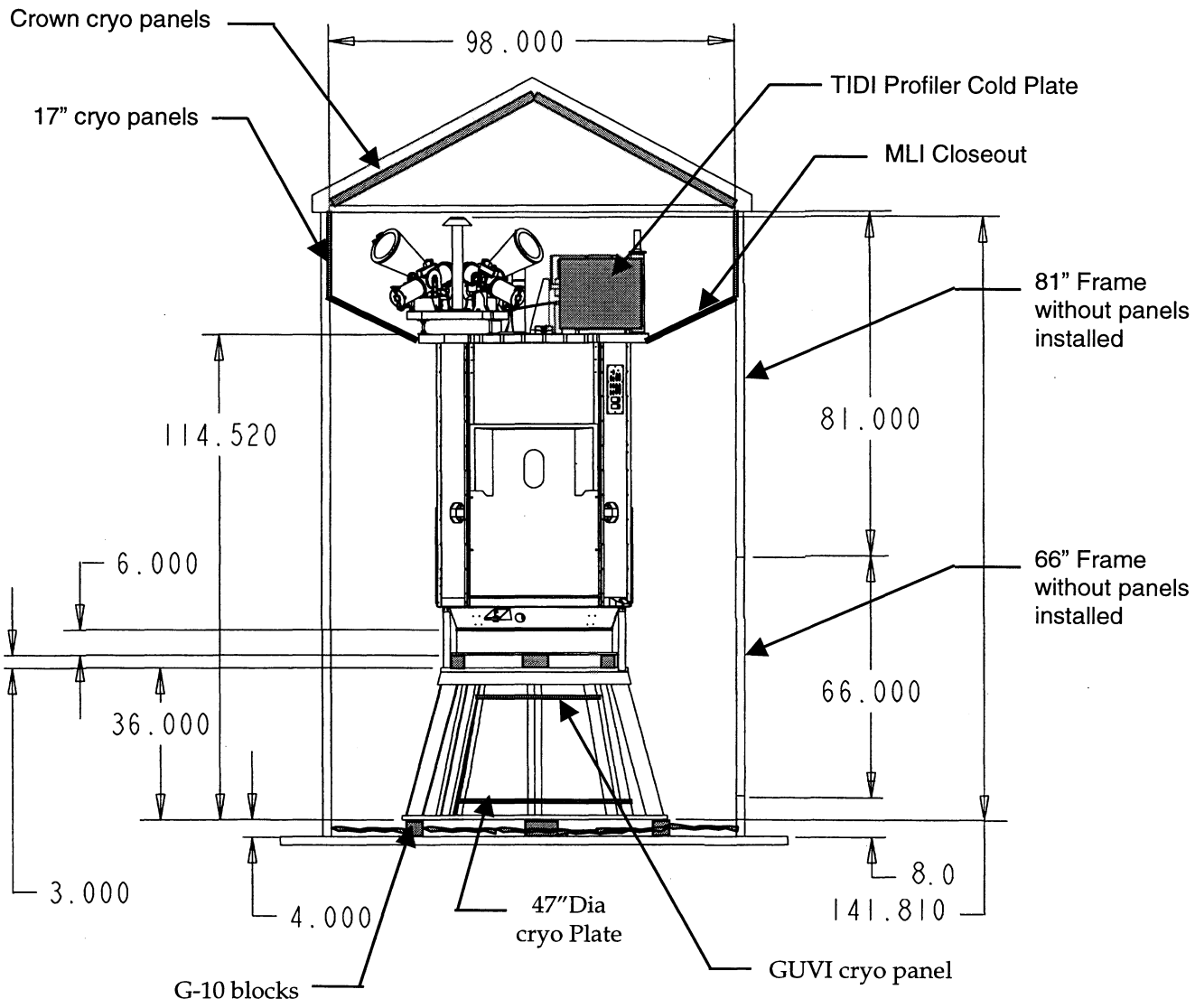

Figure 4
TIMED Spacecraft Final TV Test Configuration
(Top Cavity with Cryo Panels in frames)

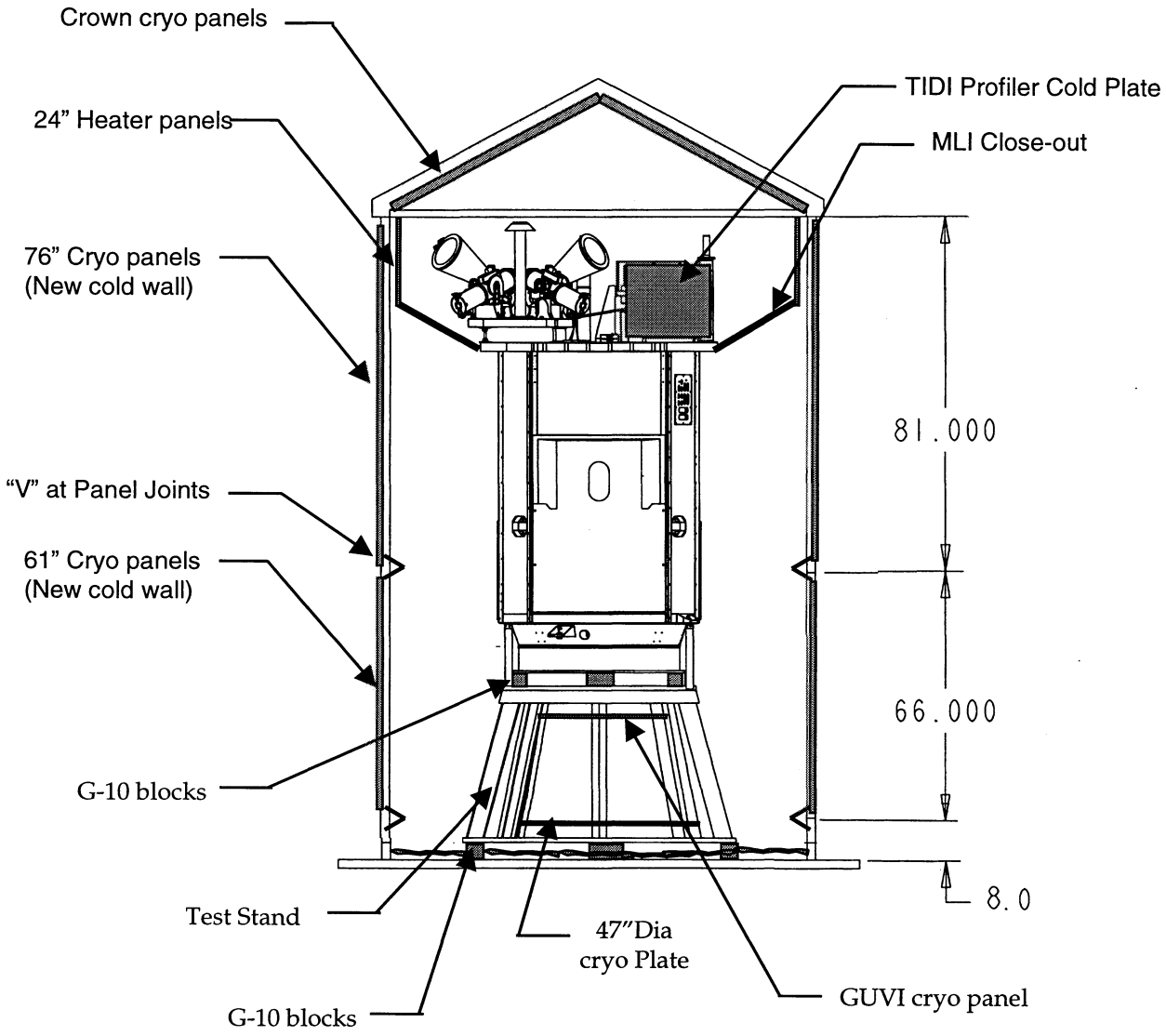

Figure 5
S/C Thermal Balance Data Versus Model Predictions
+Z Deck and Adapter Ring

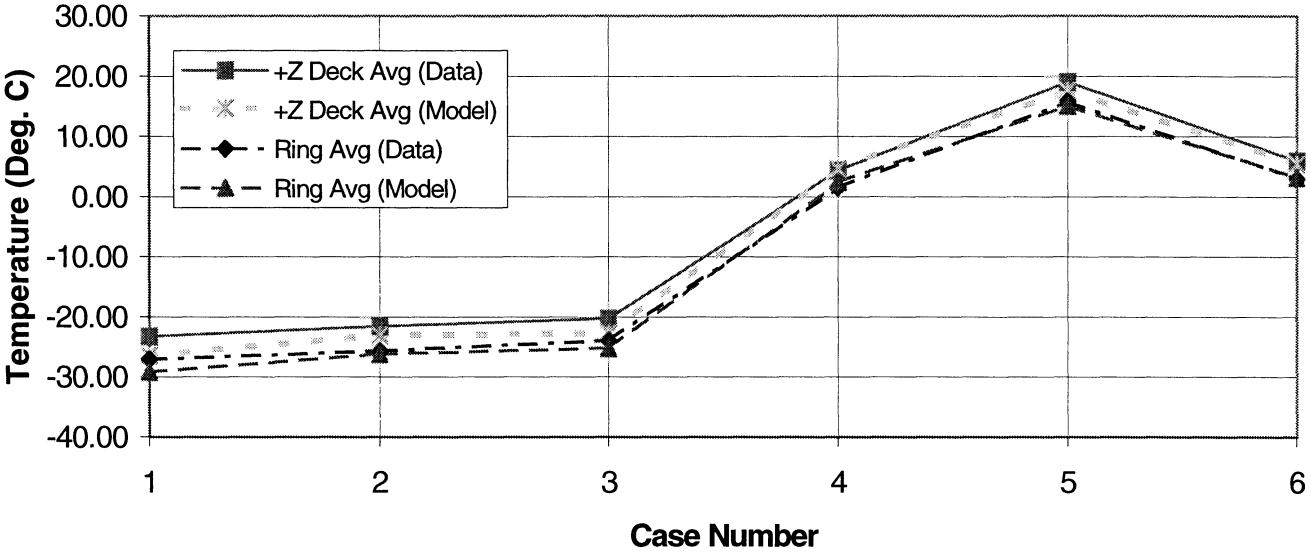

Figure 6
S/C Thermal Balance Data Versus Model Predictions
+/- X Panels

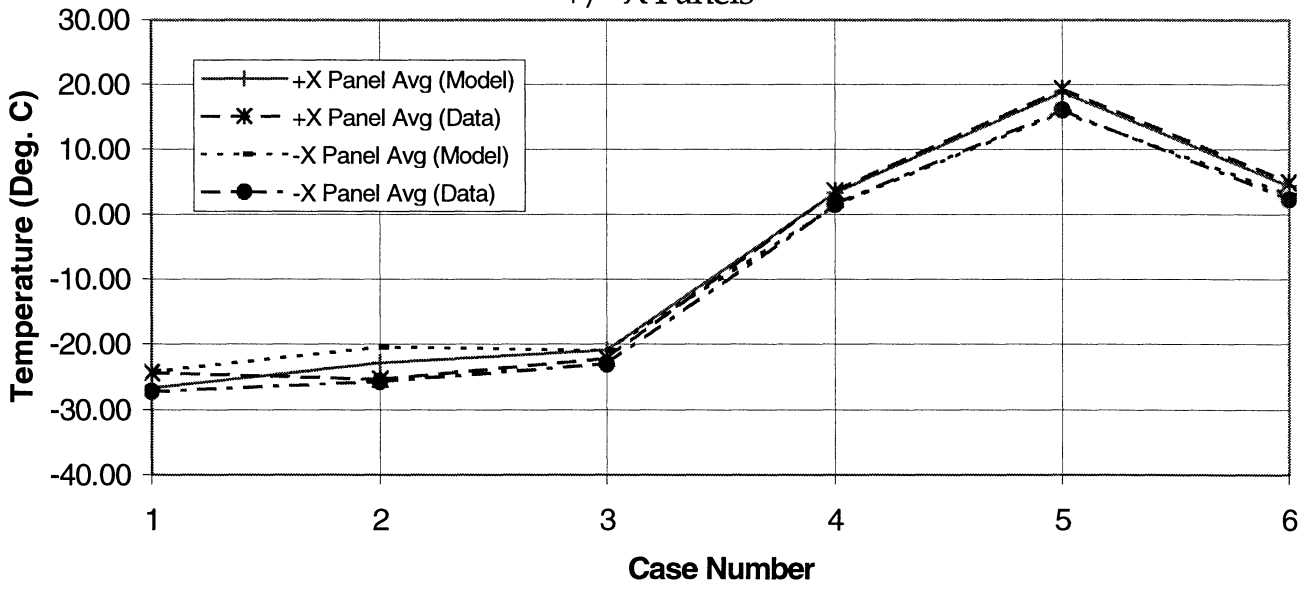

Figure 7
S/C Thermal Balance Data Versus Model Predictions
-Z deck and Optical Bench

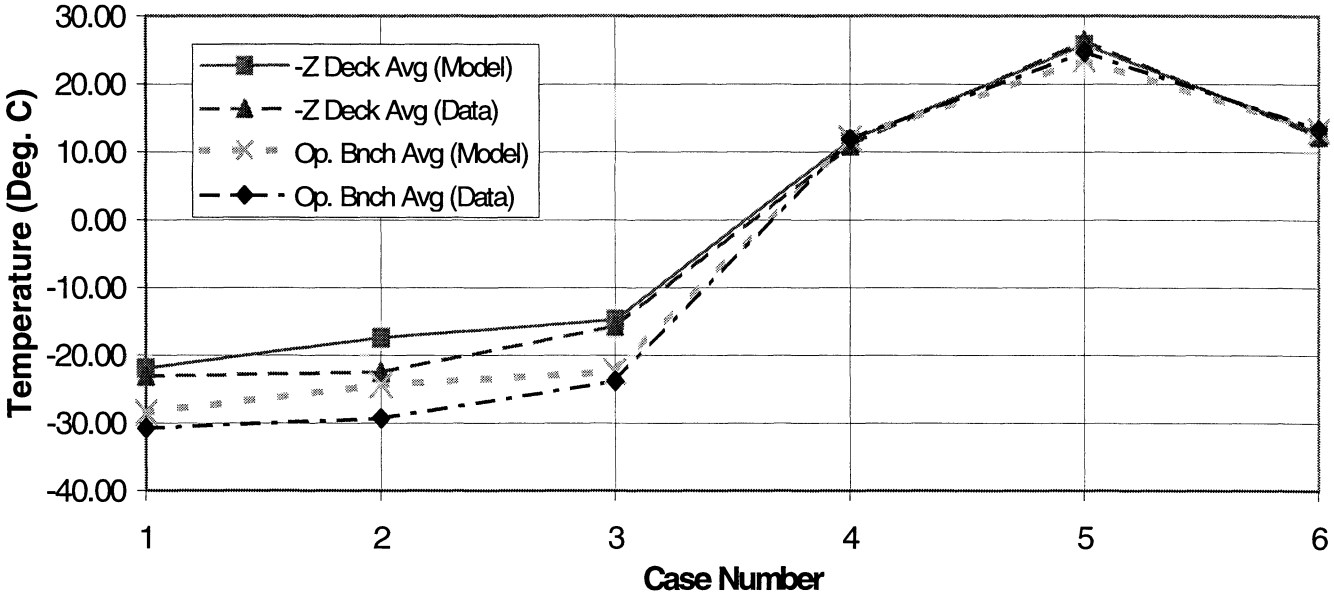

Figure 8
S/C Thermal Balance Data Versus Model Predictions
+/- Y Panels

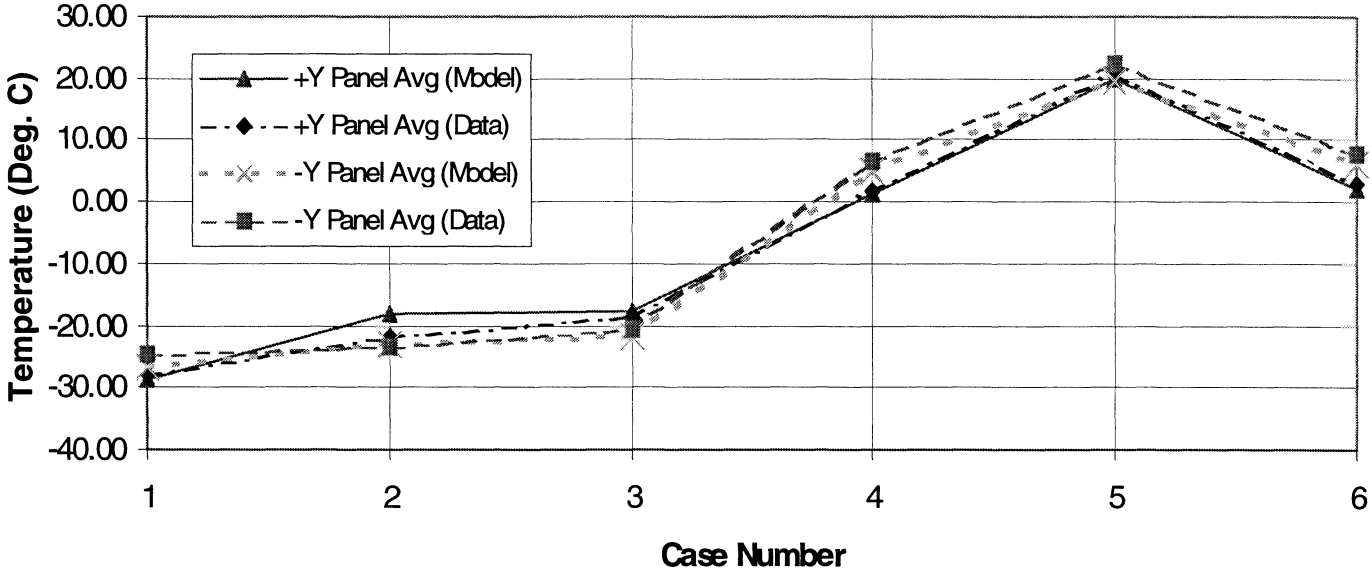

Figure 9
S/C Thermal Balance Data Versus Model Predictions
+/- X Battery Radiator

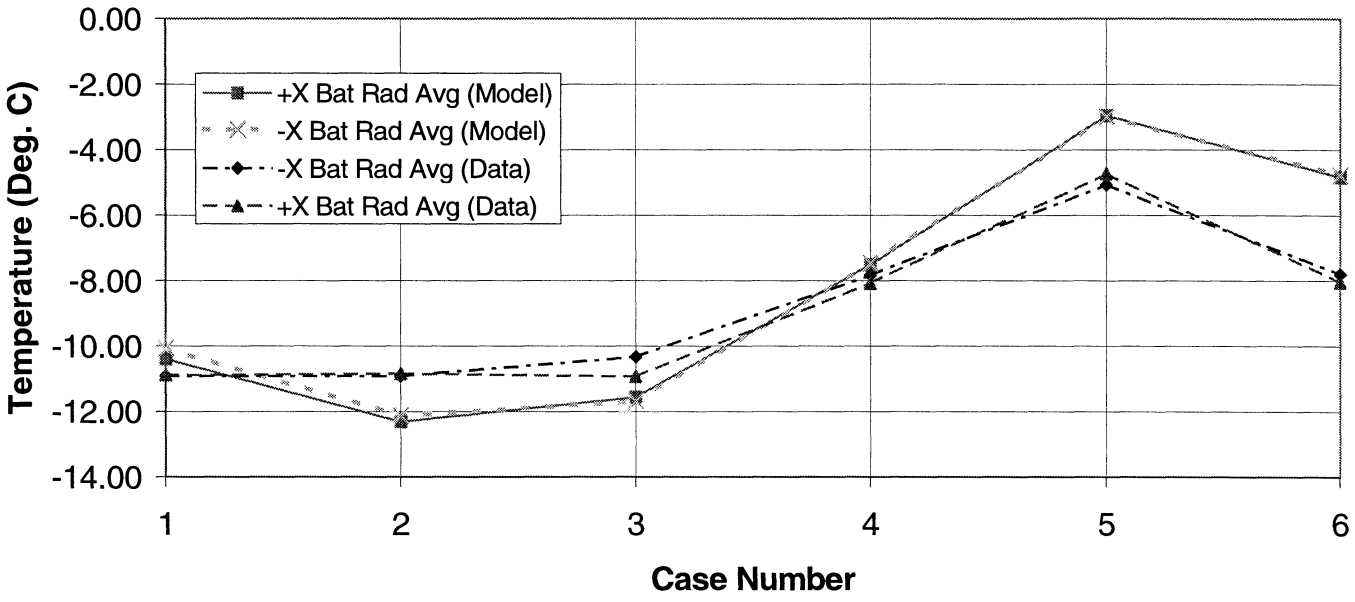

RF HIGH POWER TEST IN THERMAL VACUUM

Bernard Mauconduit

ASTRIUM Toulouse

ABSTRACT

With a communications satellite it is important, once the connection of the high power radio-frequency (RF) interfaces have been made and tested, that those interfaces are not disturbed for maintaining the RF integrity (No intrusive test). However, during the thermal vacuum test the communication's performances are required to be checked. To enable this test to be conducted without demating the RF interfaces, thus allowing antennae to emit, the RF energy has to be absorbed. This paper briefly describes the design, development, test and subsequent use of the RF caps used during the thermal vacuum test on one of our EUROSTAR 2000+.spacecrafts.

INTRODUCTION

Once one connection has been made and tested, it was required not to demate it. This very simple and safe requirement induces a lot of problems. For example, when antennae are mounted and tested, it is no longer possible to open wave-guides and derive power to classical RF loads as usual for testing the repeater. Tests with all the Travel Wave Tube Amplifiers at saturation generate high level radio-frequency emission up to 2.25 kW through either the two TX antennae or 1.1 kW through the RX/TX antenna. With such high levels, human safety of operators at ambient pressure and high electrical fields in vacuum chamber are then posing difficulties. In the other hand, this way is the only one that guarantees the entire repeater and antennae work well at full power in multi-carrier mode.

INDUCED PROBLEMS IN VACUUM CHAMBER

Emitting radio-frequency power up to 2.25 kW in a closed vacuum chamber generates very high electrical field, due to the high number of reflections of the waves by the low absorbing metallic shrouds or walls of the facility. Such an environment is not compatible with the equipment and power has to be trapped, absorbed and evacuated out of the facility.

This efficient absorption concerns two different ways. The first one is related to the power returned back to the repeater that shall be minimized for protecting the on board equipment. In other words, Voltage Standing Wave Ratio (VSWR) of the load shall be better than -20 dB. In the other hand, power loss in free room of the chamber shall be as small as possible and such that the generated maximum electrical field be compatible with the equipment Electromagnetic Compatibility (EMC) specification of the equipment.

When a load absorbs power, it warms up. Material and technology of the load shall be selected in order to minimize outgassing or coolant leaks, in order to avoid any pressure rise and then any risk of arcing either in the load or in the repeater. This heating has also to be controlled such that antennae maximum temperature will not be exceeded during the test.

Finally, introducing a RF absorbing device within the test facility shall not shadow the cooled shrouds as it could generate hot spots on the tested satellite. It means that size of the load and its support shall be as little as possible.

SELECTED SOLUTION

In order to avoid all the foreseen potential problems, we choose the following patented solution.

RF cap placed in front of the output of the horn to catch all the power directly at the source.

A cylindrical wave-guide with low absorbing walls traps the power. A reflector ends the cap and minimizes its length.

As classical absorbing material usually generate quite large outgassing and in order to minimize material heating, water is used either as absorber and coolant fluid. A tight window transparent to RF waves separates coolant and vacuum.

Fixing caps directly on the antenna masts using free strength fixtures minimizes the play between horn and cap. A RF shield with venting holes closes the space between horn and cap in order to minimize the power loss.

Figure 1, 2 and 3 present the patented design of the cap and the support of the cap onto antenna.

Designed load is 286 mm width in diameter and 450 mm long. Its mass is about 16.3 kg.

TEST SAFETY

As this system is used directly on a flight model satellite, particular attention is put on the satellite integrity. A specific safety device (see figure 4) was developed for surveying all the parameters that could permit to detect drift in the load performances before any degradation of the satellite equipment could occur. A computer acquires every second all the selected parameters, analyzes them and initiates, when required, the emergency actions.

In order to avoid any excessive heating of the load, the selected parameters to survey are pressure, temperature and flow-rate of the cooling water.

For avoiding any risk of arcing due to a pressure rise by outgassing or coolant leaks, the selected parameters are vacuum pressure in vicinity of the caps, pressure and flow rate of water. The last alarm would be detected by an increase in return power.

When software detects any parameter out of the specified range, it commands automatically the emergency actions that could be, depending on the bad parameters combination, stop RF modulation sent to the repeater, isolate one or all the water loop(s) or stop the water pump.

DEVELOPMENT PLAN

ASTRIUM Assembly Integration and Test Division with support from other departments developed the RF caps and all associated equipment, using a classical organization as follows.

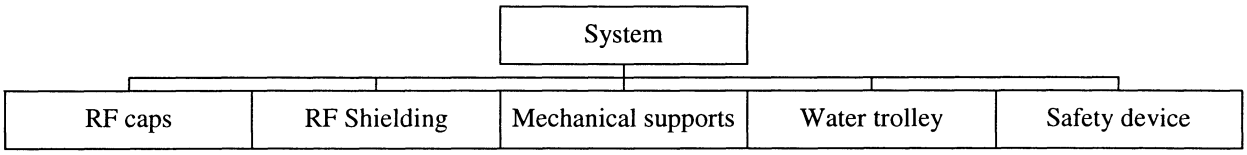

Development of each of them is based on a classical scheme including

- Specification,
- Study, sizing, material selection and definition,
- Characterization tests,
- Fabrication,
- Qualification tests for caps on a qualification model,
- Acceptance tests of each item,
- System assembly and system acceptance test.

Due to the short schedule all the devices were designed in a closed loop process that included a Failure Modes Effects and Criticality Analysis (FMECA). It permitted to improve the equipment in real time and to quickly reach the safest possible design.

In addition, RF behavior of the vacuum chamber to be used with the satellite was tested to ensure the test could be safely run. These tests confirmed that the expected electrical field was low enough to be compliant with satellite equipment and do not perturb instrumentation of the facility (vacuum gauges, temperature measurement and gas analyzer).

TESTS AND PERFORMANCES

Qualification and Acceptance Tests

RF Power and Caps Heating

The main difficulty when developing such a high power RF cap is to generate the RF high power for testing it. Generally, you do not have at your disposal a mock-up of the repeater and it is then impossible to generate multicarrier cross-polarized RF waves up to some kilowatts. We avoided this difficulty by using a theoretical approach of the cap behaviors with single carrier, multicarrier or cross-polarized waves and checks by simple tests.

All these tests were made in the ASTRIUM Stevenage EMC laboratory, which owns a high power amplifier in the required frequency band. Caps were tested with one carrier up to 1.7 kW permanently applied. According to test results with four carriers or cross-polarized waves at low power, it corresponds to a power about 2.5 kW for 28 carriers and two-crossed polarization's.

RF window maximum temperature is well in accordance with calculated one (see figures 5 and 6). Extrapolation to the maximum allowed temperature demonstrated the ability to absorb up to 3 kW with cross polarization.

VSWR

VSWR measured with a network analyzer is presented in figure 7. VSWR measured at 100 W is comprised between -21 and -30 dB depending on the frequency. The mean value all over the frequency band is about -25.5 dB. VSWR is quite independent of the power and when power increases return loss decreases a little bit.

RF Leak

Without RF shield, external electrical field was measured at 35 cm of the load output with a 100 W single carrier. In the anechoic chamber it goes from 28 to 62 V/m. In a small vacuum chamber, it rises and goes from 82 to 188 V/m. By adding a RF shield whose mean efficiency is about -20 dB, it decreases respectively down to 12 to 19 V/m in free space or 29 to 100 V/m in vacuum chamber.

Extrapolating to the large test facility we expected up to 42 V/m.

Operational Use

The spacecraft High Power test was successfully completed. The complete system worked for 28 days non-stop without any problem. Tests were made under vacuum at full power on each antenna

- For 16 hours at 2.4 kW on the West Antenna,
- For 6 hours at 2.3 kW on the East Antenna,
- For 6 hours at 1.1 kW on the Top Floor Antenna.

Return power, water pressure, water temperature at input and output of the cap are presented in figure 8 for the West antenna.

Electrical field measured in vicinity of the caps or of the external sensitive equipment was less than 7.3 V/m, that is much lower than the EMC specification of the equipment, i.e. 40 V/m.

CONCLUSION

For safely testing the repeater in high power test during the spacecraft vacuum test, the ASTRIUM Assembly Integration and Test team developed a complete system that includes patented new caps. These caps catch very efficiently up to 3 kW of RF power directly at the horn output without any excessive return loss or leak. This system was successfully used for 28 days non-stop with tests up to 6 or 16 hours at full power trough either the 3 antennae. It permits a new standard for testing the antennae at full power under vacuum.

The existing system can very easily adapted to any new spacecraft. It simply requires mechanical adaptation of support and cap. Based on our experience, this sort of cap could be improved in the future for absorbing from 5 to 10 kW RF power.

SYMBOLS

Values are given in SI Units.

FIGURES

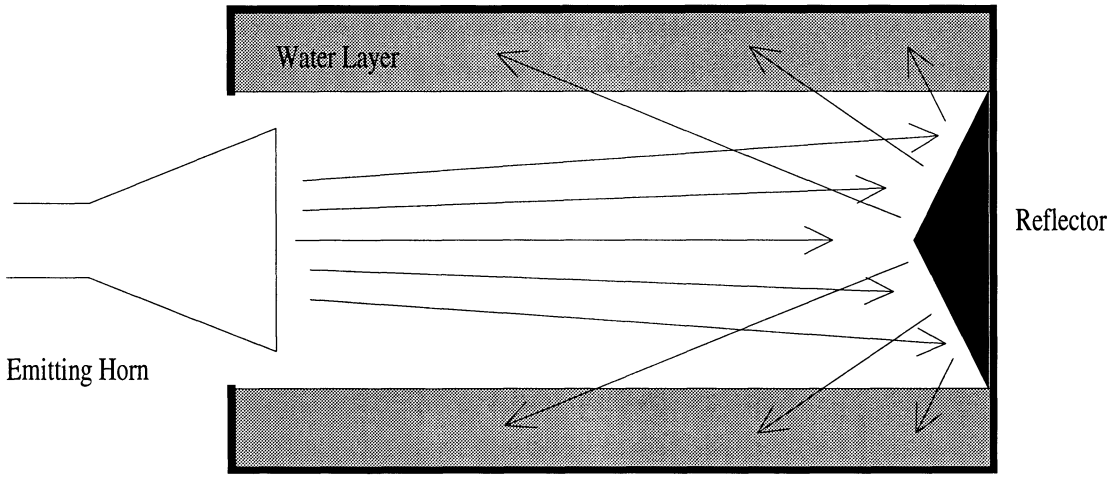

Figure 1: Schematic of the patented RF cap

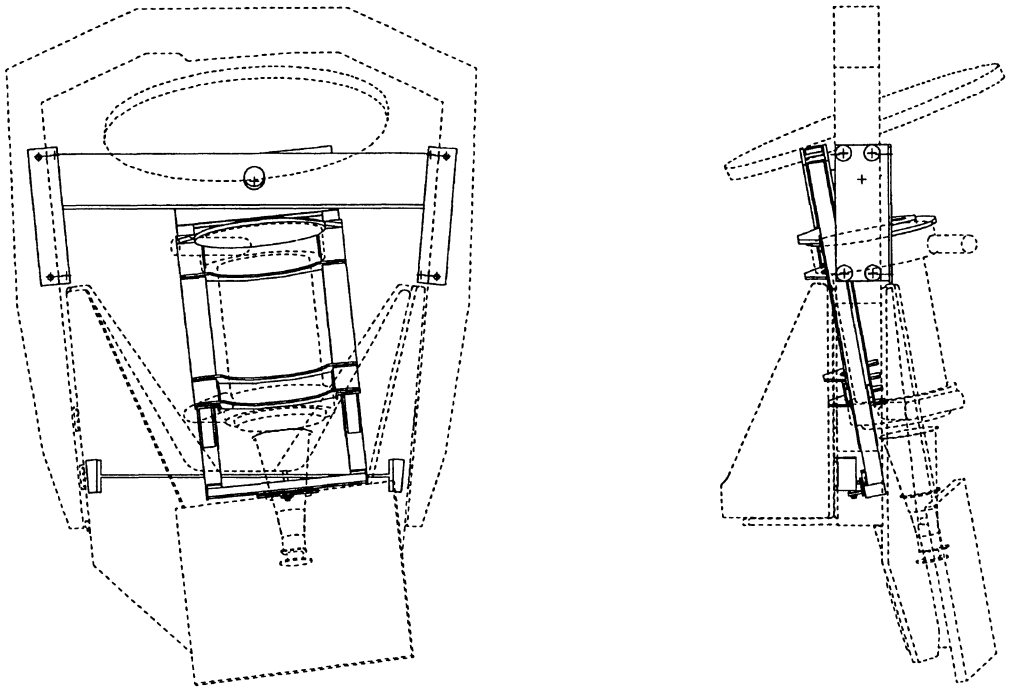

Figure 2: Cap Mechanical Support on East / West Antennae

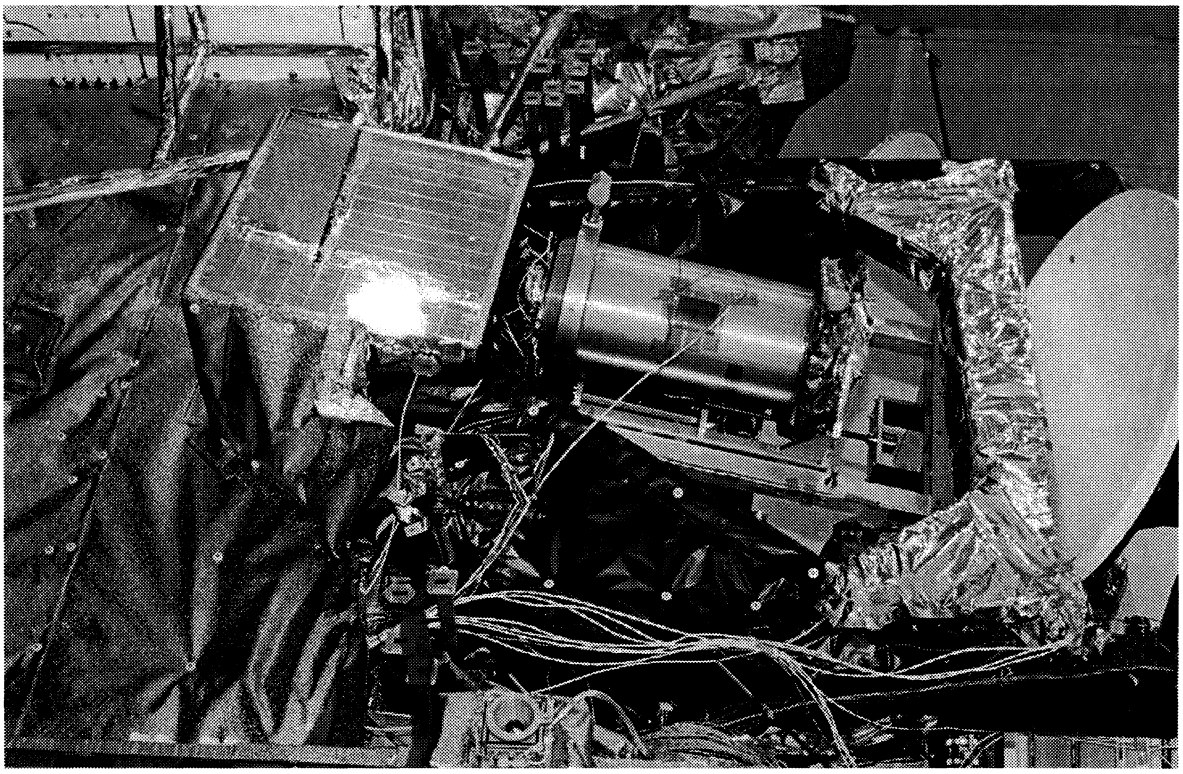

Figure 3: Photograph of Cap mounted on the West Antenna

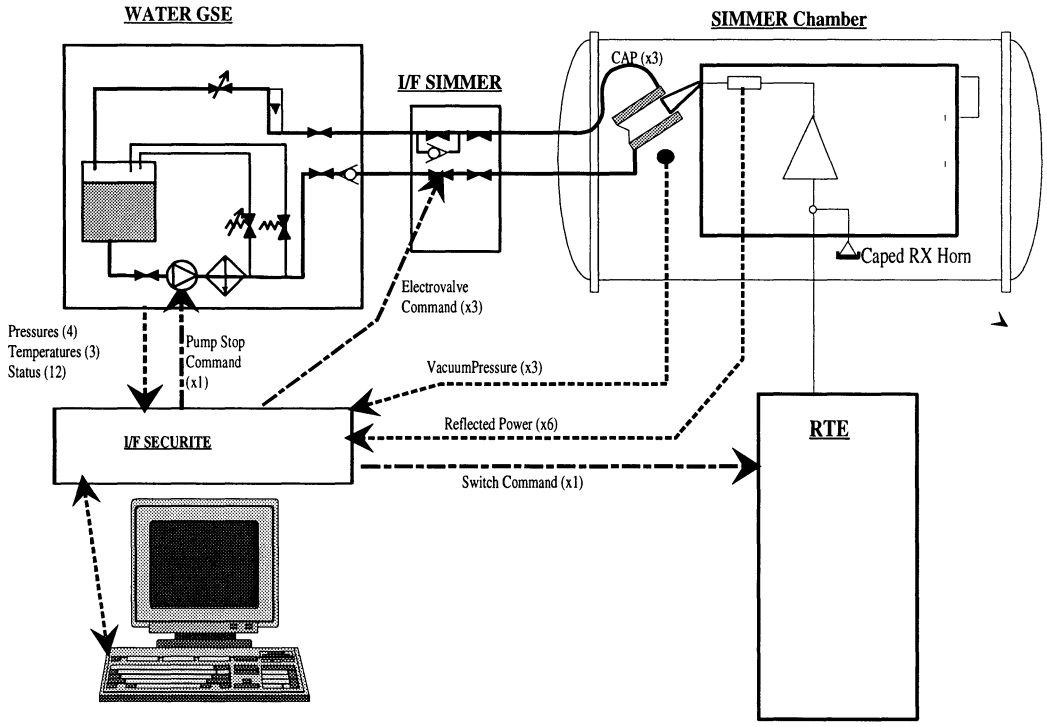

Figure 4: RF cap system with safety device in vacuum test configuration

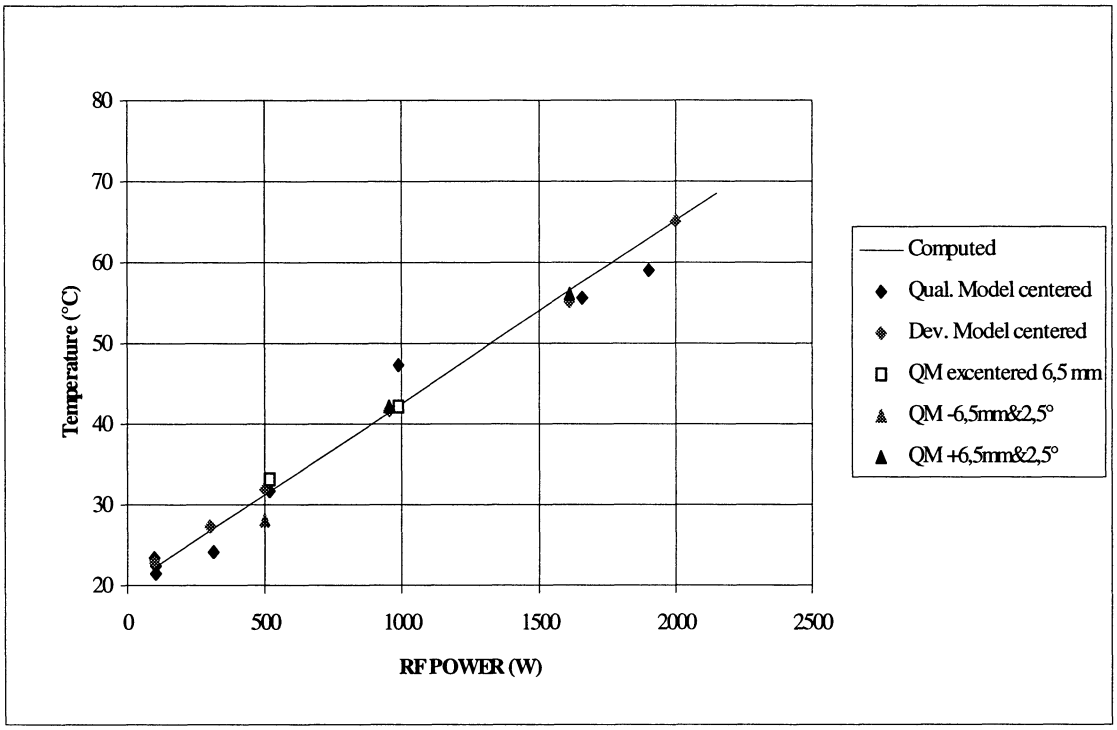

Figure 5: Maximum Temperature of the window versus one carrier RF power

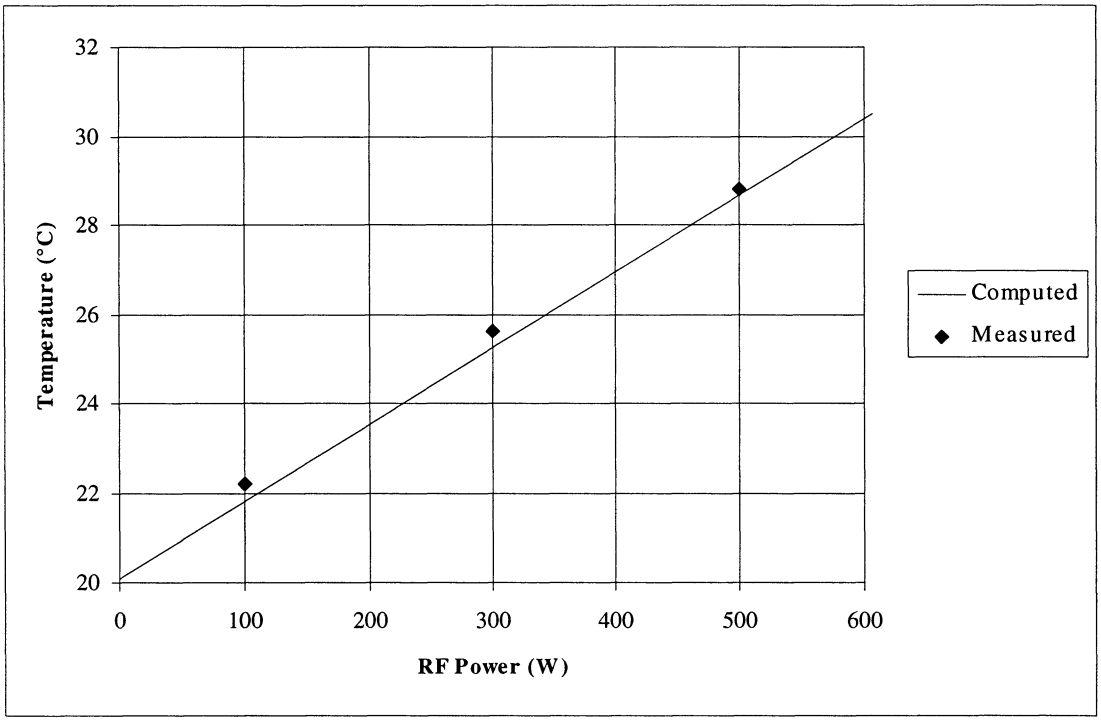

Figure6: Maximum Temperature of the window versus cross-polarized RF power

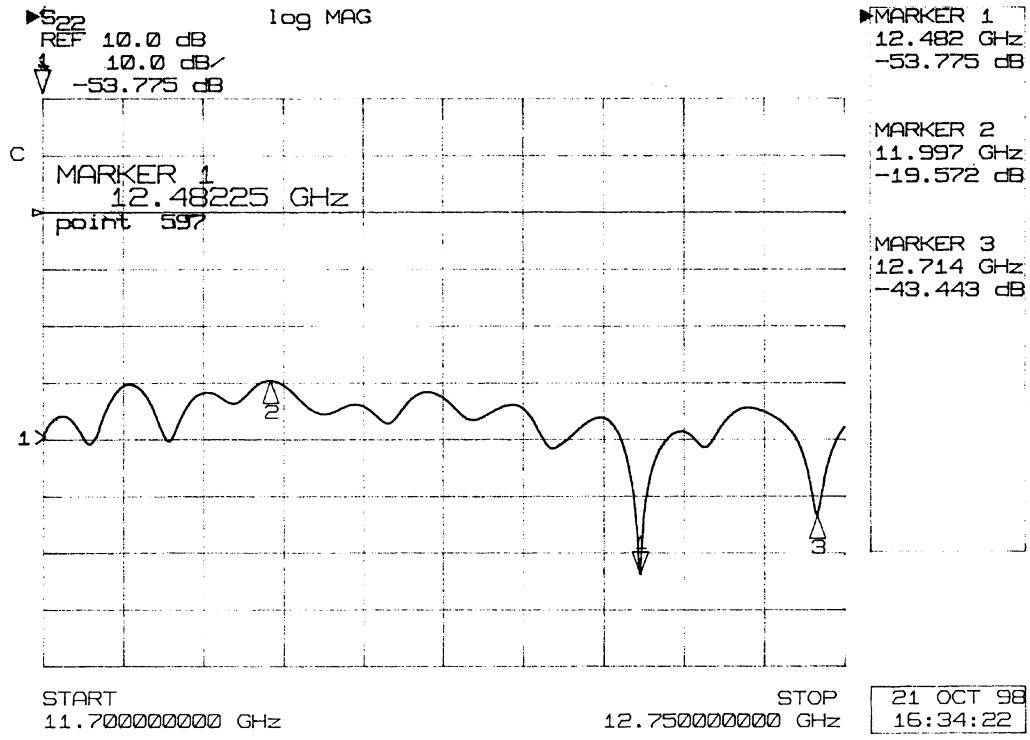

Figure7: VSWR of the cap measured with network analyzer

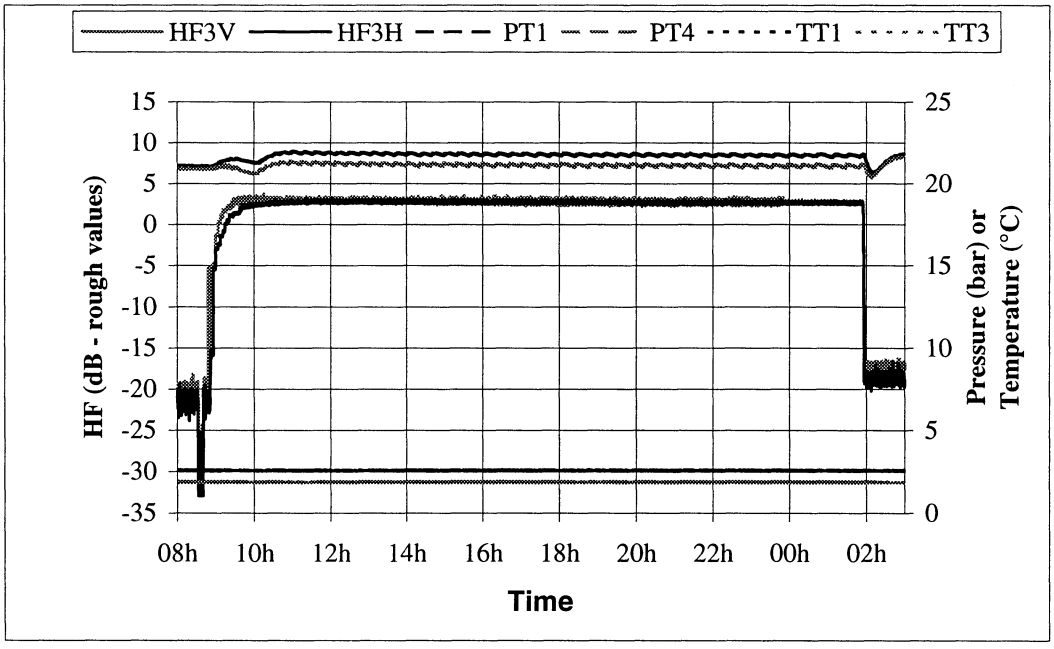

Figure 8: Registered parameters during the West Antenna High Power Test

ENVIRONMENTAL TESTING FOR A MERCURY ORBITER PROTOTYPE SOLAR PANEL

Carl J. Ercol, Jason E. Jenkins, George Dakermanji, Andrew G. Santo
The Johns Hopkins University
Applied Physics Laboratory
Laurel, MD 20723-6099

ABSTRACT

A Mercury orbiting spacecraft imposes many design challenges in the area of spacecraft thermal control and electrical power generation. The Discovery Mission MESSENGER (MErcury Surface, Space, ENvironment, GEochemistry, and Ranging), being designed and built by The Johns Hopkins University Applied Physics Laboratory (APL), will orbit and survey the planet Mercury for one year. In order to reduce cost and schedule risk while increasing the probability for mission success, the MESSENGER solar arrays will be constructed from conventional "off the shelf" materials and technologies.

INTRODUCTION

This paper describes the high temperature and high intensity illumination testing which were used to thermally evaluate a series of prototype engineering solar panel concepts. Since all of the materials, construction techniques and technologies chosen for the solar panel construction are typically used for fairly benign thermal environments, qualification or proof of concept testing was necessary to assess the risks associated with such a thermally demanding mission. The solar array concept for the MESSENGER Mission consists of two double sided rotatable wings, allowing for tailored temperature control during power generation as solar distance decreases. One side of each array is fully packed with 5.5 mil single junction gallium arsenide (GaAs/Ge) cells. The opposite side is packed with a 70%/30% mixture of Optical Solar Reflectors (OSRs) and the same type of GaAs/Ge cells. Each side of each solar panel is designed to maximize power generation and minimize operating temperature for a given solar distance range. From launch until the spacecraft reaches about 0.60 Astronomical Units (AU), where the solar constant is about 2.8 greater than at Earth, the fully packed side of each array is responsible for power generation. Once inside of 0.60 AU, the array is flipped to the 30% cell side which takes advantage of the higher solar constant while maintaining the solar panel operating temperature below 150°C.

The solar panel structure uses sandwich construction comprised of high thermal-conductivity graphite-epoxy (Gr/Ep) face-skins and an aluminum-honeycomb core. The primary thermal environment that drives the MESSENGER prototype solar panel design and the dual-sided configuration is the high solar intensity condition experienced when at planet perihelion, where the solar constant is eleven times that at Earth. The mirrored side of the array safeguards against solar panel temperatures exceeding 250°C in the event of a direct Sun pointing anomaly when at Mercury perihelion. And, the dual sided design minimizes the solar panel overall size and mass by using the fully packed face at solar distances associated with the beginning of the mission when temperatures are very benign and the solar constant is low.

A large portion of the proof of concept thermal vacuum testing was accomplished using a custom designed high temperature infrared oven to test solar panel specimens between +300°C and –105°C. The oven has allowed for accurate and repeatable component testing while proving to be very reliable and cost effective. The more expensive and complicated high intensity solar illumination tests were done only after thorough infrared temperature cycle testing and high temperature soaks verified solar panel materials and construction. The high-illumination testing was done at NASA's John H. Glenn Research Center at Lewis Field in the Tank 6 high intensity vacuum chamber. These tests were used to verify the prototype solar panel thermal design and to demonstrate ability to predict the expected test panel temperature at a high intensity solar simulated environment. The paper describes the details and results of the prototype tests conducted along with plans for the flight solar panel development and test.

BACKGROUND

Mercury has never been explored by a remote orbiting spacecraft. The only man-made space probe to visit Mercury was Mariner 10. Built and launched in the United States, Mariner 10, a 3-axis stabilized solar powered spacecraft, has provided the only images and scientific exploration of Mercury. Using three flybys, Mariner 10 was able to map only about 45% of the planet surface during a one-year period between 1974–1975. The dark side flybys were all at planet aphelion and never near the sub-solar point. Mariner 10 was designed and tested to withstand a solar-only 5 Sun (one Sun is equal to the solar flux at 1 AU or 1365 W/m^2) environment, ignoring the intense omni-directional heat radiated from Mercury's surface on the Sun-lit side.

Due to severe mass restrictions and extremely harsh thermal environments, a Mercury orbiting spacecraft poses many engineering and operational challenges. MESSENGER is a 3-axis stabilized solar powered spacecraft using a high-performance all chemical propulsion system fully integrated into an all graphite-epoxy structure. The power system will utilize two low mass dual-sided solar array wings that can be rotated and flipped as necessary to control solar panel temperatures as the spacecraft approaches Mercury perihelion. The mission design uses a ballistic trajectory with multiple Venus and Mercury gravity assists. The MESSENGER spacecraft will eventually orbit Mercury for one Earth year (or four Mercurian years) and return a wealth of scientific data and complete planet coverage, something not accomplished by Mariner 10.

The MESSENGER mission was recently selected by NASA to be the eighth program in the highly successful series of the Discovery missions. Mission cost and launch vehicle choices are very constrained under NASA Discovery guidelines. The largest acceptable launch vehicle for a NASA Discovery mission is a Boeing Delta II 7925H-9.5 (Maximum Launch Mass = 1066 kg). Driven by the 2700 meter per second mission Δ-velocity (ΔV) requirements, over one half of the launch mass is allocated to propellant. It quickly becomes apparent that due to the high ΔV nature of this mission, the spacecraft mass allocated to useful payload is limited. Spacecraft mass must be used with great discretion since the main purpose of the mission is to get maximum science return. Figure 1 illustrates the MESSENGER spacecraft. As shown, the dual-sided solar panel wings extend beyond the protective umbra created by the thermal shade, making the solar arrays the only critical component exposed to direct high intensity solar illumination. Designing the spacecraft for minimum mass will require the attention of all spacecraft sub-systems, and the seemingly vulnerable solar array is no exception. A mass saving benefit from the dual-sided approach is that the overall solar panel area is small because each face is optimized for power at the worst case solar distance and temperature. Each face of the dual sided solar array is designed to produce power at a cell operating temperature of 150°C or lower. As illustrated by Figure 2, the array is flipped from the fully packed side to the OSR side and back as the solar distance varies between approximately 0.45 and 0.60 AU. Figure 3 illustrates the variation in respective solar array face rotation angle as a function of solar distance as the array temperature is held at or below 150°C. The rotation angle is zero when the Sun line is perpendicular to the active face of the solar array.

Why Use a Dual-Sided Solar Array Concept?

The MESSENGER mission first baselined a single sided fully packed solar array using single junction GaAs/Ge cells bonded to graphite composite substrates. As illustrated by Figure 4, the fully packed solar array has to be rotated in excess of 75° to maintain the steady state solar array temperatures below the desired operating point of 150°C while at Mercury perihelion (11-Sun illumination condition). A major deficiency with this design is that a direct Sun pointing anomaly at the perihelion solar distance could easily cause the array to approach 400°C. Solar cell and Gr/Ep adhesives are only rated to maximum temperatures between 200 and 260°C. Trying to qualify this technology to temperatures in excess of 400°C was not a feasible option. Another critical deficiency with the single sided concept is that it is thermally unstable. The analysis represented by Figure 4 illustrates that controlling the solar array temperature to 150°C while at perihelion could be very difficult because of the sensitivity between tilt angle and temperature. Also, at solar panel aspect angles greater than 65°, solar cell reflectivity begins to dominate power calculations and introduce large uncertainty.

Once the single sided concept was abandoned, a trade study was done to determine the effects of adding mirrors with the cells in order to reduce the overall solar panel temperature. Power system analysis showed that the total surface area necessary to do the complete mission using only a single solar array face that combined OSRs with solar cells would be almost a factor of four larger than the original fully packed design. The OSR design also has to incorporate thicker face skins to thermally connect the solar cells to the OSRs. Although the single solar array face that utilized OSRs with solar cells was not feasible from a spacecraft mass perspective, it was from a thermal perspective. The next trade study combined a fully

packed solar array face with an OSR and solar cell face. This design would allow the MESSENGER power system to select the appropriate face depending on solar distance and solar panel temperature. Since each of the solar array faces will be designed to produce power over a defined solar distance range, the dual-sided approach allows for the panel area optimization because the worst case power condition will always dictate this parameter and set the maximum face size. This in conjunction with the deficiencies described for the single sided fully packed solar array made the dual-sided concept extremely attractive. More detailed power and thermal analysis were performed, and the dual-sided solar array became the baseline for the winning Discovery proposal, MESSENGER.

Prototype Solar Panel Construction

The prototype solar arrays were constructed of conventional materials that gave the highest probability of success for steady state temperature excursions between 200 and 260°C. The flight solar array concept calls for solar cells and OSR mirrors to be bonded to high conductivity graphite epoxy face sheets comprised of K13C2U cloth and RS3 and RS4 resin systems using conventional, NuSil Technology CV-2568, silicone adhesive, illustrated by Figure 5. The solar cells and cover glasses, Kapton™-VN, and aluminum honeycomb core as components are rated to temperatures at or above 300°C. The adhesives used to bond these different solar array components together creating the solar array assembly are the materials that have the lowest manufacturer's rated temperature. For example, Dow Corning rates DC-93500, which is used to bond cover glasses to solar cells, to only 200°C. Manufacturers of the resin systems RS3 and RS4, used to bond the individual face sheet plys together and to the honeycomb core, are only rated to 232°C. So it was decided to purchase and test multiple configurations of populated and unpopulated Gr/Ep sandwich panels that all used the same cyanide-ester resin systems and solar cell adhesives. Six different test panels were purchased and are listed in Table 1. Figures 6 and 7 depict the mirrored and non-mirrored sides of the prototype dual-sided solar array panel that was tested and is identified as Panel 4 in Table 1.

TECSTAR, Inc. did the solar cell and OSR bonding and the electrical wiring for all the test panels. The solar cells were TECSTAR 5.5 mil thick GaAs/Ge "standard" production cells cut to the required size. The solar cell interconnects end termination were all parallel gap welded and high temperature Kapton was co-cured with the GrEp to form the electrical barrier between the solar cells and the graphite panel. Ceria doped cover glass, three tenth of a millimeter thick, coated with dual anti-reflective coating was bonded to the cell using DC 93500 adhesive. NuSil 2568 adhesive was used to bond the cells and OSR to the kapton insulation on the panels.

High-Temperature Test Program Development

Development of a test program and testing philosophy was essential to verify that conventional solar array materials and manufacturing processes could be used for high temperature applications. Thermal vacuum testing of the samples would have to represent the minimum and maximum temperature excursions experienced during the expected 65-minute eclipse as well as the nominal solar panel operating temperatures when illuminated. Also, because the solar arrays represent a single point failure, the worst case steady state survival temperature would also be tested to show design robustness in the event of a Sun pointing anomaly when at Mercury perihelion.

Each prototype test panel would first be baked out for 24 hours at 80°C. This bake-out helps to remove trapped air pockets in the solar cell adhesives that could rupture at the high temperatures and damage the cells. The test program combines solar panel acceptance testing that is typical for an Earth orbiting spacecraft with the higher temperature cycle and soak testing required for a Mercury orbiting spacecraft. Electrical performance tests would be done after each set of cycle tests and after each of the high temperature soaks to verify electrical functionality and document any temperature incurred damage.

Six conventional workmanship cycles would be performed between +120°C and –105°C, establishing a test baseline. High temperature cycling would follow the workmanship cycles and would have maximum plateaus at +150°C, +180°C and +200°C and the same lower temperature of –105°C. Also, high temperature soaks representing steady state survivability in the event of a Sun pointing anomaly at perihelion had to be demonstrated. Each of the soak temperatures, 230°C, 240°C and 250°C, would be held for a minimum of one hour to verify material and construction robustness, removing any solar array recovery time constraint if an anomaly were to occur. At the completion of each level of cycle testing and after each of the high temperature soaks the test panel would be removed from the test chamber and visually inspected for damage such as substrate delamination or cracked cells or OSRs. After the visual inspection, the test panel would be taken to a laboratory for electrical performance testing if necessary. Once the inspections and electrical test is complete the prototype solar panel would be re-installed for further temperature cycle testing.

The first high temperature tests were done using a large (9 m^3) liquid nitrogen (LN_2) cooled vacuum chamber and infrared (IR) heat lamps. A dummy black aluminum test panel, which represented a typical prototype solar panel, was located inside the chamber and heated at high intensity with the IR lamps. Thermocouple measurements made on the aluminum panel showed temperature gradients in excess of 70°C when the maximum dummy panel temperature was 310°C with the chamber walls at –180°C. A few failed attempts were made to increase the flux uniformity by repositioning the IR lamps and dummy test panel. It quickly became evident that this test setup method would impose a very high risk to the sample being tested. Also, because the test samples had to be removed for inspection after each set of thermal cycles, the test setup proved to be ineffective from both cost and schedule standpoints and therefore was abandoned.

A smaller and simpler test apparatus had to be designed. The new test apparatus had to deliver uniform sample temperatures between –180 and 300°C, it had to be time and cost effective, it had to be reliable, and it had to be simple to operate. The new apparatus would be designed to operate inside the large 9-m^3 chamber so that vacuum, liquid nitrogen, thermocouple and electrical interface resources could be easily utilized. The large chamber would not have to be temperature controlled, eliminating the long transitions from vacuum to ambient conditions. The small (0.125 m^3) test apparatus, known as the "E-Box", is shown in Figure 8. The E-Box is thermally isolated from the large chamber, the east chamber, illustrated by Figure 9, using stainless steel chains and high-temperature multi-layer insulation allowing for independent temperature control. Thirteen 1000-watt resistive OMEGALUX™ strip heaters combined with an LN_2 cooling loop plumbed from an internal east chamber LN_2 feed will provide the necessary temperature control capability for the E-Box. The E-Box has two 2600 cm^2 (400 in^2) compartments that are identically heated and cooled, allowing for multiple sample testing.

Infrared Testing using the E-Box

Pathfinder infrared thermal vacuum testing in the E-Box started on April 23, 1998 using two unpopulated GrEp test panels. One test panel, identified as Panel0, was constructed from M55J fibers formed into two 0.25mm substrates using RS3 and co-cured with aluminum honeycomb as a sandwich using RS4. The second test panel, identified as Panel0A, was constructed from K13C2U fibers formed into two 1.0 mm face sheets using RS3 and co-cured with aluminum honeycomb as a sandwich using RS4. The pathfinder testing was used to verify the survivability of the RS3 and RS4 resin systems at extended high temperature before the expensive populated panels were subject to the same sequence of tests. The test procedure, which includes chamber breaks, inspections and E-Box power levels, was also refined to minimize the overall test time.

The low conductivity test panel, Panel0, shown in Figure 10, was extensively thermocoupled to measure the temperature gradients induced by heating and cooling. Since the Panel0 face sheets have very poor thermal conduction characteristics, temperature gradients measured between any two thermocouples illustrated quantitatively the heating uniformity. With an average temperature of 250°C for each test panel, the maximum differential measured between the warmest and coolest thermocouple on Panel0 was less than 5°C. The pathfinder thermal vacuum testing with the unpopulated test panels verified that the cyanide-ester resin systems could be taken to temperatures above the manufacturer's specification for extended time without damage or delamination of the sandwich construction. The pathfinder testing also verified that the heating and cooling of the test samples was very uniform and low risk while the turnaround time between cycle testing, hardware inspections and reinstallation of the sample in the E-Box was small.

Upon the satisfactory completion of the pathfinder testing, solar panel prototypes populated with mechanically-sound, electrically-rejected, but functional, GaAs/Ge cells and OSRs were then tested using the same thermal profile and inspection procedures established during the pathfinder tests. Table 2 lists a summary of the results of all the panel level infrared testing performed at APL. Figure 11 depicts the as-run thermal vacuum test data for Panel3 and Panel4, representing the prototype dual sided solar panel configuration.

Simulated High-Intensity Solar Illumination Testing

Once the dual sided prototype engineering panels were successfully temperature cycled and soaked using the E-Box, Panel3 was taken to the John H. Glenn Research Center (GRC) at Lewis Field Tank 6 thermal vacuum test facility. The Tank 6 facility is a 18.5-meter long by 7.7 meter diameter horizontal vacuum chamber with a liquid nitrogen cryogenic-wall and a solar simulator. The solar simulator uses nine 30 kW Xenon arc lamps and was designed to provide no less than 1 Sun on a 4.6 meter diameter target, 17.4 meters from the source with a subtended angle of less than 1°. In order to achieve the high intensity solar flux levels required to simulate Mercury perihelion, the targets were located at a distance of approximately 5.8 meters from the source. The vacuum system can provide ambient pressures as low as 10^{-6} torr. Tests and analysis done at APL prior to GRC solar testing indicated that heat transfer concerns are mitigated at pressures below about 150 millitorr and that

10 Suns with a room-temperature sink is equivalent to 11 Suns with a liquid nitrogen or deep space sink. Therefore all testing was conducted without high-vacuum pumps and liquid nitrogen cooling, resulting in a nominal tank pressure of 25 millitorr and an average ambient tank temperature of 22°C.

The solar array panel was installed, aligned and electrically checked on Monday, February 22, 1999. The vacuum system was started at about 10:00 am on February 23. The tank pressure was 28 millitorr at 12:49 pm when the first solar simulator lamp was started. Video and infrared cameras were mounted at window ports near the simulator window to observe the test article. A total of eight lamps were started sequentially in the following order: 5, 4, 6, 7, 2, 8, 9, 1. The lamp startup order was determined by change coupled device (CCD) imaging on a Teflon sheet prior to test panel insertion and was selected to minimize the initial flux variation on the test panel. Lamp number 3, which was planned to be used after lamp 6, failed to start and required the addition of lamp 1 as an alternative. After each lamp was started and adjusted to its operating level, solar cell I-V curves were acquired. Panel temperatures were allowed to stabilize with each lamp operation.

Figure 12 shows the maximum measured panel temperature and estimated local solar flux at that thermocouple location over the 200-minute illumination period. With four lamps operating, the maximum-recorded temperature was 174°C with a localized flux of 4.9 Suns. The eight-lamp configuration resulted in a maximum panel temperature of 257°C with a localized flux of 10.0 Suns. Both test points provided excellent agreement with pre-test analyses. No visible or electrical abnormalities were observed during the test. Post test removal and inspection of the panel showed no visible effects of the testing. Darkening of some non-optical adhesives occurred but without effect to adhesion. Pre-test and post test I-V characterizations performed at GRC's Solar Cell Measurements Lab with a Spectrolab X-25 were essentially identical.

CONCLUSIONS

The APL prototype test program met the goals of thermally evaluating the materials and processes used for conventional solar array construction. The MESSENGER prototype dual sided solar array has proven to be thermally robust and temperature tolerant. Results of the thermal testing presented verifies that the conventional adhesives typically used for the construction of cyanide-ester based GrEp solar panel substrates and solar cell bonding processes are not adversely effected by temperatures below 300°C. As illustrated, multiple solar panel samples using two different pitch based fibers passed all required cycle and dwell testing, with one sample, Panel2, being tested to high temperature failure (>310°C). The thermal modeling which was used to establish the maximum temperature limits during E-Box testing (250°C) was confirmed during the solar illumination testing at GRC (257°C). And the comprehensive prototype test program has verified that the actual maximum panel temperature is within the maximum survivable limits of the chosen materials and construction techniques by over 40°C. The infrared thermal vacuum testing with the E-Box provided inexpensive and conclusive test data regarding the integrity of the materials and construction techniques chosen for the engineering panels, avoiding the more complicated and expensive solar simulation testing until design concepts were well defined.

The prototype tests to date were intended to demonstrate that the basic material and processes used for a "standard" near Earth type solar array can also be used for a solar powered spacecraft in Mercury orbit. Tests to verify the effects of eclipse induced thermal shock, solar cell reverse biasing when shadowed during high intensity illumination, and adhesive darkening during high-temperature/high-intensity UV illumination were not conducted, but are presently being evaluated. Efforts are currently in progress to evaluate the outgassing properties of the candidate adhesives at high temperature. Also under consideration is the use of IR and UV reflective coatings, applied to solar cell cover glasses and tested at elevated temperature and with high intensity UV illumination. Although the prototype solar panel testing to date has been weighed heavily toward thermal design and panel survivability, future testing will focus on refining the flight panel electrical design, assessing long term exposure effects on solar array materials and coatings and determining solar array performance under the MESSENGER mission environments.

REFERENCES

1. MESSENGER Discovery Concept Study, The Johns Hopkins University Applied Physics Laboratory, March 1999.
2. Powe, J. S., E. L. Ralph, G. Wolf, and T. M. Trumble, On-orbit performance of CRRES/Hesp experiment, Proc 22nd IEEE Photovoltaic Specialists Conference, 2, 1409–1415, Las Vegas, NV, 1991.
3. Ercol, C. J. and A. G. Santo, Determination of optimum thermal phase angles at Mercury perihelion for an orbiting spacecraft, *Proc. SAE International Conference on Environmental Systems (ICES),* Paper 972534, July 1999.
4. Mason, L. S., High flux, solar vacuum testing of a solar array panel and heat shield, NASA John H. Glenn Research Center at Lewis Field, test report, March 1999.

Table 1. Six prototype solar panels were purchased for testing under MESSENGER thermal environments. The prototype panels were fabricated to prove that conventional solar panel construction techniques and materials could be used in the high-temperature and vacuum environment an orbiting spacecraft would experience at Mercury.

Generic Panel Identifier	Configuration Description	Construction Details
Panel 0	Unpopulated Test Panel #1	A Kapton-insulated substrate with inserts. Face sheet composition is M55J/RS3 2.5mil UDPP with RS4 sandwich film adhesive and 3.1 lb/ft^3 hexcell core.
Panel 0A	Unpopulated Test Panel #2	A Kapton-insulated substrate without inserts (UDPP K13 C2U/ RS-3, 2.5 mil, with 4.5 lb/ft^3 hexcell core.) Panel 0A is populated on one side with individually wired heater elements which are arranged as the cells and OSRs of panels 3 & 4 (below). The other side of the panels is populated by Silver Teflon to emulate OSRs.
Panel 1	Single Sided Populated Panel #1	A substrate identical to Panel 0 populated with 12 older technology GaAs/Ge "reject" cells. Cells are mechanically sound, though electrically poor. Cell size is larger than intended for MESSENGER flight.
Panel 2	Single Sided Populated Panel #2	A substrate identical to Panel 0 populated with 36 high-temperature GaAs/Ge cells and representative OSRs. The cells are larger than what will be defined for the flight panels. OSRs were placed on the panel to qualify materials and methods, and as such are not positioned to be of thermal use.
Panel 3	Dual Sided Configuration Panel #1	A substrate identical to Panel 0A is populated on a single side with 9 high-temperature GaAs/Ge cells from the Panel 2 production lot which are cut down to 4×2-cm. OSRs are cut and arranged with the cells to be representative of the flight thermo-optical design. Each string and individual corner cells of strings A and C are wired for electrical monitoring. Thermocouples are bonded between two cells each of circuits A and C and between two OSRs each of the exterior OSR strings.
Panel 4	Dual Sided Configuration Panel #2	A substrate identical to Panel 0A populated on the front side identically to Panel 3. The backside is populated with 2 by 4 cm cells cut from the Panel 2 production lot. The backside panel is also instrumented. With two flight-candidate platinum thermistors.

Table 2. MESSENGER thermal/vacuum testing at APL.

Test Report	Date	Test Item	Test Type	Test case Summary
97-032	12/18-22, 1997	Solar Panel Test Plate (Aluminum)	Engineering Development	1 Cycle (-120°C <> +310°C)
98-013	4/23–5/14, 1998	Panel0 and Panel0A Panel1 and Panel2	Thermal/Vacuum Performance	Bakeout 85°C 6 Cycles (-105°C <> +115°C) 8 Cycles (-105°C <> +150°C) 4 Cycles (-105°C <> +180°C) 4 Cycles (-105°C <> +200°C) 4 Cycles (+23°C <> 220,230, 240, 250°C)
98-023	5/22–26, 1998	Panel1	Electrical Performance T/V (Illumination)	7 Cases (+50°C <> 200°C)
98-033	8/5–24, 1998	Panel2	Long Duration T/V Test	1 Case (+23°C <> +180°C)
99-004	1/27–2/5, 1999	Panel3 and Panel4	T/V Performance Test	Bakeout 85°C 6 Cycles (-105°C <>115°C) 4 Cycles (-105°C <>150°C) 4 Cycles (-105°C <> 180°C) 4 Cycles (-105°C <> 200°C) 2 Cycles (+23°C <>230, 250°C) 6 Cycles (-105°C <>115°C)
99-008	2/8–9, 1999	Panel2	T/V Performance	1 Cycle (-100°C <> 260°C)
99-010	2/10-12, 1999	Panel3 and Panel4	Electrical Performance T/V (Electrical Continuity at High Temperature)	Bakeout +100°C Three Hour Soak @ 250°C
99-017	3/1-4, 1999	Panel2	T/V Performance	Bakeout 100°C 1 Cycle (+100°C <> 280°C) 2 Cycles (+23°C <> 300,*320°C)

*Test Panel Failed

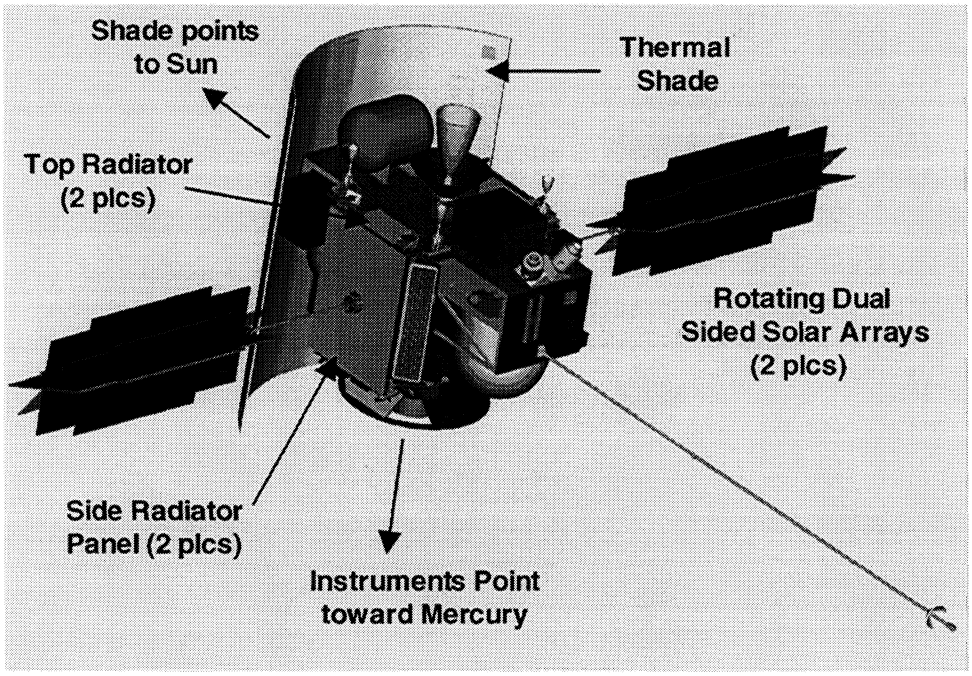

Figure 1. MESSENGER spacecraft with body mounted multi-layer insulation (MLI) removed.

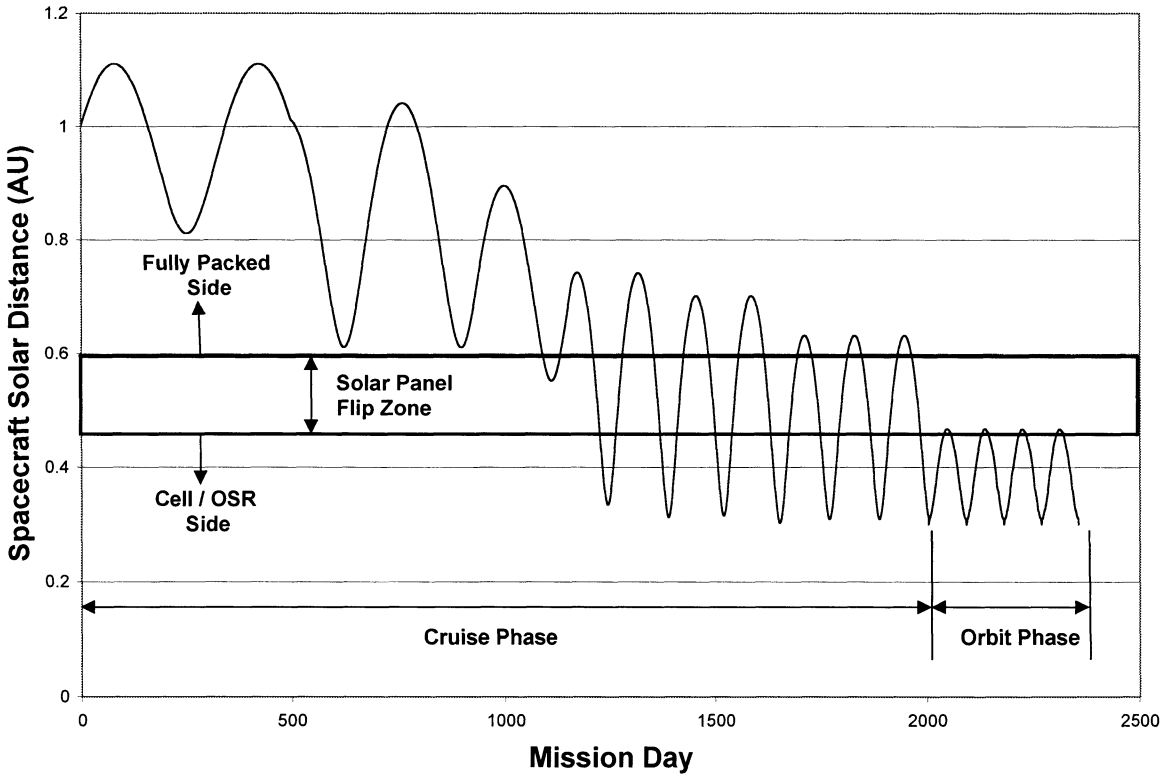

Figure 2. The MESSENGER mission profile. Cruise phase is five years and orbit phase is one year.

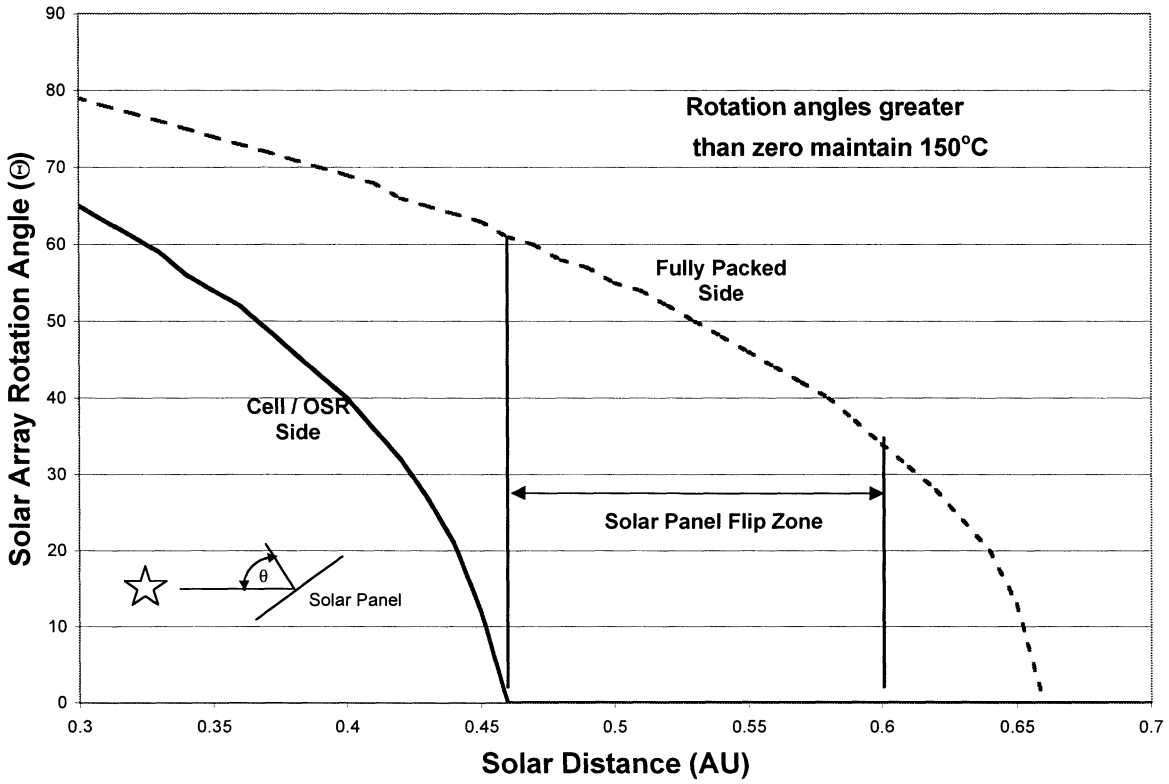

Figure 3. The solar panels are rotated to maintain the maximum temperatures at or below 150°C. The dual sided solar arrays have a wide flip zone to reduce operational constraints and minimize risks.

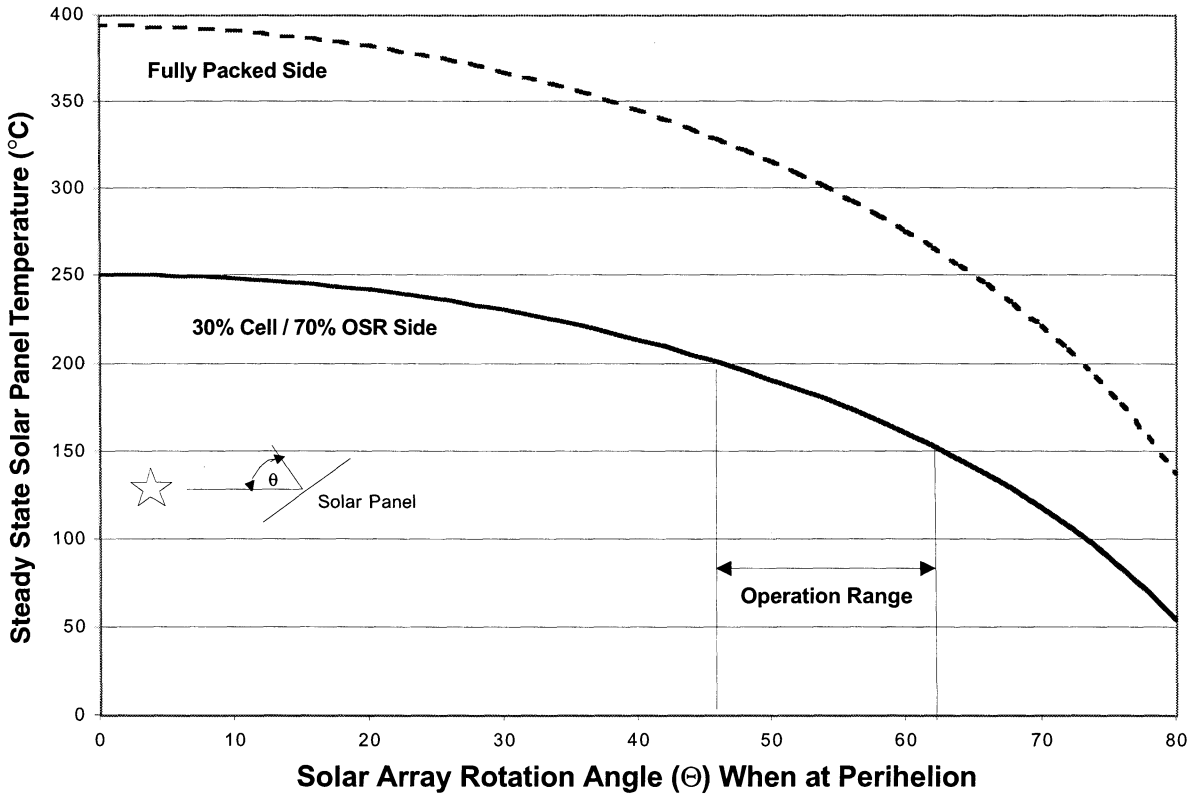

Figure 4. The OSR array side will maintain the steady state solar panel temperature below 260°C if Sun pointed when at perihelion. Note that the fully packed side could reach 400°C under the same condition.

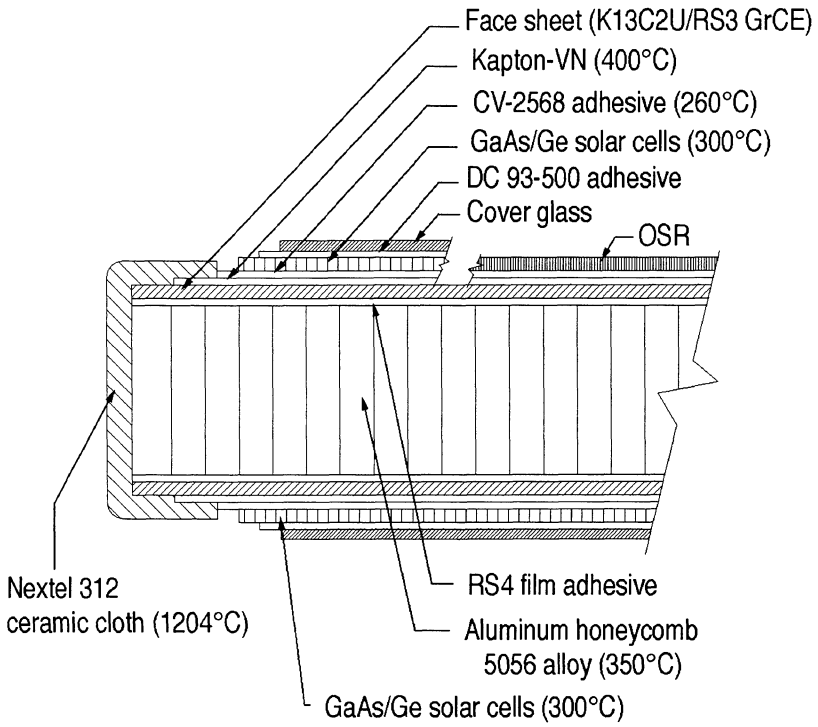

Figure 5. Solar panel cross-section showing maximum vendor recommended steady state temperatures. Solar panel materials and construction techniques were tested to temperatures in excess of 250°C.

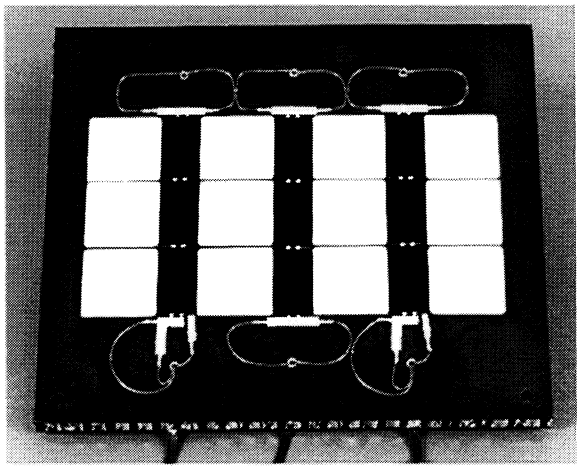

Figure 6. The prototype 30% solar cell and 70% OSR face of the dual sided array.

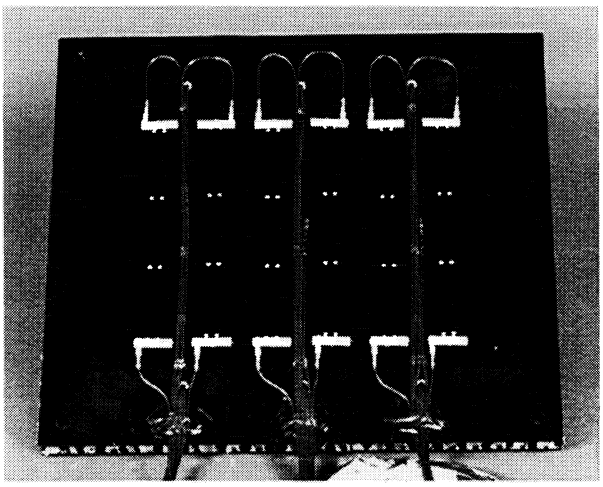

Figure 7. The prototype fully populated face of the dual sided array.

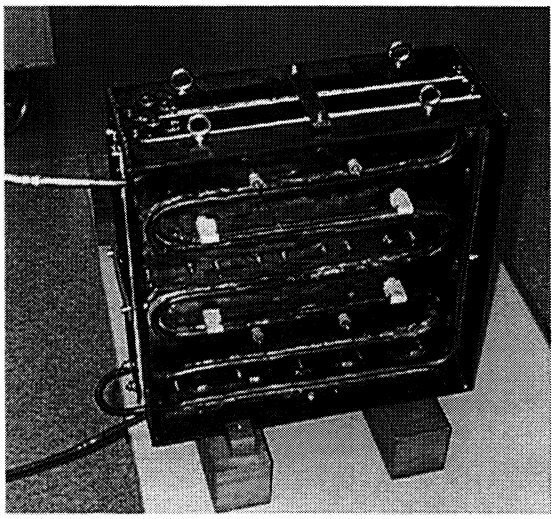

Figure 8. The E-box prior to large chamber installation. The E-box is liquid nitrogen cooled, and heated using 13 one kilowatt strip heaters.

Figure 9. The E-box in test configuration installed in the East chamber. Vacuum and high temperature kapton MLI insulate the E-Box from the room temperature walls of the East chamber.

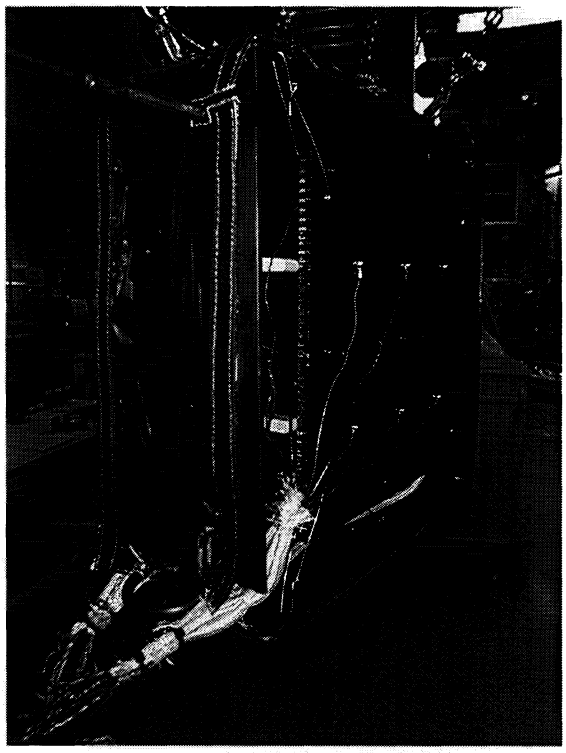

Figure 10. The E-Box being used to test Panel0 and Panel0A. Panel0 is visible in the right chamber with Panel0A (not seen) installed in the left chamber.

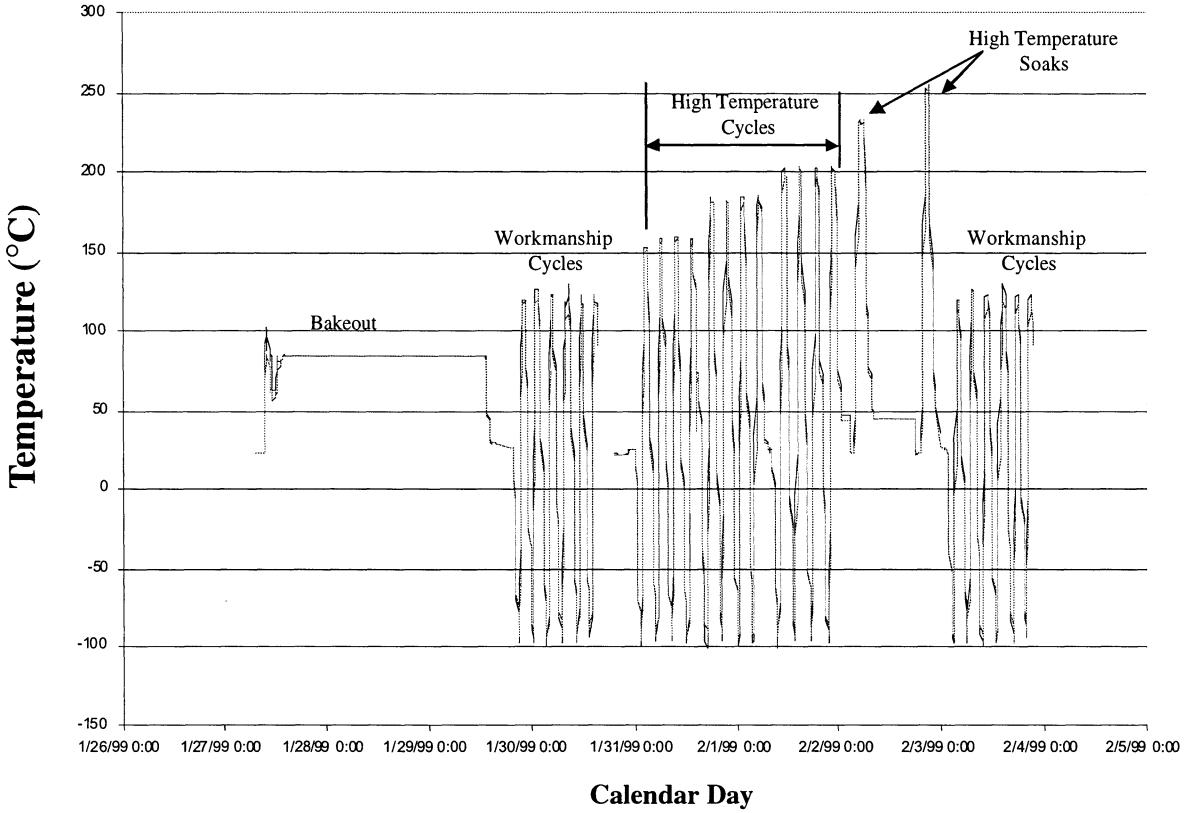

Figure 11. The actual test profile as run for Panel3 and Panel4, the dual sided prototype solar panels.

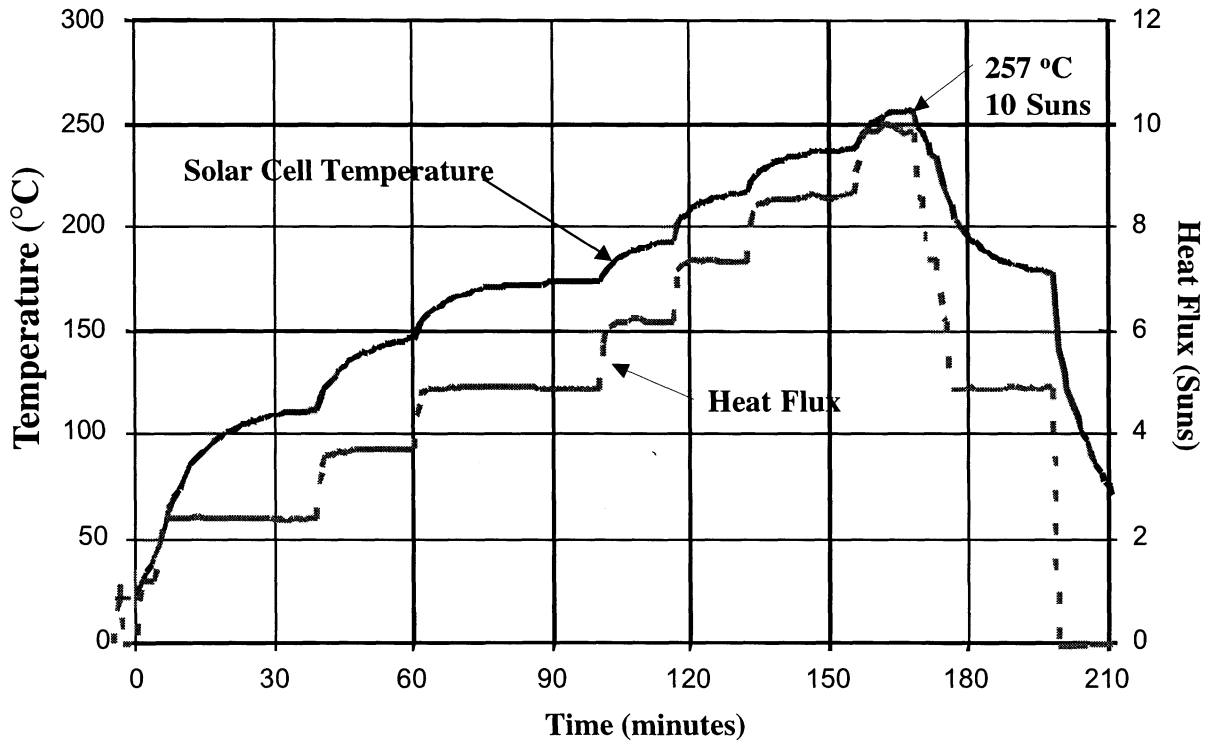

Figure 12. The results of the high-intensity illumination testing at GRC. The data represents cell temperature and simulated solar flux.

21ST SPACE SIMULATION CONFERENCE
DEVELOPMENTS IN THE INTESPACE TEST CENTRE FOR THE ARIANE 5 LAUNCHER

J.L. MARCÉ - J.C. PASQUET
INTESPACE

ABSTRACT

INTESPACE, Test Centre, is situated in Toulouse (France) and was created to test satellites launched by ARIANE 1-4 and other Russian or American launchers. This test centre is dimensioned for testing satellites up to 3.5 tonnes having a head diameter of 3.65m, that is, of the class 1/2 ARIANE 4.

Taking into account the arrival in the market of the ARIANE 5 launcher, it is necessary to make this center compatible with this new launcher and the other rival launchers. The developments envisaged will suit the needs of the ARIANE 5 (satellites with a mass of 5.5 tons having a diameter of 4.5m).

This document presents all the developments taking place at the centre, particularly:

- The setting up of a large airlock for unloading, suitable for containers of huge dimensions.
- The setting up under "one roof" of different facilities (continuity of the 100 000 class).
- The development of a compact range (modification of the positioner of the specimen and the source).
- The setting up of a very powerful anechoic wall for electromagnetic compatibility tests.
- The development of vibrations facility by the setting up of a new system of vibrations of 320kN with a large horizontal table.
- The adaptations in the thermal vacuum facilities, to make them compatible with the new satellite platforms.

These developments will be completed by early 2001 and will allow a reduction in the time taken for testing and transfers between the testing zones as well as an increase in the competitiveness of the centre in the international market. It will also ensure that INTESPACE remains the leader among independent European space testing centers.

INTRODUCTION

The INTESPACE test center is located in TOULOUSE (FRANCE) and had been created for testing space experiments and spacecrafts launched by ARIANE or others USA and Russian Rockets.

With the arrival on the market of the new Ariane 5 launcher, INTESPACE was forced to upgrade all its facilities to cater to the new generation of satellites carried on-board this launcher and similar launch vehicles.

The development strategy was aimed at telecommunications satellites, which are in the majority on the market and whose mass can reach an impressive 6.5 tonnes for a head diameter of 4.5 m and a height of up to 8 m. This category of satellites represents half the payload to be carried by Ariane 5. Full capacity Ariane satellites (eventually 11 tonnes) will be tested in the E.S.A. center in Noordwijk. INTESPACE has been selected to commercially operate this center in conjunction with IABG since 1 July 2000 through the joint subsidiary ETS (European Test Services) it has just founded with IABG.

The development of center has been carried out following three fondamental criteria :

- To offer to the customers modern facilities compatible with 6.5 tonnes satellites, services of quality, a maximal security for the hardware and staff and all of this with competitive prices, and with continuous effort in order to shorten testing duration.

- To offer a complete integrated center which enables to do the whole test under the same roof without the rupture of cleanliness class.

- To provide to every customer a center independent from the manufacturers.

PRESENTATION

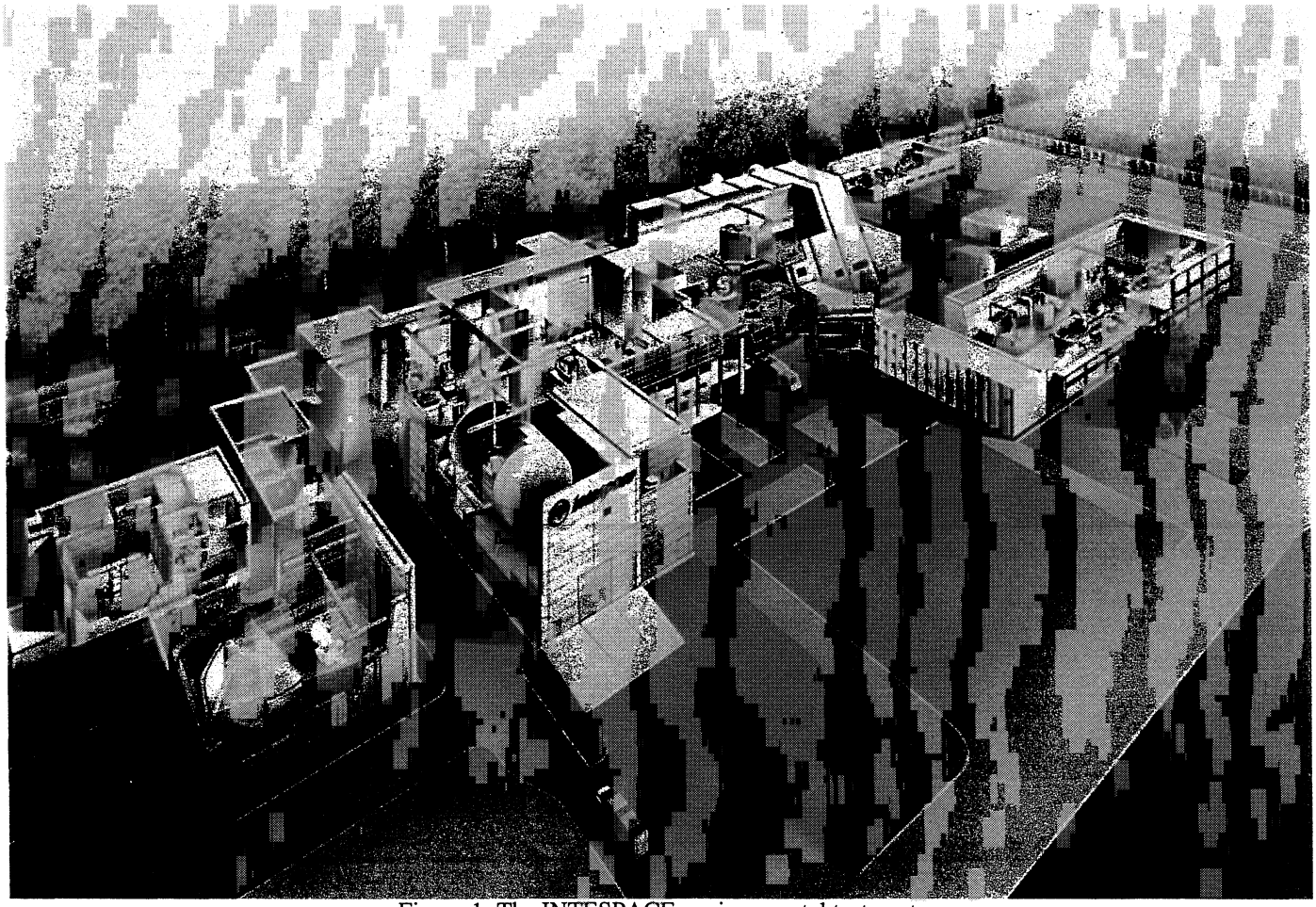

Figure 1: The INTESPACE environmental test centre

The evolution of launchers

The geostationary telecommunications satellite market is currently undergoing a major upheaval as the mass of future generation satellites increases to 6,5 tonnes providing up to a hundred channels.

To meet these new requirements, the capacities of ARIANE 4 launchers (head ∅ 3.65m, payload 4 700kg) or equivalent vehicles (ATLAS 2, PROTON) are no longer sufficient.

Tomorrow's launchers thus had to be made compatible with these new platforms.

ARIANESPACE has developed a new generation of ARIANE 5 launchers equipped with a 4.5 m diameter head and an eventual payload capacity of up to 11 tonnes with a double launch capacity of 2x5.500kg or the ability to use a «speltra» carrying 6.5 tonne satellites and a light satellite during «dissymmetric» double launches.

To respond to these objectives, INTESPACE is currently building a large-scale entry lock compatible with tomorrow's transport containers and a 100 000 class link between the environmental test centre (mechanical and thermal) and the electric test centre (anechoic chamber and compact antenna range). An overview of the centre is given below.

All facilities have been upgraded and converted to respond to these new satellite types.

By mid 2001, the test centre will include:

MECHANICAL FACILITIES

- A vibration test assembly, 320 kN horizontal (3.4 x 3 m) and 320 kN vertical fixed station with a potential of 640 kN horizontal by changing the configuration,
- An acoustic chamber of 1,100 m^3 with a new command/control system.

THERMAL FACILITIES:

- The solar vacuum (SIMLES), 6 m in diameter, is to have its thermal generator upgraded,
- The SIMMER thermal vacuum facility, 10 m in diameter, will be refitted (modifications to door screens) and its acquisition system will be brought up to 1.000 channels.

ELECTRIC FACILITIES:

- An 11 x 14 m wall will be built for full-power payload tests and the specimen positioner in the compact range will be modified to accommodate very large satellite antennae in the 5.5 x 5 m quiet zone.

INTEGRATION FACILITIES:

- Apart from the integration zones near the test facilities that will be equipped on a priority basis for the future satellites, the layout of the areas reserved for pre-test integration will be changed into a single large area of 800 m2 and the physical measurement facilities will be transferred to the vicinity of the container entry lock.

Space simulation testing at INTESPACE

INTESPACE's thermal facilities comprise two chambers in which the space environmental conditions -- -high vacuum, low temperatures, solar radiation-- can be simulated for the purposes of qualifying the thermal design of a spacecraft and performing the acceptance tests. These facilities can also be used for the mechanical tests in vacuum.

The SIMLES solar thermal vacuum facility consists of two chambers: a vertical main chamber (6 m dia. and 7 m high) and a horizontal auxiliary chamber (5.1 m dia. and 8.75 m long) placed side-by-side. The chamber's bottom loading system, at the base of the cylinder,

facilitates the installation of spacecraft of up to 3000 kg on the gimbal system.

The attitude simulator has two main functions :

- first, to simulate the satellite's movements in relation to the Sun (two-axis motion : tilt motion + to -90° and spin motion; one rotation/24 hours to 10 rpm);

- second, to provide an electrical interface and TC measurements (600 TC) between the satellite and its ESGE for the measurements to be made on the satellite itself and for temperature measurements as well (using the 220 channel-rotating collector).

The solar simulator, based on a Cassegrain system, features 36 optical blocks equipped with xenon arc lamps, a field lense, and a folding mirror as prime power sources, all of which being outside the chamber at normal atmospheric pressure. The collimation mirror, in the auxiliary chamber, is under vacuum conditions. The collimated horizontal solar beam, up to 4 m in diameter, delivers 400W/m^2 to 1600 W/m^2 per user test requirements.

The chamber is equipped with stainless steel shrouds heated and cooled by circulating gaseous nitrogen for temperatures controlled in a range from 100 to 360 K. The pumping system produces high-vacuum conditions of 10^{-5} mbar.

This facility has its own preparation bay -- 580 m^2 and 22 m high -- used to integrate the specimen prior to its testing.

The thermal generator in the facility will be upgraded by changing the turboblowers and electrical generators (250 HP engine).

The SIMMER thermal vacuum chamber consists of a large horizontal chamber (10 m dia. and 13.6 m long) equipped with a horizontal loading system. An adaptable trolley is used to install the spacecraft in either a vertical or horizontal position inside the chamber's test volume (9 m in dia. and 8.8 m long; possible extension up to 15 m).

The chamber is equipped with stainless steel shrouds that are temperature-controlled, using either gaseous or liquid nitrogen in a range from 100 to 360 K. High-vacuum conditions of 10^{-5} mbar can be achieved with the pumping system.

SIMMER also has its own preparation high bay (560 m^2 and 13 m high) used for final integration prior to testing.

The internal screens will be modified (door screens to be brought back by 2 m to accommodate 8 m high satellites on their base.

An integrated measurement system will bring the acquisition system up to 1,000 channels.

Access ways to the interior of the simulator will be fully modified to allow for final integration operations on specimens 8 metres high.

The surface of the experimenter room and back-up power will be doubled for the EGSE of future payloads.

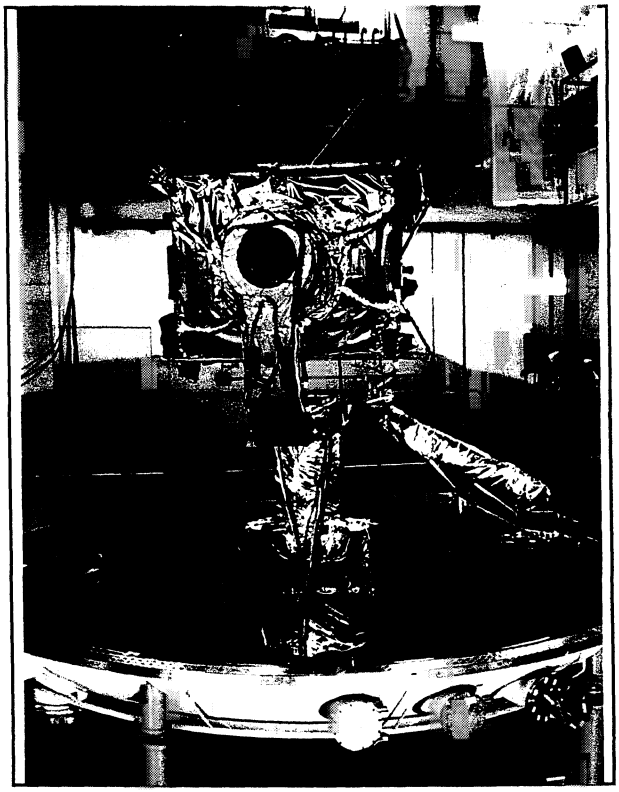

Figure 2: INTESPACE's large space simulation chamber (SIMLES)

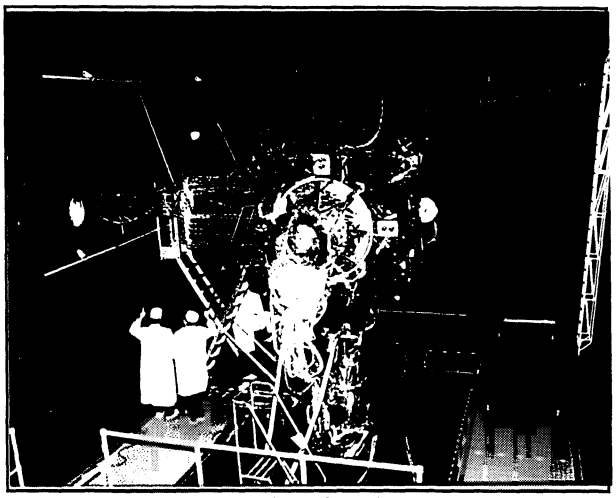

Figure 3: INTESPACE's large thermal vacuum chamber (SIMMER)

Dynamic testing at INTESPACE

INTESPACE's mechanical test facilities include a vibration test facility, an acoustic noise test facility, (reverberant acoustic chamber) and the mass properties machines to verify the integrity of the structural design of spacecraft and of their subsystems.

The controller ensures the safe operation of all subsystem and protects the specimen against excessive vibration levels via sensors placed over 15 points and at the shaker/specimen interface over eight points (as a maximum).

The acoustic noise facility simulates the noise generated by launch vehicles' engines and the vibration test facility reproduce the vibrations space vehicles are submitted to at launch. Qualification tests are performed on structural or protoflight models and acceptance tests on flight models.

The new multi-vibration system consists of four shakers. Two 160 kN shakers are coupled to a hydrostatic head expander (2.1 m in dia.) for tests in the vertical axis, and to two large slip tables (3.4 m x 3 m) for tests in the horizontal axis.

The four shakers can be coupled to the horizontal table to obtain 640 kN force. The new vibration system can test a satellite of 6.5 tonnes (plus 1.4 tonne of adaptor).

Vibration levels are programmed and the specimen monitored and safeguarded from a multi-channel controller, and its safety ensured.

A specific preparation high bay (200 m^2 and 13 m high) facilitates final integration prior to testing.

Finally, the vibration test facility satisfies the constraints due to the use of isopropyl alcohol in spacecraft pressurised tanks (2 tonnes).

The reverberant acoustic chamber simulates the spectral noise levels encountered by the spacecraft and portions of the launch vehicle during launch. An overall noise level of 156 dB can be reached in the 1100 m^3 reverberant acoustic chamber.

Figure 4: INTESPACE's large reverberant acoustic chamber

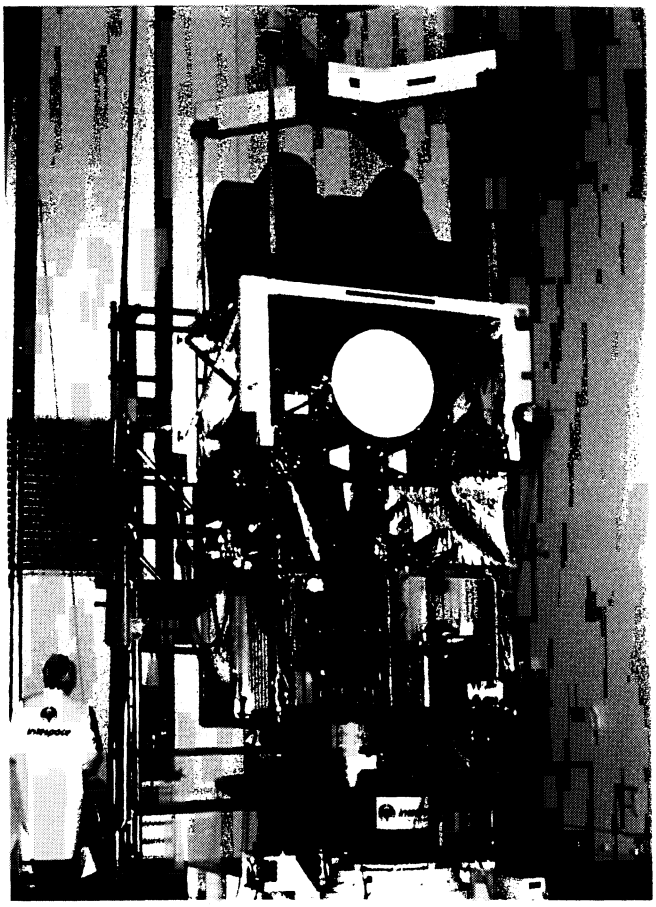

Figure 5: INTESPACE's multi-vibration system

Noise generation is ensured by pressurised gaseous nitrogen passing through three horns.

A flexible data acquisition subsystem provides for the acquisition and storage of the necessary vibroacoustic data from both the multi-vibration and the acoustic test facilities (accelerometers, strain gauges, microphones, etc).

This new subsystem consists of a 320 channel-data acquisition system and a data processing system being equipped, in addition to standard sinusoidal, random and acoustic data handling functionalities, with the DynaWorks® software package. DynaWorks® provides rapid sequences of operations for quicker visualisation, statistical comparison and analysis, permitting thereby to significantly reduce preparation times and test durations.

INTESPACE's mass properties machines are used to determine the mechanical characteristics of spacecraft (balancing, cog, moments of inertia). Specimens can be placed in either a horizontal or vertical position by means of a specific L-shaped associated with a turn-over device.

These facilities were specifically designed for the purpose of reducing test sequence durations.

The particularities of dynamic testing are :
- No changement of shakers configuration during vibration test, due to this configurationthe acceptance test duration for Telecom spacegraft is 5 days.
- No sensors disconnection between vibration and acoustic tests.
- Utilisation of the same data acquisition for vibration and acoustic tests and consequently no changement of configuration.

Electromagnetic testing at INTESPACE

INTESPACE's electromagnetic test facility is available for electromagnetic and electrostatic tests on either fully-integrated spacecraft or individual subsystems for the purpose of ensuring that mission performances will meet spacecraft specifications.

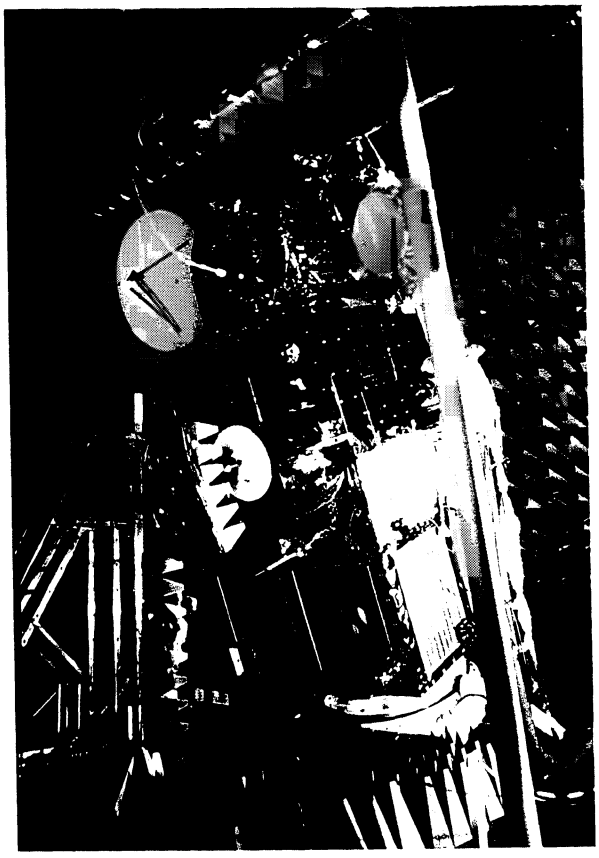

Figure 6: INTESPACE's EMC chamber

The test range consists of a large Faraday chamber with a useful test area 14 m long, 8 m wide and 10 m high. The walls and floor of the chamber are lined up with anechoïc materials. This shielded chamber is large enough to test large spacecraft with an antenna fully deployed for electromagnetic compatibility and auto-compatibility. A second Faraday cage is used for accommodation of the checkout equipment and a 200 m^2 area adjacent to the anechoïc chamber is used for spacecraft test preparation activities and accommodation of the EGSE.
Development and qualification tests are conducted according to space test specifications. Conducted and radiated emission tests and susceptibility tests are performed in the 30 Hz to 40 GHz frequency range.

Electrostatic discharge and high-field susceptibility measurements for large devices can also be performed.

INTESPACE's testing capabilities were improved to meet more stringent requirements, as defined in MIL-STD-461.

Electrical field levels are now 200V/m over 90% of the 10 kHz to 18 GHz frequency range. In the 18 to 40 GHz range, they are limited to 80 V/m. Test operations are fully automated via a real-time and closed-loop software.

High-field testing can be carried out on smaller subsystems in a third anechoïc test chamber.

INTESPACE's EMC anechoic chamber is designed to ensure that all system tests on integrated spacecraft --i.e. RF health tests, auto compatibility tests, "pimp tests"...-- are performed in the most effective way.

INTESPACE also provides EMC consultant services to the experimenters in the elaboration of the specifications and specific test procedures, and for test analysis.

Auxiliary test equipment --including antennas and antenna masts-- and microwave measuring equipment is made available to the customers. Finally, EMC test equipment is redundant on a stand-by mode to ensure test continuity and reduce test durations.

To perform full power tests on tomorrow's generation of telecommunications satellite payloads, a high-power wall measuring 11 x 14 m will be developed and will include all the safety elements needed:
- Infrared camera monitoring of hot points,
- Hot point detection before tests,
- Thermocouple instrumentation of anechoic point if required,
- Real-time monitoring of point temperature during tests.

A compact test range --MISTRAL-- is operational since 1997.

Situated in the INTESPACE's Coulomb building, the MISTRAL compact antenna test range is a test facility specifically designed for radiofrequency tests of spacecraft in their flight configuration.

The RF test range operates in the fully-controlled and isolated environment of the shielded anechoic chamber (30 x 20 x 15.5 m).

In a restricted space area, the Compact Test Range provides for the creation of a flat radiofrequency wave showing the same characteristics as those generated in a far-field range.

A series a RF sources covering the 1.47 to 40 GHz frequency band (provision is being made for 200 GHz) is placed in the focal plane of a hyperboloid subreflector which reflects RF radiations to a main paraboloid reflector. Its Cassegrain-type design provides for a test volume (5.5 x 5 x 6 m) within a short distance of the main reflector.

The spacecraft to be tested is placed on top of a 3-axis positioner.

The following measurements could be performed : antenna patterns measurements, end to end tests, transponder tests, Pimp, RF saturated flux density.

For future satellite generations, a new positioning base will be developed and the quiet zone will be extended by the addition of a rail to the specimen positioner.

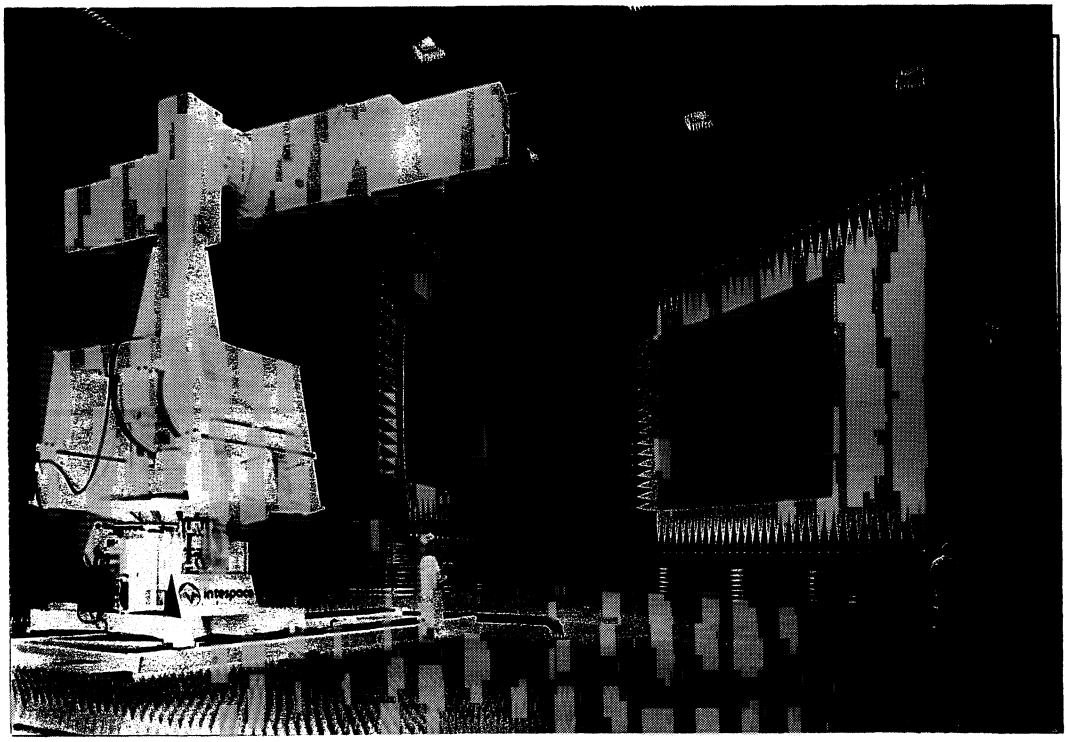

Figure 7: Compact antenna test range "MISTRAL"

INTESPACE : A UNIQUE TEST CENTRE IN EUROPE

The INTESPACE Space Test Centre features unique characteristics for satellite projects, which positions it as one of the leading test centres in Europe. The major distinctive characteristics of INTESPACE are as follows:

INTESPACE: a specialist in satellite testing

INTESPACE is a company specifically dedicated to the control of environmental conditions, with satellite and subsystem tests representing approximately two-third of the total activities of the company. The management of INTESPACE's personnel and technical facilities is entirely oriented towards space projects and turnkey test services and associated logistics support services.

INTESPACE carried out more than 100 test campaigns on satellites and large systems to the benefit of the international space community since 1984.

All the test facilities under one roof

- The major test facilities at INTESPACE are grouped under one roof, with all the test high bays beingcontrolled as per class 100 000 cleanliness conditions (Fed. Std 209).

  The integrated spacecraft to be tested can thus move smoothly and quickly from one facility to another without having to be reconfigured between the tests, thus reducing the risk of not fulfilling all cleanliness conditions. A centralised control system helps the experimenters in monitoring and verifying the cleanliness parameters, via terminals distributed in all the test areas.

- INTESPACE offers a full range of test facilities specifically adapted to the testing of spacecraft, including acoustic, vibration, thermal balance, thermal vacuum, electromagnetic compatibility, physical properties facilities.

  All integrations halls will be refitted and reconfigurable. They will provide a class 100 000 area of 800 m^2 which can be reconfigured into 3 zones of 250 m^2 each.

Optimised mechanical test facilities for a better productivity

- Vibration tests are performed on two dedicated vibration test facilities:

  - Two shakers of 160 kN each for tests in the longitudinal axis of the satellite (coupled to a vertical head expander 2.1 m in diameter);
  - Two shakers of 160 kN each for test in the lateral axis of the satellite (coupled to a horizontal slip table 3.4 x 3 m).

  This configuration is used to avoid loosing time when tilting the shaker in the case of a single shaker configuration.

- In addition, the interconnection panels of the accelerometers are mobile and maintained connected to the satellite throughout the vibration and acoustic tests. This specific characteristic offers two advantage : (1) ensuring that the test is being performed ina most riskfree manner in terms of error, connection, cable damage, and (2) contributing to reduce preparation durations and increase the overall quality of the tests.

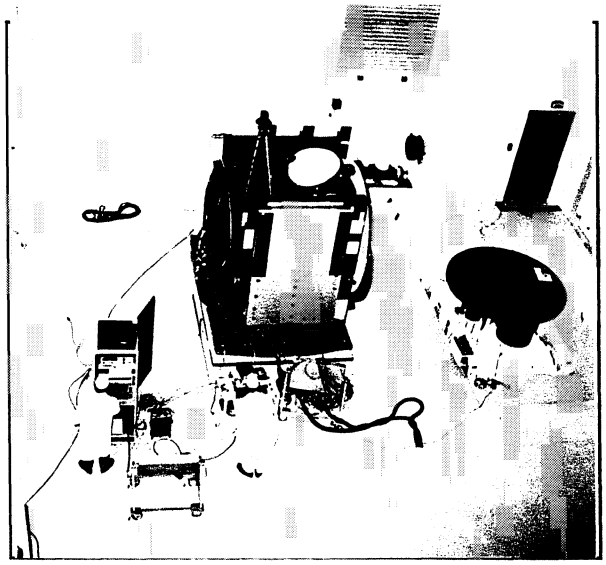

Figure 8: INTESPACE's multi-vibration system

Effectiveness increased through test predictions

The vibration tests are performed with increased effectiveness due to the use, by INTESPACE, of a test prediction tool allowing to determine the satellite/test facility interaction in advance, and thus, to adjust the test facility's control parameters.

Test predictions for tests on an electrodynamic shaker per given specifications can be obtained by coupling a model of the shaker --derived from analysis or modal survey-- with either a physical, matrix or modal-type model of the specimen and of its adapter. Control predictions can also be obtained from the simulation of the control loop and the use of previous test results or data. All of these predictions will yield analyses that will respond to any situation, i.e. from feasibility studies for such aspects as the shaker's performance

capabilities, parasitic motions, and specimen behaviours to the determination of the shaker's optimum control prior to or between the test runs.

The shaker, adapter, and specimen models together with the control parameters, feasibility test results, adapter performance, specimen behaviours, and control performance capabilities can be obtained from given test specifications to prepare the test campaign and/or ajust the test parameters prior to or between the test runs.

This methodology is likely to be applied to the INTESPACE's multi-vibration test facilities, with an updated finite element model of the moving part of the shaker. This will be achieved in two steps for taking basic requirements first into account and then for providing a general tool.

Improving test productivity : the DynaWorks® response

INTESPACE develops solutions for today's applications to ensure the successful integration of the tests in the industrial development of the product.

The DynaWorks®, software is the result of INTESPACE's eminent experience in testing.

DynaWorks®, is the response to the necessity for improved productivity and when environmental factors are extensively involved in sectors of industry such as the aeroanautics, space, defence, automation and transport, energy, shipbuilding, etc. sectors. It is a valuable tool intended to design and structure analysis departments, environmental testing laboratories, in-site environment measuring instruments, environmental engineering specialists and management teams.

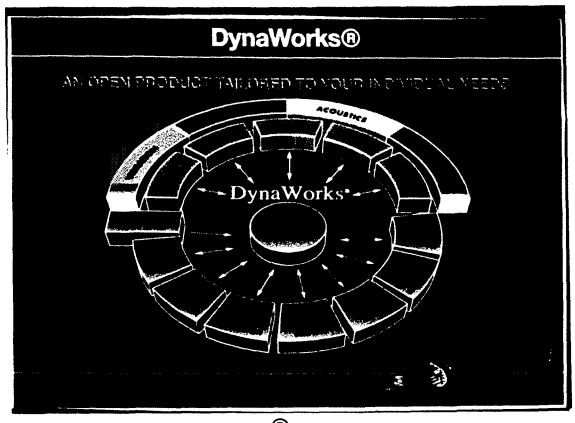

Figure 9: DynaWorks®, an open product tailored to your individual needs

DynaWorks®, is a powerful relational test data management and analysis system that allows product designers and test engineers to capture, analyse, and organise the test results generated throughout the product's life cycle. The test results obtained from heterogeneous systems during the vibration, shock, acoustic, thermal balance, ... tests can now be standardised and organised effectively with DynaWorks.

The powerful query functions of DynaWorks® provide for quick and comprehensive analysis of complex correlations such as the correlation of predicted results against experimentally obtained results, reducing thereby the development cycles of the products. With an excellent 2D and 3D graphics, a user-friendly X-WindowsTM interface, and context-sensitive on-line helps, the users will enjoy immediate increases in productivity.

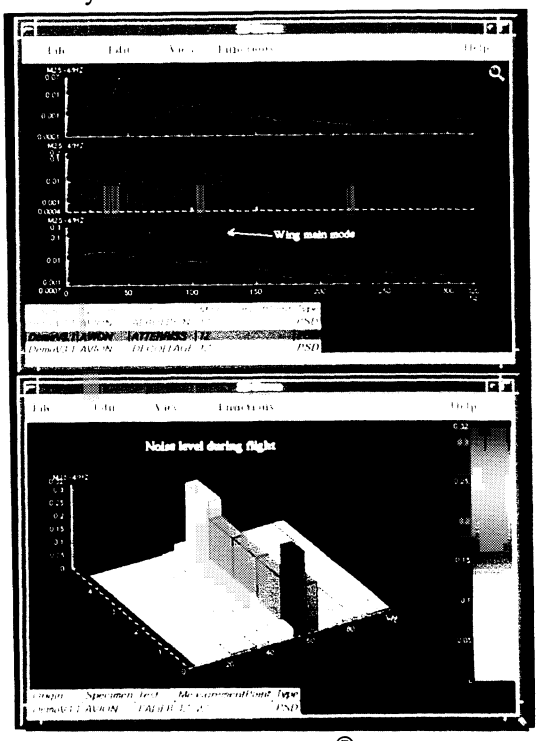

Figure 10: DynaWorks® high-level graphics capabilities

Combining physical measurement facilities for high-performance measurements

INTESPACE performs all the measurements related to the physical properties of a satellite (i.e. inertia, cog, balancing) on a combined test facility coupled with a tilt device to safely position the satellite on its three-axes.

This unique combined test facility configuration facilitates the handling of the satellite and significantly reduces the duration of the measurement campaign.

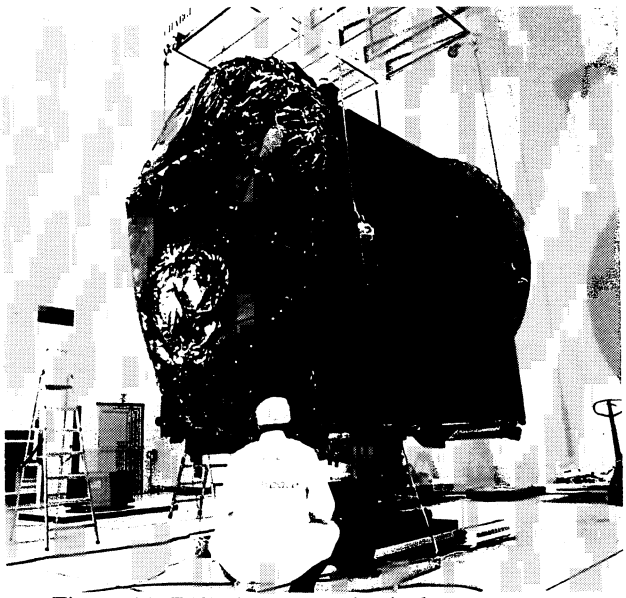

Figure 11: INTESPACE's physical measurement combined facility

Redundant and flexible thermal test facilities

INTESPACE has two large thermal-vacuum chambers, mutually compatible, dedicated to satellite acceptance tests :

- the SIMLES test chamber --a vertical chamber with a useful volume of 200m^3,
- the SIMMER test chamber --a horizontal chamber with a useful volume of 560m^3.

Both test facilities are perfectly compatible with one another in terms of mechanical and electrical interfaces with the satellite. Likewise, the measuring systems and test data processing systems are identical for both test chambers.

A high availability rate for the thermal test facilities is ensured to customers --even in the case of a failure during the test-- through the provision of redundant facilities.

Improving predictions and analysis tests results

INTESPACE offers design, research and consulting services in environmental techniques for the design of sophisticated mechanical systems and prediction of their behaviour. These activities cover the following :

- In the acoustic and vibrations tests area :
  - solving vibration and noise problems,
  - environment diagnosis,
  - verifying and readjusting previsional models in view of testing,
  - development platform of an analysis for structural dynamics,
  - vibroacoustic transmission analysis,
  - system or equipment qualification,
  - creation of environment databases.

- In the advanced dynamic tests area :
  - accurate measurement of the transfer function,
  - experimental modal analysis (multipoint excitation or shaker-induced excitation),
  - microdynamic tests (equipment or transmission characterization),
  - transient vibrations.

Calibration

Sensors and measuring equipment in the following areas :

- Acceleration.
- Temperature.
- Mass.
- Electrical quantities for which INTESPACE has COFRAC* calibration accreditation.
- Particule counters.
- Flowmeters.
- Pressure sensors.
- Acoustics, an area in which INTESPACE has earned industrywide recognition.

* COFRAC : French certification organization.

- In the development area of new thermal testing methods:
  - infrared tests,
  - tests with temperature-regulated plates.

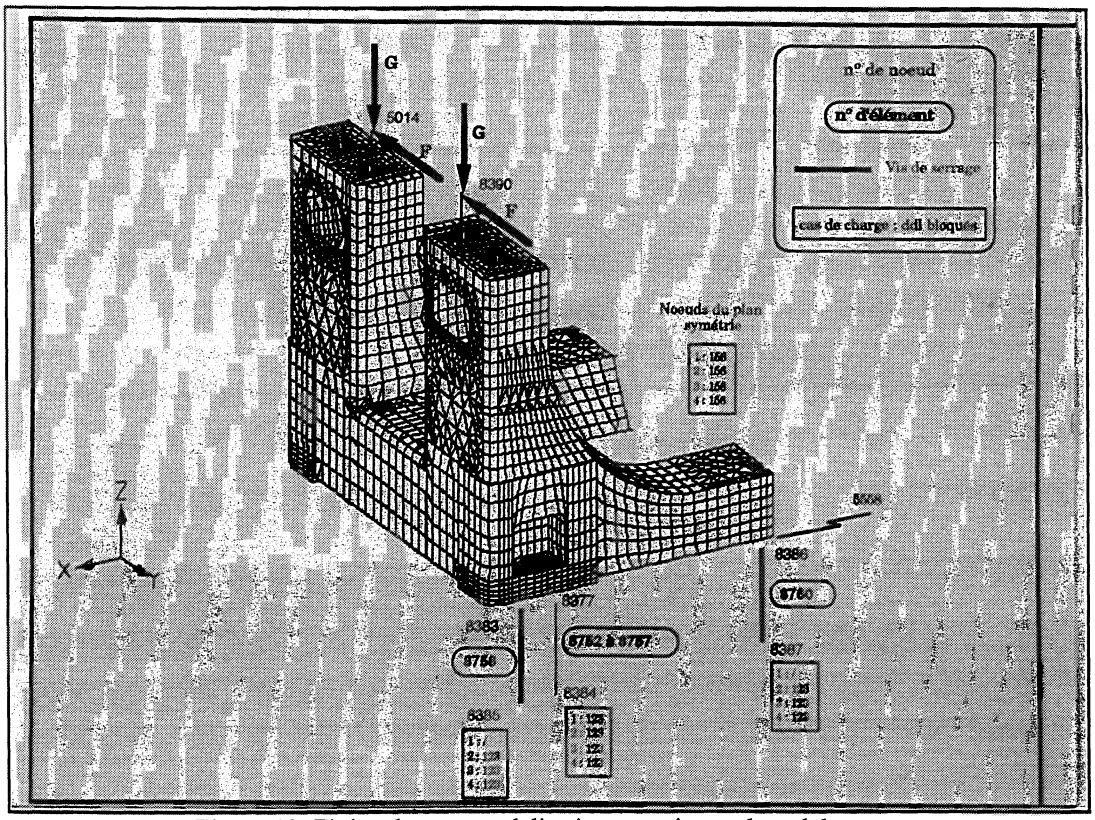

Figure 12: Finite element modelisation experimental modal survey

Improving the quality of the test

INTESPACE offers a high-quality service encomparsing calibration, verification and adjustment of out - of - tolerance measuring equipment.

Metrology

Simulating the space environment calls for highly sophisticated vacuum, cryogenic, optical and thermal technologies that must be closely monitored by skilled personnel applying a strict methodology. INTESPACE qualifies materials, paints, test facilities and other items for the space industry.

Engineering

INTESPACE also offers a variety of services relative to test centre and test facility engineering, including consulting, technical assistance, 'turnkey' missions and personnel training.

INTESPACE's competence in terms of test centre engineering is the result of :

- INTESPACE test laboratories' consolidated experience with more than 300 tests each year;

- INTESPACE's effort to establish cooperations with industrial partners, whether Prime Contractors, reasearch laboratories, universities and institutes;

- INTESPACE's participation in launch campaigns via permanent representatives in the European Space

- Launch site in Kourou (French Guiana);

- the direct payoffs from the previous installation of test centres in Europe, Brazil, Israël, South Korea and Republic of China.

INTESPACE involves the best European experts in the whole spectrum of the activities required by the polyvalence of the techniques to be implemented within an integration and test centre.

INTESPACE : INDEPENDENT CENTER

INTESPACE was created in 1983. INTESPACE shareholders are major French space industrials: CNES (39 %), ASTRIUM (38 %), ALCATEL ESPACE (13 %) - plus the Employees' Mutual Funds (10%).

INTESPACE is one of the 4 European coordinated test centres and formally approved by the European Space Agency, to conduct a number of services on behalf of the main international space industrials involved in European programmes. INTESPACE is RNE/COFRAC- and BNM/COFRAC- accredited at national level.

INTESPACE is an independent center and is a garantee for our customers and the customers of our customers. And by its new investment remains the european leader of the independant European Space Test Centers well suited to the new capability of the ARIANE 5 launch.

MAIN PARAMETERS OF THE INTESPACE FACILITIES
Electrical testing facilities

THE ELECTROMAGNETIC COMPATIBILITY TEST FACILITY

Configuration

Chamber	
. overall dimensions	16 x 10 x 11 m high
. test volume	14 x 8 x 10 m high
Door access	5 x 6 m high
Preparation bay	16 x 14.5 x 13 m high
Crane	100 kN
Cleanliness	class 100 000

EMC test capability

RF performance of the shield anechoïc chamber

• reflectivity	UHF > 30 dB
	L band > 40 dB
	C band > 50 dB
	K band > 50 dB

EMI isolation

• electric fields	14 kHz - 200 MHz
	atten. > 12 dB
• plane waves	200 MHz - 1 GHz
	atten. > 100 dB
	1 - 10 GHz, atten. > 80 dB
• magnetic fields	14 kHz, atten. > 70 dB
	250 kHz, atten. > 100 dB

Measurement system

• emission measurement	emission receivers
• spectrum analysis	30 MHz - 1 GHz
	range 100 Hz - 22 GHz
	extension to 40 GHz with mixers

Susceptibility system

• generators	10 Hz - 10 GHz
• amplifiers (range)	10 Hz - 18 GHz
	power 10 - 2000 W
	18 - 40 GHz, 3 W power

THE COMPACT ANTENNA TEST RANGE

Shielded anechoic chamber

Dimensions	30 x 20 x 15.5 m
Environmental parameters :	
• temperature	21°C ± 2°C
• humidity	50% + 10%
• cleanliness	100 000 class (Fed. Std 209)
Seismic ground isolation	
Faraday cage	

Reflectors

Dimensions	7.5 x 6 m (66 tons)
Subreflector dimensions	5.6 x 5.3 m (44 tons)
Serration length	150 cm
Surface accuracy	25 µm RMS
Equivalent focal length	130 m

Quiet zone performance

Dimensions :	
• height	5 m
• depth	6 m
• width : . focused :	5.5 m
. defocused :	up to 5.5 m left
	up to 3.3 m right
Frequency range	1.47 - 40 GHz (provision to 200 GHz)
Polarisation	linear, circular
Ripple amplitude	± 0.5 dB
Ripple phase	± 6°
Typical cross polarisation	< -40 dB
Cross polarisation accuracy at -30 dB	± .75 dB
Measurement accuracies :	
• Side lobes at -30dB	±.75 dB
• Gain	± .25 dB

Ground support equipment

Positioner	5 axes
Load capacity	6 000 kg
Travelling overhead crane capacity	10 tons
Anechoic chamber access door	6 x 11 m
Experimenters room	128 m2
Automatic access controlled area	
Fire detection and fighting systems	

THE 1100 m^3 ACOUSTIC TEST FACILITY

Configuration (chamber)

Volume	1100 m^3
Dimensions	10.3 x 8.2 x 12 m high
Door access	6 x 11.5 m high
Crane load (max.)	100 kN
Cleanliness	class 100 000

Acoustic capability

Overall sound pressure level	156 dB
Chamber suspension resonant frequency	16 Hz
Lowest frequency cut-off	13 Hz
Excited frequency	22.4 Hz - 11.2 kHz

Max. contr. frequ. bandw. random : 125 - 1000 Hz

Modal density	5 modes/1/3 oct. at 31.5 Hz
	> 100 modes per 1/3 octave at 100 Hz
Mean reverberation time	10 s

Control capability

Control	8 microph. in chamber
Processing	multiplexing, real-time analyser

THE 300 kN MULTI-VIBRATION SYSTEM

Vibration capability

Force ratings	
• longitudinal axis	320 kN sine mode
• lateral axis	
- standard	320 kN sine, random
- push pull	640 kN sine
Frequency bandwidth	
• sinusoïdal low level	2 - 2000 Hz
• sinusoïdal high level	2 - 500 Hz
• random	10 - 2000 Hz
Maximum payload	7 900 kg
Maximum velocity	1.6 m/s
Displacement	50.8 mm in random and shocks
	38 mm peak to peak in sine mode
Vertical head expander	2.1 m
Horizontal slip table	3.4 x 3 m

Control capability

Digital console	
• control channels	8 max. sine
	16 max. random
• monitoring channels	15 for notching
	and/or S/C safety

MECHANICAL DATA ACQUISITION & PROCESSING SYSTEM

Vibro-acoustic data handling system

• Accelerometer channels	240
• Strain gauge channels	64
• Microphone channels	16
Acquisition capabilities	320

Reduction capabilities

- Sine : global and/or filtered amplitude transfer function, distortion
- Random : PSD (narrow band, 1/3 octave, octave), RMS value, transfer function, coherence function
- Acoustic
  - accelerometers and others as random process
  - microphones : ASPL (narrow band, 1/3 octave, octave), OASPL

THE SIMLES SOLAR SIMULATOR

Configuration (main chamber)

Orientation	vertical
Test volume	6 m dia. x 7 m high
Access	bottom loader

Pumping system

Working pressure	$< 10^{-5}$ mbar
Roughing	mechanical : 12 000 m^3/h
Booster	turbomolecular : 6500 l/s
High vacuum (cryopumps)	20 K. 130 000 l/s

Thermal shrouds (main chamber)

Temperature range	100 - 360 K
Temperature uniformity	± 10 K at 100 K
Emissivity	≥ 0.85
Absorptivity	≥ 0.95

Solar simulation

Solar beam (horizontal)	up to 4 m dia.
Intensity	400 - 16000 W/m^2
Intensity uniformity	± 4 %
Collimation angle	± 1.9
Stability	< ± 1%
Spectrum	xenon

Gimbal system

Two-axis	S/C mass : 2500 kg
Spin axis in vertical position	S/C mass : 3000 kg
Spin motion (variable)	1 rotation/24hr to 10 rpm
Attitude motion :	
• alternating	± 90°
• speed	7.5°/min

THE SIMMER THERMAL VACUUM CHAMBER

Configuration

Orientation	horizontal
Overall dimensions	10 m dia. x 13.6 m long
Test volume	9 m dia. x 10.8 m long
Access	horizontal loader
SIMMER bay	560 m^2 x 13 m high

Pumping system

Working pressure	$< 10^{-5}$ mbar
Roughing	mechanical : 12 000 m^3/h
Booster	turbomolecular : 6500 L/s
High vacuum	130 000 L/s

Thermal shrouds

Temperature range	standard 100 - 360 K option 80 K
Temperature uniformity	± 10 K
Emissivity	≥ 0.85
Absorptivity	≥ 0.95

THERMAL DATA ACQUISITION AND PROCESSING SYSTEM

- Acquisition and storage of 396 Cu-Con thermocouple signals
- Acquisition and storage of 96 voltages and 96 currents
- Real-time analysis of test results using dedicated software packages

Multiple Pages Intentionally Left Blank

HIGH-SPEED AUTOMATED TESTER FOR VACUUM CHAMBER FEEDTHROUGH CONNECTORS AND CABLES

Robert H. Swope

NSI Technology Services Corporation
A Subsidiary of ManTech International Corporation
Goddard Space Flight Center

ABSTRACT

The Goddard Space Flight Center's thermal vacuum laboratory has developed a high-speed automated system for testing the integrity of 37-pin MIL-C-5015 cylindrical electrical feedthrough connectors used on penetration plates of thermal vacuum chambers. The system consists of a desktop P.C. driving a data acquisition front end. The latter measures the resistance through each pin of the connector and the resistance from each pin to all other pins and the connector shell. In addition to identifying unacceptable feedthroughs, the system is also used for testing cables. In the special case of Type T thermocouples, the difference in resistance between the copper and constantan wires provides positive proof of accidentally reversed connector wiring.

Computer running time to completely test a cable or feedthrough connector is less than thirty seconds. The system provides a hardcopy printout of the resistance readings. Connectors or cables with fewer wires are tested using simple adapter cables. Initial tests indicate that the performance of a given feedthrough connector can be predicted on the basis of measured resistance readings, reducing ongoing cost of connector replacement.

The opportunity to positively certify the integrity of cables, cable connectors and feedthroughs *before* the start of a thermal vacuum test minimizes the likelihood of a circuit problem that would require returning the chamber to ambient conditions for repair.

This system has two principal advantages for the Goddard thermal vacuum laboratory. Its only significant cost was the labor to fabricate the tester cable and shorting cable -- about 40 man-hours total. The system was built around a computer and data acquisition unit that were already on hand. The second advantage is that it very quickly tests both of the parameters that are essential.

HARDWARE AND SOFTWARE

The hardware components consist of the personal computer, a data acquisition/control unit, two types of modules for the data acquisition unit and a pair of thirty-foot cables to reach feedthroughs on penetration plates high above the floor on a 27 ft. x 40 ft. vertical vacuum chamber. Each of the 37 conductors (#22 AWG) in the **tester cable** connects to one pin of the mating connector on the free end of the cable. When the through-resistance of the connector pins is being measured, the 37-circuit tester cable is connected to the male side of the connector and a **shorting cable** is connected to the female side. The shorting cable shorts all 37 pins together and returns them to the resistance-measuring voltmeter module. For measuring pin-to-pin resistance, the shorting cable is removed, leaving the female side open.

Making the measurements requires two types of input modules for the data acquisition unit. Two 20-channel multiplexer modules in conjunction with the multimeter module provide the actual resistance measurement for both the through-resistance and pin-to-pin tests. In addition, the pin-to-pin test uses three 16-channel general purpose relay modules. Each conductor in the tester cable connects to one channel of the multiplexer **and** one channel of the relay module.

The desktop P.C. runs a program written in an object-oriented data acquisition application. The Ethernet port on the P.C. provides communication with the data acquisition unit and a laser printer. The LAN is converted to IEEE-488 for both units by a LAN gateway.

For the through-resistance of the connector under test, the program first establishes the through resistances of all pins of a known good connector -- a brand new one. Since a new 37-pin connector typically has resistances of less than 0.01 ohms, this step is really measuring the tester cable resistance. It stores those values in an array to be used for all subsequent measurements in a given session. Then, when the connector under test is being tested, the program subtracts the reference readings from the test readings to obtain the pin resistances.

The computer program measures pin-to-pin resistances by measuring the resistance from a given pin to *all other pins together.* It is not possible, therefore, to identify specifically which pins have a low resistance between them. The program was originally written to check from each pin to every other one individually. However, the testing took longer than four minutes per connector for the pin-to-pin test alone. For our purposes, knowing the exact pins involved is not important. If cleaning the exterior pins and glass seals does not improve the resistance, the feedthrough is set aside and marked as defective.

SYSTEM OPERATION

The operator interface for the computer program is a set of three buttons on the monitor screen for a) reference scan, b) through-resistance of connector under test, and c) pin-to-pin test. After the user has connected the tester cable to a brand new feedthrough, clicking on the first button measures the sum of the tester cable and shorting cable resistances. After the tester cable and shorting cable have been connected to the feedthrough under test, the second button repeats the resistance measurement, subtracts the cable resistance, and prints the data hardcopy. To finish the test, the user disconnects the shorting cable and clicks the pin-to-pin button on the monitor screen. All three buttons prompt the user to enter the facility number, port number, penetration plate number and feedthrough number. These items appear as a header on the hardcopy, along with the date and time.

The average time to test a connector is about two to three minutes. Most of that time is spent connecting and disconnecting the tester cable and shorting cable, which is time-consuming with threaded connectors. Program running time is approximately ten seconds for each of the three test phases.

A connector fails the through-resistance test if any pin has greater than 1 ohm resistance (for reference, 1 ohm is the approximate resistance of 60 feet of #22 AWG copper wire). In the pin-to-pin test, a connector fails if any pin measures less than 3 megohms to all other pins.

RESULTS

In the first phase of testing all feedthroughs in the lab, 137 connectors were tested (all were 37-pin). Only a small percentage showed pin-to-pin problems; some of those were corrected by cleaning the male pins and glass seals. Others apparently had internal contamination between pins.

Through-resistance test results varied widely from one feedthrough to another. Some appeared to be brand new, with all resistances ≤ 0.01 ohms. Many others passed the test with small resistances under 1 ohm. Several, however, had some pins in the range of 100K to 2 Megohms. The worst feedthrough had 11 of the 37 pins in excess of 3.3 Megohms through-resistance.

DISCUSSION

The pins in the 37-pin feedthroughs are not continuous from the room side to the vacuum side. When the feedthroughs are assembled by the manufacturer, the male pins and female pins are joined inside the body by a friction-fit pin and socket arrangement as the room-side insert is pushed into the connector shell. The room-side insert is then held in place by a spring clip.

A wide variety of voltages, currents and frequencies pass through the feedthrough connectors in thermal vacuum testing, which probably accounts for the large range of through-resistances in some of the assemblies. A likely failure scenario would be bootstrapping of corrosion at the internal joints for a circuit carrying significant current. A small increase in resistance would produce an increase in I^2R heating, which could cause further degradation and more increase in resistance. The connectors are rated at 5 amps maximum current. At that current, even as little as 1 ohm resistance would produce 25 watts of heat concentrated into a very small area, which could overheat the pin quickly.

If corrosion due to chemical reaction with the silver plated pins is the cause of increased resistance, a possible source of corrosion is air trapped inside the feedthrough shell. A Goddard failure analysis report (Ref. 1) examining arcing inside MIL-C-5015 37-pin connectors stated, "It is probable that outgassing of this cavity is sufficiently slow to allow air to remain for some time, even after the chamber has reached a relatively hard vacuum". While it is standard practice to turn off electrical circuits in a chamber during pumpdown to avoid corona (arcing), the pressure in the feedthrough cavity could conceivably still be in the corona range when circuits are activated, which could produce ions corrosive to the silver plating.

REFERENCE

1. *Failure Analysis of Cannon Connectors, Types TBFH 28-21-PS-200 and TBFH 22952-3.* Failure Analysis Section Termination Report, Serial No. 577, NASA Goddard Space Flight Center, June 4, 1966.

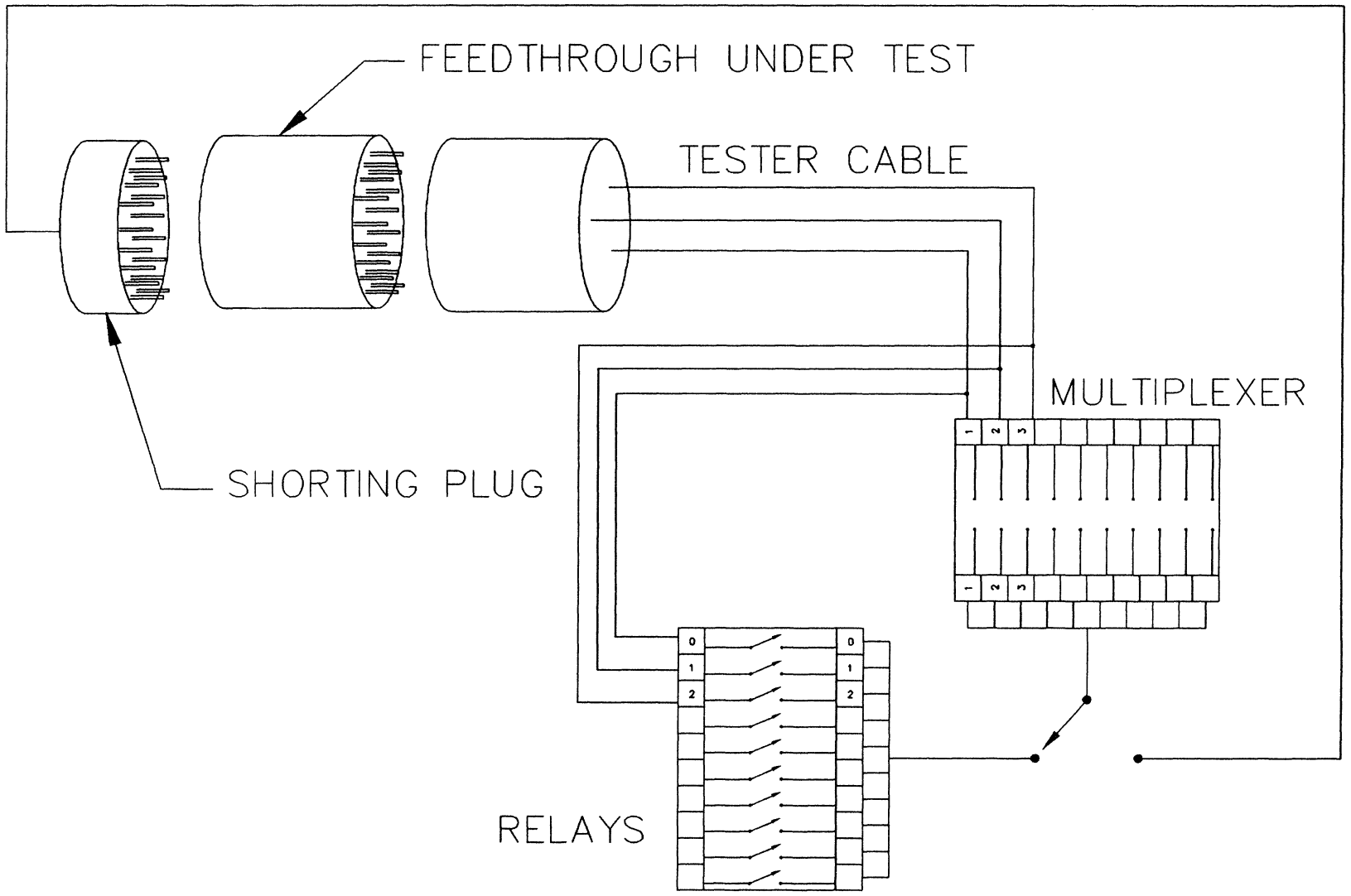

Figure 1: Schematic of Feedthrough Tester

PREPARATIONS AND PERFORMANCE OF LARGE SPACE SIMULATION CHAMBER (LSSC) DURING INSAT–2E SOLAR SIMULATION THERMAL BALANCE AND THERMAL VACUUM PERFORMANCE TESTS

R. Satish, P.Govindan, C.Kulkarni, Arvind Adhikary, R. Gopinath, D.K.Sagaraya Raj, P.Aravindakshan, S.N.Prakash, Dr. N.K.Misra, B.N.Baliga.

Environmental Test Facilities Division,
ISRO Satellite Centre, Bangalore – 560 017, India.

ABSTRACT

Solar simulation Thermal Balance and Thermal Vacuum performance tests on INSAT-2E (Indian National Satellite) were conducted in the Large Space Simulation Chamber (LSSC) available at ISRO Satellite Centre, Bangalore, India during October-November1998. The performance of the chamber system was excellent. Both tests were conducted in stabilized environments of vacuum, temperature, solar beam and motion simulator operations as required. The good performance of the chamber can be attributed to a number of modifications, trial runs and performance reviews conducted prior to the above tests. Primarily, certain deterioration in the achievable chamber vacuum was noticed over a period of time since commissioning of the chamber in 1991. A study revealed that a major reason for these degradations are development of leaks at the inter panel connections of shrouds . The panel interconnection arrangements originally provided were reviewed and modifications to the panel interconnection and shroud anchoring incorporated. Subsequently an elaborate leak rate verification of each shroud panel was conducted keeping a bench mark for the acceptable leak level as less than1x10E-8 std cc/sec. Panels with higher leak levels were rectified identifying the degraded welds at the tubes inter connecting the panels . After rectification of leaks by re welding and qualification of each panel, vacuum trial runs were conducted to ensure that the overall vacuum performance of the chamber met specifications.

During the analysis of some earlier tests conducted in the chamber it was noticed that there had been some vacuum fluctuation due to sudden release of gases by the cryo pumps. A study revealed the possibility of cryo pumps taking excessive gas load . To avoid this excessive loading and subsequent saturation of cryo pumps during extended chamber evacuation , an additional turbo molecular pump was incorporated to the pumping system of the chamber. This additional turbo molecular pump ensured a stable state lower order vacuum and an overlapped pumping regime with the cryo pumps thus relieving the cryo pumps from being loaded excessively due to out gassing from the shrouds or the test object during the pump down.

Further during the INSAT-2E thermal balance test shrouds were cooled to the required temperature of less than 100 deg K in a gaseous Nitrogen mode. The temperature uniformity achieved was comparable with that achieved in LN2 mode using sub coolers during the earlier tests . The GN2 mode of operation was adapted on a trial basis as a safeguard against the power failure kind of test interruptions . The operation

of the chamber shrouds in GN2 mode to achieve a temperature less than 100 K for conducting a thermal balance test has been found acceptable after a review of temperature distribution on shrouds and the resulted stable spacecraft temperature data. Also given in this paper are a gist of major problems encountered since commissioning of the facility and solutions provided , for the benefit of personnel who are engaged in maintenance and operation of facilities of similar capabilities elsewhere.

OVERVIEW OF LARGE SPACE SIMULATION CHAMBER

LSSC and satellite programs of ISRO

The Large Space Simulation Chamber (LSSC) Facility operational since 1991 has been installed at ISRO Satellite Centre, Bangalore, India as part of the of capabilities established to build and test large communication and remote sensing satellites indigenously. The facility has supported the thermal balance test requirements of all satellites built by ISRO since then and is also expected to support the thermal vacuum performance tests on very large communication and remote sensing satellites in future. As on date thermal balance tests on INSAT-2A ETM , IRS-1C and INSAT-2E had been successfully conducted in LSSC. The first thermal vacuum performance test to be conducted using the facility was that on INSAT-2E. The thermal vacuum performance tests of INSAT-3A and 3C space crafts are scheduled to be conducted during the first quarter of the year 2001.

System description in brief

LSSC consists of a 9 meter vertical main chamber and a 7 meter horizontal auxiliary chamber. The horizontal chamber is juxtaposed on to the vertical chamber which will accept the test satellite mounted on a vibration isolation support platform via a motion simulator. The auxiliary chamber houses the collimating mirror and the spout with chamber window provides interface with the lamp house. The lamp house houses lamp modules, transfer optics and douzer in a protected environment. The vacuum chamber is lined with shrouds through which nitrogen is circulated to attain temperature in the range of 100K to 373K. The entire facility is operated from a centrally located control console.

Chamber design

The design of the chamber is in accordance with ASME sec VIII/ BS 5500. The chamber has a 4 meter cut out on main chamber for man entry and provisions are available for loading of the test article from top of the chamber on to the motion simulator platform using an EOT Crane.

Shrouds

The shrouds are made of 304L stainless steel , single embossed, plate coil design selected based on easy weldability and very low out gassing characteristics. The outer flat side is electro polished to reduce emissivity. The inner embossed side is glass beaded

and black painted. Shrouds are designed to work for a maximum operating pressure of 100 PSI and can handle 100 KW heat load in conjunction with LN2 sub coolers. The shrouds are divided into 42 active flow control zones for the temperature control of the main and auxiliary chamber shrouds using a dedicated process controller. The LN2 circulation system is designed for heat dissipation of 100 KW inside the main chamber with a localized flux not exceeding 2 KW per meter square. LN2 is circulated in sub-cooled condition by independent centrifugal pumps for main and auxiliary chamber shrouds. The GN2 system utilizes centrifugal blowers, where in constant gas density(4.8Kg/cubic meter) is maintained over the entire working temperature range by means of the active pressure control. The system is designed for 15 KW heat load in the main chamber with a localized heat flux not exceeding 1.4 KW per meter square. Programmed warm up and cool down of the shroud is also possible in the temperature range of 100 K to 373 K at the rate of 1deg K per minute.

Vacuum system

Chamber pump down from ambient to 1 mbar is achieved using a pair of identical Roughing Skids equipped with roots type blower cascades backed by sliding vane mechanical pumps. Two turbo molecular pumps of 2200 liters per sec capacity have been originally provided to cover a vacuum range from 2.7*10E-2 down to the specified vacuum level of 1*10E-5 or better with the test object inside . One more with a similar capacity has been added after a critical evaluation of effectiveness of various pumping stages. The chamber has also been provided with two numbers of 48 inch cryo pumps with a nominal pumping speed for N2 of 55,000 liters/sec . A Helium cooled cryo panel with free N2 pumping speed of 2,50,000 liters/sec with associated helium cold gas refrigerator/liquefier provide additional pumping capabilities to cater to gas loads while the chamber being pumped down to the specified ultimate vacuum level.

Solar Simulator

The Solar simulator consists of lamp modules, transfer optics and douzer located in a protected lamp house. The segmented collimating mirror is located inside the auxiliary chamber. Eleven numbers of 20 KW Xenon arc lamp modules are used to produce a 4 meter dia collimated solar beam. The beam dia is extendable up to 4.5 meters using 14 numbers of lamp modules. The beam intensity can be set in the range 0.65 KW/sq.mtr to 1.7 KW/sq.mtr with an intensity uniformity of +/- 4% in the reference plane at the center of the main chamber.

Motion Simulator

The Motion simulator is originally a two axis mount installed on top of a vibration isolation platform ,with mechanical noise less than0.005g , inside the chamber. The motion simulator has a tilt capability of +/- 180-deg, while the spin rate can be adjusted from 1RPD to 10 RPM. The simulator has a payload capability of 3000 Kg with a static unbalance up to 100 Nm. The motion simulator can also be set in a single axis mode with the spin axis in vertical orientation on a separate pedestal in place of the tilt axis.

THERMAL BALANCE TESTS IN LSSC

Thermal balance tests in LSSC can be conducted in either solar simulation or IR simulation modes. During the solar simulation thermal balance test, the power and signal lines from the space craft are routed through slip rings housed in a vented to atmosphere housing inside the spin axis. The temperature data from the space craft is acquired using a multiplexed thermo couple measurement system through slip rings. In a typical solar simulation thermal balance test, the chamber will be evacuated to a vacuum of 1x10E-6 mbar and the shrouds cooled to –143 degC or less in GN2 mode initially. LN2 circulation is then established to attain and maintain the temperature on shrouds to less than 100 K by the circulation of sub-cooled LN2. After the shrouds are stabilized to a temperature less than 100 K the test object will be exposed to the solar beam of required intensity and the orbit conditions will be initiated operating the motion simulator spin axis at the required rate depending upon the orbital parameters of the space craft under test. The BOL, EOL scenarios and seasons are simulated by appropriate positioning of the tilt axis as applicable. Based on the information gathered from the test the thermal design of the space craft will be reviewed for necessary design modifications implemented. Thermal balance tests in LSSC have provided valuable insight into the thermal behavior of INSAT-2A, IRS-1C and INSAT-2E Space crafts. The average LN2 consumption during a thermal balance test has been around 100,000 liters per day .

IR simulation thermal balance tests at space craft level are yet to be conducted in LSSC though provisions exist as a part of chamber instrumentation. Most of the current generation of communication satellites built by ISRO beginning with INSAT-2E employ heat pipe technology for the thermal management of the space craft. This has resulted in the requirement of satellites with the heat pipe embedded panels having to be tested in a perfectly horizontal position. This required that the motion simulator be modified for operation with the spin axis in a vertical orientation. As a result tilt axis was disassembled and shifted to outside the chamber. The original two axis configuration can be regained with the re assembly of the spin axis to the tilt axis assembly whenever warranted.

THERMAL VACUUM PERFORMANCE TESTS IN LSSC

The Thermal vacuum performance (TVP) tests are being conducted in LSSC with the shrouds at 173degK and the chamber vacuum better than 1x10E-5 mbar. The shrouds are cooled in GN2 mode. The temperature environments on the space craft surfaces are simulated using IR lamps, the heat flux output of these lamps are controlled in a closed loop mode. The satellite being stationary in this case the temperature data is monitored using the direct thermocouple channels available on the chamber ports. The thermocouple data is processed with the help of a set of remote terminal units (RTU) which are individually connected to the host computer by serial links. Provisions are also available on remote terminal units to monitor strain and temperature data using RTDs. The output voltages and currents delivered by the power supplies connected to IR lamp arrays are also monitored using these RTUs. A set of control Remote terminal units (CRTUs) can control the power output to the lamps in a closed loop mode in constant

temperature , constant power or constant flux modes. The scenarios pertaining to cold soak, hot soak and transitions are simulated on space craft surfaces by controlling the thermal environment created by the lamp arrays. A typical thermal vacuum performance test may be of about 30 days duration end to end. This is inclusive of chamber preparation, time required for mating the space craft with the chamber adapter, fixing IR lamp arrays, instrumentation interface checks etc., before the test and the cryo surface warming, controlled venting of the chamber , space craft removal etc., after the test. These pre and post test activities may account roughly 2 to 3 days each . Reliable operation of machinery, uninterrupted power and other utilities, trouble free functioning of chamber sub system controllers, availability of redundancy and fall back options during emergencies etc are crucial to the test management. Functionality of each equipment will be critically reviewed during a series of facility trial runs prior to the test.

PROBLEMS NOTICED IN LSSC VACUUM SYSTEM

During commissioning of the chamber in 1991 a series of integrated trial runs were conducted prior to the thermal balance tests on INSAT-2A ETM. The specified vacuum level of 1x10E-5 mbar with the test object inside was achieved with all the vacuum pumping system installed on the chamber operational. However there were incidents of sudden vacuum degradation by one order due to sudden release of gas load either from cryo pumps or from the cryo panel when the temperature of cryo cooled surfaces drifted by 3 to 7 deg K occasionally due to GN2 gas locks in the cooling circuit of LN2 shields. This has indicated that the vacuum level achieved inside the chamber are less stable when viewed over a long period of time. This gave some suspicion about probable existence of some cold leaks on shroud panels as it was observed that data with short duration trial runs in GN2 mode with shrouds cooled to –100 degC showed stable vacuum levels.

A thorough investigation was conducted about the leak levels of each of the 42 shroud zones inside the chamber. The exercise which spanned over three months and with thorough involvement of personnel a number of locations on inter panel connections having minute leaks were identified. These locations were welded and improvements ascertained.

A detailed analysis of shroud anchoring scheme and inter panel connections were also conducted. Modifications were incorporated to the shroud anchoring and inter panel connections so as to minimize the stress during the movement of the shroud panels in horizontal or vertical directions at cryogenic temperatures. The chamber ultimate vacuum after rectification and these modifications showed marked improvement . A vacuum level of 5x10E-6 was achieved during the IRS-1C thermal balance test that followed, with the entire vacuum pumping system of the chamber operational.

It has been observed that still certain degree of instability present at the peak levels, the vacuum level of the chamber fluctuating between 1x10E-5 and 5x10E-6 with slight disturbances in cryo surface temperatures.

As a solution to the above it was felt that the overlapping turbo molecular pumping regime can be strengthened . An additional 2200 liters/sec turbo molecular pump was incorporated to the chamber. This arrangement has resulted achievement of a stable vacuum level of 1x10E-6 mbar during the INSAT-2E tests even without the use of 250000litrs/sec GHe cooled cryo panels. During the thermal vacuum performance test of INSAT-2E the peak vacuum achieved during cold soak phase was as high as 8x10E-7 mbar which can be considered significant considering 1000 cubic meters volume of the chamber and over 1200 sq. meters surface area .

IDENTIFICATION OF SHROUD LEAKS AND RECTIFICATION

LSSC Shroud Configuration

The LSSC main chamber (C1) shrouds in vertical configuration are divided into 28 zones having a total surface area of 375 sq.meters. These zones are provided with individual flow control valves controlled by the thermal control system of the facility. The main chamber (C1) shroud zones are distributed as top shroud assembly with 4 zones, bottom shroud assembly with 4 zones, 4 meter door shroud assembly with 4 zones, cylindrical shroud assembly with 13 zones. The auxiliary chamber (C2) shrouds in the horizontal configuration are divided into 14 zones having a total surface area of 150 sq.meters. Of the 14 zones 12 zones constitute the cylindrical shroud assembly and 2 zones of the solar beam port assembly. The over all distribution of shrouds inside LSSC has been given in Fig. 5.1. Developed views of main chamber and auxiliary chamber shrouds have been given in Fig 5.2, 5.3 respectively.

Location of shroud leaks and rectification

During the IRS-1C thermal balance test in March 1995 leaks were observed from the top shroud zones of the main chamber when shrouds were at liquid nitrogen temperature that led to premature end of the test. After opening the chamber and adopting various leak hunting techniques using a Helium tuned Mass Spectro meter Leak Detector (MSLD), the locations of the leaks were successfully identified and a number of corrective measures were taken to arrest these leaks, the satellite test was successfully completed with the chamber achieving a vacuum l of 1x10E-5 mbar under the test conditions.

In view of degradations noticed at the weld points of inter panel connections it was felt essential to evaluate the integrity of all rewelded joints once again prior to the INSAT-2E spacecraft thermal vacuum performance and thermal balance tests scheduled to Oct 1998 . Initially a pressure vacuum method was adapted to measure the gross leak of all the zones. The zones with an integrated leak rate of > 1x10E-5 std cc/sec were subjected to a leak test by the vacuum method to measure the individual leak rate of weld joints. Hood technique was adapted to measure the leak rate of embossed surfaces of the segments of shroud zones. A significant leak noticed was the one at the 90 deg quadrant zone of the top shroud. All welding joints and segments which indicated leak rate >1x10E-4 std cc/sec were rectified . To pinpoint the exact location of the leak on the weld joints soap the bubble method was adopted for marking. A brief reference to the

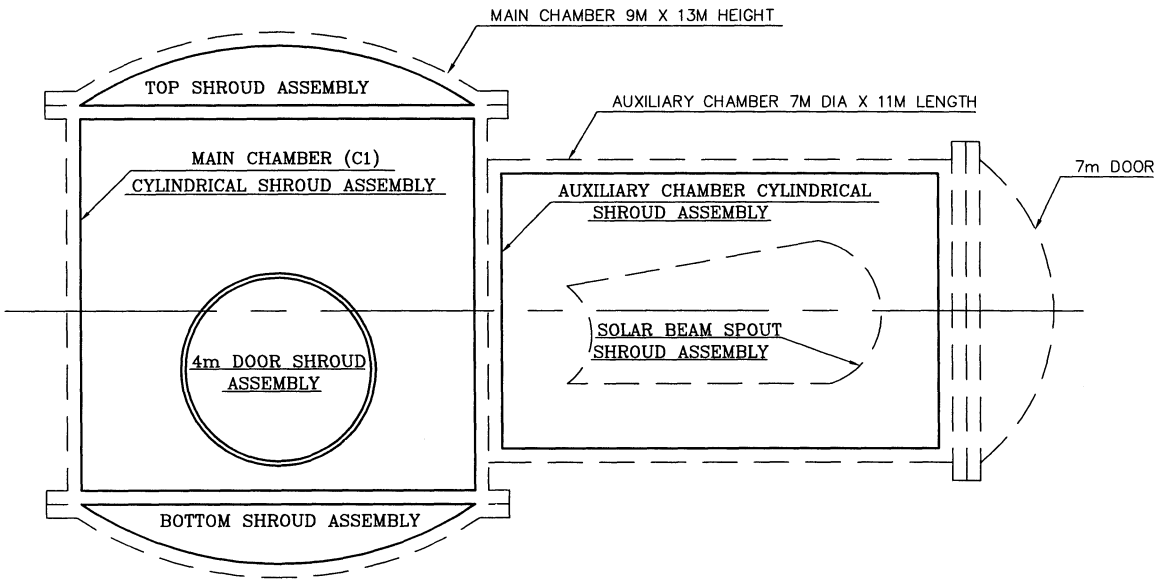

FIG.5.1 SHROUD ASSEMBLIES OF MAIN AND AUXILIARY CHAMBERS.

CCF: 22730004

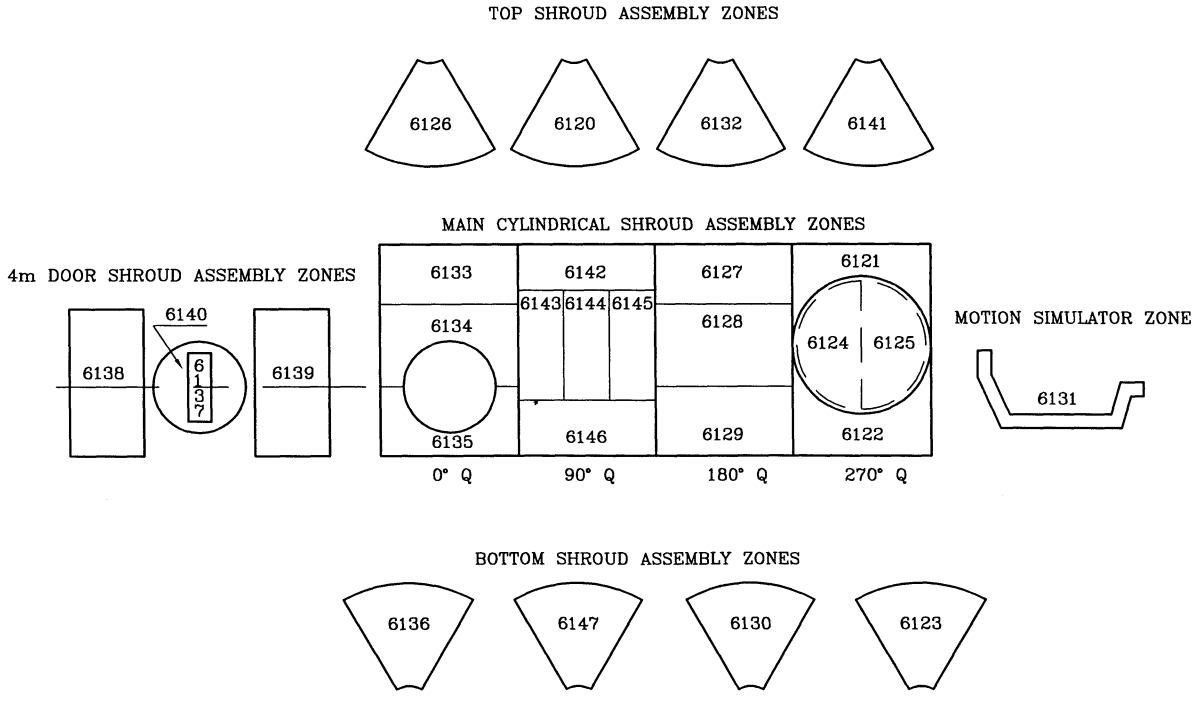

FIG.5.2 DEVELOPED VIEW OF MAIN CHAMBER SHROUD

procedures adopted for the location of zone level leak and the panel level leaks are furnished in the following sections.

Zone level leak test

Pressure vacuum method was used to measure the integrated gross leak rate of 25 zones of C1 shroud assembly and 12 zones of the C2 shroud assembly. In this method the chamber was evacuated to 1x10E-2 mbar level using Roughing pump and Helium at a pressure 1 kgf/sq.cm was maintained inside each of the zone under test . The pressurized helium leaks into the chamber through the shroud leaks, the increase in Helium concentration inside the chamber was detected by the Helium tuned Mass Spectrometer Leak Detector on the roughing port . From the difference in readings observed in MSLD the actual leak rate of the zone was estimated factoring it in to the calibration constant for a standard leak at a specified location . The calibration factor for the set up was calibrated by admitting a known and standard leak of rate 1.85x10xE-5std.cc/sec mounted at the farthest point as shown in fig5.4.

Panel level leak test

The panel level leak test was conducted to pin point the leaky points in embossed surfaces of the shroud and weld joints of the inlet and outlet header pipes, bellows and Tee connections. A typical shroud zone on top of the chamber (Zone at 90 deg quadrant) contain 9 members of trapezoidal shaped segments with inlet and outlet headers as shown in Fig 5.5.

The schematic of the panel leak test set up using both hood technique and vacuum method has been shown in Fig.5.6 . Before the leak test the calibration factor of the setup was conducted using a standard gross leak calibrator

Hood technique

The hood technique was used to determine the leak rates of the embossed surfaces of all the nine segments of the 90 deg. quadrant of top shroud . Polythene sheets cut to the shape of the embossed surface segment were fixed with the edges sealed by cellophane tapes. The fluid circulation paths of the embossed surface was evacuated to 2x10E-2 mbar. The space between the polythene sheets and embossed surface was pressurized with Helium at a pressure of 3 to 5 PSI. Leaks in the embossed surface was detected using the MSLD connected in parallel along with the pumping station. The leak rates of all the 9 segments were found to be <= 1x10E-4 std. cc/sec which was acceptable.

Vacuum method

By this method leak rates of all the 90 weld joints of inlet / outlet headers, bellows and Tees connecting all the segments were detected. The procedure followed is similar to hood technique except that Helium is sprayed on to each weld joint and a change in reading was observed in MSLD. For a particular weld joint (No.5E as shown in Fig5.5)

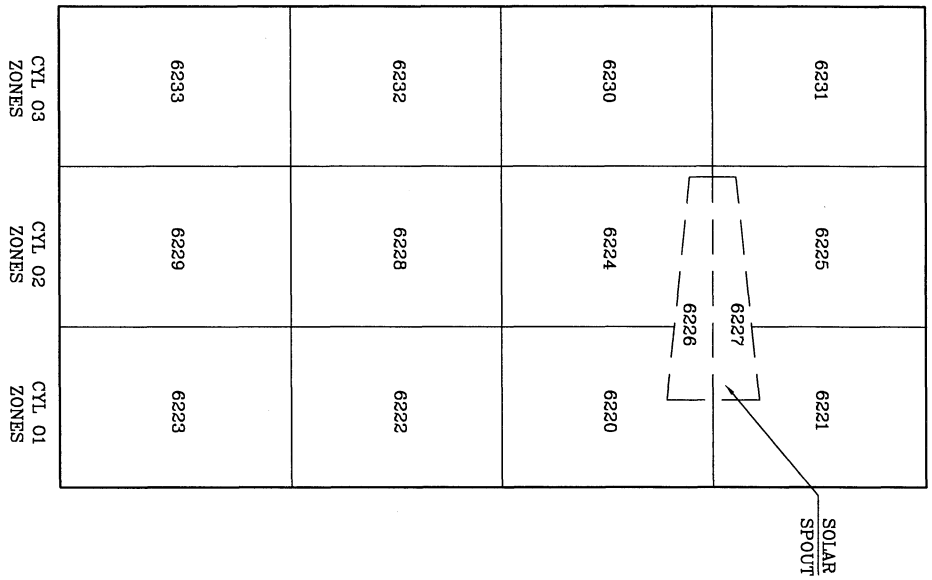

FIG.5.3 DEVELOPED VIEW OF AUXILIARY CHAMBER SHROUD

CCF: 22730007

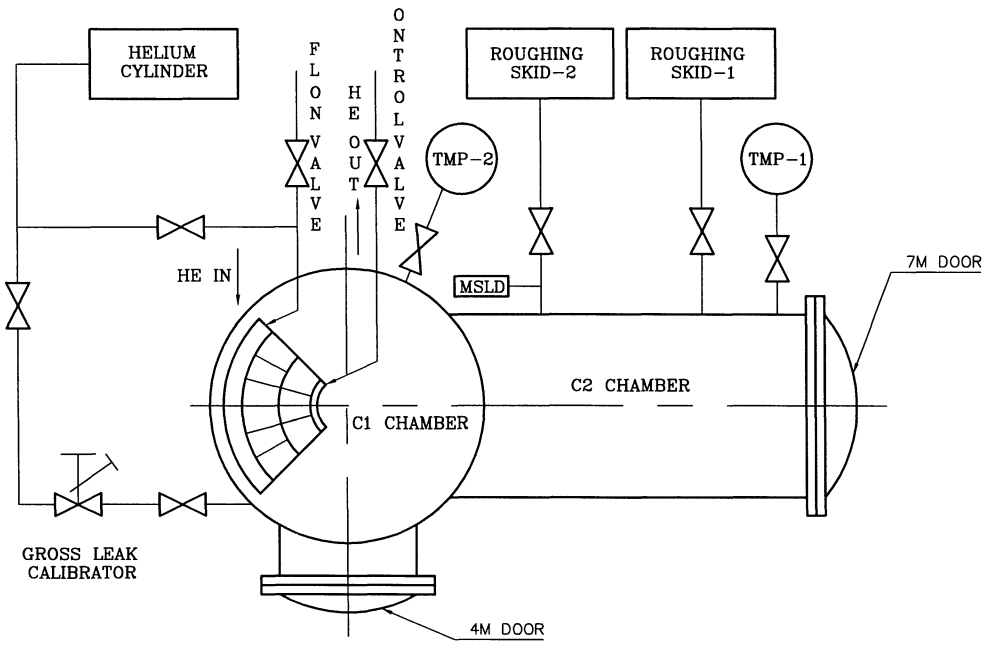

FIG.5.4 ZONE LEVEL LEAK TEST SET-UP/SCHEMATIC OF PRESSURE VACUUM METHOD

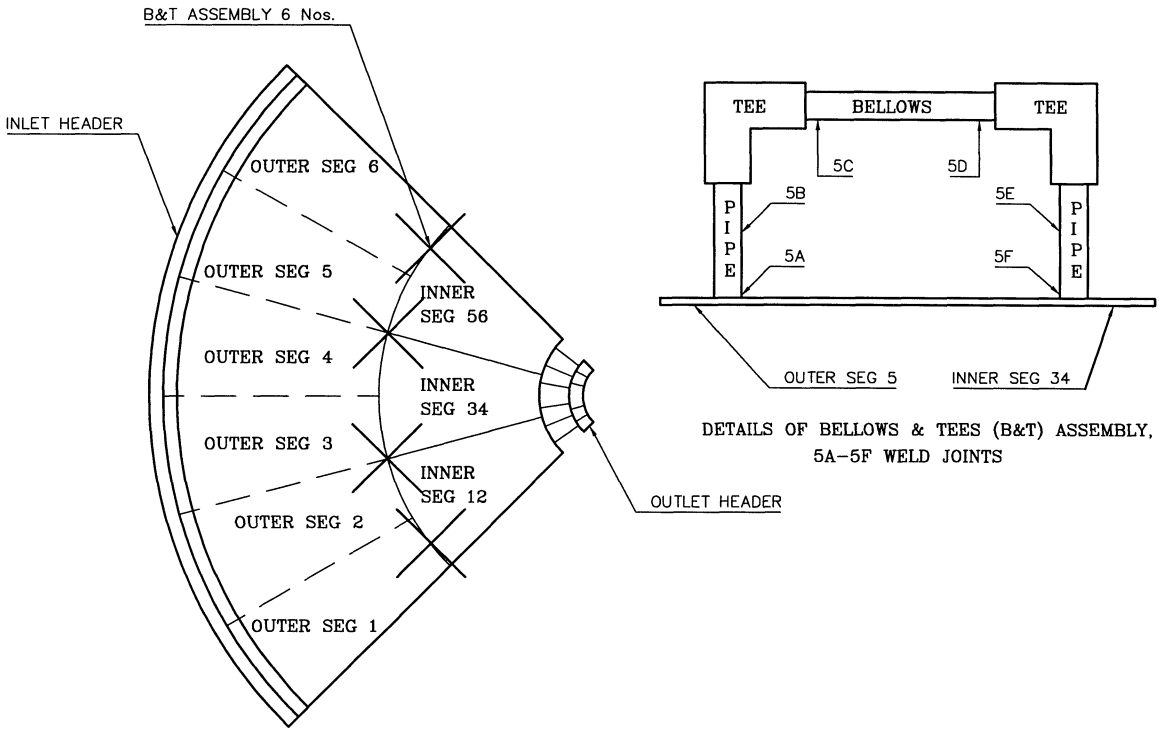

FIG.5.5 90 DEG QUADRANT TOP SHROUD ZONE DETAILS

CCF 22730002

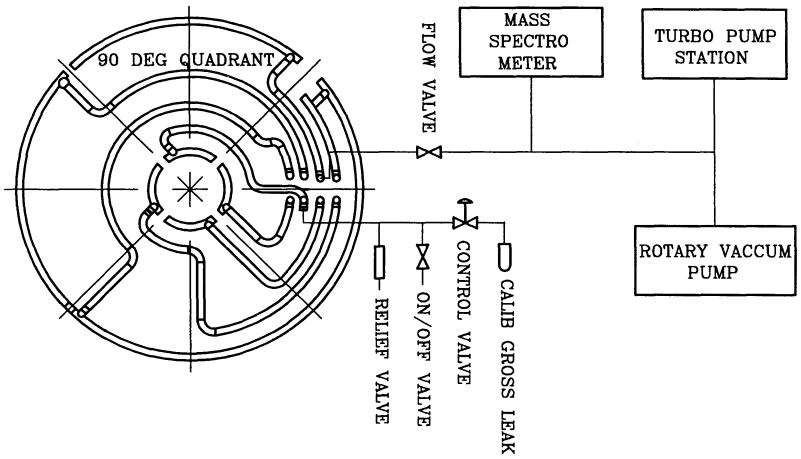

FIG.5.6 PANEL LEVEL LEAK TEST SETUP.

the leak rate was observed as 7.3xx10E-3 std. cc/sec which was not in the acceptable range.

Rectification and retest

The leaky points located was thoroughly cleaned and TIG welded .The weld location was cooled to –80 deg. C spraying LN2 and the weld integrity at low temperature was verified repeating the leak test using vacuum method .

MODIFICATIONS TO THE SHROUD ANCHORING SCHEME

Shroud Construction

The shroud is a cylinder of size 8.0 meter dia and 11.0 meter height mounted vertically and concentrically with the main chamber of size 9.0 meter dia. The top shroud and an identical bottom shroud are of truncated conical shape with a large end dia of 8.2m, small end dia of 1.0m and an intermediate dia of 4.6m mounted in co axis with the torrispherically shaped dished ends of the chamber.

There are 24 cryogenic panels in the lower part of the top shroud (i.e. between dia 8.2m and dia 4.6m) and 12 panels in the upper part (i.e. between dia 4.6m and dia 1.0m). This shroud is divided into 4 zones for fluid flow and each circuit is complete by six panels on the lower part, 3 panels on the upper part of the top shroud, inlet and outlet header lines, header to panel straight tube connections and panel to panel C-tube jumpers. The cryogenic panels are of single embossed type construction and are made out of stainless steel of grade AISI 304L. The panels are also shaped to curvature in the width direction to the chamber radius with embossing side facing test area in assembly. Two adjacent panels were overlapped and fixed together using fasteners in addition to the laterally mounted spring loaded fasteners. All four members of the inlet and outlet headers were supported by using SS turn buckles to the top dish at the both ends of the headers in addition to the adjacent headers being welded together by SS plates. Each of these headers are connected to the Chamber LN2 feed throughs using SS bellows.

Problems encountered with the shroud assembly

Leaks to a level of >1x10E-5 std cc/sec at locations such as the welded joints of inlet and outlet headers, C-tube jumpers and the straight tube connectors to a total of 560 locations were noticed. These leaks at many TIG welded locations were attributed to the thermal stress prevalent at cryogenic temperatures due to the movement constraints on the shroud panels and the attachments

Remedies and implementation

After a thorough investigation and analysis following remedies were suggested and implemented in order to provide free expansion / contraction of panels and headers at cryogenic temperatures.

FIG 6.1
TOP SHROUD
MODIFICATIONS

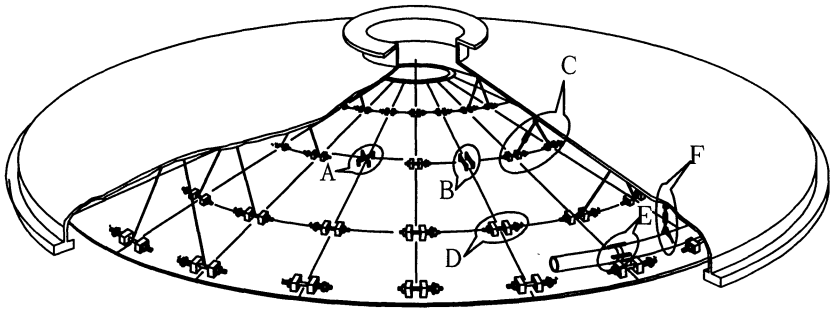

	EXISTING	MODIFIED
DETAILS-A & B SHROUD SEGMENT INTER CONNECTION	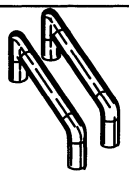	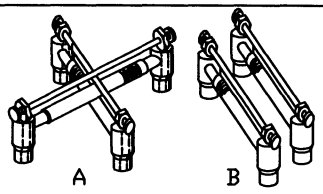
DETAIL-C SHROUD SEGMENT SUSPENSION	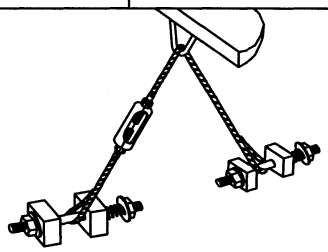	
DETAIL-D INTER SEGMENT ANCHORING	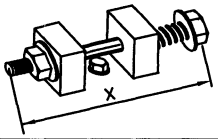	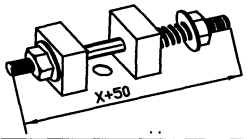
DETAIL-E MAIN HEADER ANCHORING	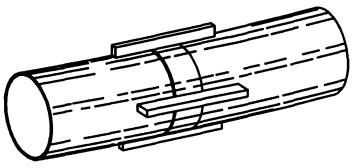	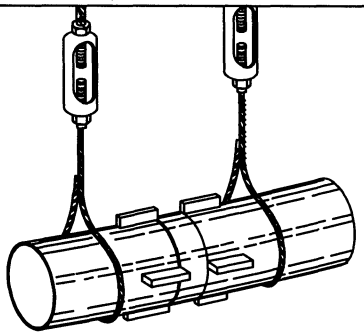
DETAIL-F MAIN HEADER SUSPENSION	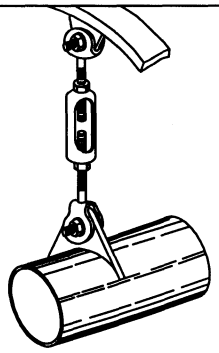	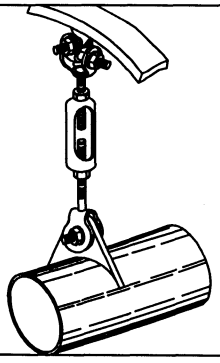

- Removal of fasteners between the two adjacent overlapped panels
- Removal end support plates of the adjacent headers
- Replacement of C-tube jumpers used for inter panel connections with SS bellows to accommodate the movement of individual panels at cryogenic temperature. See Fig. 6.1 Details A and Detail B.
- Supports to each panel to the top dish using SS wire ropes See Fig. 6.1 Details C.
- Replacement of existed springs and installation of all the spring loaded bolts laterally to the panels. See Fig.6.1 Details D
- Supports for the SS bellows provided on the header lines. See Fig 6.1 Details E.
- Modifications to the support for the inlet and outlet headers to give 3 degrees of freedom for movements. See Fig. 6.1 Details F.

The C-tube jumpers were used to provide connections between two cryogenic panels for fluid transfer from one panel to the other. For a temperature gradient of about 40 deg C between panels during transition the required height was to be 500 mm to limit the bending stress in the tube with in the allowable limit. The height provided during installation was only 125mm and there was no annular space to increase the height beyond 450mm. Hence it was decided to use SS bellows in place of the C-tube jumpers. The thermal contraction/expansion due to the thermal gradient between panels are taken best by bellows.

The springs which were used between adjacent panels for support were replaced to provide the required compression during operation by the increase of the free length of springs. Proper seating was provided on the tabs and to avoid buckling , springs with squared and ground ends were used. Some of the adjacent tab holes were not aligned and matched, the springs and fasteners were not assembled square to the tab surfaces which caused uneven compression of the springs. The mismatched and non aligned tabs on the panels were corrected for the proper installation of springs exactly lateral to the panel surface.

Performance testing

After implementation of all the remedial measures, a thorough pneumatic pressure testing, cold soak testing, MSLD testing and a thermal vacuum cycling trial was conducted. The performance of the chamber shrouds and and anchoring arrangements were found excellent proving that the analysis, measures suggested and the implementation were correct and effective. It is hoped that the solutions provided should assist in a long lasting and trouble free operation of the chamber shrouds in future.

A SUMMARY REVIEW OF VACUUM SYSTEM OPERATION PROCEDURES ADOPTED DURING INSAT-2E TESTS

The vacuum system operation procedures for the chamber has specified vacuum levels at which various vacuum pumping systems will be exposed to the chamber during the pump down from ambient to the ultimate specified vacuum level of 1x10E-5 mbar with the test object inside or 1x10E-6 mbar in the case of an empty chamber. The chamber is pumped down from ambient to a vacuum level of 3x10E-2 mbar using the roughing skids.

Roughing skids will be cut off at the ultimate and the two Turbo molecular pumps with the required fore vacuum on lines will be exposed to the chamber subsequently. The turbo molecular pumps will be in operation continuously through out the evacuating process further. When a vacuum level of 1x10E-3 mbar has been achieved the Meissner traps will be flooded with LN2. The cryopumps are then started and exposed to the chamber .This stage hence is required to concentrate distinctively on the rare gases present inside the chamber. It was noticed that three turbo molecular pumps, Meissner traps and cryo pumps in continuos operation are sufficient to achieve a peak vacuum level of 1x10E-6 mbar with the test object inside and shrouds cooled to <100degK. The vacuum level has been found quite stable for a long duration test spanning over 20 days, as in the case of a thermal vacuum performance test on INSAT-2E.

The rectification of weld leaks in shrouds and modifications to shroud interconnections have resulted considerable reduction in nitrogen leaks into the chamber at cold temperatures. As a precaution against minute GN2 leaks in the shrouds that may still be present at very low temperature(cold leaks) a third turbo molecular pump of capacity 2200 liters/sec has been augmented in addition to the originally existing two of identical capacity. Operation of these three turbo molecular pumps on a continuous basis helped significantly in pumping out a major portion of the gas that could get into the chamber from shrouds and the out gassing from the space craft under test. It is of our experience that continuous pumping down of the chamber for a substantial duration say about 4 to 6 hours up to a vacuum level of 1x10E-3 mbar or less and a resident pumping at this vacuum level for a further 2 to 3 hours duration before Meissner traps are ON can provide a stable base vacuum to the chamber.

The preparatory activities of the chamber prior to the acceptance of the test object included a thorough cleaning of the chamber floors and other polished surfaces with lint free wipes. The shroud surfaces were washed with a specified solution to remove sticking dust particles if any . Subsequently a dry run of the chamber was conducted with the shrouds baked to above 60 deg.C by the circulation of hot GN2. The contamination levels of the chamber was monitored continuously during the shroud baking using the quartz crystal micro balance contamination monitor (QCM). Sample mirror surfaces mounted at critical locations were subjected to scrape tests to monitor the composition of deposits if any noticed during the trial run , to ensure that the chamber was free of contamination and clean enough to receive the test object.

From the forgoing discussions it can be construed that the identification and rectification of leaks at the shroud inter panel connections , prevention of leaks from the shrouds at cryogenic temperatures by improving the degree of freedom to panels with modification to anchoring schemes , a review of operational procedures and augmentation of a third turbo molecular pump that resulted maximum benefits from each pumping stage etc., are the basis of excellent vacuum levels achieved inside the chamber during INSAT-2E Thermal vacuum performance and Thermal balance tests. The vacuum profile during the entire duration of the tests have been given in Fig 8.1 & Fig 8.3 respectively.

A GIST OF PROBLEMS AND SOLUTIONS PROVIDED WHILE USING CHAMBER SINCE COMMISSIONING

Vacuum system

The performance problems encountered in vacuum system and solutions attempted are listed in details in the preceding sections.

Motion simulator

In the case of Motion simulator difficulties were experienced while the multiplexed thermocouple measurement system was being used for temperature measurement. The temperature readings were fluctuating at random due to the power line noise on the input of the instrumentation amplifiers in the multiplexer boxes mounted on the motion simulator inside the chamber. By appropriate modifications to the filters at the input of the amplifiers the problem was sorted out. Additionally an averaging software was also incorporated at the data processing end to average out any random noise that may appear in the data. Secondly the readings from 50 direct thermocouple lines wired through the slip rings of motion simulator were found erratic due to the mismatch between the thermocouple wire and connector pin sizes that resulted in improper crimping and the problem was found getting aggravated at cold temperatures. As a solution the thermocouple lines through the motion simulator were replaced with a new set of wires and connectors crimped properly.

Thirdly both the tilt and spin axis motors of Motion simulator failed due to winding burn outs immediately after the first space craft test inside the chamber. The reasons for failure were analyzed as defects in the motor winding which were rectified in house after disassembly of both axes. The windings in some stator slots were found to slip out of the slots into the air gap and getting shorted. By proper insulation between phases and packing the windings tightly in stator slots during the re winding, the probability of a failure in this mode has been considered reduced. The post repair performance of the axes was normal as originally specified.

For the INSAT-2E spacecraft tests the motion simulator configuration was modified into a single axis mode with the spin axis pointing vertical, as required by the space craft in order to keep the space craft panels housing the heat pipes in a perfect horizontal orientation. The modifications called for design of an appropriate pedestal to support the spin axis apart from the task of disassembly and shifting of the tilt axis to outside the chamber..

Solar simulator

The performance of solar simulator subsystem has been satisfactory. Provision of additional flow switches in the lamp coolant flow circuit for added safety, provision of a 5 micron filter in the coolant water supply line to lamp house, provision of Y traps in vacuum window cooling line etc, are some augmentations having been done. Periodic

replacement of xenon arc lamps, alignment of source modules etc also has been carried out as and when required. The original mirror cooling system using GN2 has now been split into two independent circuits with one circuit for cooling the center zone and other circuit for heating the outer zones during thermal balance tests. This was required to maintain the temperature gradients across the mirror with in limits as the center zone would heat up fast due to the incident solar beam where as the outer zone rapidly cooled due to proximity to the cooled shrouds. The functioning of the modified mirror temperature control arrangement has been up to the requirement.

Liquid Nitrogen storage & transfer

The two one million litre liquid nitrogen storage tanks are pre cooled, inter spaces purged with dry nitrogen etc prior to the loading with LN2 for the tests. The PTFE gaskets on LN2 line valves were found to fail frequently due to temperature cycling. An innovative solution is attempted by replacing the PTFE gaskets with gaskets formed using Indium wire. The solution has worked and no LN2 leaks noticed on any of the valves provided with these gaskets.

Electrical, Instrumentation & Control System

The performance of the system has been found satisfactory. The instrumentation UPS of the facility has been provided with another UPS as an alternate source which in turn is backed up by a diesel generator ensuring availability of control supply to the facility under all exigencies.

A TRIAL THERMAL BALANCE TEST IN GASEOUS NITROGEN MODE

Ideally the thermal balance test need to be conducted with the shrouds cooled to the LN2 temperature by circulation of sub cooled LN2 through the shrouds. On previous occasions it has been observed that the temperature of shrouds opposite to the solar beam on the main chamber could be maintained at –143 deg C only inspite of the increased flow of sub cooled LN2 through these shroud zones. The temperature of remaining zones are observed reaching a temperature of –185 +/-5 deg C . The major source of heat during the thermal balance tests inside the chamber is the solar beam shining on the test object and the shrouds opposite to the beam. It has been observed that temperatures up to –180 deg C is possible to achieve on shrouds in an extended GN2 mode, the fluid content inside the shroud being a mixture of liquid and gaseous nitrogen in such a case. The pressure of gas in the cooling loop when kept around 45 PSI was found to give good temperature stability on shrouds even in the presence of solar beam. The temperature on the shrouds opposite to solar beam could be maintained at –145 +/-5 deg C which is more or less nearer to the case with sub cooled LN2 circulation also. The temperature on these zones can be maintained constant by the continuos flow of GN2 through these zones and controlled venting on to the vent header. However it has been noticed that there are chances of liquid collection at the inlet port of the GN2 blowers, the LN2 injection into the system need to be stopped during the absence of solar beam inside the chamber during the eclipse condition.

The motive of conducting a thermal balance test in GN2 mode is basically the ease of recovery of the chamber from a power failure kind of an emergency. The recovery of a system stabilized in LN2 circulation mode from a power failure require re-establishment of liquid circulation by way of venting all GN2 formed inside the shrouds during the failure duration. The delay associated in re-establishing the liquid circulation can be at least 30 to 45 minutes upon restoration of power which can result in the shroud temperature being raised to above 173deg K which may have disturbed thermal state of the spacecraft by then. The GN2 blowers on the other hand can be started and stabilized quickly the shroud temperatures can be controlled in GN2 mode very easily locating the lagging zones by regulating the flow of GN2 through these zones. From the liquid nitrogen consumption point also the GN2 mode of operation has been found economical, the LN2 consumption per day is about 80 % of that is required in LN2 mode of operation and there is an additional saving of about 1,50,000 liters of the LN2 required for conditioning of the sub-cooler and readying the unit for LN2 circulation. The LN2 consumption can be further pruned by reducing the operating pressure of GN2 in the shroud loop to an optimum value observing the temperature excursions on shrouds based on energy reflections from the space craft surfaces

A review of test results showed expected temperature stabilization on satellite sub-systems and identical variations in stabilized orbits. This has further supported the viability of conducting a thermal balance tests in a controlled GN2 circulation mode.

FACILITY PERFORMANCE DURING INSAT-2E TVP & TBT

The facility performance during thermal vacuum performance and thermal balance test of INSAT-2E were as per specifications. Both the tests were conducted in ideally stabilized environments. Plots of chamber vacuum and a representative shroud temperature during the thermal vacuum performance test have been given in Fig 8.1 and Fig 8.2 respectively. Plots of chamber vacuum, and representative shroud temperature have been given in Fig 8.3, Fig.8.4 respectively. A representative drawing of the arrangement of the space craft inside LSSC during thermal balance test has been provided in Fig 8.5.

CONCLUSION

The experience with the vacuum system of the Large Space Simulation Chamber (LSSC) since commissioning, some major problems encountered and the solutions provided are given in brief in this paper. We hope the experience shared here will of help to the people who are engaged in operation and maintenance of similar facilities else where.

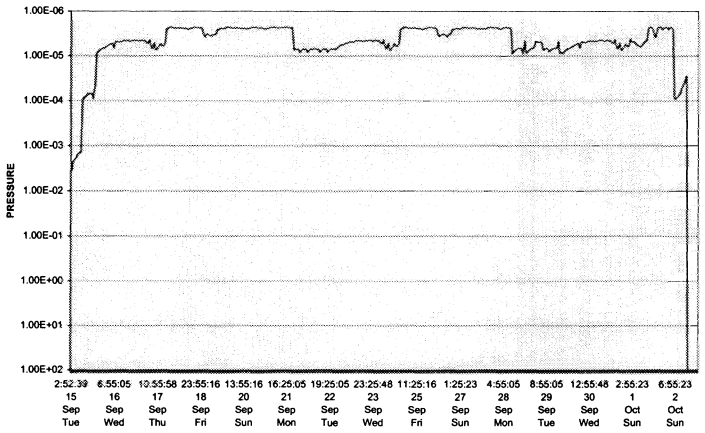

FIG 8.1 LSSC -VACUUM PLOT DURING INSAT 2E THERMOVAC TEST

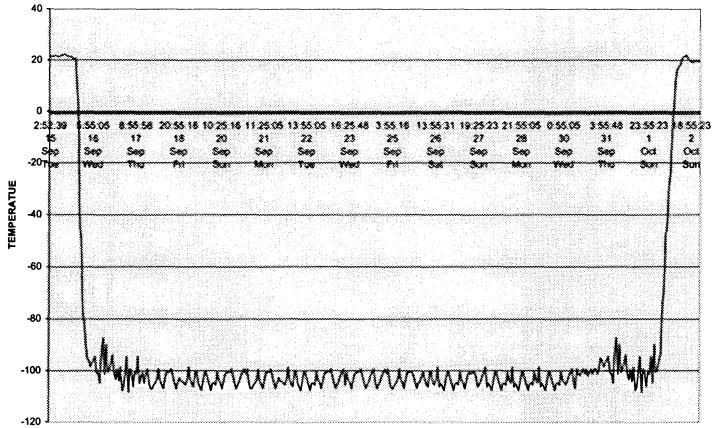

FIG 8.2 LSSC - SHROUD TEMPERATURE PLOT DURING INSAT 2E THERMOVAC TEST

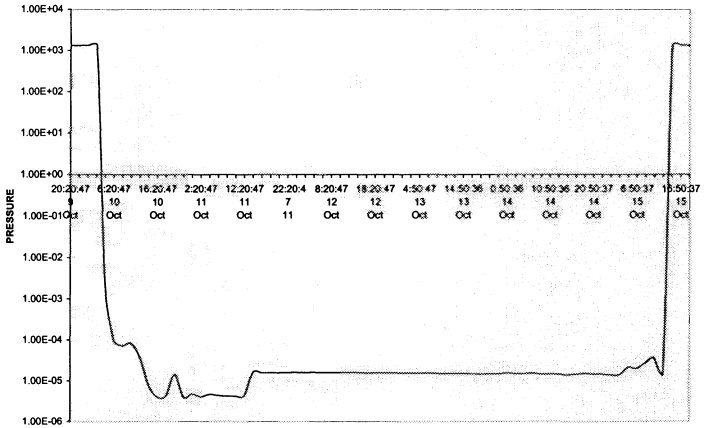

fig 8.3 LSSC - VACUUM PLOT DURING THE INSAT 2E THERMAL BALANCE TEST

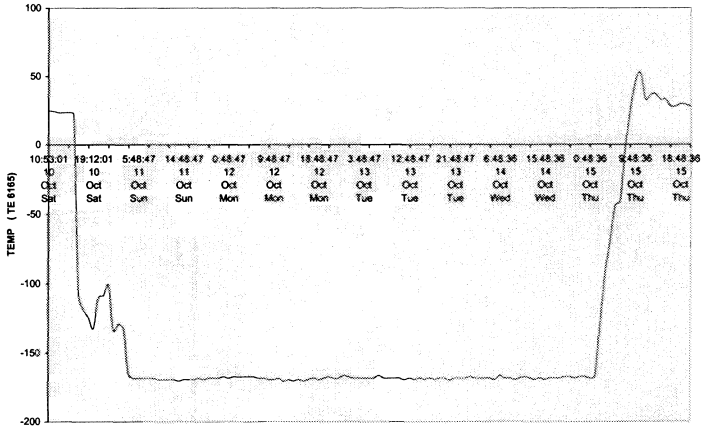

FIG 8.4 LSSC - SHROUD TEMPERATURE PLOT DURING INSAT 2E THERMAL BALANCE TEST

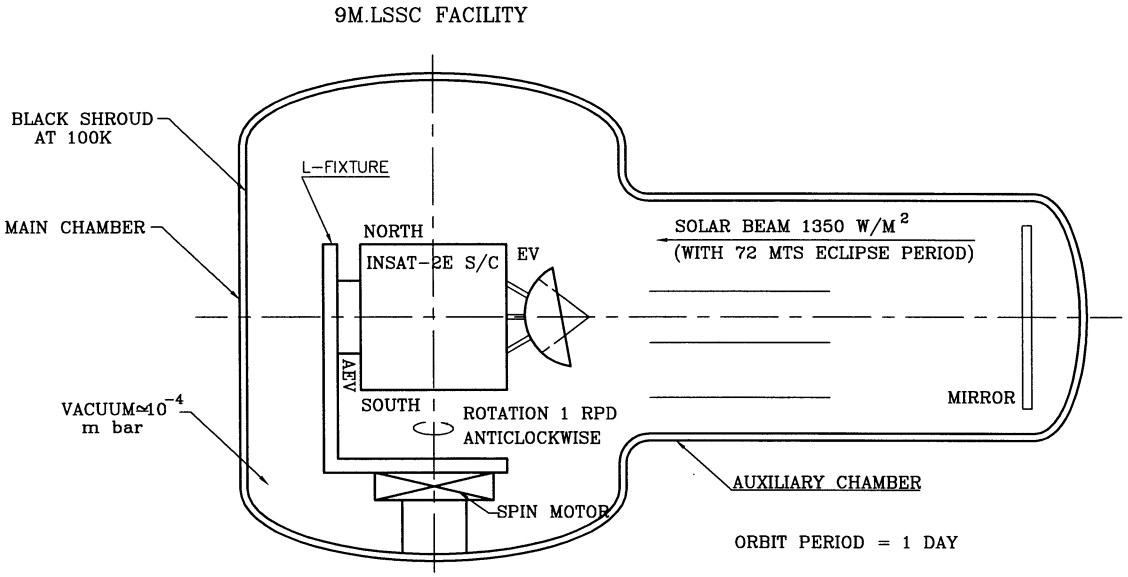

FIG.8.5 ON-ORBIT EQUINOX SIMULATION-INSAT 2E TBT

ACRONYMS

GN2	Gaseous Nitrogen
INSAT	Indian National Satellite
IRS	Indian Remote Sensing Satellite
ISRO	Indian Space Research Organisation
LSSC	Large Space Simulation Chamber
LN2	Liquid Nitrogen
MSLD	Mass Spectrometer Leak Detector
QCM	Quarts Crystal Micro Balance
TVP	Thermal Vacuum Performance
TBT	Thermal Balance Test

BIBLIOGRAPHY

1. Edwards.A.A., "Fatigue induced cracking in aluminum shroud of 39 foot vacuum chamber",13th Space simulation conference, NASA conference publication,1984.
2. Brar.A.S, Prasad Rao.V.S, Gambhir R.D, "Indian LSSC Facility",15th Space Simulation conference,NASA conference publication ,1988.
3. Edwards.A.A., "Refurbishment of a 39' Thermal vacuum chamber " 18th Space Simulation conference, NASA conference publication,1994.Seok-Weon Choi,Joon-Min Choi ,Joo-Jin Lee "Cost and performance effective design to thermal vacuum chamber",2000 Proceedings, Institute of Environmental Sciences and Technology.

****

Automation and Upgrade of Thermal System for Large 38-Year-Young Test Facility

Andrew T. Webb
Mantech International Corporation, Aerospace Application Technology Center
Goddard Space Flight Center

ABSTRACT

The Goddard Space Flight Center's Space Environment Simulator (SES) facility has been improved by the upgrade of its' thermal control hardware and software. This paper describes the preliminary design process, funding constraints, and the proposed enhancements as well as the installation details, the testing difficulties, and the overall benefits realized from this upgrade. The preliminary design process was discussed in a paper presented in October 1996 and will be recapped in this paper to provide background and comparison to actual product. Structuring the procurement process to match the funding constraints allowed Goddard to enhance its' capabilities in an environment of reduced budgets.

The installation of the new system into a location that has been occupied for over 38-years was one of the driving design factors for the size of the equipment. The installation was completed on-time and under budget. The tuning of the automatic sequences for the new thermal system to the existing shroud system required more time and ultimately presented some setbacks to the vendor and the final completion of the system. However, the end product and its' benefits to Goddard's thermal vacuum test portfolio will carry the usefulness of this facility well into the next century.

INTRODUCTION

Early in 1996, Goddard Space Flight Centers' Environmental Test Branch decided to proceed with the final phase of upgrading the Space Environment Simulator (SES) chamber and tasked Mantech International Corporation to develop, as a cooperative effort, the most cost effective approach to upgrading the thermal system. The SES is a 33-foot diameter by 60-foot tall (head to head) thermal vacuum test chamber constructed at Goddard from 1960 to 1962. The thermal system was a 35-year-old, manually operated, constant pressure, re-circulating gaseous nitrogen (GN_2) or liquid nitrogen (LN_2) system that supplied the working fluid to the chamber shrouds forming a 27-foot diameter by 40-foot high working test volume. The thermal system itself utilized a centralized GN_2 compressor or LN_2 pump, depending on the mode of operation, to circulate the working fluid through centralized heating or cooling plants to provide the necessary temperature to the chamber shrouds. The chamber shrouds consist of over 80 separate aluminum panels configured into multiple parallel/series flow paths that offer 20 to 30 psig pressure drops. Each shroud panel was formed from 1100-series ingot with graphite rods imbedded at a spacing that would yield tube spacing at 15-inch centers when the ingot was rolled and drawn to 5/32-inch thickness. The graphite was etched out and the tubes hydraulically expanded to form a 1-inch inside diameter nominal tube.

The performance of the original thermal system in the GN_2 mode was a nominal 20°C / hour at a range from –65° to +75°C. The control of the thermal system required all manual operation of temperature control valves as well as shroud zone supply and return valves. A simple bakeout required that 2-operators per shift be staffed to safely operate the thermal system.

DESIGN CRITERIA

The design criteria for the thermal system were grouped into general requirements and specific requirements. The general requirements focused on the operational and funding considerations while the specific requirements were focused on the necessary engineering requirements for the new thermal system developed in the Preliminary Design Report phase of the project.

In general, the new thermal system was required to:

- Reduce operational costs.
- Provide remote operation from another building during simple bakeouts and chamber certifications.
- Increase the functional temperature range for the shrouds to make the chamber more viable.
- Create a common control system based on programmable logic controllers (PLC's) and human machine interface (HMI) software for the vacuum and thermal systems.

The specific engineering requirements were developed during the preliminary design process and published in the Preliminary Engineering Report[i] in August, 1996. These requirements will be presented in the Design Process section.

DESIGN PROCESS

The design process started with a detailed preliminary engineering study consisting of Mantech and Code 549.4 engineers and technicians working as a team to identify the design requirements that would be most cost effective. The budget for this task was approximately $2.5 million dollars spread over a 3-year period. This required the design team to carefully evaluate all of the options and requirements. The decision tree, figure 1, summarizes the options investigated with the major decisions discussed in the following sections.

Shroud Replacement Necessary?

The first major decision was whether to replace the shrouds in this chamber or not. All of the recent upgrades of chambers with shrouds of similar manufacture were replacing them. Our dilemma was that of cost versus value. A replacement shroud with a surface area of 5000 ft^2 (465 m^2) would cost approximately $1.5 million dollars (estimated at ≈ $300/ ft^2) which would take over half of the available funds. The design team reviewed the upgrade efforts of shrouds of similar design, including a paper presented in 1984 on the Ford Aerospace 39-foot vacuum chamber[ii]. The results from these studies showed the primary point of failure to be at the welded joints where the 3300 series aluminum jumper tubes were welded to the 1100 series formed tube passages. The failures were due to stress cracks created during the rapid cool down with LN_2 and the impurities in the weld due to the high traces of carbon from the forming process. The SES shrouds have been leak free after repairing all of the failures in the infancy phase of the shrouds and after removing the gimbal sections that were plagued with leaks from the beginning.

Due to the fact that every other facility containing this style shroud had them replaced, the decision was made to conduct some non-destructive and some destructive studies on the shroud panels and weld joints. The studies were the subject of a paper presented in the October 1996 Space Simulation Conference in Baltimore, Maryland titled, "Thermal System Upgrade of the Space Environment Simulation Test Chamber.[iii]" After extensive eddy current, dye penetrant and radiographic inspection of the welds in the crossover tubes some crack development had been observed, the depths of which were no more than 10% of the wall thickness and random in occurrence. However, thermographic imaging and stress/strain measurements under thermal cycling indicated large loads on the supply and return pipes. We discovered the strain was caused by the pipe support system which did not allow the pipes to expand and contract. This problem was remedied by designing and installing a sliding pipe support system which significantly reduced the strain.

Destructive life cycle testing on some of the removed panels from the frustrum of a cone showed that the crack propagation began at approximately 900 cycles. Since the shrouds have been estimated to undergo less than 400 cycles over the first 35-years of its existence, the life remaining in the shrouds was determined to be at least another 35-years. The other thing learned was that the strain was kept low when the gradient was maintained below 100°C. The final decision was to keep the existing shrouds and limit the maximum gradient across the shrouds during transitions to 100°C.

Centralized Thermal System versus Zoned Thermal System utilizing Multiple TCU's?

Once the decision to keep the existing shrouds was reached, the issue about using a centralized compressor system versus a zoned system with multiple thermal conditioning units (TCU's) became more biased towards the compressor based system. This is due to the fact the shrouds, in their current internal piping configuration consist of zones with 400-foot long

pipe runs creating a pressure loss of 20-30 psig across the zone. Even the high pressure blowers used in most commercially available TCU's can only develop 10 psig of pressure head. This meant using the existing shrouds with TCU's would require significant manifolding changes inside the chamber and many welds at the crossover tubes; the welds most likely to fail. Some of the other considerations were the electrical requirements and space requirements of the TCU's. The TCU's use electric resistance heaters as the heat source while the centralized system could take advantage of the steam available in the building. The amount of electricity necessary to provide 400,000 btu/hr of heat to the process was not available. The space required to locate six TCU's was not available either. Based on the considerations described above, the centralized thermal system was chosen over individually zoned quadrants using multiple TCU's.

Use the Existing Nitrogen Compressor?

The heart of a centralized thermal system is the compressor. The compressor on the existing system was a Sulzers K105-1A, 125 horsepower, non-lubricated compressor rated at 10,250 lbm/hr with a 40 psig differential operating pressure. Sulzer USA was contacted to evaluate the condition of the 35-year old compressor. Their evaluation indicated that some of the seals needed replacing as well as the internal copper water tubing needed replacing with stainless steel tubing. Other than those recommendations, Sulzer USA indicated that the compressor was in excellent shape. Their compressors are very rugged and are designed to operate for 80 to 100 years. Based on the Sulzer USA report, a proven design, and reliable track record, the decision was reached to make the necessary modifications and use the existing compressor in the new thermal system.

Specific Engineering Requirements for the New Thermal System and Related Subsystems

The final engineering requirements for the new thermal system were the result of applying a systematic evaluation of the options available using a team approach and good engineering practice. Each option was examined with the pro's and con's listed and then examined as far as reasonable. The final design requirements, summarized below, were developed and included in a formal specification package.

- Temperature ramp rates of 30°C/hr on the shrouds over a gas supply temperature range of –130°C to +150°C.
- Stability of ±2°C at any control temperature in that range.
- Provide thermal conditioning to the existing top, side and bottom shrouds utilizing the existing vacuum jacketed (VJ) supply and return lines.
- New LN_2 pumping system, with warm back-up pump, to provide shroud temperatures less than –180°C while handling 50 kW of payload heat dissipation.
- Skid mounted, modular assemblies able to fit through a 9-foot by 10-foot hatch.
- Provide central heating and cooling plant using LN_2 as the coolant and available 100 psig plant steam for heat source.
- Design all heat exchangers, pipes and valves to fully utilize the existing Sulzer compressor.
- Fully automate the control system utilizing the same programmable logic controller (PLC) and human machine interface (HMI) software as the recently upgraded vacuum system to facilitate operating the chamber from other locations in the environmental test complex.
- Provide the system in a three phase procurement process to accommodate the funding available for this task over three fiscal years.
- Remove the 127 optical feedthroughs on the dome of the chamber, saving ≈$600/day in purge gas when conducting cold wall tests
- Replace the densing panels for the optical feedthroughs and the frustrum of a cone dome shroud with a single 29-foot diameter flat shroud in the dome eliminated an unnecessary circuit and providing a more uniform surface.
- Rebuild the Sulzer compressor and modify the flywheel and motor drive pulley to accept a multiple v-belt drive system.
- Upgrade all vacuum instrumentation using transducers wired directly to the PLC.
- Redesign the vacuum system SCADA to mesh with the thermal system and combine into one application.

FUNDING CONSTRAINTS

As mentioned earlier, one of the major challenges was completing this upgrade with the current fiscal constraints from NASA for these types of enhancements. The Environmental Test Branch had the vision to request facility upgrade funding based on improving the safety to payloads as well as reducing test costs. The projected allocations were phased with the first two fiscal years providing 75% of the funding and the remaining 25% in the last year with the understanding that funding could be eliminated in any of the future years. This required that the procurement be staged in fiscal efforts that would yield a deliverable at the end of each year. The first phase consisted of completing the design calculations, the fabrication drawings and procurement of major components broken out into individual milestones for the proposed system. The second phase consisted of completing the fabrication of the thermal system in modular skids, shipment to Goddard and delivery of the final fabrication drawings. The third and final phase, which was postponed several times, consisted of the installation and commissioning of the thermal system. Fortunately, funding was available every year and the project was successfully awarded to Process Systems International in January 1997. The thermal system was successfully completed in February 2000.

INSTALLATION DETAILS

The thermal system consisted of three major subsystems; the GN_2 Heat Exchanger Skid, the Valve Box Skid, and the LN_2 Skid. Each skid was fabricated to be capable of being rotated vertical and lowered through the 9-foot by 10-foot hatch opening in the floor. The opening in floor turned out to be one of the biggest engineering hurdles for the vendor supplying the equipment. This design constraint required the equipment be compact enough to fit through the opening as well as all the components in those skids be braced and supported for flipping to a vertical orientation. All three skids were successfully craned into the basement and rigged into place due as much to good design as to the skill and ingenuity of the crane operators and riggers.

Finding a window of time to install the thermal system with constantly changing project test schedules proved to be very difficult causing the installation to be postponed many times. As the actual installation grew nearer, the vendor was requested to provide an accelerated installation window from 12-weeks to 8-weeks. This was negotiated with an aggressive installation plan put into action. The actual mechanical and electrical installation went very smoothly and was completed in the schedule 5-weeks. The only exception to that was the cryogenic insulation. This process took a week longer than expected and installed with insufficient expansion joints. The insulation was replaced later during the replacement of the steam heat exchanger.

TESTING DIFFICULTIES

Mating the new thermal system to the existing shrouds and interconnecting piping required making assumptions in the design process that were not easily confirmed. The physical installation of the three major skids, the interconnecting piping and the electrical connections were completed in time on the accelerated schedule by working six 10-hour work days. The difficulties were encountered in the testing and tuning phases of the schedule. A re-occurring problem the vendor encountered centered around manufacturing debris in the manifolding of the valve box that showed up in valve seats causing valves to leak or bind producing anomalies in the process. This problem plagued the 3-inch isolation ball valves for the LN_2 pumps as well as the shroud supply and return, VJ globe valves in the valve box.

The area of automation that required the most time and testing was that of automatic transfer from the GN_2 mode of operation into the LN_2 mode of operation and back into the GN_2 mode of operation. It is always amazing how many different sensory inputs the human brain processes when operating a large system. These inputs are not easily converted into an automated process. Many rupture disks were expended in this effort until the dynamics of all of the variables that were monitored by human ears, eyes, and finger tips were translated into control algorithms that worked. The processes automated were: 1) the GN_2 Skid or compressor start, stop and pressure control functions; 2) the GN_2 mode, the process of establishing flow to the shroud zones; 3) the LN_2 Skid or pump start, stop and pressure control functions; 4) the LN_2 Mode, the process of safely establishing LN_2 flow into the shrouds after cooling the shrouds with the GN_2 mode; 5) the Purge Mode, the process of pushing the LN_2 out of the shrouds and then safely establishing the GN_2 mode again; and 6) the Safe State Mode, the process of automatically exiting whatever mode the system was in and returning the shrouds to predetermined "Safe Temperature." The control screens for these processes are included at the end of this paper.

The major factor that made it so difficult to resolve the problems in the automation of the new thermal system was the size of the system and the time lag in responding to the changes. The shrouds in the SES weigh approximately 25,000 lb (11,340 kg) with piping runs in each zone in the side shroud over 400-feet (122 m) in length. It takes about 2 hours for the return gas to change temperature after starting a transition. These time constants made it impractical to test some modes of operation more than once in a given day, thereby lengthening the process of identifying the problems and correcting them.

The biggest setback faced was during the final phase of the acceptance test in September 1999. The Safe State mode was being tested while operating in the LN_2 Mode with the shrouds flooded with LN_2. The process itself went smoothly. The problem was encountered around 10:30 pm when the steam heat exchanger was overcome by the cold process gas and froze. The transfer from Purge Mode to the GN_2 Mode had been successfully tested five times but the timing in the automated process was faster than when manually initiating the GN_2 Mode following the Purge Mode sequences. The cracks in the internal heat exchanger piping did not show up until the next run, two weeks later, when the steam was established with no GN_2 pressure in the heat exchanger. The root cause of the problem was learned in the days after finding water in the compressor. The vendor had designed the heat exchanger with steam in the tubes instead of the shell to minimize the size of the heat exchanger due to the tight size restrictions imposed by the opening in the floor. In addition, the 3-inch process valves supplying process gas to either the LN_2 or the steam heat exchangers were designed with full open or full closed actuators. When the possibility of freezing is present, good design practice for heat exchangers is to put the fluid with the freeze potential in the shell and not in the tubing. The vendors' lead process engineer, the heat exchanger manufacturer and our engineers had failed to notice this in their design. Even with many engineering controls in their design, such as an orifice sized to keep the heat exchanger hot along with free draining tubing from the heat exchanger to the steam trap, the full flow of –140°C gas cooled the steam in the tubing so rapidly, causing it to condense and form a vacuum in the drain. This allowed the condensed water to freeze and stop the steam flow (and heat) into the heat exchanger.

The vendor was very responsive and cooperative in repairing the system. The repair required redesigning a heat exchanger with the steam in the shell, procuring and installing the new heat exchange, replacing the open/closed actuators with proportional actuators, and relocating the control sensor for process control. This modification and subsequent tuning and acceptance testing was successfully completed in February 2000.

Lessons Learned

Heat Exchanger design: Spend the extra time or expense needed to have an independent heat exchanger designer or expert evaluate the design of critical heat exchangers. The design calculations are not the only things that need to be evaluated. The use of the heat exchanger in the system needs to be evaluated with respect to process fluids and engineering controls. These components are almost always custom designed, welded in place, and very costly to replace not only in the wallet but in lost time.

Automation of Processes: The time needed to properly test and tune processes that are being automated is almost universally under estimated. Take the time requested by the process/control engineer and multiply it by 2 or 3 when laying out a project schedule. Do not rush this phase – all possible scenarios should be tested. Maintain a good supply of spare rupture disks when testing LN_2 processes - they will be used. Processes that are unique to a given situation, even though typical to industry, require time to test and program in the controls to safely conduct that process. Many of the inputs used in a manual system are difficult to detect using standard instrumentation. For example, the distinct change in sound as non-cavitating LN_2 flow is established in a line versus interpreting the temperature and pressure in that line to deduce the same information. Temperature probes in a process line always have a time lag and determining the appropriate temperatures and pressures given different heat loads in the chamber is a trial and error process.

Contamination: Wherever possible, utilize low points for final weld connections in field installed process piping. No matter how careful the contractor is, cutting and grinding debris gets into the piping system that cannot be seen or cleaned out. Put this in the specification or bring it up in design reviews. Metal chips and valve seats do not get along with each other creating problems when tuning a control system by creating leaks where none are expected.

Insulation: Insulation of cryogenic process lines is a time consuming process. Use VJ process lines wherever possible. This costs more initially, but saves installation time and creates a much cleaner system. This is not always practical, so when mechanically insulating cryogenic lines, make sure the contractor uses an installer who has experience with the insulation techniques being used and multiply their estimated installation time by a factor of two when the piping runs are complex.

SYSTEM PERFORMANCE

The performance of the completed system met all of the criteria specified. The temperature ramp rate cooling is 28°C across the range and during heating is 30°C per hour. The control of the heat exchangers was greatly enhanced when the vendor went to using proportional actuators on the heat exchanger isolation valves. The factor that governs the ramp rate is the gradient across the shrouds as seen between the supply and return temperatures. To minimize the stress on the supply manifold and panel welded joints, a decision reached at the conclusion of the shroud study was to limit the gradient to 100°C. This gradient is an adjustable variable in the control system. An entry of 100°C in this field yields a ramp rate around 30°C. Smaller gradients yield slower transition rates which is a technique used to control transition rates with this system. The gradient control is a secondary control loop that takes over the control supply temperature setpoint when the differential between the return and supply gas is greater than 100°C even when the target setpoint is set at a greater value. Figure 3 depicts the gradient curve compared to the supply and return gas temperatures.

The automatic features of compressor pressure control, setpoint control and sequences to establish GN_2 and LN_2 flow have significantly minimized the demands on the operators when running the system. We now conduct chamber certifications from another building since the entire system can be monitored and controlled remotely.

CONCLUSIONS

The upgrade of the thermal system for the Space Environment Simulator at Goddard Space Flight Center combined with the final modifications to the vacuum system for remote operation was successful in meeting all of the design objectives. The success was due to the efforts of many technicians, designers and engineers from Goddard and industry working together to identify the design criteria and the solutions within the funding available for the task. The automating of the thermal system control processes has decreased the level of effort required to run the thermal system by a large factor allowing the operators more time to attend to the other duties of conducting a spacecraft level test in the SES facility. The intent of this paper is to provide a road map of possibilities that may assist others when upgrading an old system becomes necessary.

REFERENCES

[i] *Preliminary Engineering Report for the Modification of the Facility 290 Thermal System*, Andrew Webb and Janet Sushon, Mantech Systems Engineering Corporation, Document 26-09-280, August, 1996.

[ii] *Fatigue Induced Cracking in Aluminum LN_2 Shroud of 39-Foot Vacuum Chamber,* Arthur E. Edwards, Ford Aerospace and Communication Corporation, Palo Alto, CA. Presented at the 13th Space Simulation Conference by the Institute of Environmental Sciences; Orlando, FL, 1984.

[iii] *Thermal System Upgrade of the Space Environment Simulation Test Chamber,* Ashok B. Desai, Environmental Test Engineering and Integration Branch, Engineering Services Division, Goddard Space Flight Center, Greenbelt, MD. Presented at the 19th Space Simulation Conference by the Institute of Environmental Sciences; Baltimore, MD, 1996.

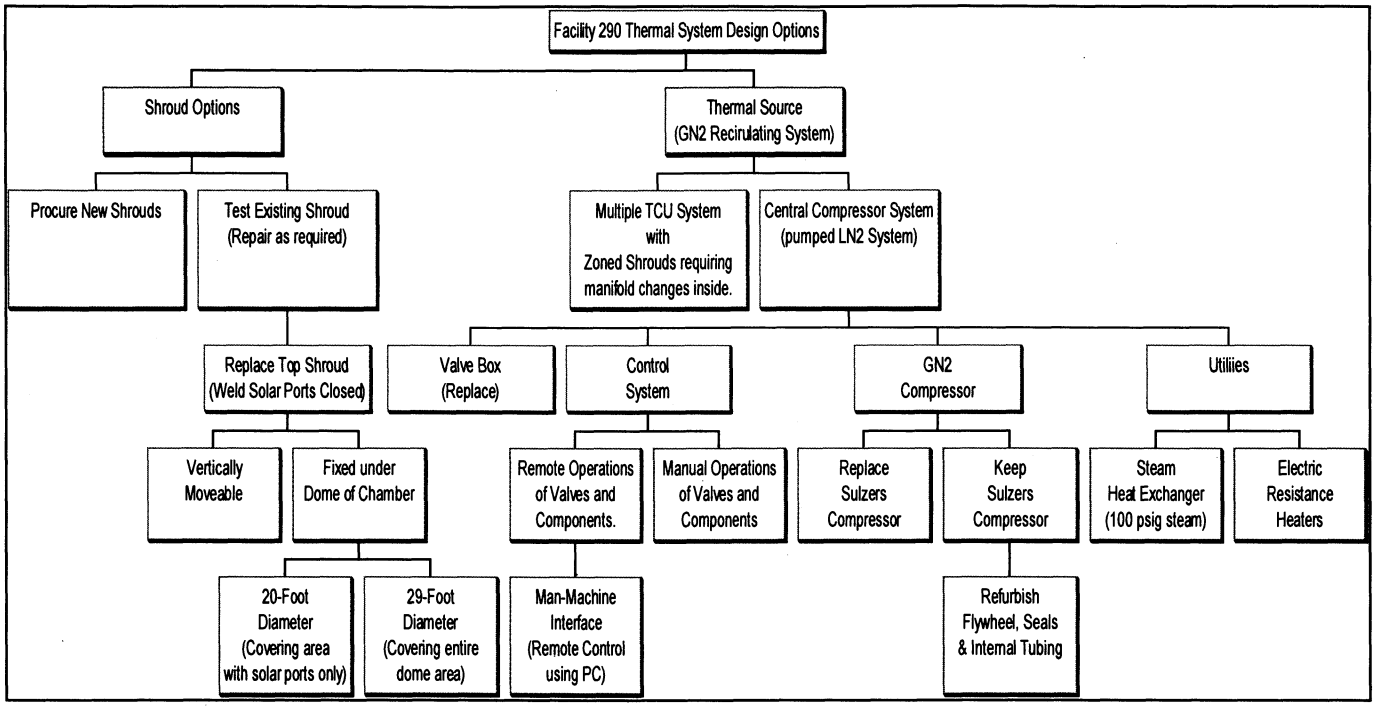

Figure 1: Decision Tree

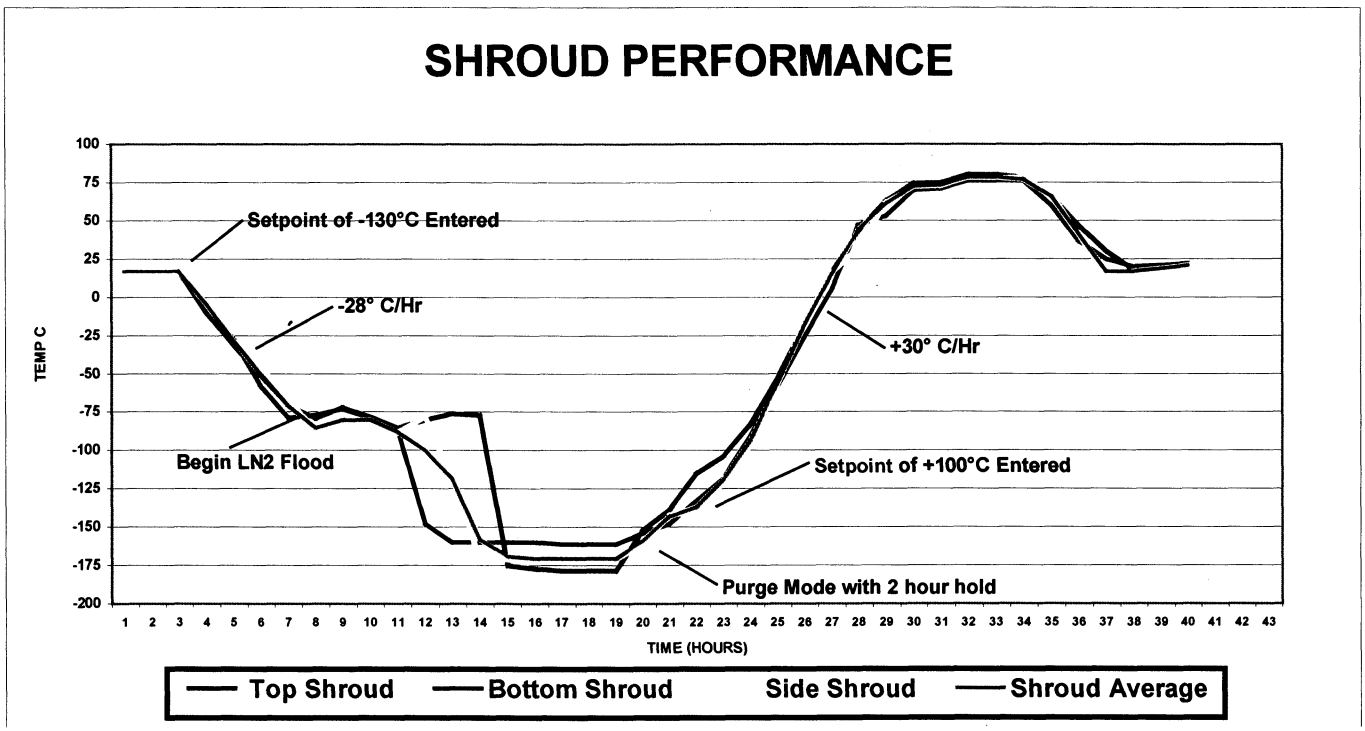

Figure 2: Shroud Performance Curve

Acceptance Test Shroud Gradient

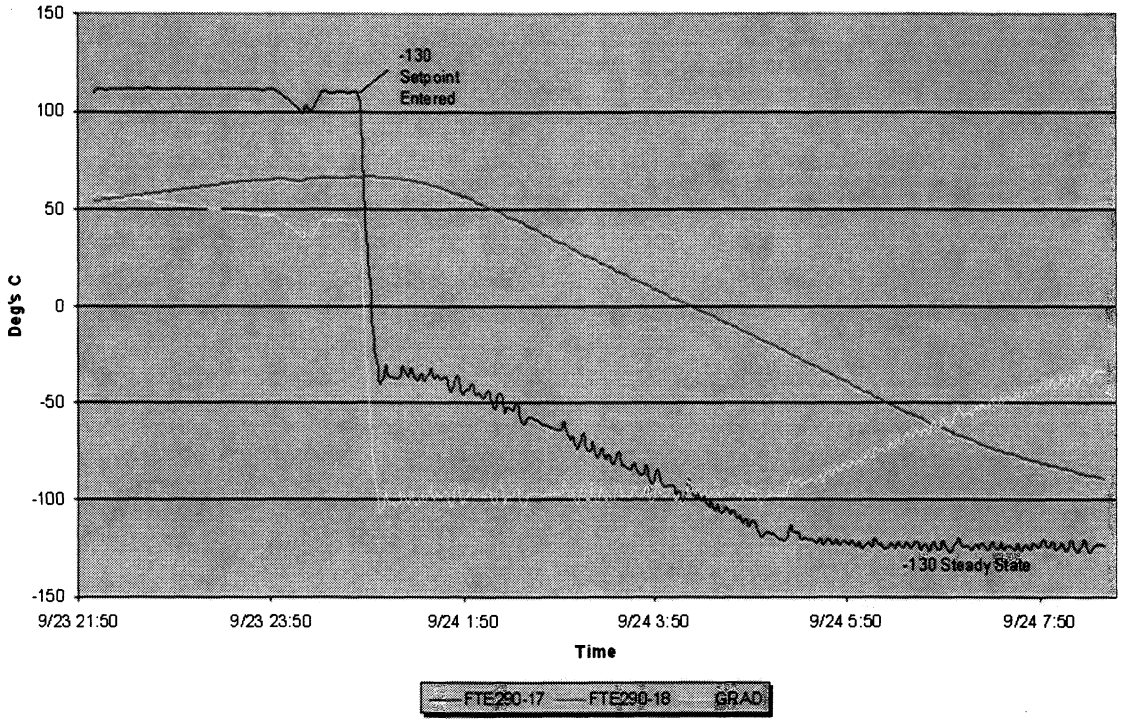

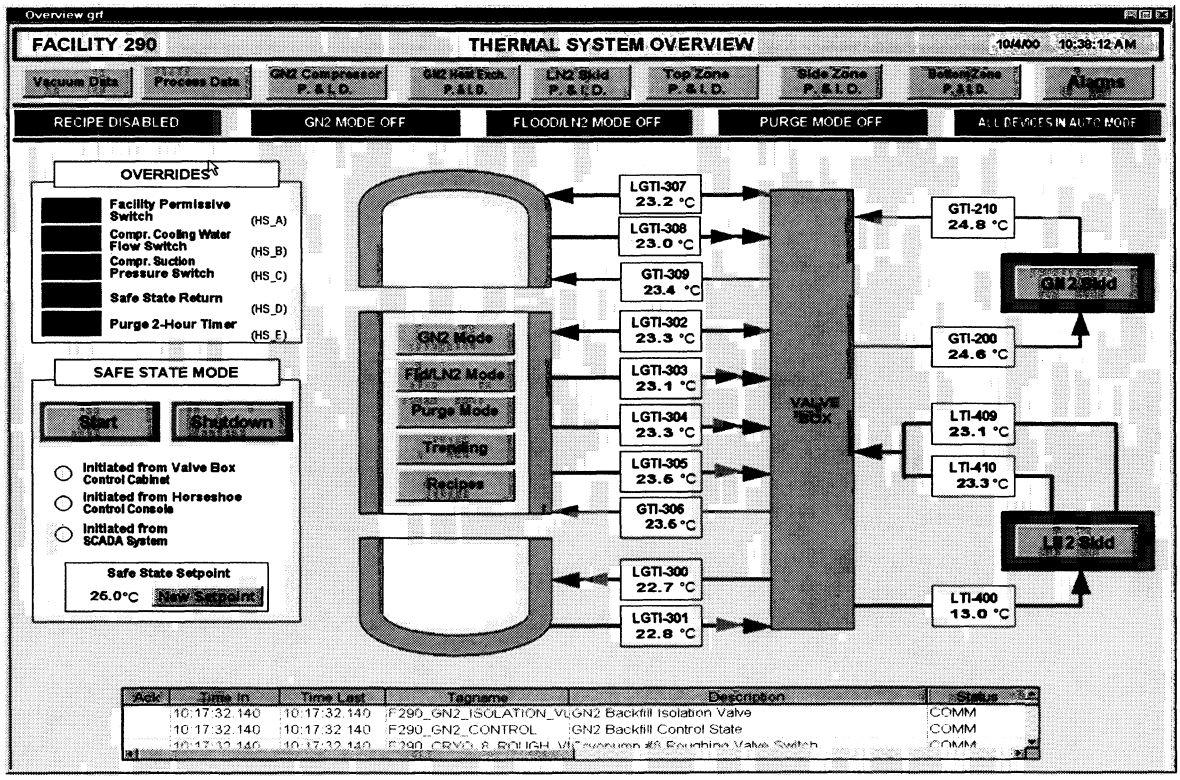

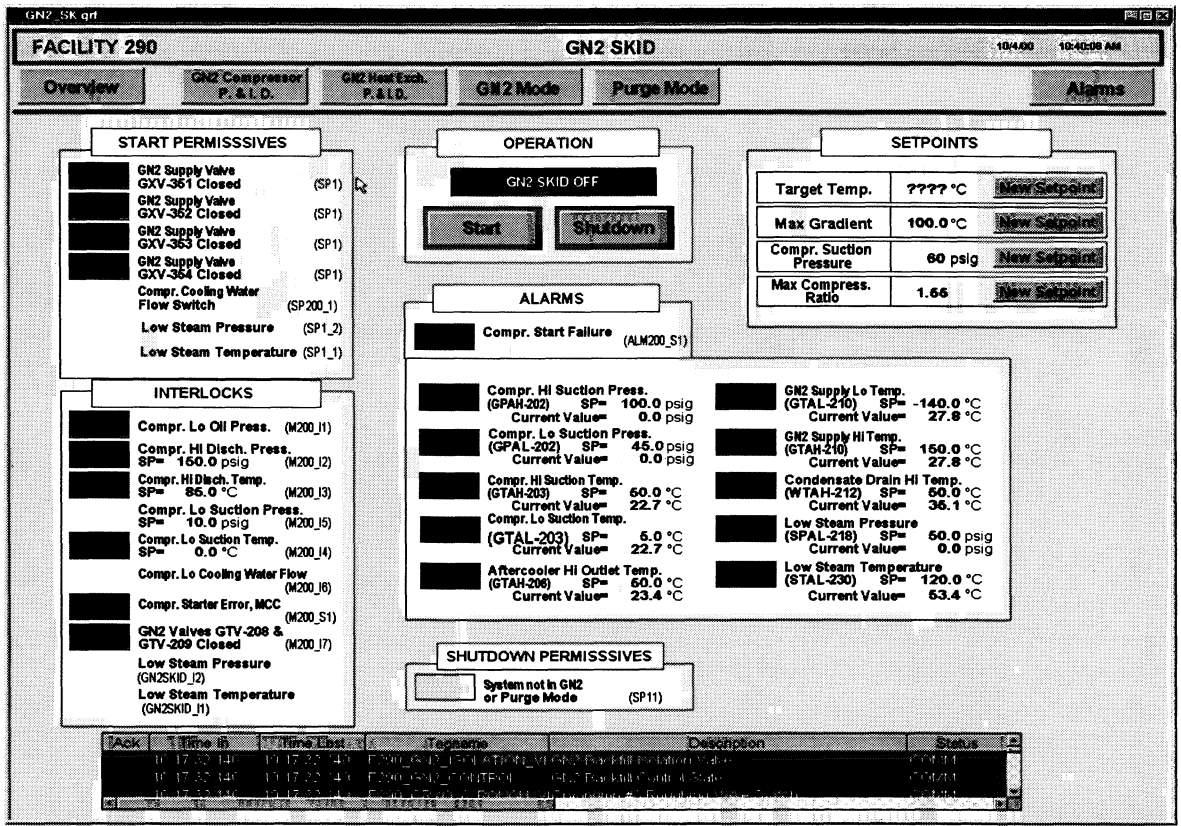
GN2_SK.grf
FACILITY 290
GN2 SKID
10/4/00 10:40:08 AM
Overview
GN2 Compressor P. & I. D.
GN2 Heat Exch. P. & I. D.
GN2 Mode
Purge Mode
Alarms
START PERMISSSIVES
GN2 Supply Valve GXV-361 Closed (SP1)
GN2 Supply Valve GXV-362 Closed (SP1)
GN2 Supply Valve GXV-363 Closed (SP1)
GN2 Supply Valve GXV-364 Closed (SP1)
Compr. Cooling Water Flow Switch (SP200_1)
Low Steam Pressure (SP1_2)
Low Steam Temperature (SP1_1)
INTERLOCKS
Compr. Lo Oil Press. (M200_I1)
Compr. HI Disch. Press. SP= 150.0 psig (M200_I2)
Compr. HI Disch. Temp. SP= 85.0 °C (M200_I3)
Compr. Lo Suction Press. SP= 10.0 psig (M200_I5)
Compr. Lo Suction Temp. SP= 0.0 °C (M200_I4)
Compr. Lo Cooling Water Flow (M200_I6)
Compr. Starter Error, MCC (M200_S1)
GN2 Valves GTV-208 & GTV-209 Closed (M200_I7)
Low Steam Pressure (GN2SKID_I2)
Low Steam Temperature (GN2SKID_I1)
OPERATION
GN2 SKID OFF
Start
Shutdown
ALARMS
Compr. Start Failure (ALM200_S1)
Compr. HI Suction Press. (GPAH-202) SP= 100.0 psig Current Value= 0.0 psig
Compr. Lo Suction Press. (GPAL-202) SP= 45.0 psig Current Value= 0.0 psig
Compr. HI Suction Temp. (GTAH-203) SP= 50.0 °C Current Value= 22.7 °C
Compr. Lo Suction Temp. (GTAL-203) SP= 5.0 °C Current Value= 22.7 °C
Aftercooler HI Outlet Temp. (GTAH-206) SP= 50.0 °C Current Value= 23.4 °C
GN2 Supply Lo Temp. (GTAL-210) SP= -140.0 °C Current Value= 27.8 °C
GN2 Supply HI Temp. (GTAH-210) SP= 150.0 °C Current Value= 27.8 °C
Condensate Drain HI Temp. (WTAH-212) SP= 50.0 °C Current Value= 35.1 °C
Low Steam Pressure (SPAL-218) SP= 50.0 psig Current Value= 0.0 psig
Low Steam Temperature (STAL-230) SP= 120.0 °C Current Value= 53.4 °C
SHUTDOWN PERMISSSIVES
System not in GN2 or Purge Mode (SP11)
SETPOINTS
Target Temp. ???? °C New Setpoint
Max Gradient 100.0 °C New Setpoint
Compr. Suction Pressure 60 psig New Setpoint
Max Compress. Ratio 1.55 New Setpoint
Ack | Time In | Time Last | Tagname | Description | Status

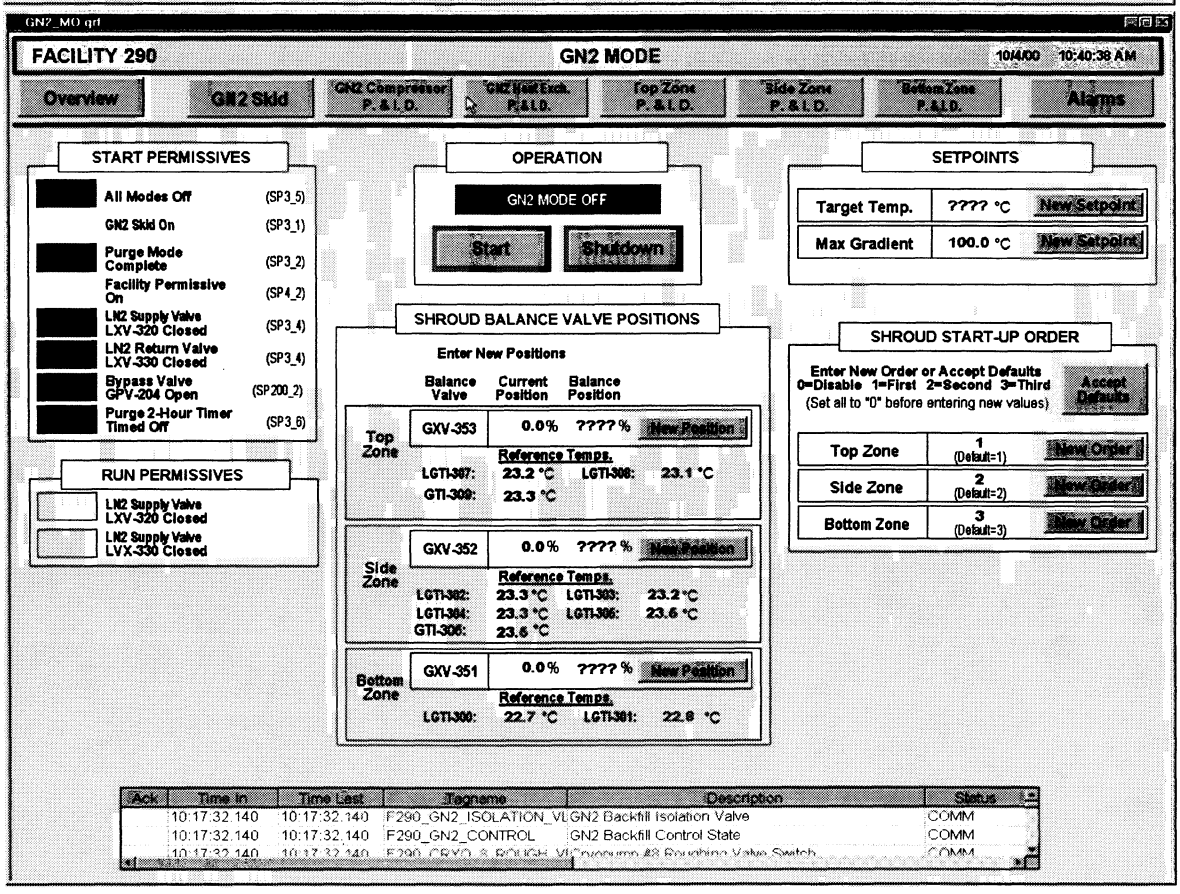
GN2_MO.grf
FACILITY 290
GN2 MODE
10/4/00 10:40:38 AM
Overview
GN2 Skid
GN2 Compressor P. & I. D.
GN2 Heat Exch. P. & I. D.
Top Zone P. & I. D.
Side Zone P. & I. D.
Bottom Zone P. & I. D.
Alarms
START PERMISSIVES
All Modes Off (SP3_5)
GN2 Skid On (SP3_1)
Purge Mode Complete (SP3_2)
Facility Permissive On (SP4_2)
LN2 Supply Valve LXV-320 Closed (SP3_4)
LN2 Return Valve LXV-330 Closed (SP3_4)
Bypass Valve GPV-204 Open (SP200_2)
Purge 2-Hour Timer Timed Off (SP3_6)
RUN PERMISSIVES
LN2 Supply Valve LXV-320 Closed
LN2 Supply Valve LVX-330 Closed
OPERATION
GN2 MODE OFF
Start
Shutdown
SHROUD BALANCE VALVE POSITIONS
Enter New Positions
Balance Valve | Current Position | Balance Position
Top Zone: GXV-353 0.0% ???? % New Position
Reference Temps. LGTI-307: 23.2 °C LGTI-308: 23.1 °C GTI-309: 23.3 °C
Side Zone: GXV-352 0.0% ???? % New Position
Reference Temps. LGTI-302: 23.3 °C LGTI-303: 23.2 °C LGTI-304: 23.3 °C LGTI-305: 23.6 °C GTI-306: 23.6 °C
Bottom Zone: GXV-351 0.0% ???? % New Position
Reference Temps. LGTI-300: 22.7 °C LGTI-301: 22.8 °C
SETPOINTS
Target Temp. ???? °C New Setpoint
Max Gradient 100.0 °C New Setpoint
SHROUD START-UP ORDER
Enter New Order or Accept Defaults 0=Disable 1=First 2=Second 3=Third (Set all to "0" before entering new values)
Accept Defaults
Top Zone 1 (Default=1) New Order
Side Zone 2 (Default=2) New Order
Bottom Zone 3 (Default=3) New Order
Ack | Time In | Time Last | Tagname | Description | Status
10:17:32.140 | 10:17:32.140 | F290_GN2_ISOLATION_VL | GN2 Backfill Isolation Valve | COMM
10:17:32.140 | 10:17:32.140 | F290_GN2_CONTROL | GN2 Backfill Control State | COMM

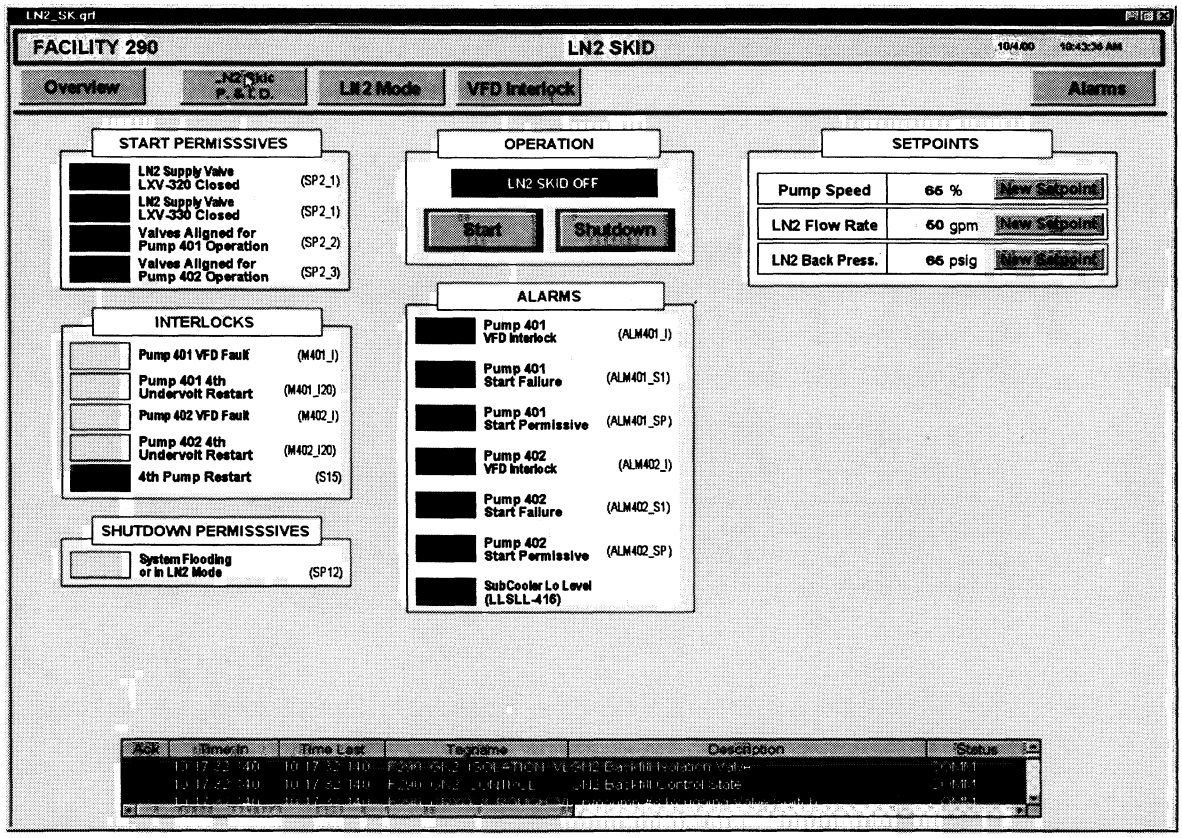
LN2_SK.grf
FACILITY 290
LN2 SKID
10/4/00
10:43:36 AM
Overview
LN2 Skid P. & I. D.
LN2 Mode
VFD Interlock
Alarms
START PERMISSSIVES
LN2 Supply Valve LXV-320 Closed (SP2_1)
LN2 Supply Valve LXV-330 Closed (SP2_1)
Valves Aligned for Pump 401 Operation (SP2_2)
Valves Aligned for Pump 402 Operation (SP2_3)
INTERLOCKS
Pump 401 VFD Fault (M401_I)
Pump 401 4th Undervolt Restart (M401_I20)
Pump 402 VFD Fault (M402_I)
Pump 402 4th Undervolt Restart (M402_I20)
4th Pump Restart (S15)
SHUTDOWN PERMISSSIVES
System Flooding or in LN2 Mode (SP12)
OPERATION
LN2 SKID OFF
Start
Shutdown
ALARMS
Pump 401 VFD Interlock (ALM401_I)
Pump 401 Start Failure (ALM401_S1)
Pump 401 Start Permissive (ALM401_SP)
Pump 402 VFD Interlock (ALM402_I)
Pump 402 Start Failure (ALM402_S1)
Pump 402 Start Permissive (ALM402_SP)
SubCooler Lo Level (LLSLL-416)
SETPOINTS
Pump Speed 65 % New Setpoint
LN2 Flow Rate 60 gpm New Setpoint
LN2 Back Press. 65 psig New Setpoint
Ack
Time In
Time Last
Tagname
Description
Status

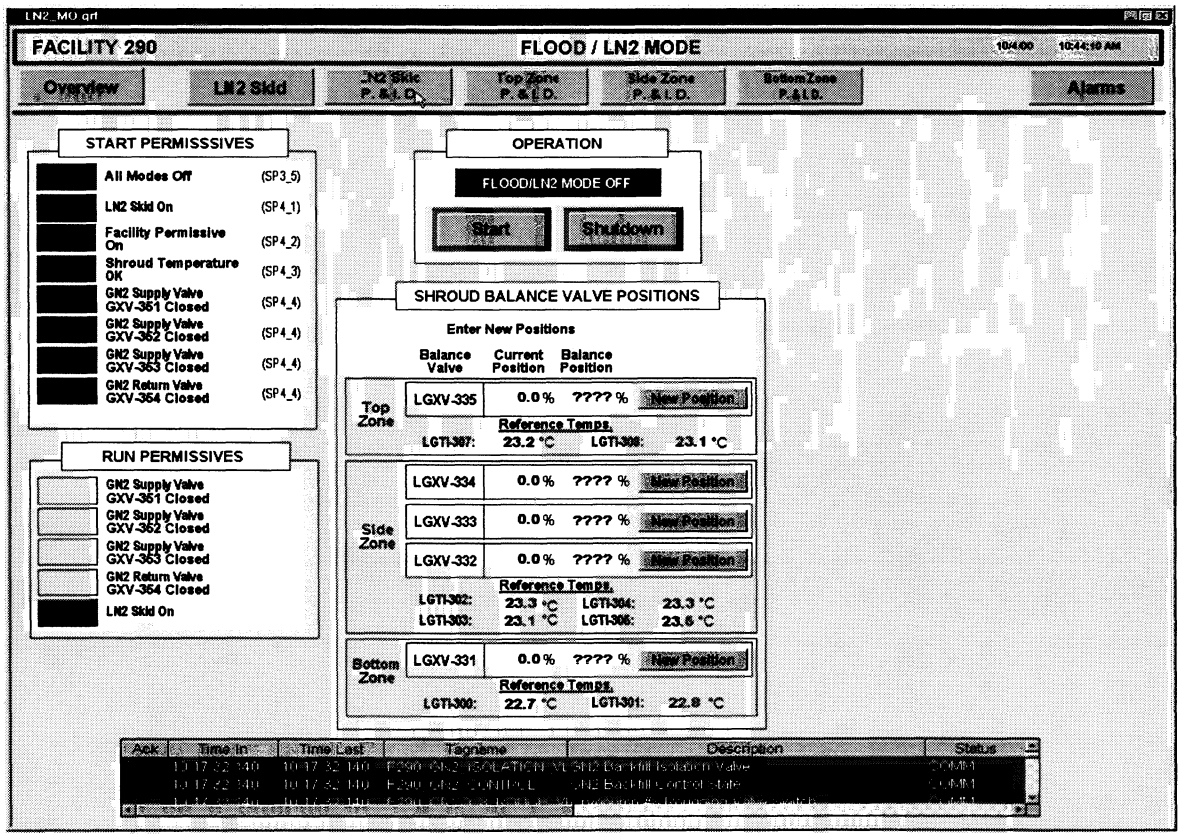
LN2_MO.grf
FACILITY 290
FLOOD / LN2 MODE
10/4/00
10:44:10 AM
Overview
LN2 Skid
GN2 Skid P. & I. D.
Top Zone P. & I. D.
Side Zone P. & I. D.
Bottom Zone P. & I. D.
Alarms
START PERMISSSIVES
All Modes Off (SP3_5)
LN2 Skid On (SP4_1)
Facility Permissive On (SP4_2)
Shroud Temperature OK (SP4_3)
GN2 Supply Valve GXV-361 Closed (SP4_4)
GN2 Supply Valve GXV-362 Closed (SP4_4)
GN2 Supply Valve GXV-363 Closed (SP4_4)
GN2 Return Valve GXV-364 Closed (SP4_4)
RUN PERMISSIVES
GN2 Supply Valve GXV-361 Closed
GN2 Supply Valve GXV-362 Closed
GN2 Supply Valve GXV-363 Closed
GN2 Return Valve GXV-364 Closed
LN2 Skid On
OPERATION
FLOOD/LN2 MODE OFF
Start
Shutdown
SHROUD BALANCE VALVE POSITIONS
Enter New Positions
Balance Valve
Current Position
Balance Position
Top Zone
LGXV-335 0.0 % ???? % New Position
Reference Temps.
LGTI-307: 23.2 °C LGTI-308: 23.1 °C
Side Zone
LGXV-334 0.0 % ???? % New Position
LGXV-333 0.0 % ???? % New Position
LGXV-332 0.0 % ???? % New Position
Reference Temps.
LGTI-302: 23.3 °C LGTI-304: 23.3 °C
LGTI-303: 23.1 °C LGTI-305: 23.6 °C
Bottom Zone
LGXV-331 0.0 % ???? % New Position
Reference Temps.
LGTI-300: 22.7 °C LGTI-301: 22.8 °C
Ack
Time In
Time Last
Tagname
Description
Status

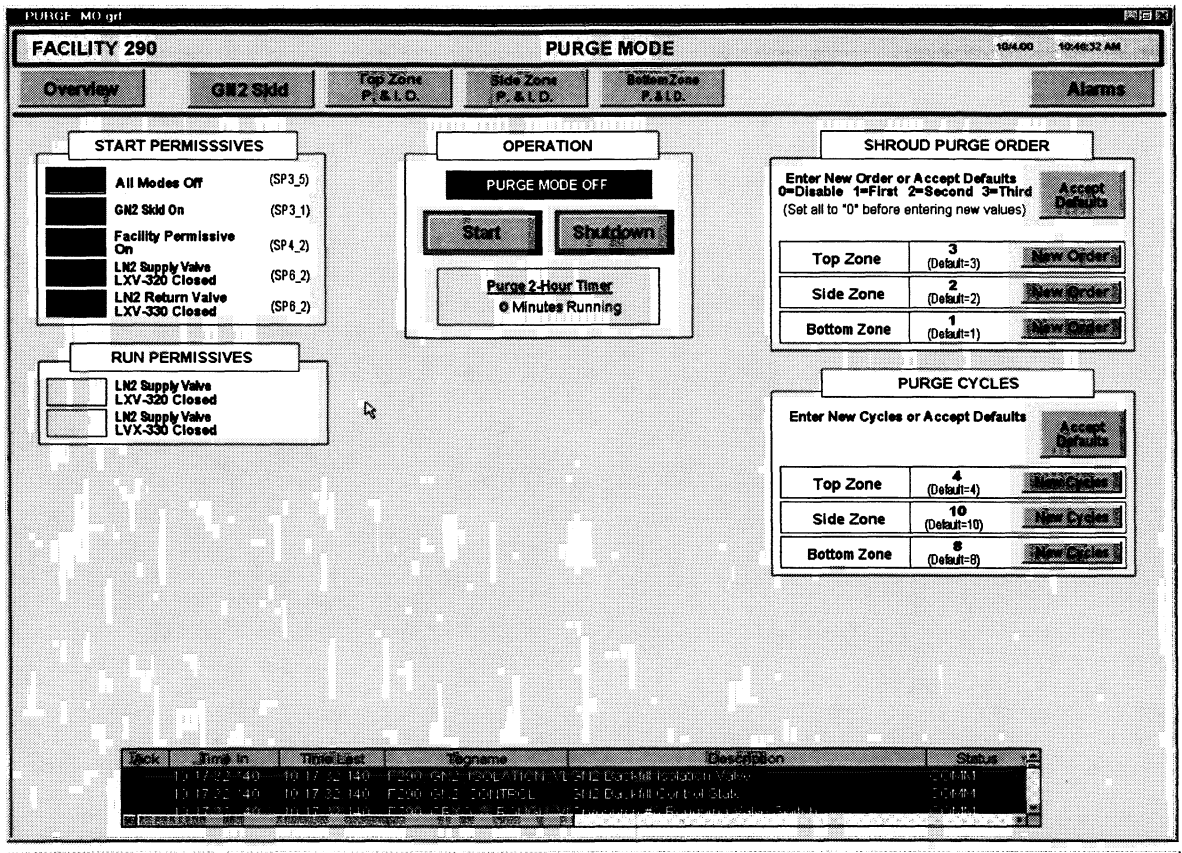
PURGE_MO.grf
FACILITY 290
PURGE MODE
Overview
GN2 Skid
Top Zone P. & I.D.
Side Zone P. & I.D.
Bottom Zone P. & I.D.
Alarms
START PERMISSSIVES
All Modes Off (SP3_5)
GN2 Skid On (SP3_1)
Facility Permissive On (SP4_2)
LN2 Supply Valve LXV-320 Closed (SP6_2)
LN2 Return Valve LXV-330 Closed (SP6_2)
RUN PERMISSIVES
LN2 Supply Valve LXV-320 Closed
LN2 Supply Valve LVX-330 Closed
OPERATION
PURGE MODE OFF
Start
Shutdown
Purge 2-Hour Timer
0 Minutes Running
SHROUD PURGE ORDER
Enter New Order or Accept Defaults
0=Disable 1=First 2=Second 3=Third
(Set all to "0" before entering new values)
Accept Defaults
Top Zone 3 (Default=3) New Order
Side Zone 2 (Default=2) New Order
Bottom Zone 1 (Default=1) New Order
PURGE CYCLES
Enter New Cycles or Accept Defaults
Accept Defaults
Top Zone 4 (Default=4) New Cycles
Side Zone 10 (Default=10) New Cycles
Bottom Zone 8 (Default=8) New Cycles
Ack | Time In | Time Last | Tagname | Description | Status

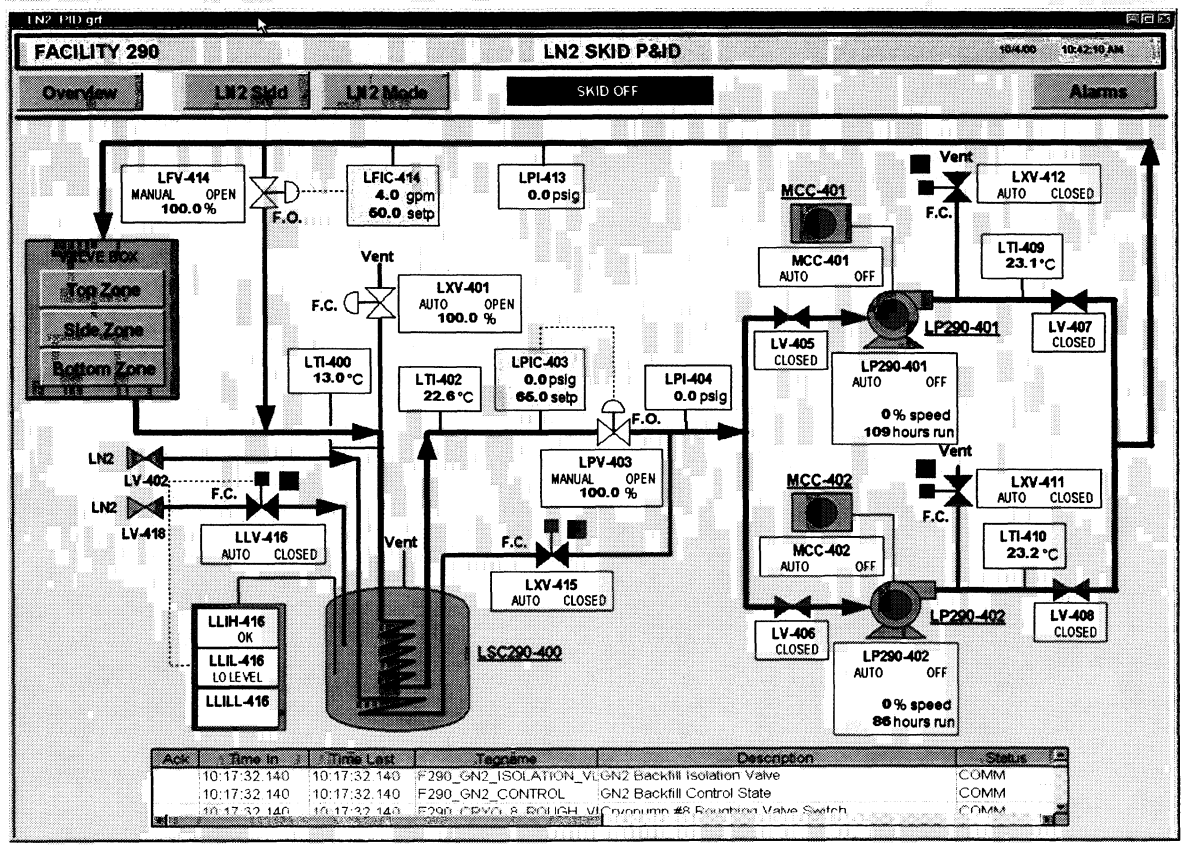
LN2_PID.grf
FACILITY 290
LN2 SKID P&ID
Overview
LN2 Skid
LN2 Mode
SKID OFF
Alarms
LFV-414 MANUAL OPEN 100.0 %
F.O.
LFIC-414 4.0 gpm 60.0 setp
LPI-413 0.0 psig
Vent
F.C.
LXV-401 AUTO OPEN 100.0 %
LTI-400 13.0 °C
LTI-402 22.6 °C
LPIC-403 0.0 psig 65.0 setp
LPI-404 0.0 psig
F.O.
LN2
LV-402
F.C.
LN2
LV-418
LLV-416 AUTO CLOSED
LLIH-416 OK
LLIL-416 LO LEVEL
LLILL-416
Vent
F.C.
LPV-403 MANUAL OPEN 100.0 %
LXV-415 AUTO CLOSED
LSC290-400
Vent
LXV-412 AUTO CLOSED
F.C.
MCC-401
MCC-401 AUTO OFF
LTI-409 23.1 °C
LV-405 CLOSED
LP290-401
LV-407 CLOSED
LP290-401 AUTO OFF
0 % speed
109 hours run
Vent
LXV-411 AUTO CLOSED
F.C.
MCC-402
MCC-402 AUTO OFF
LTI-410 23.2 °C
LV-406 CLOSED
LP290-402
LV-408 CLOSED
LP290-402 AUTO OFF
0 % speed
86 hours run
Ack | Time In | Time Last | Tagname | Description | Status
10:17:32.140 | 10:17:32.140 | F290_GN2_ISOLATION_VL | GN2 Backfill Isolation Valve | COMM
10:17:32.140 | 10:17:32.140 | F290_GN2_CONTROL | GN2 Backfill Control State | COMM

HELIUM EVOLUTION FROM THE TRANSFER OF HELIUM-SATURATED PROPELLANT IN SPACE[1]

Bich N. Nguyen
The Boeing Company
Reusable Space Systems

Dr. Frederick Best, Director
Center for Space Power
Texas A&M University

ABSTRACT

Helium evolution from the transfer of helium-saturated propellant in space is quantified to determine its impact due to creating a two-phase mixture in the transfer line. The transfer line is approximately 1.27 cm in diameter and 6096 cm in length and comprised of the fluid interconnect system (FICS), the orbiter propellant transfer system (OPTS), and the International Space Station (ISS) propulsion module (ISSPM). The propellant volumetric transfer rate is approximately between 7 and 11 liters per minute (lpm), and the supply tank pressure is maintained at approximately 1827 kPa (absolute).

The pressure drops for both monomethylhydrazine (MMH) and nitrogen tetroxide (NTO) at 11.3 lpm are approximately 202 kPa and 302 kPa, respectively. These pressure drops cause the helium-saturated propellants to release excess helium of approximately 8.8% for MMH and 15.3% for NTO at standard temperature and pressure (STP). The corresponding volume fractions of helium evolved to the propellant in the line are 0.1% for MMH and 0.6 % for NTO.

The volumes of steady-state helium evolution from helium-saturated MMH and NTO are approximately 8.19 cm^3 and 45.88 cm^3, respectively, for a total line volume of 7722 cm^3.

INTRODUCTION

One of the technical challenges in developing a propellant transfer capability in space for an unbladdered propulsion system is the helium evolution from helium-saturated propellant. The topic of gas evolution is not new; however, the effect it has on the propellant transfer in space is new. Most of us can relate to the concept of gas evolution from the experience of opening a carbonated beverage can under pressure. There is a manifestation of bubble foam discharging from the can. This bubble foam is the effect of carbon dioxide (CO_2) coming out of solution in the form of gas bubbles. Likewise, the process of helium coming out of helium-saturated propellant exhibits a similar phenomenon; however, it is to a lesser extent since the concentration of saturated gas in the two cases is significantly different. Furthermore, CO_2 is involved in a chemical equilibrium interaction with water, while helium is inert.

During propellant transfer, the propellant begins at the supply tank as a single-phase liquid. As it travels along the transfer line, it experiences a pressure drop due to line friction, restrictions, and changes in flow direction. As a result of the pressure drop, the helium-saturated propellant releases helium. Reference 1 states that: "*At a specific temperature and pressure, any liquid will hold a given quantity of gas in solution. Increasing the gas pressure will increase the quantity of gas that can be held by the liquid. Under any set of conditions of pressure and temperature, a liquid that holds the maximum quantity of gas in solution is said to be saturated. If the pressure is reduced while all other conditions remain the same, the quantity of gas that can be held in solution is reduced and the liquid then contains more gas than it can hold in solution at the new lower pressure and is over saturated. The excess dissolved gas will come out of solution; and if the pressure is reduced sufficiently, the excess gas may be observed as small bubbles.*" In addition, NASA White Sands Test Facility (WSTF) has documented helium evolution from propellants undergoing depressurization in thruster systems.[2] This clearly shows the formation of a bubble cloud in propellant.

---

[1] *This work was performed under NASA Contract No. NAS15-10000 to develop ISSPM.*

[2] *NASA WSTF Report and Vide of Hot Fire Test Series No. 3A of 12 February 1999, Run No. 19.*

When helium evolves from the propellant, it begins as tiny bubbles from nucleation sites (surfaces), turbulent eddies, and also within the liquid. Once these tiny bubbles are formed, they will grow progressively as a function of pressure drop. As the bubbles grow in size, they mix with the propellant liquid to create a two-phase flow. The process of helium evolution in the transfer line is shown in Figure 1. This figure illustrates a visual observation of de-saturating helium-saturated water from approximately 1827 kPa to 101 kPa through a 2.54-cm smooth transparent tubing.

The existence of two-phase flow will induce uncertainty in the flowmeter reading, which is used to gage the amount of transferred propellant for a single-phase flow. To eliminate the effect of helium evolution on the flowmeter uncertainty, the volume fraction of the helium to propellant is quantified so that the undesirable region of two-phase flow can be avoided. Furthermore, upon completion of propellant transfer, the transfer line must be emptied of propellant before being disconnected. This requires that the transfer line be purged. Purging in microgravity conditions already is difficult with the existence of valves and bends, and is now complicated further with the trapped helium bubbles. Under microgravity conditions, there is a tendency for the bubbles to merge and form a continuous gas passage. Reference 2 discusses the fluid behavior in microgravity conditions. The purge gas will tend to travel along the lesser resistance path, which is the gas passage. Consequently, the effectiveness of purging the residual propellant becomes questionable. Again, quantifying the volume fraction of the helium to propellant along the transfer line is necessary so that the impact of the trapped bubbles on purging can be assessed. Finally, the system pressure drop as defined by a single-phase liquid will increase with the introduction of helium evolution. The existence of gas from helium evolution will facilitate turbulence in the flow, which may change the flow regime.

In this paper, the volume fraction of helium to propellant in the transfer line is determined based on the line configurations of the FICS, OPTS, and ISSPM. The orbiter docking with ISS during the propellant transfer is shown in Figure 2.

SYMBOLS

Values are given in International System of Units (SI). The measurements and calculations were made in SI.

D	Inner diameter of the transfer line, cm.
f	Friction factor, dimensionless
G_{MMH}	Total amount of helium evolved from MMH during MMH transfer, cc at STP
G_{NTO}	Total amount of helium evolved from NTO during NTO transfer, cc at STP
He_{MMH}	Amount of helium absorbed in a given amount (cc) of MMH, cc at STP
He_{NTO}	Amount of helium absorbed in a given amount (cc) of NTO, cc at STP
Q	Volumetric flow rate, lpm
Q_{MMH}	Total amount of helium absorbed in helium saturated MMH, cc at STP
Q_{NTO}	Total amount of helium absorbed in helium saturated NTO, cc at STP
K_b	Bend loss coefficient, $K_b = \left[\left(\frac{angle}{90} - 1\right)\left(0.25\pi\frac{r}{D} + 0.5(17)\right) + 17\right]f_i$
K_v	Valve loss coefficient, $K_v = K_n f_i$
MMH	Monomethylhydrazine, fuel
NTO	Nitrogen tetroxide, oxidizer
P	Local pressure inside the transfer line, kPa (absolute)
R_{MMH}	Volume fraction of helium to propellant evolved from MMH during MMH transfer, dimensionless
R_{NTO}	Volume fraction of helium to propellant evolved from NTO during NTO transfer, dimensionless
V	Volume of the propellant element, cc
v	Velocity of the fluid flowing inside the transfer line, m/sec
x	Distance from the supply tank along the transfer line, cm
ρ	Density of the propellant, kg/m^3
ΔP	Pressure drop, kPa
$\%He_{MMH}$	Percentage of helium evolved from helium saturated MMH at 1827 kPa to a given de-saturation pressure, %
$\%He_{NTO}$	Percentage of helium evolved from helium saturated NTO at 1827 kPa to a given de-saturation pressure, %

ANALYTICAL APPROACH

The helium evolution upon de-saturation of a helium-saturated propellant is a rapid process. That is, the evolution of helium occurs nearly instantaneously with respect to decreasing pressure. It is a technical challenge to design a test apparatus to measure the transient helium evolution. Furthermore, there is a lack of test data on the kinetic helium evolution to correlate the direct effect of helium evolution with time under the proposed propellant transfer conditions. As an alternative, a steady-state condition for helium evolution was used to arrive at (1) the total amount of helium evolution and (2) the steady-state time. These results are sufficient to address the concerns of helium evolution on the flowmeter, on the effectiveness of purging, and on creating turbulence in the flow. Consequently, there is no need for the actual kinetics of helium evolution.

The pressure drop forces the helium gas to evolve from helium-supersaturated propellant. The higher the pressure drop, the more helium evolution. Thus, the characterization of helium evolution requires a complete understanding of the pressure drop characteristics of the transfer system.

PRESSURE DROP CHARACTERIZATION

Configuration

The FICS and OPTS are shown in Figure 3. The propellant can be transferred either from the forward reaction control system (FRCS), the orbiter maneuver system (OMS), or the aft reaction control system (ARCS). The FRCS is located near the lower left-hand side, and the OMS and ARCS are located near the lower right-hand side of Figure 3. As the propellant leaves the supply tanks, it enters the FICS and subsequently flows into the OPTS, which leads to the ISSPM. The OPTS is located near the upper left-hand side of Figure 3.

Pressure Drop Formulation

The pressure at any point in the transfer line is equal to the supply tank pressure minus the accumulated pressure drop from the supply tank to that point. Since the ISSPM is a bipropellant propulsion system that uses monomethylhydrazine (MMH-$CH_3N_2H_3$) as a fuel and nitrogen tetroxide (NTO-N_2O_4) as an oxidizer, the following analyses will provide derivations for both commodities. The line pressure is:

$$P_i = 1827 - \Delta P_{line} - \Delta P_{bend} - \Delta P_{valve} \tag{1}$$

where

$$\Delta P_{line} = \frac{1}{2}(4.632)\left(\frac{1}{144*32.2}\right)\frac{\rho_i}{D}\upsilon^2 f_i x^{(3)} \tag{1-1}$$

$$\Delta P_{bend} = \sum_{m=1}^{M} \frac{1}{2}(4.632)\left(\frac{1}{144*32.2}\right)\rho_i \upsilon^2 K_b(angle_m, f_i) \tag{1-2}$$

$$\Delta P_{valve} = \sum_{n=1}^{N} \frac{1}{2}(4.632)\left(\frac{1}{144*32.2}\right)\rho_i \upsilon^2 K_v(K_n, f_i) \tag{1-3}$$

i represents the commodity: MMH or NTO

The physical properties of MMH and NTO were obtained from Reference 3.

The pressure drop is a function of flow rate, which is dependent on the pressure difference between the supply tank and the receiving tank. The supply tank pressure is regulated to approximately 1827 kPa; however, the receiv-

[3] *4.632 is a conversion factor.*

ing tank pressure increases with the transferred propellant. This causes the pressure difference between tanks to decrease and the flow rate to decrease accordingly. In this report, the pressure drop analysis assumes that the flow rate is controlled to maintain a constant flow. The pressure profile during propellant transfer calculated from Equations 1, 1-1, 1-2, and 1-3 is shown in Figure 4. This figure shows that the pressure drop increases abruptly in transition from one subsystem to the next as a result of multiple redundancy isolation valves.

HELIUM CONCENTRATION AND EVOLUTION CHARACTERIZATION

Before beginning the analysis of helium evolution during propellant transfer, it is important to define the amount of helium contained in MMH and NTO and the fraction which evolves under depressurization.

Helium Concentration in Saturated Propellant and Oxidizer

When propellant is pressurized by direct contact with helium gas, the helium will be absorbed in the propellant. The amount of helium saturated at STP in MMH and NTO can be described by the following correlation (Reference 1):

$$He_{MMH}(P) = 0.0006\left(\frac{P-101}{6.895}\right) - 0.00323 \tag{2}$$

$$He_{NTO}(P) = 0.0022\left(\frac{P-101}{6.895}\right) - 0.0863 \tag{3}$$

where

$He_{MMH}(P)$ is amount of helium absorbed in a given amount (cc) of MMH, cc at STP
$He_{NTO}(P)$ is amount of helium absorbed in a given amount (cc) of NTO, cc at STP
P is the pressure, kPa (absolute)

The amount of helium contained in the propellant increases with increasing pressure. NTO can absorb 3 to 4 times more helium than MMH at a given pressure.

Helium Evolution

Helium evolves when the pressure of helium-saturated propellant is decreased. The lower the pressure, the larger the amount of helium will evolve. The percentage of helium evolution upon de-saturation can be described by the following correlation (Reference 1):

$$\%He_{MMH}(P) = -0.518\left(\frac{P-101}{6.895}\right) + 128.87$$

$$\%He_{NTO}(P) = -0.474\left(\frac{P-101}{6.895}\right) + 118.47 \tag{5}$$

where

$\%He_{MMH}(P)$ is percentage of helium evolved from helium saturated MMH at 1827 kPa to a given de-saturation pressure, %
$\%He_{NTO}(P)$ is percentage of helium evolved from helium saturated NTO at 1827 kPa to a given de-saturation pressure, %
P is the pressure, kPa (absolute)

The percentage of helium evolution increases with decreasing pressure. The percentage of helium evolution is similar for both MMH and NTO even though the relative absorption capability varies by 3 to 4 times. The propellants were initially saturated with helium at 1827 kPa.

Helium Evolution Upon Propellant Transfer

Now that the helium absorption and evolution in MMH and NTO are defined, the analysis of the helium evolution in the transfer line during propellant transfer is ready to proceed. Consider an element of propellant at a distance x from the supply tank as shown in Figure 7.

The local line pressure, P, is defined by Equation 1. This propellant element is initially saturated with a given amount of helium as defined by Equations 2 and 3. As it leaves the supply tank, it experiences a pressure drop, which causes it to release the excess helium. The percentage of helium evolution is defined by Equations 4 and 5. The amount of helium that comes out of solution can now be calculated based on Equations 2 through 5. For a given decrease in pressure, the amount of helium coming out of solution is:

$$G_{commidity} = Q_{commodity}(P)[\%He_{commodity}(P)] \tag{6}$$

Equation 6 states that, for a given elemental volume dV, the amount of helium that evolves from the propellant is a percentage of the total amount of helium saturated within that elemental volume at a given pressure.

Differentiating Equation 6 yields

$$dG_{commodity} = dQ_{commodity}(P)[\%He_{commodity}(P)] + Q_{commodity}(P)\frac{d[\%He_{commodity}(P)]}{dP}\frac{dP}{dx}dx \tag{7}$$

For a given volume of propellant, the total amount of helium saturated can be determined as follows:

$$Q_{commodity} = VHe_{commodity}(P)$$

$$dQ_{commodity} = He_{commodity}(P)dV + V\frac{dHe_{commodity}(P)}{dP}\frac{dP}{dx}dx$$

$$Q_{commodity} = \left(\frac{\pi D^2}{4}\right)\int_0^x\left[He_{commodity}(P) + \frac{dHe_{commodity}(P)}{dP}\frac{dP}{dx}x\right]dx$$

Hence, the total amount of helium evolved from an elemental volume of propellant during propellant transfer is

$$\text{For MMH, } dG_{MMH} = dQ_{MMH}(x)[\%He_{MMH}(P)] + Q_{MMH}(x)\frac{d[\%He_{MMH}(P)]}{dP}\frac{dP}{dx}dx \tag{7-1}$$

$$dG_{MMH} = \left(\frac{\pi D^2}{400}\right)\left(-0.518\left(\frac{P-101}{6.895}\right)+128.87\right)\left[\left(0.0006\left(\frac{P-101}{6.895}\right)-0.0323\right)+\frac{0.006}{6.895}\times\frac{dP}{dx}\right]dx +$$

$$\left(\frac{\pi D^2}{400}\right)\left(-\frac{0.518}{6.895}\frac{dP}{dx}\right)\left\{\int_0^x\left[\left(\frac{0.0006}{6.895}P - 0.0323\right)+\frac{0.0006}{6.895}\times\frac{dP}{dx}\right]dx\right\}dx$$

$$\text{For NTO, } dG_{NTO} = dQ_{NTO}(P)[\%He_{NTO}(P)] + Q_{NTO}(P)\frac{d[\%He_{NTO}(P)]}{dP}\frac{dP}{dx}dx \tag{7-2}$$

$$dG_{NTO} = \left(\frac{\pi D^2}{400}\right)\left(-0.474\left(\frac{P-101}{6.895}\right)+118.47\right)\left[\left(0.0022\left(\frac{P-101}{6.895}\right)-0.0863\right)+\frac{0.0022}{6.895}\times\frac{dP}{dx}\right]dx +$$

$$\left(\frac{\pi D^2}{400}\right)\left(-\frac{0.474}{6.895}\frac{dP}{dx}\right)\left\{\int_0^x\left[\left(0.0022\left(\frac{P-101}{6.895}\right)-0.0863\right)+\frac{0.0022}{6.895}\times\frac{dP}{dx}\right]dx\right\}dx$$

The total amount of helium evolved inside the propellant transfer line can now be calculated by integrating Equations 7-1 and 7-2 from x = 0 to x

$$G(x) = \int_0^x \frac{dG}{dx} dx \tag{8}$$

$$\text{For MMH, } G_{MMH}(x) = \int_0^x \frac{dG_{MMH}}{dx} dx \tag{8-1}$$

$$G_{MMH}(x) = \left(\frac{\pi D^2}{400}\right)\int_0^x \left(-0.518\left(\frac{P-101}{6.895}\right)+128.87\right)\left[\left(0.0006\left(\frac{P-101}{6.895}\right)-0.0323\right)+\frac{0.0006}{6.895}\,x\,\frac{dP}{dx}\right]dx +$$

$$\left(\frac{\pi D^2}{400}\right)\int_0^x \left(-\frac{0.518}{6.895}\frac{dP}{dx}\right)\left\{\int_0^x \left[\left(0.0006\left(\frac{P-101}{6.895}\right)-0.0323\right)+\frac{0.0006}{6.895}\,x\,\frac{dP}{dx}\right]dx\right\}dx$$

Figure 6 shows that the helium evolution from MMH increases with increasing flow rate. The pressure drop increases with increasing flow rate. Thus, the higher the flow rate, the higher the helium evolution. However, it should be noted that these results are based on STP conditions. The maximum amount of helium evolution at 11.3 lpm is approximately 100 cc at STP. The total amount of helium saturated in MMH at 1827 kPa in the transfer line is approximately 1134 cc at STP. Thus, the percentage of helium evolved inside the transfer line is approximately 8.8%.

Similarly,

$$\text{For NTO, } G_{NTO}(x) = \int_0^x \frac{dHe_{NTO}}{dx} dx \tag{8-2}$$

$$G_{NTO}(x) = \left(\frac{\pi D^2}{400}\right)\int_0^x \left(-0.474\left(\frac{P-101}{6.895}\right)+118.47\right)\left[\left(0.0022\left(\frac{P-101}{6.895}\right)-0.0863\right)+\frac{0.0022}{6.895}\,x\,\frac{dP}{dx}\right]dx +$$

$$\left(\frac{\pi D^2}{400}\right)\int_0^x \left(-\frac{0.474}{6.895}\frac{dP}{dx}\right)\left\{\int_0^x \left[\left(0.0022\left(\frac{P-101}{6.895}\right)-0.0863\right)+\frac{0.0022}{6.895}\,x\,\frac{dP}{dx}\right]dx\right\}dx$$

Figure 7 shows that the helium evolution increases with increasing transfer rate. However, the amount of helium evolution from NTO is approximately 3 to 4 times larger than that for MMH. This result is consistent with the absorption ratio between NTO and MMH. The maximum amount of helium evolution at 11.3 lpm is approximately 550 cc at STP. The total amount of helium saturated in NTO at 1827 kPa in the transfer line is approximately 3582 cc at STP. Thus, the percentage of helium evolved inside the transfer line is approximately 15.3%. Since the calculation was based on STP conditions, the volumetric amount of helium evolution will be much smaller at the actual line pressure.

Volume Fraction of Helium to Propellant Upon Propellant Transfer

It is pertinent at this time to correlate the volume fraction of the helium evolution at the local line pressure condition to gain a better perspective of the relative size of helium volume.

The volume fraction of helium to propellant is defined as the ratio of the volume of the helium evolved at line pressure to that of the line (or propellant) volume from the supply tank to x.

The line volume is $V(x) = V_{prop}(x) + V_{helium}(x)$ at pressure. Since $V_{prop}(x) >> V_{helium}(x)$, the line volume can be approximated as $V(x) \approx V_{prop}(x)$.

$$\text{For MMH, } R_{MMH}(x) = \left(\frac{1}{V}\right)\left(\frac{101}{P}\right)G_{MMH}(x) \tag{8-3}$$

$$R_{MMH}(x) = \left(\frac{1}{100}\right)\left(\frac{101}{P}\right)\left(\frac{1}{x}\right)\int_0^x\left(-0.518\left(\frac{P-101}{6.895}\right)+128.87\right)\left[\left(0.0006\left(\frac{P-101}{6.895}\right)-0.0323\right)+\frac{0.0006}{6.895}\,x\,\frac{dP}{dx}\right]dx +$$

$$\left(\frac{1}{100}\right)\left(\frac{101}{P}\right)\left(\frac{1}{x}\right)\int_0^x\left(-\frac{0.518}{6.895}\frac{dP}{dx}\right)\left\{\int_0^x\left[\left(0.0006\left(\frac{P-101}{6.895}\right)-0.0323\right)+\frac{0.0006}{6.895}\,x\,\frac{dP}{dx}\right]dx\right\}dx$$

Figure 8 shows the volume fraction of helium to MMH in the transfer line. The volume fraction of the helium gas evolution is approximately 0.1% of the line volume at 11.3 lpm. That is, for every cubic inch of the transfer line, there is a 1/1000 $in.^3$ of the helium gas. The total transfer line volume is approximately 7722 cc. The total volume of the helium gas evolution at line pressure is approximately 8.19 cc. This is equivalent to approximately 0.5 $in.^3$.

$$R_{NTO}(x) = \left(\frac{1}{V}\right)\left(\frac{101}{P}\right)G_{NTO}(x) \tag{8-4}$$

$$R_{NTO}(x) = \left(\frac{1}{100}\right)\left(\frac{101}{P}\right)\left(\frac{1}{x}\right)\int_0^x\left(-0.474\left(\frac{P-101}{6.895}\right)+118.47\right)\left[\left(0.0022\left(\frac{P-101}{6.895}\right)-0.0863\right)+\frac{0.0022}{6.895}\,x\,\frac{dP}{dx}\right]dx +$$

$$\left(\frac{1}{100}\right)\left(\frac{101}{P}\right)\left(\frac{1}{x}\right)\int_0^x\left(-\frac{0.474}{6.895}\frac{dP}{dx}\right)\left\{\int_0^x\left[\left(0.0022\left(\frac{P-101}{6.895}\right)-0.0863\right)+\frac{0.0022}{6.895}\,x\,\frac{dP}{dx}\right]dx\right\}dx$$

Figure 9 shows the volume fraction of helium to NTO in the transfer line. The volume fraction of helium is approximately 0.6% of the line volume at 11.3 lpm. That is, for every cubic inch of the transfer line, there is a 6/1000 $in.^3$ of the helium gas. For a line volume of 7722 cc, the total volume of the helium gas evolution at line pressure is approximately 45.88 cc. This is equivalent to approximately 2.8 $in.^3$.

The "homogeneous" model (Reference 5), also known as the "fog flow" model, is used to predict the effect of helium evolution on the overall pressure drop. The pressure drop due to helium evolution can be approximated by multiplying the volume fraction of gas to liquid to the frictional pressure drop. Since the volume fraction of evolved helium gas to the propellant liquid is small, the effect of helium evolution on the overall pressure drop is insignificant.

Steady-State Timeline of Helium Absorption and Evolution

As mentioned earlier, helium evolution is a dynamic process. However, concern about helium evolution during propellant transfer does not require a full understanding of the kinetic process. Furthermore, there is a lack of test data on the kinetic of helium evolution to address this concern. Therefore, the following approach was applied, which was driven by the availability of data on (1) steady-state helium absorption and evolution, and (2) steady-state timeline of helium absorption and evolution.

Boeing Reusable Space Systems[4] has conducted some preliminary de-saturation tests with helium-saturated MMH and NTO to determine the timeline of helium absorption and evolution. The test was conducted using a Hoke bottle, which was filled with MMH or NTO. The MMH or NTO was subsequently pressurized with helium gas over an extended period of time to obtain a helium-saturated propellant condition. The saturated condition was verified by either bubble point pressure or by an indication of ullage pressure drop. Reference 1 discusses the methodology of

[4] *Boeing Reusable Space Systems, 5301 Bolsa Ave., Huntington Beach, CA 92647-2099.*

bubble point pressure. The pressure drop occurs when the helium is absorbed into the solution that causes the ullage pressure to decrease. Once the saturated condition was established, the ullage gas was vented to approximately ambient pressure and the Hoke bottle was completely closed. With the new lower pressure, the helium in the solution was oversaturated and came out of solution to reestablish a new helium-saturated condition. The steady-state timeline of helium absorption and evolution is shown in Table 1. Reference 4 discusses helium absorption rate for both MMH and NTO.

Although the test de-saturation pressure is much lower than the anticipated de-saturation pressure during propellant transfer, the result suggests that the rate of helium evolution is much faster than the rate of absorption.

CONCLUSIONS

For a 6096-cm propellant transfer line, the volumes of helium evolution from helium-saturated MMH and NTO are approximately 8.19 cc and 45.88 cc, respectively. These helium volumes are distributed over the length of the line. Consequently, the impact of helium evolution on the flowmeter, on the ability to purge, and on creating turbulence in the flow is insignificant. However, it is recommended that the flowmeter be placed as close to the supply tank as practical.

The steady-state time evolution is significantly faster than that of the absorption. The steady-state evolution times for MMH and NTO are approximately 1 and 10 min, respectively. This suggests that the complete helium evolution occurs within the timeline of the propellant transfer. In addition, once the helium gas is evolved from the propellant, it will remain unsaturated from the propellant long after the transfer is complete.

REFERENCES

1. I. D. Smith, "The Determination of the Helium Saturation Level of Monomethylhydrazine and MON-3 Nitrogen Tetroxide", Lyndon B. Johnson Space Center White Sands Test Facility, Document No. TR-244-001, 1979.

2. Reynolds, W. C., and Satterlee, H. M., "Liquid Propellant Behavior at Low and Zero g" in The Dynamic Behavior of Liquids in Moving Containers with Applications to Space Vehicle Technology, Ed. H. N. Abramson, NASA Report SP-106, NASA, Scientific and Technical Information Division, Washington, DC, 1966.

3. Marsh, W. R., and Knox, B. P., "USAF Propellant Handbooks: Hydrazine Fuels," Vol. 1, Defense Technical Information Center, Cameron Station, Alexandria, VA, 1970.

4. K. Coolidge, "Helium Solubility Rates in NTO and MMH", Report No. 287-201-81-086, Rockwell International, 1981.

5. John Collier, "Convective Boiling and Condensation," second edition, McGraw-Hill Book Company, 1981.

Table 1. Steady-State Timeline of Helium Absorption and Evolution

Propellant	Amount (gram)	Beginning Pressure (kPa)	De-saturation Pressure (kPa)	Absorption Time (day)	Evolution Time (min)
NTO	95	1482	101	22	~10
MMH	59.5	1482	101	24	<1

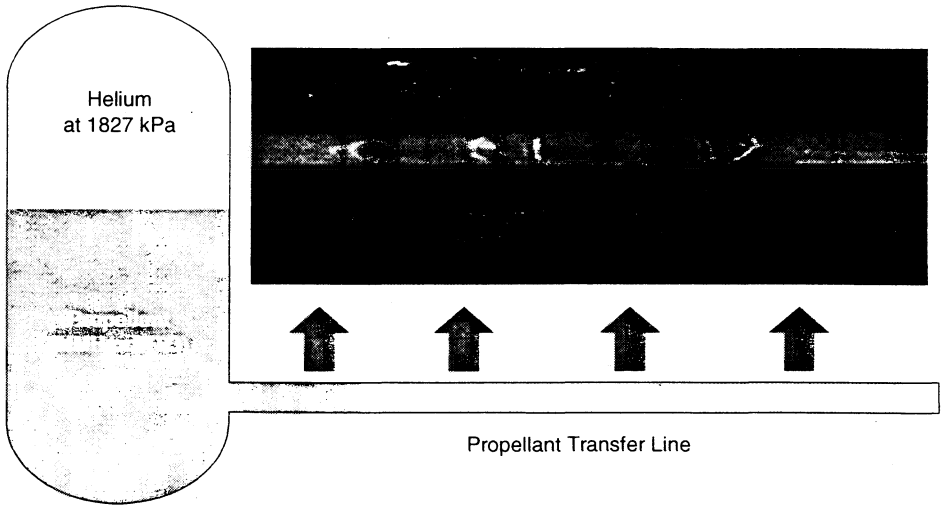

Figure 1. Process of Helium Evolution in the Transfer Line

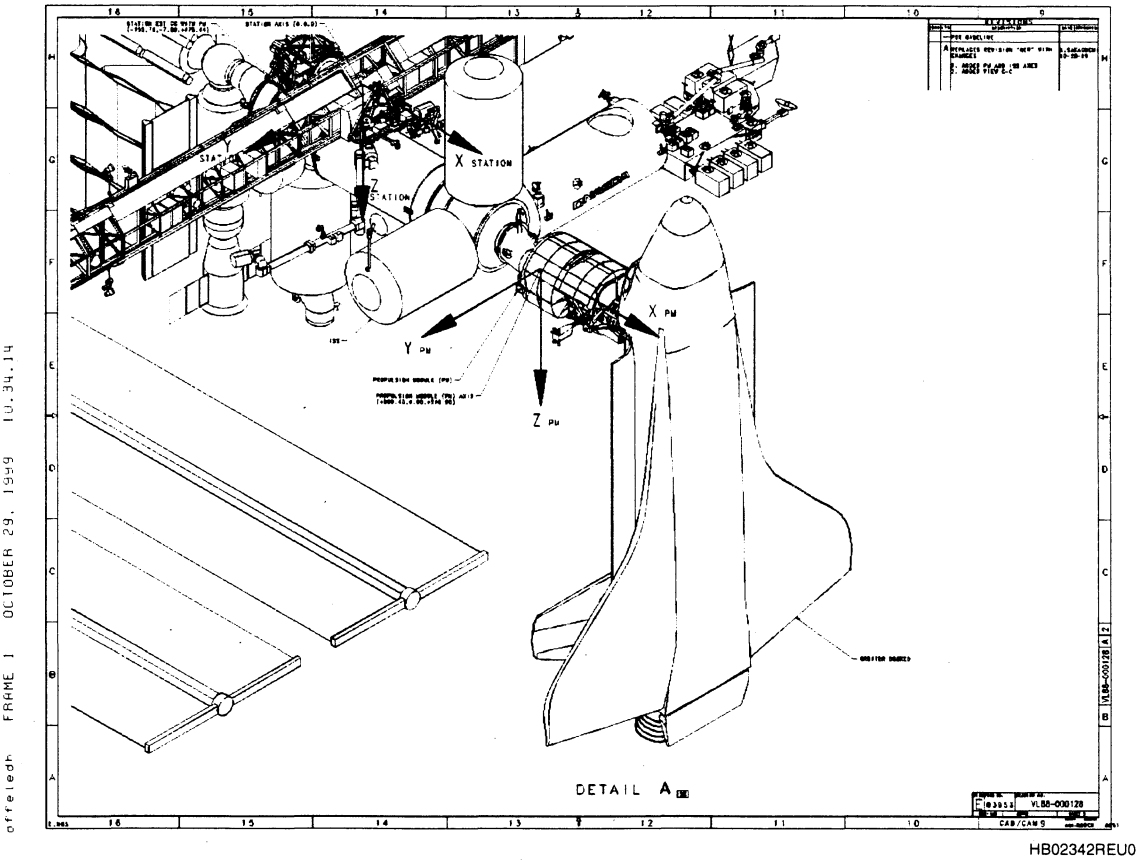

Figure 2. Orbiter Docking with the ISS

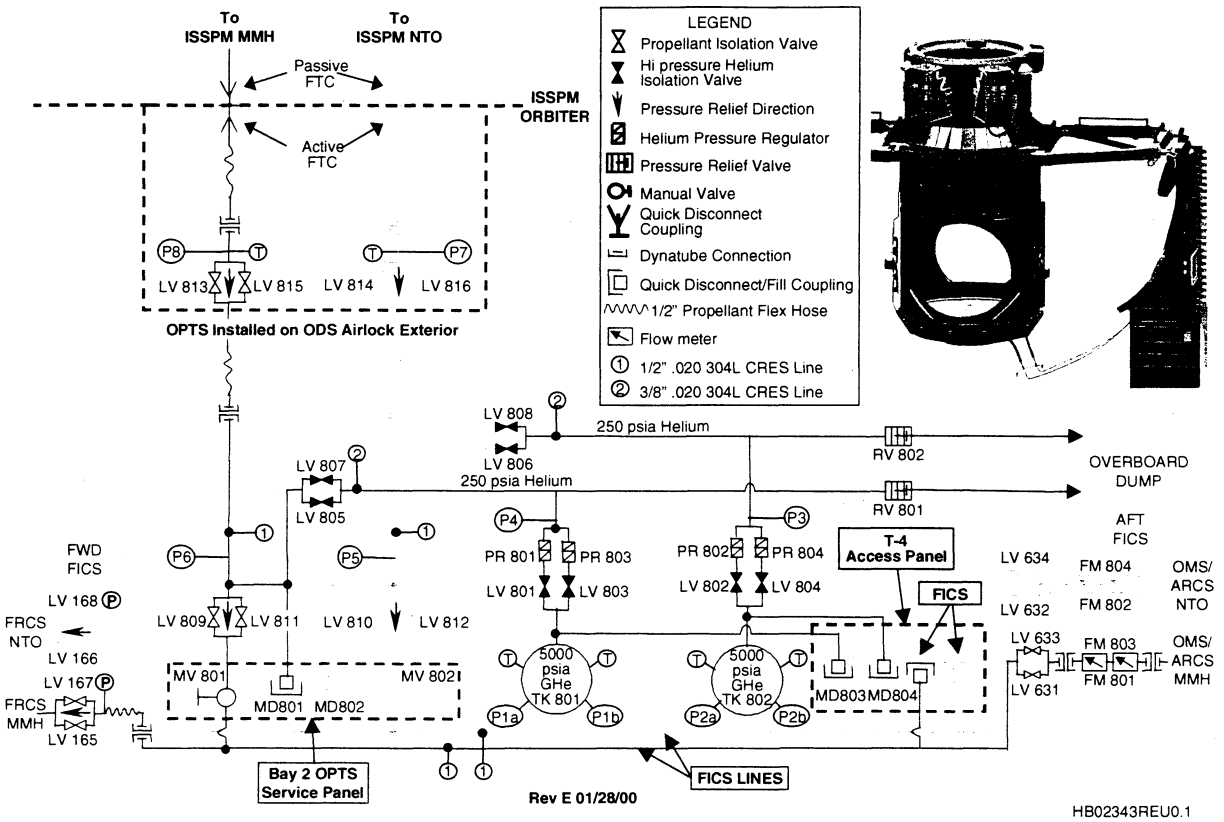

Figure 3. FICS and OPTS Fluid Transfer Line

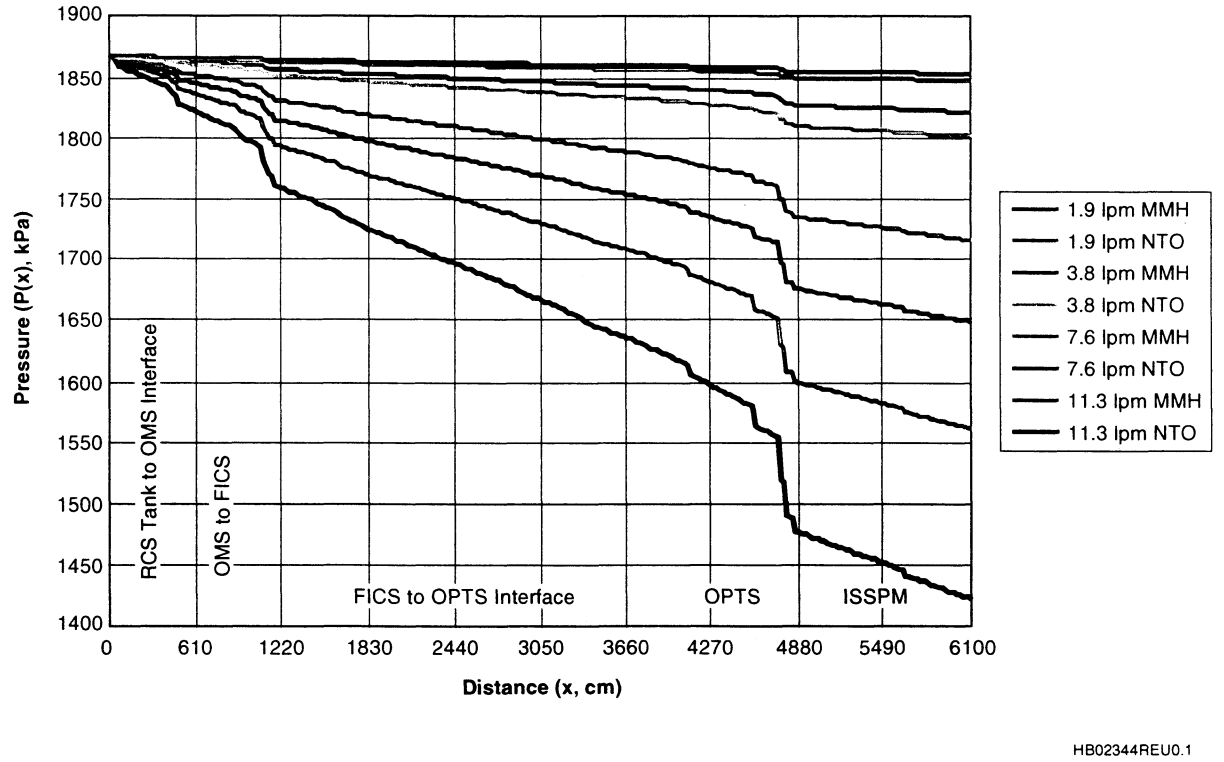

Figure 4. Pressure Profile Along the Transfer Line

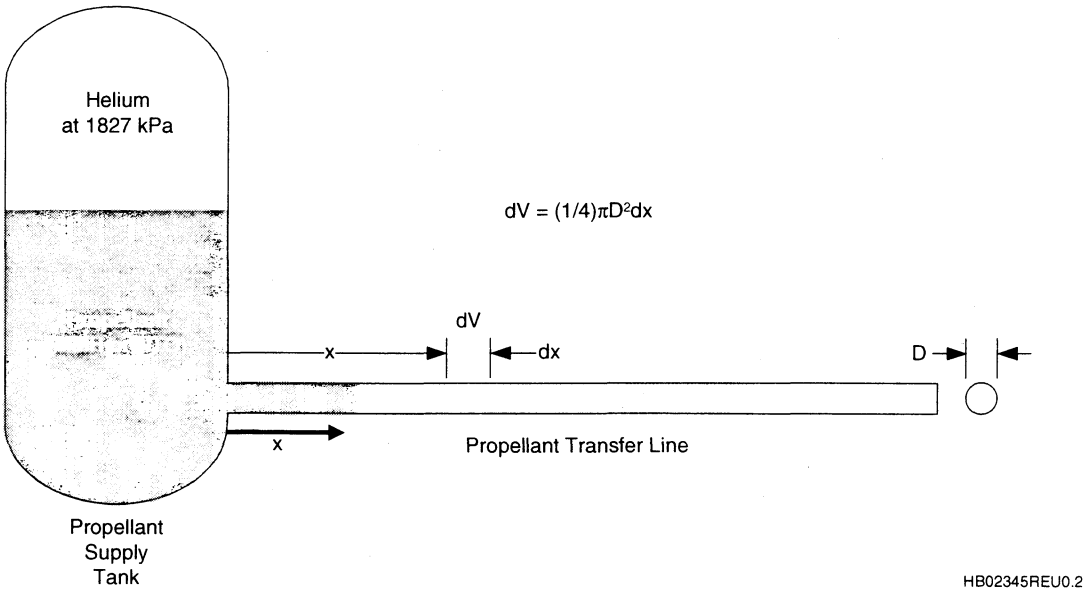

Figure 5. An Element of Propellant

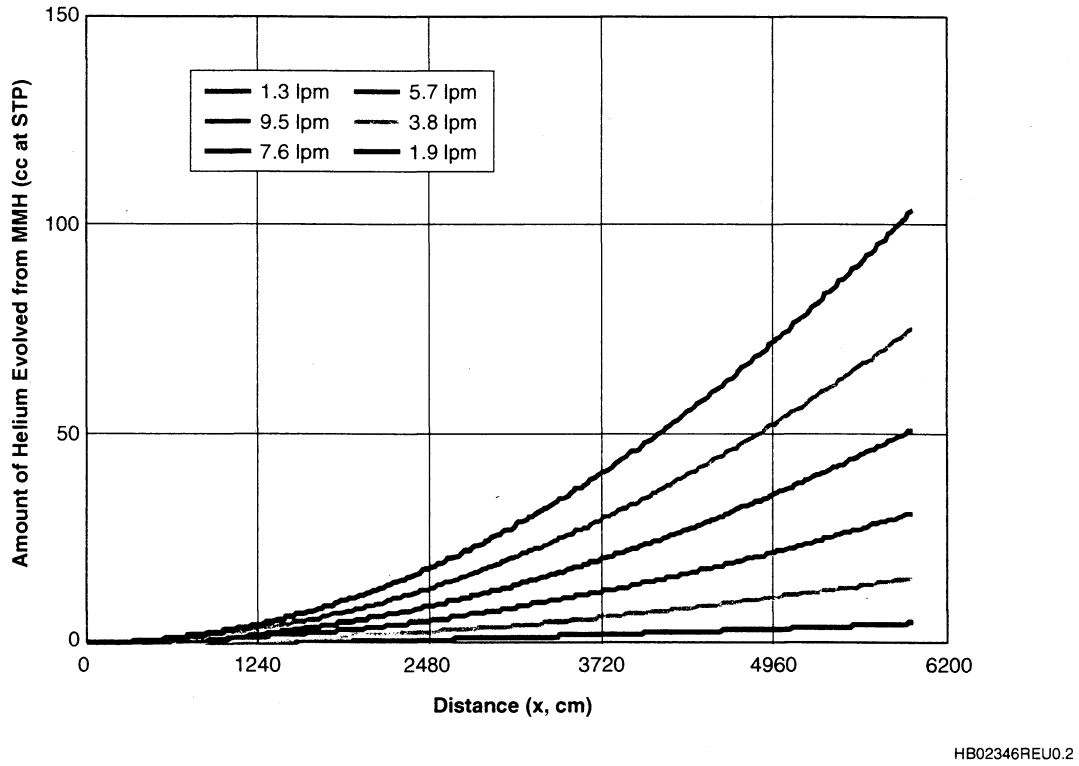

Figure 6. Amount of Helium Evolved from MMH During Propellant Transfer for Various Flow Rates (1.9 to 11.3 lpm)

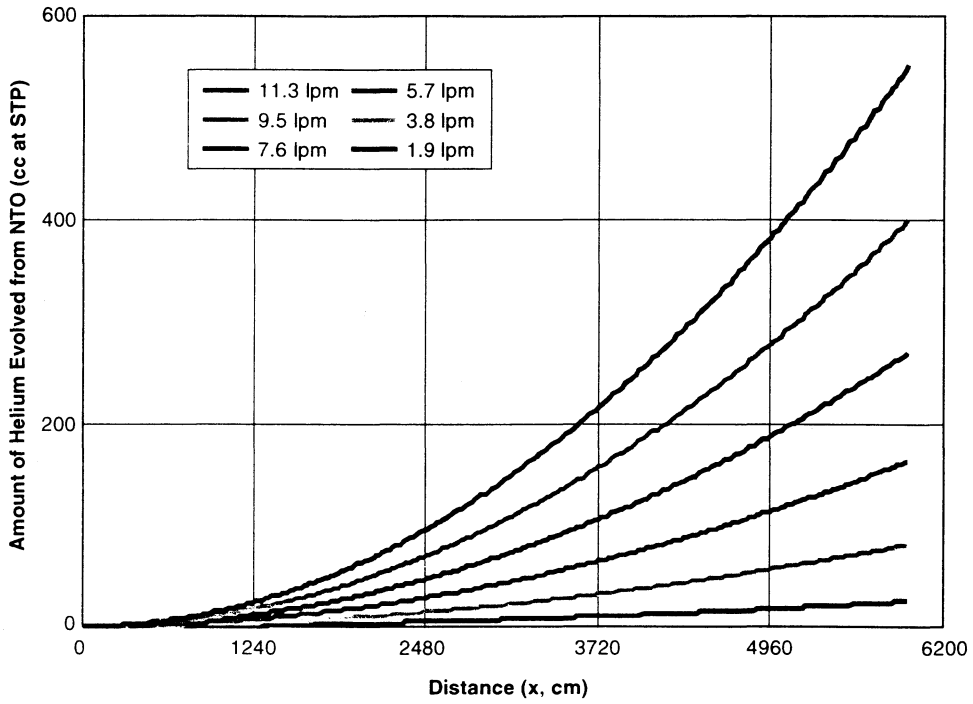

HB02347REU0.2

Figure 7. Amount of Helium Evolved from NTO During Propellant Transfer for Various Flow Rates (1.9 to 11.3 lpm)

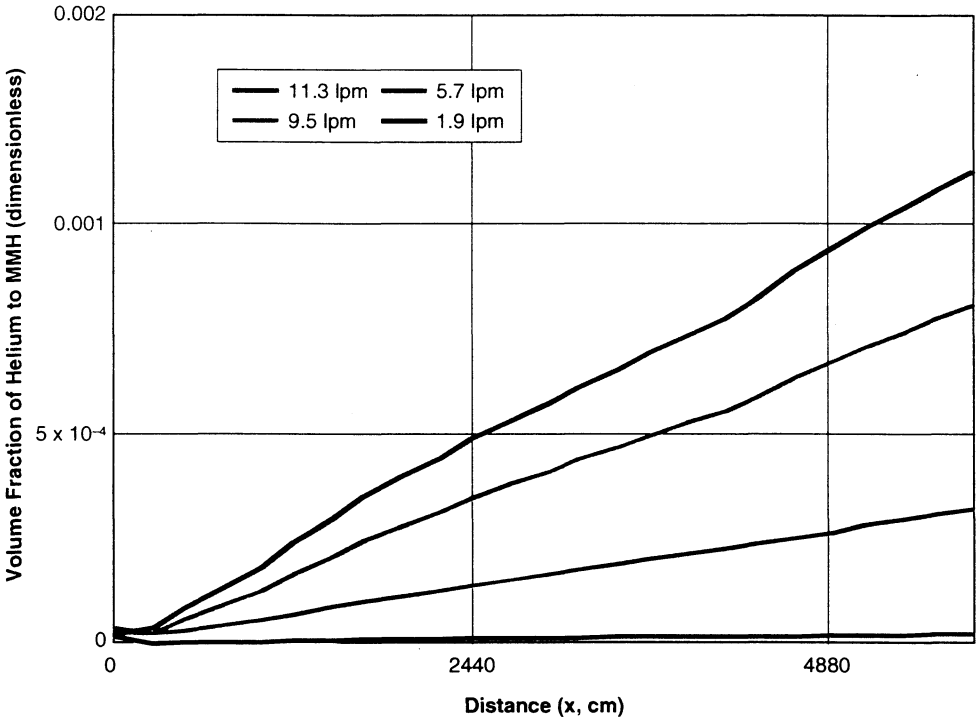

HB02348REU0.1

Figure 8. Volume Fraction of Helium to MMH During Propellant Transfer for Various Flow Rates (1.9 to 11.3 lpm)

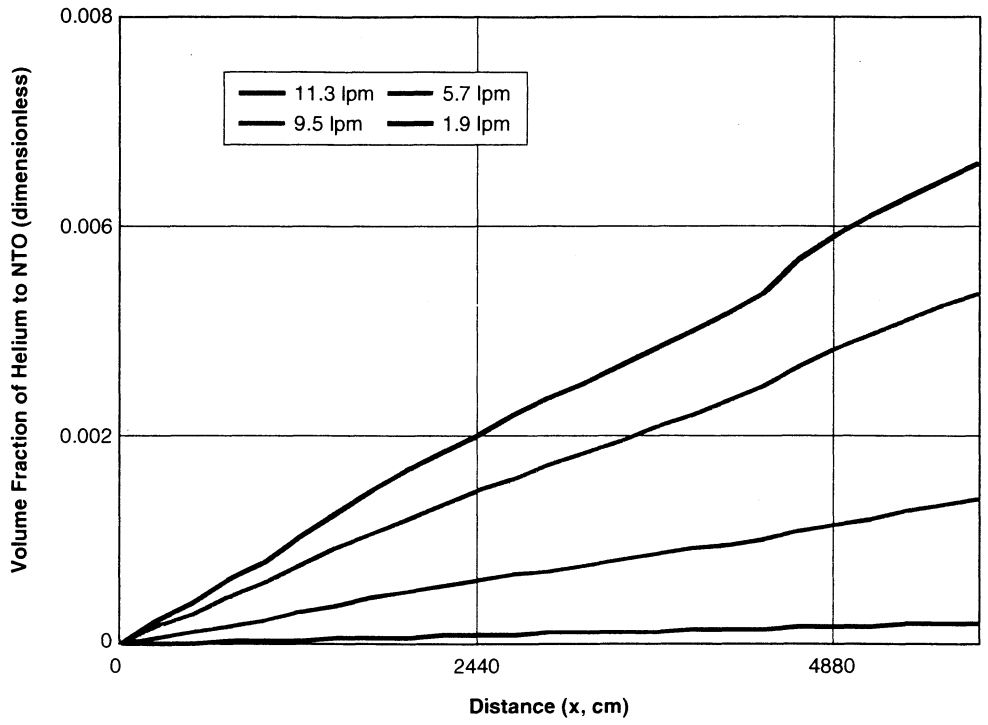

Figure 9. Volume Fraction of Helium to NTO During Propellant Transfer for Various Flow Rates (1.9 to 11.3 lpm)

Investigation on the Stability of the Flux Uniformity of the 6m Solar Simulator at ESTEC

Peter W. Brinkmann, European Space Agency
Christian Henjes, Industrieanlagen Betriebsgesellschaft mbH
Wolfgang Teichert, ATOS Netherlands

ABSTRACT

Traditionally, user programmes requested the verification of the solar intensity distribution before and after each thermal balance test in a space simulation chamber. In view of the associated cost, ESA has analysed all available results of the measured intensity distribution data of its Large Space Simulator (LSS) from 1986 until 1998, in order to provide evidence that the measurement intervals can be increased substantially.

The paper will briefly introduce the design concept of the sun simulator and the solar intensity mapping equipment. It will then describe the data collection and formatting methods applied and present the data evaluation on the basis of statistical models. The study concluded that mapping intervals in the order of a year are acceptable without undue risk for the programmes tested in the LSS within the mapping interval.

Introduction

Description of the Sun Simulator

The ESTEC solar simulator is based on an "Off-Axis Collimator System" as illustrated in Figure 1. The radiation produced by several lamps is collected by the projection optics in the **focal point** of a **collimator mirror**. The light is then projected onto the collimator mirror, which reflects a nearly parallel light beam into the **test volume**. Due to an appropriate **off-axis distance,** the optics at the focal point will not protrude into the radiation path from the collimator mirror to the test volume. This provides a shadow-free test zone.

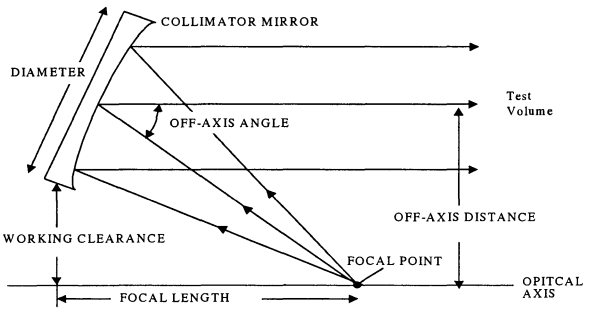

Figure 1: Off-Axis Collimator Schematic

The sun simulator (SUSI) referred to here is a subsystem of the Large Space Simulator (LSS) at ESA/ESTEC. The main beam characteristics are illustrated in Figure 2. The SUSI provides a parallel solar beam of 6 m diameter with a highly uniform intensity pattern in the test volume of the space simulator. The solar beam is parallel to the horizontal axis of the chamber.

The collector mirrors inside the lamp-modules project the radiation of the light sources (high-power xenon lamps) onto the field lens array of the projection optics, consisting of an integrator with 55 field and 55 projection lenses.

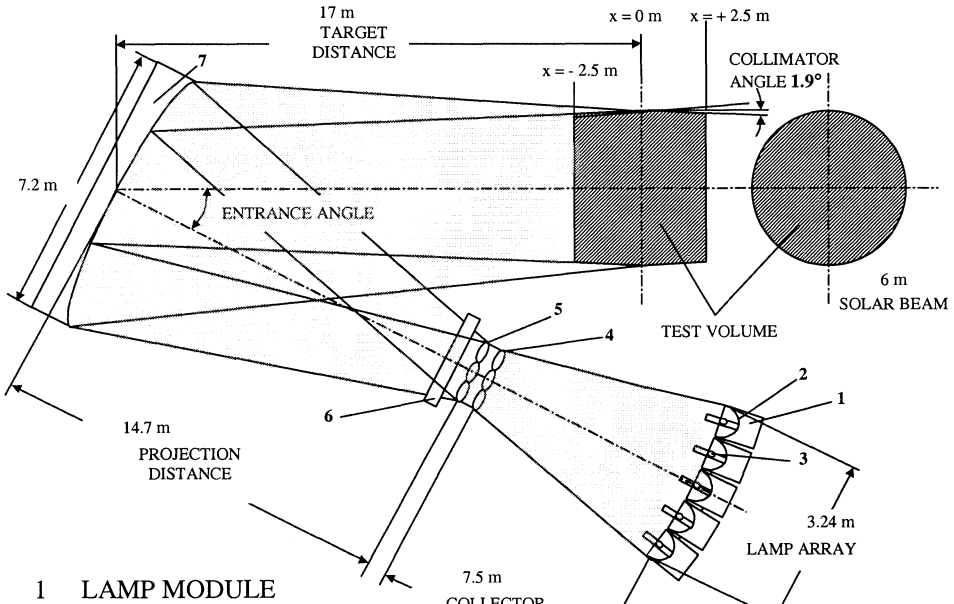

Figure 2: Main Beam Characteristics

Via the collimator mirror each projection lens forms an image of the corresponding field lens across the total target plane in the test volume. This means that each of the 55 radiation channels illuminates the total 6 m diameter plane (x=0) in the test volume. Superimposing the flux patterns of the 55 field lenses guarantees high flux uniformity in the test volume. An important requirement for achieving a good reproducibility of the intensity distribution in the test volume is a symmetrical light distribution at the field lens array of the integrator. A dedicated alignment bench permits a fast and reproducible adjustment of symmetric intensity patterns at the field lens plane. Figure 3 shows typical distribution patterns measured in the alignment bench before mounting the lamp modules to the lamp house.

The collimator mirror consists of 121 segments; each of them has been aligned correctly after mounting

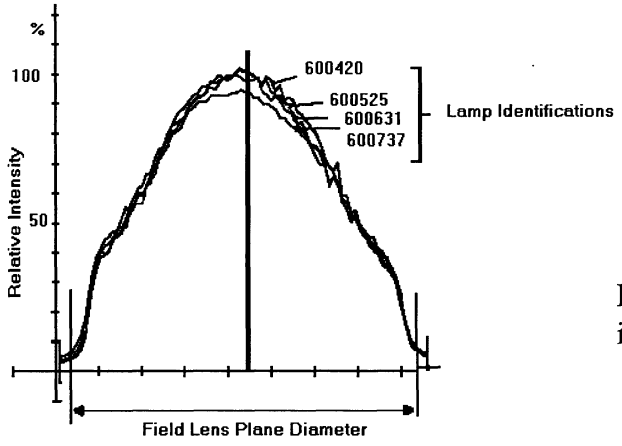

Figure 3: Intensity Distribution in the Field lens Plane

the mirror in the chamber. Mirror segments and support structure are temperature controlled using gaseous nitrogen. During its operational life it is possible to check the alignment of individual segments visually as demonstrated in Figure 4. When looking at the reflected image of the mirror even slight misalignments are easily identifiable. If one segment is not adequately aligned it will also be noticeable in the intensity distribution diagram.

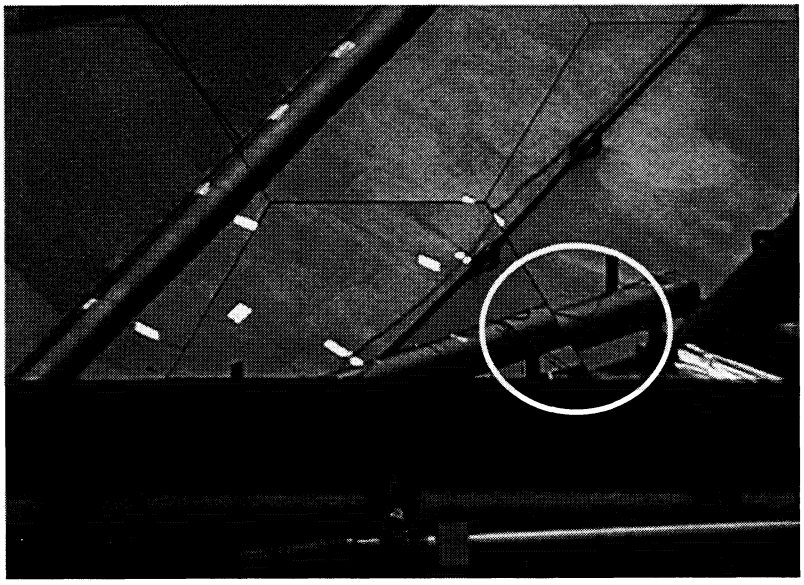

Figure 4: Visual Check of Mirror Segment Alignment

The subsequent list shows some characteristic data from the SUSI specification:

- Flux uniformity in reference plane ± 4 % (measured with a 2 x 2 cm solar cell)
- Flux uniformity in test volume ± 4 % (measured with a 2 x 2 cm solar cell)
- Nr. of lamp modules 19 (high-pressure Xenon arc)
- Lamp power rating 20 or 25 or 35 kW per lamp
- Nr. of lamps for 1 Solar constant 12 operating at approximately 20 kW

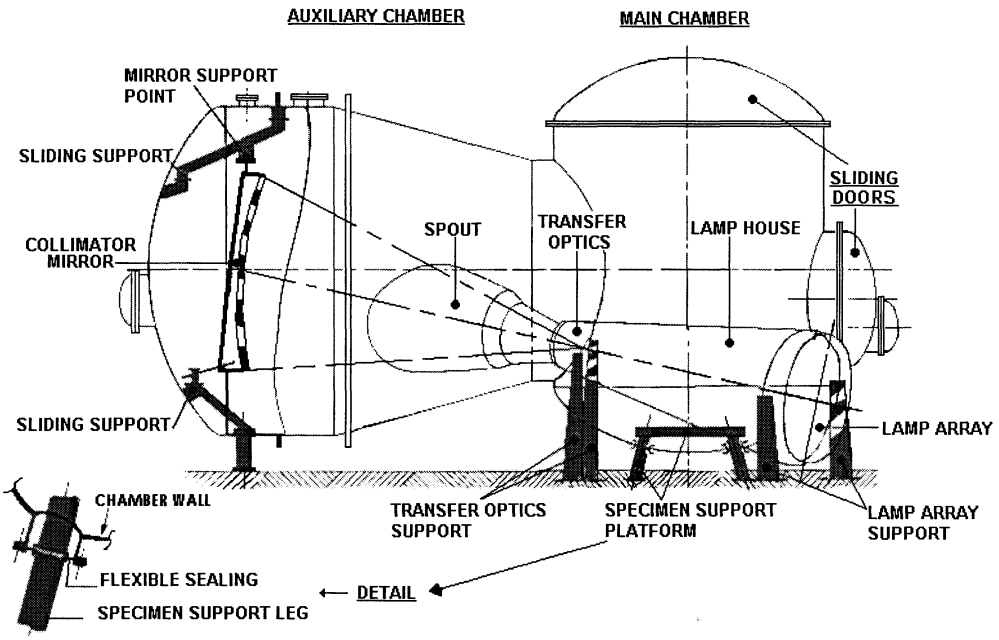

Figure 5: Optics Suspension Concept

Design Aspects for Solar Beam Stability

Stability and reproducibility of the solar radiation in the reference volume are essential performance parameters of a solar simulation facility. This includes the reproducibility of the intensity pattern during test as compared with the pattern verified during the pre-test calibration. Deficiencies in the local intensity distribution, and mismatches of the spectral distribution are less critical and can be taken into account relatively easily, as long as these effects are known and do not vary with time. The stability requirements have therefore driven layout and design of the LSS.

a) Support of optical elements and test article

The test specimen is fixed to the ground via a special support structure. This structure is mechanically isolated from the vacuum chamber by means of bellows, which prevent the transfer of mechanical loads from the vacuum vessel or the building structure to the test article.

Similarly, the lamp array and transfer optics are decoupled from the chamber and fixed to the ground, thus ensuring that test article and radiation source will maintain their relative positions independently of chamber deformations or vibrations (e.g. during pump-down). The chamber window and the collimator mirror are the only optical elements that are physically connected to

the vacuum vessel.
Movements of the window are not critical in the optical path. Nevertheless, the design of the interface structure limits axial and lateral displacements of the window during a load cycle to less than 1 mm.
The collimator mirror is at the bottom linked to the ground based chamber saddle. The top is suspended from a special bridge structure between the rear stiffener ring of the "Auxiliary Chamber" and the end-dome. A sliding support eliminates the influence of end-dome deformations during the load cycle. The displacement of the mirror support point during a pressure cycle is less than 1 mm. The suspension concept of specimen and optics is illustrated in Figure 5.

b) **Temperature control of collimator mirror**
On the one hand the stability of the collimated beam requires proper supports of the optical elements, but on the other hand it is also dependent on a stable shape of the mirror surface. The temperatures of both the mirror support structure and the mirror segments themselves are actively controlled by a GN_2 system. In calibration as well as in solar simulation mode, the temperature levels can be maintained at ambient temperature within a tolerance of ± 2 degrees C. Deformation of support structure and/or mirror elements is negligible under these conditions.

The Solar Beam Intensity Mapping System

The solar beam intensity in the test volume is scanned with the Large Intensity Scanning System (LISS) in rectangular co-ordinates (y, z). The LISS is a 6.2 m × 6.2 m stainless steel frame, which carries a temperature-controlled solar sensor (solar cell dimensions 20 mm × 20 mm). The sensor displacement in both axes is performed by means of two motors equipped with pulse encoders which deliver one pulse every 5 mm. Sensor movement and positioning, as well as the data acquisition are computer controlled. Measurements are taken in steps of 50 mm in the y and z directions. A full mapping consists of a matrix of 125 × 125 (i.e. 15625) measurements. The resolution of the measurement of each position is 5 mm. The mapping system is illustrated in Figure 6. The measurements are used to verify system performance. Apart from one collimator mirror alignment in 1993, no adaptations have been required to maintain the beam quality.
The mapping data were until 1997 handled by a HP 9826 computer using BASIC HP AP 2.0 software extended with AP 2.1 and GRAPH 2.1 (data storage, calculation of averages and flux distribution data in percent, etc.). The data were recorded on a 5 ¼ " disk, and the values were stored in mV. The format was a HP BINARY code. Two typical mapping data patterns are shown in Figures 7 and 8.

Mapping Data

For this investigation 20 mapping matrices measured in the period from 1986 to 1998 have been analysed. The mappings were made with different intensities, and with different numbers of lamps, ranging from 5 to 15.

The data were recorded with the HP 9826, which is not compatible with present PC standards. In order to analyse the data with a PC the following steps therefore had to be taken:

a) conversion of data to HP ASCII code;
b) conversion of data from the HP ASCII code to a UNIX ASCII code on a UNIX computer;
c) conversion of data to a DOS ASCII format on a UNIX computer

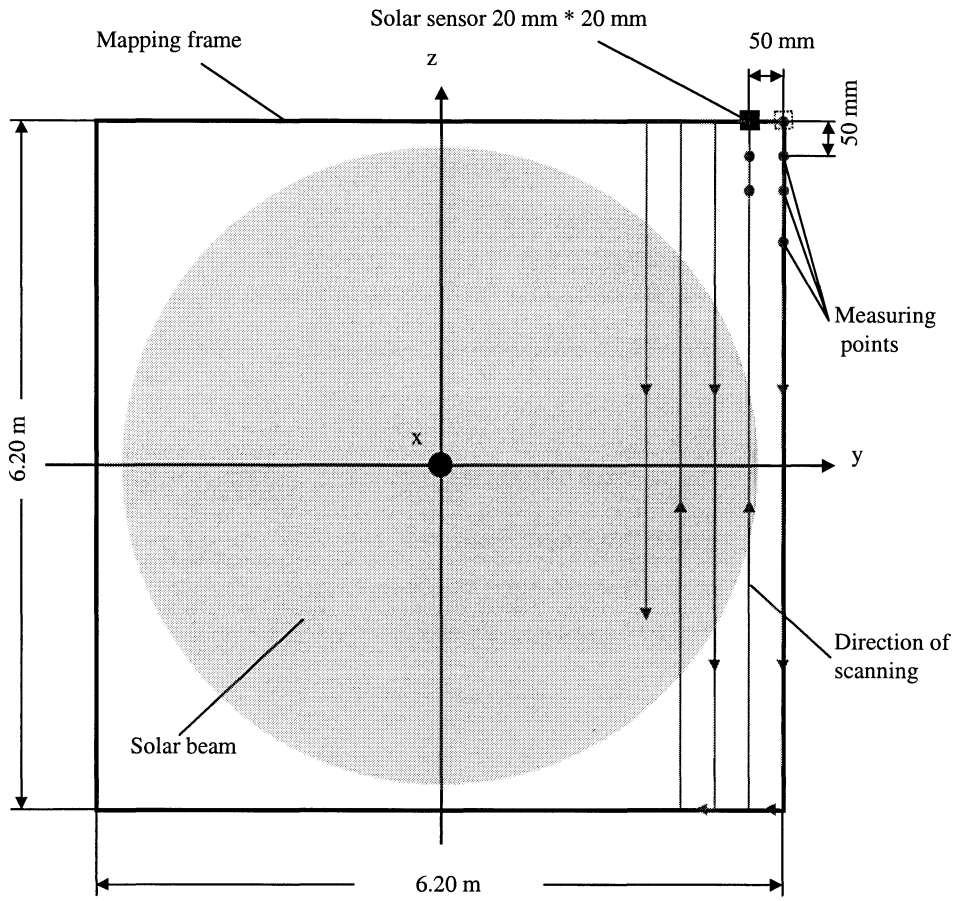

Figure 6: Schematic of the intensity mapping system

It was then possible to read and process the data via EXCEL and Matlab or other modern software.
For analysing the intensity distribution patterns, it was important to identify the centre of the beam as reference in each of the recorded data sets. The centre of the beam was evaluated by applying best-fit analysis. The resolution of the centre point matrix is 50 mm (see Figure 9).
The areas shadowed by the intensity control sensors of the LSS (illustrated in Figure 9) were discarded in the evaluation.

Evaluation of the Long Term Stability

All mapping matrices have been compared by analysing the following parameters:

- Number of points outside the nominal range (i.e. 96% – 104%).
- Standard deviation of points within the nominal range.
- Beam diameter.
- Beam centre location.

In performing the analysis the specific characteristics of the solar beam have been taken into account. Intentionally the intensity drops very rapidly at the beam edge at a radius of 3 m (see Figure 10).

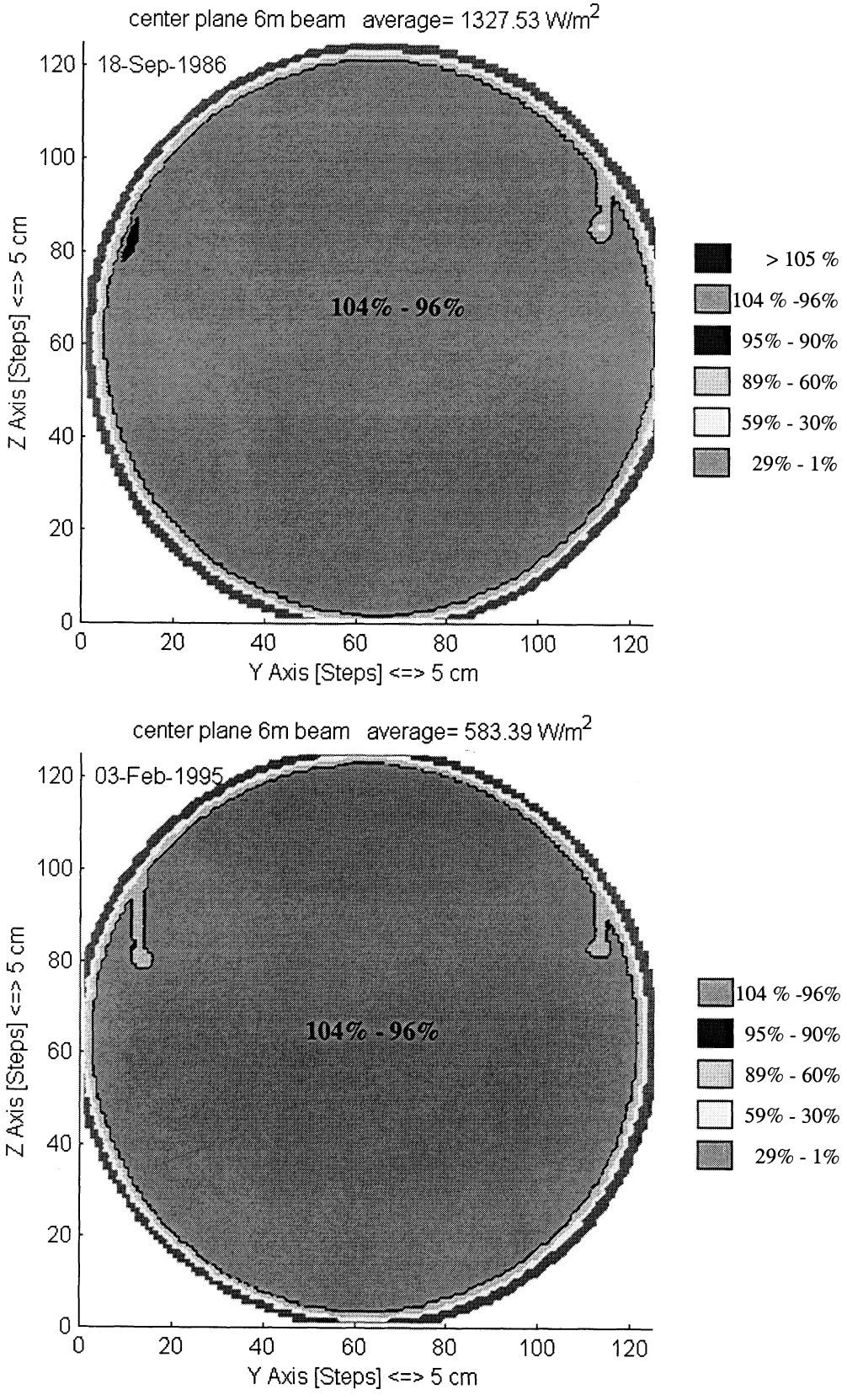

Figures 7 and 8: Typical Intensity Distribution Patterns

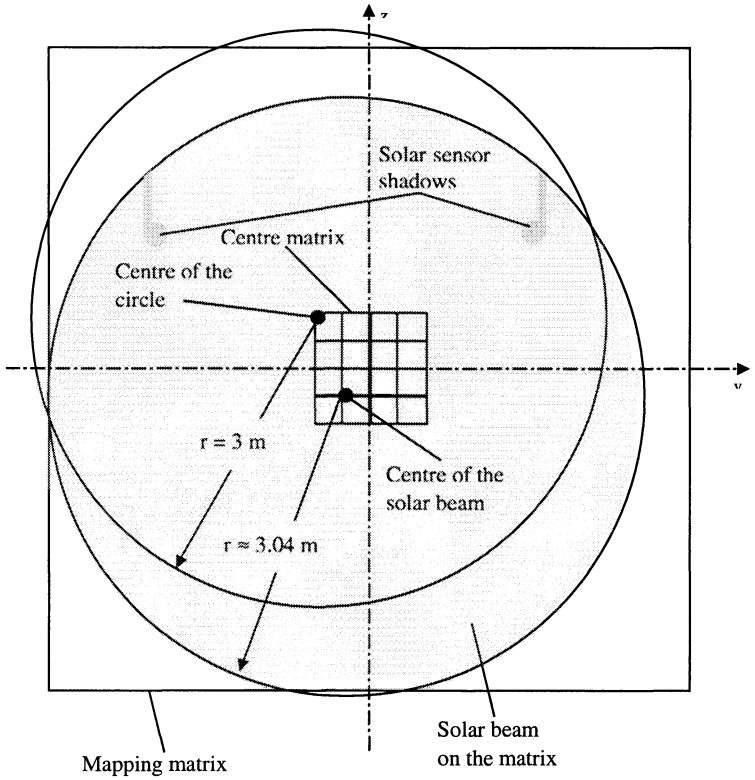

Figure 9: Beam Centre Definition

Consequently, even small tolerances in beam centre calculations and in the positioning of the measuring sensor (e.g. mounting tolerances of the Mapping System and reproducibility of sensor drive) can lead to large differences in the measured intensity from one test to another at the beam perimeter. Scanning positions even slightly beyond the nominal radius will immediately deliver data with low intensities. Therefore the probability distribution will include points well below the nominal range (i.e. 96%), while it will contain only a few points marginally above the nominal range (i.e. 104%).

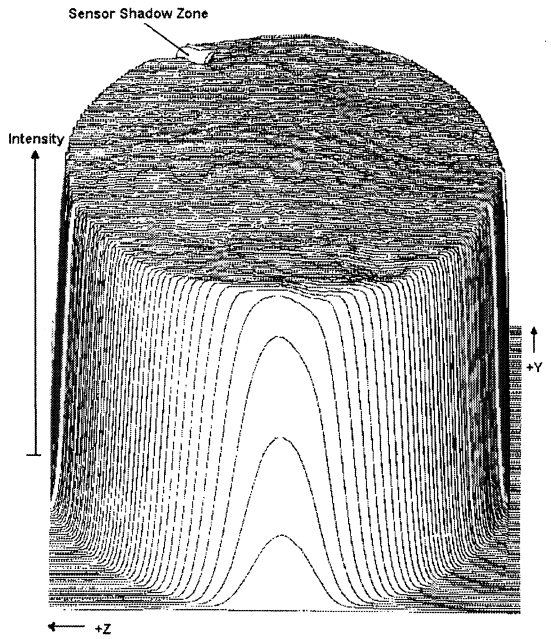

Figure 10: 3–D Illustration of Intensity Distribution

Points Outside the Nominal Range

The only quantity that has a direct link to the sun simulator requirement is the number of points outside the range from 96 % to 104 % average intensity. The results are shown in Figure 11. The number of points with intensities below 96 % is consistently around 1.5 % and shows no significant changes with time. Taking into consideration the strong impact of the sharp intensity drop at the beam perimeter (see discussion above) the data provide confidence in good reproducibility of the beam geometry over the total time period. The data also show that the beam has been practically free of "hot spots"(>104%) during the entire period from 1986 to 1998.

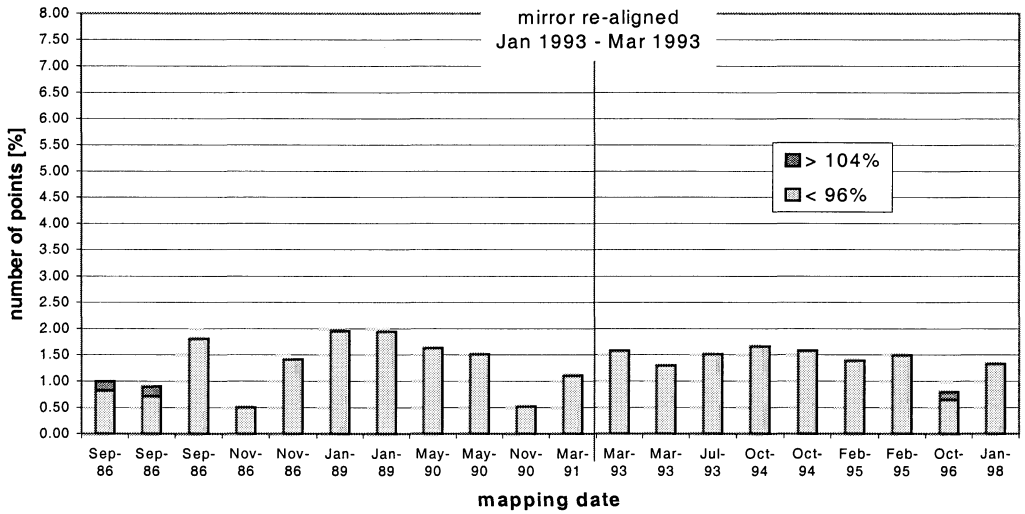

Figure 11: Number of Points out of Nominal Range

Beam Uniformity

The standard deviation of the data points inside the nominal range is taken as a measure for the beam uniformity. In the case of a uniform distribution (i.e. all values between 96 % and 104 % are equally likely), the value would be 2 %. A zero standard deviation would be obtained if all flux values were exactly 100 %.
Figure 12 shows all mapping results from 1986 to 1998.
Two physical features are visible:

1. The lowest values are identified during the mappings after the first mirror realignment in 1986 and during the first mapping after the second mirror alignment in 1993.
2. From these two points in time the measurements seem to follow an asymptotic trend.

In order to confirm this observation, the following mathematical processing is done:

- The observation interval is split in the time before and after mirror alignment. For both time intervals, an asymptotic function of the type
  $s = b_1 \cdot \left(1 - e^{-b_2 \cdot t}\right) + b_0$
  is selected for the regression line of the standard deviation s, where t is the time and b_0, to b_2 are the parameters to be fitted. These regression lines are shown in Figures 14 and 15.
- The residual error between measurements and regression line is used to define the following two intervals (with 95% confidence) for the flux uniformity:
  - an interval in which the regression line is expected for future measurements;
  - an interval within which 95% of all future measurements are expected.

  A crucial assumption in this process is to declare the residual as random, normal distributed errors of the measurements and/or the model. Then, a prediction of the future behaviour is meaningful. The size of the interval will depend on the level of fit of the historical data and on the time span of prediction.
  The essential formulas for the statistical processing are given in an annex.

- Following the alignments the data indicate that the mirror has already stabilised after having gone through the first vacuum and load cycle of the facility. With this assumption it is justified to disregard the first measurement after re-alignment in 1993. As can be seen in Figure 13, the regression line and interval predictions are all in line with the separate processing of the two time intervals.
- Finally, the comparison of the interval predictions in Figure 12 and 13 demonstrate the consequence of fitting all data without removing the point after mirror alignment. The underlying physics of the data has been disregarded. The predicted intervals for future measurements become wide. Obviously the mathematical model is therefore not adequate in that case.

Beam Diameter

The reproducibility of the beam diameter has been analysed by identifying the span of the points within the nominal range along the vertical and along the horizontal axis of the mapping matrix. The results are shown in Figures 16 and 17.

The linear regression lines show a nearly constant value over the total period. The inclination is insignificant with time. The difference between the regression values at the start and end date is well within the resolution of the measuring matrix of 50 mm. The result supports the conclusion that the beam geometry has been stable over the total period.

Beam Centre Location

The beam centre co-ordinates were calculated for each individual mapping with a resolution of 50 mm (see chapter "Mapping Data"). The identified co-ordinates are plotted as a function of time in Figures 18 and 19. The position in vertical direction is reproducible within the measurement accuracy. However, there seems to be a trend of change in the beam centre position along the horizontal axis.

Conclusion

Four different parameters have been analysed to investigate the long-term stability of the LSS sun simulator at ESTEC. The specification requires a flux uniformity of ± 4 %, which is fulfilled for 98.5 % of all data points without any sign of degradation with time.

An asymptotic trend has been identified for the standard deviation of the measured data within the nominal range. Thus there seems to be a mirror alignment settling effect, which results in a stable flux distribution after the first thermal vacuum cycling. The visual impression has been supported by statistical analysis of the available data.

The measurements made over the last 14 years also show a constant solar beam diameter.

The data indicate a horizontal displacement of the beam centre in the order of 10 to 15 mm per year. In this respect further investigations are foreseen.
For this reason it has been decided to repeat solar mapping once per year. If an explanation for the non-constant centre point is found, it would seem reasonable to increase the mapping interval further.

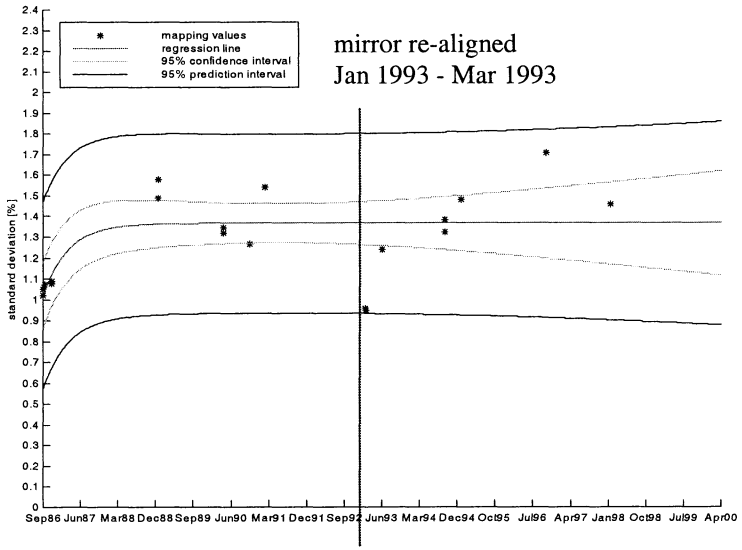

Figure 12: Beam Uniformity 1986-1998

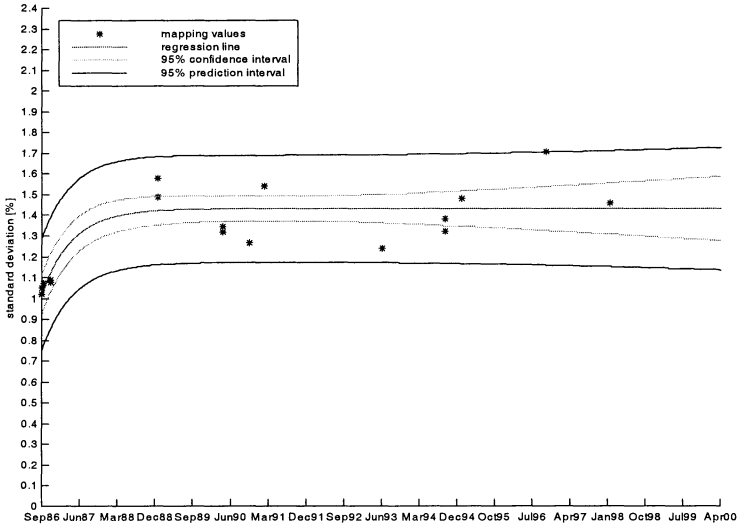

Figure 13: Beam Uniformity 1986-1998 without 1993 measurement

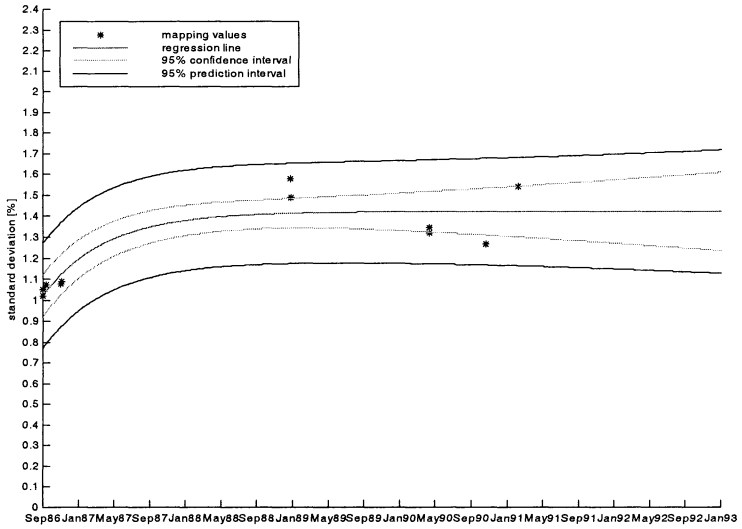

Figure 14: Beam Uniformity 1986-1991

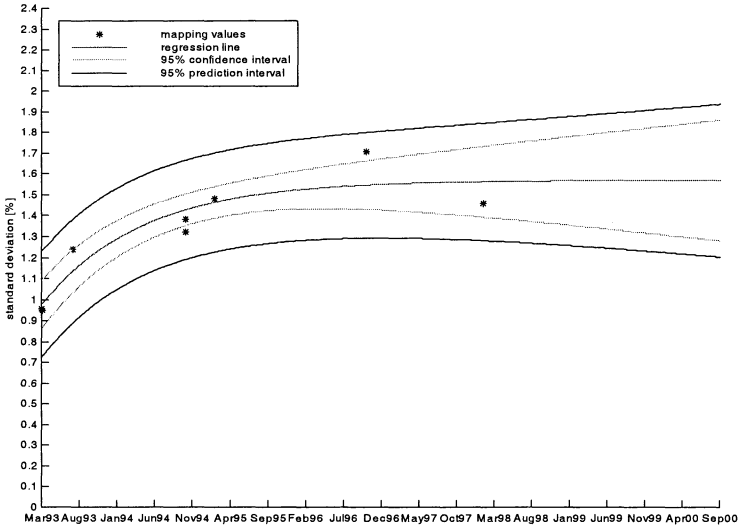

Figure 15: Beam Uniformity 1993-1998

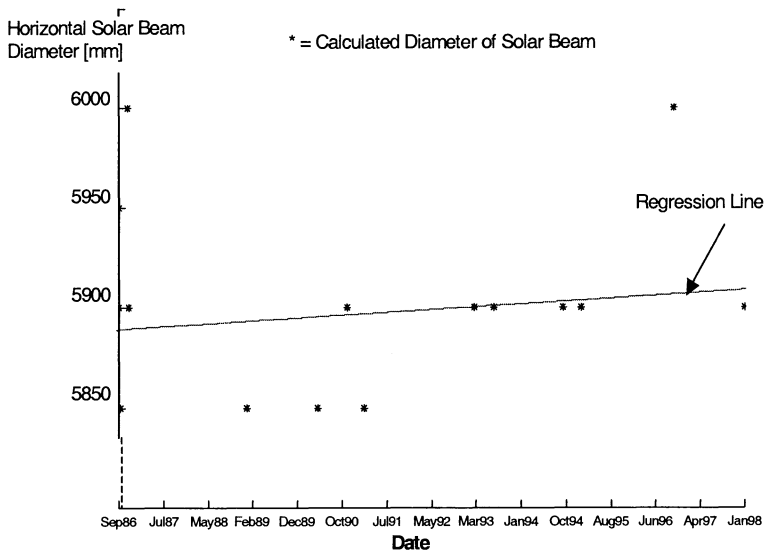

Figure 16: Diameter Horizontal Axis

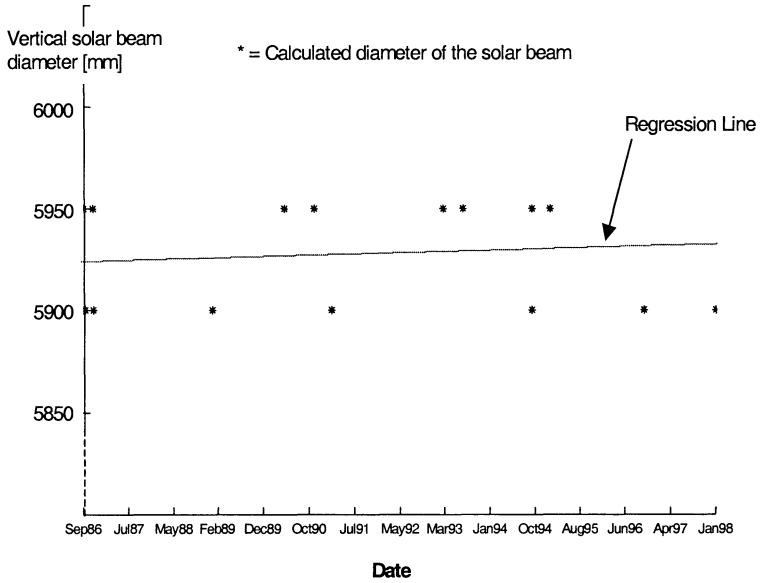

Figure 17: Diameter Vertical Axis

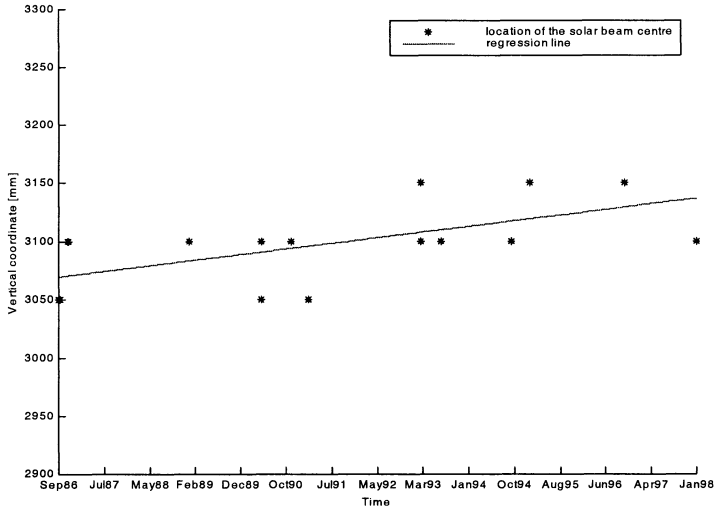

Figure 18: Beam Centre Location Vertical Axis

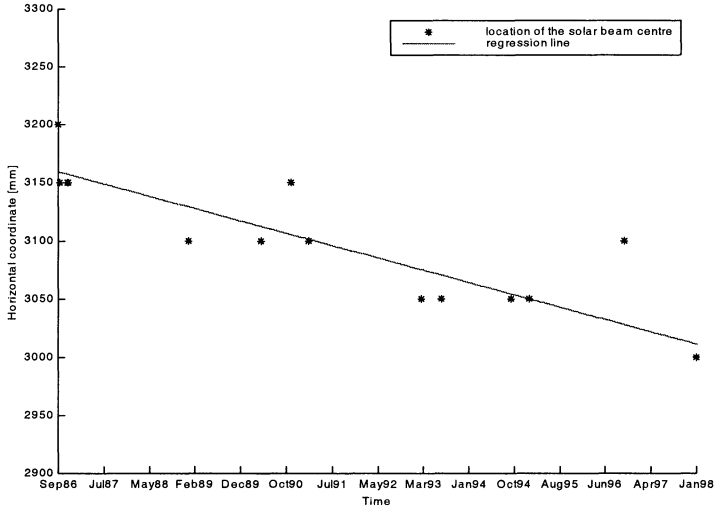

Figure 19: Beam Centre Location Horizontal Axis

Annex

The statistical evaluation is based on the linear regression analysis as described in the text book "Probability and Statistics for Engineers and Scientists"[1]

The following equations are used:

Definition of the 95% confidence interval

The 95 % confidence interval describes the range of expectation of the mean value of the measurements.

$$\hat{y}_0 - t_{\alpha/2} \cdot \sigma \cdot \sqrt{\frac{1}{n} + \frac{(x_0 - \bar{x})^2}{S_{xx}}} < \mu_{y(x_0)} < \hat{y}_0 + t_{\alpha/2} \cdot \sigma \cdot \sqrt{\frac{1}{n} + \frac{(x_0 - \bar{x})^2}{S_{xx}}}$$

Definition of the 95% prediction interval

The 95 % prediction interval describes an interval, in which 95 % of all future measurements are expected with 95 % confidence.

$$\hat{y}_0 - t_{\alpha/2} \cdot \sigma \cdot \sqrt{1 + \frac{1}{n} + \frac{(x_0 - \bar{x})^2}{S_{xx}}} < y_0 < \hat{y}_0 + t_{\alpha/2} \cdot \sigma \cdot \sqrt{1 + \frac{1}{n} + \frac{(x_0 - \bar{x})^2}{S_{xx}}}$$

were $\bar{x}$ is the mean value and S_{xx} is the variance of the measurement data

$$S_{xx} = \sum_{i=1}^{n} (x_i - \bar{x})^2$$

Finally $t_{\alpha/2}$ denotes the critical value of the t-distribution with 1 degree of freedom (i.e. the time).

[1] R.E. Walpole, R.H. Myers, S.L. Myers, 6th edition, Prentice Hall, 1998.

ON-LINE, SELF-LEARNING, PREDICTIVE TOOL FOR DETERMINING PAYLOAD THERMAL RESPONSE

At

Goddard Space Flight Center

Dr. Chian-li Jen
Computer Simulation Specialist
Mr. Leon Tilwick
Engineer, Space Simulation & Operations Support
ManTech International Corporation
Fairfax, Virginia

ABSTRACT

This paper will present the results of a joint ManTech / Goddard R&D effort, currently under way, to develop and test a computer based, on-line, predictive simulation model for use by facility operators to predict the thermal response of a payload during thermal vacuum testing. Thermal response was identified as an area that could benefit from the algorithms developed by Dr. Jen for complex computer simulations. Most thermal vacuum test setups are unique since no two payloads have the same thermal properties. This requires that the operators depend on their past experiences to conduct the test which requires time for them to learn how the payload responds while at the same time limiting any risk of exceeding hot or cold temperature limits.

The predictive tool being developed is intended to be used with the new Thermal Vacuum Data System (TVDS) developed at Goddard for the Thermal Vacuum Test Operations group. This model can learn the thermal response of the payload by reading a few data points from the TVDS, accepting the payload's current temperature as the initial condition for prediction. The model can then be used as a predictive tool to estimate the future payload temperatures according to a predetermined shroud temperature profile. If the error of prediction is too big, the model can be asked to re-learn the new situation on-line in real-time and give a new prediction. Based on some preliminary tests, we feel this predictive model can forecast the payload temperature of the entire test cycle within 5 degrees Celsius after it has learned 3 times during the beginning of the test. The tool will allow the operator to play "what-if" experiments to decide what is his best shroud temperature set-point control strategy. This tool will save money by minimizing guess work and optimizing transitions as well as making the testing process safer and easier to conduct.

INTRODUCTION

Located at Greenbelt, Maryland, the Goddard Space Flight Center (GSFC) is the lead center for NASA's Mission to Planet Earth (MTPE) program. One of its primary functions is to be "responsible for the engineering... and conduct of payload unique environmental tests simulating payload pre-launch , launch, orbit and landing thermal conditions including : thermal vacuum, solar vacuum temperature... ".

There are more than 10 thermal vacuum (T/V) chambers with the sizes ranging from 2'x2' to 27'x40' (diameter x height) located at GSFC. In general, the T/V chambers are operated at pressures around 1x10-7 torr (1.3x10-5 Pa) with the temperature ranged from –190°C to +100°C.

BACKGROUND

The standard procedures for performing thermal testing in vacuum chambers are as follows: a LN2 or GN2 shroud is used to simulate the cold environment of outer space, and a GN2 shroud or heater panels are used to simulate the sun's energy or any other heat source. In the process of T/V testing, the test operator is responsible for controlling the shroud temperature such that it meets the thermal testing requirements set by thermal engineers. A typical testing requirement is to maintain a payload's cooling or heating rate without exceeding the maximum heating/cooling rate. If the heating/cooling rate is too high, i.e. exceeds the maximum rate, the payload may be damaged by thermal stress effects. However, if the rate is too low, the time required to reach the desired temperature for testing may be too long, adding to the cost of thermal vacuum testing.

In general, the payload's heating/cooling rate is mainly determined by the difference between the shroud and payload temperatures provided that payload power is off. However, there are many other factors that may affect the payload's heating/cooling. These factors include, but are not limited to, radiation absorption, heat capacity, mass, and surface area of the payload. Therefore, in general, two different types of payloads placed in a T/V chamber will have two different heating/cooling rates even if they start with the same initial payload temperatures. If more than one payload is under test, the test operator will select the one with the faster heating/cooling rate as the reference to determine a shroud temperature set-point.

To illustrate the processes on how the shroud temperature set-point may be found by the test operator, assume that both payload and shroud temperatures start at 20°C under a vacuum condition. If the payload transition rate limit is set at 40°C/hour, the test operator may set the shroud temperature to 30°C and then observe the payload temperature response. If the observed transition rate is only 10°C/hour, the operator will confidently increase the shroud's temperature set point to ,say 50°C, and then observe the new transition rate. The operator will continue this process until the heat-up rate is close to 40°C/hour. Even if the payload temperature increase rate is about 40°C/hour, the operator has to constantly readjust the shroud temperature in order to maintain the desired rate. Overall, during initial transitions, determining the appropriate shroud temperature to maintain a transition rate is a trial and error process based on the operator's experience.

PROJECT GOALS

The goals of this project are to develop a tool by using simulation technology to support test operators by enabling them to perform payload transitions:

1. safely
2. efficiently
3. with higher quality and at lower cost

In order to meet these objectives, ManTech proposes to apply its newly developed "Learning and Predictive Simulation" technology on a Thermal Vacuum Chamber. This paper presents the phase-1, proof of the concept, results of this project.

THEORY

The heat transfer between the payload and shroud mainly comes from radiation. However, if the pressure in the chamber becomes high enough, convective heat transfer will become more and more significant. In this paper, we assume that the pressure in the chamber is low enough such that convective heat transfer between the payload and its surrounding environment is negligible. Also, the heat conduction inside the payload is assumed to be so fast that the temperature gradient inside the payload is negligible. The equation for the radiation heat transfer can be written as:

A. Heat Transfer

$$Mpl*Cpl*(\partial Tpl/\partial t) = \sigma *\varepsilon*A*(Tsh**4 - Tpl**4) + Hc(Pc)*(Tsh - Tpl) \quad \text{A-1}$$

Where :
Mpl : Payload Mass
Cpl : Payload heat capacity
Tpl : Payload average temperature (absolute)
Tsh : Shroud average temperature (absolute)
t : time in min
$\partial Tpl/\partial t$ = Payload transition rate, C/hour
σ : Stefan-Boltzmann's natural constant
ε : Emissivity or Absorptivity of a gray body
A : the radiating area
Hc(Pc) : Convective heat transfer coefficient as function of chamber pressure
Pc : Chamber pressure

Equation A-1 can be re-written as

$$Mpl*Cpl*(\partial Tpl/\partial t) = (\sigma *\varepsilon*A + Hc(Pc)/((Tsh+Tpl)*(Tsh**2+Tpl**2)))*(Tsh**4 - Tpl**4) \quad \text{A-2}$$

To lump all parameters into one, Eq. A-2 becomes

$$(\partial Tpl/\partial t) = Krc*(Tsh**4 - Tpl**4) \quad \text{A-3}$$

where Krc is the combined coefficients of convection and radiation and can be written as

$$Krc = (\sigma *\varepsilon*A + Hc(Pc)/((Tsh+Tpl)*(Tsh**2+Tpl**2)))/ Mpl*Cpl \quad \text{A-4}$$

Eq. A-3 can be solved if Krc is known and varies slowly with the time.

B. Simulation Model

There are two ways to obtain the values of Krc. To compute it from A-4 by theory or to compute it from A-3 by the actual measurements of Tsh and Tpl. For this purpose, Eq. A-3 can be rewritten as :

$$Krc = (\partial Tpl/\partial t)/ (Tsh**4 - Tpl**4) \quad \text{B-1}$$

If the first method is used to compute Krc, all coefficients or parameters in A-4 have to be known in advance. There are some difficulties in this approach because some coefficients such as ε and Cpl are functions of payload temperature. Also, it is difficult to decide area A if its surface is not flat. We choose the second method to compute Krc as long as (Tsh-Tpl) is ***not*** in the neighborhood of zero (0). Furthermore, if convective heat transfer is insignificant and ε remains as a constant in the payload temperature range, Krc will remain close to a constant during the time of testing. Unfortunately, ε does change with Tpl, so Krc will need to be readjusted if ε varies outside of a tolerable range.

B.1 Learning Mode :

Eq.B-1 can be used to derive Krc if $(\partial Tpl/\partial t)$ is reasonably large and stable, and Tsh is not close to Tpl. A more practical way to estimate Krc is to simulate Tpl by using Eq.A-3 and to find out what Krc value will give the least errors between actual Tpl's and simulated Tpl's. An example of Krc searching is given on Table B.1-1

			Krc1=3.90E-9		Krc2=4.00E-9		Krc3=4.10E-9	
Time-minutes	Tsh-data C-deg	Tpl-data C-deg	Tpl-krc1	Err1**2	Tpl-krc2	Err2**2	Tpl-krc3	Err3**2
0	-14	16.68	16.68	0	16.68	0	16.68	0
2	-14.38	16.35	16.35	1.86E-7	16.34	7.92E-5	16.33	3.02E-4
4	-14.13	16.04	16.02	4.04E-4	16.00	1.36E-3	15.99	2.88E-3
6	-14.38	15.67	15.70	7.07E-4	15.67	2.89E-6	15.65	5.37E-4
8	-14.63	15.33	15.38	2.03E-3	15.34	1.51E-4	15.31	4.20E-4
		Sum :		3.14E-3		1.59E-3		4.14E-3

Table B.1-1 : Krc Selection Matrix

From the table B.1-1, Krc2=4.00E-9 for the equation A-3 will give the least square errors fit between the actual and simulated Tpl's curve fit in the time range (0,8) minutes.

B.2 Prediction Mode

Once Krc is derived during the learning mode, there are two types of predictions which can be forecasted by this model.
Type 1: How will payload temperature respond if the shroud temperature is changed at a predetermined temperature changing (transition) rate?
In order to predict payload temperature for the next few cycles, Eq. A-3 shall be used to obtain the $(\partial Tpl/\partial t)$ payload temperature rate. Then, the payload temperature is updated by this predictive changing rate. Shroud temperature shall be updated by the predetermined transition rate. For example, if we keep shroud temperature as a constant, say –15°C, the payload temperature and its changing rate are predicted as shown in the following Table B2-1:

		Krc= 4.00E-09		
Time-minutes	Tsh-Cdeg predetermined	Tpl-rate Cdeg/hour	Tpl-Cdeg predicted	Comment
8	-14.63	-9.82	15.33	initial condition
10	-15	-9.80	15.00	
12	-15	-9.67	14.68	
14	-15	-9.55	14.35	
16	-15	-9.43	14.04	
18	-15	-9.31	13.72	
20	-15	-9.19	13.41	
22	-15	-9.08	13.10	

Table B2-1 Payload Temperature Prediction

Type 2: How shall the shroud temperature be set if payload temperature transition rate is predetermined ?
From Eq.A-3, Tsh can be rewritten as

$$Tsh = (Tpl^{**}4 + (\partial Tpl/\partial t)/Krc)^{**}(1/4) \qquad \text{B-2}$$

Since $(\partial Tpl/\partial t)$ is a predetermined value, Tpl can be updated based on this given rate. Then Tsh can be easily obtained from Eq.B-2. For example, if we set $(\partial Tpl/\partial t)$ as –10°C/hour, the following table (B2-2) gives a prediction of how shroud temperature should be set in order to maintain –10°C/hour transition rate for the payload :

	Tpl-rate	Krc=	4.00E-09	
Time-minutes	C°/hour predetermined	Tpl-C° predicted	Tsh-C° predicted	Comment
8	-9.82	15.33	-14.63	initial condition
10	-10	15.00	-15.74	
12	-10	14.67	-16.21	
14	-10	14.34	-16.68	
16	-10	14.00	-17.15	
18	-10	13.67	-17.62	
20	-10	13.34	-18.09	
22	-10	13.00	-18.57	

Table B2-2 Shroud Temperature Prediction

Actual data obtained for this prediction model analysis is as following :

			Tpl-rate
Time-Minutes	Tsh-C° data	Tpl-C° data	C°/hour data
10	-15	14.98	-10.35
12	-14.88	14.62	-10.20
14	-14.75	14.30	-10.50
16	-14.88	13.92	-10.50
18	-14.88	13.60	-10.35

Table B2-3 Actual Data From TVDS

Comparing the actual data with the predicted Tpl and Tsh, one finds that this model is very sensitive to the values selected for (∂Tpl/∂t) and Krc in predicting Tsh. However, it is less sensitive to the values selected for Tsh or Krc in predicting Tpl. These results imply that very accurate (∂Tpl/∂t) and Krc are required in order to predict Tsh with reasonable accuracy. However, even if only reasonable Krc and Tsh values are given, Tpl can still be fairly accurately predicted.

APPLICATIONS

This predictive simulation tool has been implemented in the TVDS for chambers 241, 281, and 237 at GSFC. It is used as a predictive tool to support test operators in deciding how to conduct the tests safely and efficiently. The diagrams at the end of this paper were extracted directly from TVDS for the chamber 281. The first diagram (Fig-A_1) has four parameters plotted against time. Two of the parameters are the actual and predicted payload temperatures, and the other two are the actual and the predicted shroud temperatures. The purpose of this diagram is to find out what is the best value for Krc (shown as Q in the diagram) so that it will generate the best simulated Tpl's in a formerly given time interval in comparison with observed Tpl performance obtained from the TVDS. A least-error-square method is used to define the best selection for Krc.

The next diagram, Fig.A-2, predicts shroud temperatures at the next three (3) hours if the payload temperature's predetermined transition rate is set at (-10°C/hour). Please note that the current payload transition rate is –8.86°C/hour. The predictive data begins at 11:32 and continues to 14:32. The table in Fig.A-2 contains the actual historical data in black color (from 11:10 to 11:30) and the predicted values in blue color (11:32 to 11:52). To obtain the predicted value beyond 11:52, one can simply pull down the scroll bar at the right side of the table.

BENEFITS

After the thermal properties of the test article (payload) have been determined by this learning and prediction tool, the thermal performance of the payload can be accurately predicted by the tool . This tool allows the operator to perform "what if" on-line, real time analysis. Within 30 minutes after starting a transition, the operator can quickly determine:

1. what shroud temperature should be achieved to maintain a required payload temperature transition rate,
2. when the control thermocouple will reach the required soak temperature,
3. when any payload temperature thermocouple will hit a yellow or red limit

If a payload's thermal properties change for any unknown reason, this model will no longer predict accurately; however, the operator can clearly see from the TVDS that the predicted payload temperature deviates significantly from the observed (measured) temperatures. The operator will then repeat the learning cycle to find a new value for Krc by using the last 10 to 20 minutes data. Within a few seconds, this model will accurately re-predict the payload temperature based on the new data learned in the last 10 to 20 minutes.

CONCLUSION

Capabilities of the Learning and Predictive Simulation Tool have been successfully implemented and demonstrated on GSFC's TVDS. This tool can learn the thermal properties of various types of the test articles on-line and in real time. The operator is able to effectively predict shroud temperature set points to meet the required payload heating/cooling rates. The operator can now perform without guessing or taking a trial-by-error approach.

However, the phase-1 project covers only simple payload transitions. Multiple heat sources, payload power, heat conduction effect (heat sink and source), and multiple payload testing will be implemented in the phase-2 project. An additional objective for the phase-2 project is multiple thermocouple pre-alarming. With this capability, the operator will know in advance whether his action will exceed a yellow or red payload temperature limit. Our ultimate goal is to provide test operator a fully automated test system to improve the safety, efficiency, quality, and cost of payload testing.

FIGURES :

Fig.A-1 Krc Selection

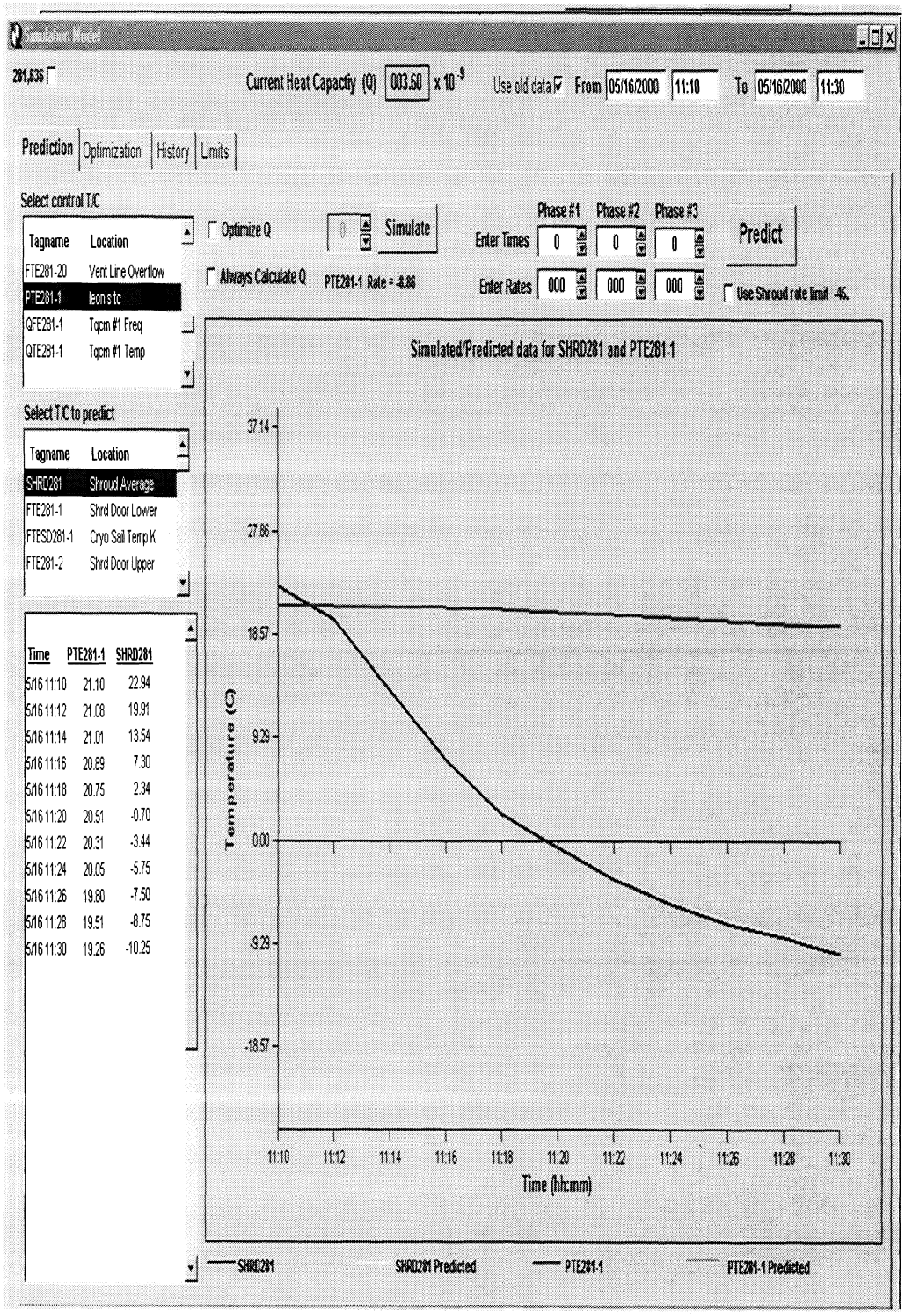

FigA-2 Tpl 3-hour Prediction

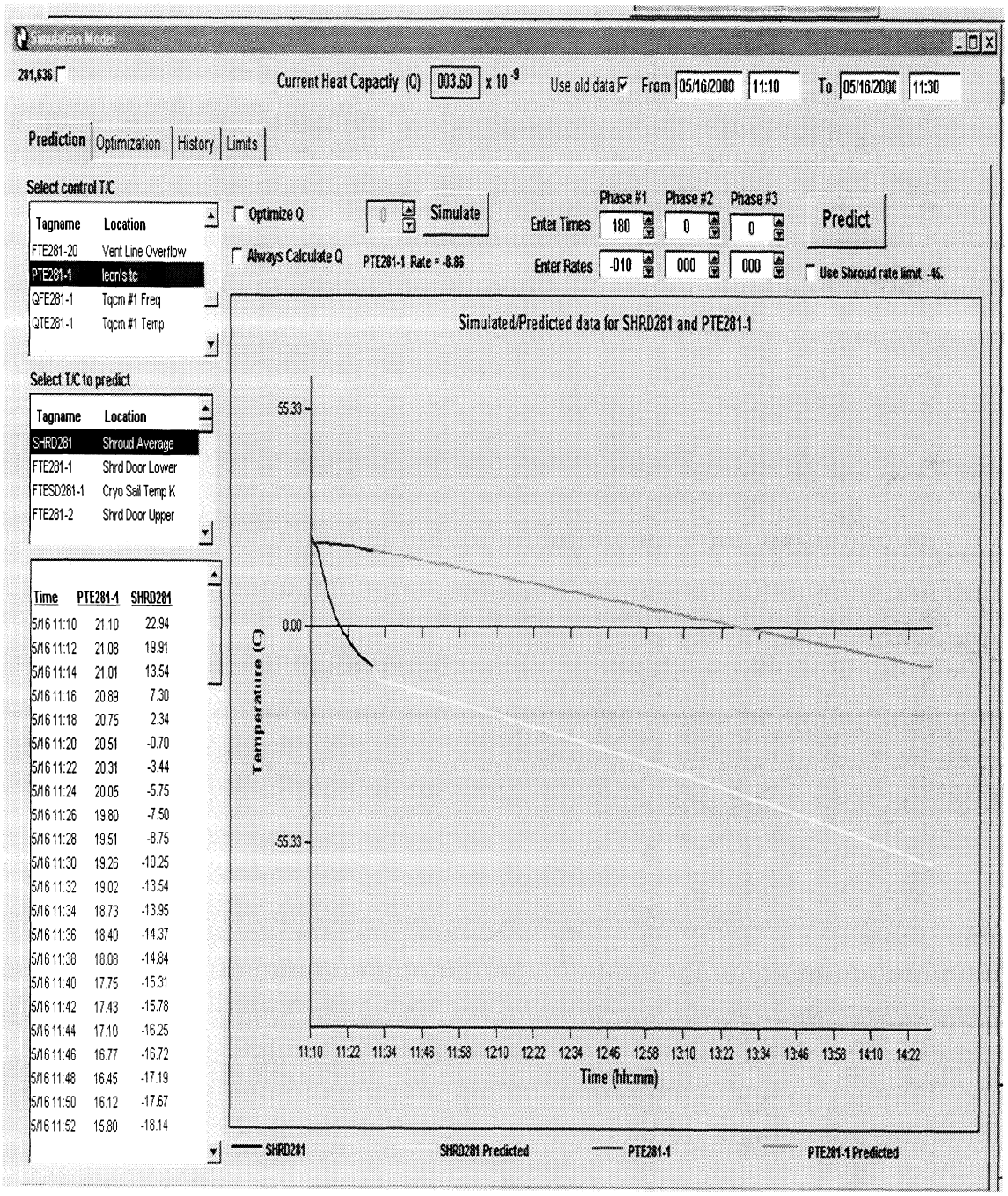

DESIGN, IMPLEMENTATION AND INSTALLATION OF A NEW ELECTRONIC TEMPERATURE DATA ACQUISITION SYSTEM (TEMPDAS) FOR THE ESTEC LARGE SPACE SIMULATOR (LSS)

W.J.C.M. van Zutphen, F.M. Fontaine
National Aerospace Laboratory NLR, PO Box 90502, 1006 BM Amsterdam, The Netherlands

B. Sarti, H.C. Vermeulen
ESTEC, Testing Division, PO Box 299, 2200 AG Noordwijk, The Netherlands

ABSTRACT

The ESTEC Large Space Simulator (LSS) provides close simulation of in-orbit environmental conditions. The LSS is equipped with a two-axis Motion System, which permits a test article to be placed within the LSS in any position relative to the angle of incidence of solar radiation. Temperature measurement signals generated by thermocouples fixed on the rotating test article are connected to the main data handling system through a Slip-Ring Unit. A high-accuracy multi-channel Temperature Data Acquisition System (TEMPDAS) has been developed for specific use in the LSS.

The concept of TEMPDAS is to multiplex, condition and measure the signals from the thermocouple sensors inside the LSS and send the digital measurement data to the data-handling unit. The National Aerospace Laboratory NLR designed, manufactured and tested two Data Collection Units, enabling TEMPDAS to measure 864 thermocouple signals.

This paper presents a full description of the main project phases and their outcomes from unit prototyping to final unit verification and installation. Special attention is paid to address some critical design and manufacturing items encountered in the course of the development and to highlight the technical solutions implemented to surmount the difficulties.

ABBREVIATIONS

ADC	Analogue to Digital Converter
DCU	Data Collection Unit
EMF	Electro-Mechanical Force
ESTEC	European Space Research and Technology Centre
FPGA	Field Programmable Gate Array
LSS	Large Space Simulator
NLR	National Aerospace Laboratory NLR
SRU	Slip Ring Unit
TC	Thermocouple
TCMB	Thermocouple Multiplexer Board
TEMPDAS	Temperature Data Acquisition System
VTR	Variable Temperature Reference

INTRODUCTION

Measurement of temperatures on a spacecraft inside ESTEC's Large Space Simulator (LSS) is generally done with thermocouples. The thermocouples are connected to a Variable Temperature Reference (VTR), which forms the cold junction. In the current situation 144 channels of the Slip Ring Unit (SRU) are used to measure 576 (compensated) thermocouple signals. The low-level signals from the thermocouples are multiplexed by mechanical relays and measured by the Data Handling System outside the Large Space Simulator [ref. 1].

A new Temperature Data Acquisition System (TEMPDAS) has been conceived [ref. 2] in order to:

- extend the thermocouple channel capacity up to 2000 channels;
- drastically reduce the required number of SRU channels from 144 to less than 20;
- have a system less prone to data corruption;
- have a system with self compensating capabilities.

TEMPDAS is made up of Data Collection Units (DCUs), placed in the LSS, and a Data Handling Unit located in the control room. Each DCU is characterised by a modular architecture and takes care of analogue thermocouple signal conditioning, digitisation and multiplexing over a MIL-STD-1553B data bus. For the realisation of the new system the National Aerospace Laboratory NLR has designed, manufactured and tested two DCUs. The absolute measurement accuracy of the system must be better than ±1 °C in all LSS operational conditions.

Besides the Data Collection Unit for the measurements of thermocouples, TEMPDAS is currently also capable of measuring Platinum sensors (Pt-DCU). ESTEC is developing a multifunctional system [ref. 3] that combines the measurement of these sensors together with thermistor sensors. This paper focuses on the thermocouple measurements only and presents the project phases and their outcomes from unit prototyping to final unit verification. Special attention is paid to address some critical design and manufacturing items encountered in the course of the development and to highlight the technical solutions implemented to surmount the difficulties.

TEMPDAS DESIGN

The "Specification for the Design and Manufacturing of a prototype Data Collection Unit" [ref. 4] forms the functional baseline for the system design (VTR). This document translates the overall accuracy requirement of ±1°C into specifications for the DCU in terms of volts, taking into account the error introduced by the sensor itself and the cold junction (VTR). The major performance specifications for the DCU are:

- Input range from –10 mV to +10 mV
- Repeatability: $3\sigma < 4{,}2\ \mu V$
- Offset between any two channels:
  - Steady-state temperature condition: < 5,7 µV
  - Transient temperature condition: < 15 µV
- Remaining System Error
  - Steady-state temperature condition: < 4,5 µV
  - Transient temperature condition: < 7,5 µV

Other design specifications are:

- Operating in vacuum between –40 °C and +50 °C
- Powered by a +28VDC external supply
- Communication via a MIL-STD-1553B bus
- Electromagnetic Compatibility in accordance with MIL-STD-461C – part3.

Figure 1 depicts the architectural design of TEMPDAS. The system is set-up to be modular extensible (up to five complete units inside the LSS). The Data Handling Unit controls the DCUs via a redundant MIL-STD-1553B bus. The software on the Data Handling Unit runs under Windows 95 and consists of Application Software (developed by ESTEC) to interface with the Data Handling System and DCU Control Software (developed by NLR).

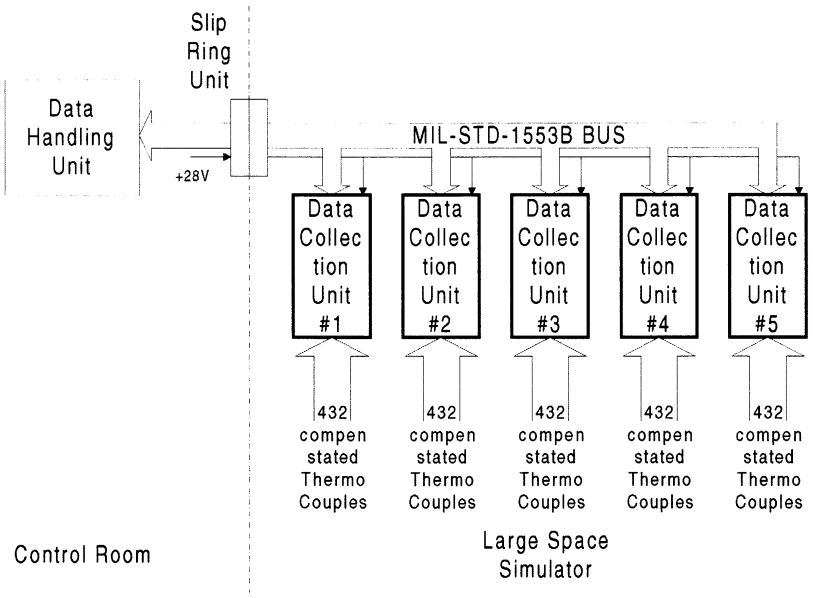

Figure 1: TEMPDAS Architectural Design

Figure 2 shows the block diagram of the DCU. Each DCU is equipped with redundant power supplies to convert the external +28 V into internal +5 V/±15 V.

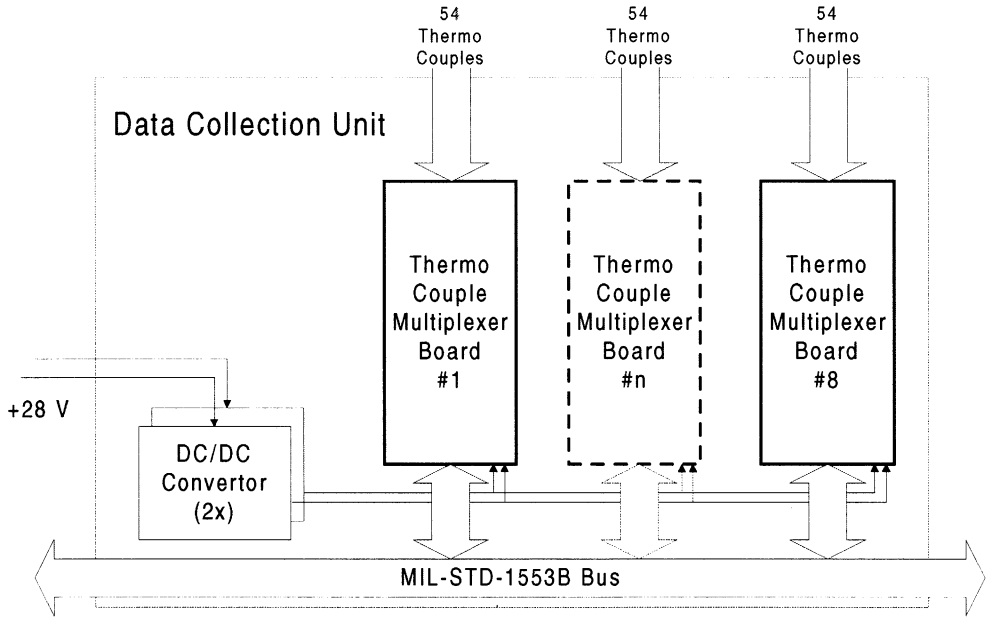

Figure 2: Block Diagram of the DCU

The actual measurements are performed on a Thermocouple Multiplexer Board (TCMB). The TCMBs work independently and are capable of measuring 54 thermocouples each. A block diagram of the TCMB is shown in ***Figure 3***.

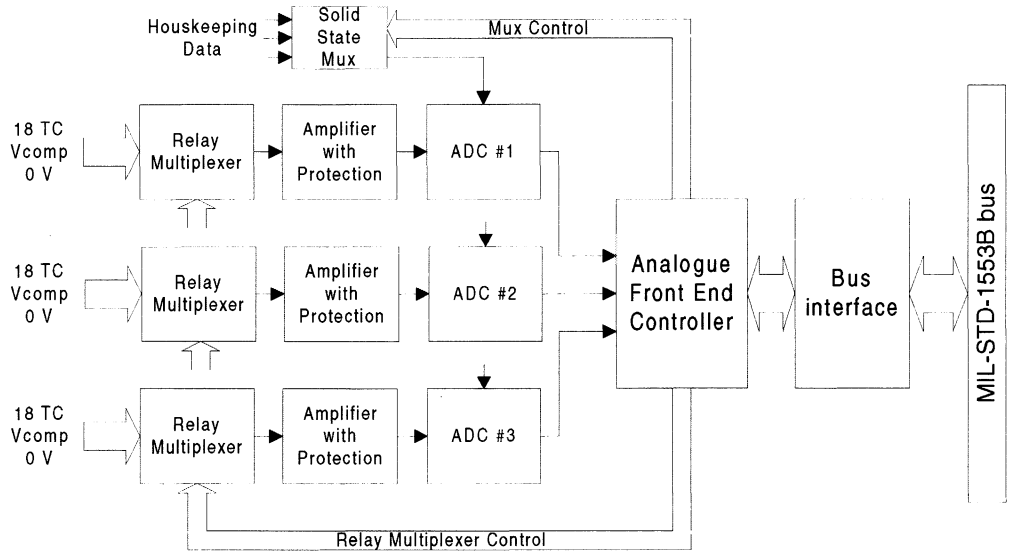

Figure 3: Block Diagram of a Thermocouple Multiplexer Board (TCMB)

The heart of the TCMB consists of an analogue front-end controller which is implemented in a Field Programmable Gate Array. Its functions are to control the multiplexers and the Analogue to Digital Converters (ADCs), store the last measurement data and provide communication with the Data Handling Unit.

Multiplexing of the low-level thermocouple signals is done with electromechanical relays because of the overall superior performance [ref. 5]. In comparison with the solid state multiplexers, relays have a lower leakage current and "on"-resistance. In the "off"-state relays also offer a protection against high common mode voltages that could be induced during isolation tests of solar panels.

A single TCMB measures 54 thermocouple signals in three parallel groups that measure 18 channels sequentially. To compensate for the offset and gain error in the amplifier and in the ADC, a measurement cycle also samples two well-known voltages; a short circuit (V_0) and a compensation voltage (V_{comp}) of about 20 mV. The compensation voltage is derived from a stable 2,5 V reference source with a 1:125 precision resistor divider. This derived voltage needs to be very stable and its value is assessed during the calibration. Each group has its own source for the compensation voltage. The compensation for the offset and gain is performed in the DCU Control Software on the Data Handling Unit according to the following formula:

$$V_{measured,TCx} = \frac{(C_{ADC,V_{TCx}} - C_{ADC,V_0})}{(C_{ADC,V_{comp}} - C_{ADC,V_0})} * V_{comp} \quad (1)$$

Where:

$C_{ADC,VTCx}$ is the ADC code while TCx was connected to the input
$C_{ADC,Vcomp}$ is the ADC code while V_{comp} was connected to the input
$C_{ADC,V0}$ is the ADC code while V_0 was connected to the input
V_{comp} is the well-known on-board compensation voltage

Housekeeping data is measured by the less accurate inputs of the ADC. Each board monitors the differences between the on-board precision voltages (V_{comp}) and four temperatures to get a good thermal overview of the board. Additional inputs are used to measure the power supply output voltages and some temperatures of the DCU housing.

TEMPDAS has been designed to minimise the effects of single point failures [ref. 6]. The MIL-STD-1553B bus has built-in features to ascertain communication in case of a single point failure in the bus hardware. The MIL-STD-1553B bus is therefore implemented as a primary bus A and a secondary bus B (redundant). This makes it possible to connect all boards in the DCU directly to the busses without jeopardising reliable operation. The power supplies of the DCU are hot redundant. At TCMB level the three independent groups have their own reference voltage, with an option to use one of another group.

ASSEMBLY

All components and materials used for the assembly of the DCU and the TCMBs were selected to have low outgassing. If available on the market, MIL-STD-883B qualified components were used. If not, the extended temperature range (-55 °C to +125°C) was selected. Due to these selection criteria the delivery times of most components was in the order of 15 to 30 weeks.

As a result of the thermal analysis [ref. 7] the layers of the PCB contained as much copper as possible to optimise thermal distribution. During the assembly of some components the boards needed to be warmed up in order to achieve good solder junctions.

Figure 4 shows the DCU with one TCMB installed and one TCMB at the front. On top of the DCU the connectors for the power supply are visible. Each TCMB has three flying wires (black cables), each for 18 TC inputs, with standard sub-D connectors. Clearly visible on the TCMB are the relay area (on top of the board) and the FPGA (on the bottom-centre). The dimensions of the housing are 217,1 mm x 180,4 mm x 151,3 mm (H x D x W).

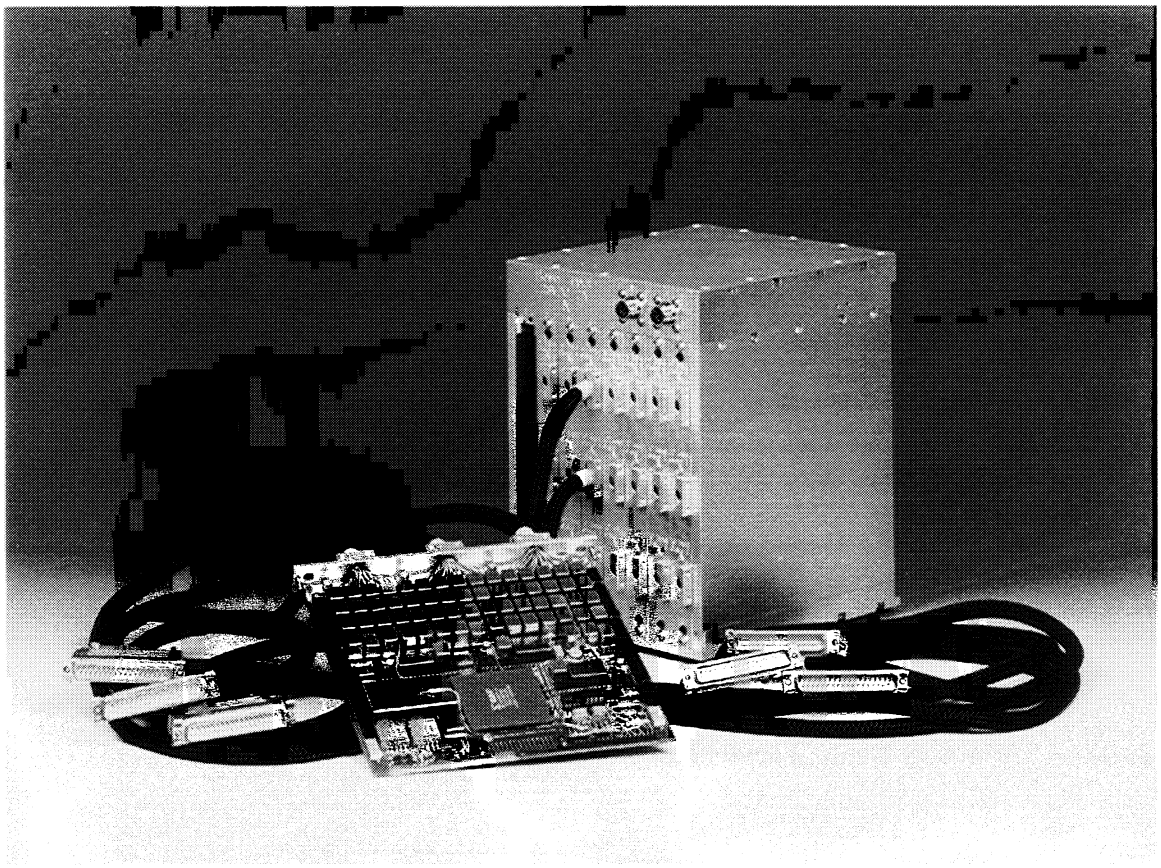

Figure 4: DCU with component side view of a TCMB at the front

CALIBRATION

After assembly and functional check, the two DCUs were powered on for about one month in order to have a burn-in period for the on-board derived precision voltages. Next, the value of these compensation voltages was determined in NLR's calibration facility, for which the set-up is depicted in ***Figure 5***. After temperature stabilisation of the DCU a stable input voltage in the order of 20 mV (i.e. 200 mA for the current source) is applied to the TC inputs of the TCMB. The same voltage is measured with a Keithley model 181 nanovolt meter. The magnitude of compensation voltages is derived from the measurements of the DCU and the Keithley 181, using equation 1 in the reversed way.

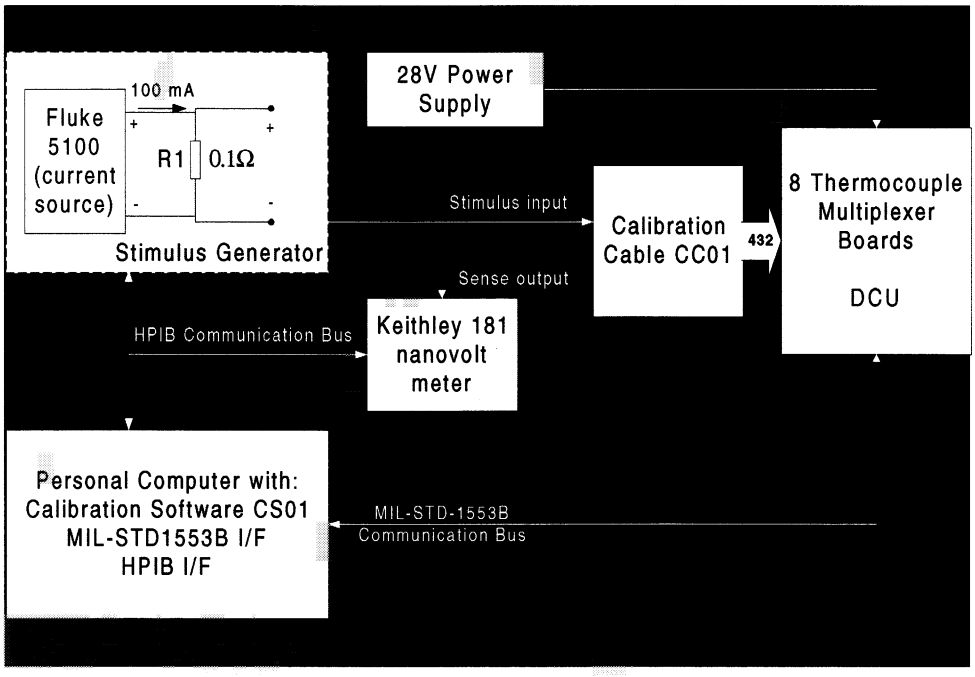

Figure 5: Calibration set-up

In order to minimise the source loading by the input impedance of the TCMBs, the output impedance of the stimulus generator has to be as low as possible. A practical value of 0,1 Ω was chosen, resulting in a stimulus current between –100 mA and +100 mA to cover the specified input range. The process is automated by a personal computer that is able to control the stimulus generator, the DCU and the Keithley 181 nanovolt meter. The results of the seven-point calibration (-10 mV, -5 mV, -2 mV, 0 mV, +2 mV, +5 mV, +10 mV) of DCU#1 is shown in ***Figure 6***. The black centre portion indicates the deviation with respect to the generated voltage of the average values measured (minimum to maximum) over all TCMBs, the red (outer) bars add the maximum two-sigma (2σ) to these values. It is shown that all measurements of the DCU are within 1μV from the generated voltage. The absolute accuracy of the Keithley 181 nanovolt meter is better than $3 \cdot 10^{-6}$ V in the range from –10 mV to +10 mV.

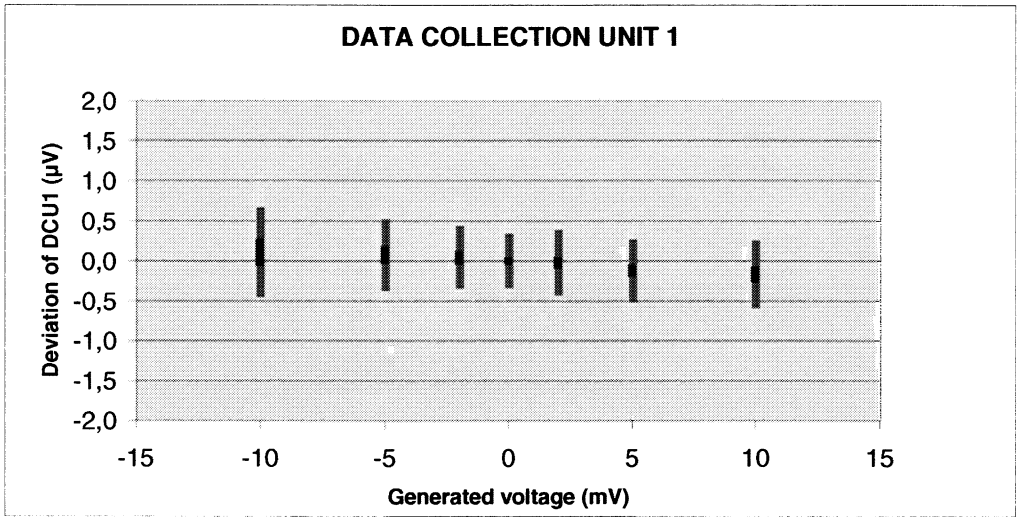

Figure 6: Calibration result of DCU#1

ENVIRONMENTAL TEST RESULTS

The two DCUs were subjected to EMC and Thermal Vacuum (TV) tests. The EMC tests were carried out at the facilities of the NLR EMC Laboratory according to MIL-STD-461C, part3 cat. A2c. With the exception of one susceptibility test (RS03 100 MHz – 1000 MHz) the units were found to be compliant. Susceptibility was however found to be less than 2 µV when the radiated field levels were halved.

The thermal vacuum tests revealed some interesting issues. A prototype DCU with only three TCMB was tested at IABG in Ottobrunn, Germany [ref 8]. Mainly the observed Offset Between Channels was out of specification. The following causes were identified for the large offset voltages:

1. **Flying Wires**: the TCMBs are equipped with flying wires, made of silver plated copper, to connect to thermocouple signals. To ease assembly, three different production batches (colours) were used. Because the connector temperature differs from the DCU temperature, a thermal Electro-Mechanical Force (EMF) is introduced as is indicated in *Figure 7*. The voltage is larger than the specification for the complete unit. Ref 9 lists a table with values for thermo-electric potentials for several materials, which shows that Cu-Cu junctions can result in up to 0,2 µV/°C. The maximum thermal EMF in *Figure 7* is about 0,1 µV/°C. In the final two DCUs the wires all come from a single batch to minimise the thermal EMF effects. The same is applicable for the Test Cable Harness used for the calibration and the environmental tests; all wires between the TCMB input connectors, the stimulus generator and the Keithley 181 nanovolt meter are from a single production batch.

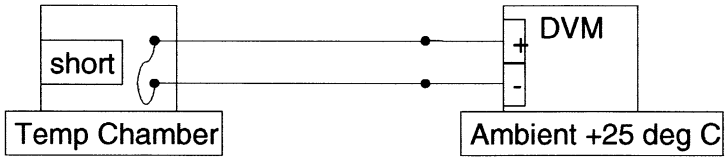

Wire Combination		Measurements (uV) at delta T of	
+	-	+75 deg C	-65 deg C
Orange	Yellow	-7	7
Yellow	Grey	5	-6
Orange	Grey	-1	1
Orange	Orange	0	0
Yellow	Yellow	0	0
Grey	Grey	0	0

Figure 7: Offset voltage due to material differences of flying wires

2. **Thermal distribution:** Figure 8 shows a thermal image of a DCU under vacuum conditions. The left side of the housing was removed to visualise the heat distribution on the TCMB. The relay area is situated on the right half of the TCMB, where also the connected flying wires are visible.
A steep temperature transient near the edges of the relay multiplexer area (right top of the TCMB in Figure 8) introduced an offset voltage in the order of 10 – 20 μV in the prototype DCU. This is mainly caused by heat flow between the flying wires and the housing through the PCB. The effect is reduced by thermally isolating the relay multiplexer area from the housing as much as possible.

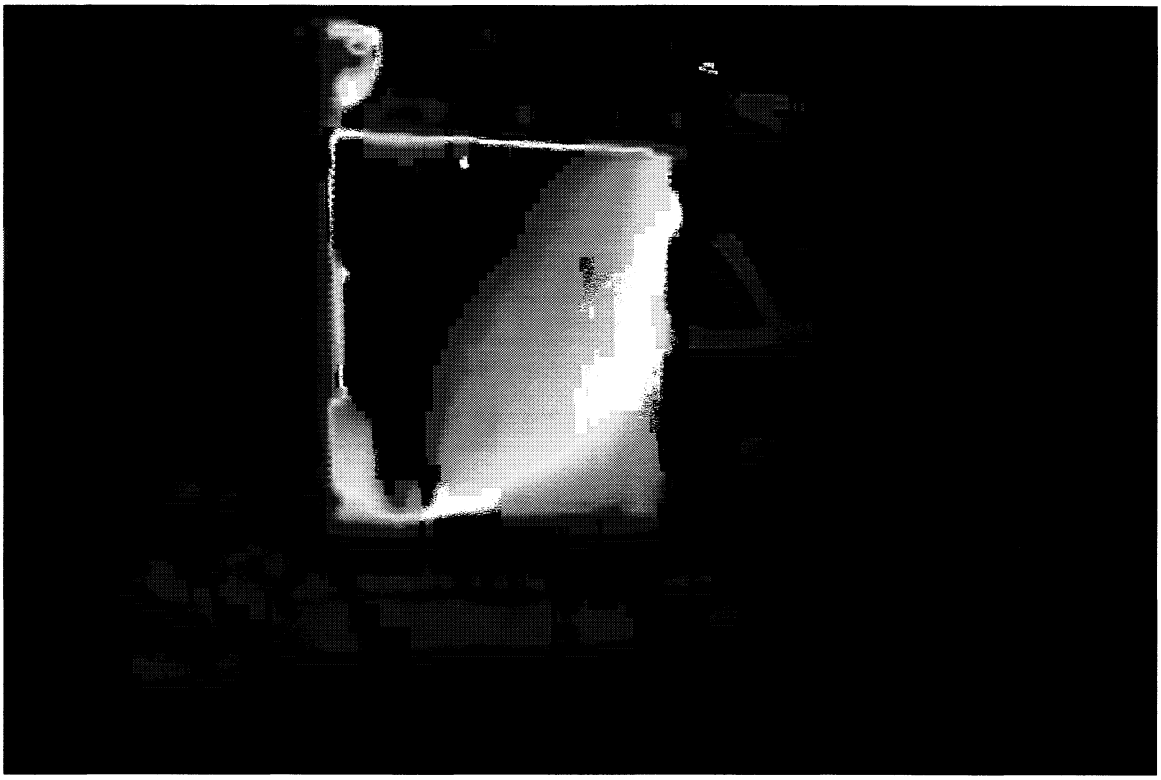

Figure 8: Thermal image of a DCU in a vacuum chamber (left side view)

The two DCUs went through a total of three thermal cycles under vacuum conditions [ref. 10]. *Figure 9* shows the temperature profile of the heatsink and shrouds during the TV test. The test set-up was basically the same as used for the calibration (See ***Figure 5: Calibration set-up***).

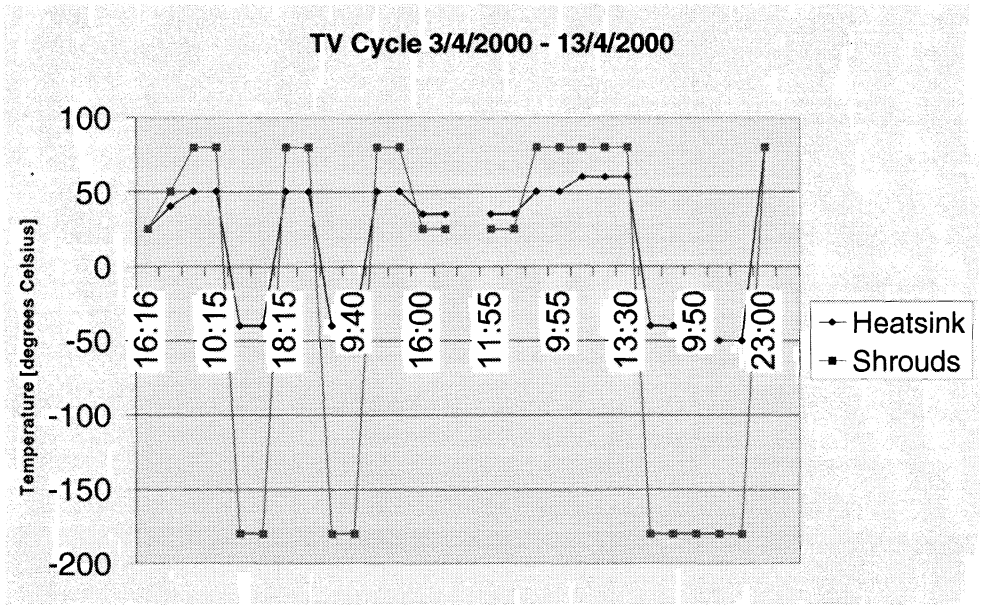

Figure 9: Temperature cycle of the thermal vacuum test

The temperature transients took place in about 2 hours. The units were continuously scanning during the cycles. The time needed for temperature stabilisation inside the DCU after a transient takes more than 8 hours.

In the first two temperature cycles a large deviation was found between the voltage of the stimulus generator and the feedback signal from the test cable harness inside the chamber. Apparently the feedthrough connector introduced a thermal offset voltage in the order of several tens of microvolts. For the investigation the test cable harness was shorted inside the chamber and the stimulus current disabled. In the last cycle the voltages on the wires coming from the feedthrough connector were measured to quantify the distortion. The offset voltage in the stimulus input lines varied between 0,4 μV and 2,3 μV while the feedback signal ranged between +31,6 μV and –62,5 μV.

To determine the accuracy of the DCU measurements, the results were corrected with the findings of the investigation on the behaviour of the feedthrough connector. Table 1 shows the overall results of the two DCUs. The repeatability and the remaining system error show to be well within specification. The offset between channels is however outside the specification.

Table 1: Results of the TV test

		Requirement	Test Result
Repeatability (3σ)		4,2 μV	1 μV (max) <0,5 μV (general)
Offset Between Channels	Steady-state	5,7 μV	10,5 μV
	Transient	15 μV	25 μV
Remaining System Error	Steady-state	4,5 μV	-1,6 μV
	Transient	7,5 μV	-2,3 μV

In the third thermal cycle the temperature limits were extended by 10 degrees. In these periods the DCUs were powered-off and powered-on after about two hours. The system started without any problem.

During the testing of the system, problems were encountered with relays that did not properly function. In the prototype DCU more than 20% of the relays failed to properly close the contacts one or more times. The failure normally showed to be intermittent; after a failure the relay would subsequently function normally for multiple consecutive scans. ESTEC and the manufacturer of the relays, Teledyne Relays, have investigated the problem. It was

concluded that the problem could very likely be attributed to contamination of the contact surface with silicone; a problem which was related to the production batches used. The functional and EMC tests of the two final DCUs were conducted without failing relays. The intermittent switching problem was however again seen in the results of thermal vacuum test. A new kind of failure was also detected; a few relays were switched on continuously for a longer period of time. Investigation of the test data showed that the number of channels with failures (about 5%) was within the specification of the relay when related to the number of unit cycles performed.

CONCLUSIONS

The test results show that the DCUs work within their specification, with the exception for the offset between channels and the EMC specification RS03. If the measurement errors were converted to temperatures, the excess offset would be in the order of 0,25 degrees (10 μV) for the temperature transient situation and 0,12 degrees (5 μV) for steady state. Susceptibility is found to be within the margins when the field levels are halved.

The temperature distribution over the relay area on the TCMB shows to have a large effect on the on the measurements. Although the board is designed for optimal thermal conductivity (without the use of a thermal frame), there will always be a small temperature gradient over the footprint of the relay. An effective improvement could be achieved by a redesign of the housing, where the boards are mounted horizontally instead of vertically.

The failures in the measurements due to the malfunctioning of the relays used make their application arguable. The accuracy that is achieved with the relays is however very high; the standard deviation is generally less than 200 nV. The results of future operational tests with the DCU shall enable a better judgement in weather to use relays or not.

REFERENCES

1. G. Beckwith et al, "Large Space Simulator", issue 1, ESTEC/YTO/DES/LSS/0315/C, 1992.
2. B. Sarti, W.J.C.M. van Zutphen et al, "The Temperature Data Acquisition System (TEMPDAS) for the ESTEC Large Space Simulator (LSS)", Third Symposium on Environmental Testing for Space Programmes, ESA SP-408, August 1997
3. K. Debeule and B. Sarti, "Development of a Multifunctional Data Acquisition Unit for the ESTEC LSS", 30th International Conference on Environmental Systems, SAE Technical Paper Series 2000-01-2530, July 2000.
4. B. Sarti et al , "Specification for the design and Manufacturing of a prototype Data Collection Unit (DCU) fot the TEMPDAS system", Issue 2 rev A, ESTEC/YTE/S/DCU/0161/C, 1996-09-20
5. R.Visser et al, "Thermal vacuum test of the analogue front-end of the TEMPDAS System", ESTEC/YTE/T/TEM/0160, Issue 1, 1995-06-28
6. W.J.C.M. van Zutphen, "Failure Modes, Effects and Criticality Analysis (FMECA) for the development of the TEMPDAS DCU", NLR/R/TEM/0005/A, Issue 1, rev A, 16 March 1998.
7. W.J.C.M. van Zutphen and F.M. Fontaine, "Thermal Analysis for the development of the TEMPDAS Data Collection Unit (DCU)", NLR/R/TEM/0004/A, Issue 2, 12 Jan 1998
8. W.J.C.M. van Zutphen, "Acceptance Test Report of the TEMPDAS prototype Data Collection Unit", NLR/R/TEM/0016/A, October 1999
9. Keithley Instruments inc., "Low Level Measurements", revised third edition, June 1984
10. W.J.C.M. van Zutphen, "Acceptance Test Report of the TEMPDAS Data Collection Unit", NLR/R/TEM/0034/A, Issue 1, July 2000

UPGRADE OF THE THERMAL VACUUM DATA SYSTEM AT NASA/GSFC

Goddard Space Flight Center
Greenbelt, Maryland

John Palmer
Mantech /NSI

ABSTRACT

The Goddard Space Flight Center's new thermal vacuum data acquisition system is a networked client-sever application that enables lab operations crews to monitor all tests from a central location. The GSFC thermal vacuum lab consists of eleven chambers in Building 7 and one chamber in Building 10. The new data system was implemented for several reasons. These included the need for centralized data collection, more flexible and easier to use operator interface, greater data accessibility, a reduction in testing time and cost, and increased payload and personnel safety. Additionally, a new data system was needed for year-2000 compliance.

This paper discusses the incorporation of the Thermal Vacuum Data System (TVDS) within the thermal vacuum lab at GSFC, its features and capabilities and lessons learned in its implementation. Additional topics include off-center (Internet) capability for remote monitoring and the role of TVDS in the efforts to automate thermal vacuum chamber operations.

INTRODUCTION

The Space Simulation Test Engineering Section at GSFC provides twelve test facilities that range in size from 2'x2' to 27'x40' and are spread out across two buildings. Nine thermal/vacuum chambers and two temperature/humidity chambers are located in Building 7. One vertical thermal/vacuum chamber is located in Building 10. All chambers can operate on a 24-hour per day schedule with three shifts of operations crews overseeing command and control for each chamber and its associated test. Because of the volume of testing and the large layout of the laboratory chambers and control systems, it is necessary to have a central point of data acquisition and test monitoring.

The previous data acquisition system was a proprietary network of terminals and scanning modules running HP-BASIC. The facility and payload data were scanned by separate modules. A typical chamber monitoring setup would include one monitor for tabular data displays and one monitor for graphical data display. Locally connected printers provided hard copies of data.

The goal of TVDS was to create a centralized, flexible, user-friendly and up to date system using off the shelf software. Required features included the following

1. Integrate facility and payload data into a single data source
2. Provide secure dependable data storage
3. System must communicate over a secure, private local area network (LAN)
4. Each client workstation must be fully customizable in terms of data display
5. System must be flexible enough to integrate with automation SCADA systems as well as be able to adapt to future needs of the lab
6. All data must be archived and readily available for user requests

Additional requirements included sensor alarming, networked printing, and the ability to connect to TVDS remotely.

DESCRIPTION

The new thermal vacuum data system (TVDS) was developed on an Oracle database using PowerBuilder for the graphical user interface. These two systems are bridged together with a custom C++ SCADA application, which acquires test data from an array of Hewlett-Packard 3852A and VXI data acquisition units. The TVDS application runs on an isolated TCP/IP network and utilizes a dedicated Digital Alpha server that allows for quick and efficient database transactions. Figure 1 shows the basic layout of the system. The network resides completely within buildings 7 and 10 and is isolated from the GSFC network. The advantage to this is limited traffic and superior speed and security.

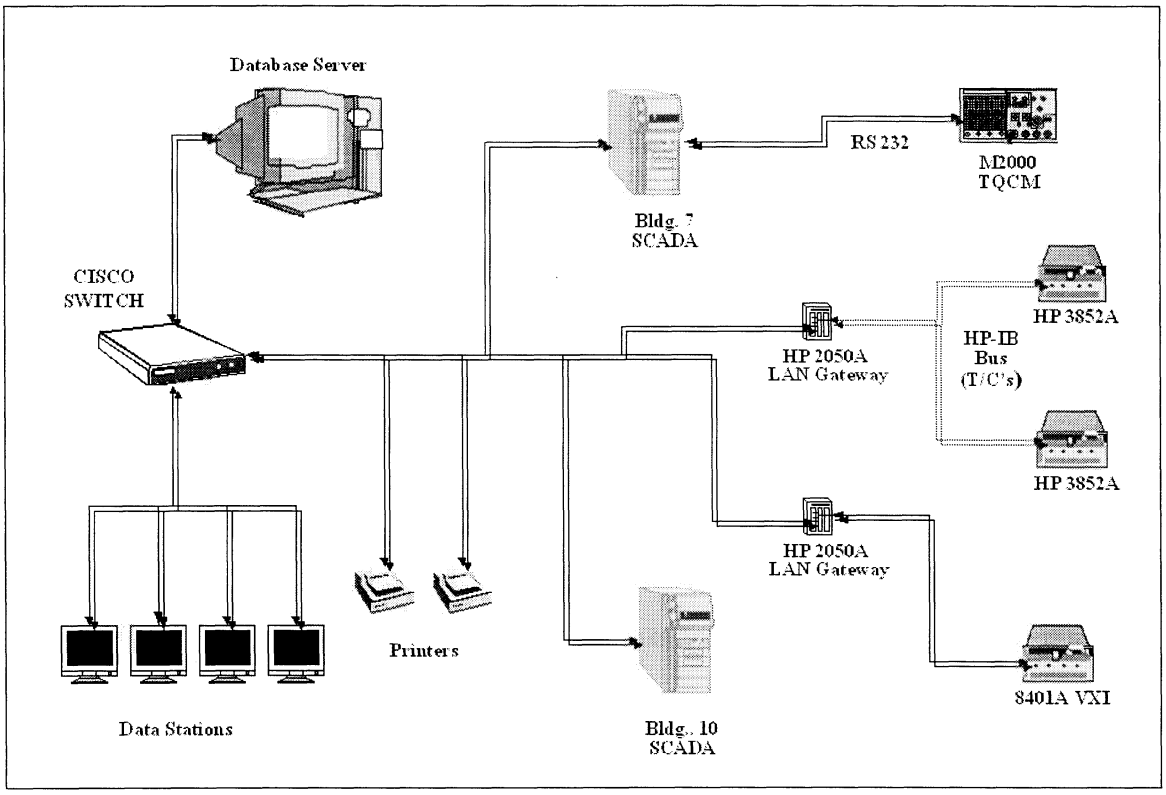

Figure 1 Overview of Thermal Vacuum Data System

Database Server

The database server is the central repository of data acquired throughout lab testing. The database engine, Oracle Server was chosen for its flexibility, robustness and multi-platform packaging. Third party software and applications can easily integrate into an Oracle database. This allows for a wide range of solutions and possibilities as the data system continues to grow. Software already integrated includes PowerBuilder, Intellution, FactoryLink and custom SCADA C++ and Visual Basic applications.

The Oracle server runs twenty-four hours a day on a UNIX platform. The computer is a Digital Alpha Server 2100 5/300 with 256 MB RAM and 18 GB hard drive space. This server uses a RAID 5 setup. All data is routed to and from the database through Cisco Fast Ethernet switch.

Database Structure

The Oracle database is structured into a series of tables based on each chamber. This was done for two reasons. By limiting tables to hold data specific to a facility, the size of the tables may be smaller and easier to maintain, and it allows for a faster retrieval of data. Because of the large volumes of data that are involved in thermal vacuum testing, the speed of data retrieval is very important.

Each chamber has a table devoted for measured test data, a directory of chamber and payload sensors, alarm limits associated with each sensor, and a list of sensors in use (active). Within each chamber's subset of tables, specific test data is referenced by a unique test number. This test number is the primary key that identifies all test parameters, recorded data, alarm limits, and user display configurations.

TVDS Network

TVDS makes use of two network systems: TCP/IP local area network (LAN) and Modbus+. Figure 2 shows how communication with the Oracle server is possible. SCADA and TVDS use TCP/IP protocol for all data transmissions, including SQL*Net transmissions from the SCADA to server and TVDS client-to-server communications. Because the LAN is only accessed by clients using TVDS, network traffic is minimal. This is important because data requests from the TVDS application can often produce large data sets. Historical data display showing data of 8 to 24 hours may take 1 to 2 seconds for retrieval. The number of connections to the system ranges from 6 to 20 connections with each instance updating every two minutes.

Using the TCP/IP protocol, it is also possible to access TVDS through and Internet browser. As shown in the bottom of Figure 2, a link from the Goddard Code 549 website gives access to an application server. This server runs multiple instances of TVDS and redirects their displays to remote connections. This will be discussed in detail in this paper.

The Modicon Modbus+ network is a token ring style system that is used by the programmable logic controllers (PLC) in buildings 7 and 10. PLCs that control valves, motors and pumps can also scan chamber sensors. Automated chambers use SCADA machines to monitor and control these systems. These SCADAs are setup to communicate on both the Modbus+ network using SA-85 network cards as well as the TVDS Ethernet LAN using standard 3Com 10/100Mb adapters.

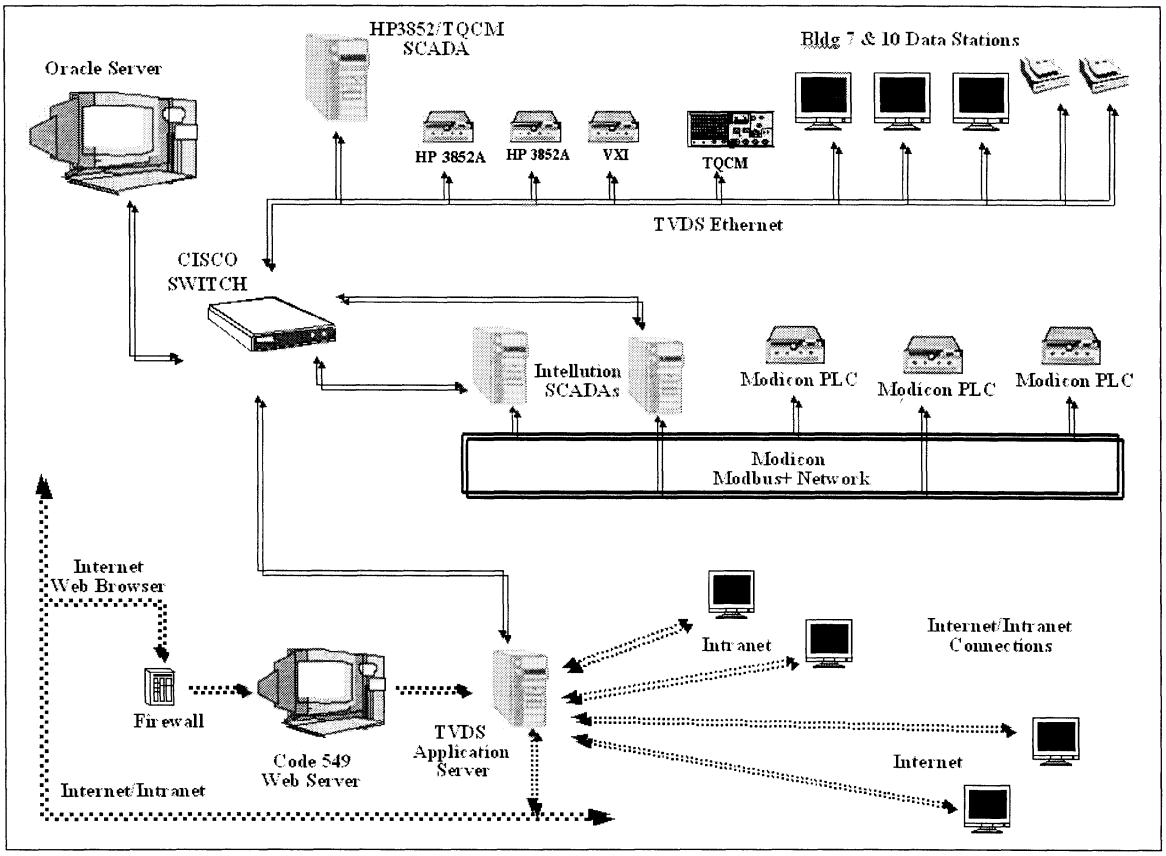

Figure 2 TVDS System Networks

Data Acquisition

Data is acquired by the Supervisory Control and Data Acquisition (SCADA) computers every two minutes and recorded in the Oracle database. Two SCADAs are utilized within the lab for facility and payload data, one for building 7 and one for building 10. Each machine is time synchronized with the database server. The SCADA applications are custom C++ or Visual Basic programs that establish and maintain communication with the acquisition hardware and Oracle database. After each data acquisition cycle, temperature averages and gradients are calculated and written to the database with other measured data. In addition, each measured sensor is compared to its sensor limits. Any sensor breeching a limit (high and low temperature, rate) is displayed in an alarm window on each client station.

Several types of sensors are used during testing including thermocouples, thermistors, silicon diodes, ionization gauges, and capacitance manometers. Four types of data acquisition units are utilized during testing: HP3852, VXI, M2000 and Modicon PLC.

HP3852

The Hewlett-Packard 3852 Data Acquisition System (DAS) is the primary acquisition unit for the lab. All facility and payload thermocouples are scanned at two-minute intervals by an array of HP3852. These units are the same as those used for the previous data system. Because some chambers have a small number of sensors (<50), their scanning is shared with other chambers on a single HP3852 unit. Larger chambers (225, 290) with large sensor libraries require dedicated units. Communication with the network is via the IEEE-488 bus and HP LAN 2050A gateway.

VXI Main Frame

Chamber 290 uses a Hewlett-Packard E8401A VXI Main Frame for acquisition of all payload sensors. Seven high-density C-size E1476A multiplexers are capable of reading up to 64 channels each which is sufficient to scan all of the chamber's payload sensors. The VXI chassis was installed as part of an effort to upgrade and standardize the data acquisition hardware. The HP3852A units, which are now obsolete, will be phased out and replaced with VXI units. VXI data acquisition offers a system-level standard design that can support a variety of hardware manufacturers, provides high transfer speeds, and plug and play flexibility.

QCM M2000

The QCM Research Model 2000 Control Data/Acquisition Unit is used for gathering all thermoelectric quartz crystal microbalance (TQCM) data. This unit is used for outgas measurement and contamination detection during testing. The M2000 communicates with the SCADA over an RS-232 link. The acquisition interface, which runs on the building 7 SCADA was developed using FactoryLink and can control up to 12 devices at once. The FactoryLink application writes all active QCM frequency, temperature and voltage measurements to the database at two-minute intervals. An example of this data is shown in Figure 3.

Modicon 984 PLC

Several of the lab chambers (225, 281, 290) make use of programmable logic controllers (PLC) for temperature and pressure measurement as well as valve, motor, and pump control. Through SCADAs, selected sensors can be written to the Oracle database. The link from Modbus+ to the TVDS LAN is established through Visual Basic scripting in the SCADA applications.

Client Stations

Client station machines are desktop computers with a CPU speed ranging from 300 to 500 MHz and RAM ranging from 64 to 128 MB. Network communication is through a 10/100MB Ethernet network adapter. The TVDS application files require approximately 2 MB of space. Additional software requirements include Oracle Client 8, any FTP utility and a time synchronization utility. The recommended monitor display setting is 1280x1024.

Each client station runs TVDS, the graphical user interface (GUI) or Human Machine Interface (HMI) that is used to display and monitor all tests within the lab. TVDS was developed using PowerBuilder from Sybase. The use of PowerBuilder for the human machine interface allows for a powerful Windows based client/server application that connects to the Oracle Database Management System (DBMS). PowerBuilder applications are developed using PowerScript, an object oriented programming language that lets the developer dynamically control objects throughout the application. Techniques such as encapsulation, polymorphism and inheritance, which object oriented programming provides, allows for efficient, powerful and reusable code. The interface is run from an executable file residing on each client computer. By running the application from each client, the server can be used exclusively for writing and retrieving data.

The interface is designed so that each chamber may be monitored from any computer at any time. Each computer independently retrieves data from the database tables. This allows for unique custom display editing of the same test for every computer

The presentation of data within the application can be customized both before and during the test without interrupting incoming data or other computer displays. Options available to the operator include activating or deactivating sensors or tags, setting alarms for any tag, configuring and monitoring multiple TQCM devices, create and edit averages and gradients dynamically, access to tag libraries and printouts of all relevant data and test information. Data can also be saved and exported to a variety of file types including text, Microsoft Excel and Data Interchange format.

Data can be presented in two formats: tabular and graphical. Both formats can present current test as well as historical data. Figure 3 shows both tabular and graphical display of TQCM data. The left side shows historical data, and calculations. The two plots on the right side show one hour of temperature and frequency data.

By allowing the operator to customize each screen through simple screen editors, relevant data can be grouped together in any fashion so that tests can be monitored safely. The tabular data format displays measured test data on tab pages in columns. Each tab page can display up to 160 tags and an unlimited number of tab pages can be defined for each chamber. Data displayed in graphical or plot form is useful for monitoring trends during a test. Up to eight tags can be displayed on each plot and an unlimited number of plots can be defined for each chamber.

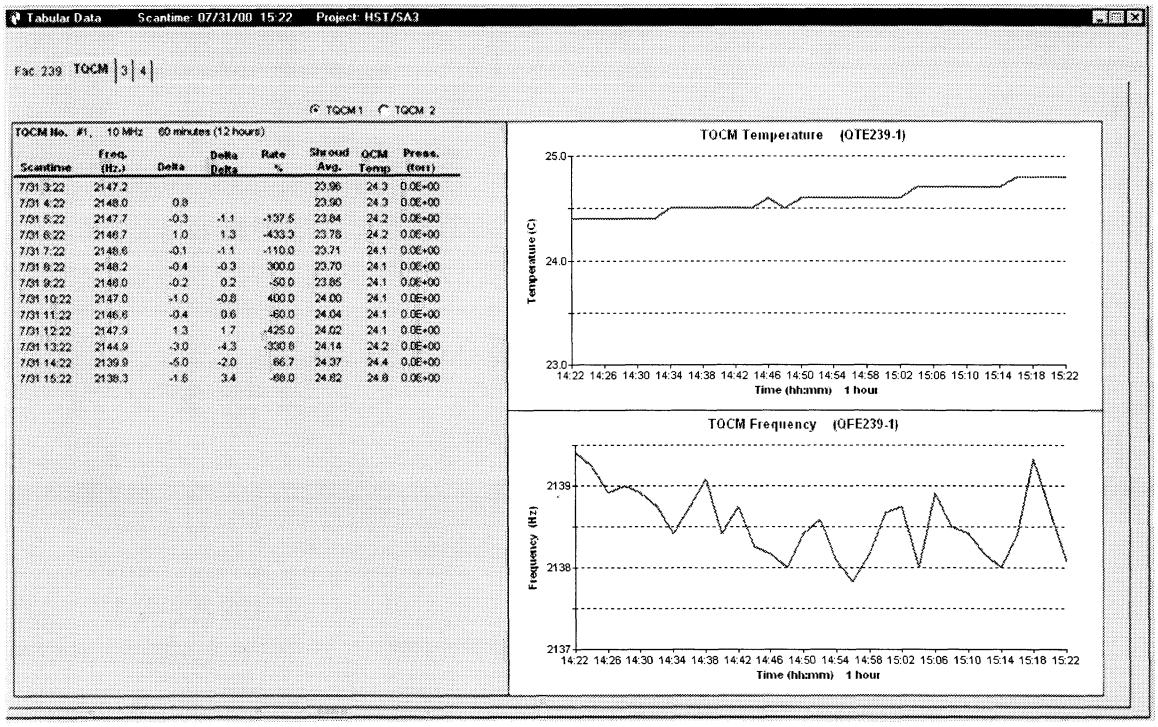

Figure 3 Tabular and Graphical display of TQCM data

TVDS FEATURES

Several features exist within TVDS that make it useful to both test operation crews as well as test projects. These features include near real-time monitoring, customized displays, shared displays, constant alarm monitoring, alarm limit editing, and remote connections.

Monitoring

Each client running TVDS automatically updates any windows showing measured data. Updates occur every two minutes on the odd minute. The SCADA machines update the database every two minutes on the even minute. Therefore, there is a one-minute lag between the data acquisition and data refresh. Because of the volume of data recorded and the necessary calculations and limit checks, it is necessary to ensure that the SCADA application has been given sufficient time to insert and update the appropriate database tables. In addition to updating data displays, any alarms associated with the monitored tests will display as well.

Alarm Limit Monitoring and Editing

As each sensor is collected by the SCADA, its value and rate of change is compared to its stored limits. Tables of limits for each chamber are configured at the beginning of a test. These limits can also be modified at any point during the test through an alarm limit editor. Font colors are used to display sensors that are under alarm. Red and yellow are used for temperature limits and blue for rate limits.

When the SCADA determines that a sensor has passed a limit, its value, limit and scantime are entered into an alarm table. For each test enabled on a client machine, TVDS checks the alarm table for each chamber. Any entries for that scantime are immediately posted in a small window, as shown in Figure 4. An audible alarm is also available and sounds for each update that has an alarm. The alarm window will remain on top of all other open windows and displays each entry in a color specific to its type of alarm: yellow or red for If the tabular display or summary page is displaying the sensor(s) under alarm, they will be shown in the alarm color as well. Note that in Figure 4 there are two sensors in blue in the first column as well as one sensor in the second column.

Customized and Shared Displays

An important requirement of TVDS was to allow each client to create and modify all tabular and graphical screens as needed. This is accomplished through a series of screen editors that can be used at any time during a test. For any chamber that is under test, a client can create two types of displays: tabular or graphical. As shown in Figure 4 tabular displays show data in four columns per tab. Within each column, the sensor or tagname is given along with its current value and location in the chamber. The user has full control over the layout of tags on each tab and may add or delete tabs as needed.

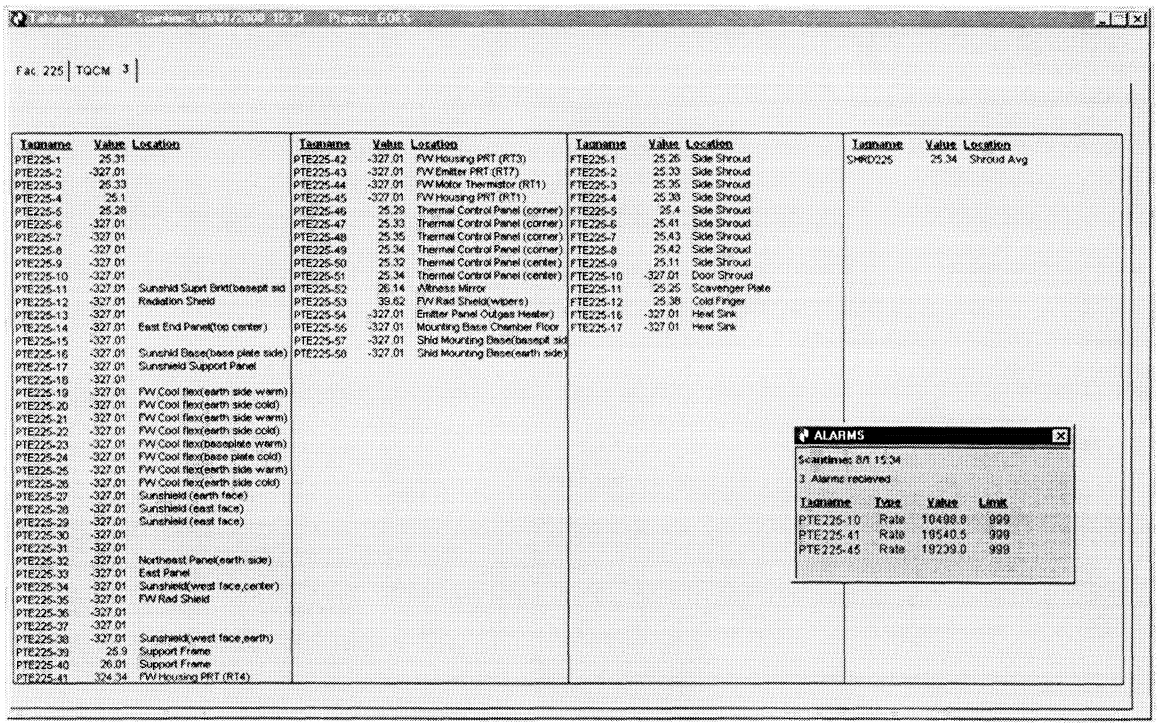

Figure 4 TVDS Tabular Display

The second method of displaying data in TVDS is graphical. Each plot can display up to twenty-four hours for eight sensors. In Figure 5, fours hours of data is shown for three payload sensors in Chamber 239. At the bottom of each plot, the legend displays the sensor name and its location within the chamber. Properties on this plot that are configurable by the user include the scale of the time and value axis, the amount of data retrieved, autoscale, auto scroll, plot title, background color, tab title and plot resize. Plots can also automatically adjust line types for black and white printing. As with the tabular displays, there is no limit to the number of plots the user can create.

Displays can also be shared or copied from other client stations. This allows projects to set up one station and quickly copy the displays over to other machines. This can be done when a display is first created or at any point during the test.

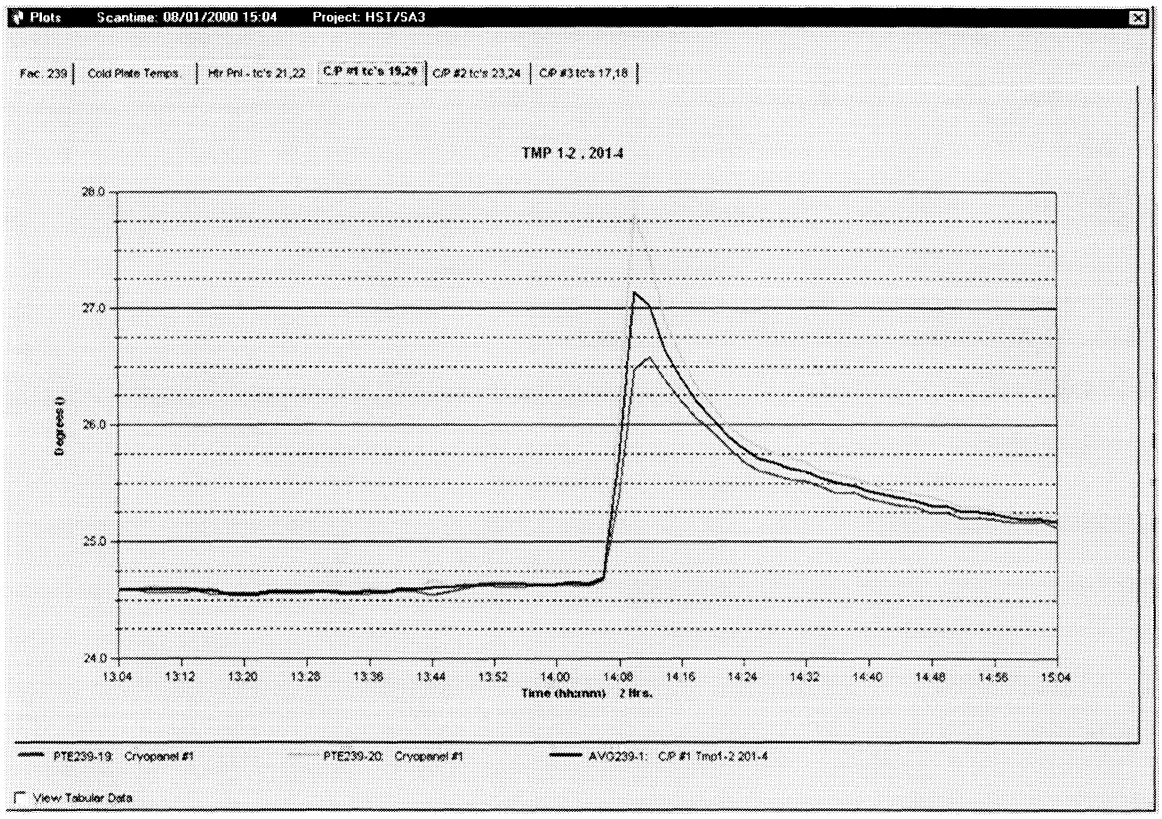

Figure 5 TVDS Graphical Display

Remote Connections

During a test, projects often require the use of several data stations. Projects members and engineers often request to have access to TVDS from their own computers. The data system operates on a private network in building 7 and 10. The obvious limitation to this is that computers on other networks cannot access test data. An additional limitation to this client-server network is that each client must have Oracle Client installed. Therefore, each client outside of the TVDS network must have access to the software as well as a license run it.

In order to provide computers outside of the TVDS network with access to the TVDS application, an application server was implemented using Sybase's Web Development Kit. As shown in the bottom of Figure 2, remote clients connect to the application server through an Internet browser. For the initial run, the client downloads a small executable that allows it to communicate with the application server. The application server then establishes a secure communication path, starts an instance of TVDS and redirects the graphics to the client. By running each instance of TVDS on the application server, data transmission remains within the TVDS network and only graphical images are transmitted to the user. In this way, the remote client can run the

application without any loss in program functionality and without any TVDS application files or Oracle software or licensing.

TVDS AND AUTOMATION

The automation of test chambers within the lab requires the design and implementation of computer interfaces that permit monitoring and command control. TVDS is designed to easily work with automation interfaces. The primary role of the data system in chamber automation is saving important data scanned by automated processes. This task is performed on a chamber's SCADA machine and runs as a background process. Integrating the data system into automation projects provides seamless transmission of data. TVDS is able to utilize this and display any data that a SCADA system can record.

ACHIEVEMENTS, PROGESS AND ISSUES

The new data system was brought online in November 1998, and by January 1999, the new system was recording data for all the lab chambers. By the summer of 1999, TVDS was integrated into the Chamber 290 automation project. This SCADA is responsible for acquiring all of the chamber thermocouple data. Additional projects that required the use of TVDS include a new remotely operated heater rack system that was brought online in March 2000, and a simulation/prediction model used for projecting thermocouple temperatures during a test. The new data system has recorded over 500 tests and over 67,000 hours of test data through July 2000.

The TVDS application has undergone several minor modifications since it was brought online. While some of these modifications involved code debugging or database table changes, the system has had no significant down time or failures. Feedback from the project members and operations crews has provided useful information regarding changes or improvements and future releases.

The thermal vacuum lab is a 24-hour, 365 days a year facility, therefore, the data system must run continuously. Because of this constant influx of data, large amounts physical storage space is needed. As in any networked database system, every effort must be made to maintain reasonable table space. Storage space is the primary issue for the new data system. Some tests may use several hundred sensors in a chamber that may run for several weeks. The measured data, along with any recorded alarms may require several hundred megabytes of space. To maintain safe levels of free disk space, the data of completed tests are backed up to tape and CD-ROM and removed from the server. The completed test data is available for requests in ASCII format. The complete test and all database tables are also backed up in a compressed Oracle export file.

FUTURE GOALS

TVDS will continue to grow and change as lab needs dictate. As part of the original design, TVDS is flexible enough to integrate with other applications and communicate with other systems and networks. The automation project of chamber 238 began in March 2000 and will require data logging with the new data system. This will require an Intellution based SCADA system similar to that of chamber 290 mentioned above that scans and writes facility data to the database.

Another goal of the data system involves the standardization of data acquisition hardware. With the rise of VXI as an industry standard and a variety of manufacturers that support VXI data acquisition, it is a logical choice for replacing the HP3852 units used throughout the lab. This step towards standardization within the lab has started with chamber 290 as mentioned earlier.

A third goal of the new data system will be to investigate and possibly incorporate fiber optic networking into the lab. While sections of the Modbus+ network already uses fiber optic, the standard twisted-pair Ethernet LAN cabling is vulnerable to electrical interference, which can often present cable routing challenges within the lab. Fiber optic cable would eliminate the issue of networking in an electrically hostile environment. In addition, because fiber optic is capable of carrying large volumes of several types of data, it may be possible to combine the data transmissions of Modbus+ and TVDS into one fiber optic system.

Additional goals of the thermal vacuum data system include modifications to TVDS that allow for quick setup of tests. This would include an automated process of updating database tables relating to sensor descriptions and alarm limit configurations. The post-test distribution of data based on user request is another feature that will be automated.

CONCLUSIONS

The upgrade of the thermal vacuum data system for Space Simulation Test engineering lab at GSFC has produced a flexible, robust and dependable system that can provide and array of test monitoring and support capabilities. By establishing a centralized acquisition system, projects and operation crews can realize an increase in data accessibility, as well as an overall reduction in testing costs and payload and personnel safety. With over 67,000 hours of test monitoring completed in less than two years, the data system has established itself as a reliable tool of GSFC's thermal vacuum testing process.

VISUALIZING SPACE SIMULATION TEST THROUGH THE INTERNET

Luiz Alexandre da Silva, Anderson Luiz Portela and Elbert E. N. Macau
Laboratório de Integração e Testes - LIT
Instituto Nacional de Pesquisas Espaciais - INPE
Brazil

ABSTRACT

With the increasing number of joint projects for spacecraft development, it is a necessity that an environmental test can be followed from remote locations. New technologies that have been created for the Internet environment, like Java and fast networking, may provide the appropriate framework to support the development of remote visualization software. However, there are fundamental issues that must be considered, like data acquisition systems interconnection, efficiency, security, and tools support the software analysis, project, and implementation. In this work we present the experience of the Brazilian Institute of Space Research/Test and Integration Laboratory (INPE/LIT) in issues that were considered for the development of a visualization software to allow the following of thermal-vacuum tests through the Internet.

I - INTRODUCTION

The number of companies that use the Internet as the highway to support their necessities for people integration and data consolidation is increasing. Around the world, employees can have access to large and on-line data base, and management systems that allow the company to operate as if everybody were working at the same place, at the same time. It is the power of technology that makes globalization easy.

In this work, we present a project that is being conducted at INPE/ LIT with the goal of allowing people in different locations of the world to follow environmental tests that are taking place at the space simulation facility as if he or she were standing at his or her computer locally. To enable this, the system is being developed in JAVA and exploits the resources that are available for Internet access and network interconnection. This system is called *System for Visualization of Space Simulation Test Through the Internet (SYSVITI).*

At this time, besides its participation in the development of the International Space Station, INPE is working together with partners from other countries (Argentine, China, French, German) in developing satellites for scientific research, remote sensing and environmental data collection. The SYSVITI will make the interaction of these multi-nation teams easier, not only by allowing the visualization of ongoing tests, but also permitting the analysis of data stored from concluded tests. Thus, this system can be considered as a key factor for the success of the ongoing project in wich INPE is engaged.

This paper is organized as follows. In the next section we describe the current visualization system at LIT. In Section III we describe the SYSVITI architecture and its resources. Section IV describes the technologies that are being used in the development of the project. In Section V we present the conclusions and general comments regarding the system.

II- CURRENT VISUALIZATION SYSTEM

The diagram of the current visualization system for environmental tests appears in Fig. 1. It was developed for the MS Windows platform using the software LabVIEW. During a test, the data acquisition system is responsible for keeping the test data in a database. The visualization system interacts with the data acquisition system to get the data requested for the clients and to show the most recent test data available. It also allows the interaction among the clients, data analysis and the recovery of stored data from finished tests. The system is an in-house development, and it is enough to support all the requests from the teams that are interested in following the environmental test or analyzing its data. Any computer connected to the local network can be used for the visualization purpose just by installing the visualization software. The drawbacks of this system in regard to remote access are that it requires a high speed network to support it, the visualization software must be installed in the remote machine, and the remote machine must use MS Windows as its operational systems.

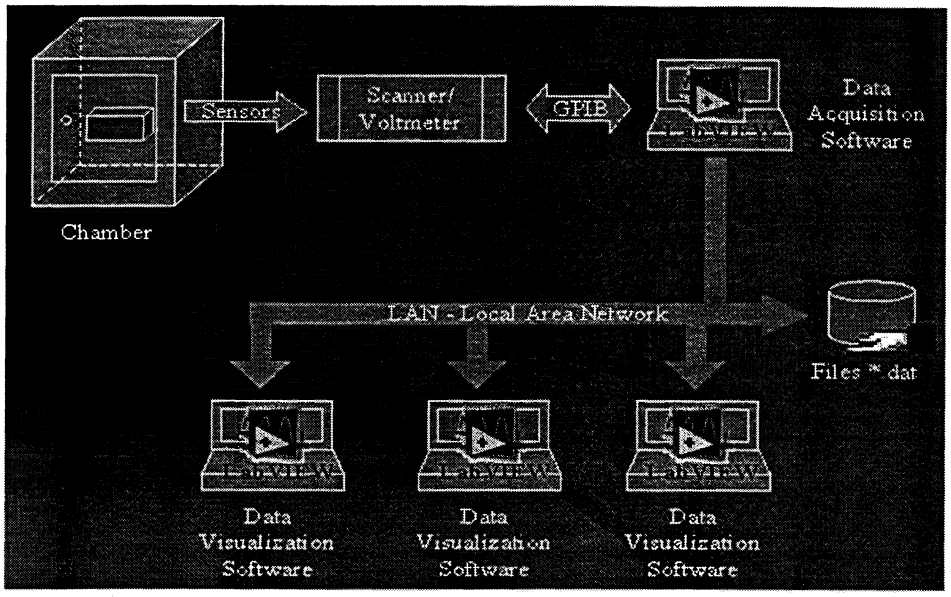

Fig. 1: Current visualization system diagram

III- SYSVITI - ARCHITECTURE AND MAIN CHARACTERISTICS

The schematic diagram of the SYSVITI is shown in Fig. 2. All its modules were developed in JAVA, with the exception of the data base which uses Oracle. It means that it was designed to be used in an Internet environment. Any computer that has access to the Internet, in principle, can be used to visualize environmental tests that are going on at LIT, independent of the operational system it uses. To accomplish this, it is just necessary to know the web site address for the system. All the modules, applets JAVA, and data are downloaded form the SYSVITI server to the visualization computer through the Internet, no matter in which part of the world this computer is located. Applet are used instead of dynamic HTML page because the applet have powerful GUI resources.

The SYSVITI is interconnected to the data acquisition system through a program interface that was made using LabVIEW. Thus, just minor changes were introduced to the data acquisition system to allow it to properly interact with the SYSVITI. This interface module continuously sends status information of ongoing tests and the data being generated by the tests to the SYSVITI.

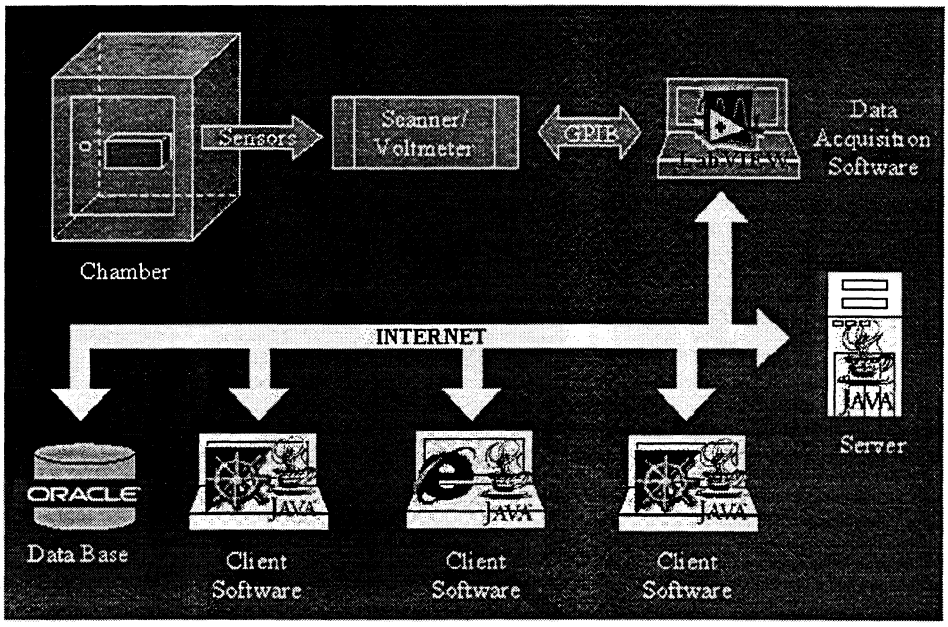

Fig. 2: SYSVITI Diagram

The system architecture of the SYSVITI can be seen in Fig. 3. It presents the following main parts:

- Data base, developed in Oracle in which all the data coming from the data acquisition system are stored;

- Server module which is responsible form the system management;

- Data acquisition interface module, which is responsible for the interaction between the SYSIVTI and the data acquisition system;

- Visualization applet, which is downloaded from the server to the visualization computer and is responsible for the visualization tasks and the interaction between the user and the visualization server.

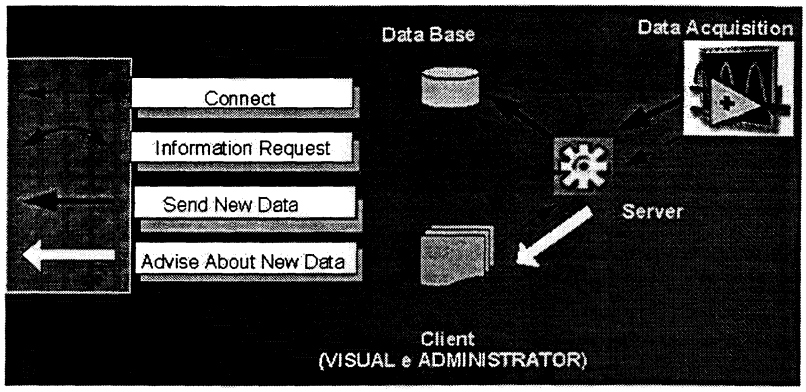

Fig. 3: SYSVITI System architecture

During a test, the data set presented to the user of the SYSVITI is updated at the same rate that is used by the data acquisition system to get and process measuring data. At any time the user can access previously recorded data, or can use system analysis tools to perform customized analysis on the data set. Additional features include multiple windows for simultaneous data visualization. Also alarm levels can be assigned to any number of channels, messages can be exchanged among the users, continuous actualization of the test status, mathematical processing over the channels, hard copies, definition of any number of user-definable channels (pseudo-channels).

The data from the data acquisition system are available to the user through entities called channels. The channels are identified by numbers and names, and can be presented to the user in four available formats: *Flash mode*, *matrix mode*, *temporal flow*, and *graphic mode*, according to the user's preference. One typical visualization window that combines different visualization formats can be seen in Fig. 4. In the flash mode, the data are presented in a two-dimensional table. In each position of the table the instantaneous value of a channel together with its number, identification, and unity of measurement is shown. Each position of the table is updated as soon as new data for the respective channel is received by the SYSVITI.

In the matrix mode, the data is also presented in a two-dimensional matrix. However, here, just the instantaneous value of a channel appears. As a result, for one specific screen resolution, a larger number of channels can be displayed in this mode than in the previous one. The identification of a specific channel and its units can be seen by just passing the cursor over the respective position of the channel in the matrix. This resource is shown in Fig. 5.

The instantaneous value of the channel together with an user definable number of previous in time measured values for the channel appear in the temporal flow mode. It is a very convenient way to follow dynamical changes in the channels. The drawback of this mode is that it is the visualization mode that presents the smaller number of different channels in a visualization window.

Graphics of the channels can be presented in the visualization window using the graphic mode. Ten channels can be plotted together in each graphic window. The dynamical evolution of the system can be followed by using the temporal auto-scale mode for the axes of time. In this mode of operation, each time one curve fills the whole axis of time, all the curves are shifted to the left with the instantaneous time plotted in the position equal to

3/4 of the next scale for the axes of time.

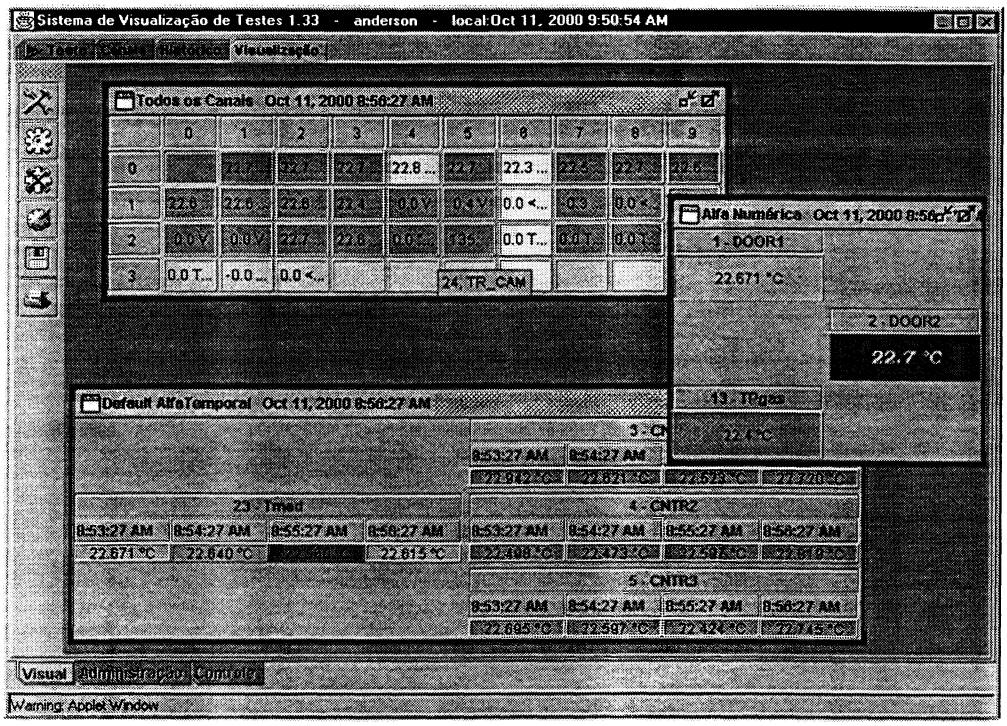

Fig. 4: Typical visualization window

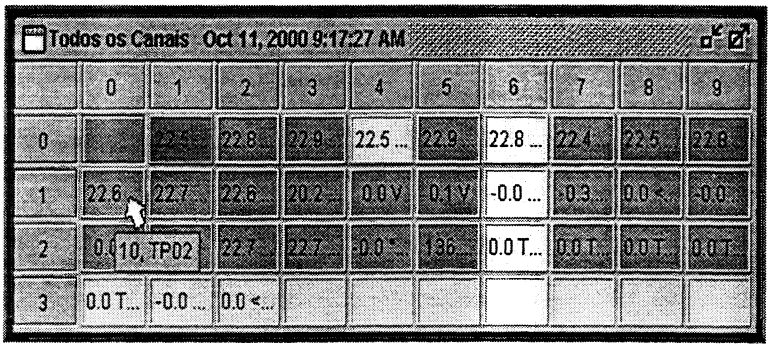

Fig.5: Toll tip function detail

The user can define as many visualization windows as he or she wants. The system allows a quick call of the defined windows, and as many windows as desired can be simultaneously presented on the screen. The use of each individual window is definable in related to its formats. Thus, the user can define the channels to be presented, the position of each channel in the visualization window, the colors and visualization resources (blinked rates, shadow effects) associated with it, the number of decimal digits, the format in which the number is presented etc. In Fig 6 the channel attribute menu associated to a specific visualization window is shown. The task bar that allows the generation of new visualization windows is presented in Fig. 7.

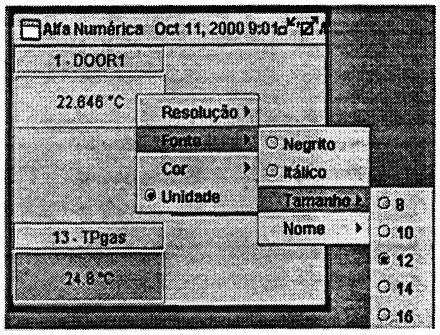

Fig. 6: Channel attribute menu detail

There is a management module through which all the administrative tasks in SYSVITI are carried out. Besides the execution of configuration changes to the system, this module allows the definition of users, groups of users, and its privileges, access codes and passwords, the specification of computers that are allowed to access data from specific tests or programs, the assignment of priority levels for sending data, status information, and routing messages.

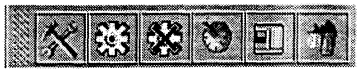

Fig. 7: Task bar detail

A user can access the system by using any browser that supports Java. When the user accesses the web page of the SYSVITI, he gets the web page that appears in Fig 8. Using it, he or she can select the language to be used for interacting with the system, and input its user code and password, which is validated by the system. After that, according to the privilege assigned to him or her by the system manager, he or she can visualize on going or already finished tests and perform analysis on the data.

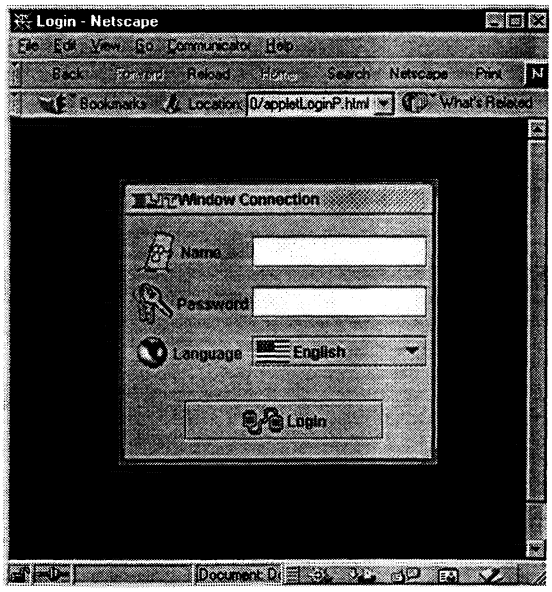

Fig. 8: Applet seem by user

IV - ENGINEERING TOLLS USED IN THE DEVELOPMENT OF SYSVITI

The system is being developed according to the software engineering methodology named *CRC/WB+* [Fernandes96]. This methodology was created by the Brazilian Aeronautical Technological Institute (ITA), located in São José dos Campos, São Paulo State, Brazil. It is an evolution derived from the methodologies CRC [Ambler95, *Fowler97*], Wirfs-Brock [WrifsBrock90] and Love [Love93] and was created to allow the full development of systems, from the designing phase to the implementation and test, based on the object oriented paradigm. During the development of this project, the CRC/WB+ methodology was extended to support the development of distributed systems.

For the code implementation, the development environment *Visual Age* from IBM, was chosen. This choice came after comparing it with other development environment available at the time when the project development started. Visual Age has unique characteristics that make the development easy, such as version control, multilingual support for messages, integrated environment, support for importation of compacted classes. Furthermore, it is a freeware, and runs in multi-platforms and operational systems.

V - CONCLUSION

The *System for Visualization of Space Simulation Test Through the Internet (SYSVITI)* is being developed to allow people in different locations of the world to follow the environmental tests that are taking place at LIT. This system facilitates the interactions of different teams in the development of cooperative space projects. The system is based on the Java language, which allows its access and operation by using any Internet browser that supports

Java.

New methodology of Software Engineering is being used in the development of the project. This methodology was extended to the development of the project to support distributed systems. The code implementation is being done by using the software Visual Age from IBM. A beta version of the *SYSVITI* was released and is being used for system test and validation.

REFERENCES

- [Ambler95] AMBLER, S., "Using Use-Case". Software Development. July 1995.
- [Flowler97] FOWLER, M. and SCOTT, K., UML "Distilled: Applying the Standard Object Modeling Language". Addison-Wesely, 1997.
- [Fernandes96] FERNANDES, C. T., "Desenvolvimento de Software Orientado a Objetos: a Metodologia CRC/WB+". II Workshop de Orientação a Objetos, Programa de Engenharia de Sistema e Computação, COPPE/UFRJ, Rio de Janeiro, RJ, 10 dezembro de 1996, pp. 14-17.
- [Love93] LOVE, T., "Object Lesson – Lessons Learned in Object-Oriented Development Projects". New York, NY:SIGs Book,1993.
- [Wirfs90] WIRFS-BROCK, R., and WILKERSON, B., and WIENER, L., "Design Object-Oriented Software". Englewood Cliffs, NJ:Prentice Hall,1990.

Automation of Space Simulation / Thermal Vacuum Test Facilities – the Basis for an Efficient and Future-oriented Test Operation

Frank Resch, Franz Kiener
IABG mbH, Einsteinstrasse 20, D-85521 Ottobrunn, Germany

ABSTRACT

For the future of space simulation testing cost efficiency and facility reliability is mandatory. Especially the operation of space simulation and thermal vacuum test facilities requires a high level of personnel involvement. Due to the 'around the clock' testing for days and weeks the cost saving potential of such kind of operation is significant. The implementation of automation systems is one prerequisite for the improvement of efficiency and reliability and is - in case of new facilities - meanwhile standard practice. However, already existing facilities based on elder control techniques require an extensive redesign of the control system in order to cope with the new technologies.

During the past 5 years the Space Simulation Facility and three other Thermal Vacuum Test Facilities of IABG were modified such that all important facility sub-systems were equipped with Programmable Logic Controllers (PLC). Further a Windows NT based command and control system was installed enabling both, operation of the facilities from a central control room as well as from a local terminal directly at the facility.

In parallel a new network based data acquisition system was developed which delivers the test data via the LAN to customer and operator workstations. The data acquisition system is linked to the command and control system such, that test data can be used for an automatic control of the test facility.

Due to the implementation of the automation system the thermal vacuum test facilities can now be operated with significantly reduced personnel and with an improved reliability and quality.

Further potential for efficiency improvements is identified on the customer side because data presentation and analysis must not necessarily be limited to the test site but can also take place outside, e.g. at the customer site. This will reduce the customer's personnel involvement during a test and therefore will result in further cost optimization. Currently IABG is deeply involved in studies for the realization of such data distribution systems.

1 Introduction

Effective test control presumes suitable facility control systems and data handling systems. The availability of the facility's housekeeping data and the test article measurement data at a central location (control room) allows an efficient control of the test facility.

In case of a parallel operation of various test facilities a central monitoring and control system combined with the test article data acquisition system reduces the need for operation personnel significantly. However, depending on the test requirements, a local control and operation of the individual test facility may also be useful.

This results in a design concept that must provide both, centralized and local facility control and operation systems combined with a network based data acquisition system for test article measurements. Furthermore the availability of test data at the customer's home base via the Internet can improve the efficiency in the field of Thermal Testing.

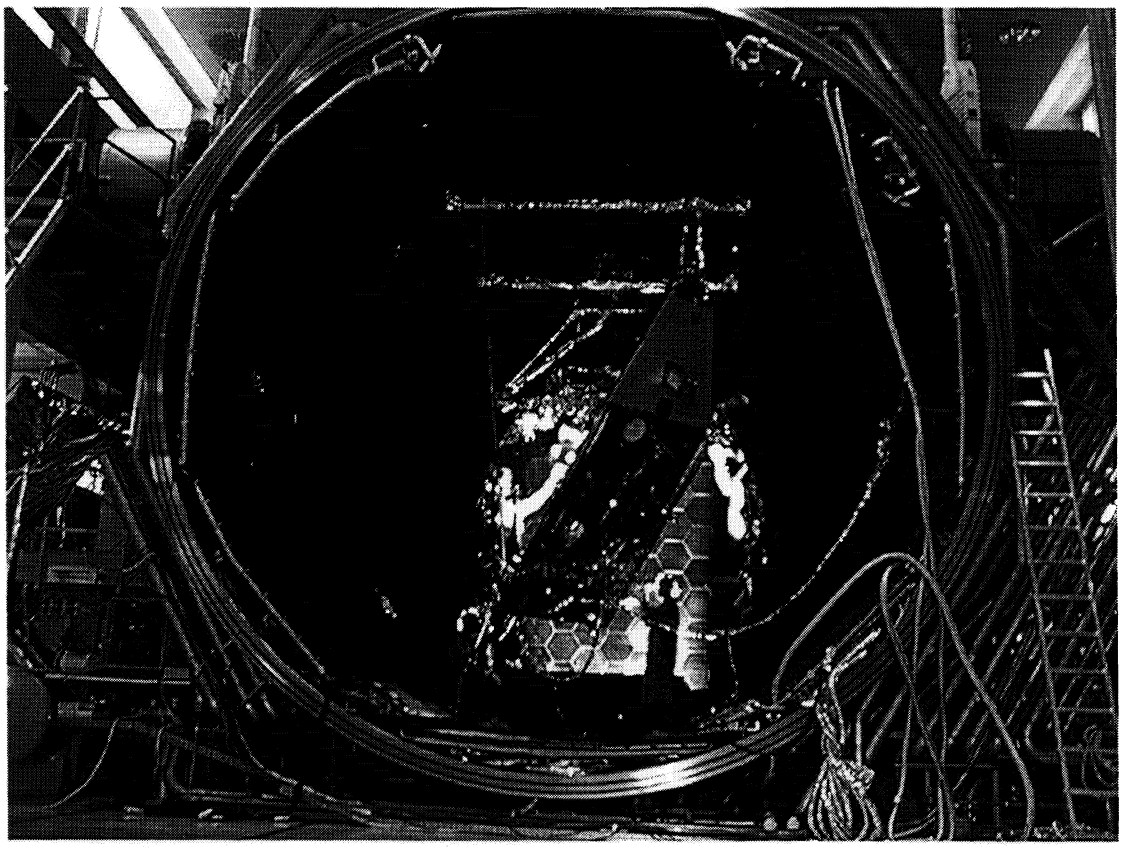

Figure 1-1: Space Simulation Facility WSA/TVA with Champ Satellite

2 Overview of the Relevant Test Facilities

IABG operates in its Space Test Centre four Thermal Vacuum Test Facilities. These facilities are used for the whole range of thermal qualification of space related products. From component level up to spacecraft level suitable facilities are available. Figure 2-1 gives an overview of the IABG TB/TV Test Facilities and their location.

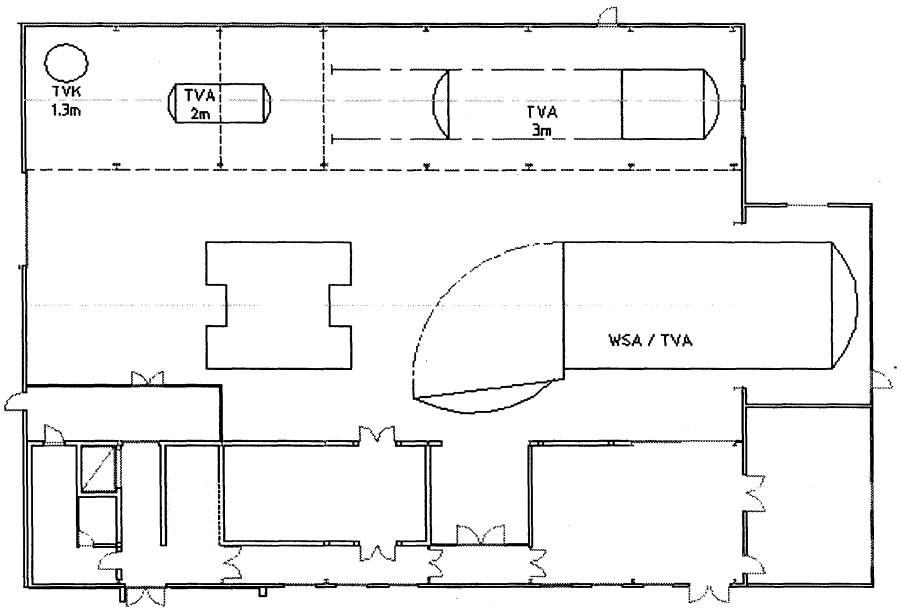

2.1 *Space Simulation Facility*

The Space Simulation Facility (WSA/TVA) is used for Thermal Vacuum and Thermal Balance Tests, which are usually performed on system level.

Vessel	- Horizontal stainless steel vessel - 7 meter diameter - 12 meter length
Thermal System	- Stainless Steel Shrouds - Central closed loop LN2/GN2 supply system - Temperature range between -180 °C and +115 °C
Vacuum System	- Central roughing pumping system - 1 turbo molecular pump (1 additional under procurement) - 6 Helium cryopumps (4 equipped with HV-valves)
Sun Simulator	- 7 x 25 kW Xenon high pressure lamps - max. 1900 W/m_ in the test plan - Circular beam with 3.6 m diameter - Rectangular beam with 4.5 m x 3.05 m
Motion Simulator	- 2-axis motion simulator - spin axis for continuos rotation - attitude axis max. 400° rotation
Auxiliary Equipment	- Infrared rig with a total electrical power of about 280 kW (DC) - Videogrammetry installation for distortion measurements under TV conditions

2.2 *Thermal Vacuum Facility 3m-TVA*

The 3m-TVA is used for Thermal Vacuum Tests on subsystem level and for Infrared Tests on solar panels and reflectors.

Vessel	- Horizontal stainless steel vessel - 3.2 meter diameter - 6 meter length
Thermal System	- Aluminum shrouds - Central closed loop LN2/GN2 supply system - Temperature range between -180 °C and +140 °C
Vacuum System	- Central roughing pumping system - 3 Helium cryopumps, all equipped with HV-valves
Motion Simulator	- 1 axis motion simulator for continuous rotation
Auxiliary Equipment	- Infrared rig with a total electrical power of about 190 kW (DC) - Videogrammetry installation for distortion measurements under TV conditions

2.3 *Thermal Vacuum Facility 2m-TVA*

The 2m-TVA is used for Thermal Vacuum Tests on subsystem level requiring specific cleanliness control or vibration de-coupling.

Vessel	- Horizontal stainless steel vessel - 2.0 meter diameter - 2.1 meter length
Thermal System	- Aluminum Shrouds - Combined LN2 - electrical heating system (open loop) - Temperature range between -180 °C and +130 °C
Vacuum System	- Local oil-free roughing pumping system - 1 Helium cryopump equipped with HV-valves
Auxiliary Equipment	- Vibration damping system (airbags) - Clean class 100 environment

2.4 *Thermal Vacuum Facility 1.3m-TVK*

The 1.3m-TVK is used for Thermal Vacuum Tests on component level.

Vessel	- Vertical stainless steel vessel - 1.5 meter diameter - 2.2 meter height
Thermal System	- Aluminum shrouds - Combined LN2 - electrical heating system (open loop) - Temperature range between -180 °C and +130 °C
Vacuum System	- Local roughing pumping system - 1 Helium cryopump equipped with HV-valve
Auxiliary Equipment	- IR rig

3 Requirements and Goals of the Automation Project

When in 1995 the automation project was launched, various subsystems of the facilities were missing the basic technical conditions for the realization of a PLC controlled operation. Controllers were still pneumatic based, sensors and actuators were not delivering compatible signals and the parts of the control system were based on relay circuit technique. One major constrain for the project was, that the availability of the facilities should not be reduced by the implementation and acceptance of the automation system. Furthermore the following upper level requirements were defined:

- Improvement of the facility's reliability and maintainability
- Integration of a standardized PLC system
- Centralized and local monitoring, command and control of all facilities
- Standardized visualization system for all facilities
- Combined visualization, command and control system
- Availability of a operator panel for local facility operation
- Combination of visualization and data acquisition system for facility monitoring
- Parallel operation of all four test facilities

4 Automation Concept and Implementation Process

During a study and trial phase one of the small test facilities (1.3m-TVK) was used as a prototype in order to develop an adequate command and control system and to gain knowledge and experience for further implementations. After successful acceptance of the prototype a program for the implementation of an entire automation system for all TB/TV test facilities was defined.

For the realization of this program the test facilities needed to be equipped with adequate sensors, controllers and actuators. All relevant facility housekeeping data, such as shroud temperatures, chamber pressure, solar intensity and other necessary data had to be made available to the PLC-system by means of electronic sensors. The implementation was done in a step by step process and subsystem oriented in order to reduce the down time of the facilities to a minimum.

In addition to the PLC-system a command and control system was necessary in order to visualize and command the entire facility via computers. Actual measured housekeeping data of all systems and their control functions are available for the operator on various window screens. Monitoring, command and control of the test facility is accessible via one computer per facility.

4.1 PLCs and Automation Network

For the control system various SIEMENS-Simatic S5/S7 PLCs were installed, programmed either with STEP5 or STEP7 language.

The smaller test facilities (1.3m-TVK and 2m-TVA) are equipped with one PLC each, for the 3m-TVA and the Space Simulation Facility each subsystem, i.e. vacuum system, thermal system, sun simulator and motion simulator is equipped with an autonomous PLC. Those are installed at different locations always close the relevant subsystem.

Each PLC is running autonomously and is independent from all other PLCs. In case of a malfunction, such as computer failures, the individual facility can be locally controlled by means of a simple operator panel.

For the standard case, where the facility is remote controlled the PLCs transfer their data via the Automation Process BUS to their visualization system in the control room. Because of the advantages of modern networks it is also possible to run the facilities via their visualization system from different locations in the test area.

The PLCs have cycle times of some ten milliseconds, so that the data processing can be achieved in adequate time periods and malfunctions of the facility are detected in real-time on PLC-level.

The Automation Process BUS is a star-shaped high speed data network (100Mbit/s). Due to the failure critical environment it is based on glass fiber technique and is equipped with SIEMENS SINEC-H1-components.

Via two HUBs all PLCs and the visualization systems are connected to the network. Each participant owns its unique address and the CSMA/CD access procedure guarantees a faultless data transfer. A bridge enables the visualization system to import housekeeping data from the standard data acquisition system. Figure 4-1 shows the schematic of the automation network.

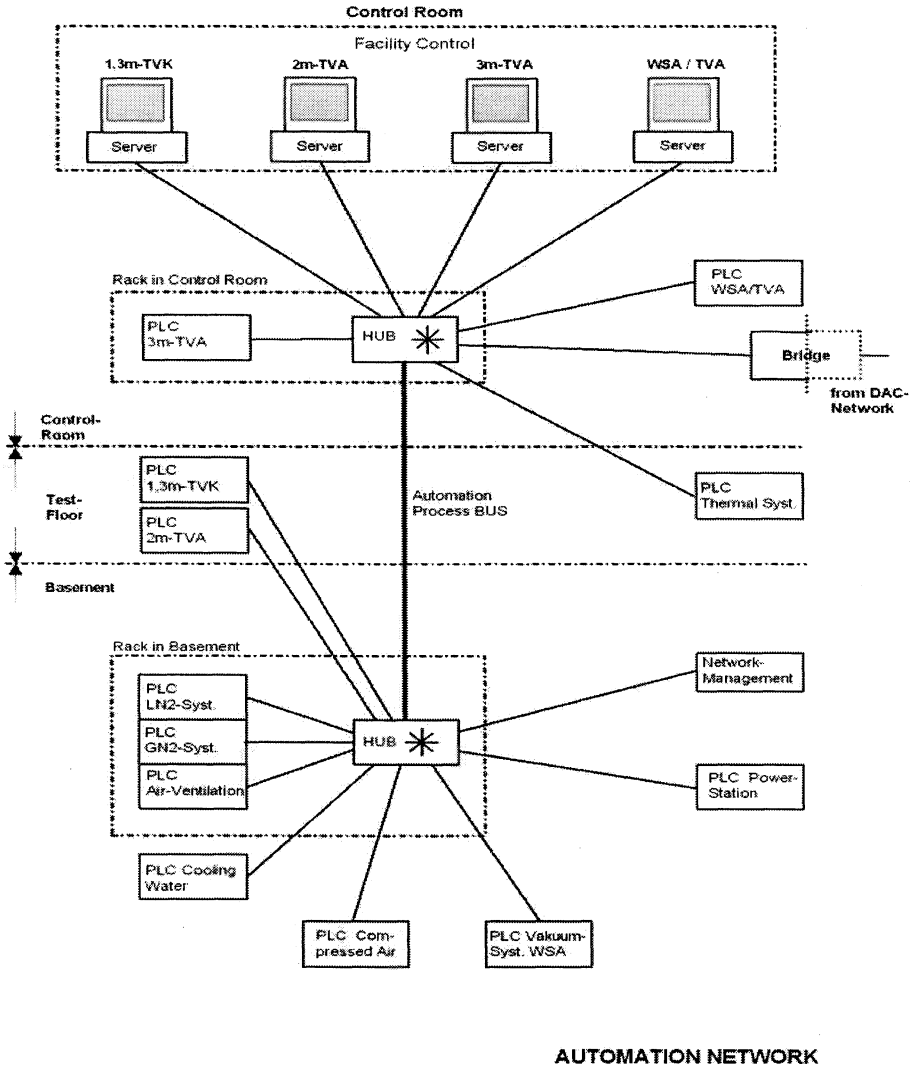

Fig. 4-1: Schematic of the Automation Network

4.2 Facility Visualization System

The remote facility control is realized by means of PC-based workstations, running under Windows-NT and a facility tailored visualization software (Siemens-SIPIOS and Siemens-WinCC).

Each of the four test facilities has its own workstation displaying in various layers and windows the facility status. All information that are necessary for the facility operation are available to the operator in real-time. Typically the small test facilities are described by about 150 signals and 10 layers, the Space Simulation Facility with all its subsystems requires about 500 signals and 30 layers.

The command system, which is directly linked to the PLCs is integrated in this displays. By mouse or keyboard the operator commands the facility. All processed PLC-data are stored in a database, so that historical data, alarms and operations can be displayed and traced

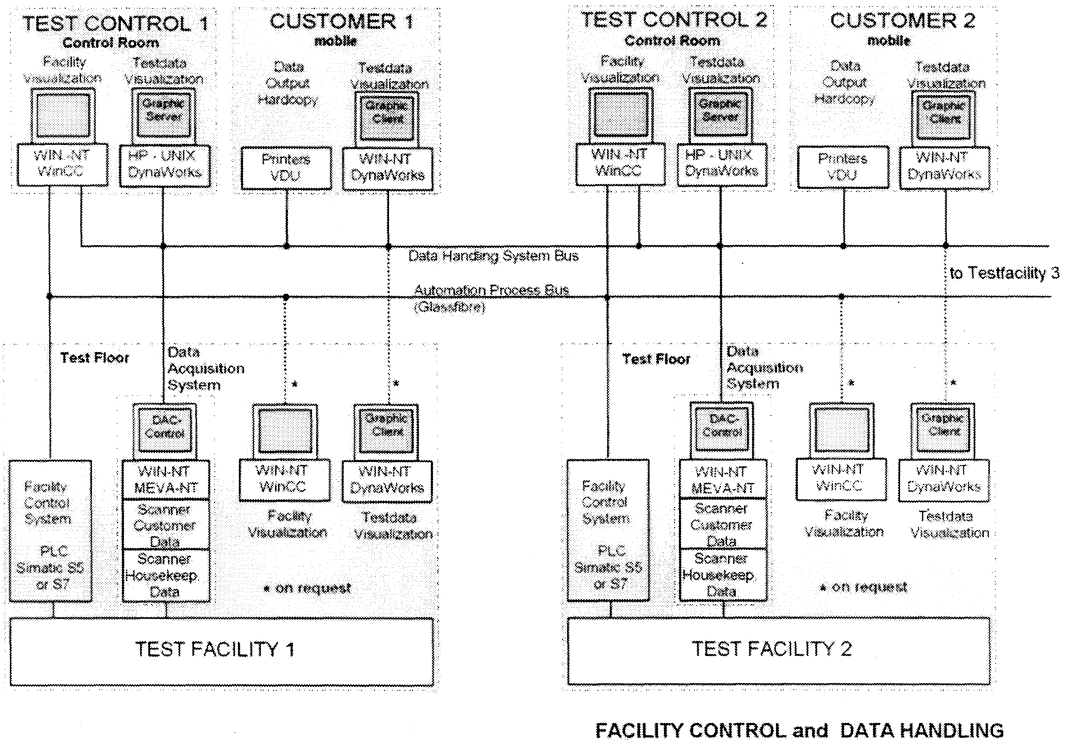

Figure 4-2: Schematic of the Visualization System

4.3 Data Acquisition System (DAC)

Comprehensive facility control in the control room requires besides the facility visualization system a powerful data acquisition system. Each of the test facilities is equipped with a stand-alone data acquisition system, based on PCs and running under Windows-NT. The network-based data acquisition software MEVA-NT, which is tailored to the specific needs of the test customers and facility operators, measures, calculates and presents the test specimen data as well as facility housekeeping data.

For special tasks two mobile DAC systems are available. Depending on the test requirements these systems can handle from 30 (1.3m-TVA) up to 1000 measuring channels (WSA / TVA). By combining the DAC systems via the network 2500 measuring channels can be handled in total.

Via the high speed (100Mbit/s) Ethernet based Data Handling System Network the preprocessed measurement data are transferred to three HP- workstations in the control room. On these servers the DynaWorks® graphical display and evaluation software is running such, that any measured data can be selected and graphically displayed in real-time. The network design as shown in Fig. 4-3 is very similar to the automation network, but is carried out in Cat.5 cable technique.

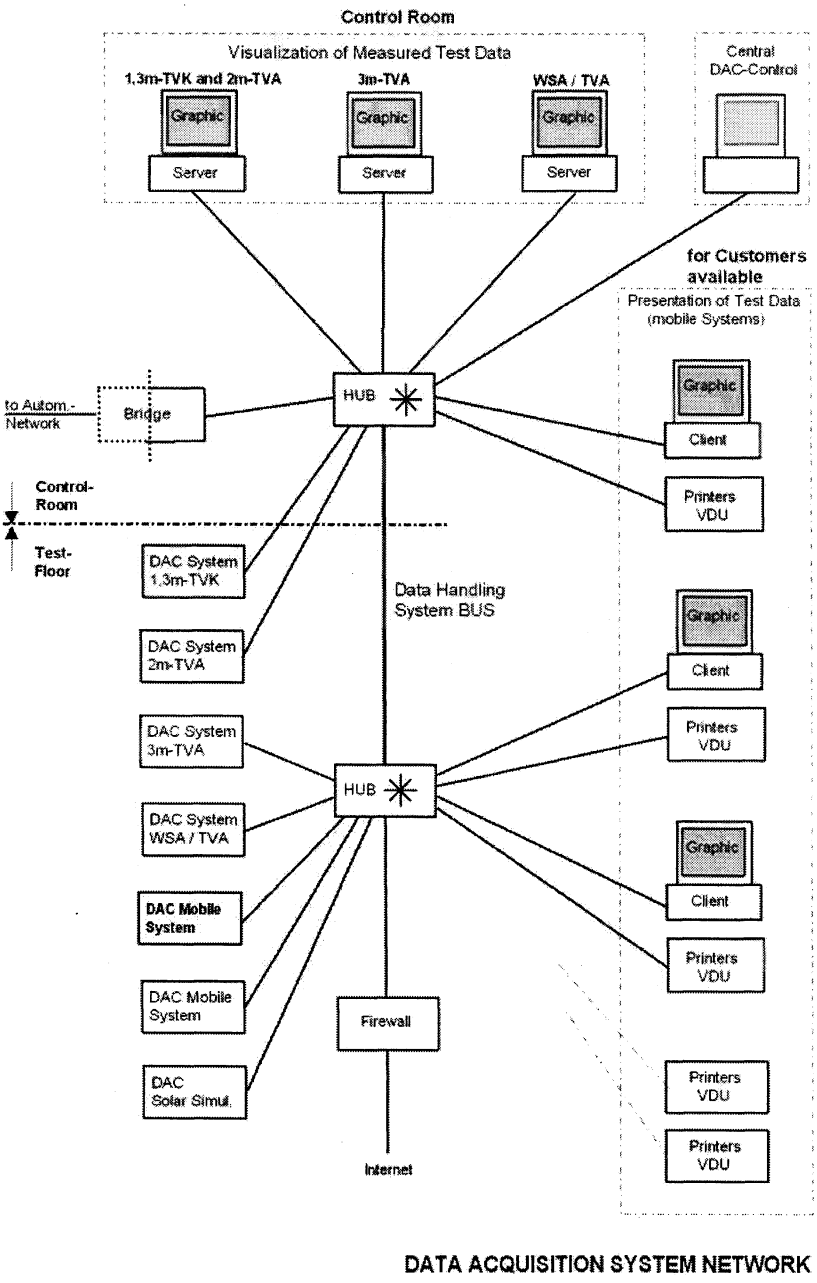

Fig. 4-3: Data Acquisition Network

Furthermore three DynaWorks® PC-clients (operated under Windows NT with Exceed) are available, which are linked to the server's database via the network. In addition pre-processed measurement data can be displayed on printers and VDUs. The DynaWorks® clients, printers and VDUs are mobile, so that the customer has access to the test data at any location in the test centre.

A central DAC control computer in the control room supervises all data handling systems. The data are locally stored on each DAC-system and in addition on a central archive computer.

4.4 Test Facility Control

Effective test control presumes suitable facility control systems and data handling systems. The common presentation of facility housekeeping data and test data at one location gives a complete overview to the current test status. Depending on the test requirements, facility control is needed in the control room or directly at test facility level.

4.4.1 Control Room Equipment for TV Test Facilities

A typical working place for on-line controlling of the small test facilities is designed such, that one operator on duty can run the facility. All test relevant activities can be carried on two monitors.

One monitor visualizes the current facility status while the other monitor displays the test specimen data. Facility control commands are given by using the mouse and the keyboard. Test specimen data can be individually selected, scaled and zoomed so that the operator on duty has a comprehensive overview to the test status at any time.

In case of emergency he is automatically alarmed by the system. By means of the central DAC control computer he is also able to control the data handling system. It runs automatically without requiring any specific data handling personnel.

This is the way how the three TV test facilities are supervised. Depending on the complexity of the test requirements one operator can normally supervise two small test facilities in parallel.

4.4.2 Control Room Equipment for the Space Simulation Facility (WSA/TVA)

Compared to the TV test facilities the Space Simulation Facility requires extended control equipment. Housekeeping data, motion simulator, sun simulator and test specimen data are supervised by an visualization system which is identical with those of the TV-facilities.

Currently not all subsystems of the WSA/TVA are completely equipped with PLC compatible sensors and control devices. Therefore the facility control is based on a mixture consisting of state-of-the-art PLC equipment with the corresponding command and control, and with equipment that is still based on old pneumatic and relay circuit technique. This means that for cases where all facility subsystems are in operation two operators are still required. Further the extensive data handling effort for such space simulation tests requires a specific data-handling operator being permanently on duty during the test execution.

In a recently launched stage 2 automation project the remaining subsystems of the Space Simulation Facility will be covered. Within the next 2 - 3 years also this test facility will be entirely operated and controlled by a state-of-the-art automation system.

4.4.3 Test Floor Equipment

Some test procedures require a local facility control directly at the test floor. In that case the facility control system and the front-end of the data acquisition systems is made available directly at the facility via the network. This provides the operator on duty exactly the same equipment as it is installed in the control room. Operation and control of the facility is identical.

5 Conclusion and Outlook

The results meanwhile gained from the automation project have proven that the initial requirements are fulfilled. The advantages of such a system in terms of reliability and maintainability are extended by the possibility to adapt easily the facility operation and control system to new requirements.

Regarding the improvement of efficiency the operational costs with respect to the manpower costs were reduced by at least 30%. This is due to the fact that the central control of all facilities enables the simultaneous operation of the test facilities without the need for a proportional reinforcement of the operator team. But also the operation itself is improved in terms of efficiency and reliability. Redundant personnel are not any longer required.

It is even possible that for standardized tests a facility is operated autonomous without the permanent presence of operators. The PLC system is built up such, that in case of malfunctions the facility goes in a safety mode, securing safe conditions for the test specimen and alarming the operator via his GSM phone.

In a recently launched stage 2 automation project the remaining subsystems of the Space Simulation Facility will be covered. The goal is that within the next 2 - 3 years also this test facility will be entirely operated and controlled by a state-of-the-art automation system.

With respect to the data handling system a project is running which will in the near future allow the transfer of selected test data via Internet to the customer's home base. The most important and critical issue is to secure a safe transfer of data and to protect the data and the system from unauthorized access.

HYDROCODE MODELS FOR THE ANALYSIS OF MULTI-LAYER THERMAL INSULATION BLANKETS AS HYPERVELOCITY SHIELDS

Shmuel Ben-Shmuel
The Aerospace Corporation

ABSTRACT

Multi-Layer Insulation (MLI) blankets are sometimes considered for space debris shielding applications. The blankets, composed of several spaced Kapton and Mylar layers, are thought to offer some penetration resistance to hypervelocity meteoroids and orbital debris. Empirical data and the physics of hypervelocity impacts suggest that the shield's mass is a critical parameter in penetration resistance. Hypervelocity impact analyses have been performed with hydrocode computational models on MLI blankets and aluminum plates. The calculations agree well with the results of impact tests on MLI blankets and aluminum plates. The results indicate that MLI blankets can provide, in certain cases, some shielding for short duration missions and for non-critical components. MLI blankets provide much less penetration protection than equal thickness metallic plates and should not be considered as an alternative to properly designed hypervelocity impact shielding. The hydrocode models developed for this study are useful for assessing the effectiveness of various barrier materials as hypervelocity impact shields.

INTRODUCTION

Space debris, which include both natural and man-made objects, come in various sizes, velocities, and orbit orientations. The largest concentration of man-made debris is in Low Earth Orbit (LEO), with lesser numbers in the intermediate and geosynchronous orbits. The clutter is getting worse with time as every launch adds more debris. Natural space debris from meteoroids and passing comets occur in all orbits. The probability of meteoroid hits also increases from occasional sources such as the Leonid showers in 1998 and 1999. Concern about the damage that hypervelocity debris impacts cause to spacecraft is as old as space flight (Ref. 1).

Hypervelocity impacts, even by small particles, can cause substantial damage up to and including loss of spacecraft. There is growing recognition for the need to incorporate shielding of critical elements in spacecraft design (Ref. 2). These concerns have resulted in experimental and numerical investigations of several spacecraft shielding concepts. The International Space Station, for example, has been designed with the debris problem in mind (Ref. 3). Typical spacecraft shields such as the Whipple incorporate a bumper shield, several layers of Nextel and Kevlar, and a back wall. Particles impacting the bumper wall break up in a cloud of fragments, which are further slowed down and broken up into smaller particles during passage through the intermediate Nextel/Kevlar barriers. The goal is to sufficiently reduce the size and velocity of the fragments so they do not possess enough kinetic energy to break through the back wall. Additional shielding can be provided for critical spacecraft components by placing them behind other parts. Some satellite makers also consider thermal insulation blankets, common in spacecraft applications, for their debris shielding capabilities in addition to their primary role. The MLI blankets carry superficial resemblance to the Whipple shield's Nextel and Kevlar intermediate layers as they too are made of multiple, spaced layers. However, the blankets are typically made of Kapton, Tedlar, and Mylar; these are light weight materials and this study demonstrates that they do not provide sufficient hypervelocity shielding.

Experimental techniques are used extensively in the study of high velocity impacts and on the effectiveness of various shielding concepts for the protection of satellites and vital components. Ground based experimental methods have limitations due to the relatively low velocities that can be achieved. While space debris can reach velocities of 70 km/sec or more, current earth-bound experiments rarely exceed 11 km/sec. Numerical methods have provided experimentally validated calculations at the low end of the impact velocity regime (Ref. 2) for metallic spheres penetrating metallic plates. These methods are extrapolated to obtain simulations at higher velocities that are beyond the range of experiments (Refs. 4, 5). The physics of hypervelocity impacts make it possible to adapt the metallic plate hydrocode models to non-metallic shields such as MLI blankets. The analysis described in this work expands the concepts of hypervelocity impact shield models to multi-layered thermal insulation blankets made of any material.

The models for both metallic plates and MLI blankets were confirmed by simulating a set of ground tests. The proven models were then used to assess the effectiveness of a MLI blanket as a debris shield for a solid state power amplifier (SSPA). The device is located inside a spacecraft but is exposed to the space environment.

High Velocity Impact Physics

The governing equations of high velocity impact dynamics are conservation of mass, conservation of momentum, and conservation of energy with inertia effects playing a dominant role (Ref. 6). Stress wave propagation in the colliding bodies determines their breakup. Finally, high velocity impact events are transient phenomena; steady state conditions may not exist at all or may be attained long after the penetrating particle and its fragments have reached the final barrier.

The colliding, sliding, and eroding surfaces of penetrator and plate generate shock waves that propagate in both bodies as stress waves. The pattern and extent of the impacting bodies' breakup depend on the impact kinetic energy, the shape of the stress waves, their velocity, and the extent of their advance. The initial stress wave generated by the impact shock wave propagates into unstressed material at the elastic wave velocity (speed of sound) which can be shown to be

$$c = \sqrt{(S/\rho)} \qquad (1)$$

where c is the elastic wave velocity, ρ is the material's density, and S is the slope of the material's stress-strain curve in the elastic regime (Ref. 6). The elastic wave velocity in aluminum, one of the materials used in the calculations, is 5.2 km/sec. Similarly, plastic stress waves are formed once the material strains are in the plastic regime. Plastic stress waves travel at the plastic wave velocity which is also defined by Equation (1) except that S is now the slope of the material's stress-strain curve in the plastic regime. Typical plastic wave velocities are lower than their elastic counterparts due to the smaller slope of the stress-strain curve in the plastic regime. The impact event depends heavily on the relative magnitude of the impact velocity and the elastic wave velocity (speed of sound). At subsonic impact velocities the stress waves will propagate deep into the colliding bodies while they are still in contact. At supersonic impact velocities the stress waves will form on the colliding surfaces and will complete their propagation into the bodies after contact has ended. The fragmentation processes will take place over largely similar times, regardless of the impact velocity, as the stress waves in the colliding bodies travel at their materials' elastic and plastic wave velocities.

Shock waves generated by high velocity impacts (Refs. 4,5) or explosive detonations (Refs. 7,8) generate high frequency, high magnitude impulse loads on structures. Solid materials under these conditions become highly deformed immediately after shock wave impact and exhibit fluid-like behavior due to the high strain rates to which they are subjected. The materials are in the extreme end of the stress-strain curve's plastic regime; their elastic properties are therefore largely irrelevant in hypervelocity impacts.

The two properties that play a significant role in high magnitude, high frequency impulsive loading events are the materials' speed of sound and density. Subsonic and supersonic impact velocities (relative to the materials' speed of sound) yield two distinctly different penetrator fragmentation mechanisms (Refs. 4, 5). Resistance to penetration, on the other hand, is proportional to the shield's mass. This leads to the interesting observation that an aluminum plate of the same areal density (weight per unit area) as the actual shield can be substituted for it in the simulation. MLI blanket materials such as Kapton or Mylar can be simulated in hypervelocity impact calculations by replacing them with aluminum plates of a thickness such that the areal density is unchanged. This is the so-called "equivalent thickness aluminum plate" assumption and it has been used in the MLI blanket models that were developed for this analysis. The blanket fragmentation pattern, however, can not be properly simulated with the equivalent thickness aluminum plate due to differences in the materials' speed of sound. This aspect of the simulation is considered to be of lesser importance in this analysis than the accurate assessment of a hypervelocity shield's penetration resistance. The penetrators, on the other hand, were simulated with their actual materials since their fragmentation determines the shield's penetration extent.

HYDROCODE MODEL

Hydrocode Overview

LS-DYNA3D, a vectorized explicit three-dimensional finite element hydrocode, has been used to construct detailed computational models for the study of the dynamic behavior of bodies undergoing high velocity impacts. The program solves the time-dependent momentum equations in Lagrangian formulation subject to position and velocity initial conditions, and to traction (force) and displacement boundary conditions (Ref. 9). Contact discontinuities on internal boundaries are handled by satisfying stress boundary conditions at these interfaces. The code is capable of simulating stress wave propagation in inelastic solids and the resulting high strain rates and large deformations. A contact-impact algorithm permits gaps and sliding along material interfaces; friction can be modeled into the simulation. Inputs for the code are geometry, material properties, and contact surface specifications. The outputs from the code for the modeled system include time histories of the positions, displacements, velocities, accelerations, pressures, densities, energies, stresses, and strains for nodes and elements of all materials. These variables completely define the analyzed system at any point in the calculated time interval.

Simulation results are given in the following units –

Velocity - cm/μsec = 10^1 km/sec
Acceleration - cm/(μsec)^2 = 10^{10} m/(sec)^2 = ~10^9 g
Pressure, stress - Megabars (Mbars) = 10^6 atmospheres
Energy - 10^7 N-cm = 10^5 Joule

Models

Two simulation models were used in this analysis, a validation model and an application case model. The model that was developed for fragmentation mechanism analyses (Refs. 4,5) was used for the verification cases of aluminum spheres penetrating aluminum plates. The model was then modified for the MLI blanket verification cases. The blankets were modeled as either a single equivalent thickness aluminum plate or as several spaced aluminum plates, having the same aggregate thickness as the single equivalent thickness plate. The important idea of the multi-layer model is to account for the effect of multiple shocks experienced by the penetrator as it passes through the MLI blanket. Inducing multiple shocks allows for more fragment spreading between layers, which in turn tends to reduce the loading on subsequent layers and the likelihood of penetration. Also, the penetrator has more time to fragment when passing through the plates and open spaces of a multi-layered model than when it penetrates a single sheet. These are the two effects that would enable a MLI blanket to have better protection capability than a single aluminum sheet of equivalent thickness. The number of equivalent thickness aluminum plates was set to the number of sub-blankets (3) in the model verification cases or to the number of blanket layers (10) in the SSPA application cases. It is shown in the verification discussion to follow that representing MLI blankets by multiple sheets of aluminum is validated by comparison with experimental data.

The penetrators for all model verification cases were aluminum spheres. The SSPA analysis modeled penetrators made of aluminum, quartz (two densities), and ice in order to consider a range of possible space debris compositions. Choice of penetrator material affects its breakup; fragmentation in hypervelocity impacts is caused solely by stress waves moving at the speed of sound in the penetrator's medium. The SSPA wall was modeled as an aluminum plate. Propagation of the impact-induced stress and shock waves plays a key role in determining whether a meteoroid fragment will successfully penetrate the MLI blanket and the SSPA wall.

The solid materials were all set up as an isotropic-elastic-plastic-hydrodynamic type material with an equation of state (Refs. 4, 5, 9). The equation of state is designed for the hypervelocity regime, which is characterized by high frequency, high magnitude pressures and accelerations. The materials fail when they reach a user selected strain level. The maximum stresses that the materials can withstand are independent of the impact velocity; only the failure strain and the materials' stress-strain relationship determine them. The interface between penetrator and plate was set up as surface

to surface eroding contact (Ref. 9). The materials' type and the interfaces are appropriate for the current problem, which is characterized by colliding, sliding, and eroding surfaces.

MODEL VERIFICATION

The validity of the numerical results depends on the validity of the model, including the assumption that aluminum sheets of equivalent thickness can represent MLI blankets. To address this issue, a set of ground tests of hypervelocity projectiles impacting aluminum plates and MLI blankets (Ref. 10) were simulated to test the agreement of hypervelocity numerical models with experimental data. Table 1 presents a description of these test cases along with both experimental and simulation results. Three cases involved aluminum plates and four involved MLI blankets. Criteria for determining agreement were aluminum plate penetration and number of MLI sub-blankets penetrated. In every case, the simulation results agreed with the test data.

Table 1. Hypervelocity Model Validation Cases (Ref. 10)

Case	1	2	3	4	5a	5b	6
Ref. 10 table #	2	2	2	1	1	1	1
Ref. 10 item #	4	11	19	1373	1338	1338	1410
Penetrator sphere diameter (cm)	.03969	.03969	.15875	.07874	.04064	.04064	.04064
Test target thickness (cm)	.127	.2032	.4826	N/A	N/A	N/A	N/A
Simulation target thickness (cm)	.127	.2032	.4826	.03653 (2)	.03653 (2)	.03653 (2)(3)	.03653 (2)(3)
Test target material	(1)	(1)	(1)	MLI (4)	MLI (4)	MLI (4)	MLI (4)
Simulation target # layers	1	1	1	1	1	3	3
Impact velocity km/sec	7.18	7.18	7.02	7.3	7.7	7.7	4.0
Test penetration (4)	Yes	No	Yes	Yes	1st sub blanket	1st sub blanket	Yes
Simulation penetration	Yes	No	Yes	Yes	No	1st sub blanket	Yes

(1) Al 6061-T6
(2) Equivalent aluminum thickness
(3) Total blanket spacing (front to back) is .635 cm (.25 inches)
(4) MLI blanket consists of three sub-blankets

Penetrator size and material (Al 1100) were the same for both test and simulation. The impact angle was normal for all cases. The MLI blankets in cases 4 through 6 are composed of 46 layers of Kapton, Mylar, and polyester netting, grouped in three sub-blankets (Ref 10). The blanket's areal density is 0.0985 g/(cm)^2. The aluminum plate equivalent thickness for this MLI blanket is 0.03653 cm. The hydrocode model simulates the MLI blankets as either a single sheet (cases 4 and 5a) or three sheets (cases 5b and 6) of equivalent thickness aluminum plates, Figure 4. The total thickness of plates and spacing was set to 0.625 cm, considered to be approximately the thickness of a typical MLI blanket. The blankets in cases 4 and 6 were penetrated while the penetrator in case 5 was stopped at the second sub-blanket, Figure 5. The maximum pressures of both penetrator and target, Figure 6, were lower in case 5b than the ones of case 3 due to the thinner plates of case 5b. The penetrator reaches pressures of up to 0.42 megabars; the first sub-blanket which absorbs most of the penetrator's kinetic energy, goes up to 0.37 megabars. The second sub-blanket attains a maximum pressure of 0.11 megabars and stops the penetrator. No fragments reach the third sub-blanket and its pressure stays at zero. A comparison of cases 5b and 6 yields an interesting observation. The projectile velocity in case 6, 4.0 km/sec,

was lower than the case 5b velocity, 7.7 km/sec, but the projectile penetrated all three MLI sub-blankets in case 6 whereas it only penetrated one sub-blanket in case 5b. The speed of sound in the aluminum projectile is 5.2 km/sec. The impact velocity in case 6 is therefore subsonic while the velocity in case 5 is supersonic. The penetrator's fragmentation mechanisms are different at subsonic and supersonic impact velocities (Ref. 5). This demonstrates that it is insufficient to conclude what constitutes effective shielding by analyzing only high velocity cases, or only low ones.

The numerical results fully agree with the experimental data. Therefore, the hypervelocity impact models for assessing penetration resistance of both metallic plates and MLI blankets have been confirmed.

SSPA - MLI BLANKET APPLICATION ANALYSIS

Issue

There is a concern regarding the space debris hazard posed to a spacecraft's Solid State Power Amplifier (SSPA). The SSPA is located inside the spacecraft, but is directly exposed to the orbital space environment. A 10-layer MLI blanket insulates the SSPA and is the only barrier shielding it from the space environment. The issue is whether the SSPA can withstand the debris fragment cloud if the blanket is located at a minimum standoff distance from the wall. The standoff allows spreading of fragments, which in turn helps to reduce the loading on the SSPA wall.

The MLI blanket's equivalent thickness is 0.0102 cm; the meteoroid diameter is 0.22 cm. The meteoroid's mass is 2.654×10^{-3} g, assuming a spherical shape and a density of 0.5 g/cm^3. Two methods, yielding 6.44×10^{-4} (Cour-Palais model) and 8.40×10^{-4} (Gruen model) calculated the probability that the SSPA panel will be struck by a meteoroid of this size or larger. A standoff distance of 20.83 cm and a 20 km/sec normal impact velocity were assumed. A meteoroid moving at 20 km/sec will take approximately 10 μsec to traverse the 20.83 cm span between the MLI blanket and the SSPA wall. For a meteoroid composed largely of ice, for which the speed of sound is 1.65 km/sec, the stress wave will traverse the diameter of the meteoroid (.22 cm) in ~1.3 μsec, the time it takes the meteoroid to travel one 8th of the distance from the MLI blanket to the SSPA panel. Hence, if the meteoroid does fragment, there will be plenty of time for fragment cloud spreading.

The assumption of 20 km/sec impact velocity at a normal angle represents one scenario. However, both the velocity and the impact angle have a considerable range of values. The average meteoroid hypervelocity impact event for this case is in reality closer to 20 km/sec at 51.8 degrees from the normal.

Hydrocode Simulation

A hydrocode analysis was performed on the MLI blanket – SSPA wall configuration. The blanket was placed at a 20.83 cm standoff distance from the SSPA panel. A meteoroid of mass 2.654×10^{-3} g was modeled at the average impact velocity of 20 km/sec at a normal impact angle. The SSPA wall was modeled as a 0.00254 cm thick aluminum sheet. The MLI blanket is composed of 10 Kapton layers and has an areal density of 0.02658 g/cm^2. The aluminum plate equivalent thickness for this blanket is 0.00986 cm. The MLI blanket was modeled in two ways. For one set of cases, the MLI blanket was represented by a single sheet of aluminum with the same areal mass density. For the second set, the MLI blanket was modeled as 10 equidistant sheets of aluminum with the same areal mass density as the MLI blanket. The total distance between the external faces of the first and last layer was set to the same value as in the validation cases' MLI blanket, .625 cm.

Table 2 shows the description and results of the six hydrocode cases that were set up to assess the effectiveness of the MLI blanket. Several different penetrator materials were considered to account for the uncertainty in material composition of the meteoroid. Cases 1 and 2 modeled the blanket as a single aluminum sheet. Cases 3 through 6 incorporated 10 sheets of aluminum. Case 6 is closest to the most likely scenario for several reasons. The 10 aluminum sheets account for the multi-shock and increased penetrator fragmentation time effects of the MLI blanket layers. Ice was considered to be a representative material because meteoroids are generally thought to be of cometary origin. In addition, the density of ice, 0.9 g/cm^3, is closest to the value of 1 g/cm^3 associated with the Gruen meteoroid model.

Table 2. MLI Blanket - SSPA Simulation Cases

Case	1	2	3	4	5	6
Penetrator material	Al 7075-T6 ρ=2.7 g/cc	Quartz ρ=.5 g/cc	Quartz ρ=.5 g/cc	Quartz ρ=.5 g/cc	Quartz ρ=2.2 g/cc	Ice ρ=.9 g/cc
Target thickness (cm)	.00986	.00986	.00986 total	.0660 total	.00986 total	.00986 total
Target # layers	1	1	10	10	10	10
MLI blanket penetration	Yes	Yes	Yes	No (stopped by 10th layer)	Yes	Yes
SSPA penetration	Yes	Yes	Yes	No	Yes	Yes

All cases have the following characteristics in common –
(1) Penetrator shape – sphere, diameter=0.217 cm
(2) Target material – Al 7075-T6
(3) Impact velocity – 20 km/sec
(4) Impact angle – normal to target
(5) MLI blanket – SSPA stand-off distance = 20.83 cm

Results

Case 1 is a baseline configuration; the aluminum penetrator and target have been tested extensively and were successfully simulated in the verification phase of this analysis. The penetrator easily perforates both the equivalent thickness aluminum sheet and the SSPA panel. Case 2 is similar to case 1 but uses different assumptions for the penetrator's material and density. Case 3 is the same as case 2 except that 10 equidistant aluminum sheets now model the MLI blanket. Case 4 represents the upper limit of possible protection – the 10 aluminum layers have the actual thickness of the MLI blanket Kapton layers. The end effect is a 10-layer barrier with 6.694 times the areal density (mass) of the MLI blanket. Case 5 explores the upper limit for a quartz penetrator's density. The last case is for an ice penetrator with a different density and material speed of sound than the quartz cases.

All but one of the hydrocode cases showed that the meteoroid easily penetrated all 10 layers of the MLI blanket as well as the SSPA wall. Case 4 showed that an MLI blanket that is at least 6.694 times thicker would be needed to stop the penetrator. If the meteoroid impacts at 51.8 deg, the amount of mass along the path of the meteoroid increases by a factor of 1.618. In this case, an MLI blanket which is at least 6.694/1.618 = 4.14 times thicker would be needed to stop the penetrator. Based on this result, it is clear that a single, 10-layer MLI blanket offers no protection against the meteoroid of the analysis case.

The hydrocode simulation of case 6, which is closest to the average scenario, is presented in Figures 7-9. The snapshots show the penetration through the MLI blanket sheets and the SSPA wall. It is clear from the Figures 8 and 9 that the meteoroid survives passage through the MLI blanket and SSPA wall mostly intact and subsequently proceeds directly into the electronics.

It should also be noted that the MLI blanket used in the model validation tests (Ref. 10) is approximately four times heavier than the MLI blanket of the SSPA application, hence resulting in effective shielding at 7.7 km/sec.

CONCLUSIONS

1. Hypervelocity impact-shielding models were developed for metallic plates and MLI blankets. The hydrocode models successfully duplicated experimental data from aluminum plates and MLI blanket tests.

2. Resistance to hypervelocity penetration is proportional to the shield's mass; hence, substitution of equivalent thickness aluminum plates for the shields' materials is valid for hypervelocity impact events.
   Note that the implication here is that there is no need to substitute aluminum (or any other material) for the shield's media if the shield's geometry and structural properties are known. The shield's composition, i.e., number of layers, their thickness, material, density, and interstitial spacing provides all the information needed for direct simulation of hypervelocity impacts, i.e., mass and geometry.
3. In the application case, the 10-layer MLI blanket does not provide the SSPA with sufficient protection from space debris impacts.
4. MLI blankets can provide some limited shielding during launch, orbit insertion, short duration missions, and for non-critical components. The blankets provide much less penetration protection than metallic plates and should not be considered as an alternative to properly designed hypervelocity impact shielding.
5. Hydrocode models provide a fast, handy tool for assessing the effectiveness of MLI blankets and other barriers as hypervelocity impact shields.

REFERENCES

1. Schonberg, W. P., "Protecting Spacecraft Against Meteoroid/Orbital Debris Impact Damage: a Historical Overview of R&D Activities", '99 Leonid Meteoroid Storm and Satellite Threat Conference, Manhattan Beach, California, May 11-13, 1999.
2. *Proceedings of the Hypervelocity Shielding Workshop.* Sponsored by NASA Johnson Space Center and the Institute for Advanced Technology at the University of Texas at Austin, Galveston, Texas, March 8-11, 1998.
3. Christiansen, E.L., *"Design Practices for Spacecraft Meteoroid/Debris (M/D) Protection",* Hypervelocity Shielding Workshop, Galveston, Texas, March 8-11, 1998.
4. Ben-Shmuel, S., "Hypervelocity Shallow Angle Impact Simulation," Leonid II Meteoroid Storm and Satellite Threat Conference, Manhattan Beach, California, May 11-13, 1999.
5. Ben-Shmuel, S., Goldstein, S., "Hypervelocity Meteorite Impact Simulation," 20th Space Simulation Conference, Annapolis, Maryland, October 27-29, 1998.
6. *High Velocity Impact Dynamics.* Edited by Jonas A Zukas, John Wiley & Sons, Inc., 1990.
7. Ben-Shmuel, S., "Sizing Bolt Cutter Assemblies for Specific Applications by Hydrocode Analysis", 36th AIAA/ASME/SAE/ASEE Joint Propulsion Conference, Huntsville, AL, July 2000.
8. Ben-Shmuel, S. and Goldstein, S., "Pyrovalve Simulation and Evaluation", 33rd AIAA/ASME/SAE/ASEE Joint Propulsion Conference, Seattle, WA, July 1997.
9. *LS-DYNA3D Theoretical Manual.* Hallquist, J.O., Livermore Software Technology Corporation, LSTC Report 1018, Revision 3, April 1994.
10. Robinson, J.H., "The Effectiveness of Multi-layer Insulation as Meteoroid and Debris Shielding," Paper No. AIAA 92-1460, AIAA Space Programs and Technologies Conference, Huntsville, AL, March 24-27, 1992.
11. Christiansen, E.L., "Design and Performance Equations for Advanced Meteoroid and Debris Shields," International Journal of Impact Engineering, Vol. 14, pp. 145-156, 1993.

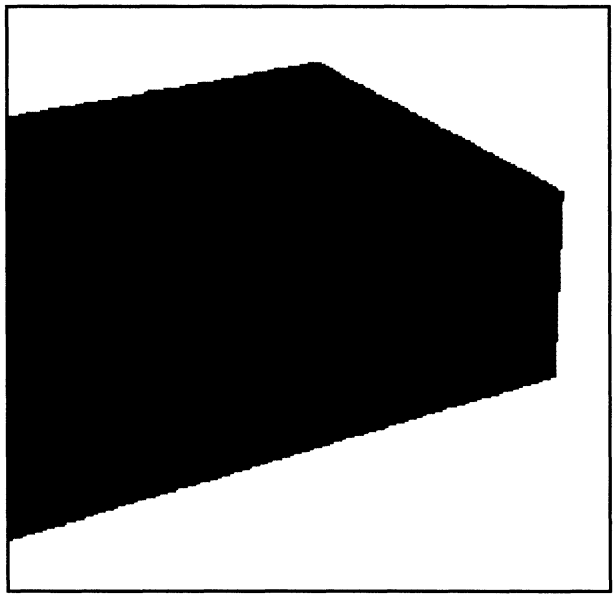

Figure 1 – Validation case 3
t=0

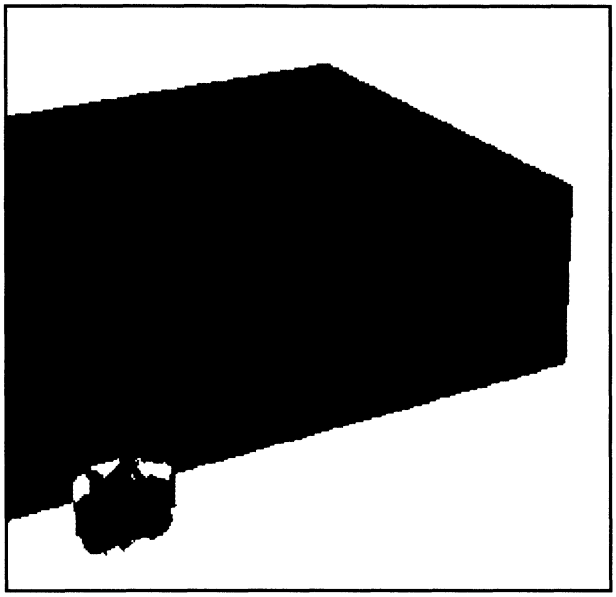

Figure 2 – Validation case 3
t=1.3 μsec

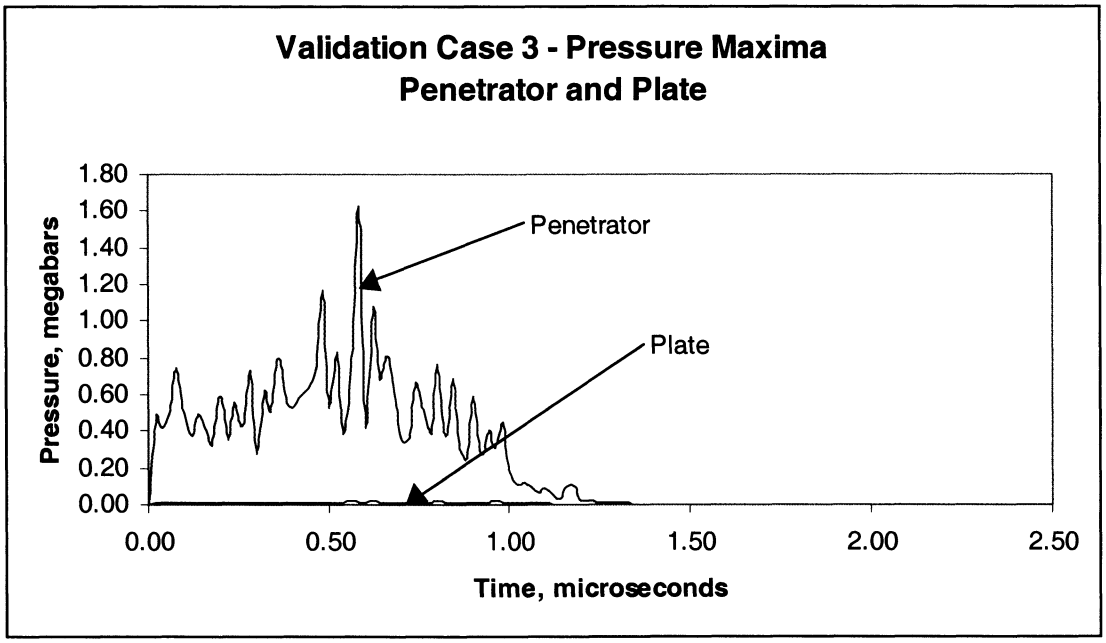

Figure 3 – Validation case 3
Pressure maxima – penetrator and plate

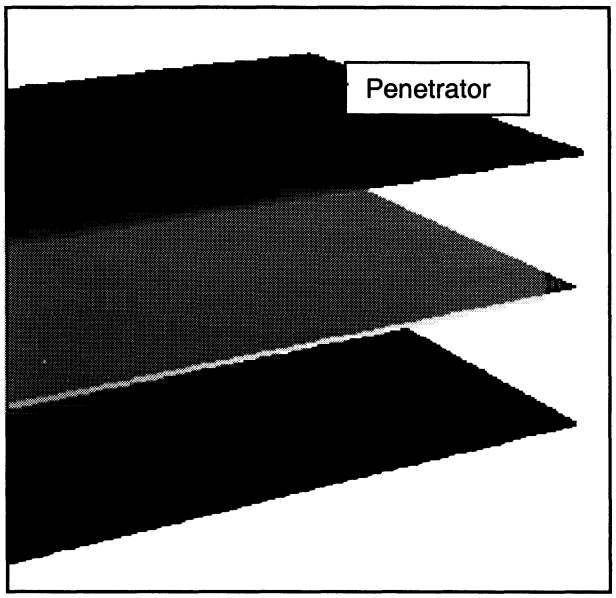

Figure 4 – Validation case 5b
t = 0

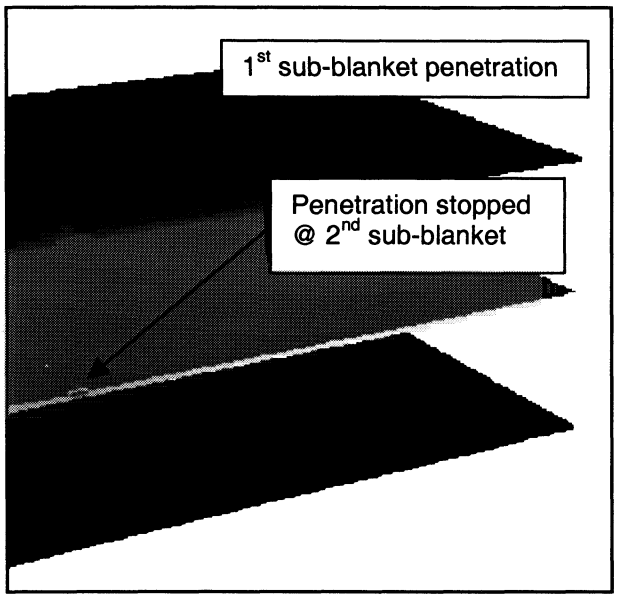

Figure 5 – Validation case 5b
t = 1.5 μsec

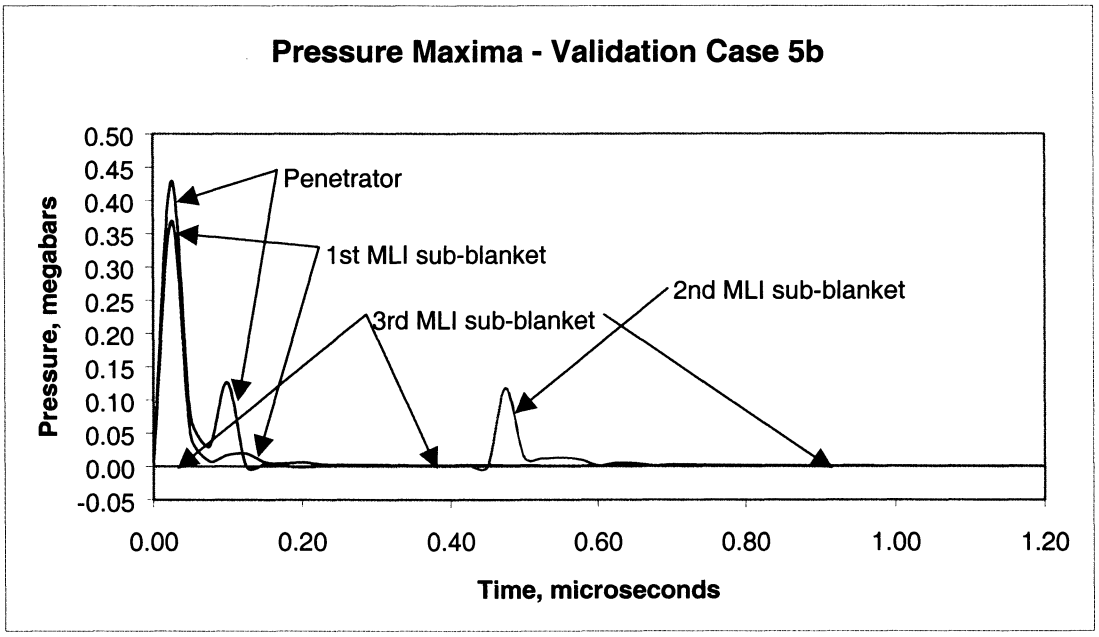

Figure 6 – Validation case 5b
Pressure maxima – penetrator and 3 plates

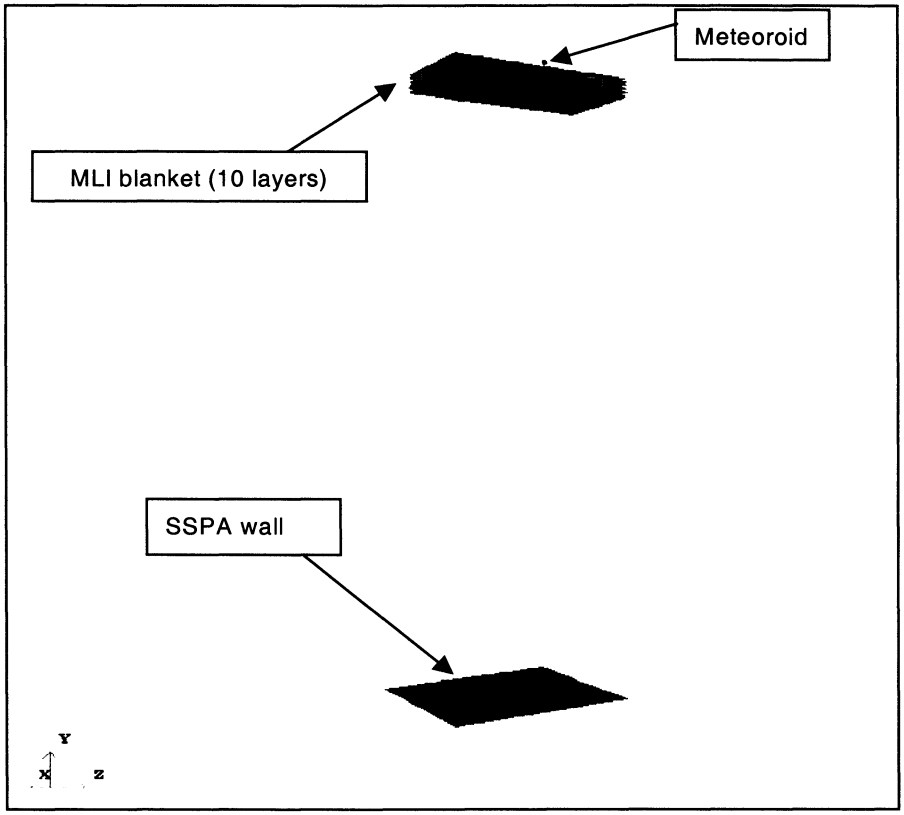

Figure 7 – SSPA case 6
View of model – MLI blanket, meteoroid, and SSPA wall

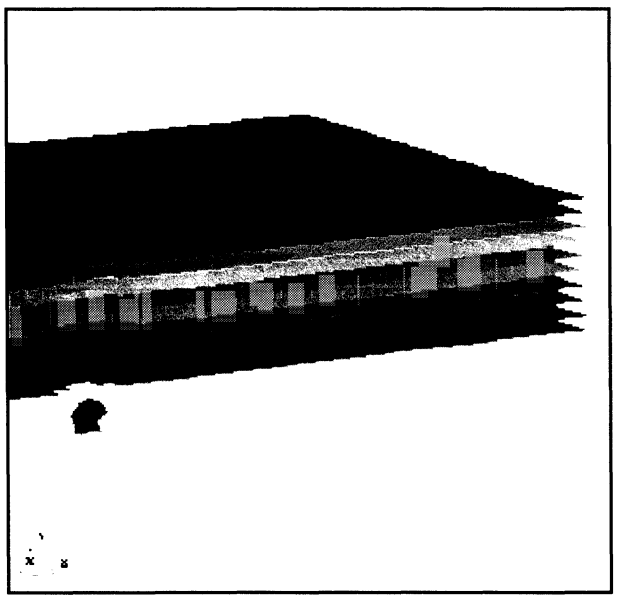

Figure 8 – SSPA case 6
MLI blanket penetration, t=0.75 μsec

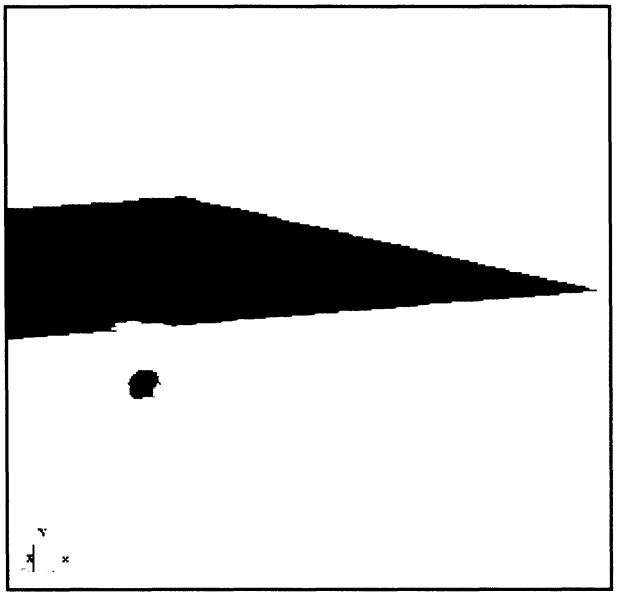

Figure 9 – SSPA case 6
SSPA wall penetration, t=10.95 μsec

OUTGASSING OF FLOWN AND UNFLOWN MIR SOLAR CELLS

Gale A. Harvey and William H. Kinard
NASA Langley Research Center

Linda A. Wilson
Middle Tennessee State University

ABSTRACT

A solar panel array with more than ten years space exposure was removed from the Mir core module in November 1997, and an eight panel section was returned to Earth in January 1998. Several solar cells were removed from panel eight of the returned array and placed in a high vacuum system with a residual gas analyzer (200 amu mass spectrometer) and a cold finger. Similar unflown solar cells of the same vintage were later obtained from Energia. Several of the unflown cells were also placed in the vacuum system and outgassed residues were collected on the LN_2 cold finger. Almost 3 mg of outgassed residue was collected from a string of three unflown solar cells over a period of 94 hours under vacuum. The collected residue was weighed with a microbalance, and then the residue was analyzed by FTIR spectroscopy, and by gas chromatograph-mass spectroscopy. About 25 outgassed constituents were separated by the gas chromatograph, and a high-resolution mass spectrum was obtained of each constituent. Molecular identifications have been made for the constituents. The constituents are primarily cyclic siloxanes, and several of the constituents are isomers of the same molecule. Most of the outgassed constituents have a molecular mass of about 500 amu.

Almost one mg of residue was extracted from one cm^2 of coverglass/adhesive from a flown solar cell by soaking in isopropyl alcohol for 30 minutes. The gas chromatograph separated about 20 constituents. The constituents are mostly cyclic siloxanes with linear branches, hydrocarbons, and phthalates. The typical molecular mass is about 600 amu.

These identifications of specific outgassing molecules have resulted in a more complete understanding of the SiO_x contamination on the Mir solar cell coverglasses, and on the MEEP experiment trays and optical specimens during the Shuttle-Mir Phase One flight experiment program. Adjusted outgassing rates based on the data reported here, and/or measured outgassing rates and specific molecular identifications of ISS hardware samples are needed to input into model predictions of induced environment effects of the ISS.

INTRODUCTION

A photograph of the first-deployed solar-panel-array on Mir is shown in Figure 1. The solar-panel-array was still attached to the Mir core module during the STS 76 photographic survey, and a close-up on-orbit photograph of the mid-section of the array showing the eighth panel of the returned portion of the array is shown in Figure 2. The whole solar array was detached from the core module in November 1997, and one of four eight-panel sections was returned to Earth in January 1998. Seven of the eight panels were returned to Russia, and the eighth panel remained in the United States. The pronounced scattering of light (as seen as bright-white areas in Figure 2) by oxidized silicone films on the solar cell coverglasses is readily apparent in bright light, and has been previously reported and discussed (ref. 1).

Study of the returned section of the solar array is part of the International Space Station (ISS) Risk Mitigation Program. The investigation plan, schedule, and preliminary results have been reported by Visentine et al. (ref. 2). Initial hardware cleanliess studies of the returned array at NASA Langley Research Center were directed toward study of the detergent-like residues on the returned array similar to those on the Mir Environmental Effects Payload (MEEP) which have been reported by Harvey et al. (ref. 3).

A second, prevalent type of contamination was very thin films consisting of irregular shaped spots of millimeter size which are readily visible in brilliant colors when the solar cell coverglasses are viewed with a 50x brightfield microscope. These prolific, overlapping, and almost ubiquitous patterns strongly suggest wetting of the coverglass surfaces and have been attributed to hydrazine thrusters residue (refs. 4, 5, and 6).

A third type of contamination is the SiO_x films produced by self-contamination from the silicone potting compound and adhesive. Silicone oils oozed from the potting compound; wetted the space-exposed coverglass surfaces; and was converted to SiO_x by atomic oxygen in low Earth orbit (LEO)(ref. 1).

A fourth type of contamination is SiO_x particles and glass fibers resulting from the degradation of silicone potting and adhesive (ref. 4). The SiO_x films and the debris SiO_x particles show that the silicone potting and adhesive undergo changes when exposed to the LEO environment. The SiO_x films indicate a uniform creep or wetting of silicone oils across the coverglass with subsequent oxidation to SiO_x. Plumes of heavier and coarser SiO_x films at some coverglass edges (figure 3) indicate microeruptions of silicone gas and particles.

OUTGASSING MEASUREMENTS AND CHEMICAL ANALYSES

Solar cell 9,5 was removed from panel eight of the returned array and placed in a small (less than 1 ft^3) high vacuum chamber equipped with a 200 amu residual gas analyzer. A mass spectrum (figure 4) obtained during high vacuum exposure of this solar cell indicates a very small amount of silicone outgassing. Nine solar cells of the same vintage as the cells in the returned array were obtained from the Russian vender Energia. Three individual cells (#25, 26, and 27) were separately placed in the small high vacuum chamber, and mass spectra obtained at lower gain. Figure 5 is the mass spectrum of unflown cell #25. Unflown cells #26 and #27 had similar mass spectra. The mass spectra from cell 9,5 and the unflown cells indicate about two orders of magnitude higher outgassing from the unflown cells than from the flown cell.

Three of the unflown cells (string 1) were place in the small vacuum chamber, and outgassed residue was collected on a LN_2 cold finger during 95 hours of vacuum exposure. Almost 3 mg of outgassed residue was collected on the cold finger. The collected residue was measured with a Cahn microbalance, and then analyzed by FTIR spectroscopy. An FTIR spectrum of the unflown cells outgassed residue is shown in Figure 6. The initial outgassing, G = mass/area-time averaged over the 95 hours of vacuum exposure can be calculated. The initial outgassing rate was about 1.40×10^{-10} gm/cm^2-sec.

The unflown outgassed residue was then analyzed by gas chromatography. A gas chromatogram of the unflown outgassed residue is shown in figure 7. Figure 7 shows that there are at least 26 constituents in the unflown outgassed residue-mixture.

The first constituent was eluted at 18.154 minutes, and has abundant mass fragments of 55 and 173 atomic mass units (amu), and may be an ether (figure 8). The second constituent was eluted at 18.384 minutes and has abundant 73 amu $Si(CH_3)_3$ and 135 amu $Si(CH_3)_2C_6H_5$ mass fragments and hence is a methyl-phenyl silicone. The 417 amu mass peak in figure 9 is probably the molecular ion. The molecular mass of most of the cyclic methyl silicones is the molecular ion plus the 15 amu methyl radical, CH_3. A possible molecular configuration of molecular mass 432 is shown in figure 10.

Constituents 4, 5, and 7 are clearly hydrocarbons with abundant alkyl mass fragments of 43, 57, 71, and 85 amu. Constituent 13 is a phthalate with the characteristic 149 amu abundant mass fragment. All of the other 21 constituents are methyl or methyl-phenyl silicones with probable molecular masses in the range 405 to 637 amu. Several isomers of molecular masses 405, 479, 503, and 553 are present. The elution times, probable molecular mass, and chemical class (including number of silicon atoms) of the 26 constituents are listed in Table 1.

Residue from one cm^2 of adhesive and scrim from flown solar cell 3,1 was extracted by soaking for 30 minutes in isopropyl alcohol. The alcohol was allowed to evaporate, and the extracted residue weighed (0.748 mg) with the Cahn microbalance. An FTIR spectrum of the extracted residue is shown in figure 10. The flown extracted residue was then analyzed by GC-MS. A gas chromatogram of the flown-extracted residue is shown in figure 11. Figure 11 shows that there are at least 19 constituents in the flown-extracted residue from solar cell 3,1.

The first constituent was eluted at 22.55 minutes, has an abundant mass fragment (base peak) at 149 amu, and hence is a phthalate. This is the same constituent as the 13^{th} constituent of the unflown outgassed residue. Constituents 2 (figure 12) and 3 are hydrocarbons. Constituents 4 and 8 are phthalates. All of the other constituents are methyl (figure 12) or methyl-phenyl silicones with seven or eight silicon atoms. Table 2 lists the elution times, probable molecular mass, and chemical class of the extracted residue constituents.

CONCLUSIONS

The initial (100-hour) outgassing rate of the Mir solar array was probably about 1×10^{-10} gm/cm^2-sec. The outgassed residue was a mixture of about 25 chemical compounds, mostly methyl-phenyl silicone oils. Several isomers of some of the silicone compounds were present. A few hydrocarbons and a phthalate were also present. The average molecular mass of the outgassing constituents was about 500 amu.

The residual oil within the flown cells (i.e. potential outgassing residue) was similar to that of the unflown solar cells, but was much less abundant, typically had one or two more silicon atoms per molecule, and was about 100 amu larger mass.

This information can be appropriately adjusted to predict short term and long term outgassing of solar arrays on the ISS. GC-MS can be well suited for detailed study of some outgassing residues. Information regarding the number of constituents in an outgassing mixture, and molecular masses and chemistry can validate assumptions regarding outgassing decay, and space exposure effects such as oxidation and polymerization. Each constituent or chemical compound in an outgassing mixture has it own outgassing rate. The chromatograms provide information on the number of outgassing rates needed to accurately characterize the outgassing of the mixture over time. The molecular weight distribution and chemistry can be used to synthesize mixtures for detailed laboratory measurements under greatly varying conditions, and to use reference library and literature search data as inputs for calculated outgassing of specific hardware under expected conditions.

REFERENCES

1. Harvey, G. A. , et al., "Optical Characterization of Returned Mir Solar Cells," AIAA 99-4488, Space Technology Conference and Exposition, Albuquerque, NM,1999.
2. Visentine, J., et al., "Mir Solar Array Return Experiment," AIAA 99-0100, 37th AIAA Aerospace Sciences Meeting and Exhibit, Reno, NV, 1999.
3. Harvey, G. A., et al., "Mir Environmental Effects Payload and Returned Mir Solar Panel Cleanliness," Proc. SAMPE 44, pp 1038-1050, 1999.
4. Harvey, G. A. et al.., "Thruster Residues on Returned Mir Solar Panel," SPIE 45th Annual Meeting, San Diego, CA, 2000.
5. Dever, J. A.., et al., "Contamination and Space Environmental Effects on Solar Cells and Thermal Control Surfaces," J. of Spacecraft and Rockets, V 32, 5, pp850-855, 1995.
6. Koontz, S. et al., SPIFEX Contamination Studies," NASA JSC Report 27399, 1996.
7. Harvey, G. A. et al., "Particle Generation by Silicone Potting Compound of Returned Mir Solar Cells," SPIE 45th Annual Meeting, San Diego, CA, 2000.

TABLE 1- Unflown Outgassed Residue

GC peak	Elution time	Probable Mass	Chemical
1.	18.154	?	HC
2.	18.384	432	5SiMO
3.	19.659	504	6SiM
4.	19.744	?	HC
5.	19.873	?	HC
6.	20.729	506	6SiMO
7.	21.072	?	HC
8.	21.228	565	7SiMO+HC
9.	21779	444	6SiM
10.	22.060	420	4SiMO
11.	22.269	420	4SiMO
12.	22.478	420	4SiMO
13.	22.546	?	phthalate
14.	22.587	420	4SiMO
15.	22.907	589	7SiMO
16.	23.665	518	7SiM
17.	23.804	494	5SiMO
18.	24.124	494	5SiMO
19.	24.292	494	5SiMO
20.	24.863	654	8SiMO
21.	25.404	518	7SiM
22.	25.638	568	6SiMO
23.	25.873	568	6SiMO
24.	25.969	568	6SiMO
25.	26.024	568	6SiMO
26.	26.093	568	6SiMO

TABLE 2- Flown Extracted Residue

GC peak	Elution time	Probable mass	Chemical
1.	22.551	?	phthalate
2.	23.647	479	HC
3.	25.866	?	HC
4.	26.693	?	phthalate
5.	26.990	518	7SiM
6.	28.138	579	7SiMO
7.	28.488	518	7SiM
8.	28.840	?	phthalate
9.	29.596	654	8SiMO
10.	29.833	518	7SiM
11.	30.930	654	8SiMO
12.	31.124	518	7SiM
13.	32.153	579	7SiMO
14.	32.332	518	7SiM
15.	33.324	654	8SiM
16.	33.324	518	7SiM
17.	34.428	579	7SiMO
18.	34.509	579	7SiMO
19.	35.566	579	7SiMO

Note: HC= hydrocarbon
SiM = methyl silicone
SiMO = methyl-phenyl silicone

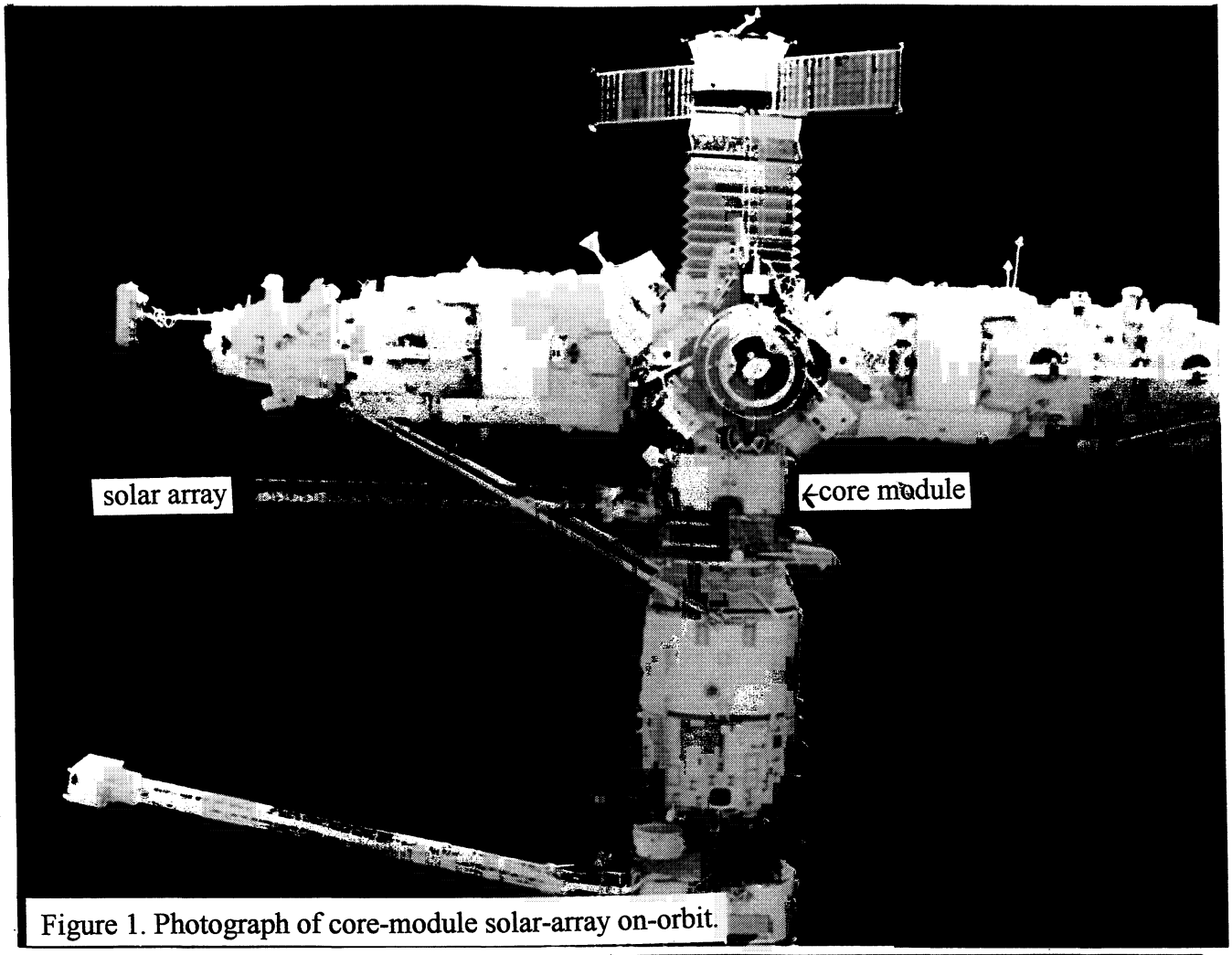

Figure 1. Photograph of core-module solar-array on-orbit.

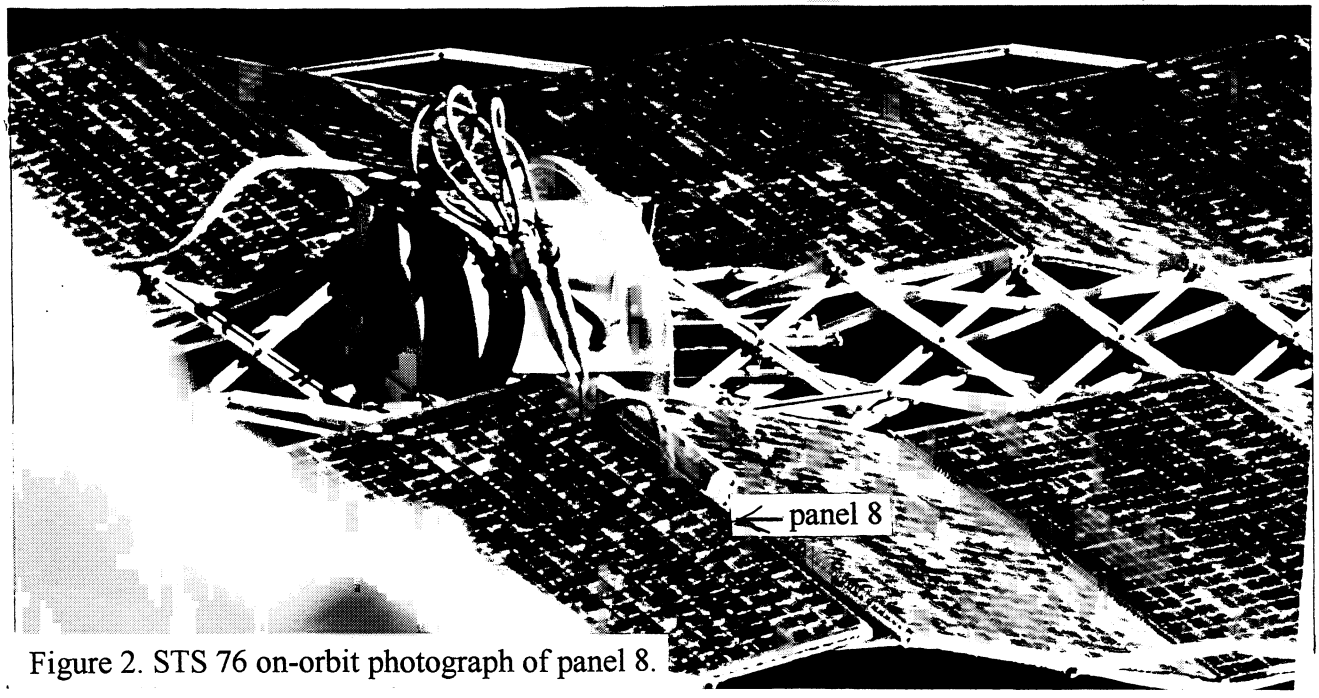

Figure 2. STS 76 on-orbit photograph of panel 8.

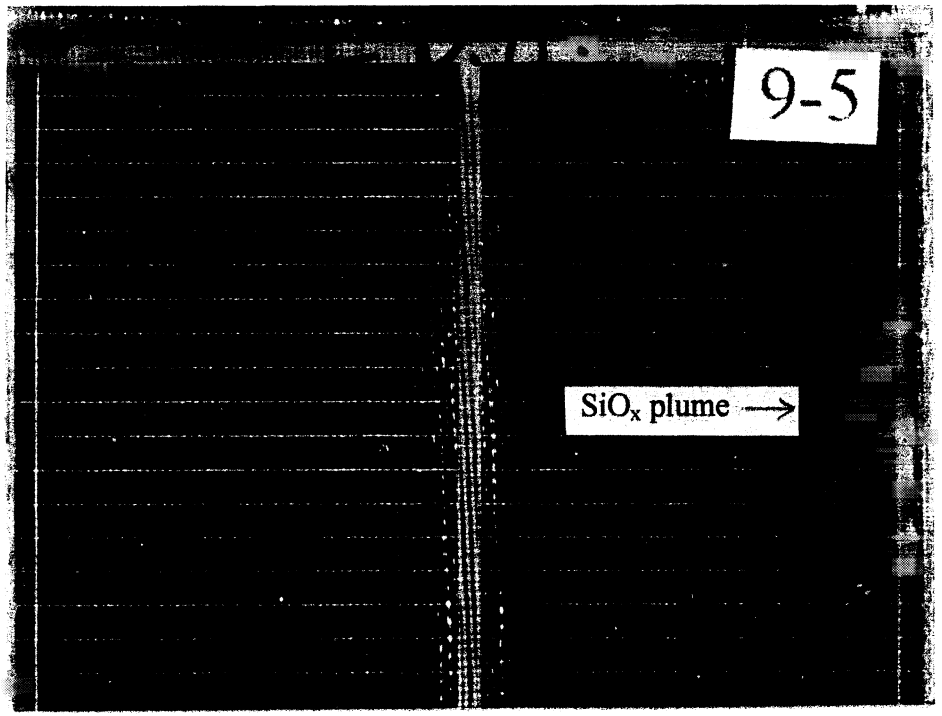

Figure 3.- Photograph of removed cell 9,5 with SiO_x plume on coverglass.

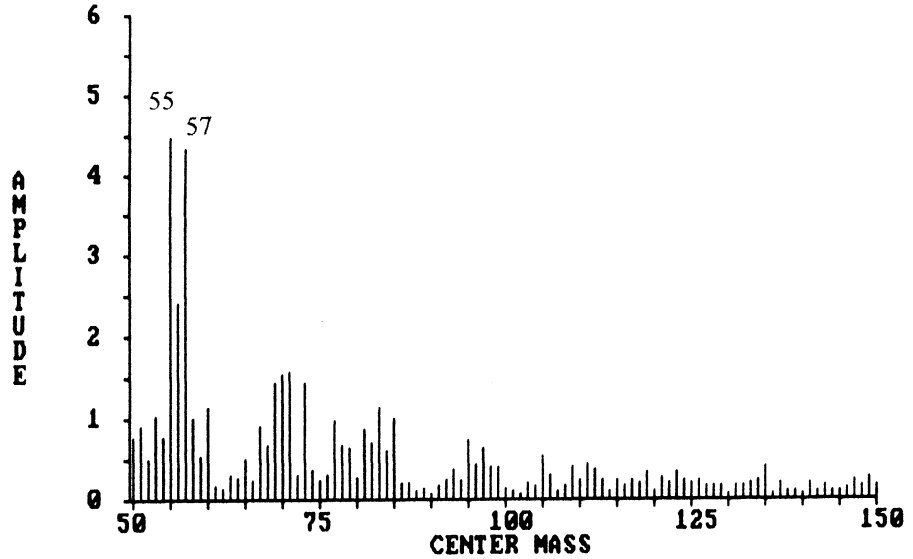

Figure 4.- RGA mass spectrum of outgassing from removed solar cell 9,5.

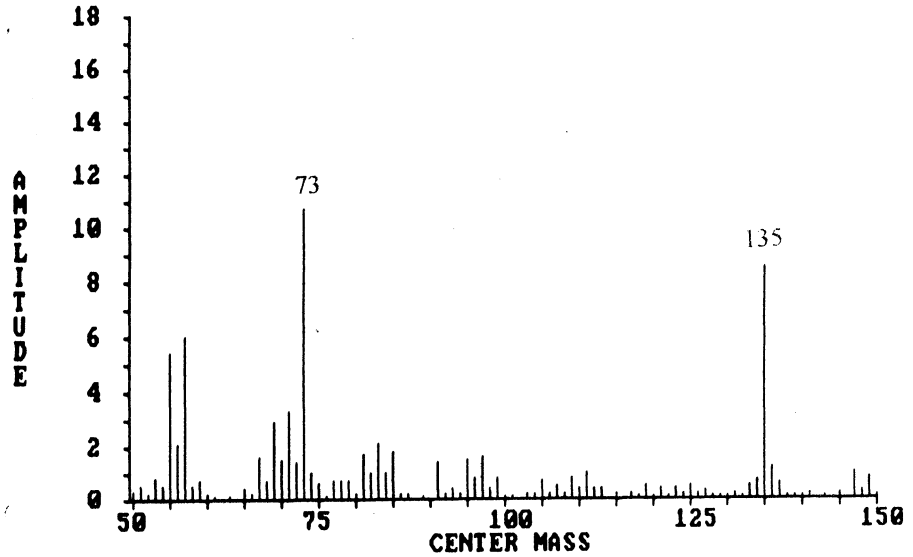

Figure 5.- RGA mass spectrum of outgassing from unflown solar cell #25

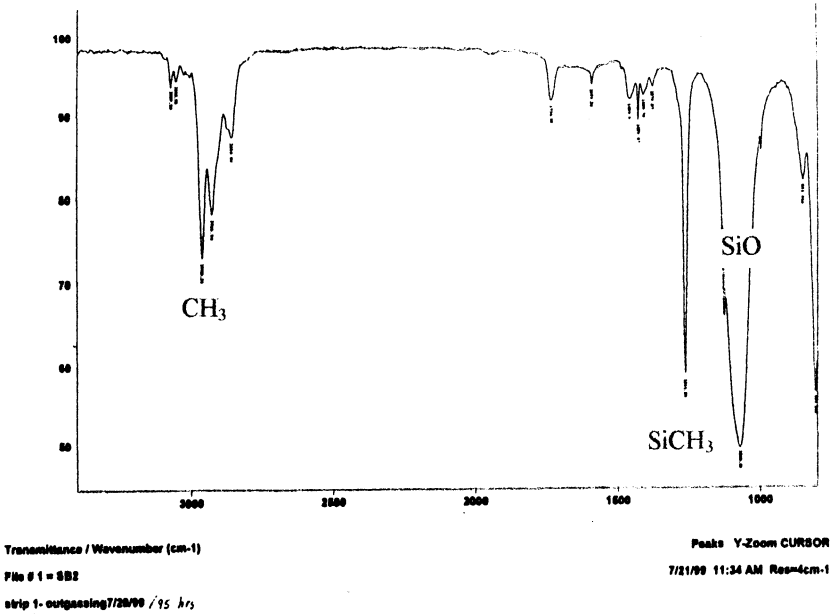

Figure 6.- FTIR spectrum of outgassed residue from three unflown solar cells.

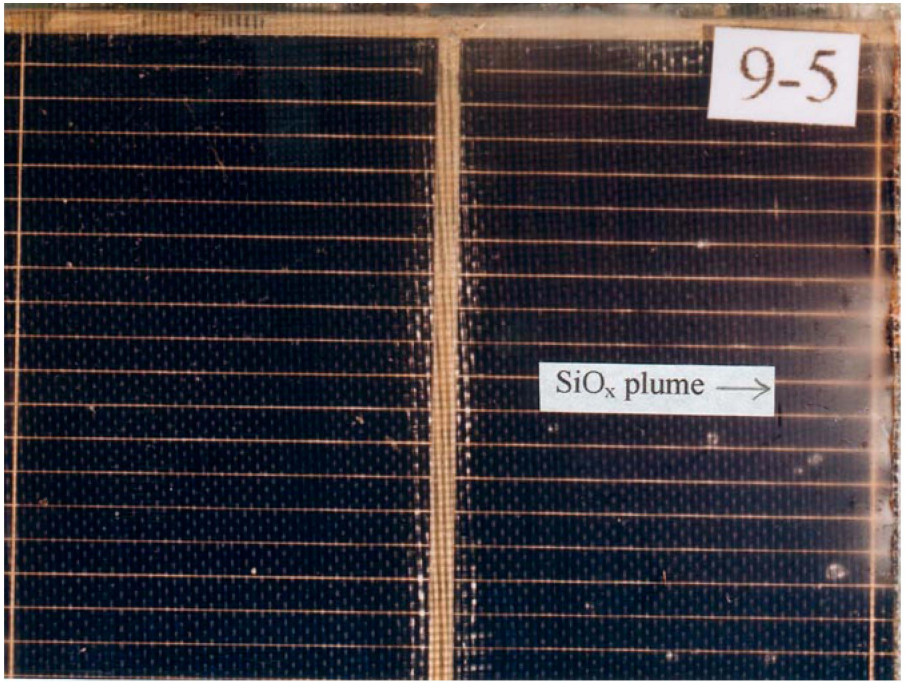

Figure 3.- Photograph of removed cell 9,5 with SiO_x plume on coverglass.

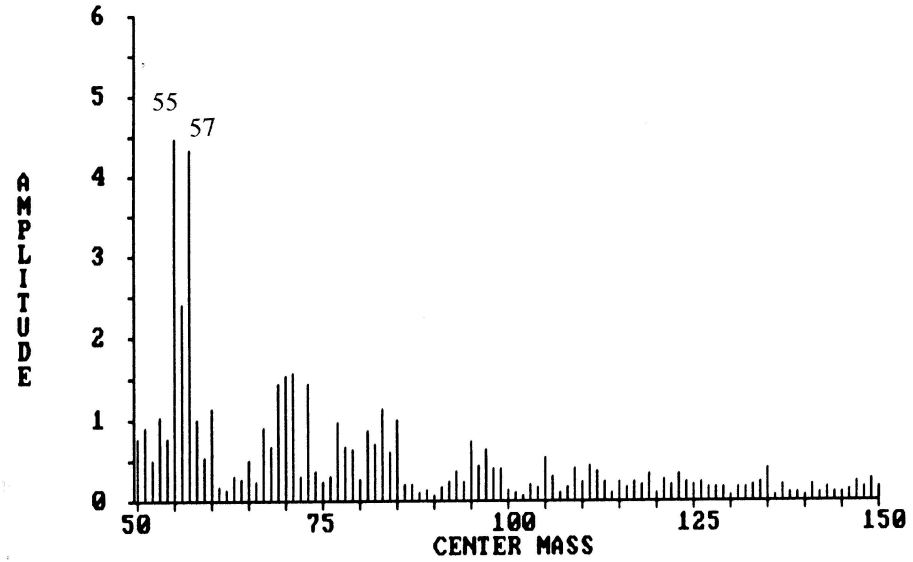

Figure 4.- RGA mass spectrum of outgassing from removed solar cell 9,5.

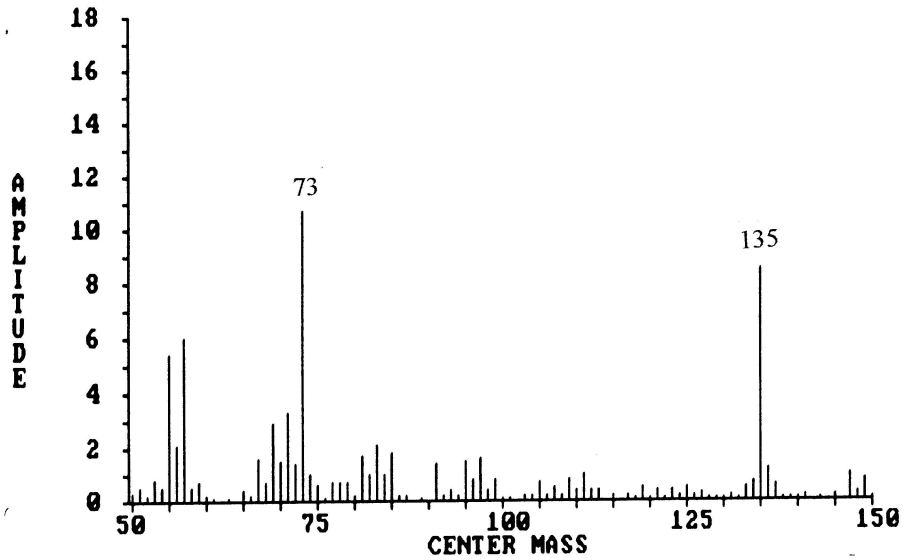

Figure 5.- RGA mass spectrum of outgassing from unflown solar cell #25.

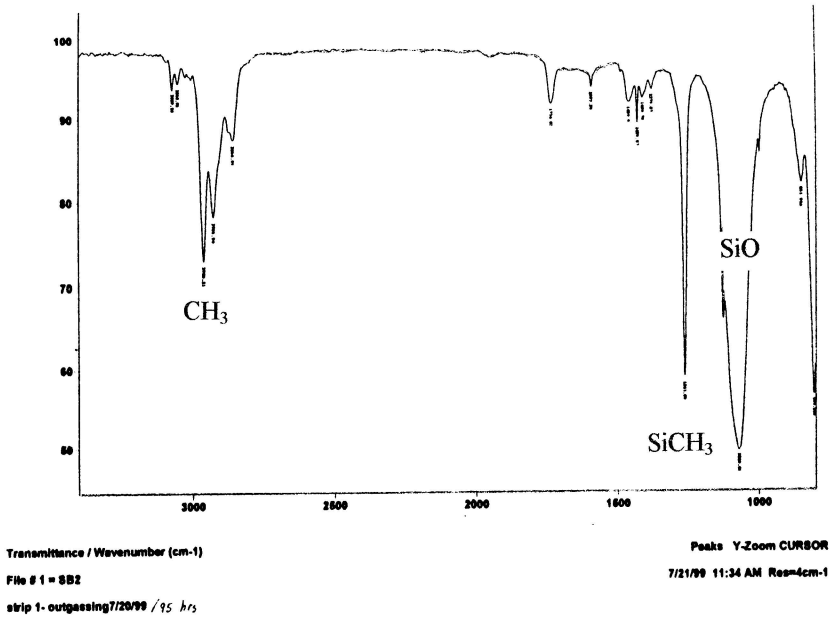

Figure 6.- FTIR spectrum of outgassed residue from three unflown solar cells.

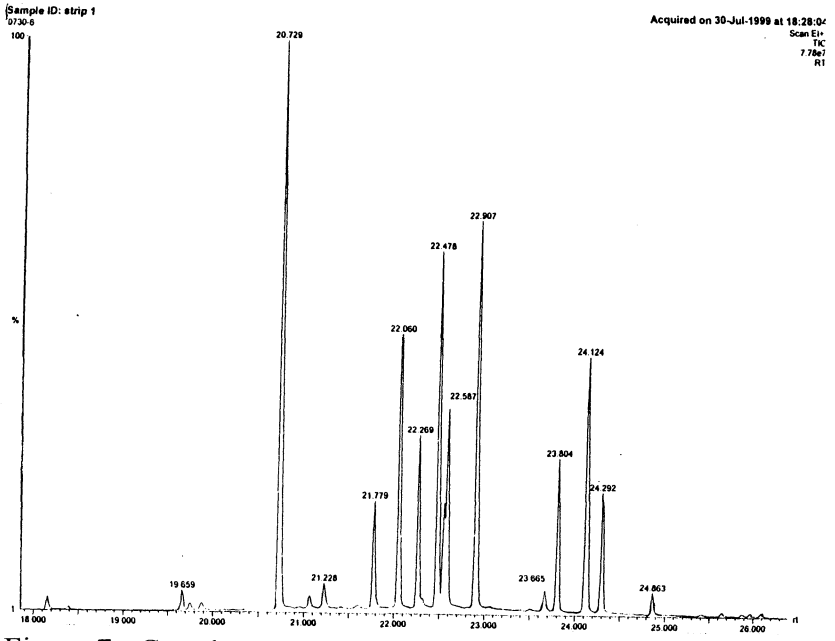

Figure 7.- Gas chromatogram of residue from three unflown solar cells.

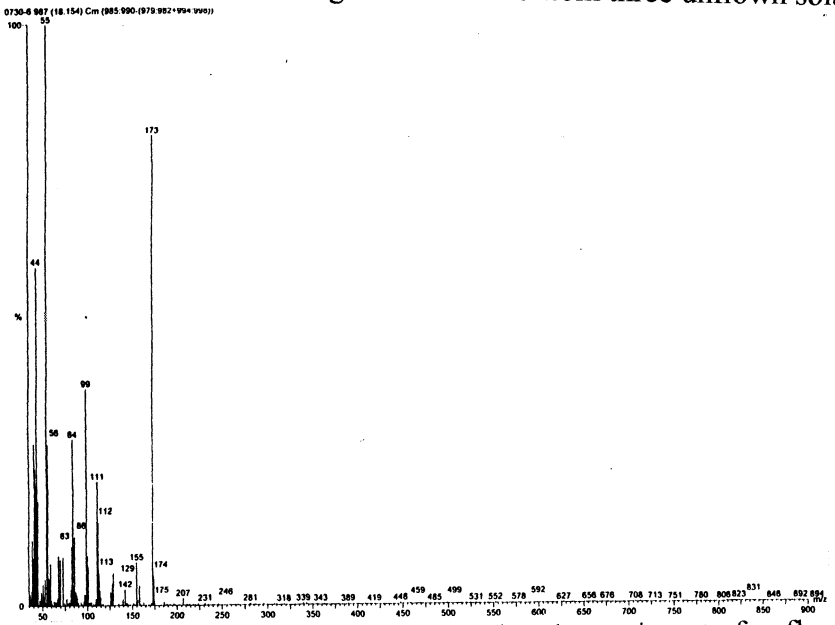

Figure 8.- Mass spectrum from first eluted constituent of unflown outgassed residue.

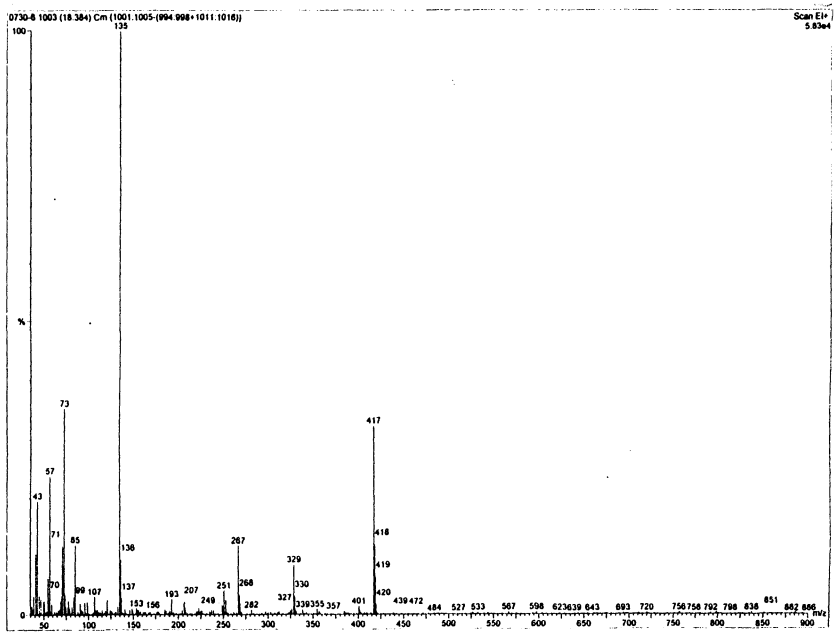

Figure 9.- Mass spectrum from second eluted constituent of unflown outgassed residue.

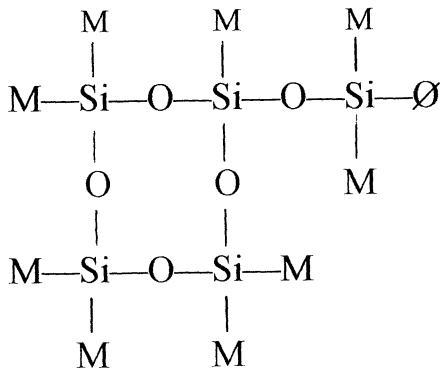

where $M=CH_3$
$Ø=C_6H_5$

Figure 10.- Possible molecular diagram of second eluted constituent of unflown outgassed residue.

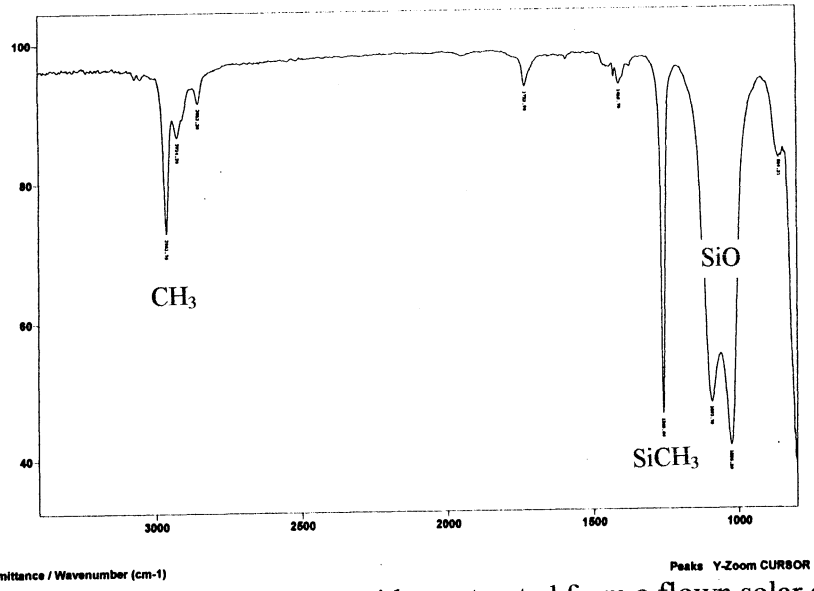

Figure 11.- FTIR spectrum of residue extracted from a flown solar cell.

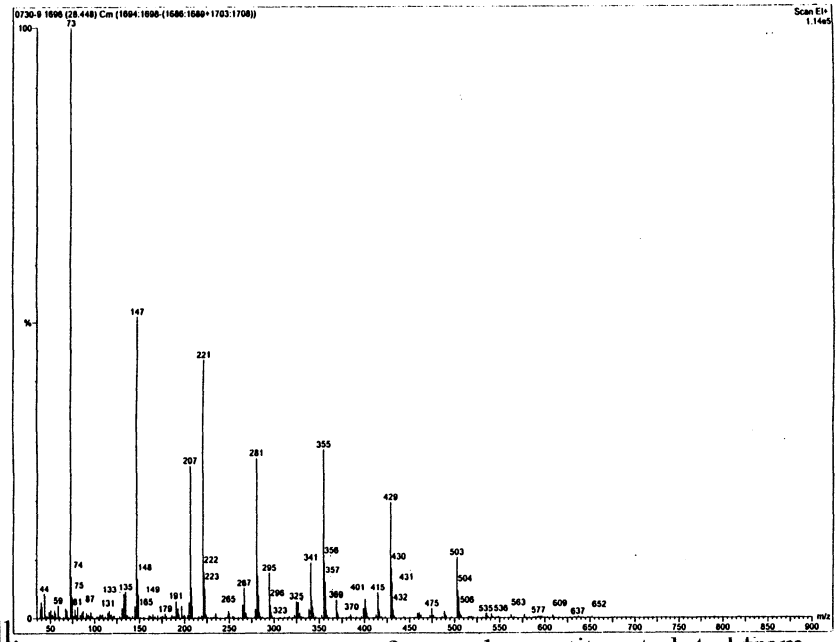

Figure 13.- Mass spectrum of seventh constituent eluted from residue extracted from a flown cell.

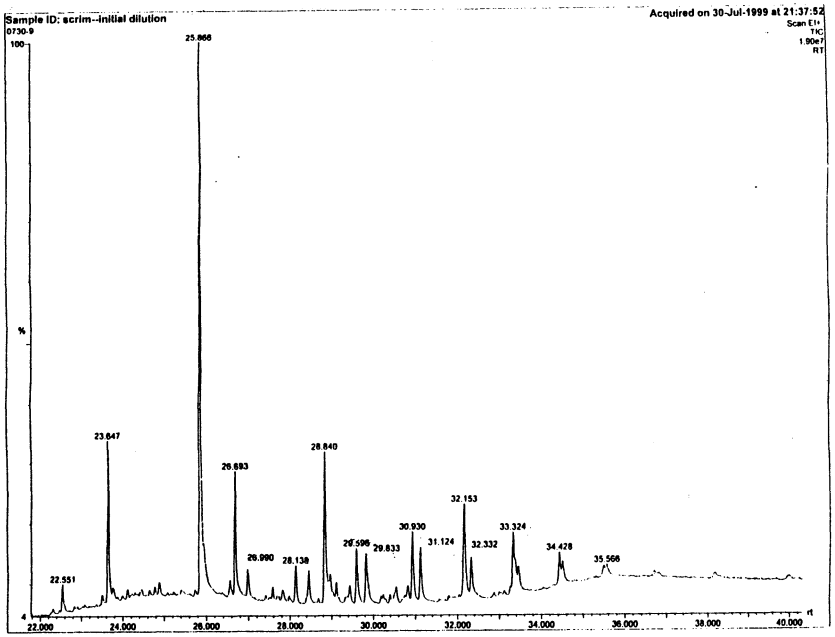

Figure 12.- Gas chromatogram of residue extracted from a flown cell.

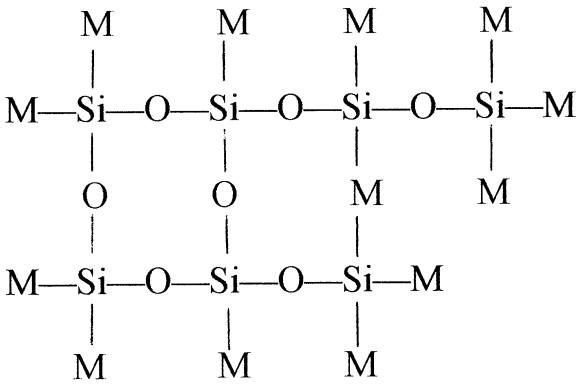

where M=CH_3

Figure 14.- Possible molecular diagram of seventh constituent eluted from extracted residue.

Page intentionally left blank

A STANDARDS- AND KNOWLEDGE-BASED APPROACH TO SPACECRAFT MODELING AND SIMULATION

David Silberberg
Andy Goldfinger
Lien Doung
Robert Hider, Jr.
John Hunt, Jr.
John Gersh
Martin Gomez
Anthony Nardo, Jr.
Gabe Rogers
Francis Weiskopf, Jr.

The Johns Hopkins University Applied Physics Laboratory
11100 Johns Hopkins Road
Laurel, MD 20723-6099
240-228-6231
david.silberberg@jhuapl.edu

ABSTRACT

The Johns Hopkins University Applied Physics Laboratory is developing a knowledge-based approach to standardizing spacecraft modeling and simulation (M&S) as well as sustaining design and design-process knowledge. The approach supports inter-organizational collaborative development, distributed simulation capabilities, plug-and-play capabilities to support rapid prototyping and software reuse, and design reuse. We define an object-oriented class decomposition of an abstract spacecraft along both functional and physical lines, and standard interfaces to each object. Mixed-fidelity spacecraft modeling and simulation software components inherit standard interfaces from the abstract classes as well as define their own unique interfaces, which enable them to be integrated seamlessly into a federated simulation of multiple simulation components. In addition, we define a knowledge base architecture that incorporates the object-oriented class decomposition, simulation component descriptions, and designs of federated simulations composed of individual simulation components. Since the knowledge base is platform-independent, its contents can be used to generate a federated simulation that runs on multiple distributed simulation platforms. Finally, we define an approach to sustaining design and design-process knowledge that extends the knowledge base to represent history, information, and experience with designs and design components.

INTRODUCTION

The current methodology for spacecraft design separates spacecraft design from testing and integration processes (refs. 1, 2). The spacecraft design process helps designers understand the behaviors of different design options and lets them pick those options that promise optimal performance. Usually, modeling and simulation is used in the design process to create conceptual architectures of spacecraft, which is later translated into a detailed design. Modeling and simulation is executed in an ad-hoc and as needed manner, and few of the simulations are ever reused or used for validation and testing. Some of the design process is performed with computer simulations, but others are performed with calculations using spreadsheets and paper. Given the ad hoc nature of the process, it is difficult to create a federation of these simulations to validate and test the integrated spacecraft. Due to the lack of consistency and standardization, the process has traditionally been slow and tedious.

The overall spacecraft design process is structured by creating design teams that are responsible for individual subsystems. Each team employs various simulations and calculations to examine the feasibility of their subsystem designs. The simulations and calculations test specific properties in specific scenarios and are often discarded after their use since they are not generally reusable. Furthermore, since subsystem teams do not usually work closely together, sub-

system simulation results and calculations are often shared through oral and data exchanges including flat files, excel spreadsheets, and word of mouth. Certainly simulations from different subsystems are not interoperable. As problems are discovered, the subsystem designs are iterated upon and checked against other subsystems until an overall system design is reached. However, the communication between design teams is ad hoc, slow, and subject to error.

Our vision is to facilitate the process of inter-organizational spacecraft design through a standards-based and knowledge-based approach. Imagine the following scenario. Two organizationally and physically separated design teams are tasked with creating a guidance, navigation, and control (GNC) system and a power system. Design engineers from both teams browse through many design cases stored in a knowledge base that describe previous spacecraft designs. The GNC team does not find a previous design that approximates the requirements of this mission, although they learn some of the pitfalls encountered by previous mission designers. In contrast, the power system team finds several examples of power system designs from previous missions that can be modified for this mission.

The GNC team creates a new design using design tools that are familiar to them. They begin by selecting and connecting components essential to the GNC system. To find the best reaction wheel for the design, they navigate to both the Acme Reaction Wheel and the Reaction Wheel Depot Web sites with their Web browsers, and download the descriptions and simulations of their respective wheels. They select the first reaction wheel and place it into their design. After all the components are selected and connected, the designers press the "Run Simulation" button to create a federated simulation that corresponds to the design. They examine the results of the simulation run and repeat the process with the second wheel. They find that the Reaction Wheel Depot's wheel performs better, but there are still modifications to be made to the design. Specifications and parameters are altered, and simulations are refined. Finally, the GNC appears to meets the requirements. During this process, simulation results and designer annotations are recorded in the knowledge base for use by other members of the mission design team and future design teams.

Simultaneously, the power system team also designs their subsystem and creates a corresponding simulation. Using a different design tool that is familiar to the power system team, the design is modified to meet the requirements of the new spacecraft. Before too much effort is placed into increasing the fidelity of both models, the subsystem designs are merged and tested until they interoperate seamlessly and without flaw. The design process continues and more functionality is added. Both subsystems are tested within the context of all spacecraft subsystems. Soon software is replaced by hardware-in-the-loop and the virtual spacecraft becomes a reality!

We have created knowledge- and standards-based architecture and prototype that enables this vision of rapid spacecraft development and validation. To fulfill this vision, the following tasks must be accomplished:

- Industry-wide acceptance of spacecraft standards for distributed and collaborative modeling and simulation.
- A knowledge-based architecture for representing standards, components, designs, and design knowledge
- A distributed simulation platform that operates over a wide area network
- A tool to capture and represent design knowledge

The next sections describe the simulation object and interface standards, the knowledge-based architecture, the knowledge base, the distributed simulation platform, and the design knowledge representation tools that are needed to support our vision.

DESIGN STANDARDS

The goal of developing spacecraft component standards is to facilitate the rapid development and validation of mixed-fidelity distributed simulations of spacecraft in a plug-and-play fashion (refs. 3, 4). The standards represent an object-oriented decomposition of a generic spacecraft both physically and functionally. The objects define standard interfaces to other objects. Spacecraft component simulations then define their interfaces by describing the objects from which they inherit. Any component simulation that adheres to the standards will automatically interface to other standard component simulations. Since the standard interfaces are not dependent on any particular implementation, the component simulations can be assembled in a plug-and-play fashion and will automatically interoperate. In addition, to encourage creativity and innovation, the standards are extensible. They will not inhibit novel component and subsystem design.

The first version of the standards (ref. 5) has been developed by studying multiple and varied candidate spacecraft that represent a rich and varied set of systems. The three spacecraft that were studied are: Thermosphere – Ionosphere – Mesosphere Energetics and Dynamics (TIMED), an scientific earth orbiting spacecraft that is in the design phase, MSX, a large and complex earth orienting spacecraft containing a variety of imaging sensors, and Near Earth Asteroid Rendezvous (NEAR), a deep space mission currently on its way to rendezvous with and orbit an asteroid. While the requirements and components of these spacecraft vary significantly, common structures and functionality have been abstracted from them. From these abstractions, a set of standard object-oriented classes and interfaces were defined that can be used to represent all of these spacecraft and we believe that the standards will fit most other mission requirements and spacecraft designs. Together, the classes and interfaces constitute the set of standards. Spacecraft designers at NASA and Jet Propulsion Laboratory (JPL) will review the standards for general community acceptance.

Based on the results of the standards study, we have created both a physical and functional decomposition of a generic spacecraft. The functional decomposition represents a generic spacecraft subsystem hierarchy. Spacecraft are decomposed into subsystems, and subsystems are decomposed into components. For example, an *attitude system* class is composed (in part) of *star camera* and *reaction wheel* classes. In contrast, the physical decomposition describes how components inherit abstract classes that are common to other components. It represents common properties that are represented in components and subsystems. For example and a *reaction wheel* object inherits from the *massive object* and *powered object* classes.

The overall functional decomposition of a spacecraft identifies the classical nine spacecraft subsystems. These are the attitude determination and control (or guidance, navigation, and control), command and data handling, instruments/payload, mechanical and structural, navigation, power, propulsion, telecommunications, and thermal control subsystems. In addition, an environment class models the physics with which spacecraft interact. Each subsystem is represented by abstract classes and interfaces. Examples of interfaces include mechanical, electrical, and data communications among the subsystems. In addition, physical interactions are modeled by interfaces among the subsystems and the environment.

The subsystems are also decomposed into common standard component classes. The component decomposition does not reflect the subsystems of any particular spacecraft. Rather, it reflects the types of components common to broad classes of spacecraft subsystems and their standard interactions. For example, an attitude control class may contain and interact with component object classes including reaction wheels, torque rods, thrusters, star trackers, gyroscopes, accelerometers, sun sensors, horizon sensors, magnetometers, and a bus interface. A telecommunications subsystem object may contain and interact with object classes including antennas, receivers, transmitters, amplifiers, transponders, diplexers, power splitters, and RF switches.

Many spacecraft components share common physical characteristics. For example, components often have mass, consume power, generate heat, generate electromagnetic noise, and communicate. Therefore, we represent abstract classes and interfaces that represent these common characteristics. Accordingly, classes like *massive object*, *powered object*, and *data source object* represent standard aggregation of and interfaces to abstract physical properties common to a wide variety of spacecraft components. The *massive object* class provides inheritance of attributes that include mass, center of mass, size, position, and orientation. The *powered object* class provides attributes that include steady state power, maximum power, heat generated, e/m noise generated, and power status. Similarly, the *data source* class provides attributes that include update rate, data rate, response time, data storage, and on/off status.

Actual component simulations that model the behavior of spacecraft components multiply-inherit from standard physical and functional classes. For example, component simulations that model the behavior of a standard reaction wheel inherit the standard interfaces of the *reaction wheel* class. In addition, since a reaction wheel has mass and is a powered object, it inherits from the standard *massive object* and *powered object* classes. Figure 1 depicts a reaction wheel with standard interfaces including *setTorqueCommandVoltage(), publishWheelSpeed(), publishWheelMomentum(),* and *publishWheelTorque().* It also inherits standard interfaces from *massive object*, such as *getMass(), getCenterOfMass(), getPosition(),* and *getOrientation();*and from *powered object*, such as *getSteadyStatePower(), getMaximumPower(),*and *getHeatGenerated().* Similarly, Figure 2 depicts a star tracker that inherits from a *star tracker* class. It

has standard star tracker interfaces including *setFieldOfView()*, *setSensitivity()*, *publishCoordinateError()*, *setNumberOfStarsTracked()*, *publishQuaternion()*, and *publishTime()*. In addition, it inherits standard interfaces from *massive object, powered object,* and *data source object.*

Actual components are not necessarily unique to individual subsystems. Some spacecraft components are dual-use and must be represented by several classes. An example of this is a battery that serves as the spacecraft chassis. The simulation of such dual-use components is facilitated by the standards since they also inherit from all applicable classes that describe their behavior and usage.

In addition, component simulations are not restricted to implementing only standard methods and interactions. They may extend the standards by specifying their additional unique capabilities. Since the simulations adhere to the base standards, their specifications need only list the incremental interactions that are supported.

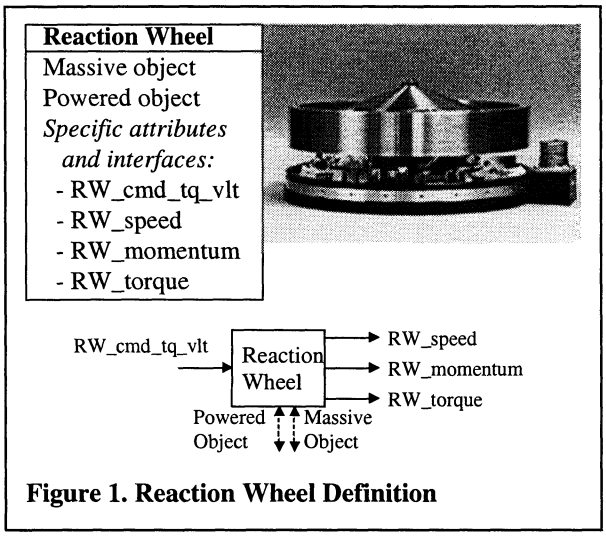

Figure 1. Reaction Wheel Definition

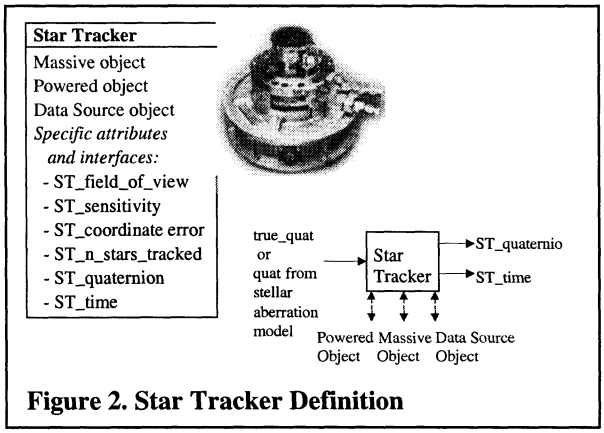

Figure 2. Star Tracker Definition

During the early stages of the design process, it is not always necessary or practical to provide high-fidelity simulations of subsystem components. Often, engineers need to focus on key component interactions to test the gross viability of a subsystem design. When the rough design is created, then the simulation software can be enhanced to provide higher fidelity modeling and simulations. Our standards approach supports this by allowing simulations to inherit from just the classes for which functionality is implemented. Thus, a low-fidelity star tracker simulation may only need to inherit from the *star tracker* and the *data source* object classes. Similarly, a low-fidelity reaction wheel simulation may need to inherit from only the *reaction wheel* class, but not the *massive object* and *data object* classes. A low-fidelity federated simulation can be assembled from low-fidelity component simulations that interact through the standard interfaces. After confirming the design viability at a rough level, the fidelity of the simulation can be enhanced to validate and test more detailed aspects of a design. The simulation software can be upgraded to higher fidelity simulations and can inherit incrementally from additional abstract classes such as *massive object* and *powered object.* As designs become more mature and detailed, the simulation standards can support the evolution and growth of increased fidelity spacecraft simulations.

ARCHITECTURAL COMPONENTS

Supporting the standards is a knowledge-based architecture that represents spacecraft designs and simulations from multiple perspectives. The standards are embodied in a knowledge base and allow multiple spacecraft designers to design, develop, modify, and validate designs in an integrated fashion. In particular, a three-tiered knowledge-based architecture is employed to represent design knowledge from three domain perspectives (ref. 6). The top layer represents knowledge from the perspective of the designers' concepts and ideas. At this level, designers interact with design tools to represent the mechanical, electronic, and environmental interactions of spacecraft components. The interfaces at this level represent and support the design concepts of spacecraft designers.

The middle layer of the architecture represents the knowledge base. This level is where the designs expressed at the top layer are stored. The knowledge base itself is three-tiered, representing the synthesis of spacecraft object-oriented modeling standards, knowledge of component capabilities, and designs. In addition, knowledge sustainment information

is stored at all tiers of the knowledge base. The representations are abstract, which ensures independence of and interoperability with multiple spacecraft design tools and simulation platforms.

The bottom layer represents knowledge from the perspective of simulations. Design information can be extracted from the knowledge base and expressed in the format of target simulation platforms. The expressions become specific directives to simulation tools, which test and validate spacecraft designs. In addition, this layer represents captured knowledge from simulation results that can be analyzed by spacecraft designers.

Multiple graphical user interface tools can be employed to design the spacecraft. The focus of this work is not to explore design tools. However, the design tools should allow the integration of components based on the standards. For example, a subsystem may be assembled via a graphical user interface, such as depicted in Figure 3, that allows designers to select the components of their design (from a palette, perhaps), place them onto a design area, and connect them according to the intended design. The connections are facilitated by the knowledge of standard component interactions that represent method calls with standard parameters. After the design is completed, it is stored in the knowledge base, which is used to validate the integration of the components.

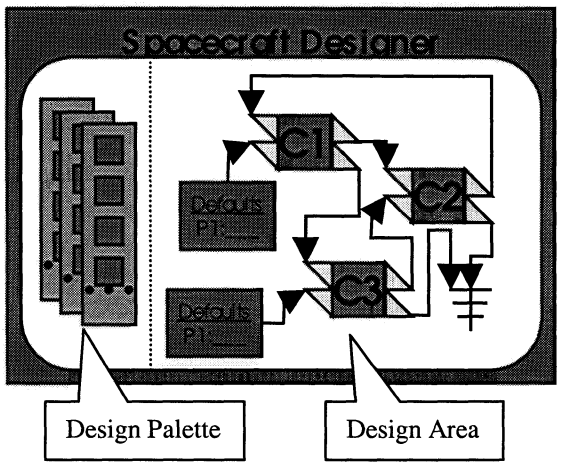

Figure 3. Example Spacecraft Design Tool

KNOWLEDGE BASE

The knowledge base is the key to providing an environment for rapid and collaborative distributed simulations (ref. 7). It embodies both design and the simulation representations. From the design perspective, it facilitates rapid subsystem design and enables integration with other subsystems. Since the representation is abstract, designers can create designs using tools that are familiar to their own domain. However, the products of the tools must express designs abstractly so that they can be stored in the knowledge base. Thus, while is our project is not recommending a specific design tool, we are developing a prototype that exemplifies the types of functionality and design capabilities that collaborative spacecraft design tools should offer.

The knowledge base is also three-tiered, as shown in Figure 4, which is modeled using the IDEF1X (ref. 8) notation. The top level represents the standards, which include both the physical and functional decomposition of generic spacecraft. In addition, it represents the structure of standard interfaces, whether interfaces call or are called in particular classes, the parameter orders, and the semantics of their parameters (e.g., type and units). For example, the standards layer represents both the *massive object* and the *structure* classes, which are stored in the "Abstract Classes" entity of the knowledge base. One of the interfaces of the *massive object* class is *getMass()*, which is called by the *structure* class. Thus, *getMass()* is stored in the "Methods" entity of the knowledge base and is associated with the *massive object* and *structure* classes by virtue of its representations in the "Standard Methods" entity. However, the knowledge base represents the *getMass()* method as a called interface in the *massive object* class, while it is represented as a caller in the *structure* class. The parameters and their order and semantics are stored in the "Parameters" entity.

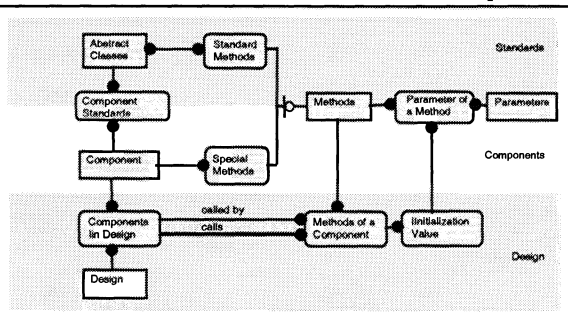

Figure 4. Knowledge Base Design

The middle layer of the knowledge base represents component simulations that are based on the standards. Component descriptions are placed in the "Component" entity. Standard abstract classes from which they inherit are

represented in the "Component Standards" entity. Unique component methods are represented in the "Methods" entity and are related to specific components in the "Special Methods" entity. The component descriptions may be acquired from different sources, including manufacturer Web sites and component simulation libraries, which must provide the abstract classes from which the associated simulations inherit, their interfaces, their additional unique methods, and component-specific properties.

The bottom layer of the knowledge base represents specific designs assembled from component simulations that adhere to the standards. Designs are captured in the "Design" entity and specific components that are employed in designs are captured in the "Design Component" entity. The calling and called-by interfaces among components and subsystems as specified by the designer are stored in the "Methods of a Component" and the "Initialization Value" entities.

The knowledge captured by the three layers describes designs in the abstract. This makes it feasible to extract specifications that drive simulations on multiple simulation platforms, including the Department of Defense (DoD) High Level Architecture (HLA) (ref. 9) and the JPL Millenia Engine. The knowledge base also captures information about requirements and experience with components and designs that can help guide future designers (not shown in Fig. 4). This knowledge will be described in the Knowledge Sustainment section of this paper.

DISTRIBUTED SIMULATION ARCHITECTURE

Since the knowledge base is an abstract representation of the standards, components, and designs, software tools can automatically extract information to drive distributed simulations on a variety of platforms. However, to demonstrate the feasibility of our knowledge-based approach, we have selected the HLA platform. HLA was developed in the mid-1990's by the Department of Defense (DoD) to support the interoperability and reuse of simulations and is used by the DoD to support war-gaming and training. However, the utility of HLA extends far beyond the military. It is applicable to a broad range of areas including spacecraft design. It provides a general and uniform environment that supports simulations involving pure software representations, man-in-the-loop simulators, hardware-in-the-loop simulators, event driven simulators, and live components. It supports an object-oriented approach to the development of distributed and interactive simulation models and environments, which is the type of environment needed to support the goals of our spacecraft M&S standardization effort.

HLA is rapidly being accepted as a general architecture for the specification of distributed simulations. In November 1998, the Object Management Group (developers of CORBA) adopted HLA as the Facility for Distributed Simulation Systems. Version 1.3 of the HLA specification has been accepted by the Simulation Interoperability Standards Organization for open standardization through the IEEE (ref. 10). Draft standards were made available in April 2000. A number of other countries are adopting HLA for their M&S activities.

As a proof of concept for our knowledge- and standards-based approach, we are developing a simulation of the TIMED satellite's attitude control system (ACS). The TIMED ACS includes flight computers (two Attitude Interface Units (AIU) and two Attitude Flight Computers (AFC)), actuators (four reaction wheels and three redundant magnetic torque rods), sensors (two star trackers, an internally redundant Inertial Reference Unit (IRU), redundant magnetometers and sun sensors), communication busses (using the 1553 protocol) and the rest of the spacecraft linked together, as shown in Figure 5. Each of the component simulations currently is being adapted to the draft standards. The simulation components are being placed on distributed and networked computers to be used by various designs. We will create multiple versions of the ACS design and show how the design descriptions can be represented in the knowledge base. Then, we will demonstrate that

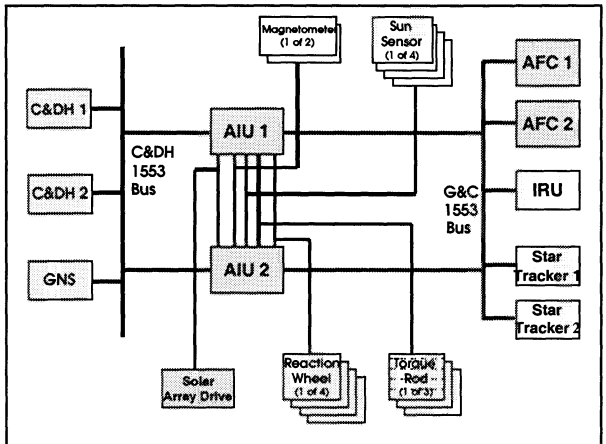

Figure 8. TIMED ACS Block Diagram

Simulation Object Model (SOM) and (Federated Object Model) FOM files can automatically be extracted from the knowledge base to drive the distributed simulations on the HLA platform. Then, we intend to demonstrate the flexibility of the approach by using the design tool to create models of the MSX and NEAR spacecraft ACS and automatically generate their simulations.

KNOWLEDGE SUSTAINMENT

Knowledge sustainment is the aspect of our approach that preserves knowledge about the design and the design process with the goal of both providing focused assistance to spacecraft designers and accelerating the design activity. Certainly, there are many aspects of knowledge sustainment that can facilitate the design process. We have chosen four areas that appear to have promise.

The first aspect of knowledge sustainment that we are addressing is a mechanism to allow designers to annotate designs with information including design rationale, experiences with designs, performance ranges, and viability for other missions. Engineers will use this capability during all phases of their design activities both for researching other designers annotations and for making annotations available to other designers on this and future missions. The approach to this tool is based on the PROSUS (PROcess-based Support System) (ref. 11).

The second aspect of knowledge sustainment that we are pursuing uses knowledge-based techniques to ensure that design specifications and behaviors meet requirements (ref. 11). Mission requirements are stored in the knowledge base and are related to the components of a design. During a distributed simulation of a design, the outputs of the component simulations relevant to the requirements are monitored and captured. Then, a tool analyzes the outputs with respect to their compliance with the requirements and displays the results to the designers. The designers will either be satisfied with the results or will iterate on the design until it complies with requirements. In either case, annotations will be made in the knowledge base that will guide the design choices of future spacecraft designers.

The third aspect of knowledge sustainment that we are pursuing captures knowledge about how to visualize the performance of a simulation. Often, the results of a simulation run are presented to designers in a rough, tabular form, which does not provide much intuition into the behavior of the simulation. Designers can make better and faster decisions when the information is presented graphically and in a way that highlights the issues that need to be addressed. To this end, we capture the visualization needs of designers in the knowledge base. After the simulation output is collected in a file, a process is executed that uses visualization knowledge to display the simulation results to the designer in the preferred format. Based on the results, the designer may choose to modify the design to best meet the design goals.

The fourth aspect of knowledge sustainment that we are addressing is a case-based reasoning capability. Engineers often can "jump start" their designs by examining similar designs employed on other spacecraft. Case-based reasoning tools provide the opportunity to search for similar designs based on component interaction configurations. The case-based tool will recognize the context of the current design and display similar designs found in the design database (refs. 12, 13). Engineers can copy all or part of similar designs into their current design. Simultaneously, they can read other engineers' design rationale and experience annotations to guide them in creating their current design.

CONCLUSION

We believe that our approach to spacecraft modeling and simulation will greatly improve the current "way of doing business." It will support collaborative modeling and simulation that is geographically and organizationally distributed. It will support rapid plug-and-play design capabilities, which will facilitate quick platform-independent modeling, simulation, integration, validation, and testing. In addition, knowledge sustainment capabilities will provide design guidance to engineers based on knowledge of other mission design efforts. It will also allow them to search for previous designs and utilize the collective wisdom and experience of spacecraft designers that have accumulated over time.

To date, we have developed the conceptual architecture and are in the process of creating a prototype to demonstrate its feasibility. Specifically, we have developed a first draft document that capture standards relevant to attitude control systems and have designed and created a knowledge base and software that automatically loads it with standards,

component descriptions, and requirements. In addition, we have commenced the coding of the spacecraft design interface, the process that automatically creates HLA object model files, the coding of ACS simulation components of the TIMED spacecraft to be used in our prototype, and the case-based reasoning tool. We expect to complete our prototype in December 2000.

REFERENCES

1. *Space Mission Analysis and Design,* Chapter 1, Wertz, J.R. and Larsen, W.J. (editors), Kluwer Academic Publishers, Dordrecht, 1991.

2. Pisacane, V.L. and Moore, R.C., *Fundamentals of Space Systems,*Oxford University Press, New York. Chapter 1, 1994.

3. Goldfinger, A., Silberberg, D., Doung, L., Gersh, J., Gomez, M., Hunt, J., Rogers, G., Weiskopf, F., "An Integrated Architecture for Spacecraft Design and Simulation," *Proceedings of the 2000 Summer Computer Simulation Conference*, Vancouver, Canada. July 16-20, 2000.

4. Goldfinger, A., Silberberg, D., Gersh, J. Hunt, J., Weiskopf, F., Spisz, T., Mou, Z.G., Rogers, G., Semmel, R., "A Knowledge-Based Approach to Spacecraft Distributed Modeling and Simulation," *International Journal of Advances in Engineering Software including Computing Systems in Engineering*, Elsevier, Oxford, U.K., 1999.

5. Rogers, G. and Hunt, J., "Draft Spacecraft Modeling Standards" *Internal JHU/APL document*, May 2000.

6. Silberberg, D., Goldfinger, A., Gersh, J., Hunt, J., Weiskopf, F., "Standards for Distributed Spacecraft Modeling, Simulation, and Knowledge Sustainment" *Proceedings of the American Institute for Aeronautics and Astronautics (AIAA) Space Technology Conference*. AIAA Press. 1999.

7. Silberberg, D., Goldfinger, A., Spisz, T., Gersh, J., Weiskopf, F., Mou, Z.G., Hunt, J., Rogers, G., Semmel, R., "Knowledge-Based Modeling and Simulation for Spacecraft Design and Development" *Fifth Symposium for Research and Development*, Johns Hopkins University Applied Physics Laboratory, 1999.

8. *Integration Definition for Information Modeling (IDEF1X)*, National Institute of Standards and Technology, Federal Information Processing Standards (FIPS) Publication 184, December 1993.

9. *High Level Architecture Object Model Template Version 1.0*, Department of Defense, 15 August 1996. http://hla.dmso.mil/portals/hla.html

10. *Draft Standard for Modeling and Simulation (M&S) High Level Architecture (HLA) - Framework and Rules*, Standard P1516, Department of Defense, [0-7381-2563-6] [DS5839-NYF], April 2000.

11. Blessing, L., "Supporting the Knowledge Life Cycle," Knowledge-Intensive CAD 3,Tokyo Japan, Dec. 1998.

12. Bilgic, T. and Fox, M., "Constraint-Based Retrieval of Engineering Design Cases," *Proceedings of the Fourth International Conference on Artificial Intelligence in Design*, Stanford California, June 1996.

13. Leake, D. and Wilson, D., "Combining CBR with Interactive Knowledge Acquisition, Manipulation and Reuse," *Proceedings of ICCBR-99*, 1999. http://www.cs.indiana.edu/~leake/INDEX.html

ASSESSING LEONID METEOROID IMPACT RISKS

Aleck L. Lee
Lockheed Martin Space Systems Company
Sunnyvale, California

ABSTRACT

The Leonid meteoroid storm produced by the passage of its parent comet, 55p/Tempel-Tuttle has been a concern for satellite operators. The recent close approach of the comet to the Earth took place around January 17, 1998. The debris cloud was expected to be several hundred to several thousand times higher than normal in the ensuing years when the Earth passes by the comet trail. Leonid meteoroid storm intensity was predicted before by analyses for satellite mission planning. The low observed Zenith Hourly Rate (ZHR) displayed in 1998 was due to the large distance between the particle and the Earth. In 1998, all of the Leonid material was located interior to the Earth's orbit at distances greater than 0.004 AU. In 1999 there will be two streams located interior to the Earth orbit; the first, consisting of material ejected from the comet in 1932, will be 0.0016 AU from the Earth, and the second composed of material ejected from Tempel-Tuttle in 1965 at 0.004 AU. More importantly, there will exist a third stream of cometary debris, located just 0.0008 AU exterior to Earth's orbit. This stream will consist of the material ejected in 1899, and its close proximity to the Earth means that the space shall be subjected to a Gaussian-like Leonid environment. The predicted probability indicates that there will certainly be a storm with ZHR higher than 1000 in November 1999. It is also likely that there will be another Leonid storm in 2000. A procedure to predict the number of hits by the meteoroids was developed using the ZHR prediction model and the orbit data of GEO communication satellites. The data include the attitude of the satellite and its projected area as a function of orbit position. The number and probability of hits are predicted for these satellites during the 1999 Leonid meteoroid storm. The worst case prediction is also included for comparison.

INTRODUCTION

The Leonid meteoroid storm produced by the passage of its parent comet, 55p/Tempel-Tuttle has been a concern for satellite operators. The recent close approach of the comet to the Earth took place around January 17, 1998. The debris cloud was expected to be several hundred to several thousand times higher than normal in the ensuing years when the Earth passes by the comet trail. Leonid meteoroid storm intensity was predicted before by analyses for satellite mission planning (Refs. 1, 2).

The observed data of Leonid meteoroid storm in 1998 were reported by several authors in the papers presented in the 1999 Leonid conference (Refs. 3, 4). The key findings in these observations were the following:

- No major meteor storm occurred in 1998,
- Peak flux occurred within one hour of the predicted expected time,
- Peak flux was approximately 0.02 meteoroid km^{-2} hr^{-1}.
- Storm produced by streamlets ejected ~100 years previously at 0.0008 AU,

The low observed Zenith Hour Rate (ZHR) displayed in 1998 was due to the large distance between the particle stream and the Earth. In 1998, all of the Leonid material was located interior to the Earth's orbit at distances greater than 0.004 AU. In 1999 there will be two streams located interior to the Earth orbit; the first, consisting of material ejected from the comet in 1932, will be 0.0016 AU from the Earth, and the second

composed of material ejected from Tempel-Tuttle in 1965 at 0.004 AU. More importantly, there will exist a third stream of cometary debris, located just 0.0008 AU exterior to Earth's orbit. This stream will consist of the material ejected in 1899, and its close proximity to the Earth means that the space shall be subjected to a Gaussian-like Leonid environment (Ref. 4). Table 1 summarizes the predicted probability of storm, P_{storm}, and the ZHR values for years 1998 to 2001.

Table 1 Predicted Leonid storm probability and ZHR

Year	P_{storm}	ZHR
1998	0.6	562
1999	1.0	1412
2000	0.25	1230
2001	> 0.33	502

The predicted probability indicates that there will certainly be a storm with ZHR higher than 1000 in November 1999. It is also likely that there will be another Leonid storm in 2000.

SPEED OF LEONID METOEROIDS

The Leonid meteoroid is well known for the high impact speed to a spacecraft. The orbit of the parent comet and the inclination angle determine the approach speed of a meteoroid to a spacecraft. Figure 1 shows a schematic of an elliptic orbit with the Sun at one of its foci.

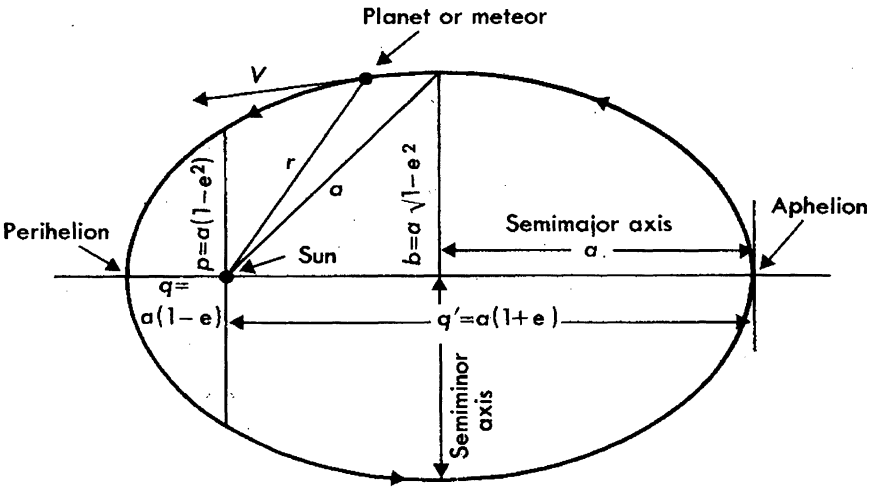

Fig. 1 The geometry of an elliptical orbit.

Kepler's unwritten fourth law gives the speed of an object V (in km/sec) as a function of its distance from the Sun, r, and the semi-major axis, a. The distances are expressed in astronomical units, AU (Ref. 5).

$$V^2 = 886 \ (2/r - 1/a) \qquad (1)$$

For a parabolic orbit, where a = ∞, the velocity of 42 km/sec represents the maximum in the solar system. For Tempel-Tuttle, being in a highly elliptic orbit, the velocity at perihelion point where it is also near the closest position to the Earth, is nearly this speed. The orbital speed of the Earth can be evaluated using this equation by setting r = a. The orbital speed of the Earth turns out to be 29.8 km/sec.

The inclination angle is the angle between the orbit plane of the Earth and that of the comet, defined in Fig. 2. In the case of Leonid meteors, the inclination angle is 17° and the comet moves in retrograde direction, i.e., head on to the Earth. The relative velocity between the comet and the Earth is therefore the sum of the two speeds, or 70 km/sec. The relative speed of the comet seen from a satellite has to be adjusted by the orbital speed of the spacecraft. In a geosynchronous orbit with a 24-hour period, the orbital speed is 3.1 km/sec. The relative speed of Leonid meteoroid to the GEO spacecraft is therefore between 67 km/sec and 73.1 km/sec.

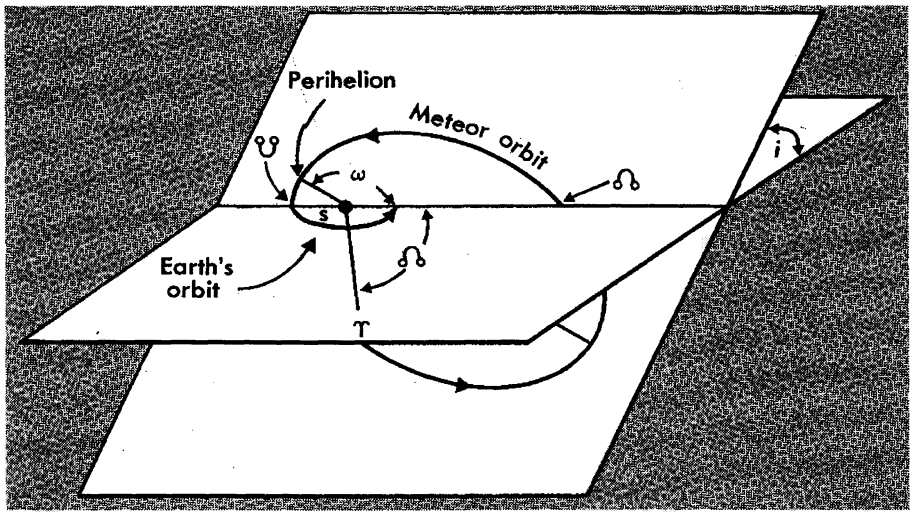

Fig. 2 The inclination angle between the orbit planes.

THE FLUX OF 1999 LEONID STORM

As mentioned earlier, there will be three streams of cometary debris in 1999 (Ref. 4). Two streams are located interior to the Earth orbit; the first, consisting of material ejected from the comet in 1932, will be 0.0016 AU from the Earth, and the second composed of material ejected from Tempel-Tuttle in 1965 at 0.004 AU. More importantly, there will be a third stream of cometary debris, located just 0.0008 AU exterior to Earth's orbit. This stream will consist of the material ejected in 1899, and its close proximity to the Earth means that the space shall be subjected to a Gaussian-like Leonid environment, with satellites closest to the stream receiving many times more flux than those situated on Earth's Sun-ward side.

The approximate relative distances between the Earth and the Leonid meteoroid streams are shown in Figure 3 (Ref. 4). In the figure, the position of the Sun is to the left along the line connecting the Earth and the Sun. The stream from 1899 comet passage is exterior to the Earth orbit shown on the right-hand side. This stream contributes most of the mass flux to the Leonid storm because of its proximity to the Earth. Therefore, it is expected that the maximum Leonid flux will take place at the satellite midnight point, i.e. at the anti-Sun side or η=180° of the orbit, as this is the point closest to the meteoroid stream.

The closest encounter in 1999 is predicted to be at 2:20 UT of November 18 (Ref. 4). Other authors predicted that the maximum takes place between 0.5 and 2.5 UT of November 18 (Ref. 3). In this analysis, the peak is assumed to be at 2:15 UT for the convenience of calculation.

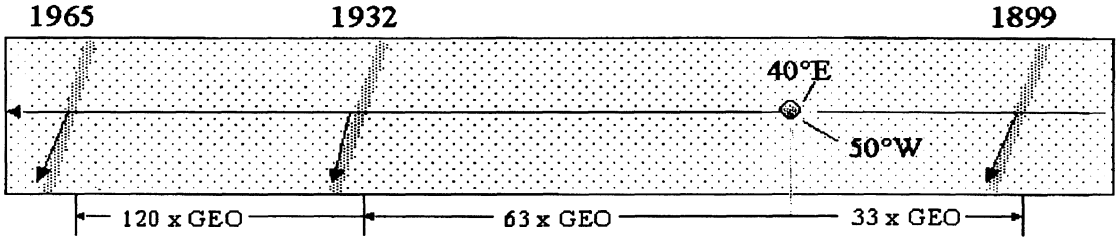

Fig. 3 Relative distance of meteoroid streams. 1899 stream is exterior of Earth orbit.

This asymmetric situation will vastly complicate calculations of the Leonid flux or fluence upon the bulk of orbiting vehicles, as both the distance from the Earth and the location of the satellite relative to the anti-Sun point must be considered. Fortunately, in the case of geostationary satellites, it is possible to construct an expression for the Leonid flux at the time of maximum as follows (Ref. 4).

$$F_{max} = 1.7\text{x}10^{-8}\ e^{\{-0.016\,[18.76 - 6.61\cos(\lambda - 35)]^2\}}\ m^{-0.8} \qquad (2)$$

Where F_{max} is the Leonid flux for particle mass greater than m (in grams) per square meter per hour, and λ is the satellite longitude (in degrees) counted west of Greenwich. Note that the greatest Leonid flux occurs at the time when the local longitude is at 35°W, which is the position at the anti-Sun point where the maximum mass flux of the Leonid stream takes place. The value of F_{max} varies between the maximum value and the minimum value at the orbit point of η=180° and 0°, respectively. The variation between the maximum and the minimum of F_{max} can be three orders of magnitude.

The formula in Eq. (2) is based on the following assumptions.

(1) The density of the 1899 stream is the same as it was in 1966 and the stream density obeys a Gaussian distribution with heliocentric distance. Figure 4 shows the intensity distribution of the 1966 Leonid storm (Ref. 6).

(2) The predicted peak time will be correct, and

(3) There is no appreciable contribution to the flux by the 1932 and 1965 streams. Either of these streams has not been encountered previously, so they are completely unknown. However, their recent ejection from the comet implies that they must be relatively dense and less dispersed than the 1899 stream. Brown's models indicate that roughly 20% of the material encountered in 1999 will be from the 1932 stream. The maximum mass flux calculated by Eq. (2) already accounts for the mass flux from the streams ejected in years 1899, 1932 and 1965.

For the convenience of calculation, let the orbit angle η be used. The equation for F_{max} will become

$$F_{max} = 1.7\text{x}10^{-8}\ e^{\{-0.016\,[18.76 - 6.61\cos(180 - \eta)]^2\}}\ m^{-0.8} \qquad (3)$$

Since the storm in 1999 is caused mostly by the mass ejected during the 1899 comet passage, as was the 1966 Leonid storm, it is expected that the shape of the 1999 storm will be similar to that of 1966 storm. Figure 4 shows the intensity in ZHR of the 1966 Leonid storm versus solar longitude.

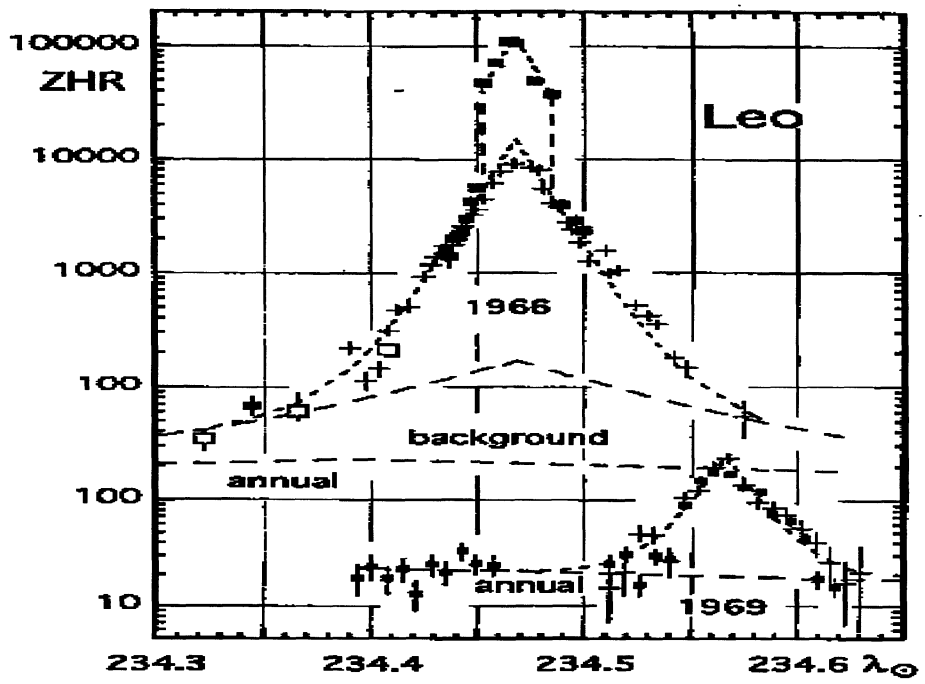

Fig. 4 The ZHR vs. time for the 1966 Leonid Storm.

Using the data from 1966 Leonid storm as a guide, the storm width at ZHR=1000 is 0.08 when measured in solar latitude λ_θ. Each 0.1-degree of λ_θ is equivalent to approximately 2.43 hours of the Earth time. The storm width at ZHR=1000 is roughly 1.94 hours, at ZHR=100 is 4.62 hour, and the total width before back to nominal background is 7.3 hours. This analysis covers a period of 12 hours, from six hours before to six hours after the peak of the storm.

THE PROBABILITY OF NO IMPACTS

The probability P_n of n hits by meteoroid is given by the following formula according to a Poisson's distribution (Ref. 7). The quantity N is the average number of hits in the given time interval.

$$P_n = N^n \cdot e^{-N} / n! \qquad (4)$$

The probability P of any number of hits, i.e. for n greater than 0, can be calculated as $(1 - P_o)$, where P_o is the probability of zero hit. Setting n equal to 0 in the above equation, the probability of any number of hits becomes unity subtracted by the probability of zero hit, as shown below.

$$P = 1 - e^{-N} \qquad (5)$$

When the number of hits N is less than 1, the probability approaches the number N. The probability of no impacts (PNI) is simply the following.

$$PNI = 1 - P = e^{-N} \qquad (6)$$

PREDICTION OF LEONID 1999 HITS

The Leonid storm impacts on two GEO spacecraft are analyzed with the orbital data from Reference 8. The position of a satellite is described by the orbit angle, η, measured from the Earth-Sun line starting from the point closest to the Sun. The value of η is 0° at the near Sun point, and 180° at the anti-Sun point. In the first case, designated as Flight-1, the satellite will be at the orbit angle, η=99° at the time when the peak storm activity is predicted. At the time of Leonid storm peak at 2:15 UT November 18, the local longitude of Flight-1 is 116°W at η=99°. In the second case, designated as Flight-2, the spacecraft is at η=221° and the longitude is 4°E at the storm peak. The predicted total number of hits accounts for the time period from six hours before the peak to six hours after. Total length of the time period covers 12 hours.

A third case, designated as Flight-3, is also considered. Since the strongest Leonid trail is outside the earth orbit, the point closest to the Leonid core would be the point opposite to the Sun. The corresponding orbit angle would be η=180°. This is the worst case when this orbit position coincides with the peak of the predicted Leonid activities.

The Leonid mass flux impinging on a spacecraft surface is a function of the mass flux density and the cross sectional area of the spacecraft. These parameters depend on orbit position, attitude, and time. At the predicted peak of the 1999 Leonid storm, the maximum mass flux expressed in number of hits per square meter per hour for particle mass greater than m is given in Eqs. (2) and (3). The size of a particle is converted from the given mass, assuming a spherical shape and a density of 1 g/cm^3. Table 2 shows the conversion of particle size to mass and the factors used in maximum mass flux predictions.

The maximum mass flux is a complex function of cosine of the orbit angle and the mass factor. Figure 5 shows the exponential function of the maximum flux equation for the covered time period – six hours before and after the Leonid peak. The time scale in the figure is centered at the peak of the storm. This figure shows the flux variation caused by the distance between the spacecraft the meteoroid trail for both Flight-1 and Flight-2. At the beginning of the covered period, the mass flux for Flight-1 is at a low point and starts to increase as it moves along the orbit, while Flight-2 begins with a high mass flux rate for the same time period. At the peak of the storm, Flight-2, being closer to the η=180° anti-Sun point, sees a much higher mass flux of the Leonid storm than Flight-1.

Table 2 Conversion of particle size to mass, assuming a density of 1 g/cm^3.

Particle Size, μm	m, g	$m^{-0.8}$	$1.7\times10^{-0.8}\ m^{-0.8}$
1	5.24×10^{-13}	6.68×10^{9}	1.136×10^{2}
5	5.55×10^{-11}	1.40×10^{8}	2.386×10^{0}
10	5.24×10^{-10}	2.66×10^{7}	4.518×10^{-1}
100	5.24×10^{-7}	1.06×10^{5}	1.799×10^{-3}
1000	5.24×10^{-4}	4.21×10^{2}	7.161×10^{-6}
10000	5.24×10^{-1}	1.68×10^{0}	2.851×10^{-8}

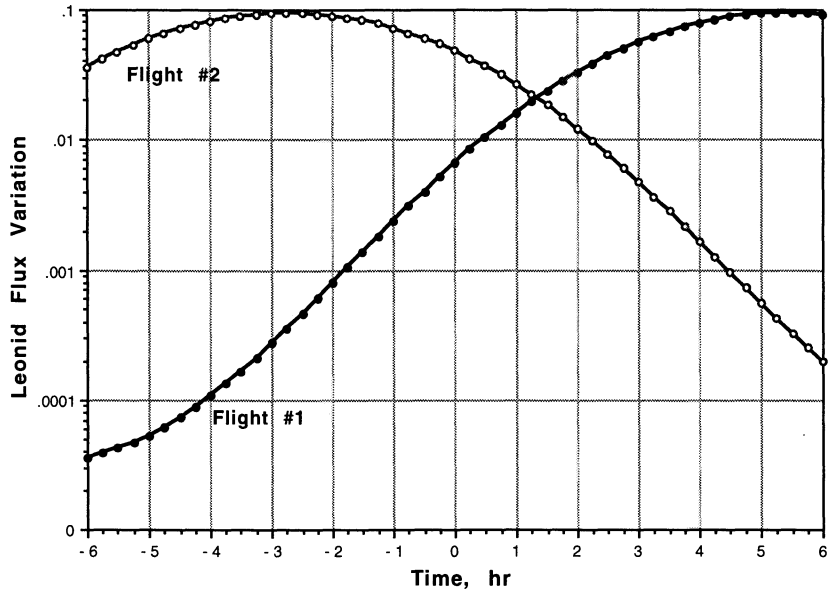

Fig. 5 Leonid maximum flux variation vs. time.

The flux at other time before or after the peak can be calculated using the maximum flux equation and adjusted according to the longitude of the location and the elapsed time. Assuming the Leonid storm of 1999 takes the same shape of the 1966 storm as shown in Figure 4, the mass flux before and after the peak has to be multiplied by a normalizing factor. A plot of the normalizing factor is shown in Figure 6. The unity coincides with the peak flux value of the 1966 Leonid storm. Figure 7 shows the projected cross-sectional areas of the spacecraft and the solar arrays of Flight-1 and Flight-2. Flight-3 uses the same projected cross-sectional areas of Flight-1 in the calculation.

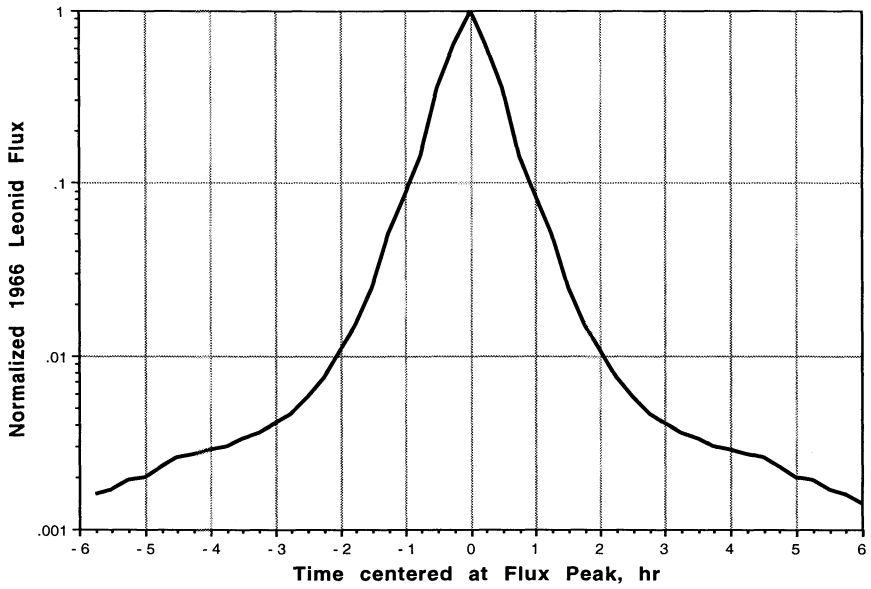

Fig. 6 Normalized 1966 Leonid flux curve.

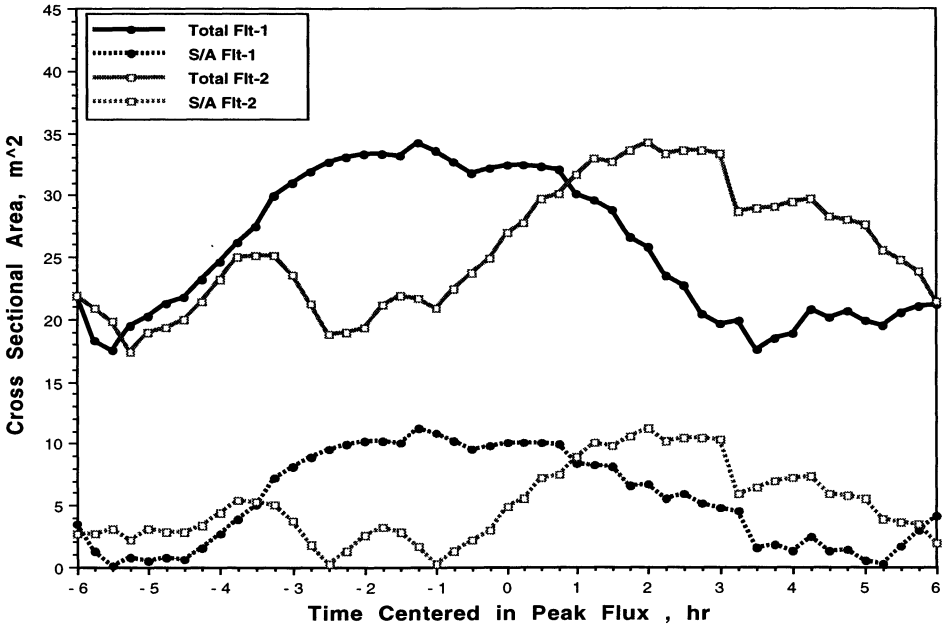

Fig. 7 Total and solar array cross-sectional areas.

A spreadsheet was developed to calculate the Leonid flux during the 12-hour period centered at the predicted peak. The first column in the spreadsheet shows the time in UT. The mass flux for particle sizes greater than 10μm, 100μm, 1000μm, and 10000μm are given in the last four columns. The total mass flux in the size ranges between 10-100, 100-1000, and 1000-10000 μm is given separately at the bottom of each column. The probability of no impact (PNI) is also calculated using Eq. (6). Table 3 summarizes the results.

Table 3 Summary of number of hits and probabalibity of no impacts.

Particle size, μm	10-100	100-1000	1000-10000	All ≥ 10μm
Flight-1				
Total Area # hits	1.033E-01	4.114E-04	1.638E-06	1.037E-01
PNI	0.9018	0.9996	1.000	0.9015
Solar Array # hits	3.045E-02	1.212E-04	4.845E-07	3.057E-02
PNI	0.9700	0.9998	1.000	0.9699
Flight-2				
Total Area # hits	5.279E-01	2.102E-03	8.401E-06	5.301E-01
PNI	0.5898	0.9979	1.000	0.5885
Solar Array # hits	8.410E-02	3.349E-04	1.338E-06	8.444E-02
PNI	0.9193	0.9997	1.000	0.9190
Flight-3				
Total Area # hits	1.237E-00	4.888E-03	1.953E-05	1.232E-00
PNI	0.2930	0.9951	1.000	0.2916
Solar Array # hits	3.776-01	1.504E-03	6.009E-06	3.791E-01
PNI	0.6855	0.9985	1.000	0.6845

Prediction shows that Flight-2 will receive more hits from the Leonid storm than Flight-1. This is consistent with the maximum mass flux variation shown in Figure 5. The portion of Flight-2 orbit at the time of storm peak is closer to the high flux region of Leonid storm than Flight-1. The bulk of mass flux comes from the short time span centered at the storm peak. The results in Table 3 show that the number of hits on Flight-2 is approximately five times that of Flight-1. Flight-3, represented the worst case, shows a mass flux more than 10 times that of Flight-1 and more than two times that of Flight-2. This is the upper bound of the number of hits.

The probability of hit, (1-PNI), by any particles greater than 10 μm is 0.10 for Flight-1 and 0.41 for Flight-2. The probability of hit on the solar array is smaller than that for the entire spacecraft, because of the smaller cross-sectional areas. The probability of getting hit by particles larger than 10 μm is 0.03 for Flight-1 and 0.08 for Flight 2. There are no hits by particles larger than 1000 μm, including the worst case, Flight-3.

The high speed of particles in Leonid meteoroid storm causes serious concerns for satellite operators. When a small particle packed with such high approaching velocity hits a spacecraft, the impact can result in structural damage or electrical damage caused by plasma production. The smaller particles are much more numerous than the larger particles in a meteoroid storm. Using the same formula given in Eq. (3), the mass flux for particles larger than 1 μm is calculated. Table 4 summarizes the predicted number of impacts by particles ranging from 1 to 5μm and from 5 μm to 10 μm, and the probability of no hit in the respective size range.

The results tallied in Table 4 show that it is almost certain that the spacecraft and its solar array will be hit by meteoroid particles of size less than 5 μm in all cases. The probability of hit by 5-10 μm particles is 0.42 for Flight-1 and 0.9 for Flight-2. The probability of hit on the solar array is 0.15 for Flight-1 and 0.3 for Flight-2. In terms of number of hits, Flight-2 will see four to five times more hits in the 1-5 μm particle size range, and two to four times more in the 5-10 μm particle size range than Flight-1. Again, the Flight-3 is the upper bound for the number of hits. This worst case shows about 10 times higher than the predicted number of hits of Flight-1 and more than two times higher than Flight-2. The variation is caused by the combination of orbit position at the time of peak Leonid activity and the orientation of the spacecraft. The latter determines the cross-sectional area of the spacecraft that intercepts the incoming meteoroid stream.

Table 4 Summary of number of hits by particles in 1~10 μm range.

Particle size range	1- 5 μm	5 - 10 μm
Flight-1		
Total Area # hits	2.598E+01	5.460E-01
PNI	0	0.5793
Solar Array # hits	7.655E+00	1.609E-01
PNI	0.0005	0.8514
Flight-2		
Total Area # hits	1.305E+02	2.269E-00
PNI	0	0.1034
Solar Array # hits	2.078E+01	3.615E-01
PNI	0	0.6966
Flight-3		
Total Area # hits	3.086E+02	6.487E-00
PNI	0	0.0015
Solar Array # hits	9.495E+01	1.966E-00
PNI	0	0.1359

CONCLUSIONS AND RECOMMENDATIONS

A procedure to compute the mass flux, number of hits, and the probability of impacts has been developed for the 1999 Leonid meteoroid storm. The results show that for the two GEO spacecraft flights, Flight-2 will see approximately five times more impacts than Flight-1. The probability of having impacts of particles larger than 10 μm is 0.1 for Flight-1 and 0.41 for Flight-2. The probability of hits by particles between 1 and 10μm is much higher, as indicated in Table 4. It is almost certain that the spacecraft will be hit during the 1999 Leonid storm by particles in the 1-10 μm size range. The number of hits is also calculated for the worst case, Flight-3, where the spacecraft is passing through the anti-Sun point of $\eta = 180°$ at the peak of Leonid storm.

It is recommended that the satellite operator use these estimates of hit to plan for mitigation measures during the period of predicted Leonid storm. It is especially pertinent to assess the potential damages that might be caused by impacts of small meteoroid particles and to develop necessary mitigation strategies (Ref. 9). There were no known reports from the spacecraft operators throughout the world during the 1999 Leonid storm.

Since Leonid meteoroid storm for year 2000 and beyond is also predicted to be a highly likely event, it is recommended that a similar mass flux prediction and probability of hit analysis be performed. The data from the analysis will be needed for mission planning when the next Leonid storm comes around.

REFERENCES

1. A. L. Lee, "Assessing Leonid Threat to a Spacecraft," LMMS TSS-586, March 12, 1998.
2. A. L. Lee, "Prediction of Leonid Storms 1998 and 1999," LMMS TSS-601, November 12, 1998.
3. P. Brown, et al, "Observations of the 1998 Leonid Shower and Model Predictions of Shower Activity for 1999-2001," Presented in 1999 Leonid Meteoroid Storm and Satellite Threat Conference, sponsored by AIAA and the Aerospace Corp., May 11-13, 1999.
4. W. J. Cooke and R. M. Suggs, "The 1998 Leonid Apparition: Satellite Fluences and Projected Values for 1999," Presented in 1999 Leonid Meteoroid Storm and Satellite Threat Conference, sponsored by AIAA and the Aerospace Corp., May 11-13, 1999.
5. G. S. Hawkins, *The Physics and Astronomy of Meteors, Comets, and Meteorites*, McGraw-Hill, 1964.
6. P. Jenniskens, "Meteor Stream Activity - II. Meteor Outbursts," *Astronomy and Astrophysics*, Vol. 295, 1995, pp. 206-235.
7. A. L. Lee, "Assessing Meteoroid and Space Debris Risks," *19th Space Simulation Conference Cost Effective Testing for the 21st Century*, NASA CP-3341, Oct. 1996.
8. J. D. Gill, Private Communication, October 1999.
9. G. E. Peterson, *Dynamics of Meteor Outbursts and Satellite Mitigation Strategies*, The Aerospace Press, 1999.

NATIONAL IGNITION FACILITY
TARGET CHAMBER

Paul Fleming
Project Manager
Pitt-Des Moines, Inc.

Richard W. Wavrik, P.E.
National Ignition Facility, Lawrence Livermore National Laboratory

James Cox
Beampath Hardware Fabrication
National Ignition Facility, Lawrence Livermore National Laboratory

ABSTRACT

On June 11, 1999 the Department of Energy dedicated the single largest piece of the National Ignition Facility (NIF) at Lawrence Livermore National Laboratory (LLNL) in Livermore, California. The ten (10) meter diameter Aluminum Target High Vacuum Chamber will serve as the working end of the largest laser in the world. The output of 192 laser beams will converge at the precise center of the Chamber. The laser beams will enter the Chamber in two by two arrays to illuminate 10 millimeter long gold cylinders called hohlraums enclosing 2 millimeter capsule containing deuterium, tritium and isotopes of hydrogen. The two isotopes will fuse, thereby creating temperatures and pressures resembling those found only inside stars and in detonated nuclear weapons, but on a minute scale. The NIF Project will serve as an essential facility to insure safety and reliability of our nation's nuclear arsenal as well as demonstrating inertial fusion's contribution to creating electrical power.

The paper will discuss the requirements that had to be addressed during the design, fabrication and testing of the Target Chamber.

A team from Sandia National Laboratories (SNL) and LLNL with input from industry performed the configuration and basic design of the Target Chamber. The method of fabrication and construction of the Aluminum Target Chamber was devised by Pitt-Des Moines, Inc. (PDM). PDM also participated in the design of the Chamber in areas such as the Target Chamber Realignment and Adjustment System, which would allow realignment of the sphere laser beams in the event of earth settlement or movement from a seismic event.

During the fabrication of the Target Chamber the sphericity tolerances had to be addressed for the individual plates. Procedures were developed for forming, edge preparation and welding of individual plates.

Construction plans were developed to allow the field construction of the Target Chamber to occur parallel to other NIF construction activities. This was necessary to achieve the overall schedule. Plans had to be developed for the precise location and alignment of laser beam ports.

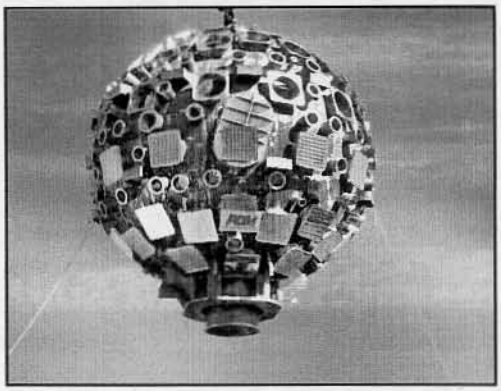

COMPLETED TARGET CHAMBER BEING LIFTED INTO PLACE

Upon completion of the fabrication of the Aluminum Target Chamber in a temporary structure the 130 ton sphere was moved from the temporary construction enclosure to its final location in the target building.

Prior to the installation of a concrete shield and after completion of the welding of the chamber penetrations vacuum leak checking was performed to insure the vacuum integrity of Target Chamber.

The entire spherical chamber external surface supports a sixteen (16) inches thick reinforced concrete shield after installation in the target building.

The final task is a total survey of the laser ports and the contour machining of spacer plates so that laser devices attached to these ports meet the alignment criteria.

This work was performed under the auspices of the U.S. Department of Energy by University of California Lawrence Livermore National Laboratory under contract No. W-7405-Eng-48.

INTRODUCTION

On December 19, 1996, the U. S. Department of Energy issued the Record of Decision for the *Programmatic Environmental Impact Statement for the Stockpile Stewardship and Management Program*, approving the construction of the National Ignition Facility (NIF). The NIF is currently under construction at Lawrence Livermore National Laboratory (LLNL) where it will be the latest in a series of high-power laser facilities used for research in inertial confinement fusion. The world-class NIF design team includes experts from LLNL, SNL, Los Alamos National Laboratory (LANL), and the University of Rochester's Laboratory for Laser Energetics (URL). When completed the NIF will house 192 laser beamlines that run the length of the facility and direct their energy inside the target chamber upon a fusion fuel capsule the size of a BB.[1]

The task facing a team of engineers from LLNL and SNL was to design and deliver a vacuum vessel that would be capable of operating at least 30 years, withstand earthquakes as well as debris and gamma radiation from experiments, maintain deep vacuum and ultrafreezing environments required for experiments, and accommodate nearly a hundred diagnostic instruments, 192 beamlines, and associated optics and equipment. All of the chamber work also had to be completed on a schedule consistent with the building schedule so that installation of the chamber could be accomplished without impacting building progress. The engineering team first consulted with laser

scientists, optical experts, target physicists, laser physicists, and facility designers at LLNL, SNL, LANL, URL, and the Defense Threat Reduction Agency about their requirements for the target chamber. These requirements included the absolute synchronization of laser beams arriving at the target simultaneously, fixed focal plane distances from the final optics to the targets, minimizing x-ray influence on the chamber walls, close proximity of myriad instruments, and ease of ingress and egress of systems to transport, hold, and freeze the tiny targets. The result was a 10 centimeter thick spherical vessel measuring 10 meters in internal diameter, with over 200 holes of varying diameters located over its surface to accommodate the beamlines, diagnostic instruments, vacuum pumping system and other equipment.[2] Sphericity was very important in this design and the stated requirement was for the inside diameter of the chamber to be within ½% of the theoretical diameter or 5 cm rather than the ASME Code requirement of 1% or 10 cm. The material chosen for the chamber was ASME A5083-0 aluminum. This is a strain-hardening alloy that is very formable and weldable. It also possesses a chemistry that will have low activation from neutrons and gamma rays formed in the destruction of the targets.

ANALYSIS

The analytical modeling of the target chamber was carried out by both SNL and LLNL using Patran and Nastran. Both static and dynamic seismic analyses were done. The seismic models also considered the interaction with the building and support pedestal. The exterior 40 cm concrete neutron/gamma ray shield was modeled as a dead weight non-supporting member (this was considered as a worst case). An initial concern was the determination of the required chamber shell plate thickness, considering the number and placement of the port holes, to produce a chamber that would not buckle and maintain a factor of safety of three (based on yield stress) under normal operating conditions. A 10 cm wall thickness met this criteria (an additional forming thickness was added for fabrication).

Due to the distribution of the optics and diagnostic ports the vertical weight of the chamber would have to be supported on a relatively small pedestal area. This would not provide adequate lateral support to the chamber during a seismic event. Thus a total of 17 lateral seismic restraints were added above and below the equator. This effectively tied the chamber to the building. The seismic analysis had to consider the interaction of these supports both on the chamber and the building.

FABRICATION

The contract for the target chamber and its neutron/gamma ray shielding was awarded to Pitt-Des Moines, Inc. (PDM) in July 1997. The method of fabrication and construction of the target chamber was PDM's responsibility. Due to the extreme thickness of the chamber shell, 111 mm – after allowance for thinning during the forming process, and the fact that final welding of the shell segments would be done in Livermore, it was determined that every effort should be made to maximize the size of the shell plate segments thereby decreasing the amount of welding. PDM used its normal spherical vessel plate layout pattern of an expanded cube (6 sides) with 3 plates per side (18 plates total). The design, looking like a giant volleyball, features 6 symmetric middle plates and 12 asymmetric outer plates. As manufactured, the 18 aluminum plates measure 2.4 by 6.9 meters and weigh about 7.5 tons each.

Accurate fabrication of the shell plate segments was essential in delivering the target chamber within the stringent tolerances prescribed by LLNL. The aluminum plates were manufactured domestically and sent to France to be warm formed in a closed die press to a calculated radius of curvature that would allow for weld shrinkage. These segments were then shipped back to the United States and after removal of the excess edge material, the edges were precisely machined to the proper dimensions with the required weld preparation applied. The first 'set' of three plates were trial fit together and inspected for dimensional accuracy. They were found to be acceptable and the remaining plate segments were machined, re-inspected for dimensional accuracy and sent to Livermore for assembly.

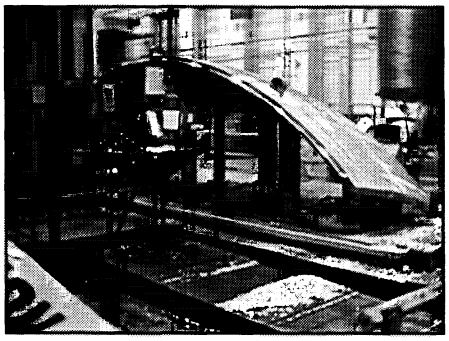

ALUMINUM PLATE SEGMENT BEING MACHINED

CONSTRUCTION

Due to the fast track nature of the project and the need to control the environment where the chamber was assembled, a protective temporary enclosure was designed and constructed. This allowed for temperature control and shielding from the wind and sun, elements that could seriously effect the quality of the welding process and precision of the installed port locations. A 2-ton polar crane was also incorporated with the enclosure to assist with the placement of the ports for welding into the chamber.

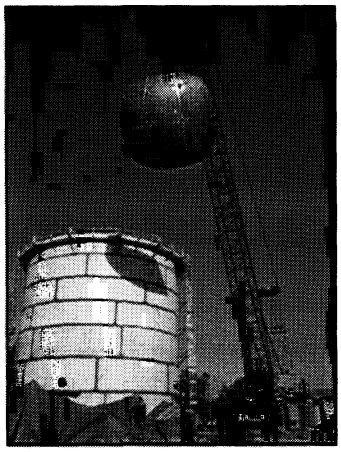

PLATE BEING LIFTED INTO TEMPORARY ENCLOSURE

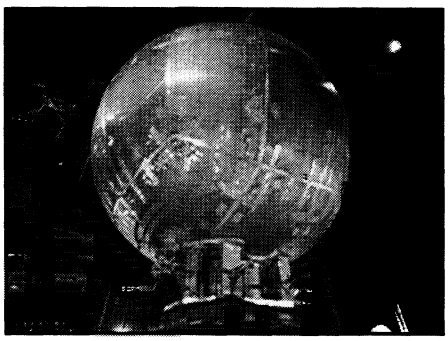

COMPLETED SPHERE

Once on site the first three plates that formed the bottom portion of the sphere were welded together as a subassembly and placed on the pre-assembled chamber support structure. All chamber welding was done using the gas metal arc welding (GMAW) process. The shell complete penetration butt welds took approximately 155 passes to complete and the welding was sequenced to control weld shrinkage/distortion in order to maintain the necessary geometrical tolerances. Once the bottom three-plate subassembly was placed on the chamber support structure the remaining plates that formed the sphere were fit together without welding and the cham-

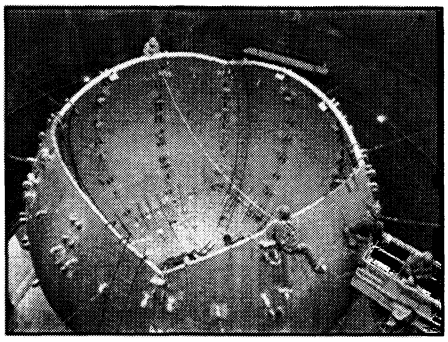

PLATES BEING FITTED

ber geometry was checked by precision survey with a laser tracker to verify proper sphericity prior to welding. Again, the sequencing of the welds was necessary to assure control of critical dimensions. During the welding process the chamber sphericity was re-checked to assure the requisite shape was being maintained.

PENETRATION INSTALLATION

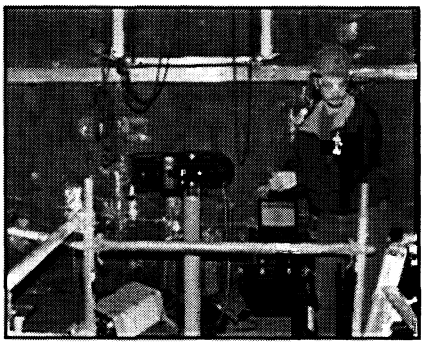

LASER TRACKER

After welding was complete, the laser tracker was again used to perform a precision survey of the interior surface. This survey verified that the chamber was well within tolerance (slightly over ¼% or 2.54 cm) and established the best-fit center of the sphere. The tracker was then used to accurately mark all port locations referenced from the best-fit center as well as over 400 beam dump brackets. PDM then developed special fixtures to bore pilot holes for the ports. These pilot holes became the reference feature used by PDM's specialty machining subcontractor to precisely bore the holes for the ports. Each hole was set specifically to a diameter not more than 3.2 mm larger than the outside diameter of the specific port designated for that location. This was done to minimize the potential for subsequent welding of the port to the chamber to cause the port to fall outside its prescribed location tolerances. PDM then used other custom designed fixtures to accurately position the ports in the holes for welding.

INSTALLING PARTS IN TARGET CHAMBER

PLACEMENT OF CHAMBER IN TARGET BAY

Once this work was complete PDM joined forces with LLNL personnel to move the target chamber from the temporary enclosure to its final location in the Target Bay of the NIF Building. At this point the target chamber weighed approximately 130 tons and the move was accomplished in two steps. First the chamber was lifted from the temporary enclosure by a 14-story-tall Manitowoc 4600 ringer crane and moved approximately halfway to the Target Bay. There it was displayed and dedicated at a ceremony attended by Energy Secretary Bill Richardson and representatives of the science communities in Great Britain and France who are pursuing similar experiments. The following week it was lifted again by the repositioned Manitowoc 4600 and set in the Target Bay on its massive concrete support pedestal.

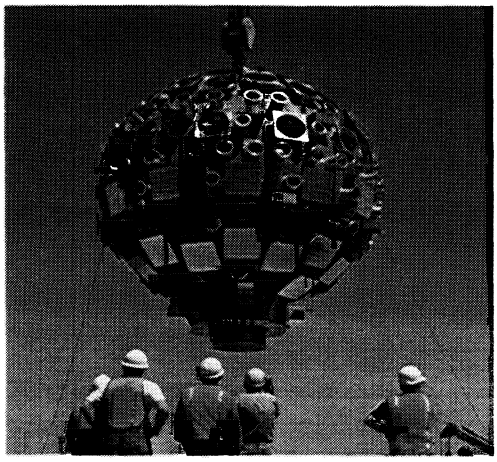

COMPLETED TARGET CHAMBER BEING LIFTED INTO PLACE

At this time the Target Bay walls were roughly half their final height thus the remaining tasks were coordinated with other subcontractors responsible for completion of the conventional building facilities. With the chamber set roughly in final position it was time to test the vacuum integrity of the chamber.

VACUUM LEAK CHECKING

The target chamber is designed to operate at 5×10^{-5} Torr for non-cryogenic target shots and 5×10^{-6} Torr for cryogenic target shots. The requirement for surface finish was mill finish or equal. After all of the fitting and welding that took place the chamber's interior surfaces were hand smoothed with fine grit flapper wheels to approximate the mill finish. The chamber was thoroughly rinsed with a high-pressure water spray. Subsequent construction dust was swept out prior to initial vacuum pumping of the chamber. Temporary o-rings were installed in all 217 flanged joints on the chamber and attached plenum.

The pumping system used for helium spray probe leak testing of the target vacuum chamber consisted of an atmospheric rotary vane pump (120 cfm) and a mechanical pump (140 cfm) that would pump the chamber from 760 Torr to 20 Torr. Then a Roots blower (1250 cfm) was turned on and backed by the mechanical pump. Below 10×10^{-3} Torr, a 6-inch turbomolecular pump (500 l/sec) was gradually valved in and the Roots/mechanical unit was valved out. Then a 10-inch turbomolecular pump (2000 l/sec) was brought on line. Once the chamber pressure was below 1×10^{-4} Torr a 20 inch cryopump was turned on. Note that during the early stages of leak testing the chamber pressure would not allow for more than just barely opening the 6-inch turbopump valve.

Testing was being performed while the building was still being constructed around the chamber and conditions were not ideal when the o-rings were installed and pumping system components mounted. Despite this, testing proceeded much as planned with repeated cycles of pumping down – leak testing – venting up to repair leaks. Each successive pump down cycle resulted in an improved base pressure and smaller leaks not visible at higher pressure were identified and corrected. The source of these leaks was about equally split between weld leaks in the ports and o-ring leaks. Once all leaks were eliminated the chamber was segmentally bagged to verify the integrity of all shell butt welds and port welds. The combination of pumps used above was able to take the target chamber repeatedly to a pressure of less than 8×10^{-7} Torr! A final rate of rise test was performed to establish a baseline. This was subsequently successfully compared to a repeated rate of rise test performed after application of the neutron/gamma ray shield to verify that the vessel was still sound.

CHAMBER SHIELDING

The neutron/gamma ray shield consists of 16 inches of borated concrete applied as layers of gunite sprayed onto the outside shell of the target chamber. Two layers of steel reinforcing bars were mounted in a grid pattern to studs welded to the chamber. A bonding agent was used to improve the tie between the concrete and the chamber shell. The tubular portions of the ports and all structural supports below the surface of the concrete were isolated from the concrete to guard against an overstressed condition in the event of a seismic occurrence. After all of the gunite layers were applied and the concrete cured for about six weeks the surface was hand worked to a smooth finish and painted with two coats of epoxy paint.

CHAMBER SURVEY

The next significant activity was to re-evaluate the spherical geometry of the chamber after placing over 200 tons of concrete on the exterior. Again, a precision survey with laser tracker was done to determine the current best-fit center based on evaluating the most critical chamber components: the location of the 72 Final Optics Assembly (FOA) or laser ports. Now knowing the location of the best-fit center and its relationship to the FOA ports, the chamber was ready to be accurately positioned on the pedestal support.

CHAMBER ALIGNMENT

Since most of the surface of the chamber has ports installed it was obvious that the equipment necessary to position the chamber could not be permanently installed. PDM developed system of hydraulic jacks and multi-ton rollers that could elevate, translate and rotate the chamber in small incremental moves. This system was installed on a substantial steel jacking ring that is supported through embedments in the chamber pedestal support. A second jacking ring is attached to the chamber support structure and lines up directly above the jacks and rollers. PDM, with the help of the precision surveyors using two laser trackers on opposite sides of the chamber, was able to place this massive structure within less than 1 mm of the desired location.

Once in position the actual gaps between the base of the chamber support and the top of the pedestal were measured and custom shims were machined and installed to lock the chamber in position. Next a number of horizontal seismic stabilizing struts were tied to the chamber. The chamber was then given a rough cleaning with warm water and a low concentration of detergent. All ports then had their covers removed and the flange faces and o-ring grooves wiped clean. The covers were reinstalled along with the vacuum pumping system components, except for the cryopump. The chamber was then pumped down to below 10×10^{-5} Torr and all flanged connections were leak tested to verify vacuum integrity.

FOA SPACERS

At this time the Target Bay is not environmentally controlled and the variation in temperature does not allow measurements with the necessary degree of accuracy to be made to verify the final position of the chamber. Another task that is related is the measurement of the position of each FOA port flange. Once the plane and location of the flange surface can be established, custom-machined spacers will be made for each of these ports. The purpose of the spacers is to correct the plane to within 0.23 degrees and the position to within 0.12 mm for the equipment that mounts to this port.

PROGRAM STATUS

The NIF construction project is scheduled for completion by the end of fiscal year 2004. Some of the beam lines will be in use well before that date, however. The current plan calls for making a few beam lines available many months before the end of project construction so that integrated beam lines can be tested and the experimental communities can begin using NIF's advanced capa-

bilities. The goal for fusion ignition and energy gain on NIF is scheduled toward the latter half of this decade.

REFERENCES

1. National Ignition Facility Poster; 40-00-0295-0563C 3/97

2. Arnie Heller, "Target Chamber's Dedication Marks Giant Milestone", Lawrence Livermore National Laboratory, Science & Technology Review – September 1999, UCRL-52000-99-9

BIOGRAPHICAL SKETCHES OF AUTHORS

Paul J. Fleming

Mr. Fleming received a Bachelors degree from Purdue University in Mechanical Engineering. He has worked for Pitt-Des Moines, Inc. for over 27 years in the areas of project management, project engineering and sales. He has been involved with storage and systems for LNG and other cryogenic fluids, composite bonding autoclave systems, thermal energy storage systems, egg shaped anaerobic digester systems as well as vacuum, fusion and high altitude simulation systems. Significant projects include ALPHA Project – San Clemente, CA; MFTF-B – Livermore, CA; Composite Bonding Autoclave Facility – Frederickson, WA; and LNG Import Terminal – Lake Charles, LA. Mr. Fleming was also responsible for the successful leak testing of a number of large thermal vacuum chambers including MFTF-A, Livermore, CA; LCTF – Oak Ridge, TN; and the prototype Neutral Beam Injector Chamber for the PPPL Tokamak Fusion Program. For the past three years he has been the Project Manager for the turnkey supply, installation and testing of the Target Chamber for the NIF Program.

Richard W. Wavrik, PE

Mr. Wavrik received a Bachelors degree from the University of Florida and a Masters of Mechanical Engineering degree from the University of Virginia. He worked on the mechanical design and development, thermal and stress analysis, and project management in positions with NASA; Research Engineering and Science Laboratory; Babcock and Wilcox Co.; Union Carbide Nuclear Division; Sandia National Laboratory; and Lawrence Livermore Laboratories. He holds several patents for innovative designs for gas centrifuges. For the past seven years, he has been the principal engineer for the NIF target chamber with responsibility for conceptual design through fabrication and installation.

James Cox

Mr. Cox is currently the System Manager for Beampath Hardware Fabrication for the National Ignition Facility at LLNL. As such, he is responsible for the design and fabrication of non-optical mechanical hardware associated with the laser beamlines for the NIF. Mr. Cox joined LLNL in 1986 as part of the Atomic Vapor Laser Isotope Separation (AVLIS) project. He has managed the installation, commissioning and operation of special equipment in several AVLIS facilities. Prior to joining NIF in September 1999, Mr. Cox served as the Refurbishment Area Design Manager for the USEC AVLIS Plant project. He holds an MS in Nuclear Engineering from the University of Wisconsin-Madison.

LIGO BEAM TUBE LEAK TESTING

A Case Study of Ultrahigh Sensitivity Vacuum Leak Testing of Very Large Structures

P. B. Shaw and Warren A. Carpenter
Chicago Bridge & Iron Co.

ABSTRACT

This Case Study presents an example of ultrahigh sensitivity leak testing of very large vacuum structures. Five key concepts are presented which can be applied to save time, trouble and money in the leak testing of vacuum systems. The case study will illustrate how these concepts were applied on the recent LIGO project, with successful outcomes of reduced cost, schedule and improved test confidence. While the details of application of the concepts will vary on other projects, observance of them can save any vacuum leak testing program time, trouble and money.

INTRODUCTION

There are two LIGO observatories, one at Hanford, Washington, and the other in Livingston Louisiana. Each LIGO observatory is a very long "L" shaped vacuum chamber with each arm of the L being a separate beam tube 1.2 meters (four feet) in diameter and 4 kilometers (2.5 miles) in length. Total internal volume of each LIGO is in excess of 332,000 cubic feet. The beam tubes are operated at vacuums of 10^{-9} torr and better. The LIGO project required the manufacture, leak test, site installation, and re-leak testing of nearly ten miles of beam tube, which contained more than 70 kilometers (44 miles) of vacuum boundary welding.

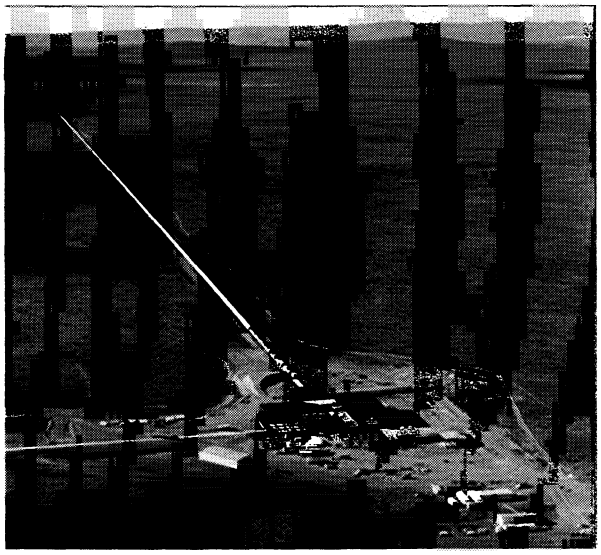

Figure 1. Aerial photograph of the Hanford LIGO X arm.

This case study demonstrates ultrahigh sensitivity leak testing. The LIGO beam tubes were tested and certified to have no single leak of 1 x 10^{-10} scc/second helium. A total air leakage (air signature) assessment of the finished structure has been performed on each 1.24 mile long module (one half of an arm) of the beam tube. Six of the 1.24 mile modules currently show total air burdens below the lower limit of detection, which is approximately 2 x 10^{-10} scc/sec. Two of the modules are indicating low 10^{-9} total air burden, although the source of that burden has not been identified, and is most likely in a valve or mechanical connection.

The LIGO project required leak testing of eight beam tube modules, each of which is 83,000 cubic feet in volume, to the sensitivity necessary to certify no leak of 1 x 10^{-10} scc/sec.

The objective of this case study is to identify key concepts that can be used to build a successful leak testing program. A "successful" leak testing program is one that controls cost, schedule and test confidence.

The LIGO beam tube section manufacturing and leak testing operations are described. That description provides examples that illustrate five key concepts, and how consideration of those concepts drove decisions and outcomes in the leak testing program.

BEAM TUBE MANUFACTURING

Beam Tube Fabrication

The beam tube was manufactured in sixty-five foot long sections. The tube sections were manufactured from a 3.2mm (one eighth inch) thick stainless steel strip that was spiraled (rather like the cardboard center to a paper towel roll) and welded.

Figure 2. A beam tube section at the fabrication plant.

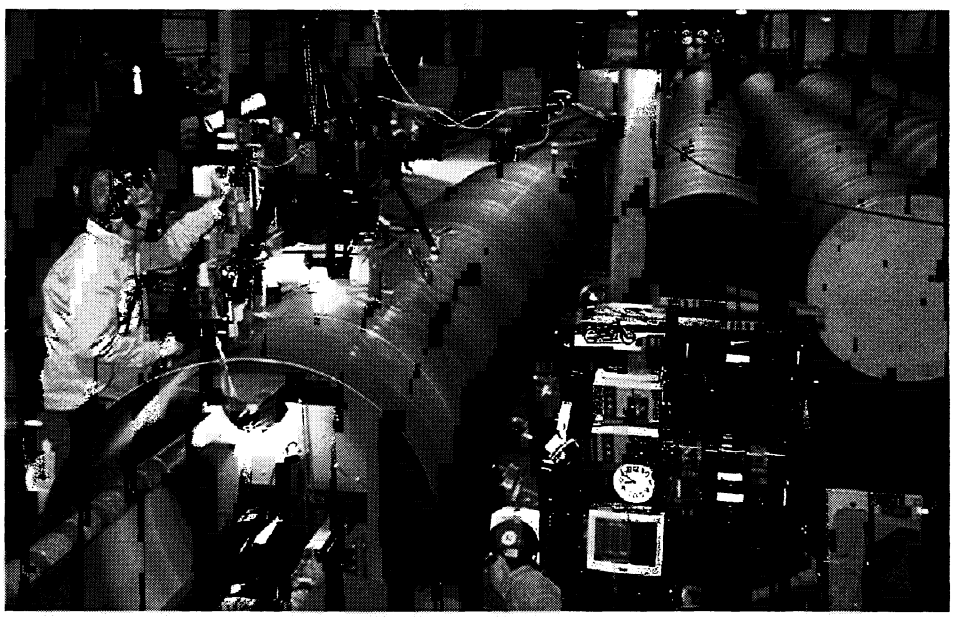

Figure 3. Welding 1/8" thick stainless steel on the spiral tube mill.

A thorough visual examination was performed on all welding. Welds examined included the welding of the spiral, welding of external stiffeners to the one eighth inch thick tube to stiffen it for vacuum service, welding of an expansion bellows to half of the tube sections, and welding of the pump ports to the tube. Visual examination was a critical element in the success of the leak-testing program, and will be discussed in detail later in this paper.

After completion of the visual inspection and repair of any observed welding anomalies, the beam tube sections were taken to the testing facility.

Beam Tube Section Test Equipment and Facility

Figure 4 is a photograph of the beam tube section testing facility located in the fabrication plant. Three identical test stations were provided in the testing facility. This permitted the pumping of three beam tube modules at one time. Figure 5 is a sketch of a tube section test station. These test stations were used for hood or bag test to confirm that the total leakage rate for a tube section was less than 1×10^{-10} scc/sec. helium.

The most obvious structures in the test facility are the large steel hoods. Steel hoods were constructed and utilized instead of using the more conventional plastic helium hood/bag. The rigid steel helium hood offered a number of important advantages:

- it significantly reduced the labor required to perform a test
- it provided a significant improvement in helium background control
- it facilitated consistent helium concentrations.

The hoods were attached to a mechanical vacuum pump, with the vacuum pump exhaust vented through the building roof. This pump was used to initially evacuate the air from the hood, and to evacuate helium from the hood at the end of the test sequence.

Figure 4. A view of the beam tube section testing facility including tests of both "standard" length and odd length tube sections.

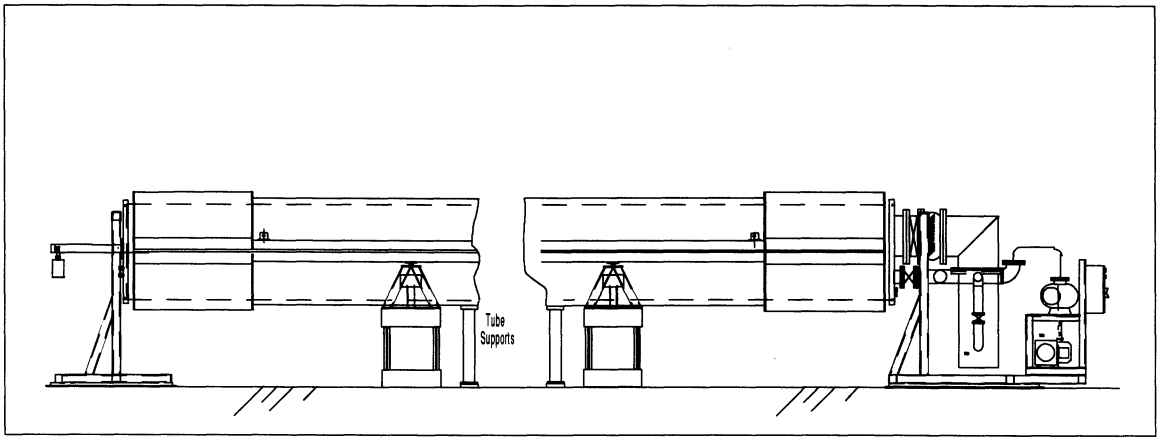

Figure 5. Sketch of a beam tube section test station.

Each test station included a pair of end heads for sealing off the open ends of the tube sections. These heads were supported on track mounted carts. The "far end" head included a vent valve for venting the tube after test completion, and a low 10^{-10} scc/sec calibrated leak for full system calibration. The "near"" end head included a six-inch roughing port, and a twenty-inch diameter high vacuum pumping port. The twenty-inch diameter high vacuum port lead to a gate valve, an LN_2 filled cold trap, and a 17,000 liter per second diffusion pump. A roots blower and rotary vane pump set was mounted on the near end cart for rough pumping and initial diffusion pump backing, and an eleven cfm vane pump was mounted to the cart to provide long term backing for the diffusion pump.

These three leak test stations were in a large, closed room within the beam tube manufacturing plant. A positive pressure room ventilation system was provided, with air supplied from outside the manufacturing facility. The air inlets were on the upwind side of the manufacturing plant, and the exhausts were to the down wind side of the plant.

A two-inch diameter branch of the diffusion pump foreline ran out through the nearest wall of the test room, through an adjacent wall into a control room. Inside the control room the foreline was connected to a small, manually fed LN_2 trap, and a manual isolation valve leading to a helium mass spectrometer. The control room was equipped with three computers for controlling the leak test stations by means of laboratory software, and three helium mass spectrometer leak detectors, one for each test station. As with the test room, this control room had positive air pressure compared to the surrounding facility, and was supplied with air from the outdoors, upwind side of the manufacturing plant.

Helium concentration sampling and return lines ran from an attachment point on each rigid hood bottom half, out of the test room to a binary gas chromatograph located in the manufacturing facility adjacent to the test room. This equipment provided a positive measurement of the helium concentration in the test hood, at an elevation below the lowest area of interest.

VACUUM PUMPING AND TEST SEQUENCE

Upon completion of manufacture, the beam tube sections were delivered to the test facility. There, each beam tube section was set on the tube stands in one of the three test stations. The end head carts were rolled up to the tube, and the tube ends sealed to the heads. The beam tube was rough pumped by the roots and vane pump set mounted on the near end cart. Then the tube section was then high vacuum pumped with the 20-inch cold trapped diffusion pump. The diffusion pump was initially backed by the roots and vane pump for a few minutes. The mass flow was then small enough to allow backing of the diffusion pump with a small eleven cfm vane pump. The tube section was vacuum conditioned with high vacuum pumping for a few hours.

While the tube was vacuum conditioning, the technicians would seal the test hood around the tube, and evacuate the helium test hood to a pressure of a few torr.

After the tube section was evacuated to a pressure in the low 10^{-6} to mid 10^{-7} torr range, the leak testing sequence was started. Immediately prior to the test sequence, the LN2 trap in the foreline and the helium mass spectrometer internal cold trap were topped off with LN2. With the helium mass spectrometer leak detector (the HMS) still isolated from the test system, the HMS auto calibration sequence was initiated, and an internal calibration of the HMS was performed. Upon completion of the HMS calibration sequence, the isolation valve to the diffusion pump foreline was opened, and the small forepump on the pumping skid was isolated. This left HMS as the only backing for the diffusion pump. The test system response was then calibrated against the signal from a low 10^{-10} scc/sec calibrated leak mounted to the far end test head.

Upon completion of the pre-test calibration, the test hood, which had been evacuated to a few torr, was filled with helium to a pressure of 720 to 740 torr. The helium concentration in the test hood was measured, and the test dwell was observed. Upon completion of the test dwell time, the system was again calibrated against the far end calibrated leak. As soon as this post test calibration was completed, the helium mass spectrometer leak detector was isolated from the test system. All readings were recorded, the test response was corrected for helium concentration and helium hood pressure, and the test was evaluated for acceptance. The helium in the hood was evacuated, vented with air and evacuated again. This air "sweep" was repeated at least two times before the hood was opened to the test room.

FIVE KEY CONCEPTS

We have identified five key concepts that are critical to any ultrahigh sensitivity leak testing program for large structures. The unifying theme underlying these concepts is to maximize the Signal to Noise ratio of tests at every opportunity. The Key Concepts are :

1. Minimize Instrument Servicing (by maximizing preservation)
2. Helium Mass Spectrometer Leak Detector Selection
3. Helium Background Control.
4. Helium Concentration Measurement.
5. Upstream Process Control.

1. Minimize Instrument Servicing (by maximizing preservation.)

When testing to 10^{-11}, and 10^{-12} scc/sec sensitivities, instrument preservation is vital. Any time you service a helium mass spectrometer leak detector, you are in for at least a one to two shift delay in getting the machine back to it's stable peak. Worse, an unfortunate percentage of the time you may be in for as much as a week of getting the machine back to peak condition. Frequently, the delays will turn out to be caused by self-inflicted issues that arise from the servicing of the instrument.

It is important to define "service" of the instrument. We are not talking about changing the air filter and the changing backing pump oils. We are speaking of any service that requires breaking the seal of the vacuum boundary.

There are some good service organizations, but very few users actually work at these sensitivities, and specifically not these sensitivities for large structures. The technicians who service your equipment are usually not accustomed to taking the precautions necessary to keep the instruments working at this fine a peak. Anytime you can prevent a major service; you are saving schedule and money.

You may note the following features that were designed to minimize the need for instrument servicing in the case study:

1.1 The amount of time that the instrument was on line with the test system is minimized. Time on line leads to mass through the instrument including contaminants. The less contamination that goes through the instrument, the less often it will need service. Typically, the HMS instruments used on the LIGO beam tube project saw less than 15 minutes exposure to the test system for any given test.

1.2 The next measure was the use of the external cold trap in the line leading to the helium mass spectrometer. Again the philosophy is to minimize the mass of contaminants going through the instrument. In the case of the mass spectrometers being used behind diffusion pumps, it is worth noting that the diffusion pump oil is an insulator. Although only minute traces of diffusion pump oil come back through the foreline, the philosophy stands: Contaminants that can be trapped before entering the instrument will never affect the instrument.

1.3 The use of an external isolation valve mounted directly to the HMS instrument test port makes it possible to isolate the helium mass spectrometer leak detector from test hardware without venting the instrument test port. The instrument was never vented to isolate it from a test. Many of these instruments were used for weeks at a time without having the test port vented. This minimizes mass flow through the instrument, and preserves the vacuum conditioning of the test port and valve block in the instrument. Although many people regard this as an extreme measure, it is all part of a philosophy that protects the instrument "in the extreme". This philosophy is meant to preserve as stable and sensitive an instrument as possible, while minimizing the need for instrument servicing.

1.4 Limit access to the test instrument. Our technicians did not service the helium mass spectrometers. When an instrument would not adequately calibrate or was not sufficiently stable to perform the required test, the technicians would summon the Testing Manager, or would exchange the instrument for another unit. The Testing Manager would make the necessary adjustment and repairs, or would arrange for repair by the instrument manufacturer's personnel. The beam tube project required six helium mass spectrometer leak detectors to support the manufacture and installation of the beam tube and it's appurtenances. The project had a total of seven leak detectors to cover the operations in the manufacturing test facility, valve tests at manufacturing, and leak testing at the installation site. Having multiple helium mass spectrometer leak detectors also provided a means to cover those instances when one of the instruments was not operating adequately.

1.5 Never use a helium mass spectrometer leak detector when a pump was all that was required. Using the helium mass spectrometer leak detectors as a pump is a common practice in many facilities. They are frequently used for roughing, and vacuum pumping test objects prior to leak testing. It is a rather expensive practice. If you can save one service call on your leak detector by using external roughing pumps, you have saved more than the cost of several vane pumps. One delay of a time critical test may easily pay for a 50 liter per second turbo pump stand. Pumps are inexpensive compared to leak detectors and their service.

A collection of mechanical roughing pumps and 50 liter per second turbo pump stands were used for all roughing, and vacuum conditioning leading up to vacuum leak tests for the LIGO beam tube project. This is consistent with the philosophy of minimizing mass flow through the instrument, and limiting HMS time on line.

The test sequence discussed previously was used for testing 800 beam tube sections that were manufactured for this project. There were more than 1000 tests of other items including valves, test ports, external hardware, pumps and other vacuum assemblies. These tests were perhaps more typical of the miscellaneous testing that is common in a space simulation test facility. The same philosophy of instrument preservation applied to all of the testing.

2. Instrument Selection

Selecting the right helium mass spectrometer can be crucial. We offer the following suggestions:

2.1 The ability to "zero" out the system background is necessity when testing in the 10^{-10}, 10^{-11} or 10^{-12} scc/sec leak sensitivity ranges on large systems. Large systems will have a background, and the zero function makes it possible to distinguish 10^{-11} and 10^{-12} signals from a stable 10^{-9} range background with a zero function.

2.2 All manufacturers claim to have first class service support. Investigate this claim carefully. CB&I owns helium mass spectrometers from four major manufacturers, and the service organizations are not equal. We were very pleased with the service and support we received from the manufacturer of our six primary helium mass spectrometer leak detectors at LIGO.

2.3 Consider carefully before purchasing a helium mass spectrometer from a manufacturer whose home market is geographically distant from your location of use. On other projects we have often been told that a needed part for one of our helium mass spectrometers is on back order on another continent. Again, we did not have these problems with our instruments at LIGO and we were very pleased with the support we received.

2.4 Investigate the manufacturer's commitment to long term support of the instrument. We have had one manufacturer stop parts and service support for an instrument that was only five years old. Again, this was not the case with the supplier of the instruments for LIGO, but it has happened with other instruments in our fleet.

3. Helium Background Control.

The design of the beam tube test facility and the rigid hoods were crucial for helium background control. To perform a test that will certify leak tightness to 1×10^{-10} scc/sec, the operational sensitivity of the system will be low 10^{-11} to mid 10^{-12} scc/sec, which is very close to the maximum instrument sensitivity commercially available from direct flow helium mass spectrometers. When working at these sensitivities, helium background control is essential. Helium background becomes noise to the test. This noise from the helium background can be nearly impossible to distinguish from the actual test signal, and can very quickly invalidate a test. Further, dealing with inadequately controlled helium background is time consuming.

There are many potential sources of helium background. The first and most obvious is the helium used in the hood during the test. A second source was the helium bottle racks and piping bringing the helium to the test room. More subtle, but a nonetheless important source is related to the use of helium in the shielding gases used for welding. In our LIGO case study, the shielding gas for welding on the spiral tube mill was 75% helium. The shielding gas for the manual GTA welding of ports, and the automated welding of the expansion bellows was also a high helium mixture. These sources were located in the same manufacturing plant as the test facility, and were sources of helium background to the testing operation.

Examples of measures used to control helium background include:

3.1 Isolating test object and test systems from facility helium sources. The case study test room was an entirely enclosed room including walls and roof. Taking the air supply for this room from the outdoors, upwind of the plant, and exhausting downwind of the plant was a helium background control measure.

3.2 Isolating the helium mass spectrometer leak detectors from the helium hood and other sources of helium. The case study HMS's were located in a separate room with a separate external air supply. Although the helium mass spectrometer control room was close to the test room, the two rooms were constructed with separate walls, with an airspace between those walls to reduce the possibility of helium background in the test room affecting the helium mass spectrometers. A further control that became necessary when operating at these sensitivities was that the room containing the helium mass spectrometers was "locked down" during each test. The helium mass spectrometers were being operated at sensitivities that were occasionally affected if the door of the room was opened and closed.

3.3 GN_2 bleed on helium mass spectrometer foreline. Although not used in the case study, other parties have testified to the effectiveness of putting a nitrogen bleed into the foreline of the helium mass spectrometer turbomolecular pump. The goal of this measure being to reduce backstreaming of helium from the surrounding environment via the forepump exhaust.

3.4 Helium background from hoods or hood bags. The use of rigid hoods instead of polyethylene bags for containing helium around the tube section during the test is a significant means of controlling helium background. In the case study test sequence, once the beam tube was satisfactorily evacuated to the low 10^{-6} or 10^{-7} torr pressure range, and the hood was sealed to the tube, then the hood would be evacuated using a mechanical pump.

a. Once the test system was calibrated, the hood would be backfilled with helium to an absolute pressure of approximately 720 to 740 torr. By keeping the hood at a net pressure lower than the surrounding test room, the net flow of helium from the hood to the room was functionally eliminated.
b. Upon completion of the test, the hood was evacuated with the mechanical pump set, and the exhaust of the pump was routed through the roof of the manufacturing facility, and exhausted above the plant roof. The hood would then be vented with air, and re-evacuated to sweep the residual helium from the hood enclosure.
c. Evacuating helium from hood bags when bags are used. There were twelve "odd length" tube sections manufactured. These sections would not fit the rigid hood, and had to be "bag" tested. The polyethylene bags were carefully made and sealed, and the helium content of the bags was evacuated from the bag through the vacuum pump vented through the roof.
d. Similar to c. above, when testing nozzles, valves and other miscellaneous fittings using helium bag hoods, we use "swimming pool hose and shop vacuums to evacuate the hood bags before test, and to evacuate the helium from the bags after test. Using the swimming pool vacuum hose, you can economically evacuate the helium from a bag to the nearest outdoor vent from a building, thereby controlling helium background in the area near a chamber or other test object.

The effects of handling helium in a facility was dramatically demonstrated in the case study. The helium background in the manufacturing test facility would rise during each of the polyethylene hood bag tests. The test facility was effectively shut down due to helium background for four or more hours after each helium bag test of an odd length tube.

4. Helium Concentration Measurement.

Actual measurement of helium concentrations in hoods and bags offers a substantial improvement in helium mass spectrometer leak detection.

Measurement of the helium concentration reduces the cost of testing, while simultaneously making a dramatic improvement in test reliability (and test confidence.) It is a genuine win-win proposition.

Traditionally, helium mass spectrometer leak testing personnel do not make actual measurements to determine the helium concentration in hoods and bags. Instead, they make an assumption concerning the helium concentration. If they are very conscientious when using a hood bag, they will evacuate the bag with a shop vacuum or other similar device. They will then fill the bag with helium while venting through a small vent hole. They will ultimately close the vent, top off the bag, and then assume a 50% concentration of helium in the bag. However, when actual measurements of the helium concentrations are made, it becomes immediately apparent that the assumption of at least 50% helium evenly distributed in the bag is entirely unfounded. The helium immediately rises to the top of the bag, and the air is in the lower elevations of the bag. The margin of error can be as much as two orders of magnitude, with concentrations in some portions of a bag being as little as 0.5% while concentration at the top of the bag will exceed 95%. The air and helium in the bag may eventually intersperse, but not within a time reasonable for a leak test.

In the LIGO Beam Tube, we used two different means of measuring helium concentrations. At our testing facility in the manufacturing plant, we had a binary gas chromatograph tuned for helium. This equipment was plumbed through a circulation pump to the test hood. The attachment point for this gas chromatograph was below the elevation of the lowest point of interest on the test object. This piece of equipment registered helium concentration directly.

An alternative means of measuring helium concentration is the portable oxygen meter. This is a small unit used by safety personnel for checking oxygen sufficiency, and by welding personnel for measuring the adequacy of purged areas for welding. This handheld, battery powered device measures oxygen content in percent. It can be used for measuring helium by means of the assumption that air is 20% oxygen, that the air concentration in a helium hood or bag is five times the oxygen, and that the balance is helium.

Figure 6. Photo of a handheld oxygen meter.

The binary gas analyzer is preferable, as it is a positive for helium test where as the oxygen meter provides a measurement of air exclusion. At the time that the LIGO project was started, binary gas analyzers were bulky, 110 VAC devices best suited to a fixed facility. Today there are handheld battery powered units available that offer the portability of a handheld unit, with the benefit of being a positive test for helium rather than a negative test for air.

The benefits of helium concentration measurement derive from a number of facts. These include:

4.1 Diffusion theory indicates that the air and helium in a bag or hood will diffuse into one another. Unfortunately, in the time frames applicable to leak testing, helium and air stratify immediately and nearly completely. We have conducted experiments with multiple detectors mounted in a helium bag on a leak test. Even though the helium fill of an evacuated bag is conducted from the bottom of the bag, there is a clear and marked stratification.

4.2 The technicians became much more adept and efficient at making hood bags when they had the "feedback" of attempting to fill the bags with an objective helium concentration measurement.

4.3 It was found that it was no longer necessary to "vent" the hood bags during fill. We now make our bags with a "dead leg" extending from the lowest elevation of the bag. The air that remains in the bag will wind up in the dead leg. The use of the dead leg results in a much lower helium background in the immediate area than the earlier "vent while filling" method.

4.4 As a consequence of the two preceding items, helium consumption for the purpose of filling most bags was reduced. The benefit being both a savings in helium, and a reduction in the helium background in the area surrounding the test.

There is another beneficial application of measuring helium concentrations. When leak hunting an object with a leak, such as a chamber shroud, it is possible to rapidly narrow the leak search by means of helium concentration measurements. The elevation of a leak can be rapidly determined by mounting multiple helium (or oxygen) sensors in the hood bag and simultaneously monitoring the leak detector and helium concentrations during the bag fill. We have done this when hunting for a leak in a large shroud. The distinct change in leak rate signal as the helium/air interface zone reaches the elevation of the leak is remarkable, and provides a nice indication of approximate elevation.

5. Upstream Process Control.

The Most Critical Concept: DON'T HAVE LEAKS! It is much less expensive to prevent a leak than to locate one that requires repair. Simply stated, if you have leaks that must be located and repaired in a large high vacuum or ultrahigh vacuum system, then you lose control of cost and schedule.

Leak hunts are notoriously difficult to estimate for direct cost and schedule impact, and the indirect cost and schedule impact will usually dwarf the immediate impacts. If the testing is part of a production sequence, then there are delays and costs to other processes that are affected by the leak hunt. Less obvious, but potentially as important is the effect of a leak hunt on your equipment. One of our concepts was to minimize service of the helium mass spectrometer leak detector. One of the most important measures in doing that is to minimize the time the instrument is on line and susceptible to contamination, and to minimize the mass flow of contaminants through the instrument. Unfortunately, leak hunts typically mean many hours of testing with the helium mass spectrometer open to a chamber, vessel, or assembly that is leaking. This greatly accelerates the need for servicing the instrument, with all of the potential delays and costs that are associated with that activity.

Fortunately, the overwhelming majority of leaks are preventable, particularly in the case of weld leaks. The visual inspections by the Welding and Quality Assurance Supervisors on the LIGO project detected and subsequently repaired hundreds of welding anomalies. These anomalies such as weld starts and stops, were repaired prior to any leak testing. The majority of these anomalies would not have produced vacuum leaks, however, the cost of making these touch up welds is far less expensive than the cost of hunting down and repair leaks during leak testing. The thoroughness and diligence of the welding supervisors and welders was a critical element of the success of the LIGO leak testing program.

For the LIGO beam tubes, the welding engineering and quality control measures utilized for the project were adequate to produce 43 miles of one eighth inch thick stainless steel weld without any one weld leak equal to or greater than 1×10^{-10} scc/second.

There were leaks detected in mechanical equipment and welds in mechanical equipment from vendors. There were also a few leaks at mechanical connections, but none in the beam tubes and the beam tube welds.

Surprisingly, a great many of the individuals and companies that work in the vacuum industry take the production of leaking components that for granted. There is a culture that assumes leaks will be produced, and that they will have to be located and repaired. This is a very expensive cultural assumption or paradigm. The cost and schedule consequences of leak hunting are so substantial that the individual or organization that will make the investment in process control to eliminate the leaks will be handsomely rewarded.

Specific, identifiable investments were made in welding engineering and quality assurance of the LIGO beam tubes to minimize the possibility of a weld leak. While these were expensive measures, there was a clear understanding that the cost and schedule consequences of producing beam tube sections with leaks was far more expensive. The net result exceeded expectations. Not only were no tubes presented for leak testing with a leak, but each of the welding engineering and quality control measures intended to prevent leaks turned out to be effective in providing greater productivity for the processes. The

purportedly "expensive" measures paid for themselves in increased productivity entirely apart from the savings against leak hunting.

CONCLUSION

The successful ultrahigh vacuum leak testing program developed on the LIGO program demonstrated the importance of five key concepts.

1. Minimize Instrument Servicing (by maximizing preservation)
2. Helium Mass Spectrometer Leak Detector Selection
3. Helium Background Control.
4. Helium Concentration Measurement.
5. Upstream Process Control.

Close attention to these concepts allowed the program to maximize the signal to noise ratio of tests. This enabled the project to achieve a high degree of test confidence while being completed at reduced cost on an accelerated testing schedule.

REPORT DOCUMENTATION PAGE

Form Approved
OMB No. 0704-0188

1. AGENCY USE ONLY *(Leave blank)*

2. REPORT DATE
October 2000

3. REPORT TYPE AND DATES COVERED
Conference Publication

4. TITLE AND SUBTITLE
Twenty-first Space Simulation Conference:
The Future of Space Testing in the 21st Century

5. FUNDING NUMBERS
Code 540

6. AUTHOR(S)
Compiled by Joseph L. Stecher III

7. PERFORMING ORGANIZATION NAME(S) AND ADDRESS (ES)
Goddard Space Flight Center
Greenbelt, Maryland 20771

8. PEFORMING ORGANIZATION REPORT NUMBER
2000-04187-0

9. SPONSORING / MONITORING AGENCY NAME(S) AND ADDRESS (ES)
National Aeronautics and Space Administration
Washington, DC 20546-0001

10. SPONSORING / MONITORING AGENCY REPORT NUMBER
CP—2000–209967

11. SUPPLEMENTARY NOTES
Co-sponsors: Institute of Environmental Sciences and Technology, American Institute for Aeronautics and Astronautics, American Society for Testing and Materials, and the Canadian Space Agency

12a. DISTRIBUTION / AVAILABILITY STATEMENT
Unclassified–Unlimited
Subject Category: 18
Report available from the NASA Center for AeroSpace Information,
7121 Standard Drive, Hanover, MD 21076-1320. (301) 621-0390.

12b. DISTRIBUTION CODE

13. ABSTRACT *(Maximum 200 words)*

The Institute of Environmental Sciences and Technology's Twenty-first Space Simulation Conference, "The Future of Space Testing in the 21st Century" provided participants with a forum to acquire and exchange information on the state-of-the-art in space simulation, test technology, atomic oxygen, programs/system testing, dynamics testing, contamination, and materials. The papers presented at this conference and the resulting discussions carried out the conference theme "The Future of Space Testing in the 21st Century."

14. SUBJECT TERMS
Space Simulation, Thermal Vacuum Testing, Contamination Control, Spacecraft Materials, New Approaches and Facilities, and Special Topics

15. NUMBER OF PAGES
280

16. PRICE CODE

17. SECURITY CLASSIFICATION OF REPORT	18. SECURITY CLASSIFICATION OF THIS PAGE	19. SECURITY CLASSIFICATION OF ABSTRACT	20. LIMITATION OF ABSTRACT
Unclassified	Unclassified	Unclassified	UL